Modern Aspects of Electrochemistry 58

T. Richard Jow
Kang Xu
Oleg Borodin
Makoto Ue *Editors*

Electrolytes for Lithium and Lithium-Ion Batteries

Springer

MODERN ASPECTS OF ELECTROCHEMISTRY

No. 58

Series Editors:
Ralph E. White
Department of Chemical Engineering
University of South Carolina
Columbia, SC 29208

Constantinos G. Vayenas
Department of Chemical Engineering
University of Patras
Patras 265 00
Greece

For further volumes:
http://www.springer.com/series/6251

Previously from Modern Aspects of Electrochemistry

Modern Aspects of Electrochemistry No. 56

Applications of Electrochemistry in Medicine

Edited by Mordechay Schlesinger, Professor Emeritus,
Department of Physics, University of Windsor, Canada.

Topics in Number 56 include:

- Electrochemistry in the design and development of medical technologies and devices
- Medical devices at the interface of biology and electrochemistry
- Sensing by screen printed electrodes for medical diagnosis
- Electrochemical glucose sensors
- Electrochemistry of adhesion and spreading of lipid vesicles on electrodes
- Bio-Electrochemistry and chalcogens
- Nanoplasmonics in medicine
- Extravascular hemoglobin: aging contusions
- Modeling tumor growth and response to radiation

Modern Aspects of Electrochemistry No. 57

Electrodeposition and Surface Finishing

Edited by Stojan S. Djokić, Professor of Chemical & Materials
Engineering at the University of Alberta

Topics in Number 57 include:

- Electrodeposition and the characterization of alloys and composite materials
- Mechanistic aspects of lead electrodeposition
- Electrophoretic deposition of ceramic materials onto metal surfaces
- Metal oxides for energy conversion and storage
- Electrochemical aspects of chemical mechanical polishing
- Surface treatments prior to metallization of semiconductors, ceramics, and polymers
- Anodization of aluminum

T. Richard Jow • Kang Xu • Oleg Borodin
Makoto Ue
Editors

Electrolytes for Lithium and Lithium-Ion Batteries

Springer

Editors
T. Richard Jow
U.S. Army Research Laboratory
Adelphi, MD, USA

Kang Xu
U.S. Army Research Laboratory
Adelphi, MD, USA

Oleg Borodin
U.S. Army Research Laboratory
Adelphi, MD, USA

Makoto Ue
Mitsubishi Chemical Corporation
Yokohama, Kanagawa, Japan

ISSN 0076-9924 ISSN 2197-7941 (electronic)
ISBN 978-1-4939-0301-6 ISBN 978-1-4939-0302-3 (eBook)
DOI 10.1007/978-1-4939-0302-3
Springer New York Heidelberg Dordrecht London

Library of Congress Control Number: 2014935230

Printed on acid-free paper

Springer is part of Springer Science+Business Media (www.springer.com)

Preface

Lithium-ion (Li-ion) batteries were first introduced into the marketplace by Sony in 1991 to power a video camera. Since then, Li-ion batteries have become part of our daily lives—powering a wide range of mobile electronic devices and power tools. The electrolyte is a key component of a Li-ion battery. Current electrolytes are the result of many years of research and development and play a key role in providing good performance for applications. New and more challenging battery requirements for power tools, hybrid electric vehicles, plug-in electric vehicles, and stand-by power sources for communications and modern airplanes require a significant advance in battery chemistry. The batteries needed are often of higher voltages and higher energy content. Furthermore, they will be exposed to extremes of temperature with the necessity of still providing long cycle and storage life and assured user safety. A new class of electrolytes is needed to meet these demands. The new electrolytes must not only provide good ionic conduction over a wide range of ambient temperatures but also provide good chemical stability and compatibility with the more reactive electrode materials that are required to achieve higher battery-specific energy and power. With the demand for higher energy density Li-ion batteries, recent development trends favor the use of higher voltage cathodes such as 4.7 V for $LiNi_{0.5}Mn_{1.5}O_4$ and 4.8 V $LiCoPO_4$, higher capacity cathodes such as layer–layer composite and layer–spinel composite made of $Li[Ni,Mn,Co]O_2$ with a capacity in the range of 250–300 mA h/g versus 140 mA h/g for $LiCoO_2$ cathodes used today in commercial cells, and higher capacity Li alloy-based anodes such as Li–Sn and Li–Si alloys. Today's state-of-the-art electrolytes made of lithium hexafluorophosphate ($LiPF_6$) dissolved in cyclic carbonate and linear carbonate solvent mixtures with functional additives are not adequate in these new higher energy density electrochemical pairs without losing capacity or power. Looking beyond the horizon, many researchers and institutions intend to utilize sulfur or air as an even higher theoretical capacity cathode and pair with pure Li as an anode pursuing even higher energy density. The need of compatible electrolytes is also imperative for developing such systems.

What we need are better electrolyte materials that are compatible with the chosen electrode materials. The development of better electrolyte materials will require a much better understanding of electrolytes and how they interact with electrode materials. This book provides an overview of electrolyte research and development in the past 10 years as a foundation for thinking about future directions.

A number of books have been devoted to the science and technology of Li-ion batteries in recent years. However, there is no single book giving a comprehensive overview of electrolytes for Li-ion batteries. With the high demand for more robust electrolytes for the improvement of performance and energy density of Li and Li-ion batteries, it is time for a book that covers the electrolyte materials and the understanding of electrolyte and electrode interactions that have been developed in the past 10 years. This book covers the materials' aspects of the electrolytes, the state of the understanding of the electrolyte and electrode interactions, and basic understandings of the electrolytes and electrode/electrolyte interaction through computation. We are pleased to provide a ten-chapter book divided in three parts to cover subjects that we believed would make a good reference for researchers and technologists in the field and also for those who are not working in the field but are interested in understanding the basics, challenges, and progress that have been made in the field.

The first part of the book comprises four chapters focusing on electrolyte materials. In Chap. 1, Professor Wesley A. Pacific Northwest National Laboratory focuses on the various lithium salts that have been developed and compares these salts with $LiPF_6$, which is the salt used in today's Li-ion batteries. A comprehensive review of the physicochemical properties of these salts in nonaqueous solvents is also provided. The developed alternative salts have potential to be useful as additives or substitute for $LiPF_6$ in new Li battery chemistry. Dr. Makoto Ue of Mitsubishi Chemicals together with Emeritus Professor Yukio Sasaki of Tokyo Polytechnic University, Professor Yasutaka Tanaka of Shizuoka University, and Professor Masayuki Morita of Yamaguchi University contribute Chap. 2, which provides a solid review of heteroatom-containing organic solvents—including sulfur, fluorine, boron, and phosphorous—applied to lithium cells in recent years. Dr. Koji Abe of Ube Industries reviews work on additives for Li-ion electrolytes since 1990. Given that the properties of additives vary widely with battery test conditions, Dr. Abe selected additives that were utilized in practical applications and tried to replace those that were less successful; he then organized the additives chronologically. As a result, the cited references are mostly patents. He left the concepts, chemistry, and mechanism for each additive to the cited references as he explained in the Background of his chapter. In Chap. 4, Dr. Hajime Matsumoto of National Institute of Advanced Industrial Science and Technology, Japan, reviews the recent progress on ionic liquids for rechargeable lithium batteries.

The second part of the book focuses on interfacial chemistry at the electrodes and the methods of characterizing the interphases. Dr. Mengqing Xu, Dr. Lidan Xing, and Professor Weishan Li of South China Normal University, China, contribute Chap. 5, a review of the understanding of the interphases between the electrolyte and the anodes including graphite anode and Li–Sn and Li–Si alloy anodes in Li-ion batteries. Dr. Francis Amalraj Susai, Dr. Ronit Sharabi, Dr. Hadar Sclar, and

Professor Doron Aurbach of Bar-Ilan University, Israel, contribute Chap. 6, which provides a review of the surface chemistry of cathode materials including transition metal spinel, transition metal layer, transition metal phosphate, and oxygen cathode materials in nonaqueous electrolytes. Dr. Jordi Cabana of Lawrence Berkeley National Laboratory wrote Chap. 7, which provides an overview of the experimental tools and the kind of information they can offer with representative examples in the literature. It is important to recognize that no single technique can currently provide the answers to these complex interfacial phenomena in Li and Li-ion batteries.

Recent advances in molecular modeling using molecular simulations—and especially density functional theory—show promise of accurate prediction of the electrolyte's electrochemical, structural, and transport properties. The third part of this book is devoted to the understanding of electrolytes and electrolyte/electrode interactions through computational and molecular modeling. In Chap. 8, Dr. Oleg Borodin of the U.S. Army Research Laboratory discusses the applications of quantum chemistry to determine electrolyte oxidative stability and oxidation-induced decomposition reactions. He uses molecular dynamics simulations and density functional theory to predict the structural and transport properties of liquid electrolytes and solid electrolyte interphase (SEI) model compounds; free energy profiles for lithium desolvation from electrolytes; and the behavior of electrolytes at charged electrodes and the electrolyte–SEI interface.

In Chap. 9, Dr. Johan Scheers and Prof. Patrik Johansson of Chalmers University of Technology, Sweden, provide a thorough, historical perspective on the prediction of electrolyte and additive electrochemical stabilities from DFT calculations, a description of the simultaneous computational modeling methods, and materials evolutions. The materials put into reduction and oxidation stability prediction investigation include carbonate solvents, salts with different anions, and additives. In Chap. 10, the final chapter, Dr. Kah Chun Lau, Dr. Rajeev Assary, and Dr. Larry Curtiss of Argonne National Laboratory review the recent progress towards understanding of aprotic electrolytes stability and decomposition mechanisms in Li-Air battery obtained from quantum chemistry calculations that were corroborated with experimental data. They also review the research that has been done on the development of stable aprotic liquid electrolytes for Li-air batteries. One of the key problems is the electrochemical stability of the presently known carbonate- and ether-based nonaqueous electrolyte systems. The Li-air battery is a relatively new system and thus there are great challenges in developing stable electrolytes that are resistant to attack by reduced O_2 species.

The development of higher energy density Li-based batteries, whether they are made of higher voltage cathodes, high capacity cathodes, carbonaceous anodes, higher capacity Li alloy anodes, pure Li anode, or air cathode, all require stable and compatible electrolytes. We need better electrolytes to match the new electrochemical pairs. This cannot be achieved without a good understanding of the electrolyte and electrode interactions in relation to the electrolyte itself. In addition to electrochemical methods, many in situ and ex situ analytical tools need to be applied to the systems. Basic understanding of the stability of the electrolytes—including

electrochemical and chemical interactions with the electrodes through molecular modeling—is much needed. Experimental techniques for the validation of the modeling are also very much in need for advancing the modeling. Research and development of Li and Li-ion batteries are on the rise. New knowledge and new understanding are increasing daily. To advance effectively, synthetic scientists, analytical scientists, and computational scientists need to work together to develop higher energy density electrochemical energy storage systems.

Adelphi, MD, USA T. Richard Jow
Adelphi, MD, USA Kang Xu
Adelphi, MD, USA Oleg Borodin
Yokohama, Japan Makoto Ue

Contents

Contributors

Koji Abe Advanced Energy Materials R&D Center, UBE Industries, Ltd., Kogushi, Ube, Yamaguchi, Japan

Advanced Electrolyte Technologies LLC, Tory, MI, USA

Susai Francis Amalraj Department of Chemistry, Bar-Ilan University, Ramat Gan, Israel

Rajeev S. Assary Materials Science Division, Argonne National Laboratory, Argonne, IL, USA

Doron Aurbach Department of Chemistry, Bar-Ilan University, Ramat Gan, Israel

Oleg Borodin U.S. Army Research Laboratory, Adelphi, MD, USA

Jordi Cabana Environmental Energy Technologies Division, Lawrence Berkeley National Laboratory, Berkeley, CA, USA

Present Address: Department of Chemistry, University of Illinois at Chicago, Chicago, IL, USA

Larry A. Curtiss Materials Science Division, Argonne National Laboratory, Argonne, IL, USA
curtiss@anl.gov

Wesley A. Henderson Electrochemical Materials & Systems, Energy & Environment Directorate, Pacific Northwest National Laboratory (PNNL), Richland, WA, USA

Patrik Johansson Department of Applied Physics, Chalmers University of Technology, Gothenburg, Sweden

Kah Chun Lau Materials Science Division, Argonne National Laboratory, Argonne, IL, USA

Weishan Li Engineering Research Center of Materials and Technology for Electrochemical Energy Storage (Ministry of Education), South China Normal University, Guangzhou, China

Hajime Matsumoto Institute for Ubiquitous Energy, Devices National Institute of Advanced Industrial Science and Technology (AIST), Ikeda, Osaka, Japan

Masayuki Morita Graduate School of science and engineering, Yamaguchi University, Tokiwadai, Ube, Japan

Yukio Sasaki Tokyo Polytechnic University, Atsugi, Kanagawa, Japan

Johan Scheers Department of Applied Physics, Chalmers University of Technology, Gothenburg, Sweden

Hadar Sclar Department of Chemistry, Bar-Ilan University, Ramat Gan, Israel

Ronit Sharabi Department of Chemistry, Bar-Ilan University, Ramat Gan, Israel

Yasutaka Tanaka Graduate School of Science and Technology, Shizuoka University, Hamamatsu, Japan

Makoto Ue Mitsubishi Chemical Corporation, Yokohama, Kanagawa, Japan

National Institute for Materials Science, Namiki, Tsukuba, Ibaraki, Japan

Lidan Xing Key Laboratory of Electrochemical Technology on Energy Storage and Power Generation of Guangdong Higher Education Institutes, South China Normal University, Guangzhou, China

Mengqing Xu School of Chemistry and Environment, South China Normal University, Guangzhou, China

About the Authors

T. Richard Jow is an ARL Fellow and Team Lead for Energy Storage Materials at the U.S. Army Research Laboratory in Adelphi, MD. His work focuses on the development of energy storage materials and devices, including high energy and high power density rechargeable lithium batteries and dielectric capacitors. He has been technical lead for the DOE-ARL joint electrolyte development program since 1999 and managed and co-managed the Army ManTech Programs on Capacitors and Li-ion Batteries, respectively. Before joining ARL in 1989, Dr. Jow was a senior chemist at Allied-Signal in Morristown, NJ, and a senior scientist at Electrochem Industries, a subsidiary of Wilson Greatbatch Limited, in Clarence, NY, developing various electrode and electrolyte materials for high energy density lithium batteries. He received his B.S. and M.S. in Physics from National Tsing Hua University and his Ph.D. in Materials Science and Engineering from Northwestern University. He has authored or coauthored over 130 journal papers and 25 patents in the areas of lithium batteries, electrochemical capacitors, and dielectric capacitors. He is a member of the Electrochemical Society and the Materials Research Society.

Kang Xu has been doing research on energy storage technologies for over 20 years. He joined U.S. Army Research Laboratory in 1997, and has been the PI/co-PI for electrolyte projects funded under US DOE Advanced Battery Research, the project leads for various DoD research projects, as well as the Contract Official Technical Representative for diversified research initiatives. His research interests cover materials development and interphasial mechanisms for electrochemical energy storage devices, including lithium and advanced battery chemistries. His recent activities also extend to emerging fronts of bio/nano-structured materials based on viral templates, and their applications in advanced battery chemistries and energy harvesting through photosynthetic routes, for which he acts as technical leads in DoD-funded programs.

He has been recognized four times by R&D Achievement Awards from the Department of the Army (1999, 2001, 2002, and 2011), the Publication Award (2005), the Army Science Conference Best Paper Award (2008), and the Science Award (2011). He has published over 130 papers in peer-reviewed journals (h-index 43),

written two book chapters, coedited a book, and currently holds 18 issued U.S. patents. He is an active member of the Electrochemical Society and Materials Research Society.

Oleg Borodin works as a scientist at the Electrochemistry Branch of the Army Research Laboratory, Adelphi, MD since 2011. After obtained a Ph.D. degree in Chemical Engineering in 2000 he worked in the area of multiscale modeling of liquid, ionic liquid and polymer electrolytes for battery and double layer capacitor applications, modeling of energetic composite materials, polymers in solutions, and polymer nanocomposites. He coauthored more than a hundred publications and four book chapters. His modeling efforts focus on the scales from electronic to atomistic and mesoscale.

Makoto Ue is a vice president and Energy 2 lab manager of Corporate R&D Center at Samsung SDI, Ltd. in Suwon, Korea. He obtained M.S. and Ph.D. from The University of Tokyo, Japan in 1981 and 1995, respectively, and studied at the University of Pittsburgh and Lawrence Berkeley National Laboratory, USA from 1988 to 1990. He worked for Tsukuba Research Center at Mitsubishi Chemical Corporation, Japan from 1981 to 2010 as the first researcher of nonaqueous electrolyte solutions (1984), the first top manager of Battery Materials Laboratory (2003–2010), the top manager of Tsukuba Research Center (2006–2010), a fellow (2007–2012), and then an adjunct researcher at National Institute for Materials Science (2011–2012). He has contributed to the growth of Li battery and capacitor industries through his steady electrolyte research and his products have been adopted in these devices for consumer and automotive applications. Dr. Ue holds about 300 papers/reviews/book chapters and about 300 patents, and is the recipient of seven academic awards including Outstanding Research Paper Award from The Electrochemical Society of Japan (1994), Research Award from International Battery Materials Association (1997), and Battery Division Technology Award from the Electrochemical Society (2004) in Li-battery fields.

Chapter 1
Nonaqueous Electrolytes: Advances in Lithium Salts

Wesley A. Henderson

Abstract The synthesis and characterization of new lithium salts has been a core component of electrolyte research for the past three decades. Upon the commercialization of Li-ion batteries with a graphite anode, $LiPF_6$ became the dominant salt for lithium battery electrolytes. But the advent of new electrodes/cell chemistries (e.g., Si alloy anodes, high-voltage cathodes, Li-air, Li-S), as well as the need for exceptional battery safety, higher/lower temperature operation, improved durability/longer lifetimes, etc., has resulted in the pressing need for new electrolyte formulations. Lithium salts, either as a substitute for $LiPF_6$ or as an additive, are one central focus for this electrolyte transformation.

Keywords Li-ion batteries • Electrolyte • Salts • Solvation • Ionic association

1.1 Introduction

Early lithium battery electrolyte research in the 1970s used available lithium salts—i.e., principally $LiClO_4$, $LiAlCl_4$, $LiBF_4$, $LiPF_6$, and $LiAsF_6$. Efforts at the time were devoted to stabilizing the stripping/plating of Li metal [1–3], as well as the use of intercalation electrodes [4]. $LiPF_6$ was reported to not provide the best Li metal stripping/plating efficiency amongst the salts studied [5, 6] and $LiPF_6$ was also found initially to be problematic for the cycling of carbon electrodes [7, 8]. $LiPF_6$ did not become the paramount salt for lithium battery electrolytes until carbon coke replaced Li metal (later to be replaced by graphite) and the solvents were optimized for the electrolyte utilized in the Li-ion batteries initially commercialized by Sony in 1991 [9–19].

W.A. Henderson (✉)
Electrochemical Materials & Systems, Energy & Environment Directorate,
Pacific Northwest National Laboratory (PNNL), 902 Battelle Boulevard, PO Box 999,
MSIN K2-44, Richland, WA 99352, USA
e-mail: Wesley.Henderson@pnnl.gov

T.R. Jow et al. (eds.), *Electrolytes for Lithium and Lithium-Ion Batteries*,
Modern Aspects of Electrochemistry 58, DOI 10.1007/978-1-4939-0302-3_1,

Many/most of the anions used for electrolyte lithium salts were initially developed in efforts to generate stronger superacids. The term superacid generally refers to acids which are more acidic than mineral Brønsted acids [20–27]. In particular, a widely used definition for superacids was given by Gillespie who defined this term to be applicable to acids which are more acidic than sulfuric acid [28–30]. The stronger the acidity, the weaker the coordination of the anions is with the associated protons (H^+ cations). The gas-phase acidity is given by:

$$HA \overset{K_a}{\rightleftarrows} A^- + H^+$$

and

$$\Delta G_{acid} = -RT \ln K_a$$

In practice, however, the determination of the acidity of superacid anions in solution is not a trivial matter as the acidity of a given acid (HA) is a function of the solvent (S) used:

$$HA + S \overset{K_a}{\rightleftarrows} A^- + SH^+$$

which is influenced by factors such as the steric bulk of the anions and solvent, ion pairing, etc. Three major substitution effects contribute to increasing the acidity of a neutral acid functional group (C–H, O–H, N–H, S–H, B–H, etc.) [20, 26]:

1. field/inductive effects
2. π-electron acceptor (resonance) and negative hyperconjugation effects
3. substituent polarization effects

The influence of these factors is evident from the acidity variations noted for different substituents (Figs. 1.1 and 1.2) [20, 26]. No simple patterns in acidity behavior are found for these effects, however, due to the interplay between them (i.e., these effects do not operate independently of one another) [20, 26]. For $=Z(X)_n$ substituents (replacing an =O: $M{=}O \rightarrow M{=}Z(X)_n$, where M=O might be $CH_3C(=O)H$, $HC(=O)NH_2$, HC(=O)OH, etc.), the acidification for the same X increases with increasing *n* [22]:

$$= N(CN) <= C(CN)_2 <= P(CN)_3 <= S(CN)_4$$
$$= NSO_2F <= C(SO_2F)_2 <= P(SO_2F)_3$$

In addition, the acidifying effect of fluorosulfonyl groups is greater than that of the corresponding cyano groups (Fig. 1.2) [22].

Classical strong mineral acids include:

$$HF(365.7) < HNO_2(330.5) < HCl(328.0) < HBr(318.2) < HNO_3(317.8)$$
$$< HI(309.3) < H_2SO_4(302.2) < HSO_3F(299.8) < HClO_4(285 \pm 8)$$

(experimental gas-phase acidity (ΔG_{acid}) values in kcal mol^{-1}) [31]. Interestingly, the gas-phase acidity may be increased somewhat by the replacement of fluorine

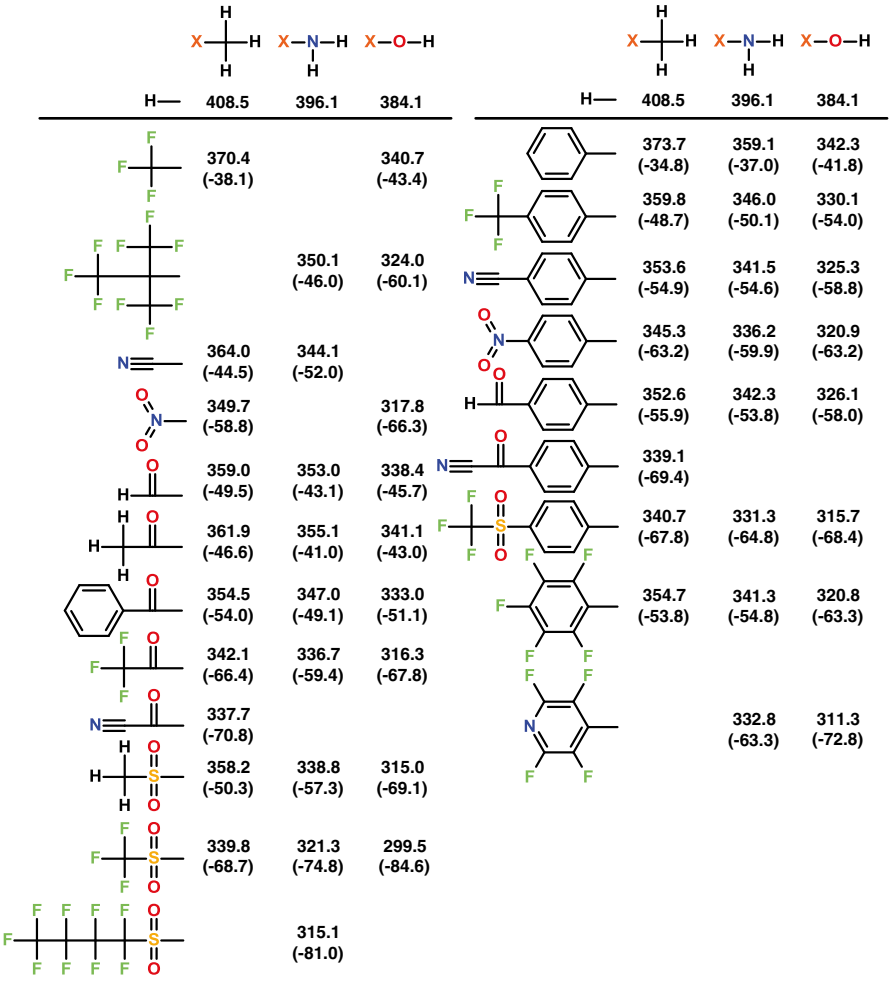

Fig. 1.1 Experimental gas-phase acidity values (kcal mol^{-1}) for various monosubstituents [20]

atoms with chlorine [32, 33]. The values noted above for HF and HCl are one example. The corresponding values for HCO_2CH_2F, HCO_2CH_2Cl, HCO_2CHF_2, and HCO_2CHCl_2 are 337.6, 335.4, 330.0, and 328.4 kcal mol^{-1}, respectively [32]. This effect, which is opposite to that expected from electronegativity alone, is attributed to the greater delocalization of the charge on the chlorine atom relative to fluorine. Thus, HSO_3Cl is expected to be a stronger acid than HSO_3F [26, 32, 33].

Replacement of the acid protons with Li^+ cations results in the corresponding lithium salts. Due to differences between the gas and condensed liquid-phase interactions, as well as the varying factors which determine proton (H^+) and Li^+ cation coordination/solvation, the exact trends noted for anion acidity do not always hold for the relative strength of lithium salt interactions. But, overall, the ionic association tendency of anions to coordinate Li^+ cations is governed by the same effects noted

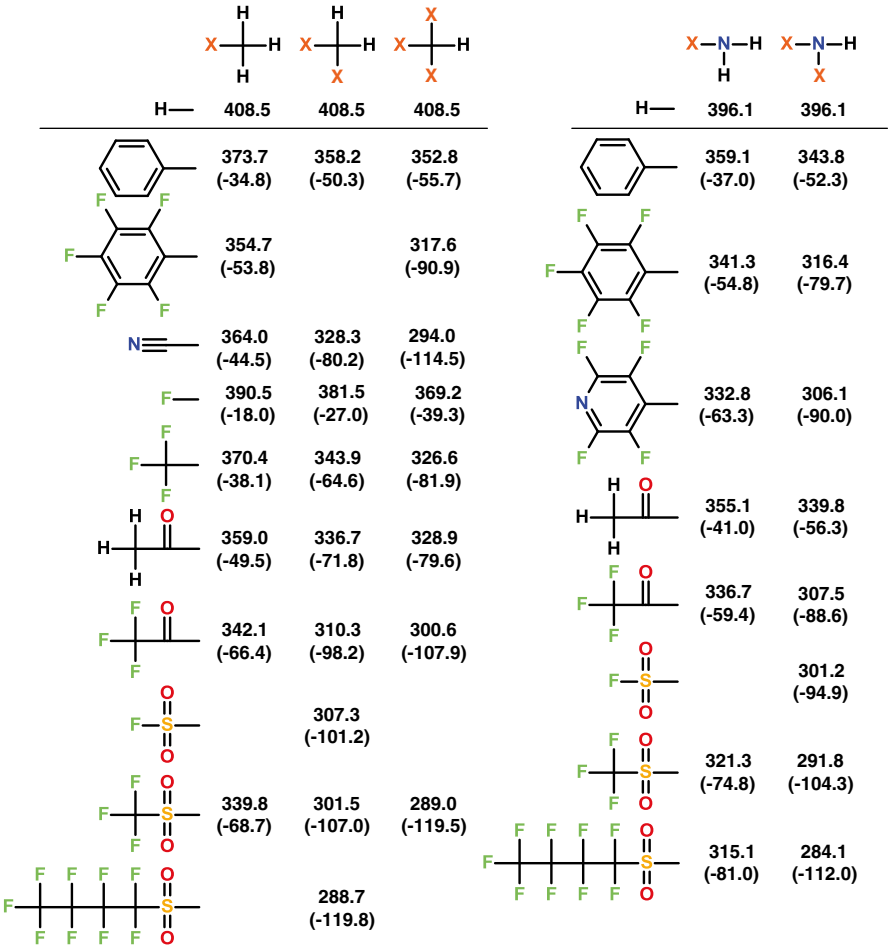

Fig. 1.2 Experimental gas-phase acidity values (kcal mol^{-1}) for various mono-, di-, and trisubstituents [20, 26]

above for acidity, as exemplified by DMSO electrolytes with lithium acetate salts with increasing anion fluorination which have the following increasing ionic association trend [34]:

$$CO_2CH_3^- > CO_2CH_2F^- > CO_2CHF_2^- > CO_2CF_3^-$$

Efforts to develop new lithium salts began in the late 1970s and 1980s with the use of perfluoroalkylsulfate (e.g., $SO_3CF_3^-$) and bis(perfluoroalkanesulfonyl)imide (e.g., $N(SO_2CF_3)_2^-$) anions. New salt development efforts gained momentum throughout the next three decades, but none of the developed salts have offered

significant advantages over—while retaining the benefits of—the $LiPF_6$ salt, which serves as the standard for industry. Thus, $LiPF_6$ continues to be the predominant salt used for most commercial Li-ion batteries.

Some of the new lithium salts, however, have been found to be very effective as electrolyte additives for the modification of electrolyte–electrode interfaces. Other lithium salts hold promise as future primary salts for lithium batteries (i.e., replacements for some or all of the $LiPF_6$), especially for demanding battery electrolyte requirements such as low/high-temperature operation and superb safety characteristics, which cannot be met by the sole use of $LiPF_6$ [35–38]. Thus, there is a continued need for rapid advances in lithium salts for the diverse range of lithium battery chemistries which are now the focus of worldwide efforts to greatly improve vehicular and stationary energy storage technologies.

1.2 Electrolyte Salt Properties

Electrolyte salts must meet a broad and demanding range of properties—some of these include [12, 37, 39, 40] the following:

1. *Ionic Conductivity*: A high Li^+ cation transport rate is necessary to achieve high power (i.e., a high rate for the overall battery reaction) as the Li^+ cation mobility within the bulk electrolyte is often one of the main sources of impedance for the battery [41]. The choice of a lithium salt's anion dramatically influences the electrolyte's conductivity due to the variations in the Li^+ cation solvation and ionic association interactions resulting from the differences in anion structure and coordination strength. Although electrolyte conductivity is the parameter most frequently considered, the Li^+ cation mobility is actually obtained from the product of the conductivity and Li^+ cation transference (or transport) number (i.e., t_{Li+}) (fraction of the current carried by the Li^+ cations). This latter parameter is frequently not reported in the literature for a given electrolyte composition. The most common t_{Li+} measurement method is that reported by Bruce and Vincent [42–44]. Caution should be exercised in interpreting results from such measurements, however, as the data can be skewed by the reaction of the electrolyte with Li metal (active electrodes) resulting in erroneous t_{Li+} values, especially for liquid electrolytes.
2. *Salt Solubility/Crystalline Solvates*: Achieving a reasonably high lithium salt solubility in the electrolyte solvent(s) is necessary to provide sufficient charge carriers for rapid ionic conduction, as well as to prevent salting out of the salt (i.e., precipitation). It is important to distinguish between salt solubility and crystalline solvates. A salt may be highly soluble, but also may readily form a crystalline solvate phase with a high melting point (T_m) resulting in the formation of solids in the electrolyte which effectively extracts the salt from the electrolyte solution (causing the conductivity to plummet). This is a particular concern for low-temperature cell operation.

3. *Stability*: Electrolytes must, in general, be robust (nonreactive with other cell components) within the electrochemical potential window utilized for the battery charge/discharge reactions [45], as well as at elevated temperature, to achieve thousands of charge/discharge cycles with low capacity loss (fade). The temperature and voltage(s) at which oxidation and/or reduction of the electrolyte components occur are not independent of one another. As for chemical stability, the electrochemical stability of electrolytes (i.e., potential stability window) is strongly temperature dependent with a modest increase in temperature, in some cases, resulting in a substantial decrease in stability [46]. The potential window is also a strong function of the materials in contact with the electrolyte [46], as well as the presence of impurities. Thus, the potential window, as measured on an inert glassy carbon electrode, is not a clear indicator of the stability of an electrolyte in contact with active electrode materials (although a poor stability on this electrode likely also indicates a poor stability with more active electrodes). Stability is a complicated factor, however, as it may also be necessary for the salt's anions to selectively degrade—e.g., to form a solid-electrolyte interface (SEI) layer on the anode and/or cathode [12] and to stabilize the Al current collector [47].
4. *SEI Formation*: The SEI is a layer formed between the electrode surface and the electrolyte through the degradation/reaction of both electrolyte components and electrode material(s) [12]. Ideally, only a limited amount of materials react, with the resulting SEI layer preventing further electrode–electrolyte reactions and enabling the facile transport of only Li^+ cations between the electrode and electrolyte (resulting in a low impedance). The lithium salt(s) present in the electrolyte, whether as a bulk salt or an additive, can dramatically influence the SEI's composition, properties, and stability [48].
5. *Al Corrosion*: The use of Al as a cathode current collector in commercial Li-ion batteries is nearly ubiquitous [47]. A given electrolyte must passivate the electrolyte–Al interface to prevent corrosive pitting of the current collector during cell cycling to high potential (>3.6 V vs. Li/Li^+).
6. *Hydrolysis Stability*: Many anions hydrolyze when exposed to water, especially at elevated temperature—often resulting in the formation of HF. This results in additional costs associated with the salt's preparation, storage, and handling. This also strongly influences the cycling behavior and lifetime of batteries, especially when cycled to high temperature and/or high potential (>4.8 V vs. Li/Li^+) [49–54]. HF formation may also result from the reaction of the anions with solvent molecules (abstraction of a hydrogen) [55].

Other desirable features include low cost and low toxicity. Failure to meet one or more of these criterions prevents the practical use of a salt in lithium and Li-ion batteries. It is important to note, however, that many of these properties are strongly dependent upon the electrolyte formulation (e.g., solvents used, salt concentration, additives). Thus, electrolyte compositions need to be tailored to specific battery applications/demands.

1.3 Established Salts

A number of lithium salts are well established as salts which are used or have been previously used for lithium battery electrolytes, although many of these do not meet the necessary criterion for commercial battery electrolytes. Frequently studied lithium salts include (Fig. 1.3) [12, 40] the following:

1. *$LiClO_4$*: Lithium perchlorate was widely used for battery electrolyte research in the 1970s and 1980s due to its high ionic conductivity, high solubility in aprotic solvents, high thermal/electrochemical stability, and favorable SEI-forming properties [12, 56]. Electrolytes with the $LiClO_4$ salt, however, typically do not passivate the Al current collector as well as those with $LiPF_6$ [38, 57–60]. The high oxidation state of the Cl^{VII} atom also makes the anion a strong oxidant and thus the salt a potential explosive [61–63]. This has largely precluded the use of $LiClO_4$ for commercial batteries.
2. *$LiAsF_6$*: Like $LiClO_4$, lithium hexafluoroarsenate was widely used for electrolyte research in the 1970s and 1980s. In particular, it was found to improve the efficiency of Li metal plating/stripping relative to electrolytes with $LiClO_4$ [12]. $LiAsF_6$ has many properties in common with $LiPF_6$ [12, 40, 64], but the potential hazards associated with the salt have largely prevented its commercial usage. Although the As^V oxidation state is not toxic, the As^{III} and As^0 states, which might be formed from electrochemical reduction, are highly toxic.
3. *$LiPF_6$*: Lithium hexafluorophosphate is used almost exclusively in commercial Li-ion batteries. This salt has thus far demonstrated the best balance of essential properties necessary for a primary Li-ion electrolyte salt [12, 40]. In aprotic solvents, the resulting electrolytes have some of the highest conductivity values measured. $LiPF_6$-based electrolytes react to form a stable interface with the Al

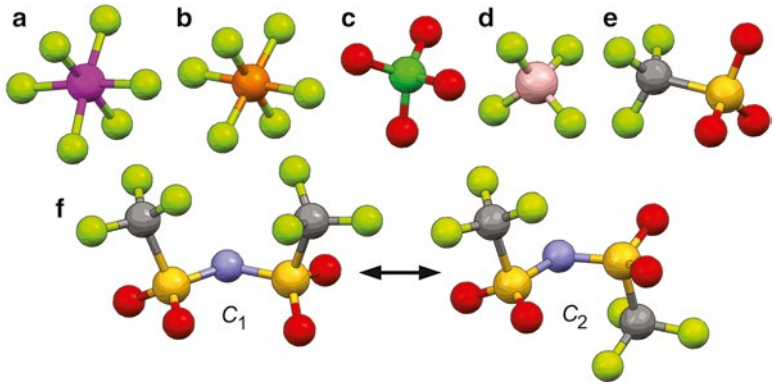

Fig. 1.3 Widely used lithium salt anions: (**a**) AsF_6^-, (**b**) PF_6^-, (**c**) ClO_4^-, (**d**) BF_4^-, (**e**) $SO_3CF_3^-$, and (**f**) $N(SO_2CF_3)_2^-$ ($TFSI^-$) (C_1 (*cis*) and C_2 (*trans*) conformations) (B—*tan*, C—*gray*, N—*blue*, O—*red*, F—*light green*, P—*orange*, S—*yellow*, Cl—*dark green*, As—*purple*)

current collector at high potential [58–60, 65–68] and a stable SEI with graphite electrodes when used with carbonate solvents [12, 40]. The P–F bond is labile, however, and the salt thus readily undergoes hydrolysis [69–73] and has a relatively low thermal stability [56, 71, 74–78]. The presence of HF in $LiPF_6$-based electrolytes, and its impact on cell performance, is one of the principal concerns associated with this salt's usage [49–54].

4. *$LiBF_4$*: Electrolytes with lithium tetrafluoroborate tend to have a significantly lower conductivity, relative to those with $LiPF_6$ [79–81], which has been a major impediment to its use in commercial Li-ion cells. The B–F bond is less labile than the P–F bond. Thus, the $LiBF_4$ salt is less susceptible to hydrolysis and more thermally stable than $LiPF_6$ [56, 82–85], but electrolytes with this salt do passivate Al well at high potential [59, 67]. Despite the lower conductivity, electrolytes with $LiBF_4$ have been shown to have improved cell cycling performance at low/high temperature, relative to cells with $LiPF_6$-based electrolytes, due to the formation of a less resistive SEI layer and improved thermal stability [81, 82, 86–89]. $LiBF_4$ may also serve as a useful additive to electrolytes with $LiPF_6$ [90] and it enables the use of γ-butyrolactone (GBL) as an electrolyte solvent (which is unstable with $LiPF_6$) [91–96].
5. *$LiSO_3CF_3$*: Lithium trifluoromethanesulfonate (triflate—most commonly abbreviated as "$CF_3SO_3^-$" in the scientific literature) was at one time widely used for electrolytes, especially for polymer electrolytes [97–107]. This salt has a high thermal stability [56] and is not susceptible to hydrolysis due to the stability of the C–F bond. Electrolytes with this salt, however, are found to be notably less conductive than those with $LiPF_6$ [5, 108–110], and $LiSO_3CF_3$-based electrolytes corrode the Al current collector at high potential [59, 65–67]. Thus, while this salt has been extensively used for research purposes, it is not used in commercial Li-ion batteries.
6. *LiTFSI* (i.e., *$LiN(SO_2CF_3)_2$*): Many acronyms are used for the lithium bis(trifluoromethanesulfonyl)imide salt: LiTFSI, LiTFSA, $LiNTf_2$, $LiTf_2N$, etc. The terms "imide" and "amide" are frequently interchanged. Much of the initial interest in the LiTFSI salt was due to its tendency to form amorphous mixtures with poly(ethylene oxide), rather than crystalline phases, when mixed to form polymer electrolytes [97, 111–113]. The bis(perfluoroalkanesulfonyl)imide anions, such as $TFSI^-$, are highly flexible with two low-energy conformations in which the $–CF_3$ groups are either *cis* (C_1) or *trans* (C_2) to one another (Fig. 1.3f) [114–117]. The combination of the strongly electron-withdrawing fluorine atoms and resonance structures due to the sulfonyl groups results in extensive negative-charge delocalization across the $–SO_2–N–SO_2–$ backbone of the anion [108, 118]. Thus, $TFSI^-…Li^+$ cation coordination occurs predominantly through oxygen atom coordination to the Li^+ cations (rather than $N…Li^+$ or $F…Li^+$ cation coordination) [119–124]. Electrolytes with this salt generally are somewhat less conductive than the corresponding $LiPF_6$ electrolytes [5, 11, 125]. The $TFSI^-$ anion has a high thermal stability and is not susceptible to hydrolysis due to the very stable C–F bonds [56, 126], but dilute aprotic solvent-base electrolytes with LiTFSI are known to strongly corrode the Al current collector at high potential [59, 60, 65–68]. This observation should be qualified with the fact that electrolytes

with ionic liquids with the $TFSI^-$ anion (with or without LiTFSI) do not corrode the Al current collector [127–132], nor do electrolytes with very high concentrations of LiTFSI [133]. Thus, simple generalizations about electrolyte salt properties (e.g., "the LiTFSI salt corrodes Al") may be flawed.

1.4 Electrolyte Characterization Tools

Rigorous electrolyte characterization requires a thorough understanding of not only the properties of the electrolyte, but also the solution structure. Anion solvation in protic solvents (e.g., water, methanol, ammonia) occurs through hydrogen-bonding interactions. Protic solvents, however, have poor electrochemical stability due to the acidic protons (i.e., O–H, N–H, S–H). The aprotic solvents useful for electrolyte applications do not have acidic protons. Thus, in general, the anions remain unsolvated (naked) in electrolytes with such solvents. Dissolution of a lithium salt therefore occurs through the solvation of the Li^+ cations by the formation of coordination bonds between the Li^+ cations and electron lone-pairs of the solvent donor atoms. Anions also form coordination bonds to the Li^+ cations using the electron lone-pairs on donor atoms (F, O, N, etc.). The competition between the solvent and anions for Li^+ cation coordination—the occupancy of the Li^+ cation's coordination shell—determines the solvate species which are present in the electrolyte. Thus, the ion solvation (solvent–Li^+ cation interactions) and ionic association tendency of the anions (anion–Li^+ cation interactions) are important features of electrolytes which are governed by the solvent/anion structure: steric factors which influence the coordination bond formation and packing around the cation, polarizability, charge delocalization, etc. The following discussion provides a short overview of a methodology which may be used to identify the electrolyte interactions and how these are determinants for electrolyte properties [134–136]:

1. *Phase Diagrams and Solvate Crystal Structures*: Solvent-lithium salt phase diagrams are an underutilized, but highly informative tool for examining electrolyte interactions. Acetonitrile (AN) is a particularly useful model solvent for comparing a salt's phase behavior as this solvent has only a single electron lone-pair and thus is either uncoordinated or coordinated to a single Li^+ cation. Figure 1.4 compares the phase diagrams of $(AN)_n$–LiX mixtures with $LiPF_6$, LiTFSI, $LiClO_4$, $LiBF_4$, and $LiCO_2CF_3$ [134, 135]. Figure 1.4 also shows the solvent/ion coordination in the solvate crystal structures determined for some of the indicated phases in the phase diagrams: $(AN)_6$:$LiPF_6$ [137], $(AN)_5$:$LiPF_6$ [138], $(AN)_1$:LiTFSI [139], $(AN)_4$:$LiClO_4$ [140], $(AN)_2$:$LiBF_4$ [141], and $(AN)_1$:$LiBF_4$ [142]. Notable features include the tendency of the $(AN)_n$–$LiPF_6$ and $(AN)_n$–$LiClO_4$ mixtures to form crystalline solvates with a high T_m. This is attributed to the small, symmetric, and relatively weakly coordinating anions which readily pack well within the solvate crystalline lattices. In contrast, dilute $(AN)_n$–LiTFSI mixtures form low T_m solvates and a crystallinity gap exists for more concentrated mixtures for which it is difficult or impossible to crystallize the

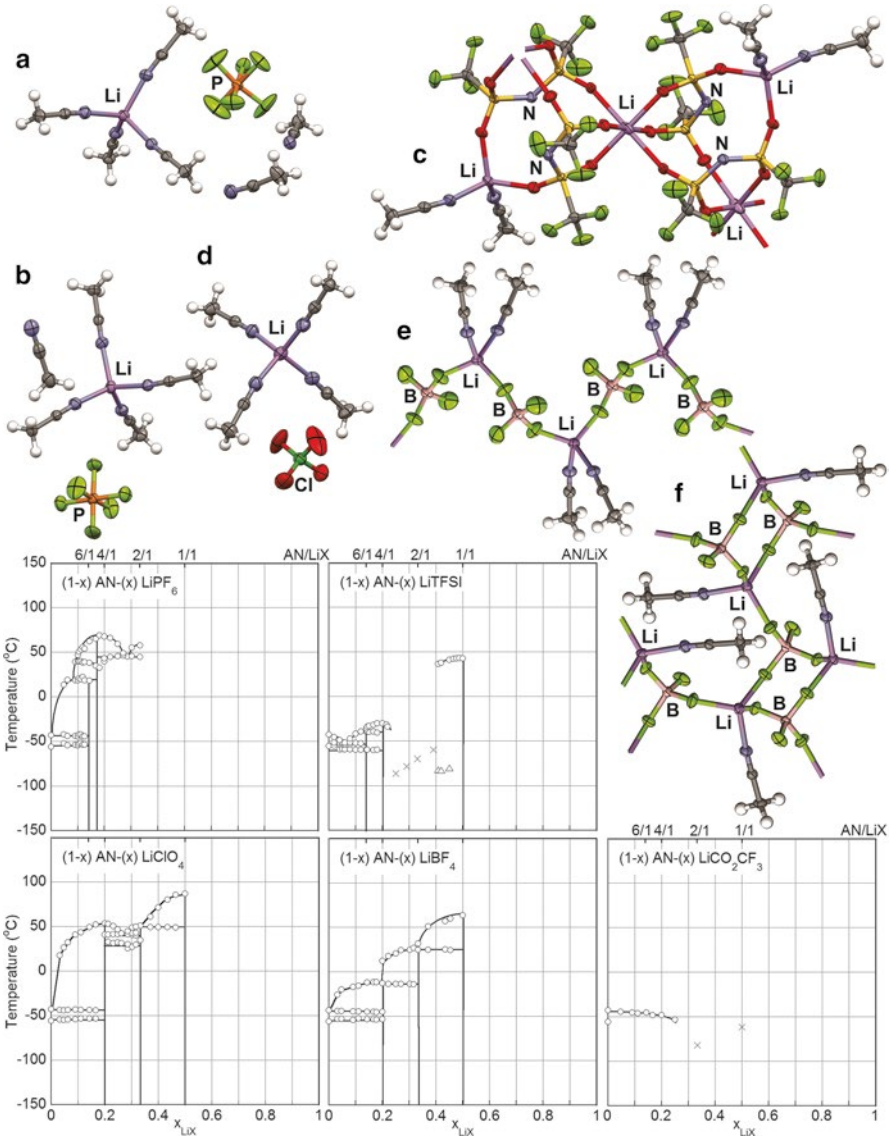

Fig. 1.4 Phase diagrams of $(AN)_n$–LiX mixtures with $LiPF_6$, LiTFSI, $LiClO_4$, $LiBF_4$, and $LiCO_2CF_3$ [134, 135] and ion/solvent coordination within the solvate crystal structures: (**a**) $(AN)_6$:$LiPF_6$ [137], (**b**) $(AN)_5$:$LiPF_6$ [138], (**c**) $(AN)_1$:LiTFSI [139], (**d**) $(AN)_4$:$LiClO_4$ [140], (**e**) $(AN)_2$:$LiBF_4$ [141], and (**f**) $(AN)_1$:$LiBF_4$ [142] (the sample T_g values are indicated by an "x" for fully amorphous samples and by a triangle for partially crystalline samples)

electrolytes—these features may be attributable to the bulky anion with lower symmetry and its influence on solvate formation. The ClO_4^- and BF_4^- anions are both tetrahedral and nearly of the same size (Fig. 1.3c, d). Interestingly, although the $(AN)_n$–$LiClO_4$ and $(AN)_n$–$LiBF_4$ mixtures form the same solvate crystalline

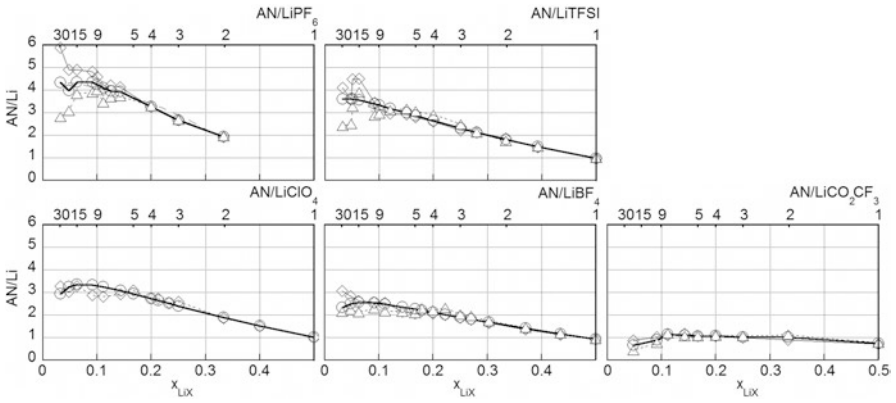

Fig. 1.5 Calculated Li^+ cation average solvation numbers (AN/Li) for $(AN)_n$–LiX electrolytes. The *dark solid line* corresponds to the average of the data obtained from the analysis of the C–C and C≡N Raman vibrational stretching bands (note that values for approximately $n > 9$ are unreliable due to a compilation of experimental errors associated with the Raman solvent band deconvolution) [134, 135]

phases (i.e., 4/1, 2/1, and 1/1 AN/LiX compositions), significant differences exist in the T_m of the 4/1 phases in which the Li^+ cations are fully solvated by four AN molecules and the anions are uncoordinated (Fig. 1.4d). This can be explained by the difference in the solvation/ionic association tendency of the two salts, as the BF_4^- anions have a greater tendency to displace the solvent molecules in the Li^+ cation coordination shells (and thus a greater tendency to disrupt the solvate structure). The 6/1 and 5/1 solvates with $LiPF_6$ also form solvates with four-fold Li^+ cation coordination (Fig. 1.4a, b), but also include uncoordinated solvent molecules to facilitate the packing of the solvated Li^+ cations and PF_6^- anions together. Finally, the $(AN)_n$–$LiCO_2CF_3$ mixtures do not form crystalline solvates. Only some of the excess AN is able to crystallize as a pure solvent phase.

2. *Li^+ Cation Solvation*: Electrolyte (average) solvation numbers are most commonly determined using vibrational spectroscopy by examining the solvent's vibrational band(s). Upon coordination to a Li^+ cation through an electron lone-pair, the electron density of the solvent molecule (and thus bond lengths/angles) changes resulting in variations in the solvent band positions [134, 135]. Integration of the peak area of the bands associated with the uncoordinated and coordinated solvent enables the calculation of the fraction of coordination solvent molecules—this number multiplied times the total number of solvent molecules in the electrolytes gives the average solvation number (Fig. 1.5). This analysis can be confounded, however, by overlapping vibrational bands, as well as variations in the relative intensity (scaling) of the peaks. Failure to account for these factors can result in a highly misleading interpretation of the experimental data. The scientific literature related to the determination of solvation numbers is rife with these problems. From an analysis of the AN Raman C–C and C≡N stretching

vibrations [134, 135], ion solvation for $(AN)_n$–LiX mixtures increases in the order:

$$LiPF_6 > LiTFSI \geq LiClO_4 > LiBF_4 >> LiCO_2CF_3$$

The maximum ion solvation number (average number of solvent molecules coordinated to the Li^+ cations) for the AN mixtures is found to be about 4 [134, 135]. Wide differences are noted for the solvation numbers for the varying anions. For example, for highly concentrated (>3 M) $(AN)_n$–LiX ($n=4$) liquid mixtures (i.e., four AN molecules present per Li^+ cation) at 60 °C, the solvation numbers are approximately 3.2 for $LiPF_6$, 2.8 for LiTFSI, 2.7 for $LiClO_4$, 2.1 for $LiBF_4$, and 1.0 for $LiCO_2CF_3$ [134, 135]. Note that these numbers are not the coordination numbers for the Li^+ cations. Rather, they represent the average number of coordinated solvent molecules with the anions making up the difference in the Li^+ cation coordination shells. Thus, the Li^+ cations in the $LiPF_6$ electrolytes are expected to be well solvated, whereas those for the $LiCO_2CF_3$ electrolytes are instead expected to be highly associated to the anions over the entire concentration range. Despite this, the solubility of $LiCO_2CF_3$ in AN is exceptionally high (>5 M). Thus, salt solubility and ionic association are not necessarily directly correlated with one another.

3. *Ionic Association*: The ionic association present in electrolytes is most commonly also determined using vibrational spectroscopy by examining one or more anion vibrational bands which shift upon coordination to the Li^+ cations [103–105, 121, 134, 135, 143, 144]. Often, the assignment of the bands to specific modes of coordination is somewhat ambiguous and the analysis of the data is simply based upon guesswork. This can be very misleading. To resolve this problem, the study of the vibrational bands for model crystalline (solid) solvates with known structure is particularly useful for assigning the vibrational band positions to particular anion…Li^+ cation coordination modes. This evaluation has been done for the salts $LiClO_4$ [145, 146], $LiBF_4$ [141], and LiDFOB [147]. Work is currently in progress to provide similar analyses for $LiPF_6$, LiTFSI, and $LiSO_3CF_3$. An example of the modes of coordination for the BF_4^- anion and the corresponding anion band positions obtained from crystalline solvates (such as AGG-I $(AN)_2$:$LiBF_4$ and AGG-II $(AN)_1$:$LiBF_4$—Fig. 1.4e, f) is shown in Fig. 1.6 [141]. This characterization "tool" is quite useful for the evaluation (deconvolution) of the Raman band data for the liquid electrolytes shown in Fig. 1.7b. This form of analysis is greatly complemented by molecular dynamics (MD) simulations (validated by the experimental data) which provide a visual representation of the solvates present in solution (Fig. 1.8) [134–136]. As an example of the utility of this marriage of methods, the solvates shown in Fig. 1.8c, d represent contact ion pairs (CIP-I and CIP-II, respectively). But the solvates in Fig. 1.8b, e, g–j also contain BF_4^- anions coordinated to a single-Li^+ cation. Thus the spectral signature of these anions would be that of CIP-I anion coordination (Fig. 1.6b). The experimental spectroscopic data, therefore, does not provide direct information about the solvates present. Instead, it indicates the fraction of the anions present

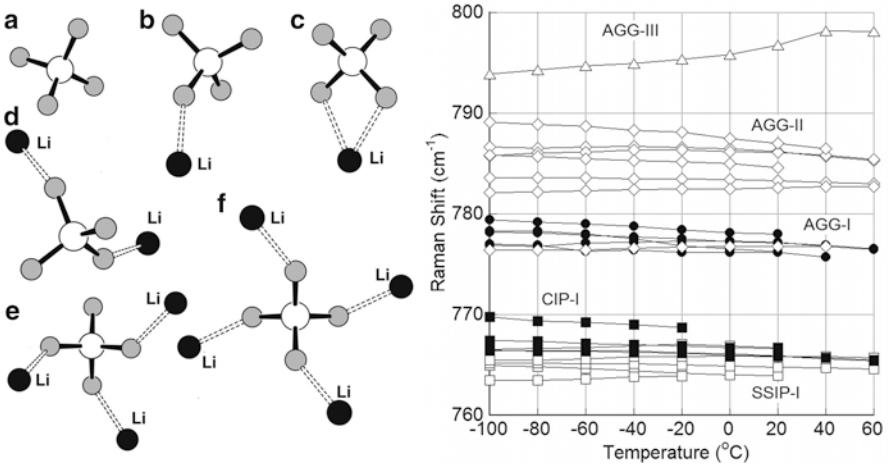

Fig. 1.6 Varying modes of BF_4^-…Li^+ cation coordination: (**a**) SSIP, (**b**) CIP-I, (**c**) CIP-II, (**d**) AGG-I, (**e**) AGG-II, and (**f**) AGG-III and Raman band peak positions for the BF_4^- anion ν_1 vibrational band for different crystalline solvates (each line corresponds to a different crystalline solvate) (no crystalline solvates with CIP-II coordination were available for analysis) [141]

with different modes of anion…Li^+ cation coordination. This is an important distinction which is generally not made throughout the published scientific literature on electrolyte characterization. The ionic association tendency of lithium salts is found to increase in the order [134–136, 148]:

$$LiAsF_6, LiPF_6 < LiTFSI \leq LiClO_4 < LiBF_4 < LiSO_3CF_3 < LiCO_2CF_3$$

A comparison of this with the Li^+ cation solvation data (Fig. 1.5) indicates that this increasing ionic association tendency is opposite to that noted for the Li^+ cation solvation. This is due to the competitive coordination of the solvent molecules and anions to the Li^+ cations. Quantum chemical (QC) calculations and MD simulations find that $(AN)_n$–LiX mixtures consist predominantly of Li^+ cations with four-fold coordination to anions and/or AN solvent molecules (very little five-fold Li^+ cation coordination is found for AN-based electrolytes) [134–136]. As noted above, aprotic solvent molecules, such as AN, have only weak interactions with anions. Thus, the Li^+ cation coordination shell in solution consists of anions and/or solvent molecules. The competitive coordination between these determines the solvate distribution present in solution (Fig. 1.8) [134–136, 141].

4. *Transport Properties*: The transport properties (e.g., viscosity and ionic conductivity) of electrolytes are one of the key metrics used to gauge electrolytes. The viscosity may be correlated with the wettability of an electrolyte with the porous separator and electrodes. Figure 1.9 shows the variation in the viscosity of $(AN)_n$–LiX mixtures at 60 °C with different lithium salts [136]. Perhaps contrary to expectations, the most dissociated salts result in the highest viscosity for the more dilute mixtures. The differences in the viscosity for the different salts and

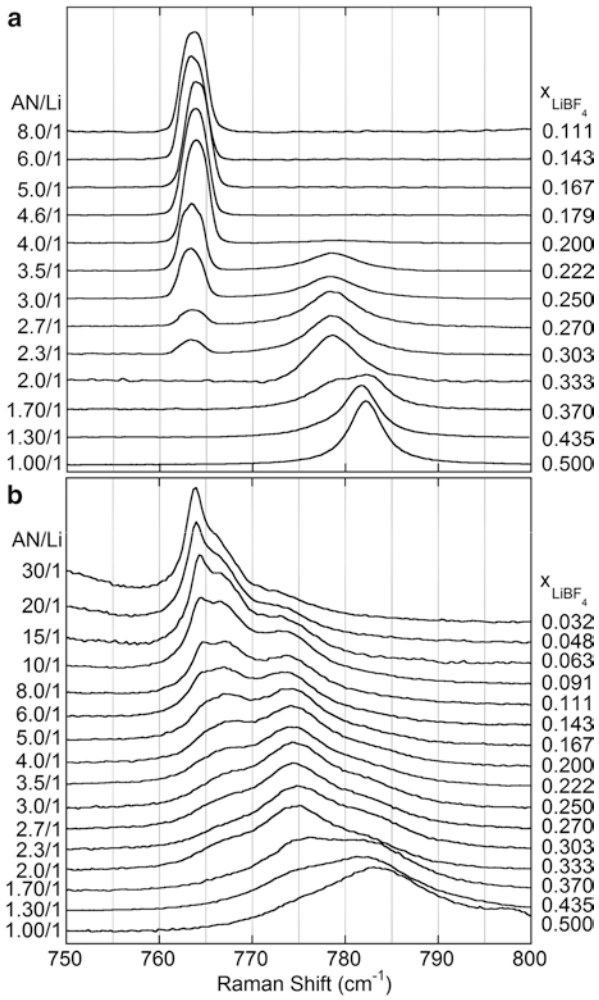

Fig. 1.7 BF_4^- anion band variation with concentration for the $(AN)_n$–$LiBF_4$ mixtures at (**a**) −80 °C and (**b**) 60 °C [134]

concentrations can be explained by the differences in solution structure (amount of uncoordinated solvent and number/distribution of solvates) (Figs. 1.8 and 1.10) [136]. Figure 1.11 shows the variation in the conductivity of the $(AN)_n$–LiX mixtures at 60 °C with the different lithium salts [136]. The differences noted in terms of both salt concentration and anion structure can once again be explained by the differences in electrolyte solution structure (types and distribution of solvates and uncoordinated anions, as well as the solvate formation/evolution dynamics) [136]. It is important to note that the AN electrolytes with $LiPF_6$ have the highest conductivity, but also the highest viscosity (Fig. 1.9). Similarly, the AN electrolytes with $LiCO_2CF_3$ have the lowest conductivity and the lowest viscosity.

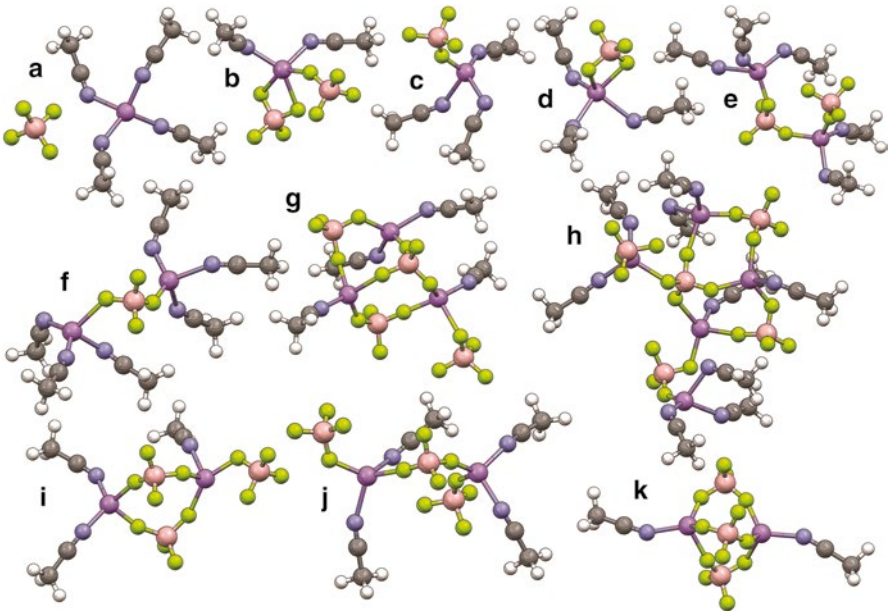

Fig. 1.8 Representative Li^+ cation solvate species (i.e., coordination shells) extracted from the MD simulations for the $(AN)_n$–$LiBF_4$ mixtures ($n = 30$, 20, and 10) at 60 °C with BF_4^- coordination: (**a**) SSIP; (**b**) CIP-I, CIP-II; (**c**) CIP-I; (**d**) CIP-II; (**e**) CIP-I, AGG-I; (**f**) AGG-I; (**g**) CIP-I, AGG-I (×3); (**h**) CIP-I, AGG-I (×3), AGG-III; (**i**) CIP-I, AGG-I (×2); (**j**) CIP-I (×2), AGG-I; and (**k**) AGG-I (×3). Only solvent and BF_4^- anions within 3.33 Å of a Li^+ cation are shown (Li—*purple*, B—*tan*, C—*gray*, N—*blue*, F—*light green*) [134]

This clearly shows that the conventional wisdom that conductivity is directly linked with viscosity—"a high conductivity is achieved for electrolytes with a low viscosity"—is inaccurate. Instead, both properties originate from the molecular-level interactions between the ions and solvent (i.e., solution structure). These properties are thus only indirectly correlated with one another. Frequently, it is found that a maximum in electrolyte conductivity is obtained near a 1 M salt concentration (Fig. 1.12) (for the AN electrolytes shown in Fig. 1.11, this corresponds to an AN/Li ratio of about 14 to 17—depending upon the salt's formula weight [136]). In addition, the choice of aprotic solvent or solvent mixtures used greatly impacts the conductivity of an electrolyte (Figs. 1.12 and 1.13) [5, 149–153], but importantly the trend in the conductivity for different salts remains largely the same irrespective of the solvent(s) used. For example, the conductivity with different lithium salts in an EC:DMC equimolar binary mixture with the solvents 3-methylsydnone (3-MSD) or 3-ethylsydnone (3-ESD) added is found to increase in the order [154]:

$$LiPF_6 > LiClO_4 > LiN\left(SO_2CF_3\right)_2 \left(LiTFSI\right) > LiN\left(SO_2C_2F_5\right)_2 > LiBF_4 > LiSO_3CF_3$$

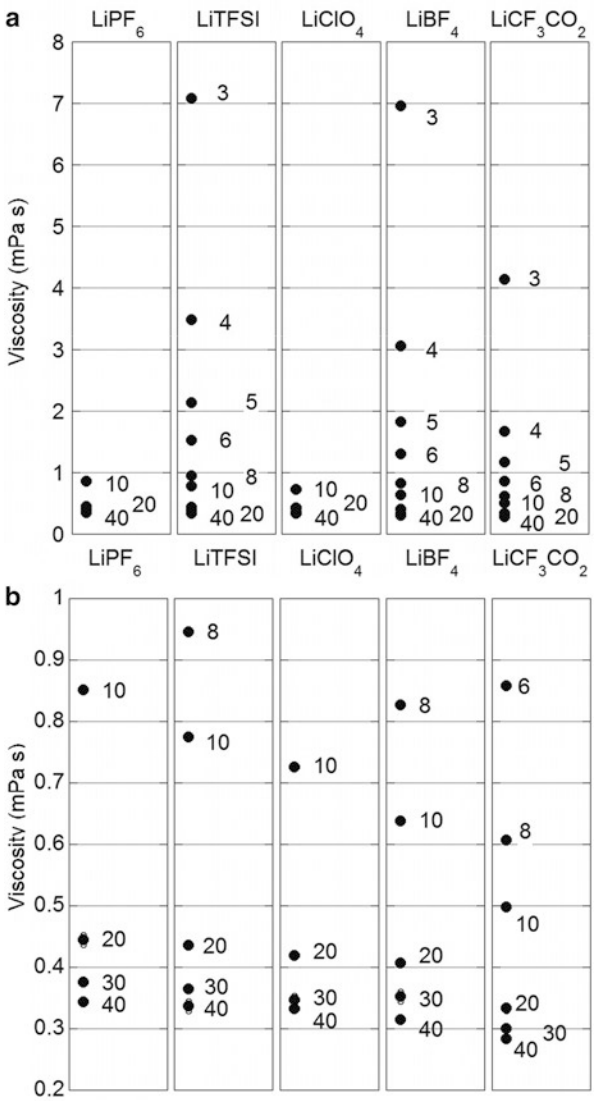

Fig. 1.9 (**a**) Viscosity of $(AN)_n$–LiX mixtures at 60 °C (AN/LiX (*n*) noted in plots) and (**b**) the same data for the dilute mixtures alone. Data for concentrated mixtures with $LiPF_6$ and $LiClO_4$ were not gathered as these samples crystallize during the measurements [136]

which is similar to the trend in Fig. 1.11 (if $LiClO_4$ and LiTFSI are interchanged). A similar order is also noted for the electrolytes in Table 1.1 and Fig. 1.14 [5, 108–110, 125, 150–153, 155, 156]. This latter figure indicates that the EC:PC electrolyte with $LiPF_6$ is slightly more conductive than the corresponding electrolyte with $LiAsF_6$, whereas the opposite is true for the 2-MeTHF:EC:PC electrolytes. Also, there is a crossover in the conductivity for the 2-MeTHF:EC:PC

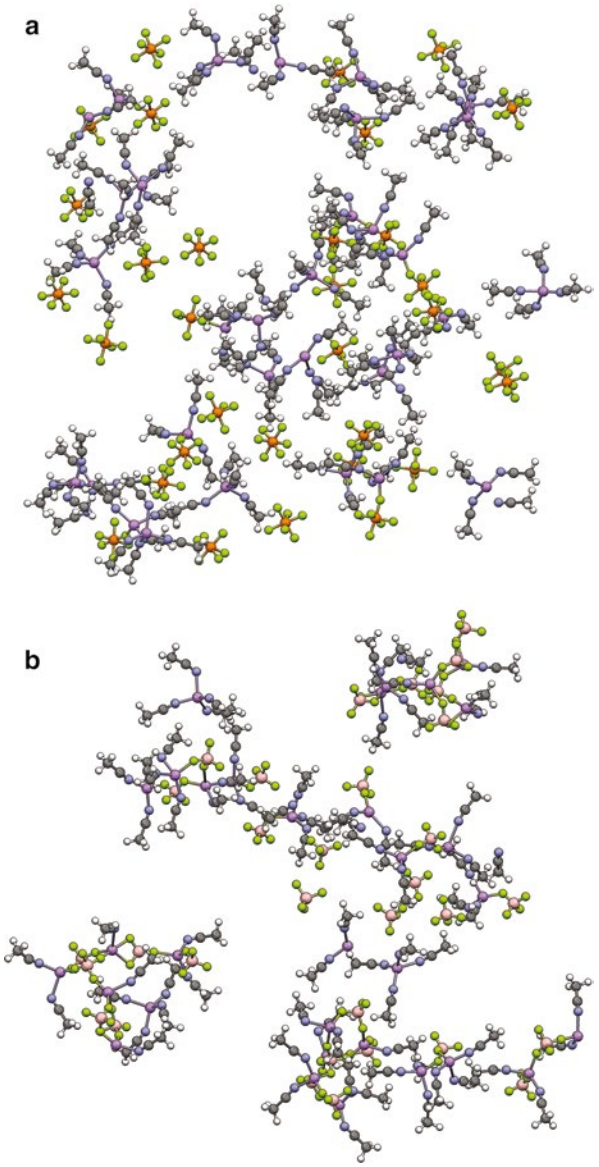

Fig. 1.10 Snapshot of the molecular simulations of $(AN)_n$–LiX mixtures ($n = 20$) with (**a**) $LiPF_6$ and (**b**) $LiBF_4$ (Li—*purple*, B—*tan*, C—*gray*, N—*blue*, F—*light green*, P—*orange*). Uncoordinated AN solvent molecules have been removed to aid in discerning the solvates present [136]

electrolytes with $LiBF_4$ or $LiSO_3CF_3$ with varying temperature. These points demonstrate that the ion solvation and ionic association interactions within the electrolytes are a function of numerous factors and generalizations about salt properties/behavior should be used with caution, as noted above.

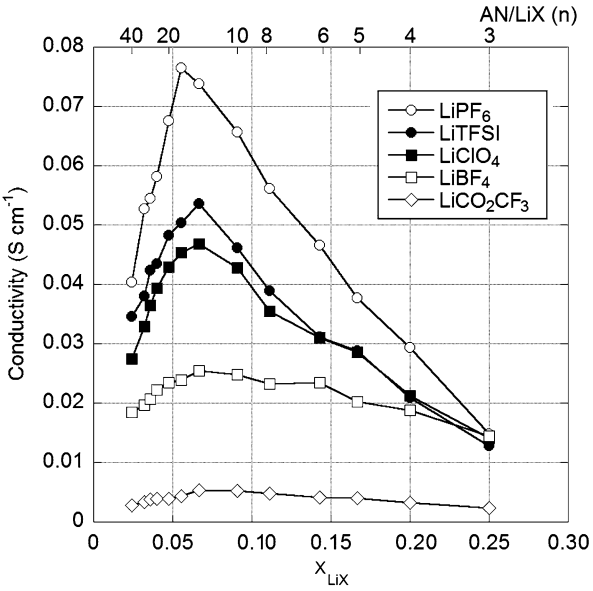

Fig. 1.11 Ionic conductivity of $(AN)_n$–LiX mixtures at 60 °C (solvent/LiX ratio (n) noted at the top of the plot) ($LiSO_3CF_3$ data not shown due to crystalline solvate formation) [136]

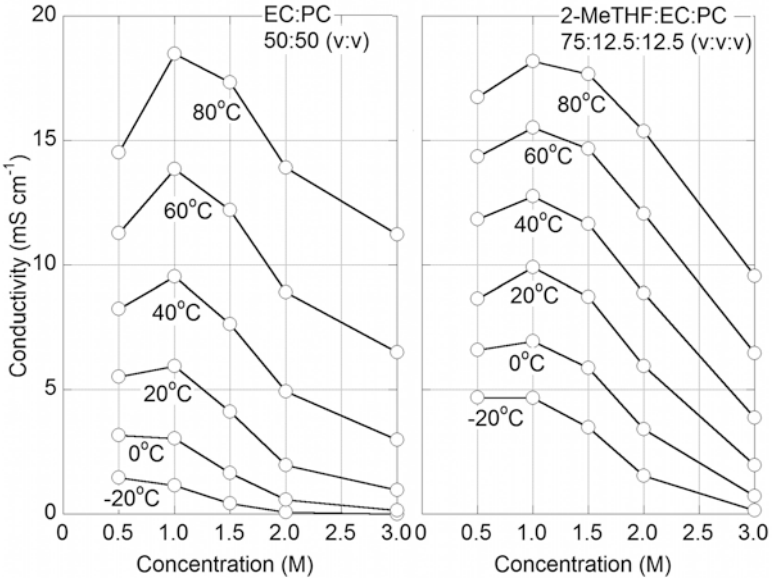

Fig. 1.12 Ionic conductivity of EC:PC (50:50 v:v) and 2-MeTHF:EC:PC (75:12.5:12.5 v:v:v) mixtures with $LiAsF_6$ for different temperatures and salt concentrations [5]

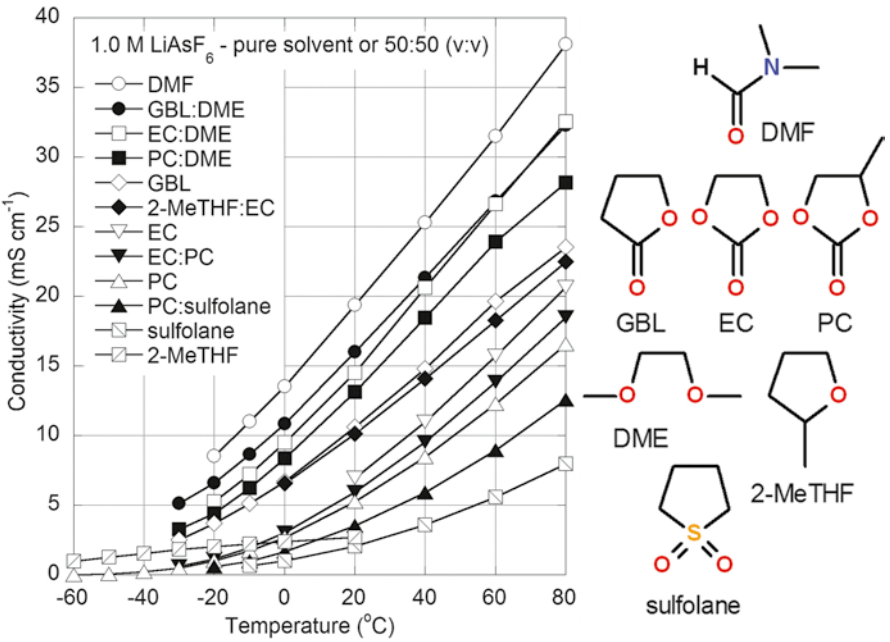

Fig. 1.13 Ionic conductivity of 1 M $LiAsF_6$ electrolytes with the indicated solvents (either a single solvent or a 50:50 v:v binary mixture) [5]

Table 1.1 Conductivity (mS cm^{-1}) of electrolytes with various lithium salts (1 M) at 25 °C ([a]v:v; [b]w:w) [108–110, 125, 155, 156]

Lithium salt (anion)	PC:DME (50:50)[a]	PC:DMC (50:50)[a]	PC:DEC (50:50)[b]	PC:EMC (50:50)[a]	EC:DMC (50:50)[a]	EC:THF (50:50)[a]	GBL
AsF_6^-	14.8	–	7.6	–	–	13.7	10.48
PF_6^-	15.3	10.0	7.1	9.33	11.2	–	11.63
ClO_4^-	13.5	6.8	4.5	6.26	10.1	13.5	–
$N(SO_2CF_3)_2^-$	12.6	–	–	7.57	–	–	9.21
BF_4^-	9.5	–	2.5	3.72	–	9.5	7.33
$SO_3CF_3^-$	6.1	2.1	–	–	3.1	5.4	–

PC propylene carbonate, *EC* ethylene carbonate, *DME* 1,2-dimethoxyethane (or monoglyme), *DMC* dimethyl carbonate, *DEC* diethyl carbonate, *THF* tetrahydrofuran, *GBL* γ-butyrolactone

1.5 Advanced Salts—Fluoroborates and -Phosphates

Lithium salts with tetraalkylborate anions are highly soluble in dioxolane (up to 3 M) [157]. This is due to the poorly coordinating tetraalkylborate anions which lack donor atoms with electron lone-pairs for Li^+ cation coordination [158]. Thus, solvent molecules readily displace the anions in the Li^+ cation coordination shells. This also accounts for the poor chemical stability of the salts [159]: lithium

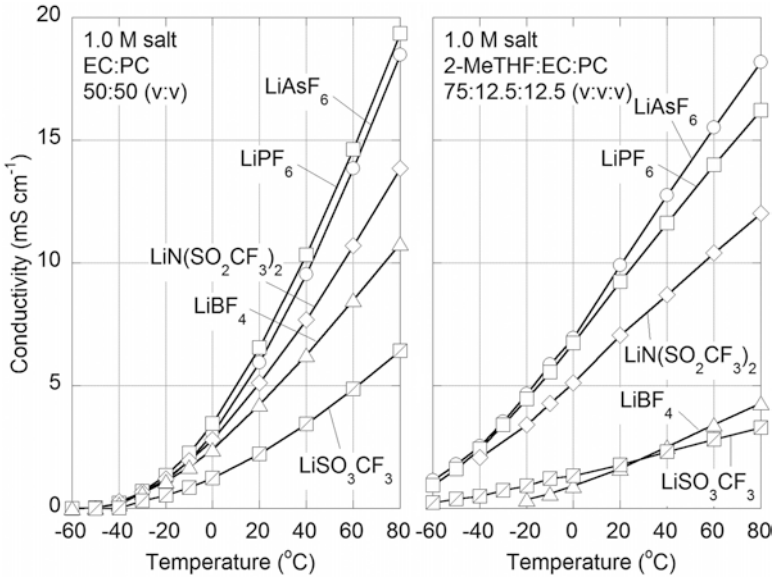

Fig. 1.14 Ionic conductivity of EC:PC (50:50 v:v) and 2-MeTHF:EC:PC (75:12.5:12.5 v:v:v) mixtures with the indicated lithium salts (1 M) [5]

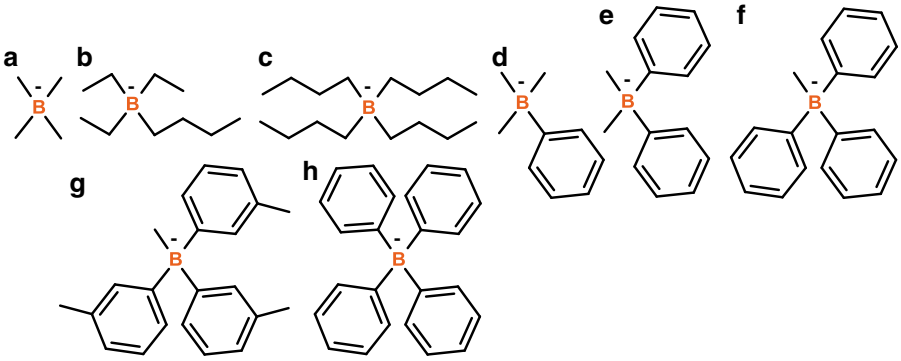

Fig. 1.15 Examples of organoborate anions: (**a**) $B(CH_3)_4^-$ [158, 160, 161], (**b**) $B(C_2H_5)_3(C_4H_9)^-$ [160, 161], (**c**) $B(C_4H_9)_4^-$ [160, 161], (**d**) $B(CH_3)_3(C_6H_5)^-$ [160, 162], (**e**) $B(CH_3)_2(C_6H_5)_2^-$ [160], (**f**) $B(CH_3)(C_6H_5)_3^-$ [160], (**g**) $B(CH_3)(C_6H_4(CH_3))_3^-$ [160], and (**h**) $B(C_6H_5)_4^-$ [160, 161]

tetramethylborate (i.e., $LiB(CH_3)_4$) (Figs. 1.15a and 1.16a) [158, 160–162] is stable in air [157], but lithium tetrabutylborate (i.e., $LiB(C_4H_9)_4$) (Fig. 1.15c) is pyrophoric [157]. In the former salt, the Li^+ cations are coordinated by the methyl hydrogens [158], but less favorable coordination may occur for anions with longer alkyl chains making the anions more reactive. Lithium tetraphenylborate (*LiBPh*$_4$) (i.e., $LiB(C_6H_5)_4$) (Figs. 1.15h and 1.16c) is stable only when the Li^+ cations are fully solvated—this

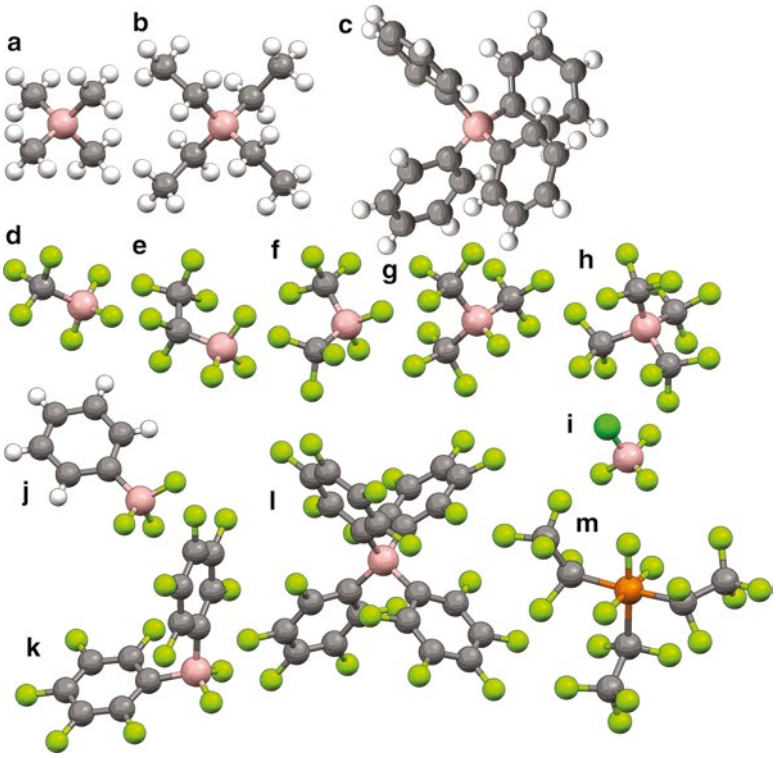

Fig. 1.16 Anion structures: (**a**) $B(CH_3)_4^-$, (**b**) $B(C_2H_5)_4^-$, (**c**) $B(C_6H_5)_4^-$ (BPh_4^-), (**d**) $BF_3(CF_3)^-$ (**e**) $BF_3(C_2F_5)^-$ (FAB^-), (**f**) $BF_2(CF_3)_2^-$, (**g**) $BF(CF_3)_3^-$, (**h**) $B(CF_3)_4^-$, (**i**) BF_3Cl^-, (**j**) $BF_3(C_6H_5)^-$, (**k**) $BF_2(C_6F_5)_2^-$, (**l**) $B(C_6F_5)_4^-$ ($BArF^-$), and (**m**) $PF_3(C_2F_5)_3^-$ (FAP^-) (B—*tan*, C—*gray*, F—*light green*, P—*orange*)

salt is typically sold commercially as the $(DME)_3$:$LiBPh_4$ solvate, while crystal structures have been reported for the $(H_2O)_4$:$LiBPh_4$ [163], $(H_2O)_2(DME)_1$:$LiBPh_4$ [164], $(H_2O)_2(THF)_2$:$LiBPh_4$ [165], $(THF)_1(12C4)_1$:$LiBPh_4$ [166], $(triglyme)_1$:$LiBPh_4$ [167], and $P(EO)_5$:$LiBPh_4$ [168] solvates—all with fully solvated Li^+ cations and uncoordinated BPh_4^- anions. The unsolvated $LiBPh_4$ salt slowly reacts with dry air. PC-based electrolytes with $LiBPh_4$ (and some DME) have a conductivity which is similar (slightly lower) to that of electrolytes with $LiBF_4$, but the conductivity of THF- and DME-based electrolytes with $LiBPh_4$ is higher than for those with $LiBF_4$ [169]. This may be attributable to variations in the ionic association interactions for the $LiBF_4$ salt with the different solvents, whereas the $LiBPh_4$ salt remains fully dissociated for all of the electrolyte formulations.

The anions from conjugate Brønsted–Lewis superacids represent the core lithium salts used for commercial lithium batteries (i.e., $LiPF_6$ and $LiBF_4$). The acidity order determined from QC calculations is as follows: HBF_4 (287.7) < HPF_6 (276.6) < $HTaF_6$ (268.3) < $HAlCl_4$ (257.4) < $HSbF_6$ (255.5) (DFT-calculated ΔG_{acid}

values in kcal mol^{-1}) [21]. $LiBF_4$ and $LiPF_6$ have both been extensively used for lithium battery research, and the latter is used in commercial Li-ion cells. The synthesis of $LiTaF_6$ and $LiNbF_6$ has been reported [170–175]. Although $LiTaF_6$ is highly soluble in THF, after the salt dissolution the electrolyte subsequently polymerized [175]. The conductivity of a 0.33 M $LiTaF_6$ electrolyte with sulfolane is 3.8×10^{-3} S cm^{-1} at 75 °C [175] (which is somewhat lower than a 0.33 M $LiPF_6$ electrolyte with sulfolane at this temperature [5]). The conductivity of PC-based electrolytes with either $LiTaF_6$ or $LiNbF_6$ was also found to be lower than the corresponding electrolytes with $LiPF_6$ [174]. Electrolytes with $LiTaF_6$ result in very poor Li metal cycling efficiency suggesting that the TaF_6^- anions may also have poor reductive stability [6]. The reductive stability of the MF_6^- anions is reported to follow the order $SbF_6^- < AsF_6^- < PF_6^-$ [176]. Electrolytes with $LiSbF_6$ have a similar conductivity to those with $LiPF_6$, but the $LiSbF_6$ salt may be corrosive to metals [6]. The Li_2SiF_6 and Li_3AlF_6 salts tend to be poorly soluble in aprotic solvents, and the resulting electrolytes have a low conductivity [6]. In contrast to these salts, $LiAsF_6$ is highly soluble and its use results in electrolytes with comparable and, in some cases, superior conductivity and properties to those with $LiPF_6$ (Table 1.1 and Fig. 1.14) [5]. But the potential to reduce the anion As^V oxidation state to the highly toxic As^{III} or As^0 oxidation states, as noted above, has largely limited the commercial use of $LiAsF_6$ [177].

$LiAlCl_4$ has been widely used for Li/SO_2Cl_2 batteries [178] (as has $LiGaCl_4$ [179–186]), but $LiAlCl_4$ has also been studied for use with intercalation cathodes. For example, an electrolyte composed of $LiAlCl_4 \cdot 3SO_2$ was used for a $Li/LiCoO_2$ cell [187, 188]. This electrolyte has a very high conductivity (70–80 mS cm^{-1} at 0–20 °C), but the salt undergoes a degradation side reaction to produce Cl_2 which then reacts with Li metal to form LiCl [187, 188]:

$$LiAlCl_4 \rightarrow AlCl_3 + 1/2\,Cl_{2(\text{dissolved})} + Li^+ + e^-$$

$$1/2\,Cl_{2(\text{dissolved})} + Li_{(s)} \rightarrow LiCl_{(s)}$$

A diverse range of analogues of BF_4^- anions (Fig. 1.17) has been reported with the replacement of fluorine atoms with perfluoroalkyl chains. The conductivity of 1 M salt in EC:EMC electrolytes with lithium salts with these anions is given in Table 1.2. Perhaps contrary to expectations, it is interesting to note that the electrolyte conductivity increases with increasing size/mass of the anions. One might instead expect that bulkier anions would be less mobile, thus decreasing the conductivity. This increase in the conductivity may be due to decreased ionic association interactions with increasing perfluoroalkyl chain lengths and numbers (Figs. 1.1 and 1.2). A separate publication, however, indicated that an electrolyte with $LiBF_3C_2F_5$ (*LiFAB*) (Figs. 1.16e and 1.17a) has a lower conductivity than the corresponding $LiBF_4$ electrolyte (1 M salt in EC:EMC 30:70 v:v) above 0 °C, but a higher conductivity at < −20 °C [190]. Yet another publication indicates that LiFAB electrolytes (EC:EMC 30:70 v:v) are more conductive than $LiBF_4$ electrolytes (but less conductive than $LiPF_6$-based electrolytes) from −10 to 25 °C [192]. The LiFAB salt has

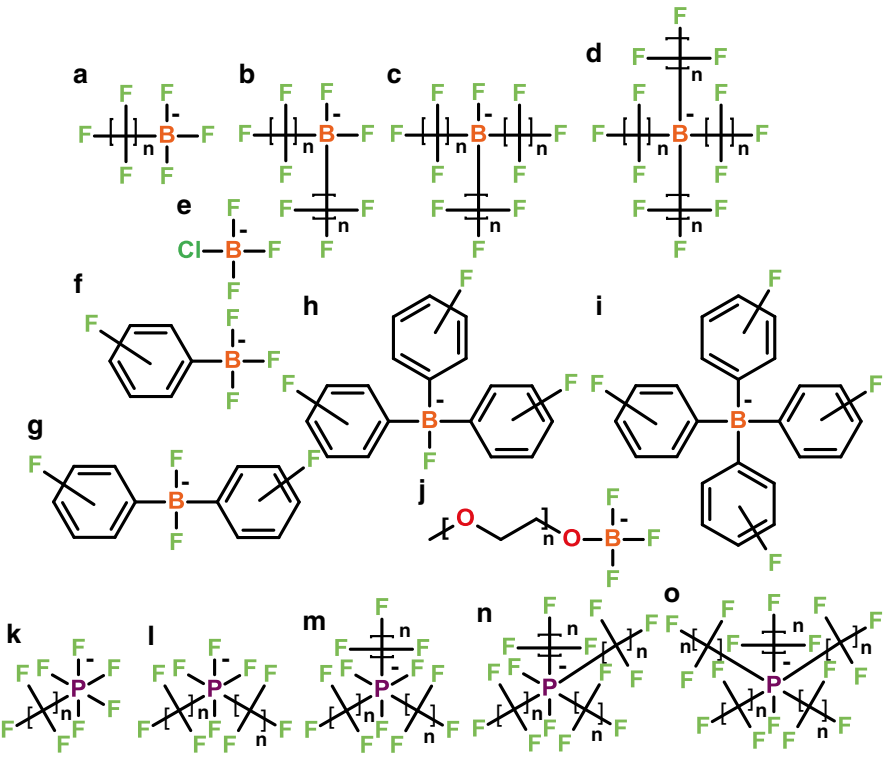

Fig. 1.17 Examples of analogues of BF_4^- and PF_6^- anions: (**a**) $BF_3(C_nF_{2n+1})^-$ [189–193], (**b**) $BF_2(C_nF_{2n+1})_2^-$ [189, 191], (**c**) $BF(C_nF_{2n+1})_3^-$ [189, 191], (**d**) $B(C_nF_{2n+1})_4^-$ [189, 194, 195], (**e**) BF_3Cl^- [196], (**f**) $BF_3(C_6H_nF_{5-n})^-$ [160, 197, 198], (**g**) $BF_2(C_6H_nF_{5-n})_2^-$ [160, 197, 198], (**h**) $BF(C_6H_nF_{5-n})_3^-$ [160, 197, 198], (**i**) $B(C_6H_nF_{5-n})_4^-$ [160, 198–201], (**j**) $BF_3O(C_2H_4O)_nCH_3^-$ [202], (**k**) $PF_5(C_nF_{2n+1})^-$ [203, 204], (**l**) $PF_4(C_nF_{2n+1})_2^-$ [203, 204], (**m**) $PF_3(C_nF_{2n+1})_3^-$ [70, 203–206], (**n**) $PF_2(C_nF_{2n+1})_4^-$ [63, 70, 203–209], and (**o**) $PF(C_nF_{2n+1})_5^-$ [204]

Table 1.2 Conductivity of electrolytes with various lithium salts at 20 °C and 1 M salt in EC:EMC (25:75 v:v) [189]

Lithium salt (anion)	Conductivity (mS cm^{-1})	Lithium salt (anion)	Conductivity (mS cm^{-1})
PF_6^-	8.52		
BF_4^-	2.91		
$BF_3(CF_3)^-$	3.21	$BF_3(C_2F_5)^-$	3.31
$BF_2(CF_3)_2^-$	4.02	$BF_2(C_2F_5)_2^-$	4.62
$BF(CF_3)_3^-$	5.11	$BF(C_2F_5)_3^-$	6.89
$B(CF_3)_4^-$	7.52	$B(C_2F_5)_4^-$	8.55
$BF_3(SO_2CF_3)^-$	4.47	$BF_3(SO_2C_2F_5)^-$	3.98
$BF_2(SO_2CF_3)_2^-$	5.83	$BF_2(SO_2C_2F_5)_2^-$	5.23
$BF(SO_2CF_3)_3^-$	7.62	$BF(SO_2C_2F_5)_3^-$	7.18
$B(SO_2CF_3)_4^-$	8.55	$B(SO_2C_2F_5)_4^-$	8.21

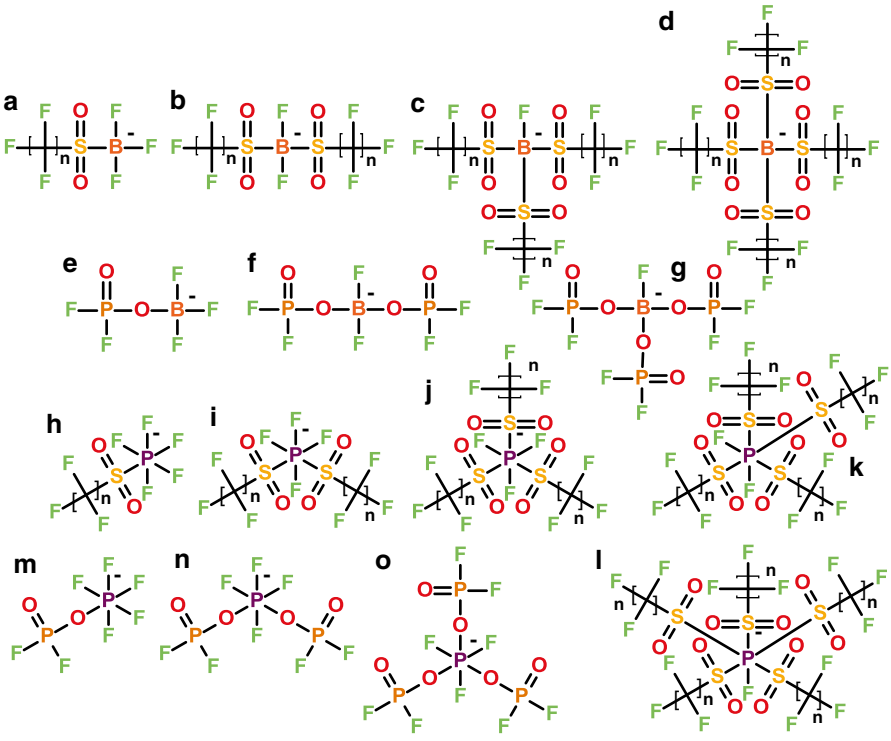

Fig. 1.18 Examples of BF_4^- and PF_6^- analogue anions with perfluoroalkylsulfonyl and phosphorodifluoridato groups: (**a**) $BF_3(SO_2C_nF_{2n+1})^-$ [189], (**b**) $BF_2(SO_2C_nF_{2n+1})_2^-$ [189], (**c**) $BF(SO_2C_nF_{2n+1})_3^-$ [189], (**d**) $B(SO_2C_nF_{2n+1})_4^-$ [189], (**e**) $BF_3(PO_2F_2)^-$ [210], (**f**) $BF_2(PO_2F_2)_2^-$ [210], (**g**) $BF(PO_2F_2)_3^-$ [210], (**h**) $PF_5(SO_2C_nF_{2n+1})^-$ [204], (**i**) $PF_4(SO_2C_nF_{2n+1})_2^-$ [204], (**j**) $PF_3(SO_2C_nF_{2n+1})_3^-$ [204], (**k**) $PF_2(SO_2C_nF_{2n+1})_4^-$ [204], (**l**) $PF(SO_2C_nF_{2n+1})_5^-$ [204], (**m**) $PF_5(PO_2F_2)^-$ [210], (**n**) $PF_4(PO_2F_2)_2^-$ [210], and (**o**) $PF_3(PO_2F_2)_3^-$ [210]

good compatibility with Al at high potential, as well as a high stability with a graphite anode and nickel oxide-based cathode. The cell cycling behavior is comparable to an electrolyte with $LiPF_6$ and far better than one with $LiBF_4$. Cells with LiFAB also had improved capacity retention relative to cells with $LiPF_6$ after storage at 60 °C [190]. For cells with graphite anodes and $LiCoO_2$ cathodes, however, comparable performance to $LiPF_6$ electrolytes was found at room temperature, but inferior performance was found at elevated temperature reportedly due to a degradation reaction of the LiFAB electrolyte with the cathode [192]. Electrolytes with variants of BF_4^- anions with perfluoroalkylsulfonyl groups ($-SO_2C_nF_{2n+1}$) (Fig. 1.18a–d) have conductivity values somewhat higher than those with anions with the corresponding perfluoroalkyl groups (Table 1.2) [189]. Analogous anions with the fluorine atoms of BF_4^- replaced with $-PO_2F_2$ groups have also been reported (Fig. 1.18e–g) [210].

The $LiBF_3Cl$ salt (Figs. 1.16i and 1.17e) has a higher solubility than $LiBF_4$ in aprotic solvents and hinders crystallization of electrolytes to a greater extent at low temperature [196]. In common with $LiBF_4$, the $LiBF_3Cl$ salt passivates Al well at high potential. The salt also makes a more favorable SEI with graphite than comparable electrolytes with $LiBF_4$ [196].

Lithium salts with fluorinated phenylfluoroborate anions have been reported (Fig. 1.17f–i) [198]. The conductivity values for 0.5 M salt in PC:DMC (v:v) electrolytes at 30 °C are reported to be $LiBF_4$ (3.7 mS cm^{-1}), $LiBF_3(C_6F_5)$ (Fig. 1.17f) (4.0 mS cm^{-1}), and $LiBF_3C_3F_7$ (Fig. 1.17a) (6.1 mS cm^{-1}), but the t_{Li+} values are 0.31, 0.71, and 0.43, respectively [198]. The lithium tetrakis(pentafluorophenyl)borate salt (*LiBArF*) (i.e., $LiB(C_6F_5)_4$) (Figs. 1.16l and 1.17i) [199, 200] has a very weakly coordinating anion with 20 fluorine atoms per Li^+ cation. Although this salt does form crystalline solvates with fully solvated Li^+ cations (i.e., $(AN)_4$:$LiB(C_6F_5)_4$ [211] and $(Et_2O)_4$:$LiB(C_6F_5)_4$ [212]), it also crystallizes as solvates in which the Li^+ cations are partially coordinated by the anion fluorine atoms (i.e., $(Et_2O)_1$:$LiB(C_6F_5)_4$·CH_2Cl_2 [212], $(toluene)_1$:$LiB(C_6F_5)_4$·toluene [212], and $(benzene)_1$:$LiB(C_6F_5)_4$ [213]). Thus, the extensive fluorination of the anion actually facilitates the coordination of the anion to the Li^+ cations (relative to $LiBPh_4$). The properties of a wide variety of different $LiBR_4$ salts with varying alkyl and/or aryl groups and substituents (–CH_3, –OCH_3, –F, –CF_3) have been extensively explored as electrolytes by researchers at Exxon Research and Engineering Company in the early 1980s [161, 214]. The anodic oxidative stability of the salts varies by more than 1.6 V depending upon the R group, with aryl groups resulting in higher stability than alkyl groups and the addition of electron-withdrawing substituents further increasing the stability [157, 160]. Related salts have been reported, such as $LiB(OC_6F_5)_4$ [215] and $LiB(SC_6F_5)_4$ [215, 216], but these salts tend to result in PEO-based electrolytes with a very low conductivity.

Lithium trifluoroalkoxyborate salts (Fig. 1.17j) are liquid at room temperature with a neat salt conductivity on the order of 10^{-4} S cm^{-1} [202]. Carbonate-based electrolytes (EC:PC:DMC 1:1:3 v:v:v) with these salts have a conductivity >3 mS cm^{-1} at 20 °C (higher than comparable electrolytes with $LiBF_4$) [202].

Analogues of PF_6^- anions (Fig. 1.17k–o) have also been reported [63, 70, 203–209]. Electrolytes (1 M salt in EC:DMC 50:50 w:w) with the $LiPF_3(C_2F_5)_3$ (*LiFAP*) salt (Figs. 1.16m and 1.17m) have a conductivity which is only slightly lower than those with $LiPF_6$ [70]. Half cells with Li metal and $LiMn_2O_4$ cycled better with the electrolyte with LiFAP (relative to those with $LiPF_6$) [70, 208]. LiFAP was found to not undergo hydrolysis (in sharp contrast to $LiPF_6$) and to have improved thermal stability relative to $LiPF_6$ [63, 70, 207, 209]. In addition, carbonate solvent-based electrolytes with a mixture of LiFAP and $LiPF_6$ were reported to have superior cycling performance (relative to comparable electrolytes with the individual LiFAP and $LiPF_6$ salts), especially at 80 °C [206]. Anions in which the PF_6^- fluorine atoms have been replaced with $–SO_2C_nF_{2n+1}$ or $–PO_2F_2$ groups have also been reported (Fig. 1.18h–o) [204, 210].

1.6 Advanced Salts—Perfluoroalkylacetates, -Sulfonates, and -Phosphates

The experimental gas-phase acidity values (ΔG_{acid} in kcal mol^{-1}) for alkyl- and perfluoroalkylacetates and sulfonates follow the order HCO_2CH_3 (341.1) < HCO_2CF_3 (316.3) ≤ HSO_3CH_3 (315.0) < HSO_3F (299.8) < HSO_3CF_3 (299.5) (Fig. 1.1) [21, 26]. The fluorocarbonate anion (i.e., CO_2F^-) is highly reactive and may be considered to be a fluorine anion, F^-, solvated by CO_2 [217]. Other perfluoroalkylacetate anions (i.e., $CO_2C_nF_{2n+1}^-$) (Figs. 1.19a and 1.20a) have not been used to any significant extent for lithium battery electrolytes. The lithium salts with these anions tend to be highly aggregated (extensive anion…Li^+ cation coordination interactions) in PC electrolytes [218]. This is in agreement with the results noted above for the $(AN)_n$–$LiCO_2CF_3$ mixtures which have a very low solvation number over the entire concentration range (Fig. 1.5) and very low conductivity relative to other $(AN)_n$–LiX mixtures (Fig. 1.11).

Fluorosulfonic acid (i.e., HSO_3F) (Fig. 1.19b) was first reported in 1918 [236]. $LiSO_3F$-based electrolytes with several aprotic solvents were found to have a similar oxidative stability to electrolytes with other lithium salts such as $LiSO_3CF_3$ [237]. The conductivity of 1 M $LiSO_3F$ electrolytes with PC and GBL is 1.4 and 3.6 mS cm^{-1}, respectively [237]. For a mixed-solvent electrolyte, 1 M $LiSO_3F$ in GBL:DME (1:1 mol:mol), however, the conductivity is 7.4 mS cm^{-1} at 25 °C [237] (to be compared with 1 M GBL:DME (1:1 mol:mol) electrolytes with $LiBF_4$, $LiPF_6$, and $LiAsF_6$ which have conductivity values of 7.7, 11.2, and 11.8 mS cm^{-1} [238]). The crystal structure for $LiSO_3F$ has been reported [239].

Trifluoromethanesulfonic acid (i.e., HSO_3CF_3) (Fig. 1.19b) and the corresponding sodium salt were first reported in 1954 [240, 241]. A 3M patent in 1956 then reported the preparation of a variety of perfluoroalkylsulfonic acids and the corresponding sodium and potassium salts [242]. The use of $LiSO_3CF_3$ in battery electrolytes began in the 1970s and early 1980s [243, 244]. Lithium salts with perfluoroalkylsulfonate anions (Figs. 1.19b and 1.20b, c) tend to be more dissociated

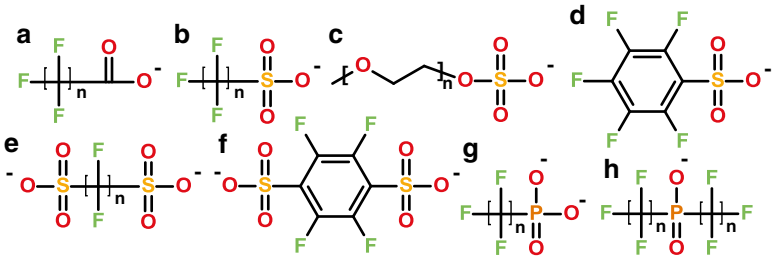

Fig. 1.19 Examples of fluoroalkylacetate, -sulfonate, and -phosphate anions: (**a**) $CO_2C_nF_{2n+1}^-$ [218], (**b**) $SO_3C_nF_{2n+1}^-$ [219–222], (**c**) $SO_4(C_2H_4O)_nCH_3^-$ [223, 224], (**d**) $SO_3(C_6F_5)^-$ [175, 221], (**e**) $SO_3(CF_2)_nSO_3^{2-}$ [175, 222, 225], (**f**) $SO_3(C_6F_4)SO_3^{2-}$ [226], (**g**) $PO_3(C_nF_{2n+1})^{2-}$ [72, 227–232], and (**h**) $PO_2(C_nF_{2n+1})_2^-$ [72, 227, 230, 233–235]

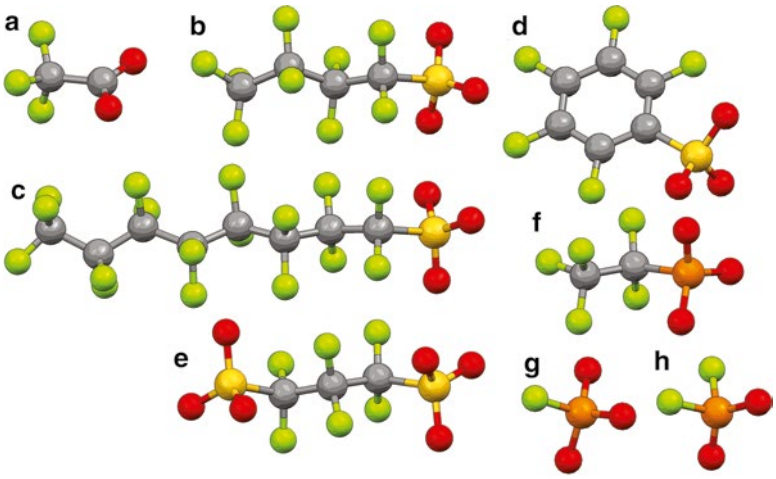

Fig. 1.20 Anion structures: (**a**) $CO_2CF_3^-$, (**b**) $SO_3C_4F_9^-$, (**c**) $SO_3C_8F_{17}^-$, (**d**) $SO_3(C_6F_5)^-$, (**e**) $SO_3C_3F_6SO_3^{2-}$, (**f**) $PO_3C_2F_5^{2-}$, (**g**) PO_3F^{2-}, and (**h**) $PO_2F_2^-$ (C—*gray*, O—*red*, F—*light green*, P—*orange*, S—*yellow*)

than those with perfluoroalkylacetate anions due to the larger size of the sulfur atoms relative to carbon (making the anion "softer") and more extensive resonance (and thus charge delocalization) due to the additional oxygen atom. This results in the sulfonate salts having a higher conductivity than the corresponding acetate salts (Table 1.3) [219, 221]. The conductivity of electrolytes with the perfluoroalkylsulfonate anions is not correlated with the mass of the anions (Table 1.3). All of the electrolytes with these salts, however, have a conductivity which is significantly lower than for the comparable electrolyte with $LiPF_6$ (Tables 1.1 and 1.3, Fig. 1.14). The crystal structure for $LiSO_3CF_3$ is known for both low- and high-temperature phases [245–247]. The conductivity of amorphous PEO-based polymer electrolytes with the perfluoroalkylsulfonate salts follows the order [220]:

$$LiSO_3C_{10}F_{21} < LiSO_3CF_3 < LiSO_3C_8F_{17} < LiSO_3C_4F_9 < LiTFSI$$

This ordering is likely due to a reduction in the partial negative charge on the anion oxygen atoms upon increasing chain length from $–CF_3$ to $–C_4F_9$ (which reduces the ionic association tendency of the anions). An additional increase in the chain length (i.e., $–C_8F_{17}$ and $–C_{10}F_{21}$), however, does not then significantly decrease the ionic association interactions further and the more bulky anions decrease the anion mobility (and perhaps the Li^+ cation mobility due to the correlated interactions of the cations with the anions), thus lowering the conductivity (relative to $LiSO_3C_4F_9$).

Note that lithium salts with nonfluorinated alkylsulfonate (e.g., $LiSO_3CH_3$) or benzenesulfonate (e.g., $LiSO_3(C_6H_5)$) anions have a very low solubility in aprotic solvents and a correspondingly low conductivity (Table 1.3) [219]. Lithium salts with oligoethersulfate anions (Fig. 1.19c) are soluble in EC:DMC mixtures, but these

Table 1.3 Conductivity of electrolytes with various lithium salts at 25 °C and 0.1 M salt in PC:DME (1:2 v:v) [219, 221]

Lithium salt (anion)	Conductivity (mS cm^{-1})	Molecular weight
PF_6^-	4.4	152
$CO_2CF_3^-$	0.4	120
$SO_3CH_3^-$	[a]	102
$SO_3CF_3^-$	2.3	156
$SO_3C_4F_9^-$	2.3	306
$SO_3(C_6H_5)^-$	0.1–0.2[b]	164
$SO_3(C_6F_5)^-$	1.1	254
$SO_3C_8F_{17}^-$	1.9	506
$N(COCF_3)_2^-$	0.8	215
$N(SO_2CF_3)_2^-$	4.0	287
$N(SO_2C_2F_5)_2^-$	3.8	387
$N(SO_2C_4F_9)(SO_2CF_3)^-$	3.5	437
$N(SO_2CF_3)(C_6F_4SO_2F)^-$	3.0	347
$N(SO_2CF_3)(SO_2C_8F_{17})^-$	3.2	637
$N(SO_2OCH_2CF_3)_2^-$	3.0	347
$N(SO_2OCH_2CF_2CF_3)_2^-$	3.0	447
$N(SO_2OCH_2CF_2CF_2H)_2^-$	2.9	411
$N(SO_2OCH(CF_3)_2)_2^-$	3.1	483
$C(SO_2CF_3)_3^-$	3.6	418
$C(SO_2OCH_2CF_3)_3^-$	2.9	508
$B(C_6H_3\text{-}3,5\text{-}(CF_3)_2)_4^-$	2.7	870
$PO_2(C_2F_5)_2^-$	0.6	308

[a]Practically insoluble
[b]ca. 0.02 M

have a much lower conductivity (<10^{-3} S cm^{-1} at 30 °C) than comparable electrolytes with $LiPF_6$ [223, 224]. The lithium salt with fluorinated benzenesulfonate anions (i.e., $LiSO_3(C_6F_5)$) (Figs. 1.19d and 1.20d) is somewhat more soluble in aprotic solvents, but the conductivity of such electrolytes is relatively low (lower than for electrolytes with $LiSO_3CF_3$) (Table 1.3) [219, 248].

Monofluorophosphoric acid (i.e., H_2PO_3F) (Figs. 1.19g and 1.20g) and difluorophosphoric acid (i.e., HPO_2F_2) (Figs. 1.19h and 1.20h) were first reported in 1929 and 1927, respectively [227–229, 235]. Lithium salts with these anions have been prepared [230, 231, 233, 234]. The related $HPHO_2F$ acid and corresponding $LiPHO_2F$ salt, however, were much more challenging to prepare [249]. Trifluoromethanephosphonic acid (i.e., $H_2PO_3CF_3$) (Fig. 1.19g) and bis(trifluoromethane)phosphonic acid (i.e., $HPO_2(CF_3)_2$) (Fig. 1.19h) were synthesized in 1954–1955 [250, 251]. The relative acidity of these anions was reported to follow the order [251]:

$$HNO_3, HCO_2CF_3, HCO_2C_3F_7 < H_2AsO_3CF_3 < HAsO_2\left(CF_3\right)_2$$

$$H_2PO_3CF_3, HCl < H_2SO_4 < HBr < HPO_2\left(CF_3\right)_2 < HClO_4$$

The lithium trifluoromethanephosphate salt (i.e., $Li_2PO_3CF_3$) (Fig. 1.19g) has also been synthesized [252]. This salt was reportedly soluble, forming a 1 M electrolyte with a PC:DME mixture which was utilized for battery cycling [252]. Perfluorodiphenylphosphinic acid (i.e., $HPO_2(C_6F_5)_2$) and the crystal structure of the corresponding potassium salt have also been reported [253].

1.7 Advanced Salts—Imides, Methides, and Phosphorylimides

The bis(fluorocarbonyl)imide acid (i.e., $H[N(COF)_2]$) (Fig. 1.21a) was first reported in 1973 [291], but anions with the X–CO–N–CO–X (X = C or F) backbone have not received much attention for battery electrolytes. In contrast, a diverse range of lithium salts with imide (sometimes called amide) anions with the $X–SO_2–N–SO_2–X$ (X = C or F) backbone have been prepared. This difference in focus is due to the difference, for example, in the acidifying capability of the $–COCF_3$ and $–SO_2CF_3$ groups (Fig. 1.2)—experimental gas-phase acidity values (ΔG_{acid} in kcal mol^{-1}) are $HN(COCF_3)_2$ (307.5) and $HN(SO_2CF_3)_2$ (291.8) (ref: H_2SO_4 (302.2)) (Fig. 1.2) [20, 26]. The $X–SO_2–N–SO_2–X$ backbone is able to adopt two low-energy conformations (Fig. 1.3f) [114–117]. This flexibility, combined with the extensive charge delocalization due to resonance and the electron-withdrawing fluorine atoms [20, 26], tends to make these lithium salts highly soluble. In addition, solvent–salt mixtures with such salts often form crystalline solvates with a low T_m (in contrast with $LiPF_6$) or crystallinity gaps (concentration ranges in which it is difficult or impossible to crystallize some or all of the electrolyte) (Fig. 1.4).

Lithium bis(methanesulfonyl)imide (or dimesylamide) (i.e., $LiN(SO_2CH_3)_2$) (Figs. 1.21b and 1.22a) [258, 292–295] and lithium bis(butanesulfonyl)imide (i.e., $LiN(SO_2C_4H_9)_2$) [258] have been reported. In sharp contrast to the lithium salts with tetraalkylborate anions which are highly soluble in aprotic solvents, lithium salts with nonfluorinated bis(alkanesulfonyl)imide anions have poor solubility in cyclic/acyclic carbonate and ether solvents [258]. This is likely due to the poor Li^+ cation-coordinating ability of the tetraalkylborate anions—thus favoring solvent coordination to the Li^+ cations, whereas the nonfluorinated bis(alkanesulfonyl)imide anions instead readily coordinate the Li^+ cations with the anion oxygen atoms and the lack of electron-withdrawing fluorine atoms results in high electron density on the oxygen atoms (i.e., strong ionic association tendency)—thus restricting the solvent coordination to the Li^+ cations. $LiN(SO_2CH_3)_2$ is insoluble in an EC:DMC mixture and has poor solubility in DMSO (<0.1 M), while $LiN(SO_2C_4H_9)_2$ has low solubility in EC:DMC (<0.1 M) and fair solubility in DMSO (~0.3 M) [258]. The conductivity at 25 °C of DMSO electrolytes with these salts (3.2 mS cm^{-1}) was considerably lower than for a 0.5 M $LiPF_6$ electrolyte with DMSO (9.8 mS cm^{-1}). In addition, ionic liquid salts with the $N(SO_2CH_3)_2^-$ anion have a higher viscosity, lower conductivity, lower thermal stability, and lower electrochemical stability than the corresponding salts with the $TFSI^-$ anion [296].

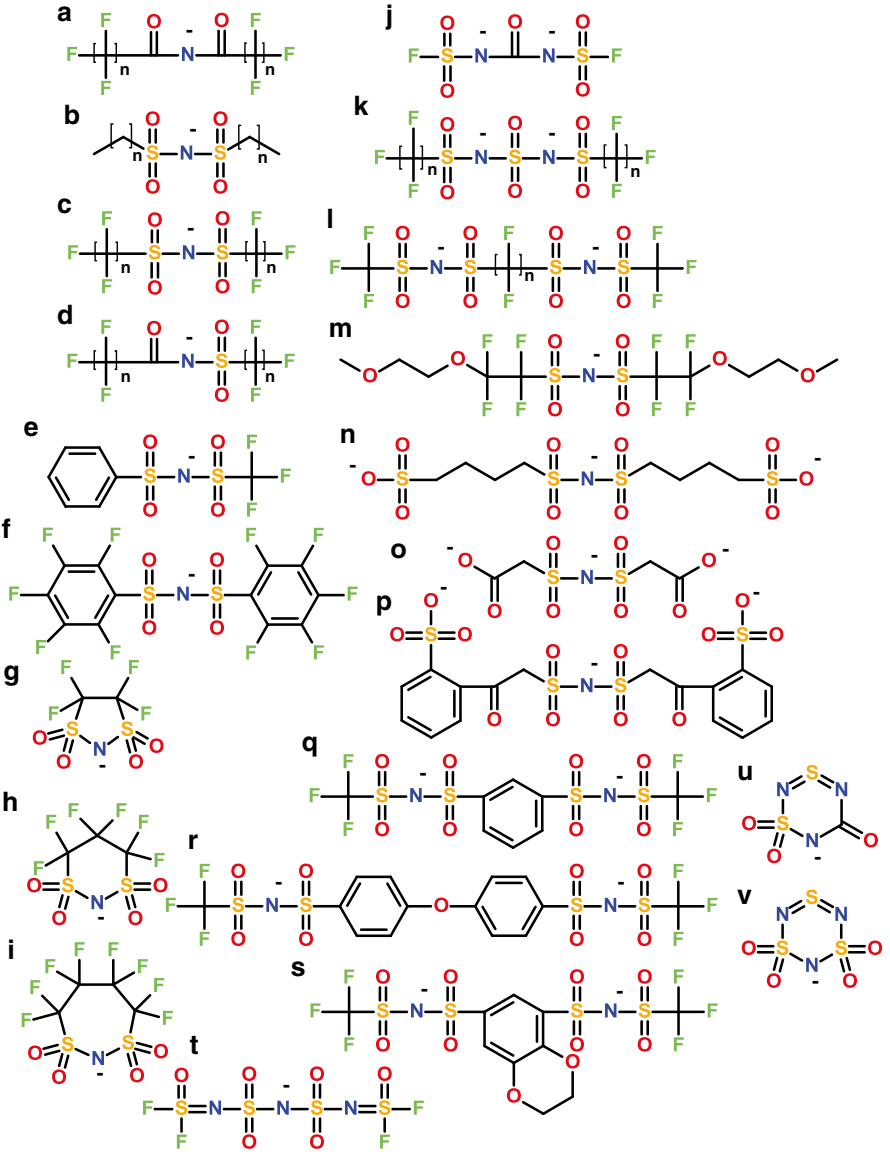

Fig. 1.21 Examples of imide anions: (**a**) $N(COC_nF_{2n+1})_2^-$ [254–257], (**b**) $N(SO_2C_nH_{2n+1})_2^-$ [258], (**c**) $N(SO_2C_nF_{2n+1})_2^-$ [259–270], (**d**) $N(COC_nF_{2n+1})(SO_2C_nF_{2n+1})^-$ [256, 257, 271–273], (**e**) $N(SO_2(C_6H_5))(SO_2CF_3)^-$ [274–276], (**f**) $N(SO_2(C_6F_5))_2^-$ [277], (**g**) $N(SO_2C_2F_4SO_2)^-$ [278, 279], (**h**) $N(SO_2C_3F_6SO_2)^-$ [269, 278, 279], (**i**) $N(SO_2C_4F_8SO_2)^-$ [278, 279], (**j**) $CO(NSO_2F)_2^{2-}$ [280], (**k**) $SO_2(NSO_2C_nF_{2n+1})_2^{2-}$ [281–283], (**l**) $(CF_2)_n(SO_2NSO_2CF_3)_2^{2-}$ [284, 285], (**m**) $N(SO_2C_2F_4O(C_2H_4O)CH_3)_2^-$ [277], (**n**) $N(SO_2C_4H_8SO_3)_2^{3-}$ [286], (**o**) $N(SO_2CH_2CO_2)_2^{3-}$ [286], (**p**) $N(SO_2CH_2CO(C_6H_4)SO_3)_2^{3-}$ [286], (**q**) $(C_6H_4)(SO_2NSO_2CF_3)_2^{2-}$ [287], (**r**) $O((C_6H_5)SO_2NSO_2CF_3)_2^{2-}$ [287], (**s**) $(C_6H_2)(OC_2H_2O)(SO_2NSO_2CF_3)_2^{2-}$ [287], (**t**) $N(SO_2NSOF_2)_2^-$ [288], (**u**) $N(CONSNSO_2)^-$ [289], and (**v**) $N(SO_2NSNSO_2)^-$ [290]

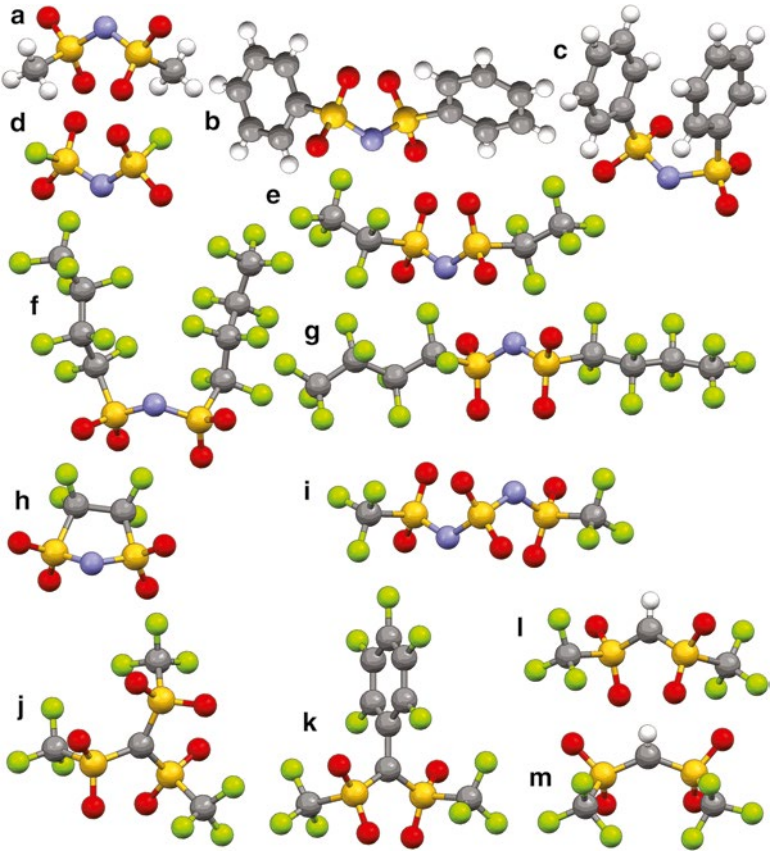

Fig. 1.22 Anion structures: (**a**) $N(SO_2CH_3)_2^-$ (*trans* conformation), (**b**) $N(SO_2(C_6H_5))_2^-$ (*trans* conformation), (**c**) $N(SO_2(C_6H_5))_2^-$ (*cis* conformation), (**d**) $N(SO_2F)_2^-$ (FSI^-), (**e**) $N(SO_2C_2F_5)_2^-$ ($BETI^-$) (*trans* conformation), (**f**) $N(SO_2C_4F_9)_2^-$ (*cis* conformation), (**g**) $N(SO_2C_4F_9)_2^-$ (*trans* conformation), (**h**) $N(SO_2C_2F_4SO_2)^-$, (**i**) $SO_2(NSO_2CF_3)_2^{2-}$, (**j**) $C(SO_2CF_3)_3^-$ ($TriTFSM^-$), (**k**) $C(SO_2CF_3)_2(C_6F_5)^-$, (**l**) $CH(SO_2CF_3)_2^-$ ($TFSM^-$) (*trans* conformation), and (**m**) $CH(SO_2CF_3)_2^-$ ($TFSM^-$) (*cis* conformation) (C—*gray*, N—*blue*, O—*red*, F—*light green*, S—*yellow*)

The $=NSO_2CF_3$ group has a very strong acidifying effect when replacing an =O [26]. The (trifluorosulfonyl)(sulfonate)imide anion [297] can be viewed as the SO_4^{2-} anion with a $=NSO_2CF_3$ group replacing an =O:

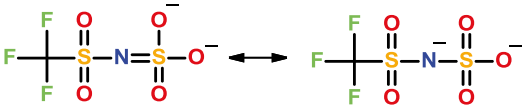

Similarly, the $TFSI^-$ anion can be viewed as the $SO_3CF_3^-$ anion with a $=NSO_2CF_3$ group replacing an =O:

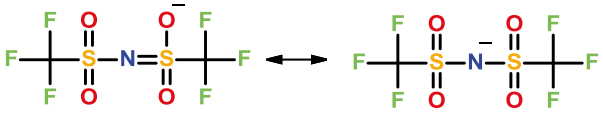

Additional $=NSO_2CF_3$ groups give [298, 299]

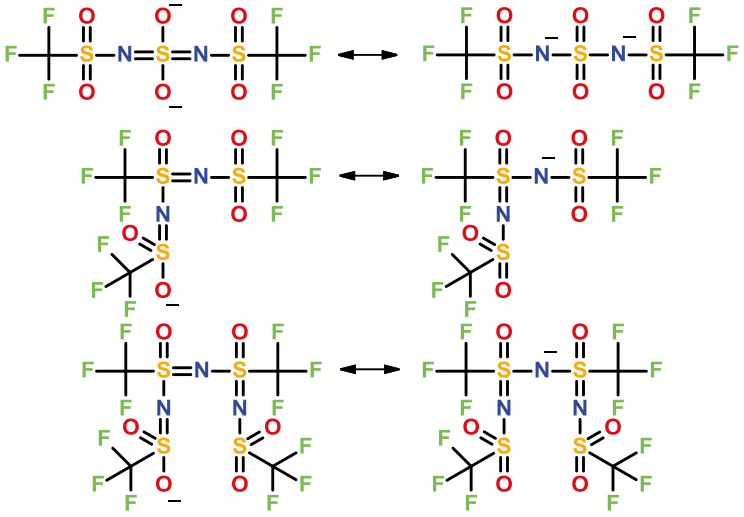

Fluorination of the imide anions results in lithium salts with exceptionally high solubility in common aprotic solvents. Bis(trifluoromethanesulfonyl)imide acid or HTFSI (i.e., $HN(SO_2CF_3)_2$) (Figs. 1.3f and 1.21c) was first reported in 1982 by Foropoulos and DesMarteau [300, 301], while the longer chain anions—$N(SO_2R_F)_2^-$—were reported a decade earlier by Meussdorffer and Niederprum [302]. In 1990, Armand patented the synthesis of LiTFSI and related fluorinated sulfonyl imide salts [303]. *LiTFSI* is now the most widely studied salt for this class of anions, but lithium bis(perfluoroethanesulfonyl)imide (*LiBETI*) (i.e., $LiN(SO_2C_2F_5)_2$) (Figs. 1.21c and 1.22e) has also been widely examined [49, 69, 207, 262, 304–310] with more than 200 publications reported for this latter salt. Electrolytes with LiBETI have a lower conductivity than those with $LiPF_6$ or LiTFSI (Table 1.4), but this salt, like LiTFSI, has an exceptionally high thermal stability and does not undergo hydrolysis due to the high stability of the C–F bonds. In addition, unlike LiTFSI, electrolytes with aprotic solvents and LiBETI are reported to not strongly corrode Al at high potential [66, 68, 311–313]. Numerous other perfluoroalkanesulfonyl imide anions have also been prepared [259, 314], including cyclic anions such as lithium cyclic-1,3-perfluoroethanedisulfonylimide (i.e., $LiN(SO_2C_2F_4SO_2)$) (Figs. 1.21g and 1.22h) and lithium cyclic-1,3-perfluoropropanedisulfonylimide (i.e., $LiN(SO_2C_3F_6SO_2)$)

Table 1.4 Conductivity of electrolytes with various lithium salts at 20 °C and 1 M salt in EC:DMC and EC:DEC (1:1 w:w) [259]

Lithium salt (anion)	Conductivity (mS cm^{-1})
In EC:DMC	
PF_6^-	9.41
$SO_3CF_3^-$	2.51
$N(SO_2CF_3)_2^-$	6.18
$N(SO_2C_2F_5)_2^-$	5.45
$N(SO_2C_4F_9)_2^-$	3.63
$N(SO_2CF_3)(SO_2C_4F_9)^-$	1.55
$N(SO_2C_2F_5)(SO_2C_4F_9)^-$	3.11
$N(SO_2C_3F_6SO_2)^-$	6.86
In EC:DEC	
PF_6^-	6.09
$SO_3CF_3^-$	1.63
$N(SO_2CF_3)_2^-$	4.24
$N(SO_2C_2F_5)_2^-$	3.95
$N(SO_2C_4F_9)_2^-$	2.34
$N(SO_2CF_3)(SO_2C_4F_9)^-$	1.10
$N(SO_2C_2F_5)(SO_2C_4F_9)^-$	2.28
$N(SO_2C_3F_6SO_2)^-$	4.95

(Fig. 1.21h)—PC:DME electrolytes with the latter have the highest conductivity of the imide salts noted in Table 1.4 [314]. The properties of most of these salts have not been extensively explored by the battery research community.

Anions with fluorosulfonyl groups ($–SO_2F$) have garnered tremendous interest in recent years. Chief among these is lithium bis(fluorosulfonyl)imide (*LiFSI*) (i.e., $LiN(SO_2F)_2$) (Figs. 1.21c and 1.22d) [156, 260, 263, 315–333]. Bis(fluorosulfonyl)-imide acid or HFSI (i.e., $HN(SO_2F)_2$) was first reported in 1962 [334], and, even though the synthesis of LiFSI was reported in 1995 [335], the limited availability and high cost of this salt have restricted its use in research studies until quite recently. Electrolytes with LiFSI typically have a conductivity equivalent to comparable electrolytes with $LiPF_6$ (making this one of the most conductive salts known) [156]. The thermal and hydrolytic stability of the FSI^- anion is lower than for the $TFSI^-$ anion due to the lower stability of the S–F bond (relative to a C–F bond), but the LiFSI salt has improved thermal/hydrolysis stability relative to $LiPF_6$ [156]. It was reported that use of the LiFSI salt in electrolytes results in severe Al corrosion at high potential [320], but it has recently been shown that this is likely due to chloride impurities in the salt rather than the LiFSI salt itself [156]. An additional favorable property (relative to $LiPF_6$) is the wide liquidus range of electrolytes with LiFSI. As for LiTFSI-based electrolytes, LiFSI-based electrolytes tend to form solvates with a low T_m or crystallinity gaps for specific electrolyte compositions.

Lithium salts with asymmetric anions may also be of interest as these tend to be more soluble and form solvates with a lower T_m than for salts with symmetric anions. Examples include lithium (fluorosulfonyl)(trifluoromethanesulfonyl)imide (*LiFTI* or LiFTA) (i.e., $LiN(SO_2F)(SO_2CF_3)$) (Fig. 1.21c) [263–265, 336] and lithium (fluorosulfonyl)(nonafluorobutanesulfonyl)imide (*LiFNFSI*) (i.e., $LiN(SO_2F)$

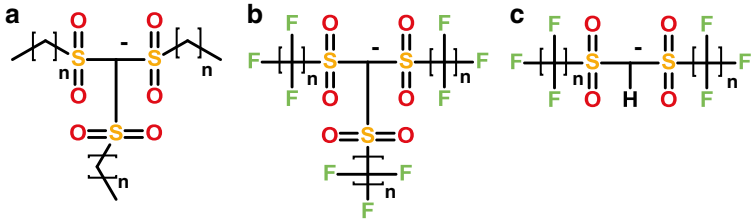

Fig. 1.23 Examples of methide anions: (**a**) $C(SO_2C_nH_{2n+1})_3^-$ [258, 339], (**b**) $C(SO_2C_nF_{2n+1})_3^-$ ($TriTFSM^-$) [111, 340–353], and (**c**) $CH(SO_2C_nF_{2n+1})_2^-$ ($TFSM^-$) [118, 341, 342, 354–360]

($SO_2C_4F_9$)) (Fig. 1.21c) [264, 265, 337]. The LiFNFSI salt has a high thermal stability (>200 °C), forms electrolytes with a high conductivity (comparable to those with $LiClO_4$), and does not significantly corrode the Al current collector at high potential. For battery testing, graphite/$LiCoO_2$ cells with LiFNFSI had a much improved cycling performance over cells with $LiPF_6$ when cycled at elevated temperature (60 °C). Asymmetric imide anions with carbonyl groups such as *TSAC*$^-$ (i.e., $N(COCF_3)(SO_2CF_3)^-$) (Fig. 1.21d) have also been reported [256, 266]. The experimental gas-phase acidity value (ΔG_{acid} in kcal mol^{-1}) for HTSAC (298.2) is somewhat higher than for HTFSI (291.8), but lower than that for HFSI (301.2) [26]. The $TSAC^-$ anion, however, has been found to have a poor electrochemical stability relative to other imide anions. The anodic oxidative stability was slightly lower relative to anions such as FTI^- and $TFSI^-$, but the cathodic reductive stability of the $TSAC^-$ anion was notably poorer (almost 1 V less stable) [273, 338].

Many other variants of imide anions have been reported (Fig. 1.21). In general, these do not have improved properties or other advantages over more widely used anions (i.e., $TFSI^-$ and $BETI^-$). One possible exception to this may be the bis(trifluoromethanesulfonamido) sulfone anion (i.e., $LiSO_2(NSO_2CF_3)_2$) (Figs. 1.21k and 1.22i) [281]. If this dilithium salt has a high solubility in aprotic solvents, then it may offer an advantage in terms of having a greater Li^+/anion mass ratio with less fluorine atoms per Li^+ cation than for $LiPF_6$ and LiTFSI. The properties of the dilithium salt with this anion, however, are not yet available. The related acid $H_2[CO(NSO_2F)_2]$ (Fig. 1.21j) and the corresponding alkali metal salts (with Na^+ or K^+) have been reported [280].

Nonfluorinated lithium tris(alkanesulfonyl)methide salts have been examined for their suitability for battery electrolytes (Fig. 1.23a) [258]. The $LiC(SO_2CH_3)_3$ salt has poor solubility in EC:DMC (<0.1 M), but good solubility in DMSO (~0.5 M). Increasing the alkyl chain length from methyl to ethyl (i.e., $LiC(SO_2C_2H_5)_3$) increases the solubility, EC:DMC (~0.3 M) and DMSO (>4 M), while using asymmetric alkyl chain lengths (i.e., $LiC(SO_2CH_3)(SO_2C_2H_5)_2$) further increases the salt solubility, EC:DMC (~0.5 M) and DMSO (>4 M). These salts have a considerably lower conductivity (4.3 mS cm^{-1}), however, in 0.5 M DMSO electrolytes at 25 °C than that for the corresponding $LiPF_6$ electrolyte (9.8 mS cm^{-1}) [258].

Lithium tris(perfluoroalkanesulfonyl)methide salts have also received some attention for battery electrolytes, especially the salt with the $C(SO_2CF_3)_3^-$ anion (*TriTFSM*$^-$) (Figs. 1.22j and 1.23b). The experimental gas-phase acidity values

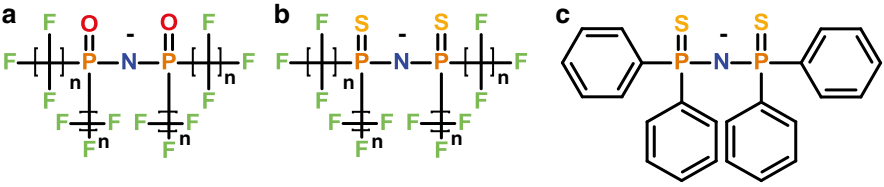

Fig. 1.24 Examples of phosphorylimide anions: (**a**) $N(PO(C_nF_{2n+1})_2)_2^-$ [361–366], (**b**) $N(PS(C_nF_{2n+1})_2)_2^-$ [367], and (**c**) $N(PS(C_6H_5)_2)_2^-$ [368–370]

(ΔG_{acid} in kcal mol^{-1}) are $HC(COCF_3)_3$ (300.6) and $HC(SO_2CF_3)_3$ (289.0) (ref: $HN(SO_2CF_3)_2$ (291.8)) (Fig. 1.2) [20, 26]. Despite the higher acidity of the TriTFSM$^-$ anion relative to TFSI$^-$ and calculations which indicate that the former anion will have a weaker Li^+ cation affinity (i.e., lower ionic association tendency), the conductivity of polyether-based electrolytes with LiTriTFSM is lower than for similar electrolytes with LiTFSI [111, 341]. This may perhaps be related to the greater size/mass of the TriTFSM$^-$ anion. For liquid 1 M electrolytes with EC:DMC (50:50 v:v), the conductivity (mS cm^{-1}) at 25 °C is $LiAsF_6$ (11.0), LiTFSI (9.0), and LiTriTFSM (7.1) [343]. Despite the recent attention devoted to LiFSI (i.e., $LiN(SO_2F)_2$), no published work is yet available regarding the properties of electrolytes with lithium tris(fluorosulfonyl)methide salt, $LiC(SO_2F)_3$ [340, 350], and the bis(fluoromethanesulfonyl)methane (i.e., $CH(SO_2F)_2^-$) anion has not yet been reported. Some limited studies have, however, been reported for the related bis(trifluoromethanesulfonyl)methide anion (*TFSM*$^-$) (i.e., $CH(SO_2CF_3)_2^-$) (Figs. 1.22l, m and 1.23c). The acid, bis(trifluoromethanesulfonyl)methane (i.e., $HCH(SO_2CF_3)_2$), was first prepared by Gramstad and Haszeldine in 1956 [355]. Poly(ethylene oxide) (PEO) electrolytes with the lithium salt (LiTFSM) (i.e., $LiCH(SO_2CF_3)_2$) were found in one report to have a lower oxidative and reductive electrochemical stability than for similar electrolytes with LiTFSI [341], whereas another study indicated that such electrolytes with LiTFSM were stable with a voltage stability window of approximately 4.5 V [359]. As for LiTFSI and LiTriTFSM, the LiTFSM salt tends to plasticize poly(ethylene oxide) resulting in amorphous electrolytes with a relatively high conductivity, although somewhat lower than for comparable LiTFSI electrolytes [341, 359].

Lithium perfluoroalkanephosphorylimide salts (Fig. 1.24a) have not yet been reported, but such anions have been explored using QC calculations [361] and the sodium and potassium salts with the $N(PO(C_2F_5)_2)_2^-$ anion (Fig. 1.25) have been prepared [365]. The lithium bis(difluorophosphoryl)imide salt (i.e., $LiN(POF_2)_2$) (Fig. 1.24a), however, has been synthesized [362, 363], as has the acid $HN(PSF_2)_2$ (Fig. 1.24b) [367]. Nonfluorinated alkyl or phenylphosphorylimide salts are also known, such as $LiN(PS(C_6H_5)_2)_2$ (Fig. 1.24c) [368–370] and $LiN(PO(C_6H_5)_2)(PS(CH_3)_2)$ [371]. No data is yet available, however, regarding the electrolyte characteristics of lithium salts with such anions.

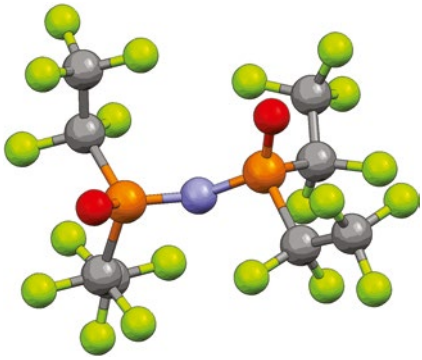

Fig. 1.25 Anion structure: $N(PO(C_2F_5)_2)_2^-$ (C—*gray*, N—*blue*, O—*red*, F—*light green*, P—*orange*)

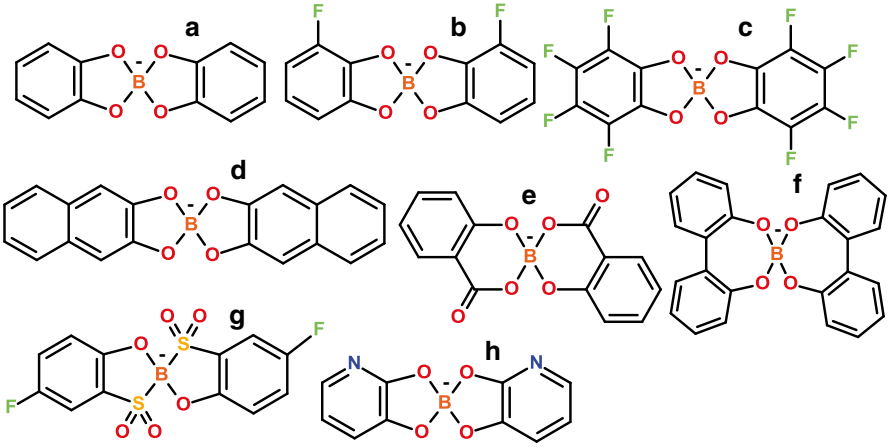

Fig. 1.26 Examples of chelated organoborate anions: (**a**) $B(O(C_6H_4)O)_2^-$ (BBB^-) [169, 372–378], (**b**) $B(O(C_6H_3F)O)_2^-$ ($FLBBB^-$) [373, 379, 380], (**c**) $B(O(C_6F_4)O)_2^-$ ($4FLBBB^-$) [373, 381], (**d**) $B(O(C_{10}H_6)O)_2^-$ (BNB^-) [56, 169, 373–375, 378], (**e**) $B(O(C_6H_4)CO_2)_2^-$ (BSB^-) [56, 373, 375, 382–385], (**f**) $B(O(C_6H_4)(C_6H_4)O)_2^-$ ($BBPB^-$) [56, 169, 373, 375], (**g**) $B(O(C_6H_3F)SO_2)_2^-$ (FSB^-) [386], and (**h**) $B(O(C_5NH_3)O)_2^-$ (BPB^-) [387]

1.8 Advanced Salts—Organoborates, -Phosphates, and -Aluminates

In 1995, Barthel and Gores reported a new class of inexpensive and chemically, electrochemically, and thermally stable salts based upon boron chelate complex anions with aromatic or aliphatic diols or carboxylic acids. The first such salt reported was lithium bis(1,2-benzenediolato(2-)-O,O′)borate (*LiBBB*) (Fig. 1.26a) [372]. The acid with this anion was originally reported in 1949 by Schafer [388]. The LiBBB salt has a high solubility in aprotic solvents (>1 M), but the oxidative stability is relatively low. A number of other nonfluorinated lithium salts with benzenediol nonfluorinated

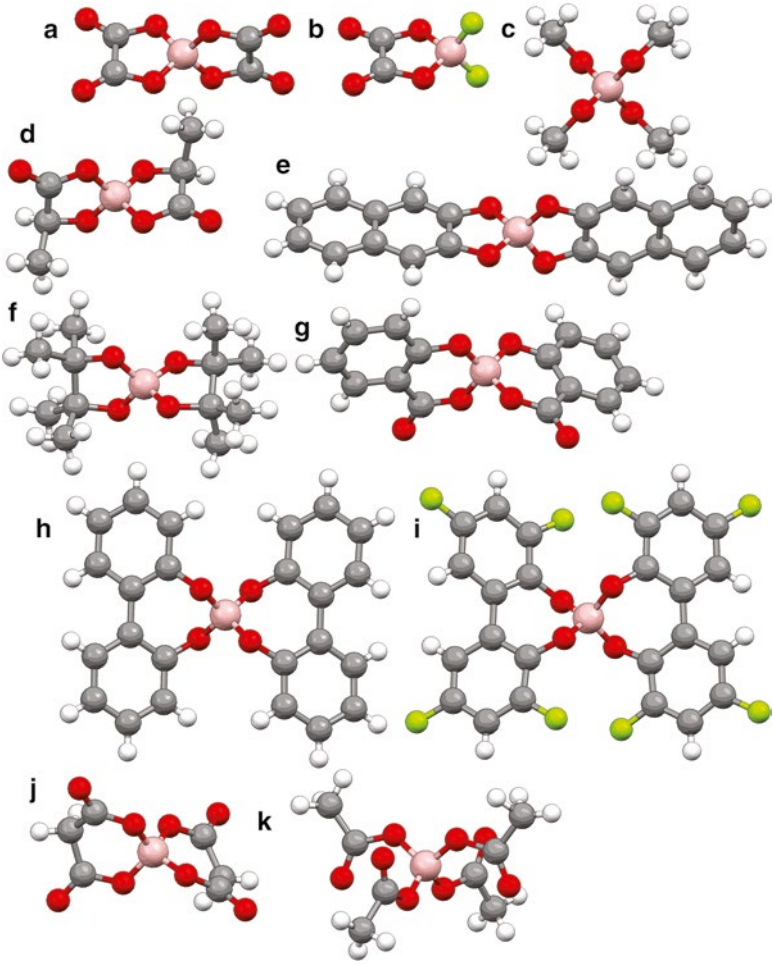

Fig. 1.27 Anion structures: (**a**) $B(CO_2CO_2)_2^-$ (BOB^-), (**b**) $BF_2(CO_2CO_2)_2^-$ ($DFOB^-$), (**c**) $B(OCH_3)_4^-$, (**d**) $B(CO_2CH(CH_3)O)_2^-$, (**e**) $B(O(C_{10}H_6)O)_2^-$ (BNB^-), (**f**) $B(OC(CH_3)_2C(CH_3)_2O)_2^-$, (**g**) $B(O(C_6H_4)CO_2)_2^-$ (BSB^-), (**h**) $B(O(C_6H_4)(C_6H_4)O)_2^-$ ($BBPB^-$), (**i**) $B(O(C_6H_2F_2)(C_6H_2F_2)O)_2^-$, (**j**) $B(CO_2CH_2CO_2)_2^-$(BMB^-), and (**k**) $B(CO_2CH_3)_4^-$ (B—*tan*, C—*gray*, O—*red*, F—*light green*)

chelates were subsequently prepared: bis(2,3-naphthalenediolato(2-)-O,O′)borate (*LiBNB*) (Figs. 1.26d and 1.27e), bis(salicylato(2-))borate (*LiBSB*) (Fig. 1.26e and 1.27g), and bis(2,2′-biphenyldiolato(2-)-O,O′)borate (*LiBBPB*) (Figs. 1.26f and 1.27h) [373]. The conductivity of electrolytes with these salts was found to increase in the order LiBBPB < LiBSB < LiBNB ~ LiBBB (Table 1.5) [169, 374, 375]. All of these electrolytes have a significantly lower conductivity than comparable electrolytes with $LiPF_6$, LiTFSI, and LiBETI (Table 1.5) [375]. The LiBSB-based electrolyte was found to have a relatively high Li cycling efficiency, however, in contrast to the other salts [375]. A number of crystalline solvates have been reported for the

Table 1.5 Conductivity of electrolytes with various lithium salts at 25 °C and 0.3 M salt in PC:DME and PC:2-MeTHF (1:1 equimolar) [375]

Lithium salt (anion)	Conductivity (mS cm^{-1})
In PC:DME	
PF_6^-	9.23
$N(SO_2CF_3)_2^-$	8.05
$N(SO_2C_2F_5)_2^-$	7.55
BBB^-	4.21
BNB^-	4.25
BSB^-	2.45
$BBPB^-$	1.09
in PC:2-MeTHF	
PF_6^-	6.57
$N(SO_2CF_3)_2^-$	5.97
$N(SO_2C_2F_5)_2^-$	5.48
BBB^-	3.07
BNB^-	2.97
BSB^-	1.28
$BBPB^-$	0.92

LiBBB and LiBSB salts: $(H_2O)_2(THF)_1$:LiBBB, $(H_2O)_1(AN)_1$:LiBBB, $(AN)_2$:LiBSB, and $(THF)_2$:LiBSB [389]. For the former solvate, the Li^+ cations are coordinated to the diol oxygen atoms, but for the latter solvate these oxygens do not participate in the cation coordination. Instead, the carbonyl oxygens are coordinated to the Li^+ cations.

The preparation of fluorinated chelated organoborate salts (i.e., $LiB(C_6H_{4-x}F_xO_2)$ demonstrated that with increasing fluorination ($x=0$, 1, or 4) (Fig. 1.26a, b, c) both the conductivity and oxidative stability increased [379, 381]. The oxidative stability limit (vs. Li/Li^+) was found to vary considerably for these salts: 3.6 V for BBB^-, 3.8 V for $FLBBB^-/BNB^-$, 4.1 V for $4FLBBB^-/BBPB^-$, and 4.5 V for BSB^- [373]. It was suggested that these anions anodically degrade on the cathode surface to form thin, electrically insulated, but Li^+ cation-conducting polymeric films which passify the electrode surface from further degradation of the salts or the solvents. A similar high salt solubility and oxidative stability limit was noted for the lithium bis(5-fluoro-2-olato-benzenesulfonato(2-)-O,O′)borate salt (*LiFSB*) (Fig. 1.26g) which has a stability limit of 4.6 V vs. Li/Li^+ [386]. The current density decreased upon repeated cycling on a Pt electrode due to electrode passivation. The salt also passivated an Al electrode at high potential. The introduction of a nitrogen to the benzenediol chelate—lithium bis(2,3-pyridinediolato(2-)-O,O′)borate (*LiBPB*) (Fig. 1.26h), however, resulted in a salt with low solubility in DMC and DEC (in contrast to the other salts prepared), but the solubility was higher in EC or PC [387]. The conductivity of electrolytes with LiBPB was lower than for the other borate salts, but the salt did passivate Pt and Al electrodes, as for the other salts studied [387].

The first organoborate salt to attract significant interest from the broader battery research community was lithium bis(oxalato)borate (*LiBOB*) (i.e., $LiB(CO_2CO_2)_2$) (Figs. 1.27a and 1.28a) [48, 79, 376, 380, 385, 390–484]. The first publication with

LiBOB was from Xu and Angell in 2001 [393], but a German patent application was filed for this salt by Metallgesellschaft AG in 1999 [548]. The acid and tetraalkylammonium salts with BOB^- (called borodicatecholate) and related anions had been reported in 1994 by Ue [549], as well as earlier by others [550]. LiBOB electrolytes have a conductivity which is comparable to or lower than that for electrolytes with $LiBF_4$ [79, 414], moderate stability to hydrolysis, high electrochemical stability (>4.5 V vs. Li/Li^+), and high thermal stability [393, 394, 414, 448]. The salt has a relatively low solubility in acyclic carbonate solvents (i.e., the solubility limit is 0.8 M in EC:DMC 3:7) but is more soluble (>1 M) in nitrile, ester, and cyclic carbonate solvents [447]. The salt has been used as both a primary salt (replacement for $LiPF_6$) and an additive (addition of small amounts to $LiPF_6$ electrolytes). Notably, the electrode surface layers formed by this salt on both the anode and cathode enable cells with LiBOB to have excellent capacity retention when cycled at elevated temperature (≥60 °C) and when cycling cathodes up to 5 V (vs. Li^+/Li).

Lithium difluoro(oxalato)borate (*LiDFOB*) (also called lithium oxalyldifluoroborate (*LiODFB*)) (i.e., $LiBF_2(CO_2CO_2)$) (Figs. 1.27b and 1.28g), like LiBOB, has also received a great deal of attention from the lithium battery research community. This salt was first reported in Central Glass Company patents filed in 2000 [390–392] and then later in a US Army Research Laboratory (ARL) publication in 2006 [491]. Many studies have now demonstrated that LiDFOB is quite useful both as a primary salt (replacement for $LiPF_6$) and as an additive to $LiPF_6$ electrolytes [491–535]. LiDFOB has a higher solubility than LiBOB in linear carbonate solvents, but it is still lower than for other salts such as $LiBF_4$, LiTFSI, and $LiPF_6$. Electrolytes with the LiDFOB salt are better than those with LiBOB at passivating the Al current collector and also tend to have a higher conductivity (i.e., the conductivity of a 1 M LiDFOB electrolyte in EC:DMC (1:1 v:v) at 25 °C is 8.6 mS cm^{-1} [506], which is somewhat lower than the conductivity of comparable electrolytes with $LiPF_6$ or $LiClO_4$ (Table 1.1)). As for LiBOB, enhanced battery performance is noted upon addition of LiDFOB to electrolytes including the cyclability/stabilization of electrode materials (such as $LiFePO_4$ and $Li_4Ti_5O_{12}$) at elevated temperature (60 °C) and of high-voltage cathode materials when cycled to 5 V due to favorable surface layers formed on the anode and cathode [40].

In addition to LiBOB and LiDFOB, a wide variety of additional organoborate anions have been synthesized (Figs. 1.28 and 1.29). Only limited information is available about the properties of the corresponding lithium salts. The $LiB(CO_2C(CF_3)_2O)_2$ salt (Fig. 1.29a), however, reportedly does not undergo hydrolysis and is thermally stable at 100 °C for 1 month, and electrolytes with this salt do not corrode Al at high potential [545]. The conductivity of electrolytes with 1 M salt in EC:DMC 1:1 at 25 °C is 7.0, 8.3, 6.3, and 1.9 mS cm^{-1}, respectively, for the $LiB(CO_2C(CF_3)_2O)_2$, $LiBF_2(CO_2C(CF_3)_2O)$, $LiB(CO_2CH(CF_3)O)_2$, and $LiB(CO_2CH_2C(CF_3)_2O)_2$ salts (Fig. 1.29a–d) [545]. Note that the concentration for the latter salt is only 0.8 M (instead of 1 M) due to its limited solubility in EC:DMC. For the fluorinated salts in Fig. 1.29h–p, the maximum conductivity (mS cm^{-1}) (differing concentrations) for DME-based electrolytes at 25 °C is 5.88 (Fig. 1.29h), 5.39 (Fig. 1.29i), 6.57 (Fig. 1.29j), 6.89 (Fig. 1.29k), 6.39 (Fig. 1.29l), 7.89 (Fig. 1.29m),

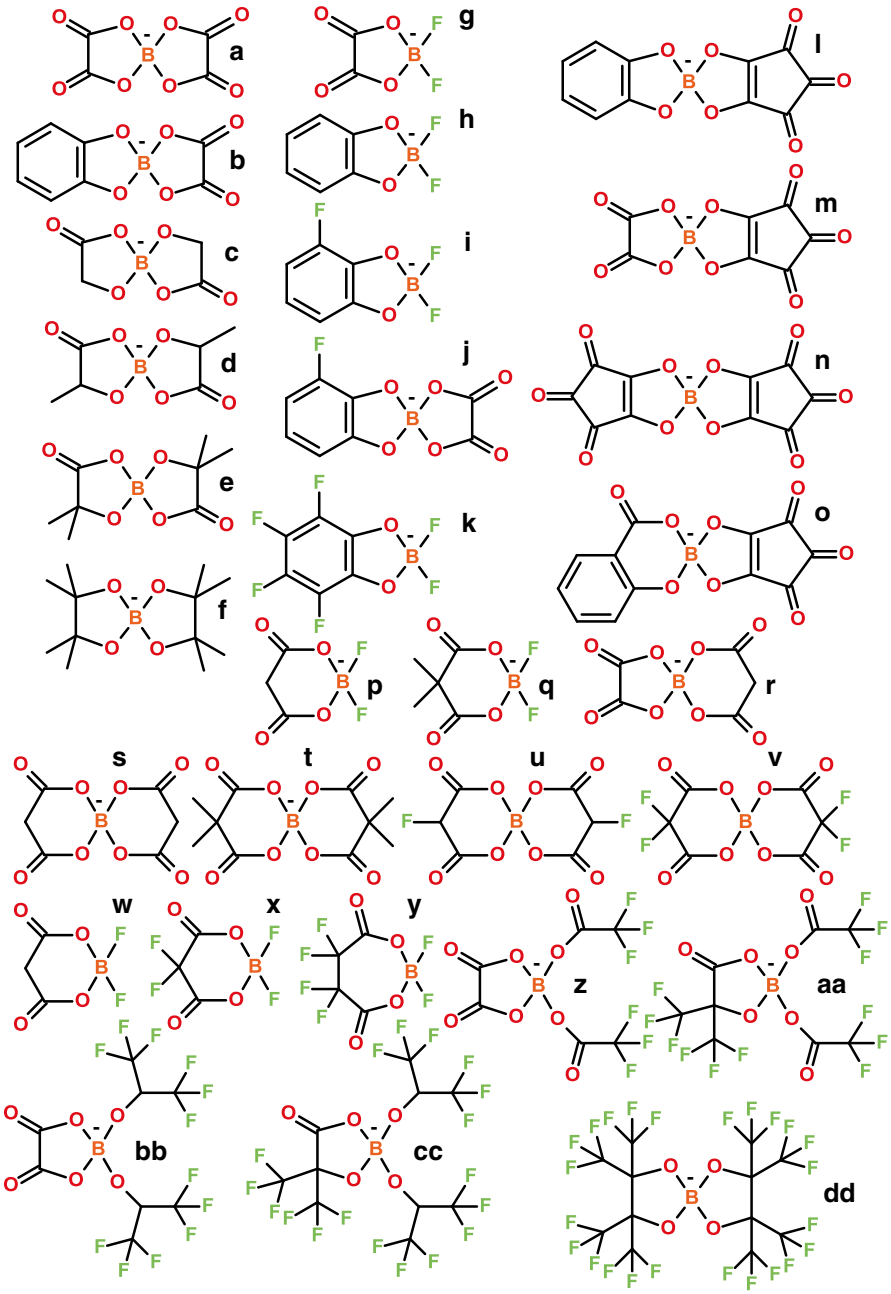

Fig. 1.28 Examples of chelated organoborate anions: (**a**) $B(CO_2CO_2)_2^-$ (BOB^-) [48, 79, 376, 380, 385, 390–484], (**b**) $B(O(C_6H_4)O)(CO_2CO_2)^-$ ($BDOB^-$) [376, 377, 485, 486], (**c**) $B(CO_2CH_2O)_2^-$ [384, 487], (**d**) $B(CO_2CH(CH_3)O)_2^-$ [384, 487, 488], (**e**) $B(CO_2C(CH_3)_2O)_2^-$ ($BMLB^-$) [385], (**f**) $B(OC(CH_3)_2C(CH_3)_2O)_2^-$ [489, 490], (**g**) $BF_2(CO_2CO_2)^-$ ($DFOB^-$) [390–392, 491–535], (**h**) $BF_2(O(C_6H_4)O)^-$ ($DFBDB^-$) [485, 536, 537], (**i**) $BF_2(O(C_6H_3F)O)^-$ ($FLDFBDB^-$) [485, 537],

7.55 (Fig. 1.29n), 7.79 (Fig. 1.29o), and 8.39 (Fig. 1.29p) [551, 552]. The conductivity of the electrolytes thus increases with increasing fluorination of the anions and is dependent upon the positioning of the fluorine atoms (with the *para* position less favorable for increasing the conductivity). Increased fluorination of the anions also increased the oxidative stability of DME- or EC:DMC-based electrolytes with the salts [551, 552]. With regard to Al passivation at high potential for these electrolytes (as well as those with EC:DMC), only the electrolytes with Fig. 1.29h, j, and n anions passivated the Al electrode—the electrolytes with the other six anions did not [551, 552]. Seemingly, the anions with fluorine atoms in the *ortho* or the *para* position on the benzene ring do not decompose to leave a passivating film on the Al surface.

The lithium bis(perfluoropinacolato)borate (LiBPFPB) salt (Fig. 1.28dd) is also reported to have a high oxidative stability [547]. No information is available about the Al corrosion behavior of electrolytes with this salt, but a 0.6 M LiBPFPB electrolyte with DME at 25 °C has a conductivity of 11.1 mS cm^{-1} [547]. The conductivity of a 1 M electrolyte with the salt in PC at 25 °C, however, is 2.1 mS cm^{-1} [547]—for comparison, the conductivity for a 1 M $LiAsF_6$ electrolyte with PC at 20 °C is 5.28 mS cm^{-1} [5].

A number of lithium salts with tetrakis(haloacyloxy)borate anions (i.e., $LiB(CO_2R)_4$) have also been synthesized (Fig. 1.30a–d) [553, 554]. These are fluorinated and/or chlorinated versions of the tetra(acetato)borate anion (i.e., $B(CO_2CH_3)_4^-$) (Figs. 1.27k and 1.30e). The acid and cesium salt with the $B(CO_2CF_3)_4^-$ anion were first reported in 1971 [561]. The lithium salt (i.e., $LiB(CO_2CF_3)_4$) was subsequently reported in 1972 [562]. Electrolytes with these non-chelate salts have a relatively high conductivity (although lower than for $LiPF_6$), high oxidative stability, and high cycle efficiency with a graphite electrode. The most conductive salt is $LiB(CO_2CF_3)_4$ (comparable to the conductivity of electrolytes with LiTFSI). Lengthening the perfluoralkyl chains from $–CF_3$ to $–C_2F_5$ decreases the conductivity, as does replacing the fluorine atoms with chlorine atoms [553]. A lithium salt with the tetrakis(chlorosulfato)borate anion (i.e., $B(SO_3Cl)_4^-$) has been reported (Fig. 1.30f) [556], as has the acid with the tetrakis-(trifluoromethanesulfonato)borate anion (i.e., $B(SO_3CF_3)_4^-$) (Fig. 1.30g) [557]. Note that this anion differs from the $B(SO_2CF_3)_4^-$ anion noted in Fig. 1.18d.

Fig. 1.28 (continued) (**j**) $B(O(C_6H_3F)O)(CO_2CO_2)^-$ (FLBDOB$^-$) [377, 380, 485, 486, 536], (**k**) $BF_2(O(C_6F_4)O)^-$ (4FLDFBDB$^-$) [486, 537], (**l**) $B(O(C_6H_4)O)(C_5O_5)^-$ (BDCB$^-$) [538], (**m**) $B(CO_2CO_2)(C_5O_5)^-$ (OCB$^-$) [538], (**n**) $B(C_5O_5)_2^-$ (BCB$^-$) [382, 383, 538], (**o**) $B(O(C_6H_4)CO_2)(C_5O_5)^-$ (CSB$^-$) [382, 383], (**p**) $BF_2(CO_2CH_2CO_2)^-$ [539], (**q**) $BF_2(CO_2C(CH_3)_2CO_2)^-$ [539], (**r**) $B(CO_2CO_2)(CO_2CH_2CO_2)^-$ (MOB$^-$) [540], (**s**) $B(CO_2CH_2CO_2)_2^-$ (BMB$^-$) [385, 484, 540, 541], (**t**) $B(CO_2C(CH_3)_2CO_2)_2^-$ [539], (**u**) $B(CO_2CHFCO_2)_2^-$ [540, 542], (**v**) $B(CO_2CF_2CO_2)_2^-$ [392, 543], (**w**) $BF_2(CO_2CH_2CO_2)^-$ [392, 543], (**x**) $BF_2(CO_2CF_2CO_2)^-$ [392, 543], (**y**) $BF_2(CO_2C_2F_4CO_2)^-$ [392, 543], (**z**) $B(CO_2CO_2)(CO_2CF_3)_2^-$ [544], (**aa**) $B(CO_2C(CF_3)_2O)(CO_2CF_3)_2^-$ [392], (**bb**) $B(CO_2CO_2)(OCH(CF_3)_2)_2^-$ [392], (**cc**) $B(CO_2C(CF_3)_2O)(OCH(CF_3)_2)_2^-$ [392, 543, 545, 546], and (**dd**) $B(OC(CF_3)_2C(CF_3)_2O)_2^-$ (BPFPB$^-$) [484, 541, 547]

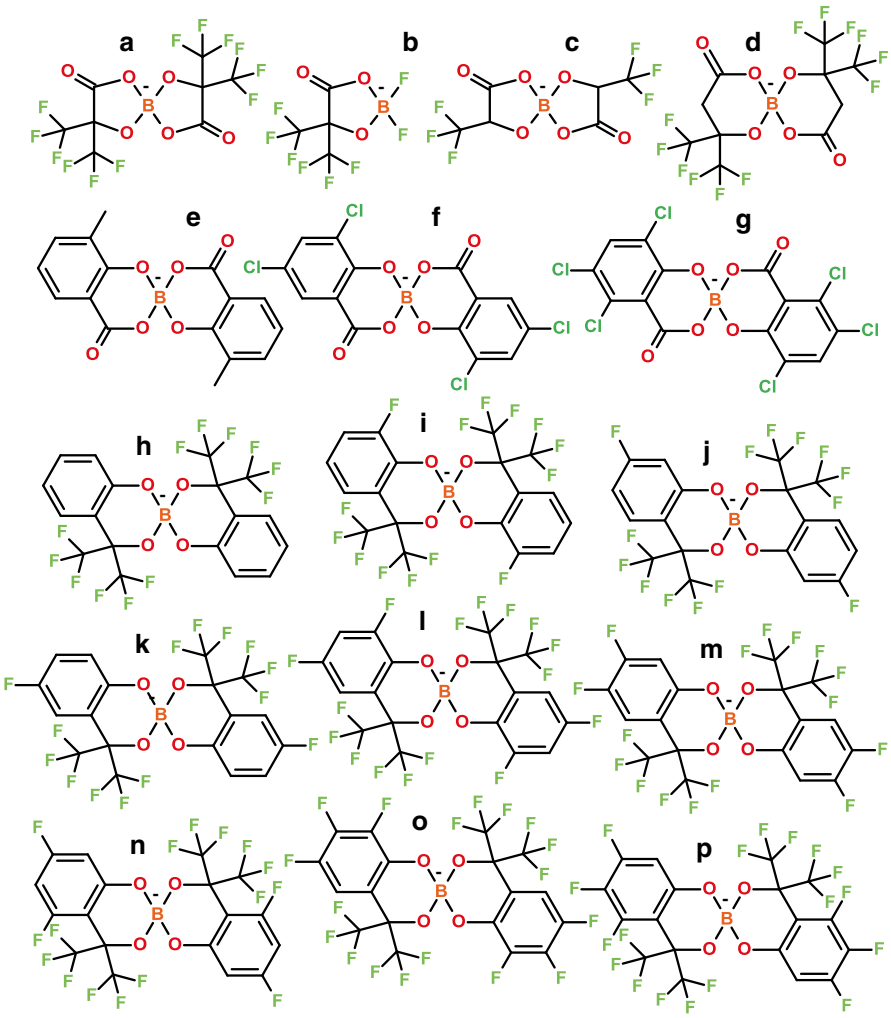

Fig. 1.29 Additional examples of chelated organoborate anions: (**a**) $B(CO_2C(CF_3)_2O)_2^-$ [392, 545, 546], (**b**) $BF_2(CO_2C(CF_3)_2O)^-$ [392, 545, 546], (**c**) $B(CO_2CH(CF_3)O)_2^-$ [392, 545, 546], (**d**) $B(CO_2CH_2C(CF_3)_2O)_2^-$ [392, 545, 546], (**e**) $B(CO_2(C_6H_3(CH_3))O)_2^-$ (3-MLBSB$^-$) [56], (**f**) $B(CO_2(C_6H_2Cl_2)O)_2^-$ (DCLBSB$^-$) [56], (**g**) $B(CO_2(C_6HCl_3)O)_2^-$ (TCLBSB$^-$) [56], (**h**) $B(O(C_6H_4)C(CF_3)_2O)_2^-$ [551, 552], (**i**) $B(O(C_6H_3F)C(CF_3)_2O)_2^-$ [551, 552], (**j**) $B(O(C_6H_3F)C(CF_3)_2O)_2^-$ [551, 552], (**k**) $B(O(C_6H_3F)C(CF_3)_2O)_2^-$ [551, 552], (**l**) $B(O(C_6H_2F_2)C(CF_3)_2O)_2^-$ [551, 552], (**m**) $B(O(C_6H_2F_2)C(CF_3)_2O)_2^-$ [551, 552], (**n**) $B(O(C_6H_2F_2)C(CF_3)_2O)_2^-$ [551, 552], (**o**) $B(O(C_6HF_3)C(CF_3)_2O)_2^-$ [551, 552], and (**p**) $B(O(C_6HF_3)C(CF_3)_2O)_2^-$ [551, 552]

The reaction of trialkoxyborates with butyllithium produces salts which are liquid (for $n \geq 2$) at ambient temperature without solvents (i.e., ionic liquids) (Fig. 1.30h) [558]. The ambient temperature conductivity for the $n=3$ salt is 2×10^{-5} S cm^{-1}, while 1 M electrolytes of the salt in EC:PC have a conductivity $<10^{-3}$ S cm^{-1}.

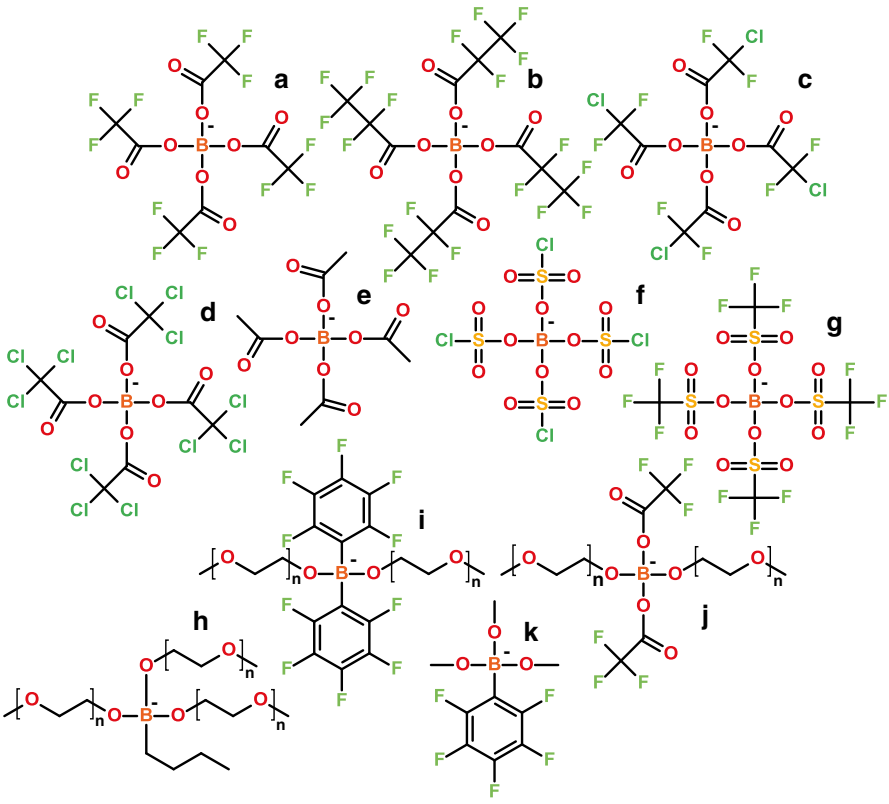

Fig. 1.30 Examples of nonchelated organoborate anions: (**a**) $B(CO_2CF_3)_4^-$ [553, 554], (**b**) $B(CO_2C_2F_5)_4^-$ [553, 554], (**c**) $B(CO_2CF_2Cl)_4^-$ [553, 554], (**d**) $B(CO_2CCl_3)_4^-$ [553, 554], (**e**) $B(CO_2CH_3)_4^-$ [554], (**f**) $B(SO_3Cl)_4^-$ [555, 556], (**g**) $B(SO_3CF_3)_4^-$ [557], (**h**) $B(O(CH_2CH_2O)_nCH_3)_3(C_4H_9)^-$ [558], (**i**) $B(C_6F_5)_2(O(CH_2CH_2O)_nCH_3)_2^-$ [559], (**j**) $B(CO_2CF_3)_2(O(CH_2CH_2O)_nCH_3)_2^-$ [559], and (**k**) $B(C_6F_5)(OCH_3)_3^-$ [560]

The nonfluorinated lithium tris(1,2-benzenediolato(2)-O,O′)phosphate (*LiTBP*) salt (Figs. 1.31a and 1.32a), reported by Sasaki and co-workers, has a relatively low thermal (<200 °C) and electrochemical (about 3.7 V (vs. Li/Li^+)) stability [378, 564, 565]. Adding a methyl group—lithium tris(4-methyl-1,2-benzenediolato(2)-O,O′) phosphate (*Li4-MLTBP*) (Fig. 1.31b)—improves the thermal stability somewhat, but decreases the electrolyte conductivity (relative to LiTBP) [566]. Adding a fluorine atom—lithium tris(3-fluoro-1,2-benzenediolato(2)-O,O′)phosphate (*Li3-FLTBP*) (Fig. 1.31c)—improves the electrolyte conductivity and thermal/electrochemical stability (relative to LiTBP and Li4-MLTBP) [564, 565]. The conductivity of 0.5 M electrolytes with EC:DMC at 25 °C is about 2.62, 2.25, and 3.16 mS cm^{-1}, respectively, for LiTBP, Li4-MLTBP, and Li3-FLTBP (as compared to 9.66 mS cm^{-1} for $LiPF_6$) [378, 564, 566]. Fully fluorinating the anion—lithium tris(3,4,5,6-tetrafluoro-1,2-benzenediolato(2)-O,O′)phosphate (Fig. 1.31d)—further increases

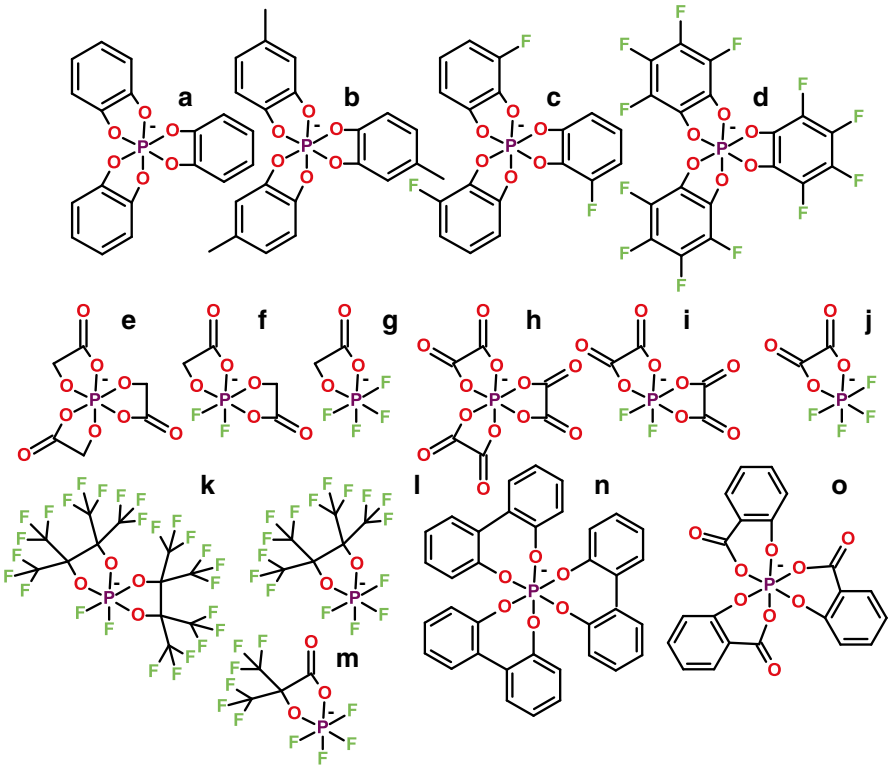

Fig. 1.31 Examples of chelated organophosphate anions: (**a**) $P(O(C_6H_4)O)_3^-$ (TBP^-) [378, 563–567], (**b**) $P(O(C_6H_3(CH_3))O)_3^-$ (4-MLTBP$^-$) [564, 566], (**c**) $P(O(C_6H_3F)O)_3^-$ (3-FLTBP$^-$) [564, 567], (**d**) $P(O(C_6F_4)O)_3^-$ [567], (**e**) $P(CO_2CH_2O)_3^-$ [568], (**f**) $PF_2(CO_2CH_2O)_2^-$ [568], (**g**) $PF_4(CO_2CH_2O)^-$ [568], (**h**) $P(CO_2CO_2)_3^-$ (TOP^-) [568, 569], (**i**) $PF_2(CO_2CO_2)_2^-$ [568], (**j**) $PF_4(CO_2CO_2)^-$ (FOP^-) [392, 543, 568, 570–576], (**k**) $PF_2(OC(CF_3)_2C(CF_3)_2O)_2^-$ [577], (**l**) $PF_4(OC(CF_3)_2C(CF_3)_2O)^-$ [577], (**m**) $PF_4(CO_2C(CF_3)_2O)_2^-$ [545, 546], (**n**) $P(O(C_6H_4)(C_6H_4)O)_3^-$ ($TBPP^-$) [578], and (**o**) $P(CO_2(C_6H_4)O)_3^-$ (TSP^-) [579]

the electrochemical stability, but the conductivity of a 0.6 mol kg^{-1} EC:DEC (2:1) electrolyte at 25 °C is relatively low (2.1 mS cm^{-1}) [567]. The high mass, high fluorination (12 F/Li$^+$), and lack of improved properties (relative to $LiPF_6$) have limited interest in this salt.

The nonfluorinated lithium tri(oxalato)phosphate (*LiTOP*) (i.e., $LiP(CO_2CO_2)_3$) salt (Figs. 1.31h and 1.32b) has a high solubility and high (oxidative) electrochemical stability [569]. The related lithium tetrafluoro(oxalato)phosphate salt (*LiFOP*) (i.e., $LiPF_4(CO_2CO_2)$) (Fig. 1.31j) was first formed in electrolytes with mixtures of $LiPF_6$ and LiBOB [576]. The properties of this salt have been extensively characterized in battery electrolytes [570–576]. In many respects, LiFOP has similar properties to $LiPF_6$. Both salts have a similar thermal stability and result in electrolytes with a high conductivity [574, 575], but a carbonate solvent-based electrolyte (i.e., 1 M in EC:DEC:DMC 1:1:1) with LiFOP may be stored at 85 °C for weeks

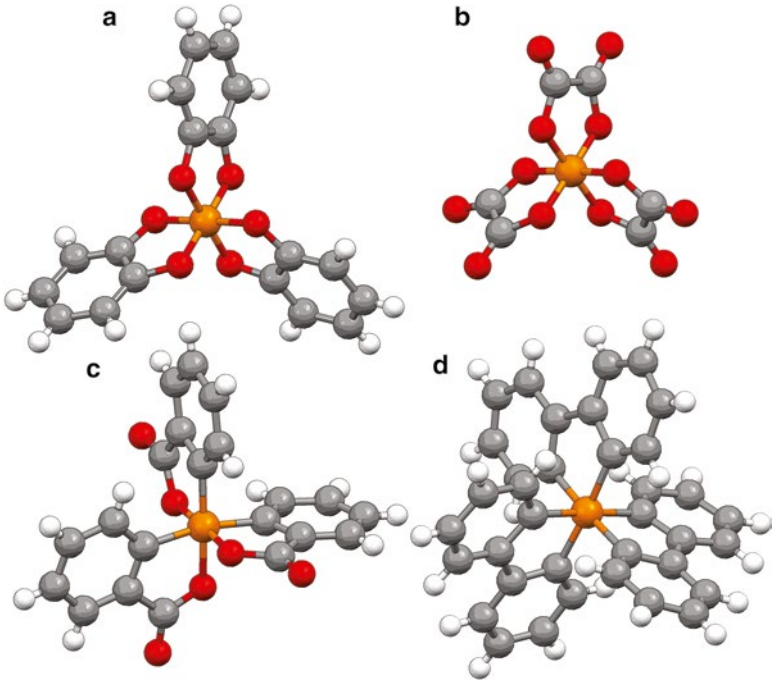

Fig. 1.32 Anion structures: (**a**) $P(O(C_6H_4)O)_3^-$, (**b**) $P(CO_2CO_2)_3^-$ (TOP^-), (**c**) $P(CO_2(C_6H_4))_3^-$ (not TSP^-), and (**d**) $P((C_6H_4)(C_6H_4))_3^-$ (not $TBPP^-$) (C—*gray*, O—*red*, P—*orange*)

with no evident degradation, whereas extensive salt degradation occurs for a similar electrolyte with $LiPF_6$ [574]. As for the LiBOB and LiDFOB salts, the addition of small amounts of LiFOP is found to improve the capacity retention of MCMB/NMC cells, as well as the stability of the lithiated negative electrode [573]. This is attributed to the oxalate group reacting to form surface layers on both the cathode and carbon anode [574]. The first cycle irreversible capacity losses due to SEI formation on the anode, however, are strongly dependent upon the type of carbon used for the anode [571, 572].

Other organophosphate anions have also been reported, such as those with perfluoropinacol (Fig. 1.31k, l), biphenylene (i.e., tris(2,2′-biphenylylene)phosphate ($TBPP^-$)) (Fig. 1.31n), and salicylate (i.e., tris(salicylato(2-))phosphate (TSP^-)) (Fig. 1.31o). No information is available about the use of these anions as lithium salts for battery electrolytes.

Fluorinated organoaluminate anions have also been examined for battery electrolytes (Figs. 1.33 and 1.34) [552, 580]. For smaller bidentate ligands (e.g., oxalate), the Al^{III} is typically coordinated by three ligands in solid-state salts, instead of two, due to its larger size relative to boron (Fig. 1.34a) [581]. This results in a six-coordinate $Al(CO_2CO_2)_3^{3-}$ trianion instead of a four-coordinate $Al(CO_2CO_2)_2^-$ anion, although there is spectroscopic evidence for the latter in aqueous solutions as the additional

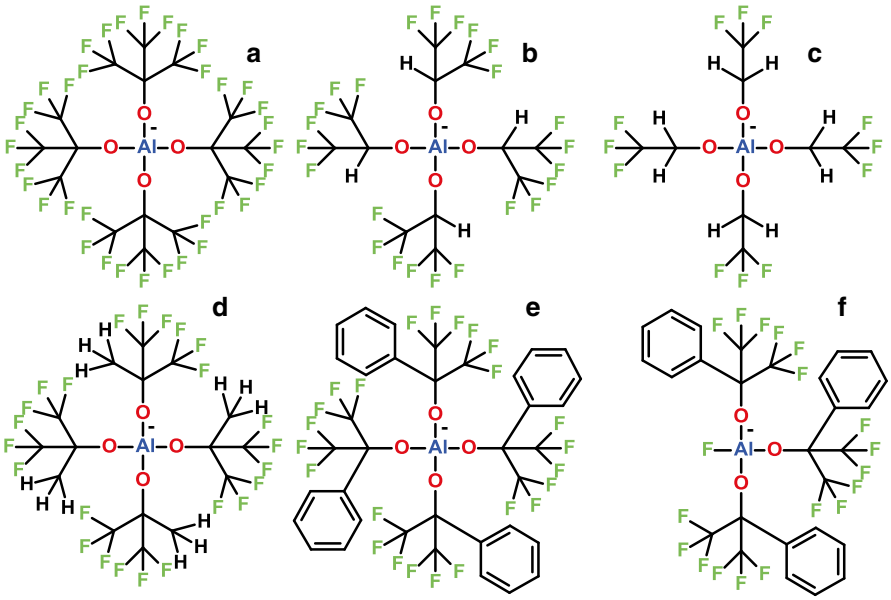

Fig. 1.33 Examples of organoaluminate anions: (**a**) $Al(OC(CF_3)_3)_4^-$ ($Al(PFTB)_4^-$) [552, 580], (**b**) $Al(OCH(CF_3)_2)_4^-$ ($Al(HFIP)_4^-$) [552, 580], (**c**) $Al(OCH_2(CF_3))_4^-$ ($Al(TFE)_4^-$) [552, 580], (**d**) $Al(OC(CH_3)(CF_3)_2)_4^-$ ($Al(HFTB)_4^-$) [552, 580], (**e**) $Al(OC(C_6H_5)(CF_3)_2)_4^-$ ($Al(HFPP)_4^-$) [552, 580], and (**f**) $AlF(OC(C_6H_5)(CF_3)_2)_3^-$ ($AlF(HFPP)_3^-$) [552, 580]

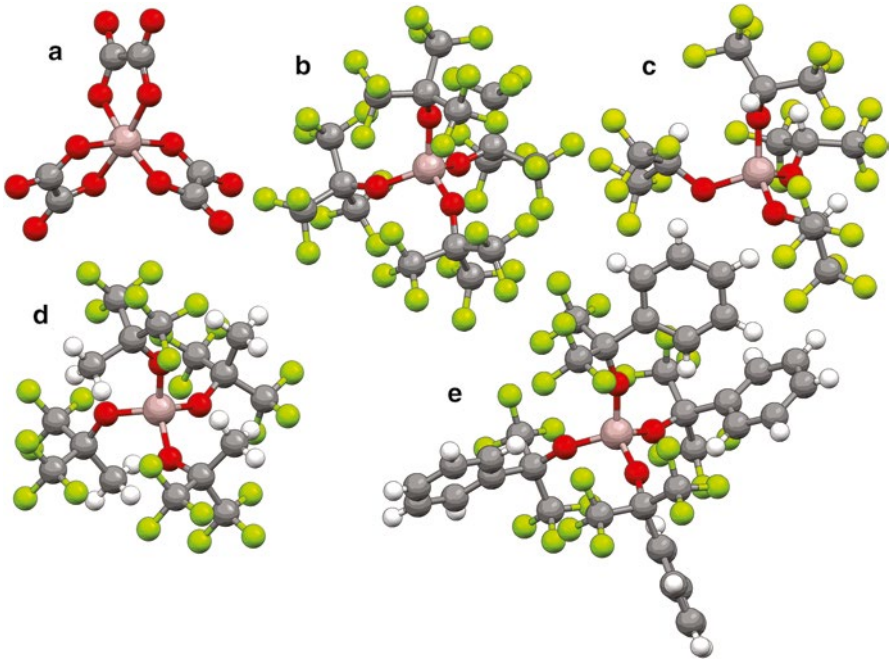

Fig. 1.34 Anion structures: (**a**) $Al(CO_2CO_2)_3^{3-}$, (**b**) $Al(OC(CF_3)_3)_4^-$ ($Al(PFTB)_4^-$), (**c**) $Al(OCH(CF_3)_2)_4^-$ ($Al(HFIP)_4^-$), (**d**) $Al(OC(CH_3)(CF_3)_2)_4^-$ ($Al(HFTB)_4^-$), and (**e**) $Al(OC(C_6H_5)(CF_3)_2)_4^-$ ($Al(HFPP)_4^-$) (C—*gray*, O—*red*, F—*light green*, Al—*tan*)

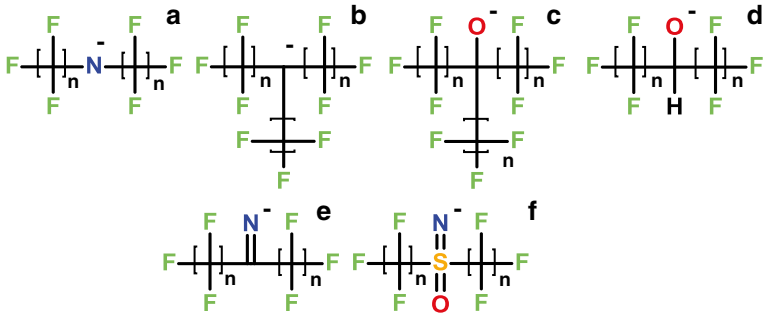

Fig. 1.35 Examples of fluorinated amide, methide, imine, alkoxide, and sulfur oxyimine anions: (**a**) $N(C_nF_{2n+1})_2^-$ [585–594], (**b**) $C(C_nF_{2n+1})_3^-$ [595, 596], (**c**) $OC(C_nF_{2n+1})_3^-$ [597–601], (**d**) $OCH(C_nF_{2n+1})_2^-$ [601–603], (**e**) $N{=}C(C_nF_{2n+1})_2^-$ [604–611], and (**f**) $N{=}S(O)(C_nF_{2n+1})_2^-$ [612–617]

coordination sites are occupied by water molecules (i.e., $Al(CO_2CO_2)_2^-{\cdot}2H_2O$) [582–584]. For more bulky ligands, however, four-coordinate anions are formed. The conductivity values (mS cm^{-1}) (0.2 M salt in DME at 25 °C) for the lithium salts with the anions shown in Fig. 1.33a–f are reported to be 6.4 (Fig. 1.33a), 6.2 (Fig. 1.33b), 1.6 (Fig. 1.33c), 6.2 (Fig. 1.33d), 3.5 (Fig. 1.33e), and 1.3 (Fig. 1.33f) [552, 580]. PC-based electrolytes with the $LiAl(HFIP)_4$ (Figs. 1.33b and 1.34c) and $LiAl(HFPP)_4$ (Figs. 1.33e and 1.34e) salts (0.3 M in PC) both passivated an Al electrode at high potential in a similar manner to a $LiPF_6$ electrolyte [552, 580].

1.9 Advanced Salts—Other Anions

HNF_2 (Fig. 1.35a) is a gas with a T_b of −24 °C [590, 591]. This gas loses hydrogen when contacted with various materials to form tetrafluorohydrazine (N_2F_4). At low temperature (crystalline solid), this acid tends to detonate spontaneously [591]. The $LiNF_2$ salt has not been reported, but it is predicted to be a dimeric complex [592, 593]. $HN(CF_3)_2$ (Fig. 1.35a) is a gas with a T_b of −6 °C [586–588]. The experimental gas-phase acidity value for $HN(CF_3)_2$ is 324.3 kcal mol^{-1}, which is significantly higher (less acidic) than the corresponding values for $HN(COCF_3)_2$ (307.5) and $HN(SO_2CF_3)_2$ (291.8) (Fig. 1.2) [26]. A German patent for Merck has been issued for the preparation of $N(CF_3)_2^-$ salts (Fig. 1.35a), but this does not include the lithium salt [589]. Another report indicates that the alkali metal bis(trifluoromethyl) amides, -phosphides, and -arsenides (i.e., $MN(CF_3)_2$, $MP(CF_3)_2$, and $MAs(CF_3)_2$) all have a high nucleophilic reactivity [594]. For the related methides, the experimental gas-phase acidity values for $HCH(CF_3)_2$ and $HC(CF_3)_3$ (Fig. 1.35b) are 343.9 and 326.6 kcal mol^{-1}, respectively (Fig. 1.2) [26]. The value for the latter is comparable to the gas-phase acidity of HCl (328.1 kcal mol^{-1}) [595, 596].

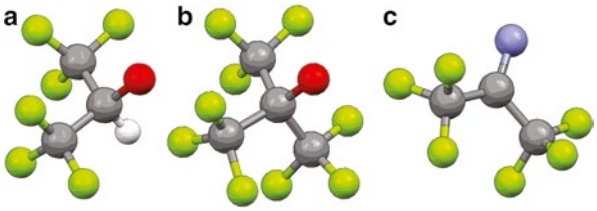

Fig. 1.36 Anion structures: (**a**) $OCH(CF_3)_2^-$, (**b**) $OC(CF_3)_3^-$, and (**c**) $N{=}C(CF_3)_2^-$ (C—*gray*, N—*blue*, O—*red*, F—*light green*)

Trifluoromethanol (i.e., $HOCF_3$) (Fig. 1.35c) is unstable at room temperature due to the elimination of HF [618, 619]:

$$HOCF_3 \rightarrow O{=}CF_2 + HF$$

$MOCF_3$ salts (M = K, Rb, and Cs) (Fig. 1.35c) have been prepared, however, by passing $O{=}CF_2$ through an acetonitrile solution of the fluoride MF [620, 621]:

$$O{=}CF_2 + MF \rightleftarrows MOCF_3$$

and the crystal structures determined [597]. No reaction occurred when LiF or NaF was used [597], and some decomposition occurred for KF, suggesting that the lithium trifluoromethoxide (or trifluoroorthocarbonate) salt is unstable (i.e., harder cations are more reactive). Additional salts with perfluoralkyl groups have also been prepared [598–600]:

$$O{=}CFR_F + MF \rightleftarrows MOCF_2R_F$$

$$O{=}C\left(CF_3\right)_2 + MF \rightleftarrows MOCF\left(CF_3\right)_2$$

with M = Rb or Cs and $R_F = -CF_3$, $-C_2F_5$, or $-C_3F_7$. It was found that the cesium salts were more thermally stable than the corresponding rubidium salts. The $LiOCH(CF_3)_2$ (Figs. 1.35d and 1.36a) and $LiOC(CF_3)_3$ (Figs. 1.35d and 1.36b) salts are both volatile with the former subliming at 50 °C under vacuum (0.05 mmHg) and the latter having a T_b of 218 °C [601].

The difluoromethanimine acid (i.e., $HN{=}CF_2$) (Fig. 1.35e) has been reported [604, 605]. This is a colorless gas which is stable at ambient temperature for hours in the gas phase at pressures lower than 5 mm Hg, but which disproportionates at higher pressure:

$$2\,HN{=}CF_2 \rightarrow H_2NCF_3 + FCN$$

The lithium hexafluoroisopropylidenimine salt (i.e., $LiN{=}C(CF_3)_2$) (Figs. 1.35e and 1.36c) has been reported [606–611]. The strong electron-withdrawing $-CF_3$

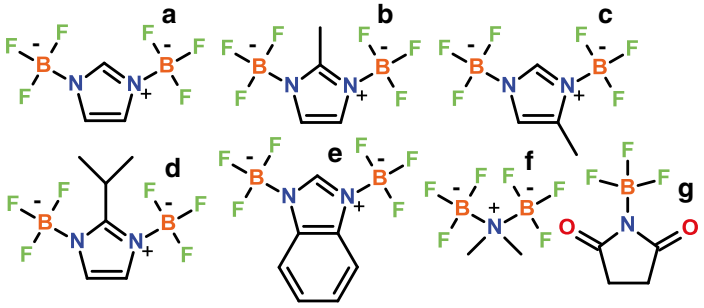

Fig. 1.37 Examples of Lewis acid–Lewis base complex anions: (**a**) $N_2C_3H_3(BF_3)_2^-$ [622–625], (**b**) $N_2C_3H_2(CH_3)(BF_3)_2^-$ [622–625], (**c**) $N_2C_3H_2(CH_3)(BF_3)_2^-$ [622–625], (**d**) $N_2C_3H_2(CH(CH_3)_2)(BF_3)_2^-$ [622–625], (**e**) $N_2C_7H_5(BF_3)_2^-$ [622–625], (**f**) $N(CH_3)_2(BF_3)_2^-$ [622–625], and (**g**) $N_2C_4H_4O_2(BF_3)^-$ [626]

groups make the double bond susceptible to nucleophilic attack. The difluorosulfur oxyimine (i.e., $HN{=}S(O)F_2$) and bis(trifluoromethyl)sulfur oxyimine (i.e., $HN{=}S(O)(CF_3)_2$) acids (Fig. 1.32f) are also known [612–617], and the lithium bis(trifluoromethyl)sulfur oxyimine salt (i.e., $LiN{=}S(O)F_2$) (Fig. 1.32f) has been prepared [615]. No information is available, however, about the properties of this latter salt. Note that none of the anions shown in Fig. 1.35 have resonance to stabilize the negative charge, except for the $N{=}S(O)(C_nF_{2n+1})_2^-$ anions.

A family of lithium salts based upon monoanionic species with one or more Lewis acid groups (i.e., BF_3) complexed to a Lewis base have also been reported (Fig. 1.37) [622–626]. The most promising of these for electrolyte applications is lithium bis(trifluoroborane)imidazolide (i.e., $LiC_3N_2H_3(BF_3)_2$) (Fig. 1.37a). This salt has a high solubility—up to 2 M solutions in EC:EMC (1:3 v:v)—and a conductivity of 5.1 mS cm^{-1} at 20 °C for a 1 M electrolyte (as compared to equivalent $LiBF_4$ and $LiPF_6$ electrolytes with conductivity values of 1.78 and 7.71 mS cm^{-1}, respectively) [622]. The salt also has a reasonably high (>4.5 V vs. Li/Li^+) oxidative stability in DMC. $Li/LiNi_{0.2}Co_{0.8}O_2$ cells with this electrolyte have a comparable performance to cells with $LiPF_6$-based electrolytes [622].

The addition of Lewis acids such as $B(OCH(CF_3)_2)_3$ and $B(OC_6F_5)_3$—the so-called anion receptors—to electrolyte solutions containing highly associated salts, such as LiF and $LiCO_2CF_3$, has been demonstrated to result in much more conductive electrolytes (than the same electrolytes without the anion receptors) [627–636]. An earlier series of publications by Brownstein explored in detail the formation, or lack of formation, in solution of complex fluoroanions when Lewis acids were added to solutions with a wide variety of fluoroanion Lewis bases [637–642]. Two of the strongest superacids known—HSO_3F-SbF_5 ("magic acid") and HF-SbF_5 (fluoroantimonic acid) [21, 557]—are also examples of complex formation between a Lewis base and Lewis acid.

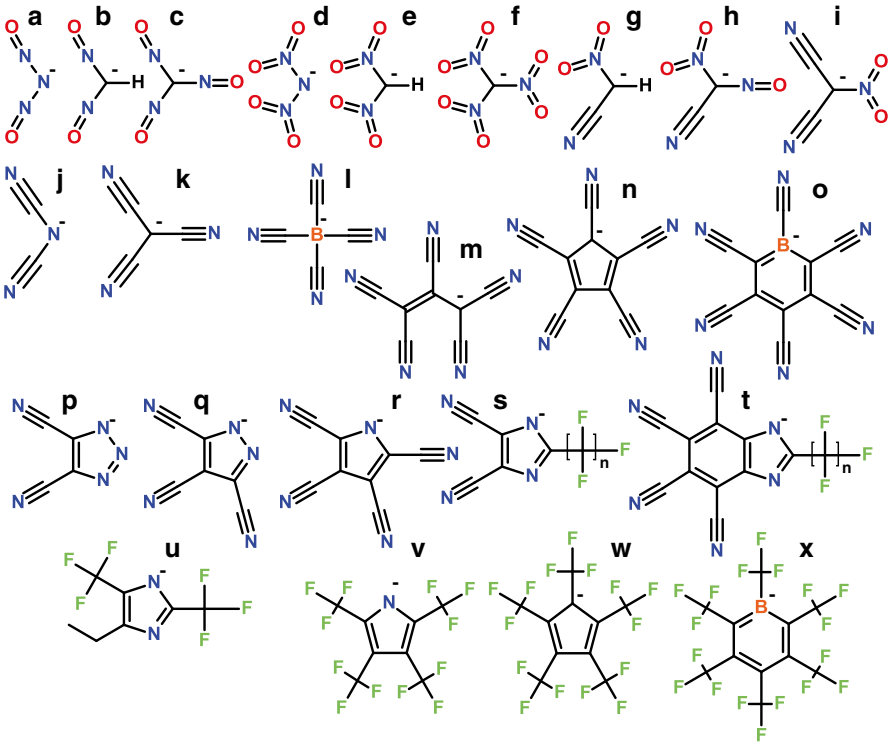

Fig. 1.38 Examples of nitroso-, nitro-, and cyano-substituted anions: (**a**) $N(NO)_2^-$ [643], (**b**) $CH(NO)_2^-$ [644], (**c**) $C(NO)_3^-$, (**d**) $N(NO_2)_2^-$ [645], (**e**) $CH(NO_2)_2^-$ [646], (**f**) $C(NO_2)_3^-$ [646], (**g**) $CH(NO_2)(CN)^-$ [646], (**h**) $C(NO)(NO_2)(CN)^-$ [646], (**i**) $C(NO_2)(CN)_2^-$ [646], (**j**) $N(CN)_2^-$ (DCA^-) [647, 648], (**k**) $C(CN)_3^-$ (TCM^-) [648, 649], (**l**) $B(CN)_4^-$ (TCB^-) [648, 650–654], (**m**) $C(CN)_2{=}C(CN)C(CN)_2^-$ [655–659], (**n**) $C_5(CN)_5^-$ [660–662], (**o**) $C_5B(CN)_6^-$ [663], (**p**) $C_2N_3(CN)_2^-$ ($DCTA^-$) [661, 664–668], (**q**) $C_3N_2(CN)_3^-$ [661, 669–671], (**r**) $C_4N(CN)_4^-$ [661, 672–674], (**s**) $C_3N_2(CN)_2(C_nF_{2n+1})^-$ (TDI^-) ($n=1$), (PDI^-) ($n=2$) and HDI^- ($n=3$) [675–686], (**t**) $C_7N_2(CN)_4(C_nF_{2n+1})^-$ [680], (**u**) $C_3N_2(C_2H_5)(CF_3)_2^-$ [687], (**v**) $C_4N(CF_3)_4^-$ [688, 689], (**w**) $C_5(CF_3)_5^-$ [688, 690–692], and (**x**) $C_5B(CF_3)_6^-$ [663]

The calculated (rather than experimental) gas-phase acidity values for methanides with –NO, $–NO_2$, and –CN substituents are as follows (QC-calculated ΔG_{acid} values in kcal mol^{-1}) relative to CH_4 (407.1): HCH_2NO (353.5), $HCH(NO)_2$ (318.5) (Fig. 1.38b), $HC(NO)_3$ (303.9) (Fig. 1.38c), HCH_2NO_2 (348.5), $HCH(NO_2)_2$ (311.5) (Fig. 1.38e), $HC(NO_2)_3$ (298.0) (Fig. 1.38f), HCH_2CN (363.9), $HCH(CN)_2$ (322.9), and $HC(CN)_3$ (288.8) (Fig. 1.38k) [693]. The addition of a single $–NO_2$ group is therefore expected to be more effective at increasing the acidity than a single –CN group. But, while double and triple substitution significantly increases the acid strength further, the gains are much smaller than for the initial substituent and vary for the different functional groups. Thus, trisubstitution with the –CN groups is more effective (as determined from the calculations) at increasing the acidity than for the –NO and $–NO_2$ groups [693]. Therefore, while resonance effects strongly

influence the acidity of these methanides, the magnitude of the effect differs markedly depending upon both the degree of substitution and the identity of the functional groups.

Lithium salts with anions having nitroso or nitro functional groups have not been used for lithium battery electrolytes, despite the strong electron-withdrawing properties of these groups. This is due to the energetic characteristics of such anions [694–697]. For example, lithium dinitrosomethanide (i.e., $LiCH(NO)_2$) (Fig. 1.38b), while stable at room temperature, is reported to be heat/shock sensitive and highly explosive, as well as highly toxic [644]. Anions with mixtures of the –NO, $–NO_2$, and –CN substituents have also been prepared (Fig. 1.38g–i) [646], but salts with the nitrosodicyanomethanide (i.e., $C(NO)(CN)_2^-$), nitrodicyanomethanide (i.e., $C(NO_2)(CN)_2^-$) (Fig. 1.38i), and other related anions are also predicted to be highly energetic and thus favorable for propellant applications [646]. Further, the trinitrogen dioxide or dinitrosamide anion (i.e., $N(NO)_2^-$) is unstable [643]. This may also be the case for the $C(NO)_3^-$ anion as there are no reports for salts with this anion in the scientific literature, although salts with the $CH(NO)_2^-$ anion are known [447]. Lithium salts with the dicyanamide anion (*LiDCA*) (i.e., $LiN(CN)_2$) (Fig. 1.38j), tricyanomethanide (*LiTCM*) (i.e., $LiC(CN)_3$) (Fig. 1.38k), and tetracyanoborate (*LiTCB*) (i.e., $LiB(CN)_4$) (Fig. 1.38l) have been little utilized for lithium battery applications [647–653]. The most likely explanation for this is the limited electrochemical stability of these anions to oxidation, relative to other lithium salt anions.

Other cyanocarbon acids are thought to be some of the strongest acids known. For example, the QC-calculated gas-phase acidity (ΔG_{acid} in kcal mol^{-1}) of 1,1,2,3,3-pentacyanopropene (i.e., $C(CN)_2{=}C(CN)CH(CN)_2$) (267.2) (Fig. 1.38m) and pentacyano-cyclo-pentadienide (i.e., $HC_5(CN)_5$) (250.1) (Figs. 1.38n and 1.39j) (as compared to a similarly calculated value for $HC(CN)_3$ (287.6)) are some of the lowest values known [21]. Sodium salts with the $C(CN)_2{=}C(CN)C(CN)_2^-$ and $C_5(CN)_5^-$ anions have been prepared [655, 656, 698–700].

The lithium salt with the 4,5-dicyano-1,2,3-triazolate anion (*DCTA*$^-$) (also known as 1,2,3-triazole-4,5-dicarbonitrile (*TADC*$^-$)) (Fig. 1.38p) was first studied by Michot in 1995 [701] and reported in two publications in 2003 [664, 665]. Little has been reported regarding the properties of the lithium salt. Alkali and alkali earth salts with the $DCTA^-$ anion have also been prepared [666, 667]. The thermal stability of these salts was found to be excellent (>350 °C) [668]. In general, triazole salts are known to be energetic. The alkali metal salts, however, were found to have low sensitivity towards impact, friction, electrostatic discharge, and fast heating [668]. The acid with the related pyrazole-3,4,5-tricarbonitrile anion (*PATC*$^-$) (Fig. 1.38q) was first reported in 1962 [669], but the lithium salt has not been investigated extensively as an electrolyte salt [661, 670, 671]. Similarly, the acid with the tetracyanopyrrolide anion (*TCP*$^-$) (Fig. 1.38r) was also reported in 1962 [672] and the sodium salt with this anion has been prepared [674]. Trifluoromethane-substituted versions of the $C_5(CN)_5^-$ and TCP^- anions have also been reported (Fig. 1.38v, w) [688–692], but the lithium salt has only been reported for $LiC_5(CF_3)_5$ (Fig. 1.39k) [692].

Lithium salts with the 4,5-dicyano-2-(trifluoromethyl)imidazole (*TDI*$^-$) (Fig. 1.39h) and 4,5-dicyano-2-(pentafluoroethyl)imidazole (*PDI*$^-$) (Fig. 1.39i)

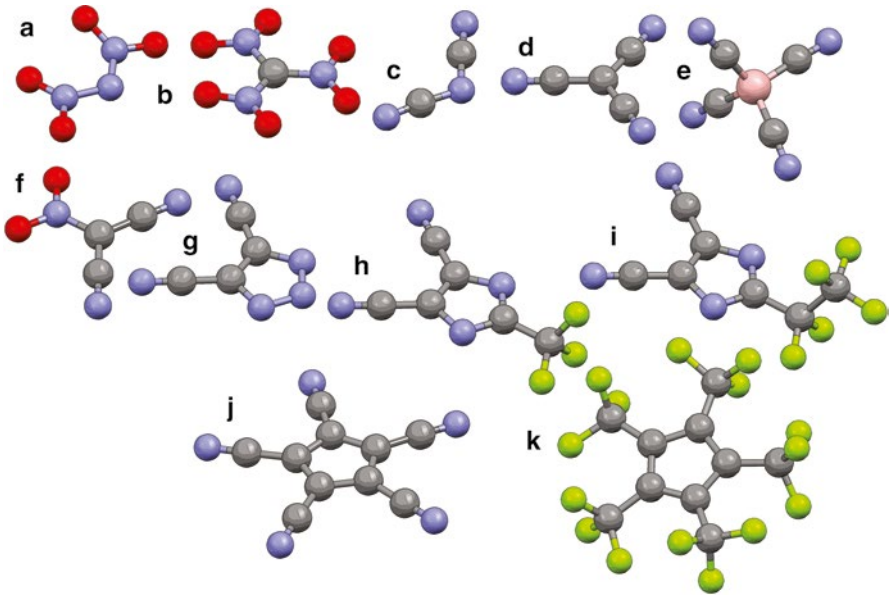

Fig. 1.39 Anion structures: (**a**) $N(NO_2)_2^-$, (**b**) $C(NO_2)_3^-$, (**c**) $N(CN)_2^-$, (**d**) $C(CN)_3^-$, (**e**) $B(CN)_4^-$, (**f**) $C(NO_2)(CN)_2^-$, (**g**) $C_2N_3(CN)_2^-$ ($DCTA^-$), (**h**) $C_3N_2(CN)_2(CF_3)^-$ (TDI^-), (**i**) $C_3N_2(CN)_2(C_2F_5)^-$ (PDI^-), (**j**) $C_5(CN)_5^-$, and (**k**) $C_5(CF_3)_5^-$ (B—*tan*, C—*gray*, N—*blue*, O—*red*, F—*light green*)

Table 1.6 Conductivity of electrolytes with various lithium salts at 20 °C and 1 M salt in EC:DMC (50:50 w:w) [681]

Lithium salt (anion)	Conductivity (mS cm^{-1})
PF_6^-	10.8
$N(SO_2CF_3)_2^-$	9.0
PDI^-	6.3
TDI^-	6.7
$DCTA^-$	2.7

anions (Fig. 1.38s) were reported by Niedzicki in 2009 [677]. The acid with TDI^- (i.e., HTDI) was first reported by Begland in 1974 [675]. A number of publications related to the use of these lithium salts for battery applications have been published [675–686], including a salt with the 4,5-dicyano-2-(n-heptafluoropropyl)imidazolide (HDI^-) anion (Fig. 1.38s). The LiTDI, LiPDI, and LiHDI salts have been found to have a high thermal stability (>250 °C), negligible hydrolysis, high oxidative stability on Pt electrodes (4.8 V vs. Li/Li^+), and passivate Al at high potential [679, 681]. Half cells with $LiMn_2O_4$ electrodes cycled (to 4.3 V vs. Li/Li^+) with electrolytes (1 M in EC:DMC 50:50 w:w) containing LiTDI or LiPDI have a similar capacity and capacity retention to the same electrode cycled with an electrolyte with $LiPF_6$ [681]. The rate performance of such cells is only slightly diminished relative to the cell with the $LiPF_6$ electrolyte due to the somewhat lower conductivity of the LiTDI and LiPDI electrolytes (Table 1.6) [681]. Although PC-based electrolytes with these salts have been tested to determine the change in impedance with time

Table 1.7 Conductivities and Al repassivation potential of electrolytes with various lithium salts at 25 °C and 1 M salt in PC:DME (1:1 v:v) [704]

Lithium salt (anion)	Conductivity (mS cm^{-1})	Al potential (V vs. Li/Li^+)
PF_6^-	15	>5
$N(SO_2CF_3)_2^-$	12	3.7
$N(SO_2C_2F_5)_2^-$	9.5	4.4
$N(SO_2CF_3)(CN)^-$	7.2	<4.2
$N(SO_2C_4F_9)(CN)^-$	5.6	>4.2
$C(SO_2CF_3)(CN)_2^-$	12.5	4.7
$C(SO_2C_4F_9)(CN)_2^-$	8.3	>5

upon storage in contact with Li metal electrodes [682], it is not yet clear if these anions are stable when charged to low potential [679] as nitriles are known to have poor reductively stability [702]. A computational study has suggested that the related 4,5,6,7-tetracyano-2-fluoroalkyl benzimidazole anions (Fig. 1.38t) may also have favorable electrolyte properties [680].

A number of other anions have also been reported which do not fit readily into the classifications noted above (Figs. 1.40 and 1.41). Little information is available about the properties of these anions (Table 1.7). The relative ionic association tendency (which influences electrolyte conductivity) for some of these may be estimated by considering the impact of different substituents on an anion's acidity (Figs. 1.1 and 1.2) and the additional information reported above. For example, the experimental gas-phase acidity values (ΔG_{acid} in kcal mol^{-1}) for $HC(C_6F_5)(SO_2CF_3)_2$ (301.3) (Fig. 1.22k) and $HC(C_6F_5)(CN)_2$ (303.6) are higher than those for $HN(SO_2CF_3)_2$ (291.8), $HC(SO_2CF_3)_3$ (289.0), and $HC(CN)_3$ (~294) due to the weaker electron-withdrawing effect of the $–C_6F_5$ group relative to $–SO_2CF_3$ and –CN for trisubstitution (in contrast to monosubstitution) (Figs. 1.1 and 1.2) [26].

Finally, a relatively unique but diverse class of anions for battery electrolytes are the carboranes and boranes [711–727]. These anions are often chemically inert and superweakly coordinating [728]. Carboranes are composed of clusters of carbon and boron atoms, whereas boranes only have boron. These carbon and boron atoms are typically bonded to H, F, Cl, Br, and/or I atoms or other groups [718]. A variety of classifications are used for carboranes and boranes including *closo-* for a complete polyhedron (e.g., $B_nX_n^{2-}$ with X = H, F, Br, Cl, I, and $6 \le n \le 12$) and for polyhedron missing one, two, or more vertices: *nido-* (e.g., B_5X_9, B_6X_{10}), *arachno-*, etc. The basicity of the dodecaborate $[B_{12}X_{12}]^{2-}$ anions increases in the order X = F < Cl < Br < I [721]. It is noteworthy that carborane synthesis is time consuming and costly, whereas *closo*-dodecaborates have similar stability, but are easier and cheaper to prepare [713]. Lithium *closo*-borane salts (i.e., $Li_2B_{10}Cl_{10}$ and $Li_2B_{12}Cl_{12}$) dissolved in $SOCl_2$ were used in electrolytes for $Li/SOCl_2$ liquid cathode cells in 1979 [729]. Johnson and Whittingham then used these salts for electrolytes for the early Exxon work with Li/TiS_2 cells in 1980 [712–714]. These salts were found to be poorly soluble in individual ether solvents, but did have a higher solubility in dioxolane: DME mixtures [712]. More recently, $Li_2B_{12}F_nH_{12-n}$ ($n = 9$ and 12) salts have been

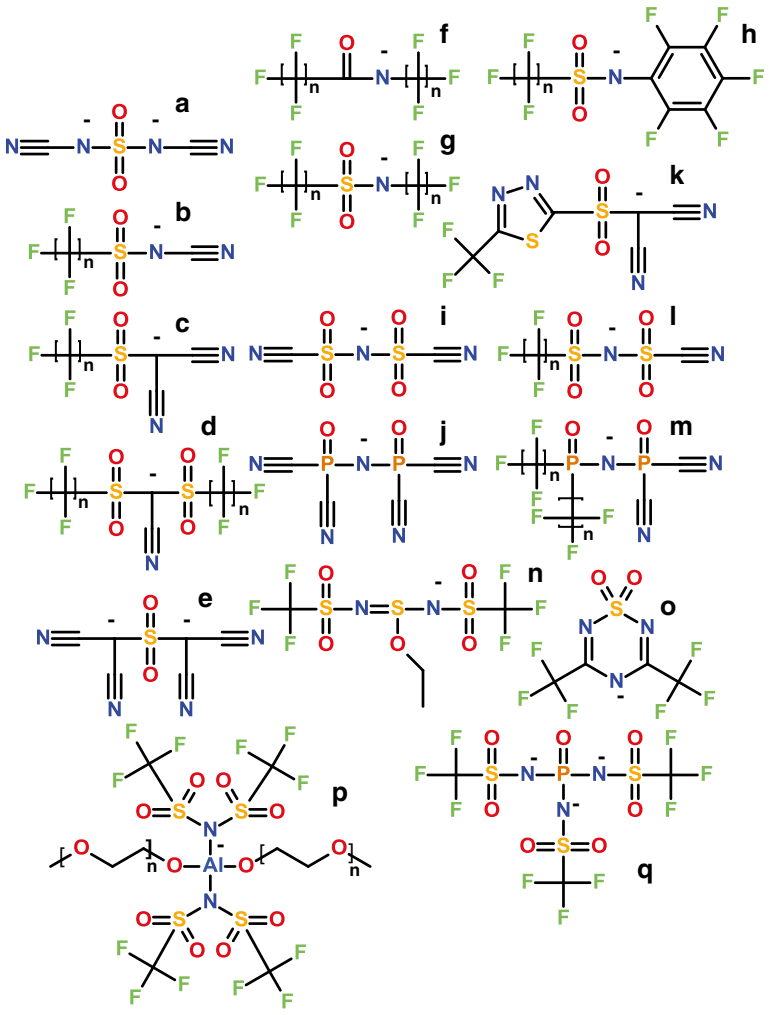

Fig. 1.40 Examples of additional anions: (**a**) $SO_2(NCN)_2^-$ [703], (**b**) $N(SO_2C_nF_{2n+1})(CN)^-$ [704], (**c**) $C(SO_2C_nF_{2n+1})(CN)_2^-$ [704–706], (**d**) $C(SO_2C_nF_{2n+1})_2(CN)^-$ [705, 706], (**e**) $SO_2(C(CN)_2)_2^-$ [706], (**f**) $N(COC_nF_{2n+1})(C_nF_{2n+1})^-$ [254], (**g**) $N(SO_2C_nF_{2n+1})(C_nF_{2n+1})^-$ [707], (**h**) $N(SO_2C_nF_{2n+1})(C_6F_5)^-$ [708], (**i**) $N(SO_2(CN))_2^-$ [361, 709], (**j**) $N(PO(CN)_2)_2^-$ [361], (**k**) $C(SO_2C_2N_2S(CF_3))(CN)_2^-$ [706], (**l**) $N(SO_2C_nF_{2n+1})(SO_2CN)^-$ [361], (**m**) $N(PO(C_nF_{2n+1})_2)(PO(CN)_2)^-$ [361], (**n**) $S(OC_2H_5)(NSO_2CF_3)_2^-$ [289], (**o**) $N(C(CF_3)NSO_2NC(CF_3))^-$ [255], (**p**) $Al(N(SO_2CF_3)_2)_2(O(CH_2CH_2O)_nCH_3)_2^-$ [559], and (**q**) $PO(NSO_2CF_3)_3^{3-}$ [710]

developed by Air Products (as the Stabilife fluorinated electrolyte salts) with a number of intriguing electrolyte properties. A TGA analysis of the $Li_2B_{12}F_{12}$ salt (*Li_2DFB*) (Figs. 1.42 and 1.43) indicates that no mass loss occurs up to 450 °C. The salt is also inert in 98 % sulfuric and 70 % nitric acid, as well as 3 M KOH (in contrast with the $B_{12}H_{12}^{2-}$ anion which reacts with sulfuric acid) [718]. The conductivity of Li_2DFB electrolytes is lower than for comparable electrolytes with $LiPF_6$ [717, 718], but the

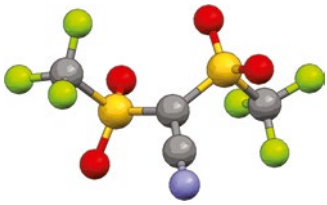

Fig. 1.41 Anion structure: $C(SO_2CF_3)_2(CN)^-$ (C—*gray*, N—*blue*, O—*red*, F—*light green*, S—*yellow*)

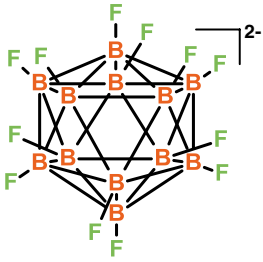

Fig. 1.42 Example of a fluorinated *closo*-dodecaborate anion: $B_{12}F_{12}^{2-}$ [715–726]

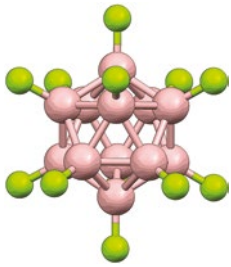

Fig. 1.43 Anion structure: $B_{12}F_{12}^{2-}$ (B—*tan*, F—*light green*)

electrolyte solvent/salt formulation can be tuned to obtain promising cell cycling performance, especially at elevated temperature (60 °C) [718]. In addition, the $B_{12}F_{12}^{2-}$ anion is not reduced at 0 V (vs. Li/Li^+) and undergoes a quasi-reversible oxidation reaction at 4.7 V (vs. Li/Li^+) to form the stable radical cation $B_{12}F_{12}^-$ [717]. The potential at which this oxidation reaction occurs can be tuned by changing the anion structure. The $Li_2B_{12}H_3F_9$ salt, for example, has a reversible oxidation reaction at 4.5 V (vs. Li/Li^+) [716, 717]. These anions are thus able to provide overcharge protection for 4+ V Li-ion batteries, as has been demonstrated for MCMB/spinel cells [716, 724]. Note that many organic molecules designed for overcharge protection have poor solubility in carbonate solvents [724]. This is not the case for the $Li_2B_{12}F_9H_3$ salt which has a reasonably high solubility (≥0.5 M) while also serving as a divalent Li^+ cation salt [717, 723].

1.10 Adoption Criterion for New Salts

Lithium salts have not been prepared for many of the anions noted above. For other anions, the corresponding lithium salts have been reported, but only in a single report with or without some limited electrolyte data provided. Such salts are often

not widely available to the greater battery research community…and many of the practitioners in this community do not have the time, resources, or expertise necessary to prepare and purify such salts. Thus, the useful properties and/or limitations of the salts often remain unknown and unutilized.

Ultimately, when developing new lithium salts, it is important to ask what advantages are sought over the widely utilized salt $LiPF_6$. This salt has been a cornerstone of Li-ion battery R&D for well over two decades. But it is clear that $LiPF_6$ has limitations. Properties or features of salts which would make them attractive candidates for commercial battery electrolytes include the following:

(a) Simplified synthesis—If low-cost and/or nontoxic reagents which are easily handled are available for salt synthesis, this may reduce the overall expense of the salt production. Waste from the synthesis/purification methods is another consideration, as is the ease of salt purification to an electrochemical-grade material. The ownership of the intellectual property (IP) rights may be another important factor.

(b) Reduced hazards—In some cases, the reagents, reaction intermediates, and/or final salts are highly toxic or have other undesirable properties (e.g., energetic materials, corrosive) which requires specialized handling of the materials and makes them undesirable for commercial batteries. The degradation products (if battery failure occurs) may also be highly toxic, as has been noted for the fluoro-organic products obtained from the reaction of $LiPF_6$ and carbonate solvents at high temperature when in contact with cathode materials [730]. Thus, the elimination of fluorine from the anions is a worthy goal, but one which is difficult to achieve based upon the information noted in this review.

(c) Hydrolysis—$LiPF_6$ readily hydrolyzes when contacted with water, especially at elevated temperature. This makes the synthesis, storage, and handling of this salt more onerous, thus adding cost to its use. A salt which is not susceptible to hydrolysis would greatly simplify the handing/transportation of the salt for large-scale battery production.

(d) Divalent anions—Divalent anions may offer a means of increasing the Li^+ cation content (for a fixed number of anions) or decreasing the amount of salt needed to retain the same number of Li^+ cations in the electrolyte. This is dependent upon both of the Li^+ cations having weak interactions with the anions, which is difficult to achieve, and the salt having a moderate–high solubility in aprotic solvents, which is also difficult to achieve.

(e) Redox shuttle mechanism—The use of a salt which has other functionality, such as a redox shuttle mechanism (e.g., $B_{12}F_{12}^{2-}$) (Figs. 1.42 and 1.43) which protects the cell against overcharging, would be desirable.

(f) Thermal stability—The use of salts, either as primary salts or as additives, which result in electrolytes with high thermal stability (alone and in contact with electrodes)—enabling cell cycling at >60 °C—is a long sought after trait.

(g) New solvents—$LiPF_6$ was optimized for use with the cyclic/acyclic carbonate solvents used for Li-ion batteries. Often the use of $LiPF_6$ for electrolytes with other solvents does result in the most conductive electrolytes (relative to other

salts), but there are exceptions. For example, $LiPF_6$ reacts with GBL (forming brown or black solutions), but this solvent has many promising features for electrolytes [91–96]. Thus, $LiPF_6$ has generally been replaced with $LiBF_4$, LiTFSI, LiBOB, LiDFOB, etc. when GBL is used as an electrolyte solvent.

(h) Low-temperature operation—The state-of-the-art carbonate-based electrolytes with $LiPF_6$ do not perform well at low temperature. Typically, approaches to optimize electrolytes for low temperature involve the addition of other solvents (e.g., methyl butyrate) to the carbonate solvents [478]. The difference in conductivity for electrolytes with different salts, however, becomes less significant at low temperature (Fig. 1.14). $LiPF_6$ tends to make high-melting crystalline solvates (Fig. 1.4) with a wide variety of solvents. This may be a factor for long running-time operation of batteries at low temperature. Thus, other salts which form solvates with a low T_m or do not crystallize (for specific compositions) (Fig. 1.4)—such as LiFSI, LiTFSI, or LiBETI—may be useful for such applications.

(i) SEI formation—Salts which preferentially decompose to form protective layers on the anode, cathode, Al current collector, etc. (i.e., LiBOB, LiDFOB) are likely to be required for electrodes such as Si alloys, sulfur, and high-voltage cathodes [54, 731, 732]. In particular, the formation of HF in electrolytes with $LiPF_6$ (perhaps due to the reaction of the anions with solvent molecules, instead of water), especially at high potentials and high temperature, is deemed to be particularly problematic [49–54]. Replacing the $LiPF_6$, the use of HF scavengers and the formation of protective layers are all ways to mitigate this problem.

Ultimately, the electrolyte formulations must meet the demanding criterion necessary for long-term battery operation (high stability with selective reactions, high safety, etc.). Conductivity remains an important consideration for high-power applications. Increasingly, salt mixtures (rather than just solvent mixtures) are being used to tailor electrolyte formulations. This trend is likely to increase in the future due to the necessity of simultaneously optimizing so many electrolyte properties which influence the battery's usable energy and power, lifetime, safety, cost, etc. New salts therefore remain one of the key variables available for the development of advanced electrolyte formulations.

1.11 Summary

A diverse range of anions have been prepared over the past three decades for lithium salts intended for lithium battery electrolyte applications. Many of these anions were originally prepared in efforts to generate stronger superacids. In general, it is found that selectively fluorinating the anions decreases the anion… Li^+ cation (ionic association) interactions, thereby increasing the conductivity of electrolyte solutions with the corresponding lithium salts. Anion fluorination also tends to increase the anodic stability of the anions to oxidation at high potential—an important

consideration for electrolyte formulations intended for use with high-voltage cathodes. In recent years, nitrile groups have also been used in lieu of fluorination. In some cases, however, salt stability is undesireable. For example, a common approach to improving electrolytes is the use of salt additives—sacrificial anions which degrade to produce interfacial layers with the anode, cathode and/or Al current collector—which stablize the interfaces with the electrolyte resulting in dramatic improvements in battery performance. New salts therefore remain one of the key variables available for the development of advanced electrolyte formulations with tailored properties for demanding energy storage applications.

Acknowledgement The author wishes to express his gratitute to the U.S. Department of Energy (DOE) Office of Basic Energy Science-Division of Materials Sciences and Engineering which supported the preparations of this review under Award DE-SC0002169.

References

1. R. Selim, P. Bro, J. Electrochem. Soc. 1974, 121, 1457-1459. Some observations on rechargeable lithium electrodes in a propylene carbonate electrolyte.
2. F. W. Dampier, S. B. Brummer, Electrochim. Acta 1977, 22, 1339-1345. The cycling behavior of the lithium electrode in $LiAsF_6$/methyl acetate solutions.
3. I. Epelboin, M. Froment, M. Garreau, J. Thevenin, D. Warin, J. Electrochem. Soc. 1980, 127, 2100-2104. Behavior of secondary lithium and aluminum-lithium electrodes in propylene carbonate.
4. K. Brandt, Solid State Ionics 1994, 69, 173-183. Development of secondary lithium batteries.
5. J. T. Dudley, D. F. Wilkinson, G. Thomas, R. LeVae, S. Woo, H. Blom, C. Horvath, M. W. Juzkow, B. Denis, P. Juric, P. Aghakian, J. R. Dahn, J. Power Sources 1991, 35, 59-82. Conductivity of electrolytes for rechargeable lithium batteries.
6. S.-I. Tobishima, K. Hayashi, K.-I. Saito, J.-I. Yamaki, Electrochim. Acta 1995, 40, 537-544. Ethylene carbonate-based ternary mixed solvent electrolytes for rechargeable lithium batteries.
7. M. Ishikawa, M. Morita, M. Asao, Y. Matsuda, J. Electrochem. Soc. 1994, 141, 1105-1108. Charge/discharge characteristics of carbon fiber with graphite structure in organic electrolytes containing lithium trifluoromethanesulfate and lithium hexafluorophosphate.
8. K. Zaghib, K. Tatsumi, H. Abe, T. Ohsaki, Y. Sawada, S. Higuchi, J. Power Sources 1995, 54, 435-439. Electrochemical behavior of an advanced graphite whisker anodic electrode for lithium-ion rechargeable batteries.
9. C.-K. Huang, S. Surampudi, D. H. Shen, G. Halpert, Proc. Electrochem. Soc. 1994, 94-4, 105-110. Effect of electrolyte composition on carbon electrode performance.
10. K. Sekai, H. Azuma, A. Omaru, S. Fujita, H. Imoto, T. Endo, K. Yamaura, Y. Nishi, S. Mashiko, M. Yokogawa, J. Power Sources 1993, 43–44, 241-244. Lithium-ion rechargeable cells with $LiCoO_2$ and carbon electrodes.
11. J. M. tarascon, D. Guyomard, Solid State Ionics 1994, 69, 293-305. New electrolyte compositions stable over the 0 to 5 V voltage range and compatible with the $Li_{1+x}Mn_2O_4$/carbon Li-ion cells.
12. K. Xu, Chem. Rev. 2004, 104, 4303-4417. Nonaqueous liquid electrolytes for lithium-based rechargeable batteries.
13. A. Yoshino, Angew. Chem. Int. Ed. 2012, 51, 5798-5800. The birth of the lithium-ion battery.

14. M. S. Whittingham, Proc. IEEE 2012, 100, 1518-1536. History, evolution, and future status of energy storage.
15. B. Scrosati, J. Solid-State Electrochem. 2011, 15, 1623-1630. History of lithium batteries.
16. K. Brandt, Solid State Ionics 1994, 69, 173-183. Historical development of secondary lithium batteries.
17. Z.-I. Takehara, K. Kanamura, Electrochim. Acta 1993, 38, 1169-1177. Historical development of rechargeable lithium batteries in Japan.
18. B. Scrosati, J. Electrochem. Soc. 1992, 139, 2776-2781. Lithium rocking chair batteries: An old concept?
19. J. M. Tarascon, D. Guyomard, Electrochim. Acta 1993, 38, 1221-1231. The $Li_{1-x}Mn_2O_4$/C rocking-chair system: A review.
20. I. A. Koppel, R. W. Taft, F. Anvia, S.-Z. Zhu, L.-Q. Hu, K.-S. Sung, D. D. Desmarteau, L. M. Yagupolskii, Y. L. Yagupolskii, N. V. Igat'ev, N. V. Kondratenko, A. Y. Volkonskii, V. M. Vlasor, R. Notario, P.-C. Maria, J. Am. Chem. Soc. 1994, 116, 3047-3057. The gas-phase acidities of very strong neutral Brønsted acids.
21. I. A. Koppel, P. Burk, I. Koppel, I. Leito, T. Sonoda, M. Mishima, J. Am. Chem. Soc. 2000, 122, 5114-5124. Gas phase acidities of some neutral Bronsted superacids: A DFT and ab initio study.
22. I. A. Koppel, P. Burk, I. Koppel, I. Leito, J. Am. Chem. Soc. 2002, 124, 5594-5600. Generalized principle of designing neutral superstrong Brønsted acids.
23. E. S. Stoyanov, K.-C. Kim, C. A. Reed, J. Am. Chem. Soc. 2006, 128, 8500-8506. An infrared *v*NH scale for weakly basic anions. Implications for single-molecule acidity and superacidity.
24. I. Leito, E. Raamat, A. Kütt, J. Saame, K. Kipper, I. A. Koppel, I. Koppel, M. Zhang, M. Mishima, L. M. Yagupolskii, R. Y. Garlyauskayte, A. A. Filatov, J. Phys. Chem. A 2009, 113, 8421-8424. Revision of the gas-phase acidity scale below 300 kcal mol^{-1}.
25. A. Kütt, T. Rodima, J. Saame, E. Raamat, V. Mäemets, I. Kaljurand, I. A. Koppel, R. Y. Garlyauskayte, Y. L. Yagupolskii, L. M. Yagupolskii, E. Bernhardt, H. Willner, I. Leito, J. Org. Chem. 2011, 76, 391-395. Equilibrium acidities of superacids.
26. P. Burk, I. A. Koppel, I. Koppel, L. M. Yagupolskii, R. W. Taft, J. Comp. Chem. 1996, 17, 30-41. Superacidity of neutral Brönsted acids in gas phase.
27. G. A. Olah, G. K. Surya Prakash, J. Sommer, Science, 1979, 206, 13-20. Superacids.
28. G. A. Olah, G. K. S. Prakash, Á. Molnár, J. Sommer, Superacid Chemistry, Wiley, Hoboken, NJ, 2009.
29. R. J. Gillespie, T. E. Peel, Adv. Phys. Org. Chem. 1971, 9, 1-24. Superacid systems.
30. R. J. Gillespie, T. E. Peel, J. Am. Chem. Soc. 1973, 95, 5173-5178. The Hammett Acidity function for some superacid systems. 11. The systems H_2SO_4-HSO_3F, KSO_3F-HSO_3F, HSO_3F-SO_2, HSO_3F-AsF_5, HSO_3F-SbF_5, and HSO_3F-SbF_5-SO_2.
31. I. A. Koppel, V. Pihl, J. Koppel, F. Anvia, R. W. Taft, J. Am. Chem. Soc. 1994, 116, 8654-8657. Thermodynamic acidity of $(CF_3)_3CH$ and ^{1}H-undecafluorobicyclo[2.2.1]heptane: The concept of anionic (fluorine) hyperconjugation.
32. A. H. Otto, S. Schrader, T. Steiger, M. Schneider, J. Chem. Soc. Faraday Trans. 1997, 93, 3927-3930. Gas-phase deprotonation of sulfuric acid, perchloric acid, chlorosulfonic acid and fluorosulfonic acid.
33. R. Steudel, A. H. Otto, Eur. J. Inorg. Chem. 2000, 2379-2386. Geometries, acidities, and dissociation reactions of the gaseous superacids $H_2S_2O_3$, H_2SO_5, HSO_3F, and HSO_3Cl.
34. J. Barthel, H.-J. Gores, L. Kraml, J. Phys. Chem. 1996, 100, 1283-1287. Effects of electronegative substituents of anions on ion-pair formation. 1. Temperature dependence of the conductivity of lithium fluoroacetate and alkali-metal acetate solutions in dimethyl sulfoxide.
35. D. Lisbona, T. Snee, Proc. Saf. Environ. 2011, 89, 434-442. A review of hazards associated with primary lithium and lithium-ion batteries.
36. P. G. Balakrishnan, R. Ramesh, T. Prem Kumar, J. Power Sources 2006, 155, 401-414. Safety mechanisms in lithium-ion batteries.

37. J. B. Goodenough, Y. Kim, Chem. Mater. 2010, 22, 587-603. Challenges for rechargeable Li batteries.
38. L. Hu, Z. Zhang, K. Amine, J. Power Sources 2013, 236, 175-180. Electrochemical investigation of carbonate-based electrolytes for high voltage lithium-ion cells.
39. D. Aurbach, Y. Talyosef, B. Markovsky, E. Markevich, E. Zinigrad, L. Asraf, J. S. Gnanaraj, H.-J. Kim, Electrochim. Acta 2004, 50, 247-254. Design of electrolyte solutions for Li and Li-ion batteries: a review.
40. V. Aravindan, J. Gnanaraj, S. Madhavi, H.-K. Liu, Chem. Eur. J. 2011, 17, 14326-14346. Lithium-ion conducting electrolyte salts for lithium batteries.
41. C.-K. Park, Z. Zhang, Z. Xu, A. Kakirde, K. Kang, C. Chai, G. Au, L. Cristo, J. Power Sources 2007, 165, 892-896. Variables study for the fast charging lithium ion batteries.
42. P. G. Bruce, C. A. Vincent, J. Electroanal. Chem. 1987, 255, 1-17. Steady state current flow in solid binary electrolyte cells.
43. P. G. Bruce, J. Evans, C. A. Vincent, Solid State Ionics 1988, 28–30, 918-922. Conductivity and transference number measurements on polymer electrolytes.
44. F. M. Gray, Solid Polymer Electrolytes Fundamentals and Technological Applications, VCH, New York, NY 1991.
45. M. Ue, M. Takeda, M. Takehara, S. Mori, J. Electrochem. Soc. 1997, 144, 2684-2688. Electrochemical properties of quaternary ammonium salts for electrochemical capacitors.
46. H. Zheng, J. Qin, Y. Zhao, T. Abem Z. Ogumi, Solid State Ionics 2005, 176, 2219-2226. Temperature dependence of the electrochemical behavior of $LiCoO_2$ in quaternary ammonium-based ionic liquid electrolyte.
47. C. Iwakura, Y. Fukumoto, H. Inoue, S. Ohashi, S. Kobayashi, H. Tada, M. Abe, J. Power Sources 1997, 68, 301-303. Electrochemical characterization of various metal foils as a current collector of positive electrode for rechargeable lithium batteries.
48. M.-H. Ryou, J.-N. Lee, D. J. Lee, W.-K. Kim, Y. K. Jeong, J. W. Choi, J.-K. Park, Y. M. Lee, Electrochim. Acta 2012, 83, 259-263. Effects of lithium salts on thermal stabilities of lithium alkyl carbonates in SEI layer.
49. H. Lee, J.-J. Cho, J. Kim, H.-J. Kim, J. Electrochem. Soc. 2005, 152, A1193-A1198. Comparison of voltammetric responses over the cathodic region in $LiPF_6$ and LiBETI with and without HF.
50. E. Markevich, R. Sharabi, H. Gottlieb, V. Borgel, K. Fridman, G. Salitra, D. Aurbach, G. Semrau, M. A. Schmidt, N. Schall, C. Bruenig, Electrochem. Commun. 2012, 15, 22-25. Reasons for capacity fading of $LiCoPO_4$ cathodes in $LiPF_6$ containing electrolyte solutions.
51. J. Wu, N. Membreno, W.-Y. Yu, J. D. Wiggins-Camacho, D. W. Flaherty, C. B. Mullins, K. J. Stevenson, J. Phys. Chem. C 2012, 116, 21208-21215. Influence of hydrofluoric acid formation on lithium ion insertion in nanostructured V_2O_5.
52. R. Sharabi, E. Markevich, V. Borgel, G. Salitra, G. Gershinsky, D. Aurbach, M. A. Schmidt, N. Schall, C. Stinner, J. Power Sources 2012, 203, 109-114. Raman study of structural stability of $LiCoPO_4$ cathodes in $LiPF_6$ containing electrolytes.
53. S. F. Lux, I. T. Lucas, E. Pollak, S. Passerini, M. Winter, R. Kostecki, Electrochem. Commun. 2012, 14, 47-50. The mechanism of HF formation in $LiPF_6$ based organic carbonate electrolytes.
54. H. Zheng, Q. Sun, G. Liu, X. Song, V. S. Battaglia, J. Power Sources 2012, 207, 134-140. Correlation between dissolution behavior and electrochemical cycling performance for $LiNi_{1/3}Co_{1/3}Mn_{1/3}O_2$-based cells.
55. O. Borodin, W. Behl, T. R. Jow, J. Phys. Chem. C 2013, 117, 8661-8682. Oxidative stability and initial decomposition reactions of carbonate, sulfone, and alkyl phosphate-based electrolytes.
56. Y. Sasaki, M. Handu, K. Kurashima, T. Tonuma, K. Usami, J. Electrochem. Soc. 2001, 148, A999-A103. Application of lithium organoborate with salicyclic ligand to lithium battery electrolyte.
57. R. Marom, O. Haik, D. Aurbach, I. C. Halalay, J. Electrochem. Soc. 2010, 157, A972-A983. Revisiting $LiClO_4$ as an electrolyte for rechargeable lithium-ion batteries.

58. B. Markovsky, F. Amalraj, H. E. Gottlieb, Y. Gofer, S. K. Martha, D. Aurbach, J. Electrochem. Soc. 2010, 157, A423-A429. On the electrochemical behavior of aluminum electrodes in nonaqueous electrolyte solutions of lithium salts.
59. S. S. Zhang, T. R. Jow, J. Power Sources 2002, 109, 458-464. Aluminum corrosion in electrolyte of Li-ion battery.
60. K. Kanamura, J. Power Sources 1999, 81–82, 123-129. Anodic oxidation of nonaqueous electrolytes on cathode materials and current collectors for rechargeable lithium batteries.
61. G. H. Newman, R. W. Francis, L. H. Gaines and B. M. Rao, J. Electrochem. Soc. 1980, 127, 2025-2027. Hazard investigations of $LiClO_4$/dioxolane electrolyte.
62. R. Jasinski, S. Carroll, J. Electrochem. Soc. 1970, 117, 218-219. Thermal stability of a propylene carbonate electrolyte.
63. J. S. Gnanaraj, E. Zinigrad, L. Asraf, H. E. Gottieb, M. Sprecher, D. Aurbach, M. Schmidt, J. Power Sources 2003, 119–121, 794-798. The use of accelerating rate calorimetry (ARC) for the study of the thermal reactions of Li-ion battery electrolyte solutions.
64. Y. Ein-Eli, S. R. Thomas, R. Chadha, T. J. Blakley, V. R. Koch, J. Electrochem. Soc. 1997, 144, 823-829. Li-ion battery electrolyte formulated for low-temperature applications.
65. K. Kanamura, T. Umegaki, S. Shiraishi, M. Ohashi, Z.-I. Takehara, J. Electrochem. Soc. 2002, 149, A185-A194. Electrochemical behavior of Al current collector of rechargeable lithium batteries in propylene carbonate with $LiCF_3SO_3$, $Li(CF_3SO_2)_2N$, or $Li(C_4F_9SO_2)(CF_3SO_2)N$.
66. L. J. Krause, W. Lamanna, J. Summerfield, M. Engle, G. Korba, R. Loch, R. Atanasocki, J. Power Sources 1997, 68, 320-325. Corrosion of aluminum at high voltages in non-aqueous electrolytes containing perfluoroalkylsulfonyl imides; new lithium salts for lithium-ion cells.
67. H. Yang, K. Kwon, T. M. Devine, J. W. Evans, J. Electrochem. Soc. 2000, 147, 4399-4407. Aluminum corrosion in lithium batteries. An investigation using the electrochemical quartz crystal microbalance.
68. M. Morita, T. Shibata, N. Yoshimoto, M. Ishikawa, Electrochim. Acta 2002, 47, 2787-2793. Anodic behavior of aluminum in organic solutions with different electrolytic salts for lithium batteries.
69. C. G. Barlow, Electrochem. Solid-State Lett. 1999, 2, 362-364. Reaction of water with hexafluorophosphates and with Li bis(perfluoroethylsulfonyl)imide salt.
70. M. Schmidt, U. Heider, A. Kuehner, R. Oesten, M. Jungnitz, N. Ignat'ev, P. Sartori, J. Power Sources 2001, 97–98, 557-560. Lithium fluorophosphates: A new class of conducting salts for electrolytes for high energy lithium-ion batteries.
71. T. Kawamura, S. Okada, J. Yamaki, J. Power Sources 2006, 156, 547-554. Decomposition reaction of $LiPF_6$-based electrolytes for lithium ion cells.
72. A. V. Plakhotnyk, L. Ernst, R. Schmutzler, J. Fluor. Chem. 2005, 126, 27-31. Hydrolysis in the system $LiPF_6$—propylene carbonate—dimethyl carbonate—H_2O.
73. R. Yazami, A. Martinent, in Fluorinated Materials for Energy Conversion, Chap. 9 (T. Nakajima, H. Groult, Eds.), Elsevier, New York, 2005. Fluorinated anions and electrode/electrolyte stability in lithium batteries.
74. H. Yang, G. V. Zhuang, P. N. Ross Jr., J. Power Sources 2006, 161, 573-579. Thermal stability of $LiPF_6$ salt and Li-ion battery electrolytes containing $LiPF_6$.
75. B. Ravdel, K. M. Abraham, R. Gitzendanner, J. DiCarlo, B. Lucht, C. Campion, J. Power Sources 2003, 119–121, 805-810. Thermal stability of lithium-ion battery electrolytes.
76. N.-S. Choi, I. A. Profatilova, S.-S. Kim, E.-H. Song, Thermochim. Acta 2008, 480, 10-14. Thermal reactions of lithiated graphite anode in $LiPF_6$-based electrolyte.
77. W. Li, B. L. Lucht, J. Electrochem. Soc. 2006, 153, A1617-A1625. Lithium-ion batteries: Thermal reactions of electrolyte with the surface of metal oxide cathode particles.
78. H. Yang, X.-D. Shen, J. Power Sources 2007, 167, 515-519. Dynamic TGA–FTIR studies on the thermal stability of lithium/graphite with electrolyte in lithium-ion cell.
79. M. S. Ding, T. R. Jow, J. Electrochem. Soc. 2004, 151, A2007-A2015. How conductivities and viscosities of PC-DEC and PC-EC solutions of $LiBF_4$, $LiPF_6$, LiBOB, Et_4NBF_4, and Et_4NPF_6 differ and why.

80. T. R. Jow, M. S. Ding, K. Xu, S. S. Zhang, J. L. Allen, K. Amine, G. L. Hendriksen, J. Power Sources 2003, 119–121, 343-348. Nonaqueous electrolytes for wide-temperature-range operation of Li-ion cells.
81. J. Li, C. F. Yuan, Z. H. Guo, Z. A. Zhang, Y. Q. Lai, J. Liu, Electrochim. Acta 2012, 59, 69-74. Limiting factors for low-temperature performance of electrolytes in $LiFePO_4$/Li and graphite/Li half cells.
82. S. S. Zhang, K. Xu, T. R. Jow, J. Electrochem. Soc. 2002, 149, A586-A590. Study of $LiBF_4$ as an electrolyte salt for a Li-ion battery.
83. E.-S. Hong, S. Okada, T. Sonoda, S. Gopukumar, J. Yamaki, J. Electrochem. Soc. 2004, 151, A1836-A1840. Thermal stability of electrolytes with mixtures of $LiPF_6$ and $LiBF_4$ used in lithium-ion cells.
84. N. Katayama, T. Kawamura, Y. Baba, J. Yamaki, J. Power Sources 2002, 109, 321-326. Thermal stability of propylene carbonate and ethylene carbonate-propylene carbonate-based electrolytes for use in Li cells.
85. P. Ping, Q. Wang, J. Sun, H. Xiang, C. Chen, J. Electrochem. Soc. 2010, 157, A1170-A1176. Thermal stabilities of some lithium salts and their electrolyte solutions with and without contact to a $LiFePO_4$ electrode.
86. N. Takami, M. Sekino, T. Ohsaki, M. Kanda, M. Yamamoto, J. Power Sources 2001, 97–98, 677-680. New thin lithium-ion batteries using a liquid electrolyte with thermal stability.
87. N. Takami, T. Ohsaki, H. Hasebe, M. Yamamoto, J. Electrochem. Soc. 2002, 149, A9-A12. Laminated thin Li-ion batteries using a liquid electrolyte.
88. S. S. Zhang, K. Xu, T. R. Jow, Electrochem. Commun. 2002, 4, 928-932. A new approach toward improved low temperature performance of Li-ion battery.
89. S. S. Zhang, K. Xu, T. R. Jow, J. Solid State Electrochem. 2003, 7, 147-151. Low-temperature performance of Li-ion cells with a $LiBF_4$-based electrolyte.
90. X. Zuo, C. Fan, J. Liu, X. Xiao, J. Wu, J. Nan, J. Electrochem. Soc. 2013, 160, A1199-A1204. Lithium tetrafluoroborate as an electrolyte additive to improve the high voltage performance of lithium-ion battery.
91. A. Chagnes, B. Carré, P. Willmann, R. Dedryvère, D. Gonbeau, D. Lemordant, J. Electrochem. Soc. 2003, 150, A1255-A1261. Cycling ability of γ-butyrolactone-ethylene carbonate based electrolytes.
92. J. Kasnatscheew, R. W. Schmitz, R. Wagner, M. Winter, R. Schmitz, J. Electrochem. Soc. 2013, 160, A1369-1374. Fluoroethylene carbonate as an additive for γ-butyrolactone based electrolytes.
93. D. Belov, D.-T. Shich, J. Solid State Electrochem. 2012, 16, 603-615. GBL-based electrolyte for Li-ion battery: thermal and electrochemical performance.
94. K. Zaghib, K. Striebel, A. Guerfi, J. Shim, M. Armand, M. Gauthier, Electrochim. Acta 2004, 50, 263-270. $LiFePO_4$/polymer/natural graphite: Low cost Li-ion batteries.
95. T. Ohsaki, N. Takami, M. Kanda, M. Yamamoto, Stud. Surf. Sci. Catal. 2001, 132, 925-928. High performance thin lithium-ion battery using an aluminum-plastic laminated film bag.
96. K. Zaghib, M. Dontigny, A. Guerfi, J. Trottier, J. Hamel-Paquet, V. Gariepy, K. Galoutov, P. Hovington, A. Mauger, H. Groult, C.M. Julien, J. Power Sources 2012, 216, 192-200. An improved high-power battery with increased thermal operating range: C-$LiFePO_4$//C-$Li_4Ti_5O_{12}$.
97. A. Vallée, S. Besner, J. Prud'homme, Electrochim. Acta 1992, 37, 1579-1583. Comparative study of poly(ethylene oxide) electrolytes made with $LiN(CF_3SO_2)_2$, $LiCF_3SO_3$ and $LiClO_4$: Thermal properties and conductivity behavior.
98. M. Minier, C. Berthier, W. Gorecki, J. Phys. 1984, 45, 739-744. Thermal analysis and NMR study of a poly(ethylene oxide) complex electrolyte: $PEO(LiCF_3SO_3)_x$.
99. D. Fauteux, Solid State Ionics 1985, 17, 133-138. Formation of a passivating film at the lithium poly(ethylene oxide) (PEO)-lithium trifluoromethanesulfonate ($LiCF_3SO_3$) interface.
100. R. Neat, M. Glasse, R. Linford, A. Hooper, Solid State Ionics 1986, 18–19, 1088-1092. Thermal history and polymer electrolyte structure: implications for solid-state battery design.
101. P. Lightfoot, M. A. Mehta, P. G. Bruce, Science 1993, 262, 883-885. Crystal structure of the polymer electrolyte poly(ethylene oxide)$_3$:$LiCF_3SO_3$.

102. T. Shodai, B. B. Owens, H. Ohtsuka, J. Yamaki, J. Electrochem. Soc. 1994, 141, 2978-2981. Thermal stability of the polymer electrolyte $(PEO)_8LiCF_3SO_3$.
103. S. Chintapalli, R. Frech, Electrochim. Acta 1998, 43, 1395-1400. Kinetic effects in the ionic association of poly(ethylene oxide)-lithium triflate complexes.
104. R. Frech, S. Chintapalli, P. G. Bruce, C. A. Vincent, Macromolecules 1999, 32, 808-813. Crystalline and amorphous phases in the poly(ethylene oxide)-$LiCF_3SO_3$ system.
105. C. P. Rhodes, R. Frech, Macromolecules 2001, 34, 2660-2666. Local structures in crystalline and amorphous phases of diglyme-$LiCF_3SO_3$ and poly(ethylene oxide)-$LiCF_3SO_3$ systems: Implications for the mechanism of ionic transport.
106. G. B. Appetecchi, F. Alessandrini, R. G. Duan, A. Arzu, J. Power Sources 2001, 101, 42-46. Electrochemical testing of industrially produced PEO-based polymer electrolytes.
107. W. A. Henderson, Solid State Ionics 2012, 217, 1-5. Influence of polymer chain length and chains ends on polyelectrolyte solvate structure and melting point.
108. A. Webber, J. Electrochem. Soc. 1991, 138, 2586-2590. Conductivity and viscosity of solutions of $LiCF_3SO_3$, $Li(CF_3SO_2)N$, and their mixtures.
109. S.-I. Tobishima, T. Okada, Electrochim. Acta 1985, 30, 1715-1722. Lithium cycling efficiency and conductivity in high dielectric solvent/low viscosity solvent mixed systems.
110. M. Morita, O. Yamada, M. Ishikawa, J. Power Sources 1999, 81–82, 425-429. Charge and discharge performances of lithiated metal oxide cathodes in organic electrolyte solutions with different compositions.
111. L. A. Dominey, V. R. Koch, T. J. Blakley, Electrochim. Acta 1992, 37, 1551-1554. Thermally stable lithium salts for polymer electrolytes.
112. S. Sylla, J.-Y. Sanchez, M. Armand, Electrochim. Acta 1992, 37, 1699-1701. Electrochemical study of linear and crosslinked PEO-based polymer electrolytes.
113. M. Armand, W. Gorecki, R. Andreani, Int. Symp. Polym. Electrolytes 1990, 91-97. Perfluorosulfonimide salts as solute for polymer electrolytes.
114. P. Johansson, S. P. Gejji, J. Tegenfeldt, J. Lindgren, Electrochim. Acta 1998, 43, 1375-1379. The imide ion: Potential energy surface and geometries.
115. I. Rey, P. Johansson, J. Lindgren, J. C. Lassègues, J. Grondin, L. Servant, J. Phys. Chem. A 1998, 102, 3249-3258. Spectroscopic and theoretical study of $(CF_3SO_2)_2N^-$ ($TFSI^-$) and $(CF_3SO_2)_2NH$ (HTFSI).
116. S. P. Gejji, C. H. Suresh, K. Babu, S. R. Gadre, J. Phys. Chem. A 1999, 103, 7474-7480. Ab initio structure and vibrational frequencies of $(CF_3SO_2)_2N^-Li^+$ ion pairs.
117. L. Xue, C. W. Padgett, D. D. DesMarteau, W. T. Pennington, Solid State Sci. 2002, 4, 1535-1545. Synthesis and structures of alkali metal salts of bis[(trifluoromethyl)sulfonyl]imide.
118. D. Benrabah, R. Arnaud, J.-Y. Sanchez, Electrochim. Acta 1995, 40, 2437-2443. Comparative ab initio calculations on several salts.
119. W. A. Henderson, F. McKenna, M. A. Khan, N. R. Brooks, V. G. Young Jr., R. Frech, Chem. Mater. 2005, 17, 2284-2289. Glyme-lithium bis(trifluoromethanesulfonyl)imide and glyme-lithium bis(perfluoroethanesulfonyl)imide phase behavior and solvate structures.
120. M. G. Davidson, P. R. Raithby, A. L. Johnson, P. D. Bolton, Eur. J. Inorg. Chem. 2003, 18, 3445-3452. Structural diversity in Lewis-base complexes of lithium triflamide.
121. D. Brouillette, D. E. Irish, N. J. Taylor, G. Perron, M. Odziemkowski, J. E. Desnoyers, Phys. Chem. Chem. Phys. 2002, 4, 6063-6071. Stable solvates in solution of lithium bis(trifluoromethylsulfone)imide in glymes and other aprotic solvents: Phase diagrams, crystallography and Raman spectroscopy.
122. Q. Zhou, P. D. Boyle, L. Malpezzi, A. Mele, J.-H. Shin, S. Passerini, W. A. Henderson, Chem. Mater. 2011, 23, 4331-4337. Phase behavior of ionic liquid-LiX mixtures: Pyrrolidinium cations and $TFSI^-$ anions - Linking structure to transport properties.
123. J. L. Nowinski, P. Lightfoot, P. G. Bruce, J. Mater. Chem. 1994, 4, 1579–1580. Structure of $LiN(CF_3SO_2)_2$, A novel salt for electrochemistry.
124. W. A. Henderson, D. M. Seo, Q. Zhou, P. D. Boyle, J.-H. Shin, H. C. De Long, P. C. Trulove, S. Passerini, Adv. Energy Mater. 2012, 2, 8014-8019. An alternative ionic conductivity mechanism for plastic crystalline salt–lithium salt electrolyte mixtures.

125. A. Chagnes, B. Carré, P. Willmann, D. Lemordant, J. Power Sources 2002, 109, 203-213. Modeling viscosity and conductivity of lithium salts in γ-butyrolactone.
126. S. Steudte, J. Neumann, U. Bottin-Weber, M. Diedenhofen, J. Arning, P. Stepnowski, S. Stolte, Green Chem. 2012, 14, 2474-2483. Hydrolysis study of fluoroorganic and cyano-based ionic liquid anions – consequences for operational safety and environmental stability.
127. J. L. Goldman, A. B. McEwen, Electrochem. Solid-State Lett. 1999, 2, 501-503. EMIIm and EMIBeti on aluminum. Anodic stability dependence on lithium salt and propylene carbonate.
128. B. Garcia, M. Armand, J. Power Sources 2004, 132, 206-208. Aluminium corrosion in room temperature molten salt.
129. R.-S. Kühnel, M. Lübke, M. Winter, S. Passerini, A. Balducci, J. Power Sources 2012, 214, 178-184. Suppression of aluminum current collector corrosion in ionic liquid containing electrolytes.
130. C. Peng, L. Yang, Z. Zhang, K. Tachibana, Y. Yang, J. Power Sources 2007, 173, 510-517. Anodic behavior of Al current collector in 1-alkyl-3-methylimidazolium bis[(trifluoromethyl) sulfonyl] amide ionic liquid electrolytes.
131. C. Peng, L. Yang, Z. Zhang, K. Tachibana, Y. Yang, S. Zhao, Electrochim. Acta 2008, 53, 4764-4772. Investigation of the anodic behavior of Al current collector in room temperature ionic liquid electrolytes.
132. J. L. Allen, D. W. McOwen, S. A. Delp, E. T. Fox, J. S. Dickmann, S.-D. Han, Z.-B. Zhou, T. R. Jow, W. A. Henderson, J. Power Sources 2013, 237, 104-111. *N*-Alkyl-*N*-methylpyrrolidinium difluoro(oxalato)borate ionic liquids: Physical/electrochemical properties and Al corrosion.
133. D. W. McOwen, D. M. Seo, O. Borodin, J. Vatamanu, P. D. Boyle, W. A. Henderson, Energy Environ. Sci. 2014, 7, 416-426. Concentrated electrolytes: Decrypting electrolyte properties and reassessing Al corrosion mechanisms.
134. D. M. Seo, O. Borodin, Sang-Don Han, Q. Ly, P. D. Boyle, W. A. Henderson, J. Electrochem. Soc. 2012, 159, A553-A565. Electrolyte solvation and ionic association. I. Acetonitrile-lithium salt mixtures: Intermediate and highly associated salts.
135. D. M. Seo, O. Borodin, S.-D. Han, P. D. Boyle, W. A. Henderson, J. Electrochem. Soc. 2012, 159, A1489-A1500. Electrolyte solvation and ionic association. II. Acetonitrile-lithium salt mixtures: Highly dissociated salts.
136. D. M. Seo, O. Borodin, D. Balogh, M. O'Connell, Q. Ly, S.-D. Han, S. Passerini, W. A. Henderson, J. Electrochem. Soc. 2013, 160, A1061-A1070. Electrolyte solvation and ionic association. III. Acetonitrile-lithium salt mixtures—Transport properties.
137. D. M. Seo, P. D. Boyle, O. Borodin, W. A. Henderson, RSC Adv. 2012, 2, 8014-8019. Li^+ cation coordination by acetonitrile—Insights from crystallography.
138. D. M. Seo, P. D. Boyle, W. A. Henderson, Acta Crystallogr. 2011, E67, m1148. Tetrakis(acetonitrile-kN)lithium hexafluoridophosphate acetonitrile monosolvate.
139. D. M. Seo, P. D. Boyle, W. A. Henderson, Acta Crystallogr. 2011, E67, m534. Poly[bis(acetonitrile-*κN*) bis[μ_3-bis(trifluoromethanesulfonyl)imido-κ_4O, O':O'':O''']dilithium].
140. Y. Yokota, V. G. Young Jr., J. G. Verkade, Acta Crystallogr. 1999, C55, 196-198. The homoleptic lithium complex $[Li(CH_3CN)_4]ClO_4$.
141. D. M. Seo, P. D. Boyle, J. L. Allen, S.-D. Han, E. Jónsson, P. Johansson, W. A. Henderson, J. Phys. Chem. C 2013, in-press. Solvate structures and computational/spectroscopic characterization of $LiBF_4$ electrolytes.
142. D. M. Seo, P. D. Boyle, W. A. Henderson, Acta Crystallogr. 2011, E67, m547. Poly[[(acetonitrile)-lithium(I)]-μ_3-tetrafluoridoborato].
143. W. A. Alves, Vib. Spectrosc. 2007, 44, 197-200. Vibrational spectroscopic and conductometric studies of lithium battery electrolyte solutions.
144. W. Huang, R. Frech, P. Johansson, J. Lindgren, Electrochim. Acta 1995, 40, 2147-2151. Cation-polymer interaction and ionic association in diglyme-$LiCF_3SO_3$ and diglyme-propylene carbonate-$LiCF_3SO_3$ complexes.
145. J. Grondin, D. Talaga, J.-C. Lassègues, W. A. Henderson, Phys. Chem. Chem. Phys. 2004, 6, 938-944. Raman study of crystalline solvates between glymes $CH_3(OCH_2CH_2)nOCH_3$ (n = 1, 2 and 3) and $LiClO_4$.

146. J. Grondin, J.-C. Lassègues, M. Chami, L. Servant, D. Talaga, W. A. Henderson, Phys. Chem. Chem. Phys. 2004, 6, 4260-4267. Raman study of tetraglyme–$LiClO_4$ solvate structures.
147. S.-D. Han, J. L. Allen, E. Jonsson, P. Johansson, D. W. McOwen, P. D. Boyle, W. A. Henderson, J. Phys. Chem. C 2013, 117, 5521-5531. Solvate structures and computational/spectroscopic characterization of lithium difluoro(oxalato)borate (LiDFOB) electrolytes.
148. W. A. Henderson, J. Phys. Chem. B 2006, 110, 13177-13183. Glyme-lithium salt phase behavior.
149. Y. Matsuda, M. Morita, F. Tachihara, Bull. Chem. Soc. Jpn. 1986, 59, 1967-1973. Conductivity of lithium salts in the mixed systems of high permittivity solvents and low viscosity solvents.
150. Y. Matsuda, M. Morita, K. Yamada, K. Hirai, J. Electrochem. Soc. 1985, 132, 2538-2543. Characteristics of sulfolane-based electrolytes for rechargeable lithium batteries.
151. M. Morita, F. Tachihara, Y. Matsuda, Electrochim. Acta 1987, 32, 299-305. Dimethyl sulfoxide-based electrolytes for rechargeable lithium batteries.
152. Y. Matsuda, M. Morita, J. Power Sources 1987, 20, 273-278. Organic electrolyte solutions for rechargeable lithium batteries.
153. M. Morita, Y. Matsuda, J. Power Sources 1987, 20, 299-304. Effect of solvent blending on cycling characteristics of lithium.
154. Y. Sasaki, H. Miura, K. Tominaga, N. Nanbu, Electrochemistry 2002, 70, 334-336. Electrolytic properties and application to a lithium battery of ternary solvent electrolytes with ethylene carbonate - dimethyl carbonate - 3-methylsydnone and 3-ethylsydnone.
155. G. Moumouzias, G. Ritzoulis, D. Siapkas, D. Terzidis, J. Power Sources 2003, 122, 57-66. Comparative study of $LiBF_4$, $LiAsF_6$, $LiPF_6$, and $LiClO_4$ as electrolytes in propylene carbonate-diethyl carbonate solutions for Li/$LiMn_2O_4$ cells.
156. H.-B. Han, S.-S. Zhou, D.-Z. Zhang, S.-W. Feng, L.-F. Li, K. Liu, W.-F. Feng, J. Nie, H. Li, X.-J. Huang, M. Armand, Z.-B. Zhou, J. Power Sources 2011, 196, 3623-3632. Lithium bis(fluorosulfonyl)imide (LiFSI) as conducting salt for nonaqueous liquid electrolytes for lithium-ion batteries: Physicochemical and electrochemical properties.
157. L. P. Klemann, G. H. Newman, J. Electrochem. Soc. 1981, 128, 13-18. $LiB(CH_3)_4$-dioxolane electrolyte in rechargeable Li/TiS cells.
158. W. E. Rhine, G. Stucky, S. W. Peterson, J. Am. Chem. Soc. 1975, 97, 6401-6406. Stereochemistry of polynuclear compounds of the main group elements. A neutron and x-ray diffraction investigation of lithium-hydrogen-carbon interactions in $LiB(CH_3)_4$.
159. A. Haag, G. Hesse, Liebigs Ann. Chem. 1971, 751, 95-108. Uber die umsetzung von lithium-tetraalkylboranaten mit alkylierungsmitteln.
160. H. H. Horowitz, J. I. Haberman, L. P. Klemann, G. H. Newman, E. L. Stogryn, T. A. Whitney, Proc. Electrochem. Soc. 1981, 81–4, 131-143. The anodic oxidation stability of lithium electrolytes.
161. L. P. Klemann, G. H. Newman, U.S. Patent 4,060,674, 1977. Alkali metal anode-containing cells having electrolytes of organometallic-alkali metal salts and organic solvents.
162. L. P. Klemann, G. H. Newman, E. L. Stogryn, U.S. Patent 4,139,681, 1978. Electrochemical cells having alkali metal anodes and electrolyte salt complex compositions including halo-organometallic alkali metal salt complexes.
163. P. K. Bakshi, S. V. Sereda, O. Knop, Can. J. Chem. 1994, 72, 2144-2152. Crystal chemistry of tetraradial species. Part 6. Embarras de richesses: Lithium cation coordinated by eight 0-H…phenyl bonds.
164. J. M. Butler, G. M. Gray, J. Chem. Crystallogr. 2002, 32, 171-175. Diaquo(1,2-dimethoxyethane)lithium tetraphenylborate.
165. H. Schödel, T. Vaupel, H. Bock, Acta Crystallogr. 1996, C52, 637-640. Lithium tetraphenylborate·2THF·$2H_2O$.
166. B. Wilde, A. Jaenschke, F. Olbrich, Z. Anorg. Allg. Chem. 2008, 634, 166-172. Komplexe der alkalimetalltetraphenylborate mit makrocyclischen kronenethern.
167. W. A. Henderson, N. R. Brooks, W. W. Brennessel, V. G. Young Jr., Chem. Mater. 2003, 15, 4679-4684. Triglyme-Li^+ cation solvate structures: Models for amorphous concentrated liquid and polymer electrolytes (I).

168. W. A. Henderson, N. R. Brooks, V. G. Young Jr., J. Am. Chem. Soc. 2003, 125, 12098-12099. Single-crystal structures of polymer electrolytes.
169. Y. Sasaki, S. Sekiya, M. Handa, K. Usami, J. Power Sources 1999, 79, 91-96. Chelate complexes with boron as lithium salts for lithium battery electrolytes.
170. V. Gutmann, H. J. Emeléus, J. Chem. Soc. 1950, 1046-1050. The preparation of hexafluoroniobates, hexafluorotantalates, and hexafluorobismuthates by means of bromine trifluoride.
171. B. Cox, J. Chem. Soc. 1956, 876-878. Complex fluorides. Part IV. The structural chemistry of complex fluorides of the general formula ABF_6.
172. V. T. Kalinnikov, Y. I. Balabanov, L. A. Agulyanskaya, A. I. Agulyanskii, Y. A. Serebryakov, Zh. Obshch. Khim. 1984, 54, 1929-1932. Physicochemical study of the reaction of lithium metatantalate with ammonium hydrogen difluoride.
173. E. G. Rakov, M. V. Melkumyants, V. F. Sukhoverkhov, Zh. Neorg. Khim. 1990, 35, 1123-1126. Reaction of lithium niobate and tantalate with bromine trifluoride.
174. J.-H. Kim, S. Yonezawa, M. Takashima, J. Fluor. Chem. 2006, 127, 1054-1057. Reaction between LiF and MF_5 (M = Ta, Nb) in a fluorine atmosphere.
175. V. R. Koch, L. A. Dominey, J. L. Goldman, M. E. Langmuir, J. Power Sources 1987, 20, 287-291. New anions as supporting electrolytes for rechargeable lithium batteries.
176. C. Nanjundiah, J. L. Goldman, L. A. Dominey, V. R. Koch, J. Electrochem. Soc. 1988, 135, 2914-2917. Electrochemical stability of lithium M hexafluoride (M = P, As, Sb) in tetrahydrofuran and sulfolane.
177. V. R. Koch, J. Electrochem. Soc. 1979, 126, 181-187. Reactions of tetrahydrofuran and lithium hexafluoroarsenate with lithium.
178. M. Alamgir, K. M. Abraham, J. Appl. Electrochem. 1994, 24, 288-297. Studies to improve the Li/SO_2Cl_2 cell.
179. W. L. Bowden, J. S. Miller, D. Cubbison, A. N. Dey, J. Electrochem. Soc. 1984, 131, 1768-1772. New electrolyte salts for $Li/SOCl_2$ cells.
180. K. A. Klinedinst, R. A. gary, J. Electrochem. Soc. 1987, 134, 1884-1890. Performance and abuse resistance of a high-rate prismatic lithium/sulfuryl chloride cell.
181. T. J. Lee, P. C. Yao, G. T.-K. Fey, J. Power Sources 1991, 35, 143-151. Raman and ^7Li NMR spectroscopic studies of Li/SO_2 rechargeable cells.
182. W. P. Kilroy, C. Schlakikjer, P. Polsonetti, M. Jones, J. Power Sources 1993, 43–44, 715-723. Optimized lithium oxyhalide cells.
183. M. M. Morrison, N. Marincic, J. Power Sources 1993, 45, 343-352. Studies in lithium oxyhalide cells for downhole instrumentation. Use of lithium tetrachlorogallate electrolyte in $Li/SOC1_2$ cells.
184. M. Goledzinowski, R. J. Doré, I. R. Hill, J. Power Sources 1995, 54, 356-361. Cyclic voltammetric and Raman spectroscopic studies of the $Li/LiAlCl_4/SO_2$ and $Li/LiGaCl_4/SO_2$ rechargeable systems.
185. I. R. Hill, B. G. Anderson, M. Goledzinowski, R. J. Doré, J. Electrochem. Soc. 1995, 142, 3267-3273. Investigations of the chemistry of rechargeable Li/SO_2 cells containing retrachlorometallate:SO_2 electrolytes.
186. W. C. West, A. Shevade, J. Soler, J. Kulleck, M. C. Smart, B. V. Ratnakumar, M. Moran, R. Haiger, K. O. Christie, G. K. Surya Prakash, J. Electrochem. Soc. 2010, 157, A571-A577. Sulfuryl and thionyl halide-based ultralow temperature primary batteries.
187. J. Dreher, B. Haas, G. Hambitzer, J. Power Sources 1993, 43–44, 583-587. Rechargeable $LiCoO_2$ in inorganic electrolyte solution.
188. C. P. Park, S. M. Oh, J. Power Sources 1997, 68, 338-343. Performances of Li/Li_xCoO_2 cells in $LiAlCl_4{\cdot}3SO_2$ electrolyte.
189. K. Sonoda, A. Ueda, K. Iwamoto, Eur. Patent Appl. EP 1174941 A2, 2002. Non-aqueous electrolyte and electrochemical device comprising the same.
190. Z.-B. Zhou, M. Takeda, T. Fujii, M. Ue, J. Electrochem. Soc. 2005, 152, A351-A356. $Li[C_2F_5BF_3]$ as an electrolyte salt for 4 V class lithium-ion cells.

191. G. Pawelke, H. Bürger, Coord. Chem. Rev. 2001, 215, 243-266. Perfluoroalkyl borates: Congeners of perfluoroalkanes.
192. M. Ue, T. Fujii, Z.-B. Zhou, M. Takeda, S. Kinoshita, Solid State Ionics 2006, 177, 323-331. Electrochemical properties of $Li[C_nF_{2n+1}BF_3]$ as electrolyte salts for lithium-ion cells.
193. Z.-B. Zhou, M. Takeda, M. Ue, J. Fluor. Chem. 2003, 123, 127-131. Novel electrolyte salts based on perfluoroalkyltrifluoroborate anions 1. Synthesis and characterization.
194. E. Bernhardt, G. Henkel, H. Willner, G. Pawelke, H. Bürger, Chem. Eur. J. 2001, 7, 4696-4705. Synthesis and [properties of the tetrakis(trifluoromethyl)borate anion, $[B(CF_3)_4]^-$: Structure determination of $Cs[B(CF_3)_4]$ by single-crystal x-ray diffraction.
195. T. Kubota, M. Adachi, S. Fujita, Eur. Patent Appl. EP 1465267 A2, 2004. Battery with specified electrolyte.
196. S. S. Zhang, J. Power Sources 2008, 180, 586-590. $LiBF_3Cl$ as an alternative salt for the electrolyte of Li-ion batteries.
197. H.-J. Frohn, H. Franke, P. Fritzen, V. V. Bardin, J. Organomet. Chem. 2000, 598, 127-135. (Fluoroorgano)fluoroboranes and -fluoroborates I: Synthesis and spectroscopic characterization of potassium fluoroaryltrifluoroborates and fluoroaryldifluoroboranes.
198. H. S. Lee, X.-Q. Yang, J. McBreen, Int. Patent WO 2011/031401 A2, 2011. Lithium nonfluorinated and fluorinated phenyl trifluoro borate salts for non-aqueous battery electrolytes.
199. A. G. Massey, A. J. Park, J. Org. Chem. 1964, 2, 245-250. Perfluorophenyl derivatives of the elements. I. Tris(pentafluorophenyl)boron.
200. B. Zhang, M. Köberl, A. Pöthig, M. Cokoja, W. A. Hermann, F. E. Kühn, Z. Naturforsch. 2012, 67b, 1030-1036. Synthesis and characterization of imidazolium salts with the weakly coordinating $[B(C_6F_5)_4]^-$ anion.
201. M. Kuprat, M. Lehmann, A. Schulz, A. Villinger, Organometallics 2010, 29, 1421-1427. Synthesis of pentafluorophenyl silver by means of Lewis Acid catalysis: Structure of silver solvent complexes.
202. E. Zygadło-Monikowska, Z. Florjańczyk, J. Ostrowska, P. Bołtromiuk, J. Frydrych, W. Sadurski, N. Langwald, Electrochim. Acta 2011, 57, 66-73. Synthesis and characterization of new trifluoroalkoxyborates lithium salts of ionic liquid properties.
203. F. Kita, H. Sakata, A. Kawakami, H. Kamizori, T. Sonoda, H. Nagashima, N. V. Pavlenko, Y. L. Yagupolskii, J. Power Sources 2001, 97–98, 581-583. Electronic structures and electrochemical properties of $LiPF_{6-n}(CF_3)_n$.
204. A. Omaru, T. Nirasawa, Eur. Patent Appl. EP1318562 A2, 2002. Secondary battery and electrolyte used therefore.
205. R. Oesten, U. Heider, M. Schmidt, Solid State Ionics 2002, 148, 391-397. Advanced electrolytes.
206. J. S. Gnanaraj, E. Zinigrad, L. Asraf, M. Spreche, H. E. Gottlieb, W. Geissler, M. Schmidt, D. Aurbach, Electrochem. Commun. 2003, 5, 946-951. On the use of $LiPF_3(CF_2CF_3)_3$ (LiFAP) solutions for Li-ion batteries. Electrochemical and thermal studies.
207. J. S. Gnanaraj, E. Zinigrad, M. D. Levi, D. Aurbach, M. Schmidt, J. Power Sources 2003, 119–121, 799-904. A comparison among $LiPF_6$, $LiPF_3(CF_2CF_3)_3$ (LiFAP), and $LiN(SO_2CF_2CF_3)_2$ (LiBETI) solutions: Electrochemical and thermal studies.
208. J. S. Gnanaraj, M. D. Levi, Y. Gofer, D. Aurbach, M. Schmidt, J. Electrochem. Soc. 2003, 150, A445-A454. $LiPF_3(CF_2CF_3)_3$: A salt for rechargeable lithium ion batteries.
209. E. Zinigrad, L. Larush-Asraf, J. S. Gnanaraj, H. E. Gottieb, M. Sprecher, D. Aurbach, J. Power Sources 2005, 146, 176. Calorimetric studies of the thermal stability of electrolyte solutions based on alkyl carbonates and the effect of the contact with lithium.
210. S. Tsujioka, T. Mitsui, K. Kondo, A. Fujiwara, Int. Patent WO 2010122867 A1, 2010. Electrolyte for electrochemical device, electrolyte solution using same, and nonaqueous electrolyte battery.
211. B. Zhang, M. Köberl, A. Pöthig, M. Cokoja, W. A. Herrmann, F. E. Kühn, Z. Naturforsch. 2012, 67b, 1030-1036. Synthesis and characterization of imidazolium salts with the weakly coordinating $[B(C_6F_5)_4]^-$ anion.

212. M. Kuprat, M. Lehmann, A. Schulz, A. Villinger, Organometallics 2010, 29, 1421-1427. Synthesis of pentafluorophenyl silver by means of Lewis Acid catalysis: Structure of silver solvent complexes.
213. M. Bolte, I. Ruderfer, T. Müller, Acta Crystallogr. 2005, E61, m1581-m1582. Lithium–tetrakis(pentafluorophenyl)borate–benzene (1/1/2).
214. L. P. Klemann, G. H. Newman, T. A. Whitney, E. L. Stogryn, D. Farcasiu, Proc. Electrochem. Soc. 1981, 81–4, 79-88. Investigations of anion structure in lithium tetraorganoborate salts - steps toward the design of an organic electrolyte.
215. T. Aoki, T. Fujinami, J. Electrochem. Soc. 2005, 152, A2352-A2356. Lithium ion conductivity of polymer electrolytes based on insoluble lithium tetrakis(pentafluorobenzenethiolato) borate and poly(ethylene oxide).
216. T. Aoki, A. Konno, T. Fujinami, J. Power Sources 2005, 146, 412-417. Polymer electrolytes composed of lithium tetrakis(pentafluorobenzenethiolato)borate and poly(fluoroalkylcarbon) s.
217. X. Zhang, U. Gross, K. Seppelt, Angew. Chem. Int. Ed. Engl. 1995, 34, 1858-1860. Fluorocarbonate, $[FCO_2]^-$: Preparation and structure.
218. M. Hojo, T. Ueda, H. Hamada, Z. Chen, S. Umetani, J. Mol. Liq. 2009, 145, 24-32. Conductometric studies on higher ion-aggregation from lithium fluoroalkanoates in propylene carbonate and *N*,*N*-dimethylformamide.
219. F. Kita, H. Sakata, S. Sinomoto, A. Kawakami, H. Kamizori, T. Sonoda, H. Nagashima, J. Nie, N. V. Pavlenko, Y. L. Yagupolskii, J. Power Sources 2000, 90, 27-32. Characteristics of the electrolyte with fluoro organic lithium salts.
220. G. Nagasubramanian, D. H. Shen, S. Surampudi, Q. Wang, G. K. Surya Prakash, Electrochim. Acta 1995, 40, 2277-2280. Lithium superacid salts for secondary lithium batteries.
221. F. Kita, A. Kawakami, J. Nie, T. Sonoda, H. Kobayashi, J. Power Sources 1997, 68, 307-310. On the characteristics of electrolytes with new lithium imide salts.
222. S. A. Ullrich, G. L. Gard, R. L. Nafshun, M. M. Lerner, J. Fluor. Chem. 1996, 79, 33-38. Lithium salts of bis (perfluoroalkyl) sulfonic acids: synthesis, characterization and conductivity studies.
223. C. Chauvin, F. Alloin, P. Judeinstein, C. P. del Valle, J.-Y. Sanchez, ChemPhysChem 2006, 7, 1921-1929. NMR and electrochemical study on lithium oligoether sulfate in polymeric and liquid electrolytes.
224. C. Chauvin, X. Ollivrin, F. Alloin, J.-F. LeNest, J.-Y. Sanchez, Electrochim. Acta 2005, 50, 3843-3852. Lithium salts based on oligoether sulfate esters.
225. W. M. Lamanna, A. Xiao, M. J. Triemert, P. T. Pham, Int. Patent Appl. WO 2012170240 A1, 2012. Lithium ion electrochemical cells including fluorocarbon electrolyte additives.
226. P. Sartori, G. Bauer, J. Fluor. Chem. 1978, 12, 203-210. 2,3,5,6-Tetrafluorbenzoldisulfonsäure aus pentafluorbenzolsulfonsäure.
227. M. B. Herath, S. E. Creager, A. Kitaygorodskiy, D. D. DesMarteau, ChemPhysChem 2010, 11, 2871-2878. Perfluoroalkyl phosphonic and phosphinic acids as proton conductors for anhydrous proton-exchange membranes.
228. W. Lange, Ber. Dtsch. Chem. Ges. 1929, 62B, 793-801. Monofluorophosphoric acid and the similarity between its salts and the sulfates.
229. W. Lange, Ber. Dtsch. Chem. Ges. 1927, 60B, 962-970. The resemblance of the fluorosulfonates to the perchlorates in chemical and crystallographic relationships, and a fluorophosphate.
230. U. Schülke, R. Kayser, Z. Anorg. Allg. Chem. 1991, 600, 221-226. Herstellung von fluorophosphaten, difluorophosphaten, fluorophosphonaten und fluorophosphiten in fluoridhaltigen harnstoffschmelzen.
231. G. A. Bukhalova, I. V. Mardirosova, Izv. An. SSR Neorg. Mater. 1966, 2, 2015-2019. Complex formation in binary systems of alkali metal fluorides and metaphosphates.
232. F. W. Bennett, H. J. Emeléus, R. N. Haszeldine, J. Chem. Soc. 1954, 3598-3603. Organometallic and organometalloidal fluorine compounds. Part X. Trifluoromethylphosphonous and -phosphonic acids.

233. R. C. Thompson, W. Reed, Nucl. Chem. Lett. 1969, 5, 581-585. Preparation and infrared spectra of alkali metal difluorophosphates.
234. P. Vast, A. Semmoud, A. Addou, G. Palavit, J. Fluor. Chem. 1988, 38, 297-302. Etude methodologique de la synthese des difluorodioxophosphates metalliques a partir de l'oxyde du difluorure de phosphoryle.
235. W. Lange, Ber. Dtsch. Chem. Ges. 1929, 62B, 786-792. Difluophosphoric acid and formation from it of salts similar to those of perchloric acid.
236. W. Traube, J. Hoerenz, F. Wunderlich, Ber. Dtsch. Chem. Ges. 1918, 52B, 1272-1284. Fluorosulfonic acid, fluorosulfonates and sulfuryl fluoride.
237. V. I. Sirenko, V. D. Prisyazhnyi, T. A. Zmievskaya, A. A. Kramarenko, Russ. J. Electrochem. 1999, 35, 1133-1136. Aprotic electrolytes containing lithium fluorosulfonate.
238. A. Bałkowska, G. Szymański, L. Werblan, J. Electroanal. Chem. 1990, 287, 229-238. Conductivities of lithium salts in a mixed solvent: Comparison of conductance equations for their analysis.
239. Z. Žák, M. Kosiŭka, Acta Crystallogr. 1978, B34, 38-40. The crystal structure of lithium fluorosulphaste $LiSO_3F$.
240. R. N. Haszeldine, J. M. Kidd, J. Chem. Soc. 1954, 4228-4232. Polyfluoroalkyl derivatives of sulfur. Part I. Trifluoromethanesulfphonic acid.
241. T. Gramstad, R. N. Haszeldine, J. Chem. Soc. 1956, 173-180. Perfluoroalkyl derivatives of sulphur. Part IV. Perfluoroalkanesulphonic acids.
242. T. J. Brice, P. W. Trott, U.S. Patent 2,732398, 1956. Fluorocarbon sulfonic acids and derivatives.
243. W. H. Tiedemann, D. N. Bennion, J. Chem. Engr. Data 1971, 16, 368-370. Density, viscosity, and conductivity of lithium triflormethanesulfonate solutions in dimethylsulfite.
244. T. Fujinaga, I. Sakamoto, Pure Appl. Chem. 1980, 52, 1387-1396. Electrochemical characteristics of trifluoromethanesulfphonic acid and its salts in non-aqueous solvents.
245. M. Tremayne, P. Lightfoot, M. A. Mehta, P. G. Bruce, K. D. M. Harris, K. Shankland, C. J. Gilmore, G. Bricogne, J. Solid State Chem. 1992, 100, 191-196. Ab initio structure determination of $LiCF_3SO_3$ from X-ray powder diffraction data using entropy maximization and likelihood ranking.
246. M. Bolte, H.-W. Lerner, Acta Crystallogr. 2001, E57, m231-m232. Lithium trifluoromethanesulfonate.
247. R. Dinnebier, N. Sofina, M. Jansen, Z. Anorg. Allg. Chem. 2004, 630, 1613-1616. The structure of the high temperature modification of lithium triflate (γ-$LiSO_3CF_3$).
248. G. Hirankumar, C. Iojoiu, F. Alloin, J. Y. Sanchez, T. Pagnier, J. Raman. Spectrosc. 2007, 38, 1570-1576. Dissociation of $C_6F_5SO_3Li$ in two organic solvents with different dielectric constants: A Raman spectroscopic study.
249. H. Falius, Angew. Chem., Int. Ed. 1970, 9, 733-734. Simple synthesis of phosphorofluoridous acid, $H[PHO_2F]$.
250. R. N. Haszeldine, Angew. Chem. 1954, 693-728. Neuere chemie des fluors. Organometall- und organometalloid-verbindungen des fluors.
251. H. J. Emeléus, R. N. Haszeldine, R. C. Paul, J. Chem. Soc. 1955, 563-574. Organometallic and organometalloidal fluorine compounds. Part XII. Bistrifluoromethylphos-phinic acid and related phosphorus oxy-acids.
252. S. Furukawa, S. Yoshimura, M. Takahashi, Jap. Patent JP 03040372, 1991. Nonaqueous lithium batteries with new electrolytes.
253. K. W. Oliver, S. J. Rettig, R. C. Thompson, J. Trotter, S. Xia, J. Fluor. Chem. 1997, 83, 47-50. Synthesis of perfluorodiphenylphosphinic acid and its potassium and oxonium salts; Crystal structure of oxonium perfluorodiphenylphosphinate.
254. G. H. Sprenger, K. J. Wright, J. M. Shreeve, Inorg. Chem. 1973, 12, 2890-2893. Polar additions of chlorine monofluoride and chlorine fluorosulfate to fluorinated isocyanates.
255. H. W. Roesky, Angew. Chem. Int. Ed. 1969, 8, 510. 3,5-Bis(trifluorornethyl)-1,2,4, 6-thiatriaza-2,5-cyclohexadiene-1,1-dione.
256. F. Ye, R. E. Noftle, J. Fluor. Chem. 1997, 81, 193-196. Preparation of fluorinated imides.
257. F. Ye, R. E. Noftle, D. D. DesMarteau, Syn. Met. 1993, 60, 141-144. Preparation and properties of conducting polypyrrole doped with fluorinated imides.

258. B. Mandal, T. Sooksimuang, B. Griffin, A. Padhi, R. Filler, Solid State Ionics 2004, 175, 267-272. New lithium salts for rechargeable battery electrolytes.
259. L. Conte, G. P. Gambaretto, G. Caporiccio, F. Alessandrini, S. Passerini, J. Fluor. Chem. 2004, 125, 243-252. Perfluoroalkanesulfonylimides and their lithium salts: Synthesis and characterisation of intermediates and target compounds.
260. A. Vij, R. L. Kirchmeier, J. M. Shreeve, R. D. Verma, Coord. Chem. Rev. 1997, 158, 413-432. Some fluorine-containing nitrogen acids and their derivatives.
261. M. Beran, J. Příhoda, J. Taraba, Polyhedron, 2010, 29, 991-994. A new route to the syntheses of *N*-(fluorosulfuryl)fulfonamide salts: Crystal structure of Ph_4P^+ $[CF_3SO_2NSO_2F]^-$.
262. W. Xianming, E. Yasukawa, S. Kasuya, Electrochim. Acta 2001, 46, 813-819. Electrochemical properties of tetrahydropyran-based ternary electrolytes for 4 V Lithium metal rechargeable batteries.
263. K. Kubota, J. Matsumoto, Chem. Lett. 2011, 40, 1105-1106. Melting and crystallization behaviors of alkali metal (fluorosulfonyl)(trifluoromethylsulfonyl)amides.
264. R. D. Howells, W. M. Lamanna, A. D. Fanta, J. E. Waddell, Int. Patent Appl. WO 97/23448, 1997. Preparation of bis(fluoroalkylenesulfonyl) imides and (fluoroalkylsulfonyl) (fluorosulfonyl) imides.
265. R. D. Howells, W. M. Lamanna, A. D. Fanta, J. E. Waddell, U.S. Patent WO 5,874,616, 1999. Preparation of bis(fluoroalkylenesulfonyl) imides and (fluoroalkylsulfonyl) (fluorosulfonyl) imides.
266. H. V. Venkatasetty, Annual Battery Conference on Applications and Advances, 16th, Long Beach, CA, United States, Jan. 9-12, 2001, 277-282. New and novel lithium imide electrolytes and copolymers: Synthesis and characterization for lithium rechargeable batteries.
267. H. W. Roesky, H. H. Giere, Inorg. Nucl. Chem. Lett. 1971, 7, 171-175. Sulfur-nitrogen compounds. 33. Preparation of *N*-(trifluoromethylsulfonyl)sulfamoyl fluoride and some reactions.
268. H. V. Venkatasetty, J. Power Sources 2001, 97–98, 671-673. Novel superacid-based lithium electrolytes for lithium ion and lithium polymer rechargeable batteries.
269. W. M. Lamana, L. J. Krause, J. W. Summerfield, Int. Patent WO 9711504 A1, 1997. Battery containing bis(perfluoroalkylsulfonyl)imide and cyclic perfluoroalkylenedisulfonylimide.
270. W. Gorecki, C. Roux, M. Clémancey, M. Armand, E. Belorizky, ChemPhysChem 2002, 620-625. NMR and conductivity study of polymer electrolytes in the imide family: P(EO)/ $Li[N(SO_2CnF_{2n+1})(SO_2C_mF_{2m+1})]$.
271. J. A. Roderiguez, R. E. Noftle, Inorg. Chem. 1971, 10, 1874-1877. The reaction of fluorosulfuryl isocyanate with alkali metal fluorides.
272. R. E. Noftle, J. W. Green, S. K. Yarbro, J. Fluor. Chem. 1976, 7, 221-227. Reaction of fluorosulfuryl isocyanate with group IIb metal fluorides.
273. H. Matsumoto, H. Sakaebe, K. Tatsumi, J. Power Sources 2005, 146, 45-50. Preparation of room temperature ionic liquids based on aliphatic onium cations and asymmetric amide anions and their electrochemical properties as a lithium battery electrolyte.
274. M. B. Herath, S. E. Creager, R. V. Rajagopal, O. E. Geiculescu, D. D. DesMarteau, Electrochim. Acta 2009, 54, 5877-5883. Ionic conduction in polyether-based lithium arylfluorosulfonimide ionic melt electrolytes.
275. S. Hamrock, P. Pham, Int. Patent Appl. WO 98/50349, 1997. Fluorinated sulphonamide and sulphone derivatives.
276. A. Chakrabarti, R. Filler, B. Mandal, ECS Trans. 2007, 6, 77-88. Synthesis and characterization of a new class of mono-lithium salts for PEO-based solid polymer electrolytes.
277. B. K. Mandal, R. Filler, J. Fluor. Chem. 2005, 126, 845-848. New fluorine-containing plasticized low lattice energy lithium salt for plastic batteries.
278. R. J. Koshar, Eur. Patent EP 57327 A1, 1982. Cyclic perfluoroaliphatic disulfonimides.
279. L. J. Krause, J. W. Summerfield, U.S. Patent 5,691,081, 1997. Battery containing bis(perfluoroalkylsulfonyl)imide and cyclic perfluoroalkulene disulfonylimide salts.
280. H. W. Roesky, A. Hoff, Chem. Ber. 1968, 101, 162-173. Darstellung und untersuchung von fluorsulfurylverbindungen.

281. J. Taraba, Z. Žak, Acta Crystallogr. 2004, C60, o79-o81. The polysulfonylamines bis(methylsulfonamido) sulfone and bis(trifluoromethylsulfonamido) sulfone.
282. R. Appel, H. Rittersbacher, Chem. Ber. 1964, 97, 849-851. Reaction of sulfuryl diisocyanate with halosulfuric acids. A simple method for the preparation of fluorosulfonyl isocyanate and imidobis(sulfuryl fluoride).
283. Z.-B. Zhou, H. Han, J. Nie, W. Song, H. Zhang, Chin. Patent CN 102786443, 2012. Dibasic or tribasic fluoro-containing sulfonylimide alkaline metal salt and ionic liquid, and application thereof.
284. O. E. Geiculescu, Y. Xie, R. Rajagopal, S. E. Creager, D. D. DesMarteau, J. Fluor. Chem. 2004, 125, 1179-1185. Dilithium bis[(perfluoroalkyl)sulfonyl]diimide salts as electrolytes for rechargeable lithium batteries.
285. R. Jüschke, M. Koeckerling, P. Sartori, Z. Naturforsch. B 1998, 53, 135-144. Synthesis of novel lithium salts with doubly charged anions for secondary batteries.
286. K. Luo, R. Filler, B. K. Mandal, Solid State Ionics 2006, 177, 857-861. Synthesis and characterization of novel non-fluorinated tri-lithium imide salts for use in lithium-ion battery electrolytes.
287. A. Chakrabarti, R. Filler, B. K. Mandal, Solid State Ionics 2010, 180, 1640-1645. Synthesis and properties of a new class of fluorine-containing dilithium salts for lithium-ion batteries.
288. W. Buckendahl, O. Glemser, Chem. Ber. 1977, 110, 1154-1158. Some substitution reactions of nitrogen-sulfur-chlorine compounds.
289. H. W. Roesky, W. Schmieder, W. Isenberg, W. S. Sheldrick, G. M. Sheldrick, Chem. Ber. 1982, 115, 2714-2727. Anions of sulfur with the coordination number 3: Synthesis, structure, and range of existence.
290. H. W. Roesky, W. G. Böwing, J. Chem. Soc. Chem. Comm. 1975, 735-736. Preparation and x-ray structure of sulfur-nitrogen oxides.
291. C. Jäckh, W. Sundermeyer, Chem. Ber. 1973, 106, 1752-1757. Darstellung und reaktionen von carbonylhalogeniden und -pseudohalogeniden.
292. D. Schomburg, A. Blaschette, S. Kassomenakis, Z. Anorg. Allg. Chem. 1991, 604, 47-51. Polysulfonyl amines. XXVI. A polymeric lithium amide with alternating tetra- and hexacoordinate lithium atoms: Crystal structure of lithium dimesylamide monohydrate.
293. S. Ukawa, Y. Yamamoto, Jap. Patent JP 2005209523 A, 2005. Lithium batteries inhibiting self discharge under high-temperature environment, and their electrolytes.
294. O. Moers, A. Blaschette, J. G. Jones, Z. Anorg. Allg. Chem. 2002, 628, 2086-2090. Polysulfonylamines. Part 161. Crystal structures of metal di(methanesulfonyl)amides. Part 8. A surprising pair of isostructural compounds. Crystal structure of $AgNa[(CH_3SO_2)_2N]_2{\cdot}H_2O$ and space-group revision for $Li[(CH_3SO_2)_2N]{\cdot}H_2O$.
295. A. Blaschette, K. H. Nagel, P. G. Jones, Z. Naturforsch. B 1994, 49, 36-42. Polysulfonylamines. LIV. (12-Crown-4)lithium dimesylamide-acetonitrile (3/2): A crystal with two fundamentally different conformations of the same coronand.
296. J. M. Pringle, J. Golding, K. Baranyai, C. M. Forsyth, G. B. Deacon, J. L. Scott, D. R. MacFarlane, New J. Chem. 2003, 27, 1504-1510. The effect of anion fluorination in ionic liquids—physical properties of a range of bis(methanesulfonyl)amide salts.
297. A. Scozzafava, M. D. Banciu, A. Popescu, C. T. Supuran, J. Enzym. Inhib. 2000, 15, 443-453. Carbonic anhydrase inhibitors: Inhibition of isozymes I, II and IV by sulfamide and sulfamic acid derivatives: 85.
298. Z.-B. Zhou, H. Han, J. Nie, W. Song, H. Zhang, Chin. Patent CN 102786443, 2012. Dibasic or tribasic fluoro-containing sulfonylimide alkaline metal salt and ionic liquid, and application thereof.
299. R. Y. Garlyauskayte, A. N. Chernega, C. Michot, M. Armand, Y. L. Yagupolskii, L. M. Yagupolskii, Org. Biomol. Chem. 2005, 3, 2239-2243. Synthesis of new organic super acids—*N*-(trifluoromethylsulfonyl)imino derivatives of trifluoromethanesulfonic acid and bis(trifluoromethylsulfonyl)imide.
300. J. Foropoulos Jr., D. D. DesMarteau, J. Am. Chem. Soc. 1982, 104, 4260-4261. Bis[bis-(trifluoromethanesulfonyl)imido]xenon: A new compound possessing xenon-nitrogen bonds.

301. J. Foropoulos Jr., D. D. DesMarteau, Inorg. Chem. 1984, 23, 3720-3723. Synthesis, properties, and reactions of bis((trifluoromethyl)sulfonyl) imide, $(CF_3SO_2)_2NH$.
302. J. N. Meussdorffer, H. Niederprum, Chem. Ztg. 1972, 96, 582-583. Bis(perfluoralkanesulfonyl) imides $(R_fSO_2)_2NH$.
303. M. Armand, Int. Patent WO 90/11999, 1990. Process for the synthesis of sulfonylimidides.
304. J. Grondin, D. Talaga, J. C. Lassègues, P. Johansson, W. A. Henderson, J. Raman Spectrosc. 2007, 38, 53-60. Spectroscopic and ab initio characterization of the conformational states of the bis(perfluoroethanesulfonyl) imide anion ($BETI^-$).
305. W. A. Henderson, F. McKenna, M. A. Khan, N. R. Brooks, V. G. Young Jr., R. Frech, Chem. Mater. 2005, 17, 2284-2289. Glyme-lithium bis(trifluoromethanesulfonyl)imide and glyme-lithium bis(perfluoroethanesulfonyl)imide phase behavior and solvate structures.
306. P. Johansson, J. Tegenfeldt, J. Lindgren, J. Phys. Chem. A 2000, 104, 954-961. Vibrational spectroscopy and ab initio calculations on $[N(C_2F_5SO_2)_2]^-$ and the corresponding superacid $HN(C_2F_5SO_2)_2$.
307. K. Naoi, M. Mori, Y. Naruoka, W. M. Lamanna, R. Atanasoski, J. Electrochem. Soc. 1999, 146, 462-469. The surface film formed on a lithium metal electrode in a new imide electrolyte, lithium bis(perfluoroethylsulfonylimide) $[LiN(C_2F_5SO_2)_2]$.
308. C. Capiglia, Y. Saito, H. Kageyama, P. Mustarelli, T. Iwamoto, T. Tabuchi, H. Tukamoto, J. Power Sources 1999, 81–82, 859-862. ^7Li and ^{19}F diffusion coefficients and thermal properties of non-aqueous electrolyte solutions for rechargeable lithium batteries.
309. X. Wang, E. Yasukawa, S. Mori, J. Electrochem. Soc. 1999, 146, 3992-3998. Electrochemical behavior of lithium imide/cyclic ether electrolytes for 4 V lithium metal rechargeable batteries.
310. X. Wang, E. Yasukawa, S. Kasuya, J. Electrochem. Soc. 2000, 147, 2421-2426. Lithium imide electrolytes with two-oxygen-atom-containing cycloalkane solvents for 4 V lithium metal rechargeable batteries.
311. L. J. Krause, W. Lamanna, J. Summerfield, M. Engle, G. Korba, R. Loch, R. Atanasoski, J. Power Sources 1997, 68, 320-325. Corrosion of aluminum at high voltages in non-aqueous electrolytes containing perfluoroalkylsulfonyl imides; New lithium salts for lithium-ion cells.
312. L. Péter, J. Arai, J. Appl. Electrochem. 1999, 29, 1053-1061. Anodic dissolution of aluminium in organic electrolytes containing perfluoroalkylsulfonyl imides.
313. X. Wang, E. Yasukawa, S. Mori, Electrochim. Acta 2000, 45, 2677-2684. Inhibition of anodic corrosion of aluminum cathode current collector on recharging in lithium imide electrolytes.
314. L. J. Krause, J. W. Summerfield, U.S. Patent 5,691,081, 1997. Battery containing bis(perfluoroalkylsulfonyl)imide and cyclic perfluoroalkylene disulfonylimide salts.
315. K. Zaghib, P. Charest, A. Guerfi, J. Shim, M. Perrier, K. Striebel, J. Power Sources 2004, 134, 124-129. Safe Li-ion polymer batteries for HEV applications.
316. K. Zaghib, P. Charest, A. Guerfi, J. Shim, M. Perrier, K. Striebel, J. Power Sources 2005, 146, 380-385. $LiFePO_4$ safe Li-ion polymer batteries for clean environment.
317. M. Beran, J. Prihoda, Z. Zak, M. Cernik, Polyhedron 2006, 25, 1292-1298. A new route to the syntheses of alkali metal bis(fluorosulfuryl)imides: Crystal structure of $LiN(SO_2F)_2$.
318. A. Guerfi, S. Duchesne, Y. Kobayashi, A. Vijh, K. Zaghib, J. Power Sources 2008, 175, 866-873. $LiFePO_4$ and graphite electrodes with ionic liquids based on bis(fluorosulfonyl)imide $(FSI)^-$ for Li-ion batteries.
319. K. Kuboto, T. Nohira, T. Goto, R. Hagiwara, Electrochem. Commun. 2008, 10, 1886-1888. Novel inorganic ionic liquids possessing low melting temperatures and wide electrochemical windows: Binary mixtures of alkali bis(fluorosulfonyl)amides.
320. A. Abouimrane, J. Ding, I. J. Davidson, J. Power Sources 2009, 189, 693-696. Liquid electrolyte based on lithium bis-fluorosulfonyl imide salt: Aluminum corrosion studies and lithium ion battery investigations.
321. A. Guerfi, M. Gontigny, Y. Kobayashi, A. Vijh, K. Zaghib, J. Solid State Electrochem. 2009, 13, 1003-1014. Investigations on some electrochemical aspects of lithium-ion ionic liquid/gel polymer battery systems.

322. K. Kuboto, T. Nohira, R. Hagiwara, J. Chem. Engr. Data 2010, 55, 3142-3146. Thermal properties of alkali bis(fluorosulfonyl)amides and their binary mixtures.
323. A. S. Best, A. I. Bhatt, A. F. Hollehkamp, J. Electrochem. Soc. 2010, 157, A903-A911. Ionic liquids with the bis(fluorosulfonyl)imide anion: Electrochemical properties and applications in battery technology.
324. J. Huang, A. F. Hollenkamp, J. Phys. Chem. C 2010, 114, 21840-21847. Thermal behavior of ionic liquids containing the FSI anion and the Li^+ cation.
325. S. Tsuzuki, K. Hayamizu, S. Seki, J. Phys. Chem. B 2010, 114, 16329-16336. Origin of the low viscosity of [emim][$(FSO_2)_2N$] ionic liquid and its lithium salt mixture: Experimental and theoretical study of self-diffusion coefficients, conductivities, and intermolecular interactions.
326. K. Hiyamizu, S. Tsuzuki, S. Seki, K. Fujii, M. Suenaga, Y. Umebayashi, J. Chem. Phys. 2010, 133, 194505/1-194505/13. Studies on the translational and rotational motions of ionic liquids composed of *N*-methyl-*N*-propyl-pyrrolidinium (P13) cation and bis(trifluoromethanesulfonyl) amide and bis(fluorosulfonyl)amide anions and their binary systems including lithium salts.
327. L. Li, S. Zhou, H. Han, H. Li, J. Nie, M. Armand, Z. Zhou, X. Huang, J. Electrochem. Soc. 2011, 158, A74-A82. Transport and electrochemical properties and spectral features of non-aqueous electrolytes containing LiFSI in linear carbonate solvents.
328. S. Seki, K. Takei, H. Miyashiro, M. Watanabe, J. Electrochem. Soc. 2011, 158, A769-A774. Physicochemical and electrochemical properties of glyme-$LiN(SO_2F)_2$ complex for safe lithium-ion secondary battery electrolyte.
329. M. Nadherna, J. Reiter, J. Moskon, R. Dominko, J. Power Sources 2011, 196, 7700-7706. Lithium bis(fluorosulfonyl)imide-PYR_{14}TFSI ionic liquid electrolyte compatible with graphite.
330. K. Hayamizu, S. Tsuzuki, S. Seki, Y. Umebayashi, J. Chem. Phys. 2011, 135, 084505/1-084505/11. Nuclear magnetic resonance studies on the rotational and translational motions of ionic liquids composed of 1-ethyl-3-methylimidazolium cation and bis(trifluoromethanesulfonyl)amide and bis(fluorosulfonyl)amide anions and their binary systems including lithium salts.
331. K. Kubota, T. Nohira, R. Hagiwara, Electrochim. Acta 2012, 66, 320-324. New inorganic ionic liquids possessing low melting temperatures and wide electrochemical windows: Ternary mixtures of alkali bis(fluorosulfonyl)amides.
332. J. Reiter, M. Nadherna, R. Dominko, J. Power Sources 2012, 205, 402-407. Graphite and $LiCo_{1/3}Mn_{1/3}Ni_{1/3}O_2$ electrodes with piperidinium ionic liquid and lithium bis(fluorosulfonyl) imide for Li-ion batteries.
333. G. G. Eshetu, S. Grugeon, G. Gachot, D. Mathiron, M. Armand, S. Laruelle, Electrochim. Acta 2013, 102, 133-141. LiFSI vs. $LiPF_6$ electrolytes in contact with lithiated graphite: Comparing thermal stabilities and identification of specific SEI-reinforcing additives.
334. R. Appel, G. Eisenhauer, Chem. Ber. 1962, 95, 246-248. The synthesis of $HN(SO_2F)_2$.
335. C. Michot, M. Armand, J.-Y. Sanchez, Y. Choquette, M. Gauthier, Int. Patent WO 95/26056, 1995. Ionic conducting material having good anticorrosive properties.
336. K. Kubota, T. Nohira, R. Hagiwara, H. Matsumoto, Chem. Lett. 2010, 39, 1303-1304. Thermal properties of alkali (fluorosulfonyl)(trifluoromethylsulfonyl)amides.
337. H. Han, J. Guo, D. Zhang, S. Feng, W. Feng, J. Nie, Z. Zhou, Electrochem. Commun. 2011, 13, 265-168. Lithium (fluorosulfonyl)(nonafluorobutanesulfonyl)imide (LiFNFSI) as conducting salt to improve the high-temperature resilience of lithium-ion cells.
338. H. Matsumoto, N. Terasawa, T. Umecky, S. Tsuzuki, H. Sakaebe, K. Asaka, K. Tatsumi, Chem. Lett. 2008, 37, 1020-1021. Low melting and electrochemically stable ionic liquids based on asymmetric fluorosulfonyl(trifluoromethylsulfonyl)amide.
339. J. V. Silverton, D. T. Gibson, Acta Crystallogr. 1965, 19, 651-658. The disordered crystal and molecular structure of tris(methylsulfonyl)methane.
340. G. Klöter, H. Pritzkow, K. Seppelt, Angew. Chem. Int. Ed. Engl. 1980, 19, 942. Tris(fluorosulfonyl)methane, $HC(SO_2F)_3$.

341. F. Alloin, J.-Y. Sanchez, J. Power Sources 1999, 81–82, 795-803. Electrochemical investigation of organic salts in polymeric and liquid electrolytes.
342. P. Johansson, J. Phys. Chem. A 2001, 105, 9258-9264. Ab initio structures and vibrational spectra of $Li[C(CF_3SO_2)_3]$ and $Li[CH(CF_3SO_2)_2]$.
343. C. W. Walker Jr., J. D. Cox, M. Salomon, J. Electrochem. Soc. 1996, 143, L80-L82. Conductivity and electrochemical stability of electrolytes containing organic solvent mixtures with lithium tris(trifluoromethanesulfonyl)methide.
344. Y. L. Yagupolskii, T. I. Savina, Zh. Obshch. Khim. 1983, 19, 79-81. Methanetrisulfonic acid derivatives.
345. Y. L. Yagupolskii, T. I. Savina, Zh. Obshch. Khim. 1985, 21, 2048-2054. Aryl ethers of the aci-forms of methanetrisulfonyl trifluoride and their reactions.
346. Y. L. Yagupolskii, I. I. Gerus, T. I. Savina, Zh. Obshch. Khim. 1988, 24, 73-77. Addition of methanetris(sulfonyl fluoride) to unsaturated compounds.
347. Y. L. Yagupolskii, T. I. Savina, I. I. Gerus, R. K. Orlova, Zh. Obshch. Khim. 1990, 26, 2030-2031. New Friedel-Crafts reaction catalyst: tris(fluorosulfonyl)methane.
348. Y. L. Yagupolskii, T. I. Savina, N. O. Pavlenko, A. A. Pankov, S. V. Pazenok, Zh. Obshch. Khim. 1991, 61, 1512-1518. Tris(fluorosulfonyl)methanide $-C(SO_2F)_3$ - an effective stabilizing nonnucleophilic carbanion.
349. P. Burk, I. A. Koppel, J. Tapfer, F. Anvia, R. W. Taft, J. Mol. Struct. 1994, 121, 191-196. Theoretical study of prototropic tautomerism and acidity of tris(fluorosulfonyl)methane.
350. G. Klöter, H. Pritzkow, K. Seppelt, Angew. Chem. Int. Ed. 1980, 19, 942. Tris(fluorosulfonyl) methane, $HC(SO_2F)$.
351. Y. L. Yagupolskii, W. Tyrra, R. Gnann, N. Maggiarosa, D. Naumann, J. Fluor. Chem. 2002, 113, 143-146. 2,6-Difluorophenylxenon(II)bis(fluorsulfonyl)amid, -bis(trifluormethylsulfonyl)amid, -tris(fluorsulfonyl)methanid und -bis(trifluormethylsulfonyl)methanid-neue C-Xe-N- und C-Xe-C-verbindungen?
352. L. Turowsky, K. Seppelt, Inorg. Chem. 1988, 27, 2135-2137. Tris((trifluoromethyl)sulfonyl)-methane, $HC(SO_2CF_3)_3$.
353. D. Aurbach, O. Chusid, I. Weissman, P. Dan, Electrochim. Acta 1996, 41, 747-760. $LiC(SO_2CF_3)_3$, a new salt for Li battery systems. A comparative study of Li and non-active metal electrodes in its ethereal solutions using in situ FTIR spectroscopy.
354. R. Arnaud, D. Benrabah, J.-Y. Sanchez, J. Phys. Chem. 1996, 100, 10882-10891. Theoretical study of CF_3SO_3Li, $(CF_3SO_2)_2NLi$, and $(CF_3SO_2)_2CHLi$ ion pairs.
355. T. Gramstad, R. N. Haszeldine, J. Chem. Soc. 1957, 4069-4079. Perfluoroalkyl derivatives of sulphur. Part VII. Alkyl trifluoromethanesulphonates as alkylating agents, trifluoromethanesulphonic anhydride as a promoter for esterification, and some reactions of trifluoromethanesulphonic acid.
356. R. J. Koshar, R. A. Mitsch, J. Org. Chem. 1973, 38, 3358-3363. Bis(perfluoroalkylsulfonyl) methanes and related disulfones.
357. D. D. Desmarteau, W. T. Pennington, K. S. Sung, S. Z. Zhu, R. Scott, Eur. J. Solid State Inorg. Chem. 1991, 28, 905-917. Novel layered structures in metal salts of bis(sulfonyl)methanes.
358. D. Benrabah, D. Baril, J.-Y. Sanchez, M. Armand, G. G. Gard, J. Chem. Soc. Faraday Trans. 1993, 89, 355-359. Comparative electrochemical study of new poly(oxyethylene)-Li salt complexes.
359. N. R. Holcomb, P. G. Nixon, G. L. Gard, R. L. Nafshun, M. M. Lerner, J. Electrochem. Soc. 1996, 143, 1297-1300. Synthesis of $LiCH(SO_2CF_3)_2$ and ionic conductivity of polyether-saIt complexes.
360. R. Jüschke, P. Häsel, P. Sartori, J. Fluor. Chem 1998, 91, 9-12. Comparative study of physical properties of bis(trifluoromethylsulfonyl) dihalogenomethanes and bis(fluorosulfonyl) dihalogenomethanes.
361. J. Scheers, E. Jonsson, P. Jacobsson, P. Johansson, Electrochemistry 2012, 80, 18-25. Novel lithium imides; Effects of -F, $-CF_3$, and $-C\equiv N$ substituents on lithium battery salt stability and dissociation.

362. E. Fluck, E. Beuerle, Z. Anorg. Allg. Chem. 1975, 412, 65-70. Bis(difluorophosphoryl)amine and some *N*-derivatives.
363. Z.-B. Zhou, H. Han, J. Nie, Chin. Patent CN 101654229, 2010. Method for preparation of fluorine-containing sulfonimide (phosphonimide) and its alkali metal salt.
364. E. Fluck, E. Beuerle, Z. Anorg. Allg. Chem. 1975, 412, 65-70. Bis(difluorophosphoryl)amine and some *N*-derivatives.
365. D. Bejan, H. Willner, N. Ignatiev, C. W. Lehmann, Inorg. Chem. 2008, 47, 9085-9089. Synthesis and characterization of bis[bis(pentafluoroethyl)phosphinyl]imides, $M^+N[(C_2F_5)_2P(O)]_2^-$, M = H, Na, K, Cs, Ag, Me_4N.
366. L. Kling III, C. B. Colburn, W. E. Hill, Inorg. Nucl. Chem. - Herbert H. Hyman Mem. Vol. 1976, 5-7. The reactions of phosphorus fluorides with lithium bis(trimethylsilyl)amide.
367. T. L. Charlton, R. G. Cavell, Inorg. Chem. 1970, 9, 379-387. Preparation and properties of some oxygen-, sulfur-, and nitrogen-bridged phosphoryl and thiophosphoryl difluorides.
368. A. Schmidpeter, H. Groeger, Z. Anorg. Allg. Chem. 1966. 345, 106-118. Über phosphazene. II. Darstellung und struktur der tetraphenyl-dithio-imidodiphosphinsäure.
369. M. Hernández-Arganis, S. Hernández-Ortega, R. A. Toscano, V. García-Montalvo, R. Cea-Olivares, Chem. Commun. 2004, 310-311. A powerful novel strategy for the preparation of discrete inorganic carbon-free rings containing alkaline cations.
370. F. Chen, M. Kapon, J. D. Woollins, M. S. Eisen, Organometallics 2009, 28, 2391-2400. Bis(imidodithiodiphosphinato) titanium and zirconium complexes: Synthesis, characterization, and their catalytic activity in the polymerization of α-olefins.
371. I. Ghesner, C. palotas, A. Silvestru, C. Silvestru, J. E. Drake, Polyhedron 2001, 20, 1101-1105. Lithium tetraorganodichalcogenoimidodiphosphinates. Crystal structure of $[Li\{(OPPh_2)(SPMe_2)N\}\cdot 2H_2O]_2$, a dimer formed through oxygen-bridging phosphorus ligands.
372. J. Barthel, M. Wühr, R. Buestrich, H. J. Gores, J. Electrochem. Soc. 1995, 142, 2527-2531. A new class of electrochemically and thermally stable lithium salts for lithium battery electrolytes I. Synthesis and properties of lithium bis[1,2-benzenediolato(2-)-O,O']borate.
373. J. Barthel, R. Buestrich, H. J. Gores, M. Schmidt, M. Wühr, J. Electrochem. Soc. 1997, 144, 3866-3870. A new class of electrochemically and thermally stable lithium salts for lithium battery electrolytes IV. Investigations of the electrochemical oxidation of lithium organoborates.
374. M. Handa, S. Fukuda, Y. Sasaki, K. Usami, J. Electrochem. Soc. 1997, 144, L235-L237. Use of a chelate complex with boron as a lithium salt for lithium battery electrolytes.
375. Y. Sasaki, M. Handa, S. Sekiya, K. Kurashima, K. Usami, J. Power Sources 2001, 97–98, 561-565. Application to lithium battery electrolyte of lithium chelate compound with boron.
376. Z.-M. Xue, J.-F. Zhao, J. Ding, C.-H. Chen, J. Power Sources 2010, 195, 853-856. LBDOB, a new lithium salt with benzenediolato and oxalato complexes of boron for lithium battery electrolytes.
377. Z.-M. Xue, W. Zhou, J. Ding, C.-H. Chen, Electrochim. Acta 2010, 55, 5342-5348. Electronic structures and molecular properties of FLBDOB and its derivatives: A combined experimental and theoretical study.
378. M. Handa, M. Suzuki, J. Suzuki, H. Kanematsu, Y. Sasaki, Electrochem. Solid-State Lett. 1999, 2, 60-62. A new lithium salt with a chelate complex of phosphorus for lithium battery electrolytes.
379. J. Barthel, R. Buestrich, E. Carl, H. J. Gores, J. Electrochem. Soc. 1996, 143, 3565-3571. A new class of electrochemically and thermally stable lithium salts for lithium battery electrolytes II. Conductivity of lithium organoborates in dimethoxyethane and propylene carbonate.
380. Z.-M. Xue, C.-Q. Ji, W. Zhou, C.-H. Chen, J. Power Sources 2010, 195, 3689-3692. A new lithium salt with 3-fluoro-1,2-benzenediolato and oxalato complexes of boron for lithium battery electrolytes.
381. J. Barthel, R. Buestrich, E. Carl, H. J. Gores, J. Electrochem. Soc. 1996, 143, 3572-3575. A new class of electrochemically and thermally stable lithium salts for lithium battery electrolytes III. Synthesis and properties of some lithium organoborates.

382. Z.-M. Xue, K.-N. Wu, B. Liu, C.-H. Chen, J. Power Sources 2007, 171, 944-947. New lithium salts with croconato-complexes of boron for lithium battery electrolytes.
383. Z.-M. Xue, Y.-Z. Ding, C.-H. Chen, Electrochim. Acta 2007, 53, 990-997. A DFT study of electronic structures, energies, and molecular properties of lithium bis[croconato]borate and its derivatives.
384. O. Hiruta, M. Mizutani, Y. Takeuchi, Y. Ukyo, K. Kaneko, S. Iida, K. Torii, Jap. Patent JP 2009266644 A, 2009. Nonaqueous electrolyte solutions and lithium ion secondary batteries.
385. W. Xu, L.-M. Wang, R. A. Nieman, C. A. Angell, J. Phys. Chem. B 2003, 107, 11749-11756. Ionic liquids of chelated orthoborates as model ionic glassformers.
386. J. Barthel, M. Schmidt, H. J. Gores, J. Electrochem. Soc. 1998, 145, L17-L20. Lithium bis[5-fluoro-2-olato-1-benzenesulfonato (2-)-O,O']borate(l-), a new anodically and cathodically stable salt for electrolytes of lithium-ion cells.
387. J. Barthel, A. Schmid, H. J. Gores, J. Electrochem. Soc. 2000, 147, 21-24. A new class of electrochemically and thermally stable lithium salts for lithium battery electrolytes V. Synthesis and properties of lithium bis[2,3-pyridinediolato(2-)-O,O´]borate.
388. H. Schafer, Z. Anorg. Chem. 1949, 259, 86-91. Boric acid and hydroxy compounds. IV. New salts of dipyrocatechol boric acid.
389. A. Downard, M. Nieuwenhuyzen, K. R. Seddon, J.-A. van den Berg, Cryst. Growth Des. 2002, 2, 111-119. Structural features of lithium organoborates.
390. S. Tsujioka, H. Takase, M. Takahashi, H. Sugimoto, Jap. Patent JP 2001247306 A, 2001. Synthesis and purification of ionic metal complexes.
391. S. Tsujioka, H. Takase, M. Takahashi, H. Sugimoto, Jap. Patent JP 2001302675 A, 2001. Preparation of lithium bis(oxalato)borate as ionic metal complex.
392. S. Tsujioka, H. Takase, M. Takahashi, Y. Isono, Eur. Patent EP 1308449 A2, 2003. Preparation of lithium (alkanoato)borates and (alkanoato)phosphates.
393. W. Xu, C. A. Angell, Electrochem. Solid-State Lett. 2001, 4, E1-E4. LiBOB and its derivatives. Weakly coordinating anions, and the exceptional conductivity of their nonaqueous solutions.
394. K. Xu, S. Zhang, T. R. Jow, W. Xu, C. A. Angell, Electrochem. Solid-State Lett. 2002, 5, A26-A29. LiBOB as salt for lithium-ion batteries.
395. K. Xu, S. Zhang, B. A. Poese, T. R. Jow, Electrochem. Solid-State Lett. 2002, 5, A259-A262. Lithium bis(oxalato)borate stabilizes graphite anode in propylene carbonate.
396. K. Xu, S. Zhang, T. R. Jow, Electrochem. Solid-State Lett. 2003, 6, A117-A120. Formation of the graphite/electrolyte interface by lithium bis(oxalato)borate.
397. K. Xu, U. Lee, S. Zhang, M. Wood, T. R. Jow, Electrochem. Solid-State Lett. 2003, 6, A144-A148. Chemical analysis of graphite/electrolyte interface formed in LiBOB-based electrolytes.
398. T. R. Jow, M. S. Ding, K. Xu, S. S. Zhang, J. L. Allen, K. Amine, G. L. Henriksen, J. Power Sources 2003, 119–121, 343-348. Nonaqueous electrolytes for wide-temperature-range operation of Li-ion cells.
399. J. Jiang, J. R. Dahn, Electrochem. Solid-State Lett. 2003, 6, A180-A182. Comparison of the thermal stability of lithiated graphite in LiBOB EC/DEC and in $LiPF_6$ EC/DEC.
400. J. Jiang, J. R. Dahn, Electrochem. Commun. 2004, 6, 39-43. ARC studies of the thermal stability of three different cathode materials: $LiCoO_2$; $Li[Ni_{0.1}Co_{0.8}Mn_{0.1}]O_2$; and $LiFePO_4$, in $LiPF_6$ and LiBoB EC/DEC electrolytes.
401. P. Y. Zavalij, S. Yang, M. S. Whittingham, Acta Crystallogr. 2003, B59, 753-759. Structures of potassium, sodium and lithium bis(oxalato)borate salts from powder diffraction data.
402. Y. Aihara, T. Bando, H. Nakagawa, H. Yoshida, K. Hayamizu, E. Akiba, W. S. Price, J. Electrochem. Soc. 2004, 151, A119-A122. Ion transport properties of six lithium salts dissolved in γ-butyrolactone studied by self-diffusion and ionic conductivity measurements.
403. Z. Chen, J. R. Dahn, Electrochim. Acta 2004, 49, 1079-1090. Methods to obtain excellent capacity retention in $LiCoO_2$ cycled to 4.5 V.
404. J. Jiang, H. Fortier, J. N. Reimers, J. R. Dahn, J. Electrochem. Soc. 2004, 151, A609-A613. Thermal stability of 18650 size Li-ion cells containing LiBOB electrolyte salt.

405. J. Jiang, J. R. Dahn, Electrochim. Acta 2004, 49, 2661-2666. Effects of particle size and electrolyte salt on the thermal stability of $Li_{0.5}CoO_2$.
406. K. Amine, J. Liu, S. Kang, I. Belharouak, Y. Hyung, D. Vissers, G. Hendriksen, J. Power Sources 2004, 129, 14-19. Improved lithium manganese oxide spinel/graphite Li-ion cells for high-power applications.
407. J. Jiang, J. R. Dahn, Electrochem. Commun. 2004, 6, 724-728. ARC studies of the reaction between Li_0FePO_4 and $LiPF_6$ or LiBOB EC/DEC electrolytes.
408. J. Jiang, J. R. Dahn, Electrochim. Acta 2004, 49, 4599-4604. Effects of solvents and salts on the thermal stability of LiC_6.
409. G. V. Zhang, K. Xu, T. R. Jow, P. N. Ross Jr. Electrochem. Solid-State Lett. 2004, 7, A224-A227. Study of SEI layer formed on graphite anodes in PC/LiBOB electrolyte using IR spectroscopy.
410. K. Xu, U. Lee, S. Zhang, J. L. Allen, T. R. Jow, Electrochem. Solid-State Lett. 2004, 7, A273-A277. Graphite/electrolyte interface formed in LiBOB-based electrolytes.
411. T. R. Jow, K. Xu, M. S. Ding, S. S. Zhang, J. L. Allen, K. Amine, J. Electrochem. Soc. 2004, 151, A1702-A1706. LiBOB-based electrolytes for Li-ion batteries for transportation applications.
412. J. Jiang, J. Chen, J. R. Dahn, J. Electrochem. Soc. 2004, 151, A2082-A2087. Comparison of the reactions between $Li_{7/3}Ti_{5/3}O_4$ or LiC_6 and nonaqueous solvents or electrolytes using accelerating rate calorimetry.
413. K. Xu, U. Lee, S. Zhang, J. L. Allen, T. R. Jow, J. Electrochem. Soc. 2004, 151, A2106-A2112. Graphite/electrolyte interface formed in LiBOB-based electrolytes.
414. M. S. Ding, J. Electrochem. Soc. 2005, 152, A132-A140. Conductivity and viscosity of PC-DEC and PC-EC solutions of LiBOB.
415. H.-G. Schweiger, M. Multerer, U. Wietelmann, J.-C. Panitz, T. Burgermeister, H. J. Gores, J. Electrochem. Soc. 2005, 152, A622-A627. NMR determination of trace water in lithium salts for battery electrolytes.
416. K. Xu, S. Zhang, R. Jow, J. Power Sources 2005, 143, 197-202. Electrochemical impedance study of graphite/electrolyte interface formed in LiBOB/PC electrolyte.
417. K. Amine, J. Liu, I. Belharouak, Electrochem. Commun. 2005, 7, 669-673. High-temperature storage and cycling of C-$LiFePO_4$/graphite Li-ion cells.
418. K. Xu, S. Zhang, T. R. Jow, Electrochem. Solid-State Lett. 2005, 8, A365-A368. LiBOB as additive in $LiPF_6$-based lithium ion electrolytes.
419. M. S. Ding, T. R. Jow, J. Electrochem. Soc. 2005, 152, A1199-A1207. Properties of PC-EA solvent and its solution of LiBOB comparison of linear esters to linear carbonates for use in lithium batteries.
420. K. Amine, J. Liu, I. Belharouak, S.-H. Kang, I. Bloom, D. Vissers, G. Henriksen, J. Power Sources 2005, 146, 111-115. Advanced cathode materials for high-power applications.
421. H. Kaneko, K. Sekine, T. Takamura, J. Power Sources 2005, 146, 142-145. Power capability improvement of LiBOB/PC electrolyte for Li-ion batteries.
422. K. Striebel, J. Shim, A. Sierra, H. Yang, X. Song, R. Kostecki, K. McCarthy, J. Power Sources 2005, 146, 33-38. The development of low cost $LiFePO_4$-based high power lithium-ion batteries.
423. K. Xu, S. S. Zhang, U. Lee, J. L. Allen, T. R. Jow, J. Power Sources 2005, 146, 79-85. LiBOB: Is it an alternative salt for lithium ion chemistry?
424. B.-T. Yu, W.-H. Qiu, F.-S. Li, G.-X. Xu, Electrochem. Solid-State Lett. 2006, 9, A1-A4. The electrochemical characterization of lithium bis(oxalato)borate synthesized by a novel method.
425. W. Larsson, J.-C. Panitz, A. Cedergren, Talanta 2006, 69, 276-280. Interference-free coulometric titration of water in lithium bis(oxalato)borate using Karl Fischer reagents based on Nmethylformamide.
426. J.-C. Panitz, U. Wietelmann, M. Wachtler, S. Stroebele, M. Wohlfahrt-Mehrens, J. Power Sources 2006, 153, 396-401. Film formation in lithium bis(oxalato)borate-containing electrolytes.
427. K. Amine, Q. Wang, D. R. Vissers, Z. Zhang, N. A. A. Rossi, R. West, Electrochem. Commun. 2006, 8, 429-433. Novel silane compounds as electrolyte solvents for Li-ion batteries.

428. S. S. Zhang, K. Xu, T. R. Jow, J. Power Sources 2006, 154, 276-280. LiBOB-based gel electrolyte Li-ion battery for high temperature operation.
429. Z. Chen, W. Q. Lu, J. Liu, K. Amine, Electrochim. Acta 2006, 51, 3322-3326. $LiPF_6$/LiBOB blend salt electrolyte for high-power lithium-ion batteries.
430. S. S. Zhang, K. Xu. T. R. Jow, J. Power Sources 2006, 156, 629-633. Enhanced performance of Li-ion cell with $LiBF_4$-PC based electrolyte by addition of small amount of LiBOB.
431. X. Zhang, T. M. Devine, J. Electrochem. Soc. 2006, 153, B365-B369. Passivation of aluminum in lithium-ion battery electrolytes with LiBOB.
432. S. S. Zhang, K. Xu, T. R. Jow, J. Power Sources 2006, 159, 702-707. An improved electrolyte for the $LiFePO_4$ cathode working in a wide temperature range.
433. S. Wang, W. Qiu, T. Li, B. Yu, H. Zhao, Int. J. Electrochem. Sci. 2006, 1, 250-257. Properties of lithium bis(oxalato)borate (LiBOB) as a lithium salt and cycle performance in $LiMn_2O_4$ half cell.
434. M. Wachtler, M. Wohlfahrt-Mehrens, S. Stroebele, J.-C. Panitz, U. Wietelmann, J. Appl. Electrochem. 2006, 36, 1199-1206. The behaviour of graphite, carbon black, and $Li_4Ti_5O_{12}$ in LiBOB-based electrolytes.
435. W. Lu, Z. Chen, H. Joachin, J. Prakash, J. Liu, K. Amine, J. Power Sources 2007, 163, 1074-1079. Thermal and electrochemical characterization of MCMB/$LiNi_{1/3}Co_{1/3}Mn_{1/3}O_2$ using LiBOB as an electrolyte additive.
436. B.-T. Yu, W.-H. Qiu, F.-S. Li, L. Cheng, J. Power Sources 2007, 166, 499-502. Comparison of the electrochemical properties of LiBOB and $LiPF_6$ in electrolytes for $LiMn_2O_4$/Li cells.
437. S. Wang, W. Qiu, Y. Guan, B. Yu, H. Zhao, W. Liu, Electrochim. Acta 2007, 52, 4907-4910. Electrochemical characteristics of $LiM_xFe_{1-x}PO_4$ cathode with LiBOB based electrolytes.
438. E. Zinigrad, L. Larush-Asraf, G. Salitra, M. Sprecher, D. Aurbach, Thermochim. Acta 2007, 457, 64-69. On the thermal behavior of Li bis(oxalato)borate LiBOB.
439. N.-S. Choi, K. H. Yew, H. Kim, S.-S. Kim, W.-U. Choi, J. Power Sources 2007, 172, 404-409. Surface layer formed on silicon thin-film electrode in lithium bis(oxalato) borate-based electrolyte.
440. L. Larush-Asraf, M. Bliton, H. Teller, E. Zinigrad, D. Aurbach, J. Power Sources 2007, 174, 400-407. On the electrochemical and thermal behavior of lithium bis(oxalato)borate (LiBOB) solutions.
441. D.-T. Shieh, P.-H. Hsieh, M.-H. Yang, J. Power Sources 2007, 174, 663-667. Effect of mixed LiBOB and $LiPF_6$ salts on electrochemical and thermal properties in $LiMn_2O_4$ batteries.
442. J. Liu, Z. Chen, S. Busking, I. Belharouak, K. Amine, J. Power Sources 2007, 174, 852-855. Effect of electrolyte additives in improving the cycle and calendar life of graphite/$Li_{1.1}[Ni_{1/3}Co_{1/3}Mn_{1/3}]_{0.9}O_2$ Li-ion cells.
443. H. Xie, Z. Tang, Z. Li, Y. He, H. Wang, Y. Liu, Electrochem. Solid-State Lett. 2008, 11, C19-C22. Aluminum corrosion behavior of LiBOB in composite polymer electrolyte for Li-polymer batteries.
444. D. P. Abraham, M. M. Furczon, S.-H. Kang, D. W. Dees, A. N. Jansen, J. Power Sources 2008, 180, 612-620. Effect of electrolyte composition on initial cycling and impedance characteristics of lithium-ion cells.
445. J. C. Arrebola, A. Caballero, L. Hernan, J. Morales, J. Power Sources 2008, 183, 310-315. A high energy Li-ion battery based on nanosized $LiNi_{0.5}Mn_{1.5}O_4$ cathode material.
446. Y. Guo, Z. Yin, Z. Tao, X. Li, Z. Wang, J. Power Sources 2008, 184, 513-516. An advanced electrolyte for improving surface characteristics of $LiMn_2O_4$ electrode.
447. K. Xu, J. Electrochem. Soc. 2008, 155, A733-A738. Tailoring electrolyte composition for LiBOB.
448. M. Amereller, M. Multerer, C. Schreiner, J. Lodermeyer, A. Scmid, J. Berthel, H. J. Gores. J. Chem. Engr. Data 2009, 54, 468-471. Investigation of the hydrolysis of lithium bis[1,2-oxalato(2-)-O,O'] borate (LiBOB) in water and acetonitrile by conductivity and NMR measurements in comparison to some other borates.
449. K. Xu, B. Deveney, K. Nechev, Y. Lam, T. R. Jow, J. Electrochem. Soc. 2008, 155, A959-A964. Evaluating LiBOB/lactone electrolytes in large-format lithium-ion cells based on nickelate and iron phosphate.

450. Y. Abu-Lebdeh, I. Davidson, J. Electrochem. Soc. 2009, 156, A60-A65. High-voltage electrolytes based on adiponitrile for Li-ion batteries.
451. A. Xiao, L. Yang, B. L. Lucht, S.-H. Kang, D. P. Abraham, J. Electrochem. Soc. 2009, 156, A318-A327. Examining the solid electrolyte interphase on binder-free graphite electrodes.
452. J.-Y. Huang, X.-J. Liu, X.-L. Kang, Z.-X. Yu, T.-T. Xu, W.-H. Qiu, J. Power Sources 2009, 189, 458-461. Study on γ-butyrolactone for LiBOB-based electrolytes.
453. M.-Q. Li, M.-Z. Qu, X.-Y. He, Z.-L. Yu, Electrochim. Acta 2009, 54, 4506-4513. Effects of electrolytes on the electrochemical performance of Si/graphite/disordered carbon composite anode for lithium-ion batteries.
454. S. Santee, A. Xiao, L. Yang, J. Gnanaraj, B. L. Lucht, J. Power Sources 2009, 194, 1053-1060. Effect of combinations of additives on the performance of lithium ion batteries.
455. L. Yang, M. M. Furxzon, A. Xiao, B. L. Lucht, Z. Zhang, D. P. Abraham, J. Power Sources 2010, 195, 1698-1705. Effect of impurities and moisture on lithium bisoxalatoborate (LiBOB) electrolyte performance in lithium-ion cells.
456. B. Markovsky, F. Amalraj, H. E. Gottlieb, Y. Gofer, S. K. Surendra, D. Aurbach. J. Electrochem. Soc. 2010, 157, A423-A429. On the electrochemical behavior of aluminum electrodes in nonaqueous electrolyte solutions of lithium salts.
457. Z. Yu, T. Xu, T. Xing, L.-Z. Fan, F. Lian, Q. Qiu, J. Power Sources 2010, 195, 4285-4289. A Raman spectroscopy investigation of the interactions of LiBOB with γ-BL as electrolyte for advanced lithium batteries.
458. C. Täubert, M. Fleischhammer, M. Wohlfahrt-Mehrens, U. Wietelmann, T. Buhrmester, J. Electrochem. Soc. 2010, 157, A721-A728. LiBOB as electrolyte salt or additive for lithium-ion batteries based on $LiNi_{0.8}Co_{0.15}Al_{0.05}O_2$/graphite.
459. L. Yang, M. M. Furczon, A. Xiao, B. L. Lucht, Z. Zhang, D. P. Abraham, J. Power Sources 2010, 195, 1698-1705. Effect of impurities and moisture on lithium bisoxalatoborate (LiBOB) electrolyte performance in lithium-ion cells.
460. S. Dalavi, M. Xu, B. Ravdel, L. Zhou, B. L. Lucht, J. Electrochem. Soc. 2010, 157, A1113-A1120. Nonflammable electrolytes for lithium-ion batteries containing dimethyl methylphosphonate.
461. S.-T. Myung, H. Natsui, Y.-K. Sun, H. Yashiro, J. Power Sources 2010, 195, 8297-8301. Electrochemical behavior of Al in a non-aqueous alkyl carbonate solution containing LiBOB salt.
462. P. Ping, Q. Wang, J. Sun, X. Feng, C. Chen, J. Power Sources 2011, 196, 776-783. Effect of sulfites on the performance of LiBOB/γ-butyrolactone electrolytes.
463. P. Ping, Q. Wang, J. Sun, X. Feng, C. Chen, J. Electrochem. Soc. 2010, 157, A1170-A1176. Thermal stabilities of some lithium salts and their electrolyte solutions with and without contact to a $LiFePO_4$ electrode.
464. L. Yang, T. Markmaitree, B. L. Lucht, J. Power Sources 2011, 196, 2251-2254. Inorganic additives for passivation of high voltage cathode materials.
465. J. Dong, Z. Zhang, Y. Kusachi, K. Amine, J. Power Sources 2011, 196, 2255-2259. A study of tri(ethylene glycol)-substituted trimethylsilane (1NM3)/LiBOB as lithium battery electrolyte.
466. L.-Z. Fan, T. Xing, R. Awan, W. Qiu, Ionics 2011, 17, 491-494. Studies on lithium bis(oxalato) borate/propylene carbonate-based electrolytes for Li-ion batteries.
467. Y. Kusachi, J. Dong, Z. Zhang, K. Amine, J. Power Sources 2011, 196, 8301-8306. Tri(ethylene glycol)-substituted trimethylsilane/lithium bis(oxalate)borate electrolyte for $LiMn_2O_4$/graphite system.
468. K. Amine, Z. Chen, Z. Zhang, J. Liu, W. Lu, Y. Qin, J. Lu, L. Curtis, Y.-K. Sun, J. Mater. Chem. 2011, 21, 17754-17759. Mechanism of capacity fade of MCMB-$Li_{1.1}[Ni_{1/3}Mn_{1/3}Co_{1/3}]_{0.9}O_2$ cell at elevated temperature and additives to improve its cycle life.
469. Z. Chen, A. Jansen, K. Amine, Energy Environ. Sci. 2011, 4, 4567-4571. Novel functionalized electrolyte for MCMB/$Li_{1.156}Mn_{1.844}O_4$ lithium-ion cells.
470. M. C. Smart, F. C. Krause, C. Hwang, W. C. West, J. Soler, G. K. S. Prakash, B. V. Ratnakumar, ECS Trans. 2011, 35, 1-11. The evaluation of triphenyl phosphate as a flame retardant additive to improve the safety of lithium-ion battery electrolytes.

471. D.-J. Lee, J. Hassoun, S. Panero, Y.-K. Sun, B. Scrosati, Electrochem. Commun. 2012, 14, 43-46. A tetraethylene glycol dimethylether-lithium bis(oxalate)borate (TEGDME-LiBOB) electrolyte for advanced lithium ion batteries.
472. S. Dalavi, M. Xu, B. Knight, B. L. Lucht, Electrochem Solid-State Lett. 2012, 15, A28-A31. Effect of added LiBOB on high voltage ($LiNi_{0.5}Mn_{1.5}O_4$) spinel cathodes.
473. S. Xiong, X. Kai, X. Hong, Y. Diao, Ionics 2012, 18, 249-254. Effect of LiBOB as additive on electrochemical properties of lithium-sulfur batteries.
474. M. Cuisinier, J.-F. Martin, P. Moreau, T. Epicier, R. Kanno, D. Guyomard, N. Dupre, Solid St. Nuc. Mag. Res. 2012, 42, 51-61. Quantitative MAS NMR characterization of the $LiMn_{1/2}Ni_{1/2}O_2$ electrode/electrolyte interphase.
475. S. Li, Y. Zhao, X. Shi, B. Li, X. Xu, W. Zhao, X. Cui, Electrochim. Acta 2012, 65, 221-227. Effect of sulfolane on the performance of lithium bis(oxalato)borate-based electrolytes for advanced lithium ion batteries.
476. S. Li, B. Li, X. Xu, X. Shi, Y. Zhao, L. Mao, X. Cui, J. Power Sources 2012, 209, 295-300. Electrochemical performances of two kinds of electrolytes based on lithium bis(oxalate) borate and sulfolane for advanced lithium ion batteries.
477. S. Y. Li, X. L. Cui, X. L. Xu, X. M. Shi, G. X. Li, Russ. J. Electrochem. 2012, 48, 518-524. Quantitative MAS NMR characterization of the $LiMn_{1/2}Ni_{1/2}O_2$ electrode/electrolyte interphase.
478. M. C. Smart, B. L. Lucht, S. Dalavi, F. C. Krause, B. V. Ratnakumar, J. Electrochem. Soc. 2012, 159, A739-A751. The effect of additives upon the performance of MCMB/$LiNi_xCo_{1-x}O_2$ Li-ion cells containing methyl butyrate-based wide operating temperature range electrolytes.
479. M. Matsui, K. Dokko, Y. Akita, H. Munakata, K. Kanamura, J. Power Sources 2012, 210, 60-66. Surface layer formation of $LiCoO_2$ thin film electrodes in non-aqueous electrolyte containing lithium bis(oxalate)borate.
480. V. Aravindan, Y. L. Cheah, W. C. Ling, S. Madhavi, J. Electrochem. Soc. 2012, 159, A1435-A1439. Effect of LiBOB additive on the electrochemical performance of $LiCoPO_4$.
481. C. Li, Y. Zhao, H. Zhang, J. Liu, J. Jing, X. Cui, S. Li, Electrochim. Acta 2013, 104, 134-139. Compatibility between $LiNi_{0.5}Mn_{1.5}O_4$ and electrolyte based upon lithium bis(oxalate)borate and sulfolane for high voltage lithium-ion batteries.
482. X. Cui, H. Zhang, S. Li, Y. Zhao, L. Mao, W. Zhao, Y. Li, X. Ye, J. Power Sources 2013, 240, 476-485. Electrochemical performances of a novel high-voltage electrolyte based upon sulfolane and γ-butyrolactone.
483. Y. Zhu, Y. Li, M. Bettge, D. P. Abraham, Electrochim. Acta 2013, 110, 191–199. Electrolyte additive combinations that enhance performance of high-capacity $Li_{1.2}Ni_{0.15}Mn_{0.55}Co_{0.1}O_2$-graphite cells.
484. W. Xu, A. J. Shuysterman, M. Videa, V. Velikov, R. Marzke, C. A. Angell, J. Electrochem. Soc. 2003, 150, E74-E80. Structures of orthoborate anions and physical properties of their lithium salt nonaqueous solutions.
485. Z.-M. Xue, B.-B. Sun, W. Zhou, C.-H. Chen, J. Power Sources 2011, 196, 8710-8713. A new lithium salt with dihydroxybenzene and lithium tetrafluoroborate for lithium battery electrolytes.
486. X.-Y. Li, Z.-M. Xue, J.-F. Zhao, C.-H. Chen, J. Power Sources 2013, 235, 274-279. A new lithium salt with tetrafluoro-1,2-benzenediolato and oxalato complexes of boron for lithium battery electrolytes.
487. R. Pizer, P. J. Ricatto, Inorg. Chem. 1994, 33, 2402-2406. Thermodynamics of several 1:1 and 1:2 complexation reactions of the borate ion with bidentate ligands. ^{11}B NMR spectroscopic studies.
488. S. Dhanuskodi, P. A. Angeli Mary, S. Thamotharan, V. Parthasarathi, Acta Crystallogr. 2002, E58, m212-m214. Lithium borodilactate.
489. V. G. Kalacheva, E. Svarcs, V. G. Ben'kovskii, I. D. Leonov, Zh. Neorg. Khim. 1970, 15, 401-403. Dipinacolborates of alkali metals.

490. J. Dale, J. Chem. Soc. 1961, 922-930. The stereochemistry of polyborate anions and of borate complexes of diols and certain polyols.
491. S. S. Zhang, Electrochem. Commun. 2006, 8, 1423-1428. An unique lithium salt for the improved electrolyte of Li-ion battery.
492. S. S. Zhang, J. Power Sources 2006, 162, 1379-1394. A review on electrolyte additives for lithium-ion batteries.
493. Z. Chen, J. Liu, K. Amine, Electrochem. Solid-State Lett. 2007, 10, A45-A47. Lithium difluoro(oxalato)borate as salt for lithium-ion batteries.
494. J. Liu, Z. Chen, S. Busking, K. Amine, Electrochem. Commun. 2007, 9, 475-479. Lithium difluoro(oxalato)borate as a functional additive for lithium-ion batteries.
495. S. S. Zhang, J. Power Sources 2007, 163, 713-718. Electrochemical study of the formation of a solid electrolyte interface on graphite in a $LiBC_2O_4F_2$-based electrolyte.
496. V. Aravindan, P. Vickraman, Solid State Sci. 2007, 9, 1069-1073. A novel gel electrolyte with lithium difluoro(oxalato)borate salt and Sb_2O_3 nanoparticles for lithium ion batteries.
497. J. Liu, Z. Chen, S. Busking, I. Belharouak, K. Amine, J. Power Sources 2007, 174, 852-855. Effect of electrolyte additives in improving the cycle and calendar life of graphite/ $Li_{1.1}[Ni_{1/3}Co_{1/3}Mn_{1/3}]_{0.9}O_2$ Li-ion cells.
498. H.-Q. Gao, Z.-A. Zhang, Y.-Q. Lai, J. Li, Y.-X. Liu, J. Cent. South Univ. Technol. 2008, 15, 830-834. Structure characterization and electrochemical properties of new lithium salt LiODFB for electrolyte of lithium ion batteries.
499. V. Aravindan, P. Vickraman, K. Krishnaraj, Polym. Int. 2008, 57, 932-938. Lithium difluoro(oxalate)borate-based novel nanocomposite polymer electrolytes for lithium ion batteries.
500. S.-H. Kang, D. P. Abraham, A. Xiao, B. L. Lucht, J. Power Sources 2008, 175, 526-532. Investigating the solid electrolyte interphase using binder-free graphite electrodes.
501. D.P. Abraham, M. M. Furczon, S.-H. Kang, D. W. Dees, A. N. Jansen, J. Power Sources 2008, 180, 612-620. Effect of electrolyte composition on initial cycling and impedance characteristics of lithium-ion cells.
502. V. Aravindan, P. Vickraman, K. Krishnaraj, Curr. Appl. Phys. 2009, 9, 1474-1479. Li^+ ion conduction in TiO_2 filled polyvinylidenefluoride-co-hexafluoropropylene based novel nanocomposite polymer electrolyte membranes with LiDFOB.
503. M. Amereller, M. Multerer, C. Schreiner, J. Lodermeyer, A. Schmid, J. Barthel, H. J. Gores, J. Chem. Eng. Data 2009, 54, 468-471. Investigation of the hydrolysis of lithium bis[1,2-oxalato(2-)-O,O′] borate (LiBOB) in water and acetonitrile by conductivity and NMR measurements in comparison to some other borates.
504. A. Xiao, L. Yang, B. L. Lucht, S.-H. Kang, D. P. Abraham, J. Electrochem. Soc. 2009, 156, A318-A327. Examining the solid electrolyte interphase on binder-free graphite electrodes.
505. Z. Chen, Y. Qin, J. Liu, K. Amine, Electrochem. Solid-State Lett. 2009, 12, A69-A72. Lithium difluoro(oxalato)borate as additive to improve the thermal stability of lithiated graphite.
506. J. Li, K. Xie, Y. Lai, Z. Zhang, F. Li, X. Hao, X. Chen, Y. Liu, J. Power Sources 2010, 195, 5344-5350. Lithium oxalyldifluoroborate/carbonate electrolytes for $LiFePO_4$/artificial graphite lithium-ion cells.
507. Z. Zhang, X. Chen, F. Li, Y. Lai, J. Li, P. Liu, X. Wang, J. Power Sources 2010, 195, 7397-7402. $LiPF_6$ and lithium oxalydifluoroborate blend salts electrolyte for $LiFePO_4$/artifical graphite lithium-ion cells.
508. E. Zygadło-Monikowska, Z. Florjańczyk, P. Kubisa, T. Biedroń, A. Tomaszewska, J. Ostrowska, N. Langwald, J. Power Sources 2010, 195, 6202-6206. Mixture of $LiBF_4$ and lithium difluoro(oxalato)borate for application as a new electrolyte for lithium-ion batteries.
509. M. H. Fu, K. L. Huang, S. Q. Liu, J. S. Liu, Y. K. Li, J. Power Sources 2010, 195, 862-866. Lithium difluoro(oxalato)borate/ethylene carbonate + propylene carbonate + ethyl (methyl) carbonate electrolyte for $LiMn_2O_4$ cathode.
510. D. Moosbauer, S. Zugmann, M. Amereller, H. J. Gores, J. Chem. Eng. Data 2010, 55, 1794-1798. Effect of ionic liquids as additives on lithium electrolytes: Conductivity, electrochemical stability, and aluminum corrosion.

511. J. Huang, L.-Z. Fan, B. Yu, T. Xing, W. Qiu, Ionics 2010, 16, 509-513. Density functional theory studies on the B-containing lithium salts.
512. S. Zugmann, D. Moosbauer, M. Amereller, C. Schreiner, F. Wudy, R. Schmitz, R. Schmitz, P. Isken, C. Dippel, R. Müller, M. Kunze, A. Lex-Balducci, M. Winter, H. J. Gores, J. Power Sources 2011, 196, 1417-1424. Electrochemical characterization of electrolytes for lithium-ion batteries based on lithium difluoromono(oxalato)borate.
513. J. L. Allen, S.-D. Han, P. D. Boyle, W. A. Henderson, J. Power Sources 2011, 196, 9737-9742. Crystal structure and physical properties of lithium difluoro(oxalato)borate (LiDFOB or $LiBF_2Ox$).
514. S. Li, X. Xu, X. Shi, X. Cui, Adv. Mater. Res. 2011, 197–198, 1121-1124. Electrochemical performance of lithium difluoro(oxalate)borate synthesized by a novel method.
515. S. Zugmann, M. Fleischmann, M. Amereller, R. M. Gschwind, M. Winter, H. J. Gores, J. Chem. Eng. Data 2011, 56, 4786-4789. Salt diffusion coefficients, concentration dependence of cell potentials, and transference numbers of lithium difluoromono(oxalato)borate-based solutions.
516. S. Zugmann, M. Fleischmann, M. Amereller, R. M. Gschwind, H. D. Wiemhöfer, H. J. Gores, Electrochim. Acta 2011, 56, 3926-3933. Measurement of transference numbers for lithium ion electrolytes via four different methods, a comparative study.
517. L. Zhou, W. Li, M. Xu, B. Lucht, Electrochem. Solid-State Lett. 2011, 14, A161-A164. Investigation of the disproportionation reactions and equilibrium of lithium difluoro(oxalato) borate (LiDFOB).
518. J. L. Allen, P. D. Boyle, W. A. Henderson, Acta Crystallogr. 2011, E67, m533. Lithium difluoro(oxalato) borate tetramethylene sulfone disolvate.
519. K. Amine, Z. Chen, Z. Zhang, J. Liu, W. Lu, Y. Qin, J. Lu, L. Curtis, Y.-K. Sun, J. Mater. Chem. 2011, 21, 17754-17759. Mechanism of capacity fade of MCMB/$Li_{1.1}[Ni_{1/3}Mn_{1/3}Co_{1/3}]_{0.9}O_2$ cell at elevated temperature and additives to improve its cycle life.
520. M. Xu, L. Zhou, L. Hao, L. Xing, W. Li, B. L. Lucht, J. Power Sources 2011, 196, 6794-6801. Investigation and application of lithium difluoro(oxalate)borate (LiDFOB) as additive to improve the thermal stability of electrolyte for lithium-ion batteries.
521. L. Yang, T. Markmaitree, B. L. Lucht, J. Power Sources 2011, 196, 2251-2254. Inorganic additives for passivation of high voltage cathode materials.
522. Y. Zhu, Y. Li, M. Bettge, D. P. Abraham, J. Electrochem. Soc. 2012, 159, A2109-A2118. Positive electrode passivation by LiDFOB electrolyte additive in high-capacity lithium-ion cells batteries and energy storage.
523. S. Li, X. Xu, X. Shi, B. Li, Y. Zhao, H. Zhang, Y. Li, W. Zhao, X. Cui, L. Mao, J. Power Sources 2012, 217, 503-508. Composition analysis of the solid electrolyte interphase film on carbon electrode of lithium-ion battery based on lithium difluoro(oxalate)borate and sulfolane.
524. H. Zhou, F. Liu, J. Li, Appl. Mech. Mater. 2012, 152–154, 1106-1111. Preparation, thermal stability and electrochemical properties of LiODFB.
525. X. Wu, Z. Wang, X. Li, H. Guo, Y. Zhang, W. Xiao, J. Power Sources 2012, 204, 133-138. Effect of lithium difluoro(oxalato)borate and heptamethyldisilazane with different concentrations on cycling performance of $LiMn_2O_4$.
526. C. Yang, Y. Ren, B. Wu, F. Wu, Adv. Mater. Res. 2012, 455–456, 258-264. Formulation of a new type of electrolytes for $LiNi_{1/3}Co_{1/3}Mn_{1/3}O_2$ cathodes working in an ultra-low temperature range.
527. V. Aravindan, P. Vickaman, Ind. J. Phys. 2012, 86, 341-344. Effect of aging on the ionic conductivity of polyvinylidenefluoride–hexafluoropropylene (PVdF–HFP) membrane impregnated with different lithium salts.
528. M. Hu, J. Wei, L. Xing, Z. Zhou, J. Appl. Electrochem. 2012, 42, 291-296. Effect of lithium difluoro(oxalate) borate (LiDFOB) additive on the performance of high-voltage lithium-ion batteries.
529. S. Dalavi, P. Guduru, B. L. Lucht, J. Electrochem. Soc. 2012, 159, A642-A646. Performance enhancing electrolyte additives for lithium ion batteries with silicon anodes.

530. Q. Wu, W. Lu, M. Miranda, T. K. Honaker-Schroeder, K. Y. Lakhsassi, D. Dees, Electrochem. Commun. 2012, 24, 78-81. Effects of lithium difluoro(oxalate)borate on the performance of Li-rich composite cathode in Li-ion battery.
531. T. Schedlbauer, S. Krueger, R. Schmitz, R. W. Schmitz, C. Schreiner, H. J. Gores, S. Passerini, M. Winter, Electrochim. Acta 2013, 92, 102-107. Lithium difluoro(oxalato)borate: A promising salt for lithium metal based secondary batteries?
532. F. Wu, Q. Zhu, L. Li, R. Chen, S. Chen, J. Mater. Chem. A 2013, 1, 3659-3666. A diisocyanate/sulfone binary electrolyte based on lithium difluoro(oxalate)borate for lithium batteries.
533. S. Li, W. Zhao, X. Cui, Y. Zhao, B. Li, H. Zhang, Y. Li, G. Li, X. Ye, Y. Luo, Electrochim. Acta 2013, 91, 282-292. An improved method for synthesis of lithium difluoro(oxalato) borate and effects of sulfolane on the electrochemical performances of lithium-ion batteries.
534. H. Zhou, Z. Fang, J. Li, J. Power Sources 2013, 230, 148-154. $LiPF_6$ and lithium difluoro(oxalato)borate/ethylene carbonate + dimethyl carbonate + ethyl(methyl)carbonate electrolyte for $Li_4Ti_5O_{12}$.
535. J. Xiang, F. Wu, R. Chen, L. Li, H. Yu, J. Power Sources 2013, 233, 115-120. High voltage and safe electrolytes based on ionic liquid and sulfone for lithium-ion batteries.
536. Z.-M. Xue, B.-H. Zhao, C. H. Chen, J. Power Sources 2011, 196, 6478-6482. A new lithium salt with 3-fluoro-1,2-benzenediolato and lithium tetrafluoroborate for lithium battery electrolytes.
537. Z.-M. Xue, X.-F. Zhang, W. Zhou, C.-H. Chen, J. Power Sources 2012, 202, 336-340. A new lithium salt with tetrafluoro-1,2-benzenediolato and lithium tetrafluoroborate for lithium battery electrolytes.
538. Y.-N. Tang, Z.-M. Xue, J. Ding, C.-H. Chen, J. Power Sources 2012, 218, 134-139. Two unsymmetrical lithium organoborates with mixed-ligand of croconato and oxalicdiolato or benzenediolato for lithium battery electrolytes.
539. L. Yang, H. Zhang, P. F. Driscoll, B. Lucht, J. B. Kerr, ECS Trans. 2011, 33, 57-69. Six-membered-ring malonatoborate-based lithium salts as electrolytes for lithium ion batteries.
540. W. Xu, A. J. Shusterman, R. Marzke, C. A. Angell, J. Electrochem. Soc. 2004, 151, A632-A638. LiMOB, an unsymmetrical nonaromatic orthoborate salt for nonaqueous solution electrochemical applications.
541. M. Videa, W. Xu, B. Geil, R. Marzke, C. A. Angell, J. Electrochem. Soc. 2001, 148, A1352-A1356. High Li^+ self-diffusivity and transport number in novel electrolyte solutions.
542. S. Tsujioka, H. Takase, M. Takahashi, H. Sugimoto, M. Koide, U.S. Patent 20020061450 A1, 2002. Electrolyte for electrochemical device.
543. S. Tsujioka, H. Takase, M. Takahashi, H. Sugimoto, M. Koide, Eur. Patent EP 1195834 A2, 2002. Electrolyte containing ionic metal complex for electrochemical device.
544. M. Schmidt, N. Ignatiev, W.-R. Pitner, J. Eichhorn, Ger. Patent DE 102008021271 A1, 2010. Reactive ionic liquids.
545. S. Tsujioka, H. Takase, M. Takahashi, Eur. Patent EP 1075036 A2, 2001. Electrolyte for electrochemical device.
546. S. Tsujioka, H. Takase, M. Takahashi, Eur. Patent EP 1074555 A2, 2001. Ionic metal complex and process for synthesizing same.
547. W. Xu, C. A. Angell, Electrochem. Solid-State Lett. 2000, 3, 366-368. A fusible orthoborate lithium salt with high conductivity in solutions.
548. U. Lischka, U. Wietelmann, M. Wegner, Ger. Patent DE 19829030 C1, 1999. Lithium bis(oxalato)borate, method for its production and application.
549. M. Ue, K. Shima, S. Mori, Electrochim. Acta 1994, 39, 2751-2756. Electrochemical properties of quaternary ammonium borodiglycolates and borodioxalates.
550. M. Finkelstein, E. A. Mayeda, S. D. Ross, J. Org. Chem. 1975, 40, 804-805. Preparation and anodic peak potentials of salts of coordination compounds derived from boric acid and polyhydric phenols.
551. B. G. Nolan, S. H. Strauss, J. Electrochem. Soc. 2003, 150, A1726-A1734. Nonaqueous lithium battery electrolytes based on bis(polyfluorodiolato)borates.

552. B. G. Nolan, S. Tsujioka, S. H. Strauss, in Fluorinated Materials for Energy Conversion, Chap. 9 (T. Nakajima, H. Groult, Eds.), Elsevier, New York, 2005. Electrochemical properties of lithium electrolytes based on bis(polyfluorodiolato)borate and tetrakis(polyfluoroalkoxy) aluminate superweak anions.
553. H. Yamaguchi, H. Takahashi, M. Kato, J. Arai, J. Electrochem. Soc. 2003, 150, A312-A315. Lithium tetrakis(haloacyloxy)borate: An easily soluble and electrochemically stable electrolyte for lithium batteries.
554. J. Arai, Eur. Patent Appl. EP1197494 A2, 2002. New organic borate compounds and the nonaqueous electrolytes and lithium secondary batteries using the compounds.
555. M. Drache, B. Vandorpe, J. Heubel, Bull. Soc. Chim. Fr. 1976, 1749-1754. Reactions of alkaline tetrachloroborates with sulfur trioxide in liquid sulfur dioxide. Mixed alkali metal boron chlorosulfates.
556. G. Mairesse, M. Drache, Acta Crystallogr. 1980, B36, 2767-2768. Lithium tetrakis(chlorosulfato)borate.
557. G. A. Olah, K. Laali, O. Farooq, J. Org. Chem. 1984, 49, 4591-4594. Chemistry in superacids. 6. Perfluoroalkanesulfonic acid-boron perfluoroalkanesulfonates: New superacid systems for generation of carbocations and catalysts for electrophilic transformations of hydrocarbons.
558. E. Zygadło-Monikowska, Z. Florjańczyk, K. Służewska, J. Ostrowska, N. Langwald, A. Tomaszewska, J. Power Sources 2010, 195, 6055-6061. Lithium conducting ionic liquids based on lithium borate salts.
559. R. Tao, T. Fujinami, J. Power Sources 2005, 146, 407-411. Application of mixed-salts composed of lithium borate and lithium aluminate in PEO-based polymer electrolytes.
560. N. Y. Adonin, V. V. Bardin, U. Floerke, H.-J. Hermann, Z. Anorg. Allg. Chem. 2005, 631, 2638-2646. Polyfluoroorganoboron-oxygen compounds. 4. Lithium pentafluorophenyltrimethoxyborate, $Li[C_6F_5B(OMe)_3]$, reactions with selected electrophiles and nucleophiles.
561. M. G. Harriss, J. B. Milne, Can. J. Chem. 1971, 49, 3612-3616. Trifluoroacetic acid solvent system. III. Acid, $HB(OOCCF_3)_4$, and the solvent autoprotolysis constant.
562. M. G. Harriss, J. B. Milne, Can. J. Chem. 1972, 50, 3789-3798. Trifluoroacetic acid solvent system. IV. Triple ions.
563. H. R. Allcock, E. C. Bissell, J. Am. Chem. Soc. 1973, 95, 3154-3157. Triethylammonium tris(o-phenylenedioxy)phosphate. Crystal and molecular structure.
564. N. Nanbu, K. Tsuchiya, T. Shibazaki, Y. Sasaki, Electrochem. Solid-State Lett. 2002, 5, A202-A205. Lithium tris[3-fluoro-1,2-benzenediolato(2-)-O,O']phosphate as a novel lithium salt for lithium battery electrolytes.
565. N. Nanbu, K. Tsuchiya, Y. Sasaki, J. Power Sources 2005, 142, 333-338. Electrolytic properties of lithium chelatophosphates and application to lithium batteries. A new lithium salt with a chelate complex of phosphorus for lithium battery electrolytes.
566. N. Nanbu, T. Shibazaki, Y. Sasaki, Chem. Lett. 2001, 30, 862-863. A novel lithium salt with a chelate complex of phosphorus for lithium battery electrolytes.
567. M. Eberwein, A. Schmid, M. Schmidt, M. Zabel, T. Burgemeister, J. Barthel, W. Kunz, H. J. Gores, J. Electrochem. Soc. 2003, 150, A994-A999. Synthesis and electrochemical properties of some lithium chelatophosphates.
568. S. Zhang, C. Xu, T. R. Jow, U.S. Patent 2010/0267984 A1, 2010. Oxyfluorophosphate synthesis process and compound therefrom.
569. U. Wietelmann, W. Bonrath, T. Netscher, H. Nöth, J.-C. Panitz, M. Wohlfahrt-Mehrens, Chem. Eur. J. 2004, 10, 2451-2458. Tris(oxalato)phosphorus acid and its lithium salt.
570. L. Zhou, B. L. Lucht, J. Power Sources 2012, 205, 439-448. Performance of lithium tetrafluorooxalatophosphate (LiFOP) electrolyte with propylene carbonate (PC).
571. L. Zhou, S. Dalavi, M. Xu, B. L. Lucht, J. Power Sources 2011, 196, 8073-8084. Effects of different electrode materials on the performance of lithium tetrafluorooxalatophosphate (LiFOP) electrolyte.
572. M. Xu, L. Zhou, D. Chalasani, S. Dalavi, B. L. Lucht, J. Electrochem. Soc. 2011, 158, A1202-A1206. Investigation of the solid electrolyte interphase on MCMB and NG electrodes in lithium tetrafluorooxalatophosphate $[LiPF_4C_2O_4]$ based electrolyte.

573. Y. Qin, Z. Chen, J. Liu, K. Amine, Electrochem. Solid-State Lett. 2010, 13, A11-A14. Lithium tetrafluoro oxalato phosphate as electrolyte additive for lithium-ion cells.
574. M. Xu, A. Xiao, W. Li, B. L. Lucht, J. Electrochem. Soc. 2010, 157, A115-A120. Investigation of lithium tetrafluorooxalatophosphate [$LiPF_4(C_2O_4)$] as a lithium-ion battery electrolyte for elevated temperature performance.
575. M. Xu, A. Xiao, W. Li, B. L. Lucht, Electrochem. Solid-State Lett. 2009, 12, A155-A158. Investigation of lithium tetrafluorooxalatophosphate as a lithium-ion battery electrolyte.
576. A. Xiao, L. Yang, B. L. Lucht, Electrochem. Solid-State Lett. 2007, 10, A241-A244. Thermal reactions of $LiPF_6$ with added LiBOB. Electrolyte stabilization and generation of LiF_4OP.
577. U. Heider, M. Schmidt, A. Kuehner, D. Petigk, Eur. Patent Appl. 1143548 A2, 2001. Method of preparation of lithium salts for nonaqueous electrolyte batteries.
578. D. Hellwinkel, Chem. Ber. 1965, 98, 576-587. at-Complexes with six-coordinated phosphorus.
579. A. Chandrasekaran, Roberta O. Day, Robert R. Holmes, Inorg. Chem. 2002, 41, 1645-1651. P-O donor action from carboxylate anions with phosphorus in the presence of hydrogen bonding. A model for phosphoryl-transfer enzymes.
580. S. Tsujioka, B. G. Nolan, H. Takase, B. P. Fauber, S. H. Strauss, J. Electrochem. Soc. 2004, 151, A1418-A1423. Conductivities and electrochemical stabilities of lithium salts of polyfluoroalkoxyaluminate superweak anions.
581. A. K. Powell, S. L. Heath, Coord. Chem. Rev. 1996, 149, 59-80. X-ray structural analysis of biologically relevant aluminium(III) complexes.
582. S. N. Mhatre, R. K. Iyer, P. N. Moorthy, Magn. Res. Chem. 1993, 31, 169-175. Characterization of aluminum complexes in tea extract.
583. A. J. A. Aquino, D. Tunega, G. Haberhauer, M. Gerzabek, H. Lischka, Phys. Chem. Chem. Phys. 2000, 2, 2845-2850. A density functional theoretical study on solvated Al^{3+}-oxalate complexes: Structures and thermodynamic properties.
584. X. Jin, Y. Yan, W. Shi, S. Bi, Environ. Sci. Technol. 2011, 45, 10082-10090. Density functional theory studies on the structures and water-exchange reactions of aqueous Al(III)oxalate complexes.
585. K. E. Peterman, J. M. Shreeve, Inorg. Chem. 1975, 14, 1223-1228. Reactions and photochemistry of some fluorinated amines and imines.
586. C. W. Tullock, U.S. Patent 3077499, 1963. Preparation of bis(trifluoromethyl)amine.
587. J. A. Young, S. N. Tsoukalas, R. D. Dresdner, J. Am. Chem. Soc. 1958, 80, 3604-3606. Fluorocarbon nitrogen compounds. III. Some reactions of bis(trifluoromethyl)amine.
588. D. A. Barr, R. N. Haszeldine, J. Chem. Soc. 1955, 2532-2534. Perfluoroalkyl derivatives of nitrogen. II. Bis(perfluoroalkyl)amines.
589. N. Ignatiev, U. Welz-Biermann, M. Schmidt, M. Weiden, U. Heider, H. Willner, A. Kucheryna, Ger. Patent DE 10258671 A1, 2004. Procedure for the production and use of ionic liquids with $[N(CF_3)_2]^-$ anion.
590. A. Kennedy, C. B. Colburn, J. Am. Chem. Soc. 1959, 81, 2906-2907. Difluoroamine.
591. E. A. Lawton, J. Q. Weber, J. Am. Chem. Soc. 1959, 81, 4755. Direct fluorination of urea: Synthesis and properties of difluoramine.
592. A. M. Sapse, D. C. Jain, Chem. Phys. Lett. 1984, 110, 251-255. Ab initio studies of the lithium difluoroamide (NF_2Li) and dilithium imide ($NHLi_2$) dimers.
593. A. M. Sapse, D. C. Jain, J. Phys. Chem. 1987, 91, 3923-3925. Solvent effect on the dimerization of some lithium compounds.
594. R. Minkwitz, A. Liedtke, Inorg. Chem. 1989, 28, 1627-1630. Preparation and spectroscopic characterization of CF_3-substituted amides, phosphides, and arsenides, $M(CF_3)_2^-$ (M = N, P, As).
595. A. Guerrero, R. Herrero, J. Z. Dávalos, I. Koppel, J.-L. M. Abboud, A. Chana, I. A. Koppel, J. Phys. Chem. A 2009, 113, 6422-6429. Hydrogen-bonding interactions of $(CF_3)_3CH$ and $(CF_3)_3C^-$ in the gas phase. An experimental (FT-ICR) and computational study.
596. P. Marshall, M. Schwartz, J. Phys. Chem. A 1997, 101, 2906-2909. Computational study of C-H bond strengths in polyfluoralkanes.

597. J. S. Francisco, I. H. Williams, Chem. Phys. 1985, 98, 105-114. Structural and spectral consequences of ion pairing: A theoretical study of $CF_3O^-Li^+$ and $CF_3O^-Na^+$.
598. M. E. Redwood, C. J. Willis, Can. J. Chem. 1967, 45, 389-395. Fully fluorinated alkoxides. II. Ethoxides, propoxides, and butoxides.
599. F. Seel, R. Budenz, W. Gombler, Angew. Chem. Int. Ed. 1967, 6, 256. Cesium and rubidium pentafluoroethoxide.
600. C. T. Ratcliffe, J. M. Shreeve, Chem. Commun. 1966, 674-675. A simple method for the preparation of nitrosyl fluoride.
601. R. E. Dear, W. B. Fox, R. J. Fredericks, E. E. Gilbert, D. K. Hubbins, Inorg. Chem. 1970, 9, 2590-2591. Volatile fluorinated alkoxides of the alkali metals.
602. L. O. Müller, R. Scopelliti, I. Krossing, Chimia 2006, 60, 220-223. Chasing an elusive alkoxide: Attempts to synthesize $[OC(tBu)(CF_3)_2]^-$.
603. R. Francke, D. Cericola, R. Kötz, D. Weingarth, S. R. Waldvogel, Electrochim. Acta 2012, 62, 372-380. Novel electrolytes for electrochemical double layer capacitors based on 1,1,1,3,3,3-hexafluoropropan-2-ol.
604. H. Bürger, G. Pawelke, J. Chem. Soc. Chem. Commun. 1988, 105-106. Difluoromethanimine, F_2C=NH, a novel unstable molecule.
605. G. Pawelke, R. Dammel, W. Poll, Z. Naturforsch. B 1992, 47, 351-357. Preparation of difluoromethanimine F_2C:NH and F_2C:ND by hydrolysis of CF_3NCO.
606. Y. V. Zeifman, N. P. Gambaryan, I. L. Knunyants, Dokl. Akad. Nauk. SSSR, Ser. Khim. 1963, 153, 1334-1337. Hexafluoroacetonimines.
607. W. J. Middleton, C. G. Krespan, J. Org. Chem. 1965, 30, 1398-1402. Fluorimines.
608. K. Niedenzu, K. E. Blick, C. D. Miller, Inorg. Chem. 1970, 9, 975-977. Boron-nitrogen compounds. XXXI. The interaction of boron trihalides with hexafluoroisopropylidenimine.
609. R. F. Swindell, T. J. Oullette, D. P. Babb, J. M. Shreeve, Inorg. Nucl. Chem. Lett. 1971, 7, 239-241. Reactions of $LiN=C(CF_3)_2$ with halides.
610. R. F. Swindell, D. P. Babb, T. J. Oullette, J. M. Shreeve, Inorg Chem. 1972, 11, 242-245. Hexafluoropropylideniminolithium reacts with halides.
611. S. G. Metcalf, J. M. Shreeve, Inorg. Chem. 1972, 11, 1631-1634. Bis(hexafluoroisopropyl idenimino) disulfide, chloro(hexafluoroisopropylidenimino)sulfur(II), and some derivatives.
612. G. W. Parshall, R. Cramer, R. E. Foster, Inorg. Chem. 1962, 1, 677-679. Iminosulfur oxydifluoride and poly(oxofluorosulfur nitride).
613. H. W. Roesky, O. Glemser, A. Hoff, W. Koch, Inorg. Nucl. Chem. Lett. 1967, 3, 39-42. Über das azyldifluorosulfation NSF_2O^-.
614. R. D. Cramer, U.S. Patent 3,410,669, 1968. Iminosulfur oxydifluoroides and the process for their preparation.
615. M. Feser, R. Hoefer, O. Glemser, Z. Naturforsch. B 1974, 29, 716-718. Preparation and properties of sulfur oxide difluoride imide salts and their reaction with dimethyltin dihalides.
616. D. T. Sauer, J. M. Shreeve, Inorg. Chem. 1972, 11, 238-242. Bis(perfluoroalkyl)sulfur oxyimines and silver bis(trifluoromethyl)sulfur oxyimine.
617. T. Kitazume, J. M. Shreeve, Inorg. Chem. 1978, 17, 2173-2176. Stable fluorinated sulfuranes and sulfurane oxides. Synthesis and reactions.
618. V. K. Seppelt, Angew. Chem. 1977, 89, 325. Trifluoromethanol, CF_3OH.
619. G. Klöter, K. Seppelt, J. Am. Chem. Soc. 1979, 101, 347-349. Trifluoromethanol (CF_3OH) and trifluoromethylamine (CF_3NH_2).
620. M. E. Redwood, C. J. Willis, Can. J. Chem. 1965, 43, 1893-1898. Fully fluorinated alkoxides. part I. Trifluoromethoxides of alkali metals.
621. J. Arlt, M. Jansen, Chem. Ber. 1991, 124, 321-327. The crystal structures of potassium, rubidium and cesium trifluoroorthocarbonates with a similarity to barium sulfate type.
622. T. J. Barbarich, P. F. Driscoll, Electrochem. Solid-State Lett. 2003, 6, A113-A116. A lithium salt of a Lewis acid-base complex of imidazolide for lithium-ion batteries.

623. T. J. Barbarich, P. F. Driscoll, S. Izquierdo, L. N. Zakharov, C. D. Incarvito, A. L. Rheingold, Inorg. Chem. 2004, 43, 7764-7773. New family of lithium salts for highly conductive nonaqueous electrolytes.
624. T. J. Barbarich, U.S. Patent Appl. US 2003/0108800 A1, 2003. Non-aqueous electrolytes for lithium electrochemical cells.
625. T. J. Barbarich, U.S. Patent Appl. US 2009/0269676 A1, 2009. Non-aqueous electrolytes for lithium electrochemical cells.
626. M. Ihara, T. Kubota, U.S. Patent Appl. US 2011/0214895 A1, 2011. Lithium secondary battery, electrolytic solution for lithium secondary battery, electric power tool, electric vehicle, and electric power storage system.
627. H. S. Lee, X. Q. Yang, C. L. Xiang, J. McBreen, J. Electrochem. Soc. 1998, 145, 2813-2818. The synthesis of a new family of boron-based anion receptors and the study of their effect on ion pair dissociation and conductivily of lithium salts in nonaqueous solutions.
628. X. Sun, H. S. Lee, S. Lee, X. Q. Yang, J. McBreen, Electrochem. Solid-State Lett. 1998, 1, 239-240. A novel lithium battery electrolyte based on lithium fluoride and a tris(pentafluorophenyl) borane anion receptor in DME.
629. X. Sun, H. S. Lee, X. Q. Yang, J. McBreen, J. Electrochem. Soc. 1999, 146, 3655-3659. Comparative studies of the electrochemical and thermal stability of two types of composite lithium battery electrolytes using boron-based anion receptors.
630. J. McBreen, H. S. Lee, X. Q. Yang, X. Sun, J. Power Sources 2000, 89, 163-167. New approaches to the design of polymer and liquid electrolytes for lithium batteries.
631. H. S. Lee, X. Q. Yang, X. Sun, J. McBreen, J. Power Sources 2001, 97–98, 566-569. Synthesis of a new family of fluorinated boronate compounds as anion receptors and studies of their use as additives in lithium battery electrolytes.
632. X. Sun, H. S. Lee, X. Q. Yang, J. McBreen, J. Electrochem. Soc. 2002, 149, A335-A359. A new additive for lithium battery electrolytes based on an alkyl borate compound.
633. X. Sun, H. S. Lee, X.-Q. Yang, J. McBreen, Electrochem. Solid-State Lett. 2002, 5, A248-A251. Using a boron-based anion receptor additive to improve the thermal stability of $LiPF_6$-based electrolyte for lithium batteries.
634. H. S. Lee, Z. F. Ma, X. Q. Yang, X. Sun, J. McBreen, J. Electrochem. Soc. 2004, 151, A1429-A1435. Synthesis of a series of fluorinated boronate compounds and their use as additives in lithium battery electrolytes.
635. B. Xie, H. S. Lee, H. Li, X. Q. Yang, J. McBreen, L. Q. Chen, J. Power Sources 2008, 10, 1195-1197. New electrolytes using Li_2O or Li_2O_2 oxides and tris(pentafluorophenyl) borane as boron based anion receptor for lithium batteries.
636. L. F. Li, H. S. Lee, H. Li, X. Q. Yang, K. W. Nam, W. S. Yoon, J. McBreen, X. J. Huang, J. Power Sources 2008, 184, 517-521. New electrolytes for lithium ion batteries using LiF salt and boron based anion receptors.
637. S. Brownstein, Inorg. Chem. 1973, 12, 584-589. Complex fluoro anions in solution, I. Homo- and heteropolyfluoro anions of niobium and tantalum.
638. S. Brownstein, J. Inorg. Nucl. Chem. 1973, 35, 3567-3574. Complex fluoroanions in solution—II. Reactions of boron trifluoride and phosphorous pentafluoride with group VB hexafluoroanions.
639. S. Brownstein, Can. J. Chem. 1978, 56, 343-347. Complex fluoroanions in solution. VII. Replacement of fluoride by trifluoroacetate.
640. S. Brownstein, J. Bornais, G. Latremouille, Can. J. Chem. 1978, 56, 1419-1422. Complex fluoroanions in solution. VIII. Mixed anions containing fluoride and trifluoromethanesulfonate or fluorosulfate.
641. S. Brownstein, G. Latremouille, Can. J. Chem. 1978, 56, 2764-2767. Complex fluoroanions in solution. IX. BF_3-anion complexes and their disproportionation.
642. P. J. Chevrier, S. Brownstein, J. Inorg. Nucl. Chem. 1980, 42, 1397-1405. Complex fluoroanions in solution—X. Complexes of phosphorus and arsenic fluorides with simple anions.
643. A. Alijah, E. S. Kryachko, J. Mol. Struct. 2007, 844–845, 193-199. On the $N_3O_2^-$ paradigm.

644. H. Brand, P. Mayer, K. Polborn, A. Schulz, J. J. Weigand, J. Am. Chem. Soc. 2005, 127, 1360-1361. Blue alkali dinitrosomethanides: Synthesis, structure, and bonding.
645. A. Gorkovenko, S. Jaffe, U.S. Patent Appl. 2006/0154144 A1, 2006. Novel enhanced electrochemical cells with solid-electrolyte interphase promoters.
646. H. Brand, J. F. Liebman, A. Schulz, P. Mayer, A. Villinger, Eur. J. Inorg. Chem. 2006, 4294-4308. Nonlinear, resonance-stabilized pseudohalides: From alkali methanides to ionic liquids of methanides.
647. A. P. Purdy, E. Houser, C. F. George, Polyhedron 1997, 16, 3671-3679. Lithium dicyanamide, its reactions with cyanuric chloride, and the crystal structures of $LiN(CN)_2(MeCN)_2$ and $LiCN(C_5H_5N)_2$.
648. H. Yoon, G. H. Lane, Y. Shekibi, P. C. Howlett, M. Forsyth, A. S. Best, D. R. MacFarlane, Energy Environ. Sci. 2013, 6, 979-986. Lithium electrochemistry and cycling behaviour of ionic liquids using cyano based anions.
649. S. A. Forsyth, S. R. Batten, Q. Dai, D. R. MacFarlane, Aust. J. Chem. 2004, 57, 121-124. Ionic liquids based on imidazolium and pyrrolidinium salts of the tricyanomethanide anion.
650. J. Scheers, P. Johansson, P. Jacobsson, J. Electrochem. Soc. 2008, 155, A628-A634. Anions for lithium battery electrolytes: A spectroscopic and theoretical study of the $B(CN)_4^-$ anion of the ionic liquid $C_2mim[B(CN)_4]$.
651. T. Küppers, E. Bernhardt, H. Willner, H. W. Rohm, M. Köckerling, Inorg. Chem. 2005, 44, 1015-1022. Tetracyanoborate salts $M[B(CN)_4]$ with M = singly charged cations: Properties and structures.
652. R. Younesi, M. Hahlin, M. Treskow, J. Scheers, P. Johansson, K. Edström, J. Phys. Chem. C 2012, 116, 18597-18604. Ether based electrolyte, $LiB(CN)_4$ salt and binder degradation in the $Li–O_2$ battery studied by hard X-ray photoelectron spectroscopy (HAXPES).
653. T. Küppers, E. Bernhardt, H. Willner, H. W. Rohm, M. Köckerling, Inorg. Chem. 2005, 44, 1015-1022. Tetracyanoborate salts $M[B(CN)_4]$ with M = singly charged cations: Properties and structures.
654. J. Scheers, J. Pitawala, F. Thebault, J.-K. Kim, J.-H. Ahn, A. Matic, P. Johansson, P. Jacobson, Phys. Chem. Chem. Phys. 2011, 13, 14953-14959. Ionic liquids and oligomer electrolytes based on the $B(CN)_4^-$ anion; Ion association, physical and electrochemical properties.
655. W. J. Middleton, U.S. Patent US 2766243, 1956. Tetracyanoethylene and 1,1,2,3,3-pentacyanopropene.
656. W. J. Middleton, E. L. Little, D. D. Coffman, V. A. Engelhardt, J. Am. Chem. Soc. 1958, 80, 2795-2806. Cyanocarbon chemistry. V. Cyanocarbon acids and their salts.
657. C. E. Looney, J. R. Downing, J. Am. Chem. Soc. 1958, 80, 2840-2844. Cyanocarbon chemistry. XII. Some physical characteristics of cyanocarbon derivatives.
658. R. H. Boyd, J. Am. Chem. Soc. 1961, 83, 4288-4290. Strengths of cyanocarbon acids and a H-acidity scale for concentrated acid solutions.
659. R. H. Boyd, J. Phys. Chem. 1963, 67, 737-744. Cyanocarbon chemistry. XXIII. The ionization behavior of cyanocarbon acids.
660. C. Richardson, C. A. Reed, Chem. Commun. 2004, 706-707. Exploration of the pentacyanocyclopentadienide ion, $C_5(CN)_5^-$, as a weakly coordinating anion and potential superacid conjugate base. Silylation and protonation.
661. P. Johansson, H. Nilsson, P. Jacobsson, M. Armand, Phys. Chem. Chem. Phys. 2004, 6, 895-899. Novel Hückel stabilised azole ring-based lithium salts studied by ab initio Gaussian-3 theory.
662. R. Vianello, J. F. Liebman, Z. B. Maksić, Chem. Eur. J. 2004, 10, 5751-5760. In search of ultrastrong Brønsted neutral organic superacids: A DFT study on some cyclopentadiene derivatives.
663. A. Kütt, I. Koppel, I. A. Koppel, I. Leito, ChemPhysChem 2009, 10, 499-502. Boratabenzene anions $C_5B(CN)_6^-$ and $C_5B(CF_3)_6^-$ and the superacidic properties of their conjugate acids.
664. P. Johansson, S. Beranger, M. Armand, H. Nilsson, P. Jacobsson, Solid State Ionics 2003, 156, 129-139. Spectroscopic and theoretical study of the 1,2,3-triazole-4,5-dicarbonitrile anion and its lithium ion pairs.

665. M. Egashira, B. Scrosati, M. Armand, S. Beranger, C. Michot, Electrochem. Solid-State Lett. 2003, 6, A71-A73. Lithium dicyanotriazolate as a lithium salt for poly(ethylene oxide) based polymer electrolytes.
666. M. J. Crawford, K. Karaghiosoff, T. M. Klapötke, F. A. Martin, Inorg. Chem. 2009, 48, 1731-1743. Synthesis and characterization of 4,5-dicyano-2H-1,2,3-triazole and its sodium, ammonium, and guanidinium salts.
667. C. M. Sabaté, E. Jeanneau, H. Delalu, Dalton Trans. 2012, 41, 3817-3825. Metal salts of the 4,5-dicyano-2H-1,2,3-triazole anion ($[C_4N_5]^-$).
668. C. M. Sabaté, H. Delalu, New Trends in Research of Energetic Materials, Proceedings (Pardubice, Czech Republic, Apr. 18-20, 2012) 2012, 747-750. Study of metal salts of the 4,5-dicyano-2H-1,2,3-triazole anion as pyrotechnic ingredients.
669. C. D. Weiss, J. Org. Chem. 1962, 27, 3695-3696. 3,4,5-Tricyanopyrazole.
670. H. Markusson, S. Béranger, P. Johansson, M. Armand, P. Jacobsson, J. Phys. Chem. A 2003, 107, 10177-10183. Lithium-pyrazole-3,4,5-tricarbonitrile: Ion pairing and lithium ion affinity studies.
671. O. W. Webster, Ger. Patent DE 2317453 A1, 1973. 4,5-Dicyanoimidazoles.
672. H. E. Simmons, U.S. Patent 1962-223825, 1962. Cyanopyrroles.
673. H. E. Simmons, R. D. Vest, S. A. Vladuchick, O. W. Webster, J. Org. Chem. 1980, 45, 5113-5121. Thiacyanocarbons. 5. Reactions of tetracyano-l,4-dithiin and tetracyanothiophene with nucleophiles: Synthesis of tetracyanopyrrole and tetracyanocyclopentadiene salts.
674. M. Becker, J. Harloff, T. Jantz, A. Schulz, A. Villinger, Eur. J. Inorg. Chem. 2012, 5658-5667. Structure and bonding of tetracyanopyrrolides.
675. R. W. Begland, D. R. Hartter, F. N. Jones, D. J. Sam, W. A. Sheppard, O. W. Webster, F. J. Weigert, J. Org. Chem. 1974, 39, 2341-2350. Hydrogen cyanide chemistry. VIII. New chemistry of diaminomaleonitrile. Heterocyclic synthesis.
676. M. Bukowska, J. Prejzner, P. Szczecinski, Pol. J. Chem. 2004, 78, 417-422. Synthesis of 4,5-dicyanoimidazoles.
677. L. Niedzicki, M. Kasprzyk, K. Kuziak, G. Z. Żukowska, M. Armand, M. Bukowska, M. Marcinek, P. Szczecinski, W. Wieczorek, J. Power Sources 2009, 192, 612-617. Modern generation of polymer electrolytes based on lithium conductive imidazole salts.
678. M. Bukowska, P. Szczecinski, W. Wieczorek, L. Nidzicki, B. Scrosati, S. Panero, P. Reale, M. Armand, S. Laruelle, S. Grugeon, Int. Patent Appl. WO 2010023413 A1, 2010. Pentacyclic anion salt used as electrolyte for batteries.
679. L. Niedzicki, G. Z. Żukowska, M. Bukowska, P. Szczeciński, S. Grugeon, S. Laruelle, M. Armand, S. Panero, B. Scrosati, M. Marcinek, W. Wieczorek, Electrochim. Acta 2010, 55, 1450-1454. New type of imidazole based salts designed specifically for lithium ion batteries.
680. J. Scheers, P. Johansson, P. Szczeciński ,W. Wieczorek, M. Armand, P. Jacobsson, J. Power Sources 2010, 195, 6081-6087. Benzimidazole and imidazole lithium salts for battery electrolytes.
681. L. Niedzicki, S. Grugeon, S. Laruelle, P. Judeinstein, M. Bukowska, J. Prejzner, P. Szczeciński, W. Wieczorek, M. Armand, J. Power Sources 2011, 196, 8696-9700. New covalent salts of the 4+ V class for Li batteries.
682. L. Niedzicki, M. Kasprzyk, K. Kuziak, G. Z. Żukowska, M. Marcinek, W. Wieczorek, M. Armand, J. Power Sources 2011, 196, 1386-1391. Liquid electrolytes based on new lithium conductive imidazole salts.
683. J. Scheers, L. Niedzicki, G. Z. Żukowska, P. Johansson, W. Wieczorek, P. Jacobsson, Phys. Chem. Chem. Phys. 2011, 13, 11136-11147. Ion–ion and ion–solvent interactions in lithium imidazolide electrolytes studied by Raman spectroscopy and DFT models.
684. M. Dranka, L. Niedzicki, K. Kasprzyk, M. Marcinek, W. Wieczorek, J. Zachara, Polyhedron 2013, 51, 111-116. An insight into coordination ability of dicyanoimidazolato anions toward lithium in presence of acetonitrile. Crystal structures of novel lithium battery electrolyte salts.

685. G. Schmidt, M. Flasque, Int. Patent Appl. WO 2013072591 A1, 2013. Method for the preparation of a salt of a pentacyclic anion, particularly lithium 4,5-dicyano-2-fluoroalkylimidazolates, useful for manufacturing of an electrolyte composition for batteries.
686. S. Schmidt, Int. Patent Appl. WO 2013083894 A1, 2013. Use of lithium salt mixtures as electrolytes for lithium batteries.
687. Y. Kamitori, J. Heterocyclic. Chem. 2001, 38, 773-776. A facile synthesis of fluorine-containing heterocycles - Use of 1,1,1-trifluoro-2-alkanones as a convenient synthetic intermediate.
688. E. D. Laganis, D. M. Lemal, J. Am. Chem. Soc. 1980, 102, 6634-6636. 5H-Perfluoropentamethylcyclopentadiene, an extraordinary carbon acid.
689. Y. Kobayashi, A. Ando, K. Kaeada, A. Ohsawa, I. Kumadaki, J. Org. Chem. 1980, 45, 2962-2966. Organic fluorine compounds. 32.' A 1,3-dipolar cycloaddition reaction of tetrakis(trifluoromethyl)(dewar thiophene) and some reactions of the cycloadducts.
690. R. D. Chambers, S. J. Mullins, A. J. Roche, J. F. S. Vaughan, J. Chem. Soc., Chem. Commun. 1995, 841-842. Direct syntheses of pentakis(trifluoromethyl)cyclopentadienide salts and related dienes.
691. R. D. Chambers, A. J. Roche, J. F. S. Vaughan, Can. J. Chem. 1996, 74, 1925-1929. Direct syntheses of pentakis(trifluoromethyl)cyclopentadienide salts and related systems.
692. R. D. Chambers, W. K. Gray, J. F. S. Vaughan, S. R. Korn, M. Médebielle, A. S. Batsanov, C. W. Lehmann, J. A. K. Howard, J. Chem. Soc., Perkin Trans. 1997, 1, 135-145. Reactions involving fluoride ion. Part 41. Synthesis of hexakis(trifluoromethyl)cyclopentadiene and derived cyclopentadienide salts.
693. H. Brand, J. F. Liebman, A. Schulz, Eur. J. Chem. 2008, 4665-4675. Cyano-, nitro- and nitrosomethane derivatives: Structures and gas-phase acidities.
694. V. G. Kiselev, N. P. Gritsan, J. Phys. Chem. A 2008, 112, 4458-4464. Theoretical study of the nitroalkane thermolysis. 1. Computation of the formation enthalpy of the nitroalkanes, their isomers and radical products.
695. M. D. Cliff, M. W. Smith, J. Energetic Mater. 1999, 17, 69-86. Thermal characteristics of alkali metal dinitramide salts.
696. S. B. Babkin, A. N. Pavlov, G. M. Nazin, Russ. Chem. Bull. 1997, 46, 1844-1847. Anomalous decomposition of dinitramide metal salts in the solid phase.
697. R. Gilardi, J. Flippen-Anderson, C. George, R. J. Burcher, J. Am. Chem. Soc. 1997, 119, 9411-9416. A new class of flexible energetic salts: The crystal structures of the ammonium, lithium, potassium, and cesium salts of dinitramide.
698. R. J. Less, T. C. Wilson, M. McPartlin, P. T. Wood, D. S. Wright, Chem. Commun. 2011, 47, 10007-10009. Transition metal complexes of the pentacyanocyclopentadienide anion.
699. R. J. Less, B. Guan, N. M. Muresan, M. McPartlin, E. Reisner, T. C. Wilson, D. S. Wright, Dalton Trans. 2012, 41, 5919-5924. Group 11 complexes containing the $[C_5(CN)_5]^-$ ligand; 'Coordination-analogues' of molecular organometallic systems.
700. R. J. Less, T. C. Wilson, B. Guan, M. McPartlin, A. Steiner, P. T. Wood, D. S. Wright, Eur. J. Inorg. Chem. 2013, 1161-1169. Solvent direction of molecular architectures in Group 1 metal pentacyanocyclopentadienides.
701. C. Michot, PhD Thesis, Institut National Polytechnique de Grenoble Publisher, 1995.
702. N. Chaix, F. Alloin, J.-P. Bélières, J. Saunier, J.-Y. Sanchez, Electrochim. Acta 2002, 47, 1327-1334. Electrochemical study of polymethacrylonitrile electrolytes Comparative investigation of polynitriles electrochemical stability through model molecules. Part II.
703. L. Jäger, B. Freude, R. Skirl, K. Schubert, H. Köhler, Z. Anorg. Allg. Chem. 1993, 619, 711-717. Pseudoelement compounds. IV. Modification of the ions sulfite $[SO_2Y]^{2-}$, sulfate $[SO_{4-n}Y_n]^{2-}$, and sulfonate $[RSO_2Y]^-$ by introducing pseudochalcogen groups NCN and $C(CN)_2$.
704. A. D. Fanta, P. T. Pham, W. M. Lamanna, Int. Patent WO 00/11742, 2000. Cyano-substituted methide and amide salts.
705. Y. L. Yagupolskii, N. V. Pavlenko, E. Lork, Heteroatom Chem. 1998, 9, 565-570. Trifluoromethylsulfonylmethanides functionalized by a CN group.

706. M. Armand, Y. Choquette, M. Gauthier, C. Michot, Eur. Patent, EP 0 850 921 A1, 1998. Sels d'anions dérivés du malonitrile, et leurs utilisations comme matériaux à conduction ionique.
707. H. W. Roesky, Angew. Chem. Int. Ed. 1968, 7, 63-64. Preparation of *N*-(trifluoromethyl) fluorosulfonamide and its salts.
708. B. Huber, T. Linder, K. Hormann, T. Frömling, J. Sundermeyer, B. Roling, Z. Phys. Chem. 2012, 226, 377-390. Synthesis of novel lithium salts containing pentafluorophenylamido-based anions and investigation of their thermal and electrochemical properties.
709. S. Maeda, S. Hayakawa, S. Kawada, Y. Aoki, Jap. Patent JP 2008251530 A, 2008. Electrolyte solution and secondary lithium battery using the electrolyte solution.
710. H. Yamamoto, M. Matsui, Int. Patent Appl. WO 2008069207, 2008. Preparation of lithium salts as supporting salts for electrolyte solutions.
711. V. Geis, K. Guttsche, C. Knapp, H. Scherer, R. Uzun, Dalton Trans. 2009, 2687-2694. Synthesis and characterization of synthetically useful salts of the weakly-coordinating dianion $[B_{12}Cl_{12}]^{2-}$.
712. J. W. Johnson, M. S. Whittingham, J. Electrochem. Soc. 1980, 127, 1653-1654. Lithium closoboranes as electrolytes in solid cathode lithium cells.
713. J. W. Johnson, A. H. Thompson, J. Electrochem. Soc. 1981, 128, 932-933. Lithium closoboranes. II. Stable nonaqueous electrolytes for elevated temperature lithium cells.
714. J. W. Johnson, J. F. Brady, J. Electrochem. Soc. 1982, 129, 2213-2219. Lithium closoborane electrolytes. III. Preparation and characterization.
715. G. GirishKumar, W. H. Bailey III, B. K. Peterson, W. J. Casteel Jr., J. Electrochem. Soc. 2011, 158, A146-A153. Electrochemical and spectroscopic investigations of the overcharge behavior of StabiLife electrolyte salts in lithium-ion batteries.
716. Z. Chen, A. N. Jansen, K. Amine, Energy Environ. Sci. 2011, 4, 4567-4571. Novel functionalized electrolyte for MCMB/$Li_{1.156}Mn_{1.844}O_4$ lithium-ion cells.
717. Z. Chen, J. Liu, A. N. Jansen, G. GirishKumar, B. Casteel, K. Amine, Electrochem. Solid-State Lett. 2010, 13, A39-A42. Lithium borate cluster salts as redox shuttles for overcharge protection of lithium-ion cells.
718. S. V. Ivanov, S. M. Miller, O. P. Anderson, K. A. Solntsev, S. H. Strauss, J. Am. Chem. Soc. 2003, 125, 4694-4695. Synthesis and stability of reactive salts of dodecafluoro-closo-dodecaborate(2-).
719. D.V. Peryshkov, S.H. Strauss, J. Fluor. Chem. 2010, 131, 1252-1256. $K_2B_{12}F_{12}$: A rare A_2X structure for an ionic compound at ambient conditions.
720. D. V. Peryshkov, R. Friedemann, E. Goreshnik, Z. Mazej, K. Seppelt, S. H. Strauss, J. Fluor. Chem. 2013, 145, 118-127. Anion packing, hole filling, and HF solvation in $A_2(HF)nB_{12}F_{12}$ and $K_2(HF)TiF_6$ (A = K, Cs).
721. J. Derendorf, M. Kessler, C. Knapp, M. Ruhle, C. Schulz, Dalton Trans. 2010, 39, 8671-8678. Alkali metal-sulfur dioxide complexes stabilized by halogenated closo-dodecaborate anions.
722. K. Hayamizu, A. Matsuo, J. Arai, J. Electrochem. Soc. 2009, 156, A744-A750. A divalent lithium salt $Li_2B_{12}F_{12}$ dissolved in propylene carbonate studied by NMR methods.
723. J. Arai, A. Matsuo, T. Fujisaki, K. Ozawa, J. Power Sources 2009, 193, 851-854. A novel high temperature stable lithium salt ($Li_2B_{12}F_{12}$) for lithium ion batteries.
724. Z. Chen, Y. Qin, K. Amine, Electrochim. Acta 2009, 54, 5605-5613. Redox shuttles for safer lithium-ion batteries.
725. Z. Chen, Y. Ren, A. N. Jansen, C. Lin, W. Weng, K. Amine, Nat. Commun. 2013, 4, 1513-1520. New class of nonaqueous electrolytes for long-life and safe lithium-ion batteries.
726. S. V. Ivanov, W. J. Casreel Jr., G. P. Pez, M. Ulman, U.S. Patent US 2005/0064288, 2005. Polyfluorinated boron cluster anions for lithium electrolytes.
727. C. M. Ionica-Bousquet, D. Muñoz-Rojas, W. J. Casteel, R. M. Pearlstein, G. GirishKumar, G. P. Pez, M. R. Palacín, J. Power Sources 2010, 195, 1479-1485. Polyfluorinated boron cluster-based salts: A new electrolyte for application in $Li_4Ti_5O_{12}$/$LiMn_2O_4$ rechargeable lithium-ion batteries.

728. L. Lipping, I. Leito, I. Koppel, I. A. Koppel, J. Phys. Chem. A 2009, 113, 12972-12978. Gas-phase Brønsted superacidity of some derivatives of monocarba-closo-borates: A computational study.
729. A. N. Dey, J. Miller, J. Electrochem. Soc. 1979, 126, 1445-1451. Primary Li/$SOCl_2$ cells. VII. Effect of $Li_2B_{10}Cl_{10}$ and $Li_2B_{12}Cl_{12}$ electrolyte salts on the performance.
730. A. Hammami, N. Raymond, M. Armand, Nature 2003, 424, 635-636. Runaway risk of forming toxic compounds.
731. T. Ohzuku, R. J. Brodd, J. Power Sources 2007, 174, 449-456. An overview of positive-electrode materials for advanced lithium-ion batteries.
732. J. Choi, A. Manthiram, J. Electrochem. Soc. 2005, 152, A1714-A1718. Role of chemical and structural stabilities on the electrochemical properties of layered $LiNi_{1/3}Mn_{1/3}Co_{1/3}O_2$ cathodes.

Chapter 2
Nonaqueous Electrolytes with Advances in Solvents

Makoto Ue, Yukio Sasaki, Yasutaka Tanaka, and Masayuki Morita

Abstract Most of the liquid electrolytes used in commercial lithium-ion (Li-ion) cells are nonaqueous solutions, in which roughly 1 mol dm^{-3} of lithium hexafluorophosphate ($LiPF_6$) salt is dissolved in a mixture of carbonate solvents selected from cyclic carbonates—ethylene carbonate and propylene carbonate—and linear carbonates—dimethyl carbonate, ethyl methyl carbonate, and diethyl carbonate. In Sect. 2.1, the physicochemical properties of these carbonate solvents are listed and the phase diagrams and electrolytic conductivity data of mixed carbonate solvent systems are given. However, recent market demands for Li-ion cells with higher energy, higher power, and higher safety requires new solvents to improve the performance of cells in electrolytes based on carbonate solvents only. New heteroatom-containing organic solvents including fluorine, boron, phosphorous, and sulfur, which have been applied to lithium cells in recent years, are reviewed from the viewpoints of synthesis, physicochemical properties, and cell performance by four authors.

M. Ue (✉)
Mitsubishi Chemical Corporation, 1000 Kamoshida, Aoba, Yokohama, Kanagawa 227-8502, Japan

National Institute for Materials Science, Namiki, Tsukuba, Ibaraki 305-0044, Japan
e-mail: macue01@gmail.com

Y. Sasaki
Tokyo Polytechnic University, 1583 Iiyama, Atsugi, Kanagawa 243-0297, Japan
e-mail: sasaki2045@gmail.com

Y. Tanaka
Graduate School of Science and Technology, Shizuoka University, Hamamatsu 432-8561, Japan
e-mail: tcytana@ipc.shizuoka.ac.jp

M. Morita
Graduate School of Science and Engineering, Yamaguchi University, 2-16-1, Tokiwadai, Ube 755-8611, Japan
e-mail: morita@yamaguchi-u.ac.jp

T.R. Jow et al. (eds.), *Electrolytes for Lithium and Lithium-Ion Batteries*, Modern Aspects of Electrochemistry 58, DOI 10.1007/978-1-4939-0302-3_2,

Section 2.2 mainly reviews the papers on novel fluorinated organic solvents, which include fluorinated lactones, fluorinated linear carboxylates, fluorinated cyclic carbonates, fluorinated linear carbonates, fluorinated monoethers, fluorinated diethers, and others. The physicochemical properties of typical fluorinated compounds are summarized in comparison with nonfluorinated counterparts.

Section 2.3 summarizes the recent promising progress of electrolyte solvents that contain boron atoms, particularly borate esters and cyclic borate esters. The authors also introduce some boron compounds acting as additives and supporting salts in electrolytes.

Section 2.4 reviews organophosphorous compounds as nonflammable or flame-retardant electrolytes for lithium-ion batteries. These include organic phosphates, phosphites, phosphonates, or phosphazenes, and a phosphonamidate as co-solvents or additives. The author introduces polymeric gel electrolytes containing these flame-retardant components.

Section 2.5 reviews papers on lithium and lithium-ion cells using sulfur-containing organic solvents, including sulfide, sulfoxide, sulfone, sulfite, sulfonate, and sulfate. Particularly, the performance of sulfones such as ethyl methyl sulfone and sulfolane as electrolyte solvents for high-voltage cells is introduced.

2.1 General Remarks

Most lithium cells available in the market utilize nonaqueous electrolyte solutions, where lithium salts are dissolved in organic solvents. The gelled electrolytes used in lithium-ion polymer batteries are also regarded as an organic electrolyte immobilized with a high molecular weight polymer.

There are numerous organic solvents and lithium salts; however, a very limited number of materials fulfill the following physicochemical requirements for practical use.

1. High electrolytic conductivity
2. High chemical and electrochemical stability
3. Wide operational temperature range
4. High safety

The selection of the electrolyte materials is also dependent on the kind of negative and positive electrodes.

Most liquid electrolytes used in commercial lithium-ion cells are nonaqueous solutions, in which roughly 1 mol dm^{-3} of lithium hexafluorophosphate ($LiPF_6$) salt is dissolved in a mixture of carbonate solvents selected from cyclic carbonates, e.g., ethylene carbonate (EC) and propylene carbonate (PC), and linear carbonates, e.g., dimethyl carbonate (DMC), ethyl methyl carbonate (EMC), and diethyl carbonate (DEC), as listed in Table 2.1 [1].

Regarding the practical carbonate solvents, the phase diagrams of mixed-carbonate solvent systems were investigated by Ding [2]. Since these data are very important, a brief explanation is given here. Figure 2.1 shows phase

Table 2.1 Physical properties of carbonate solvents

Solvent	FW	ε_r	η_0 (mPa s)	d_0 (g cm^{-3})	mp (°C)	bp (°C)	fp (°C)	κ^a (mS cm^{-1})	$E_{red}{}^a$ (V vs. Li/Li$^+$)	$E_{ox}{}^a$ (V vs. Li/Li$^+$)
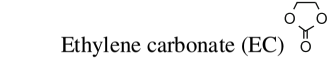 Ethylene carbonate (EC)	88.1	90[b]	1.9[b]	1.32[b]	36	238	143	17	0.0	+6.2
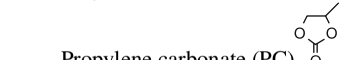 Propylene carbonate (PC)	102.1	65	2.5	1.20	−49	242	138	13	0.0	+6.6
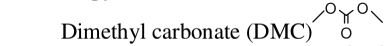 Dimethyl carbonate (DMC)	90.1	3.1	0.59	1.06	5	90	17	2.0[c]	0.0[c]	+6.5[c]
 Ethyl methyl carbonate (EMC)	104.1	3.0	0.65	1.01	−53	108	23	1.1[c]	0.0[c]	+6.7[c]
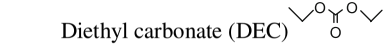 Diethyl carbonate (DEC)	118.1	2.8	0.75	0.97	−74	127	25	0.6[c]	0.0[c]	+6.7[c]

[a]1 mol dm^{-3} Et_4NBF_4 ([c]0.65 mol dm^{-3} Bu_4NBF_4), GC, 5 mV s^{-1}, 1 mA cm^{-2}

25°C ([b]40°C)

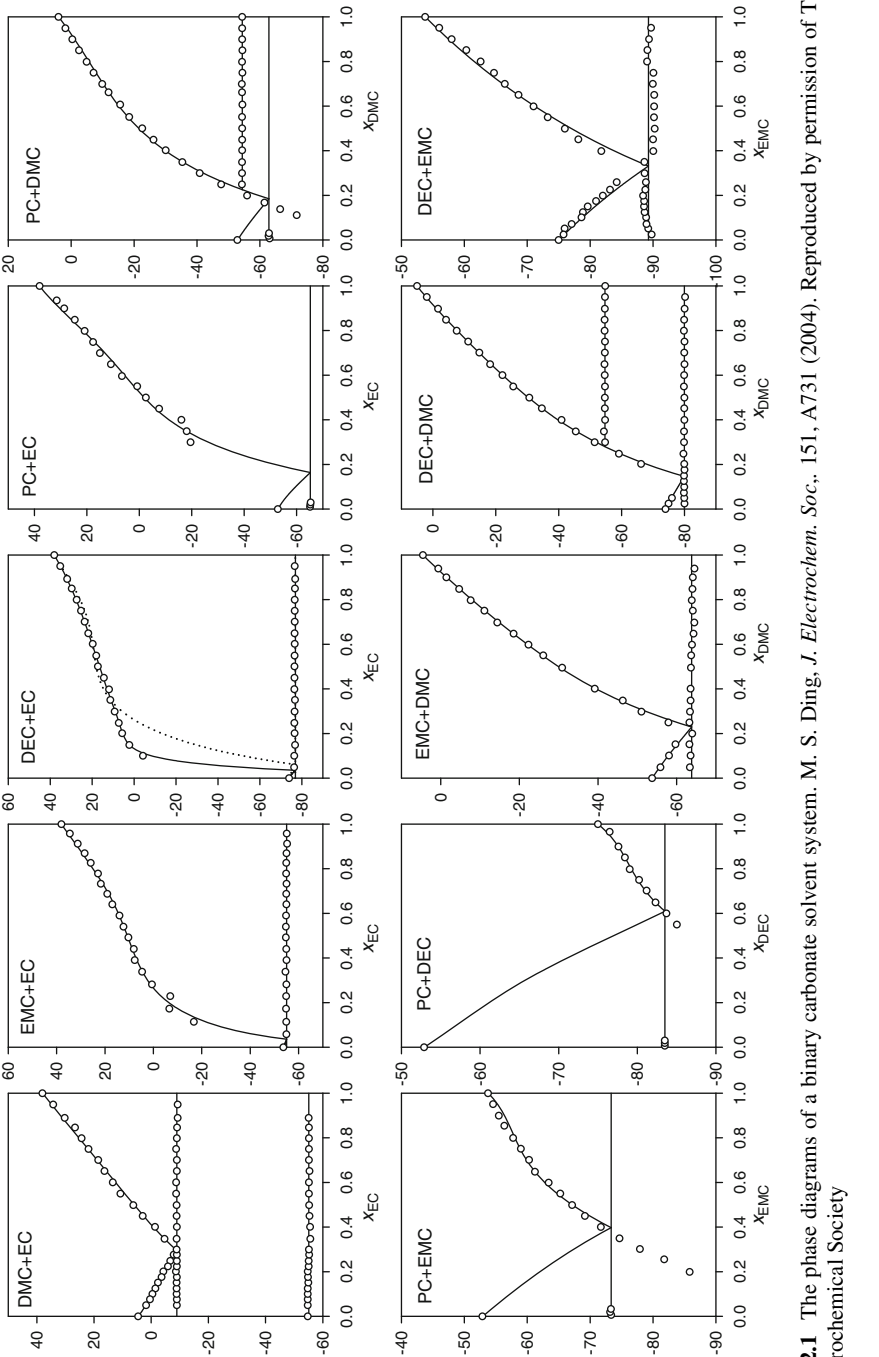

Fig. 2.1 The phase diagrams of a binary carbonate solvent system. M. S. Ding, *J. Electrochem. Soc.*, 151, A731 (2004). Reproduced by permission of The Electrochemical Society

diagrams of binary solvent systems selected from five carbonate solvents, where χ and θ are mole fraction and temperature, respectively. All systems exhibit a eutectic point and a typical phase diagram of binary systems, where both components mutually dissolve in the liquid state and do not dissolve in the solid state. Compositions near the eutectic point are preferred to expand the lower limit of the operation temperature. The eutectic point falls remarkably when both components have similar freezing points and molecular structures (chain or cyclic). Figure 2.2 shows the phase diagram of an EC-DMC-EMC ternary system as (a) a liquidus surface plot and (b) a contour plot of temperature over the composition triangle of the mole fraction. In the surface plot, the binary eutectic temperatures are indicated with the numbers near the respective solidus lines, and the ternary eutectic temperature is also indicated in the figure. In the contour plot, the temperature values of selected contours are indicated by the numbers near them. As shown in the surface plot, the melting point of EC falls progressively with the addition of DMC until it reaches the eutectic point (−8.6 °C) of the EC-DMC binary, thus tracing the solubility curve of EC in DMC on the EC-DMC binary phase diagram as an end-member to the ternary. It does the same with the addition of EMC, forming the solubility curve of EC in EMC with the eutectic point (−55.1 °C) on the EC-EMC binary. With the addition of DMC and EMC together, the melting point of EC expands into a falling solubility surface of EC in DMC-EMC, bounded on the two binary end-members by the solubility curves of EC in DMC and in EMC. It is further bounded within the composition triangle by two more space curves formed when the solubility surface of EC intersects those of DMC and EMC. Further, the three solubility surfaces meet at the eutectic point (−64.7 °C) of the ternary system EC-DMC-EMC, thus forming a complete liquidus surface above which any composition of the ternary is a thermodynamically stable liquid. Below the eutectic temperature of the ternary, which is lower than any of the three binary eutectic temperatures, any composition will be composed of nothing but solid phases. The most striking and important feature in the topography of the liquidus surface of the EC-DMC-EMC ternary is the slow descent of the melting point of EC with the addition of, or the flat solubility surface of EC in, DMC and EMC.

The electrolytic conductivity of $LiPF_6$ in the EC-EMC binary solvent system is given in Table 2.2 over a range of salt concentrations and temperatures [1, 3]. The content of EC is usually less than 50 vol.%, preferably 30 vol.%, because higher EC content causes its precipitation at low temperatures. For high-rate (high-power) applications, further high electrolytic conductivity is required. The addition of DMC is an effective solution to increase the electrolytic conductivity as shown in Fig. 2.3.

In addition to carbonate solvents, much effort has been made to introduce new solvents in order to improve cell performance. In the following section, heteroatom-containing organic solvents applied to lithium cells in recent years are reviewed by each author. The heteroatom includes fluorine, phosphorous, boron, and sulfur.

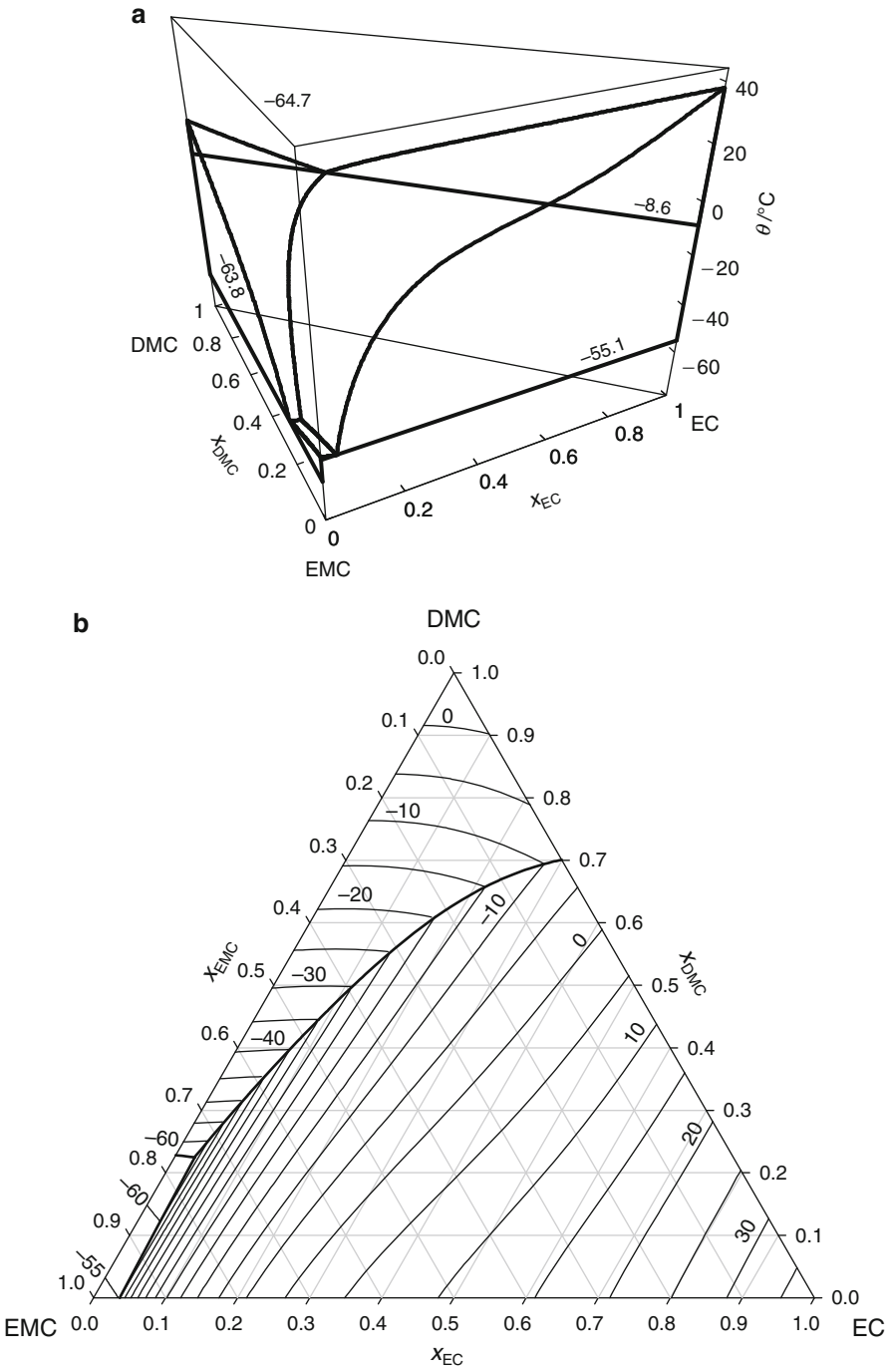

Fig. 2.2 The phase diagram of an EC-DMC-EMC ternary solvent system. M. S. Ding, *J. Electrochem. Soc,*. 151, A731 (2004). Reproduced by permission of The Electrochemical Society

Table 2.2 Electrolytic conductivity of $LiPF_6$ in an EC-EMC binary solvent system

$LiPF_6$, C (M)	EC, χ (vol.%)	EMC, χ (vol.%)	t (°C)											
			−40	−30	−20	−10	0	10	20	25	30	40	50	60
0.50	10	90	0.9	1.4	1.9	2.4	3.0	3.6	4.2	4.4	4.7	5.3	5.8	6.3
0.75	10	90	1.2	1.8	2.6	3.3	4.1	5.0	5.9	6.3	6.7	7.5	8.3	9.1
1.00	10	90	1.0	1.7	2.6	3.5	4.4	5.4	6.5	6.9	7.4	8.4	9.4	10.4
1.25	10	90	1.0	1.7	2.6	3.7	4.8	5.9	7.2	7.6	8.3	9.5	10.7	11.8
1.50	10	90	0.7	1.3	2.1	3.1	4.1	5.4	6.7	7.3	8.0	9.3	10.7	12.0
0.50	30	70		*p*	3.0	4.0	5.1	6.3	7.5	8.0	8.6	9.8	11.1	12.3
0.75	30	70	*p*	2.1	3.1	4.3	5.6	7.0	8.6	9.3	10.0	11.5	13.1	14.6
1.00	30	70	1.1	1.8	2.9	4.1	5.6	7.2	8.8	9.6	10.5	12.2	14.0	15.8
1.25	30	70	0.7	1.3	2.3	3.4	4.8	6.5	8.2	9.0	9.9	11.8	13.7	15.6
1.50	30	70	0.4	1.0	1.8	3.0	4.4	6.0	7.7	8.5	9.4	11.3	13.3	15.5
0.50	50	50			*p*	3.8	4.9	6.3	7.6	8.3	9.0	10.4	11.9	13.4
0.75	50	50		*p*	2.9	4.2	5.6	7.2	8.9	9.8	10.7	12.5	14.5	16.4
1.00	50	50		*p*	2.7	4.0	5.4	7.0	8.8	9.7	10.6	12.6	14.8	16.9
1.25	50	50		*p*	1.9	3.1	4.7	6.4	8.4	9.3	10.4	12.6	14.9	17.3
1.50	50	50							Insoluble					
0.50	60	40						*p*	7.4	8.1	8.8	10.3	11.8	13.3
0.75	60	40				*p*	5.4	7.0	8.8	9.7	10.6	12.5	14.5	16.5
1.00	60	40			*p*	3.5	5.1	6.8	8.6	9.5	10.5	12.6	14.8	17.0
1.25	60	40			*p*	2.9	4.3	6.2	8.2	9.2	10.2	12.5	15.0	17.5
1.50	60	40							Insoluble					

in mS cm^{-1}, *p*: EC precipitation

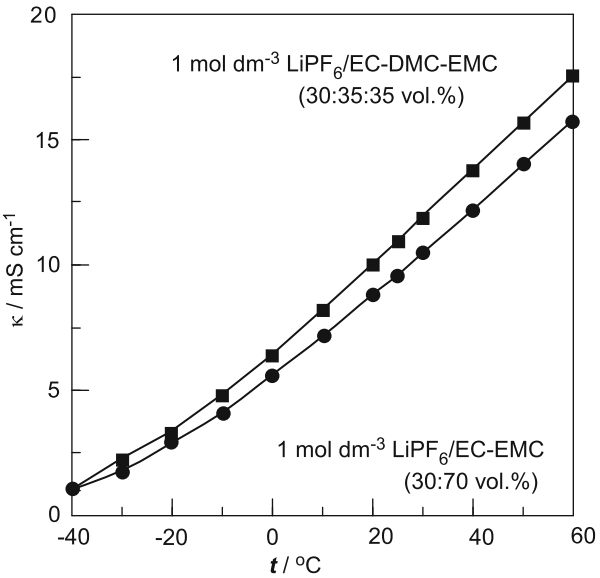

Fig. 2.3 Conductivity increases by the addition of DMC

2.2 Fluorine-Containing Organic Solvents

2.2.1 Introduction

One of the recent methodologies for finding a new appropriate solvent for advanced lithium batteries is the introduction of fluorine atoms into the solvent molecules, because it will improve the various electrochemical properties such as solvent polarity, oxidation durability, liquidus temperature range, and nonflammability, which would result in better cell performances [4, 5]. In general, fluorinated organic solvents show very different physical properties compared to the common organic solvents because of very high electronegativity and low polarizability of the fluorine atom. In addition, partially fluorinated organic solvents show fairly high polarity in comparison with that of fully fluorinated (perfluoro-) organic solvents.

There are three methods for the introduction of fluorine atoms into the solvent molecules, which are common organic chemical synthesis, electrolytic fluorination, and direct fluorination using elemental fluorine (F_2 gas), respectively. The direct fluorination is the simplest method to prepare partially fluorinated organic solvents. It makes possible to obtain many interesting fluorinated organic solvents. Among the important solvents for practical lithium batteries, the direct fluorination has already been applied to propylene carbonate (PC) [6] and 1,2-dimethoxyethane (DME) [7] in the late 1960s.

This section mainly reviews the papers on the novel fluorinated organic solvents, which were investigated for lithium batteries in the past decade. Although their chemical structures were drawn in Schemes, it was difficult to include all detailed data on physical and electrochemical properties of fluorinated solvents. The physical properties of typical fluorinated compounds and non-fluorinated counterparts were summarized in Tables 2.3 and 2.4, respectively [4, 5], where FW, d, ε_r, η, E_{homo}, and E_{lumo} are formula weight, density, relative permittivity, viscosity, and frontier orbital energies, respectively. The frontier orbital energies were recalculated by RHF/6-311+G(2d,p) with structure optimization.

2.2.2 Fluorinated Lactones

γ-Butyrolactone (γ-BL) is one of the good solvents for lithium batteries because of its well-balanced relative permittivity and viscosity, and wide liquidus temperature range. Therefore, it is interesting to modify γ-BL by fluorination. Three kinds of mono-fluorinated γ-butyrolactones, α-fluoro-γ-BL (α-F-γ-BL), β-fluoro-γ-BL (β-F-γ-BL), and γ-fluoro-γ-BL (γ-F-γ-BL) were prepared by direct fluorination as shown in Scheme 2.1 [8]. A mixture of α-F-γ-BL and β-F-γ-BL was obtained by fractional distillation (3:7 in molar ratio, F-γ-BL_{mix}). γ-F-γ-BL was easily decomposed by HF produced during the reaction. It was possible to obtain α-F-γ-BL by direct fluorination using α-acetyl-γ-BL as a starting material [5]. In addition, γ-F-γ-BL was selectively produced by electrolytic fluorination [9].

Table 2.3 Physical properties of fluorinated solvents

Name	FW	d, g cm^{-3}	ε_r	η, mPa s	E_{homo}, eV	E_{lumo}, eV
α-Fluoro-γ-butyrolactone (α-F-γ-BL)	104	1.30	73	3.4	−12.16	1.55
β-Fluoro-γ-butyrolactone (β-F-γ-BL)	104				−12.19	1.52
γ-Fluoro-γ-butyrolactone (γ-F-γ-BL)	104				−12.31	1.61
3:7 mixture of α-and β-Fluoro-γ-butyrolactone (F-γ-BL$_{mix}$)	104	1.30	80	3.9	–	–
Methyl fluoroacetate (MFA)	92	1.17	18	1.2	−12.58	1.71
Methyl difluoroacetate (MDFA)	110	1.26			−12.90	1.67
Ethyl fluoroacetate (EFA)	106	1.09	15	0.89	−12.47	1.75
Ethyl difluoroacetate (EDFA)	124	1.24			−12.78	1.73
2-Fluoroethyl acetate (2FEA)	106	1.09	7.8	0.97	−12.46	1.75
2,2-Difluoroethyl acetate (DFEA)	124	1.20	9.4	1.0	−12.64	1.74
2,2,2-Trifluoroethyl acetate (TFEA)	142	1.24	6.7	0.70	−12.80	1.76
4-Fluoro-1,3-dioxolan-2-one (FEC)	106	1.50	107	4.1	−13.30	1.45
cis-4,5-Difluoro-1,3-dioxolan-2-one (*cis*-DFEC)[a]	124	1.59		2.3 (60 °C)	−13.91	1.34
trans-4,5-Difluoro-1,3-dioxolan-2-one (*trans*-DFEC)[a]	124	1.51	37	2.5	−13.91	1.63
4,4-Difluoro-1,3-dioxolan-2-one (*gem*-DFEC)[a]	124	1.57	34	2.1	−13.70	1.56
4-Fluoromethyl-1,3-dioxolan-2-one (FPC)	120	1.41	190	7.6	−13.00	1.39
4-Trifluoromethyl-1,3-dioxolan-2-one (TFPC)	156	1.58	67	5.0	−13.39	1.31
trans-4-Fluoromethyl-5-methyl-1,3-dioxolan-2-one (F-*t*-BC)	134	1.33	150	13	−12.86	1.44
Fluoromethyl methyl carbonate (FDMC)	108	1.24	9.0	0.92	−13.25	1.79
Bis(fluoromethyl) carboante (DFDMC)	126	1.40	14	1.4	−13.68	1.80
Difluoromethyl fluoromethyl carboante (TFDMC)	144	1.47	11	0.99	−13.75	1.76
2-Fluoroethyl methyl carbonate (FEMC)	122	1.19	7.3	1.4	−12.98	1.84
2,2-Difluoroethyl methyl carbonate (DFEMC)	140	1.29	9.3	2.7	−13.21	1.78
Methyl 2,2,2-trifluoroethyl carbonate (TFEMC)	158	1.33	7.1	0.82	−13.33	1.75
Ethyl 2-fluoroethyl carbonate (FDEC)	136	1.12	6.5	1.3	−12.80	1.86
2,2-Difluoroethyl ethyl carbonate (DFDEC)	154	1.29	6.6	1.3	−13.01	1.82
Ethyl 2,2,2-trifluoroethyl carbonate (TFDEC)	172	1.33	7.1	0.93	−13.11	1.80
3-Fluoropropyl methyl carbonate (FPMC)	136	1.14	7.1	1.7	−12.98	1.83
Methyl 3,3,3-trifluoropropyl carbonate (TrFPMC)	172	1.30	7.5	1.7	−13.13	1.77
Methyl 2,2,3,3-tetrafluoropropyl carbonate (TeFPMC)	190	1.40	8.8	2.6	−13.28	1.73
Methyl 2,2,3,3,3-pentafluoropropyl carbonate (PeFPMC)	208	1.41	6.2	1.3	−13.06	1.75
Methyl nanofluorobutyl ether (MFE)	250	1.52		0.38	−14.03	1.70
Ethyl nanofluorobutyl ether (EFE)	264	1.43		0.38	−13.26	1.77
2-Trifluoromethyl-3-methoxyperfluoropentane (TMMP)[b]	350	1.66	6.1	1.2	−13.08	1.68
2-(Trifluoro-2-fluoro-3-difluoropropxy)-3-difluoro-4-fluoro-5-trifluoropentane (TPTP)[b]	346	1.54	6.3	1.7	−13.81	1.47
2-Fluoroethoxymethoxyethane (FEME)	122	1.01	17	1.0	−11.68	1.95
2,2-Difluoroethoxymethoxyethane (DFEME)	140	1.10	17	1.1	−11.88	1.87
Methoxy-2,2,2-trifluoroethoxyethane (TFEME)	158	1.15	17	0.79	−11.98	1.84
Ethoxy-2-fluoroethoxyethane (EFEE)	136	0.97	14	1.1	−11.58	1.97
2,2-Difluoroethoxyethoxyethane (EDFEE)	154	1.05	14	1.1	−11.77	1.91
Ethoxy-2,2,2-trifluoroethoxyethane (ETFEE)	172	1.10	14	0.85	−11.87	1.89

[a]Reference [20]
[b]Reference [50]

Table 2.4 Physical properties of typical organic solvents

Name	FW	d, g cm^{-3}	ε_r	η, mPa s	E_{homo}, eV	E_{lumo}, eV
γ-Butyrolactone (γ-BL)	86	1.13	39	1.7	−11.86	1.67
Methyl acetate (MA)	74	0.93	6.7	0.36	−12.21	1.85
Ethyl acetate (EA)	88	0.89	6.0	0.43	−12.09	1.87
Ethylene carbonate (EC)	88	1.32 (40 °C)	90 (40 °C)	1.9 (40 °C)	−12.86	1.51
Propylene carbonate (PC)	102	1.20	65	2.5	−12.72	1.52
trans-Butylene carbonate (*t*-BC)	116	1.14	64	3.2	−12.60	1.55
Dimethyl carbonate (DMC)	90	1.06	3.1	0.59	−12.85	1.88
Ethyl methyl carbonate (EMC)	104	1.01	3.0	0.65	−12.71	1.91
Diethyl carbonate (DEC)	118	0.97	2.8	0.75	−12.59	1.93
Propyl methyl carbonate (PMC)	118	0.98	3.0	1.1	−12.67	1.91
Dimethoxyethane (DME)	90	0.86	5.5	0.46	−11.49	2.02
Ethoxymethoxyethane (EME)	104	0.85	5.7	0.52	−11.40	2.03
Diethoxyethane (DEE)	118	0.84	5.0	0.60	−11.36	2.05

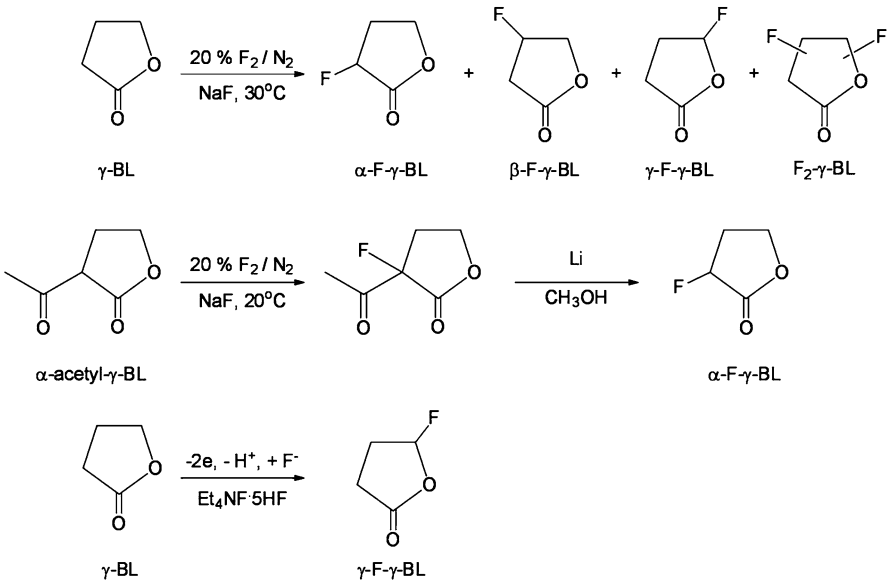

Scheme 2.1 Preparation methods of fluorinated γ-butyrolactones

The melting point of α-F-γ-BL is 26.5 °C, which is very different from that of γ-BL (−43.4 °C) [5]. The relative permittivities of α-F-γ-BL and F-γ-BL$_{mix}$ at 25 °C were 72.6 and 80.3, respectively, and about twice of that of γ-BL in a temperature range from 10 to 80 °C [5, 10]. At the same time, the viscosities of α-F-γ-BL and F-γ-BL$_{mix}$ became much higher than that of γ-BL. The electrolytic conductivities of lithium salts in α-F-γ-BL and F-γ-BL$_{mix}$ in a temperature range from 10 to 80 °C

were in the order; $LiPF_6 > LiClO_4 > LiBF_4$ and F-γ-BL_{mix} > α-F-γ-BL, and always lower than those in γ-BL due to their high viscosities. α-F-γ-BL and F-γ-BL_{mix} showed higher oxidation potentials than γ-BL on Pt electrode. In general, the introduction of fluorine atoms to organic solvents tends to increase their oxidation potentials and decrease their reduction potentials as expected from HOMO and LUMO energies. The lithium cycling efficiency (charge–discharge coulombic efficiency for a lithium electrode) on a Ni electrode was examined as the first step to know the possibility of applying F-γ-BL_{mix} to rechargeable lithium cells. The cycling efficiency is highly dependent on the morphology of the film on the lithium electrode. Among three kinds of solvents tested, F-γ-BL_{mix}, γ-BL, and PC, the lithium cycling efficiency became in the order; F-γ-BL_{mix} > PC > γ-BL and $LiPF_6 > LiBF_4 > LiClO_4$. Furthermore, 1 moldm^{-3} $LiPF_6$/F-γ-BL_{mix}-EC equimolar binary solution showed higher efficiency more than 75 % during 100 cycles, and better than α-F-γ-BL-EC equimolar binary solution. 1 moldm^{-3} $LiPF_6$/F-γ-BL_{mix} electrolyte showed much higher capacity retention in a Li/$LiCoO_2$ cell than γ-BL counterpart, but not as good as PC counterpart [10].

2.2.3 *Fluorinated Linear Carboxylates*

Fluorinated compounds of linear carboxylates were examined for low temperature application. The electrochemical behavior of a graphite electrode at low temperatures was investigated in 1 moldm^{-3} $LiClO_4$/EC-DEC-X (10:10:1 in volume) solution containing a fluorinated carboxylate (X) selected form CHF_2COOCH_3 (methyl difluoroacetate, MDFA), $CF_3CF_2COOCH_2CH_3$, $CF_3CF_2CF_2COOCH_3$, $(CF_3)_2CHCOOCH_3$, $CF_3CF_2CF_2CF_2COOCH_2CH_3$, $CF_3CF_2CF_2CF_2CF_2CF_2COOCH_3$, $CF_3CF_2CF_2CF_2$ $CF_2CF_2CF_2COOCH_2CH_3$ [11], and 1 moldm^{-3} $LiClO_4$/EC-DEC-PC-X (4:4:2:1 in volume) selected from CHF_2COOCH_3, $CF_3CF_2COOCH_2CH_3$, $CF_3CF_2CF_2COOCH_3$, $(CF_3)_2CHCOOCH_3$, $CF_3CF_2CF_2CF_2COOCH_2CH_3$, $CF_3CF_2CF_2CF_2COOCH(CH_3)_2$, $CF_3CF_2CF_2CF_2COOC(CH_3)_3$ [12] in Scheme 2.2.

The electrolytic conductivities of 1 moldm^{-3} $LiClO_4$/EC-DEC-MDFA (10:10:1 in volume) and EC-DEC-PC-MDFA (4:4:2:1 in volume) solutions were a little bit higher than those of EC-DEC and EC-DEC-PC baseline solutions, respectively, and other fluorinated carboxylates gave inferior conductivities in a temperature range from 0 to 50 °C [12]. The reduction potentials of these fluorinated carboxylates (0.87–1.41 vs. Li/Li$^+$) were more positive than that of EC (0.60 V). With decreasing reduction potential of the fluorinated carboxylates, the reversibility of the graphite electrode increased, resulting in higher charge capacity. The lowest reduction potential was observed for a low molecular weight MDFA. 1 moldm^{-3} $LiClO_4$/EC-DEC-MDFA (10:10:1 in volume) solution provided larger charge capacities than EC-DEC baseline solution at 0 and −4 °C. The study was extended to fluorinated graphite electrodes using 1 moldm^{-3} $LiClO_4$/EC-DEC-PC (1:1:1 in volume) solution with 0.15 vol.% MDFA at −10 °C [13].

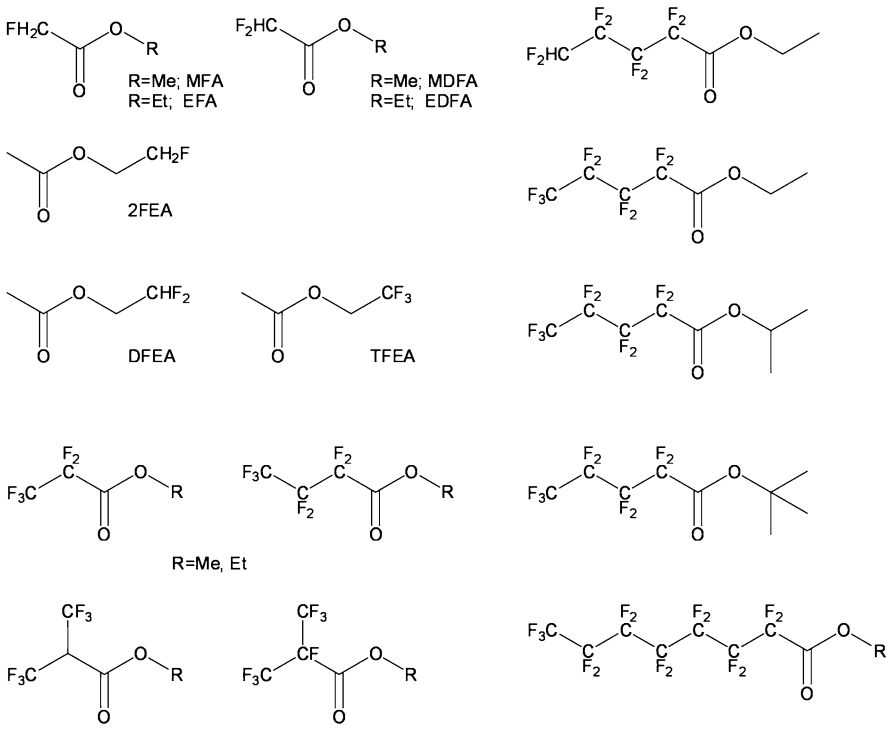

Scheme 2.2 Fluorinated linear carboxylates

Thermal stability and electrochemical properties of fluorinated carboxylates selected from CHF_2COOCH_3 (MDFA), $CHF_2COOCH_2CH_3$ (ethyl difluoroacetate, EDFA), $CF_3CF_2COOCH_3$, $CF_3CF_2COOCH_2CH_3$, $CF_3CF_2CF_2COOCH_3$, $CF_3CF_2CF_2COOCH_2CH_3$, $(CF_3)_2CFCOOCH_3$, $(CF_3)_2CFCOOCH_2CH_3$, $HCF_2CF_2CF_2CF_2COOCH_2CH_3$, and $CF_3CF_2CF_2CF_2CF_2CF_2CF_2COOCH_2CH_3$ in Scheme 2.2 were investigated [14–17]. Most fluorinated carboxylates including 0.2 moldm^{-3} or saturated $LiPF_6$ showed an exothermic reaction peak at higher temperatures in differential scanning calorimetry (DSC) than the corresponding non-fluorinated solvent counterparts even at the coexistence of Li or $Li_{0.5}CoO_2$ [14]. Among these fluorinated carboxylates, 1 moldm^{-3} $LiPF_6$/EC-DMC-MDFA (1:1:2 in volume) solution showed the highest onset temperature and smallest amount of exothermic heat at the coexistence of lithium [15]. However, the volume ratio of MDFA in 1 moldm^{-3} $LiPF_6$/EC-DMC-MDFA, PC-MDFA solutions should be more than 50 % to show the remarkable improvement of the thermal stability. This kind of good behavior was observed only in MDFA and not in EDFA, because the main component of SEI in the MDFA solution was CHF_2COOLi, which dissolved in EC, PC, DMC, DEC, and EDFA solution [16]. The main exothermic peak of 1 moldm^{-3} $LiPF_6$/MDFA solution at the coexistence of a lithiated graphite is around 400 °C and about 100 °C higher than that of EC-DMC (1:1 in volume) solution [17].

The relative permittivities and viscosities of methyl acetate (MA) and ethyl acetate (EA) increased by the introduction of one or two fluorine atoms, which resulted in the decrease of electrolytic conductivity of 1 moldm^{-3} $LiPF_6$ solutions as usual [16, 18]. The oxidation potentials on Pt were also increased by the introduction of fluorine atoms. Depending on the position of fluorine atom, the properties of 2-fluoroethyl acetate (2FEA) and ethyl fluoroacetate (EFA) varied. The electrolytic conductivities of 1 moldm^{-3} $LiPF_6$ solutions at 25 °C were in the order; MA > EA > MDFA > EFA > EC-DMC (1:1 in volume) >2FEA > EDFA >> EMC. However, the electrolytic conductivities of 1 moldm^{-3} $LiPF_6$/EFA and 2FEA solutions became higher than that of EA counterpart at high temperatures [18]. The lithium cycling efficiency of 1 moldm^{-3} $LiPF_6$/MDFA solution was more than 80 % and higher than those of EDFA, MA, or EA solutions [14]. The lithium cycling efficiency of 1 moldm^{-3} $LiPF_6$/EC-2FEA equimolar binary solution was higher than those of EC-EFA, EC-EA, or EC-EMC solutions [18]. The discharge capacity of carbons was smaller in 1 moldm^{-3} $LiPF_6$/MDFA solution than EC-DMC (1:1 in volume) counterpart due to the large resistance of SEI, while the cycling performance was similar to EC-DMC counterpart. A graphite/$LiCoO_2$ cells containing 1 moldm^{-3} $LiPF_6$/MDFA electrolyte exhibited a good cycling performance without any oxidation of the electrolyte on the $LiCoO_2$ cathode [17]. Furthermore, by adding 3 vol.% of vinylene carbonate (VC) in 1 moldm^{-3} $LiPF_6$/MDFA electrolyte resulted in satisfactory reversible capacity and cycling performance in a graphite/$LiCoO_2$ cell [19].

2.2.4 Fluorinated Cyclic Carbonates

Ethylene carbonate (EC) and propylene carbonate (PC) have favorable physical and electrochemical properties such as high relative permittivity, high donicity, and relatively wide potential window. The direct fluorination of EC was successfully carried out to provide 4-fluoro-1,3-dioxolan-2-one (fluoroethylene carbonate, FEC) as shown in Scheme 2.3 [20]. The fluorination of EC was strongly dependent on a choice of a reaction medium and no solvent was preferred from the viewpoint of conversion. FEC was further fluorinated to give three di-fluorinated derivatives. On the other hand, FEC was also prepared from 4-chloroethylene carbonate by exchange with KF [21]. FEC was tested as an electrolyte additive for rechargeable lithium cells [21, 22] and is now practically used [23, 24].

The melting point of FEC was 17 °C and lower than that of EC (37 °C). The relative permittivity and viscosity of FEC were higher than those of EC (Fig. 2.4a, b) [25]. The electrolytic conductivity of $LiPF_6$ in FEC was always lower than that in EC due to its high viscosities (Fig. 2.4c) [4]. FEC showed a higher oxidation potential on Pt than EC (Fig. 2.4d). The lithium cycling efficiency of 1 moldm^{-3} $LiPF_6$/FEC was as high as 90 % (Fig. 2.4e). The cycling efficiency of a graphite/$LiCoO_2$ cell containing 1 moldm^{-3} $LiPF_6$/FEC-PC-EC (1:3.5:3.5 in volume) electrolyte was higher than 99.5 % and the discharge capacity retention of the cell was 63 % at the 200th cycle [5].

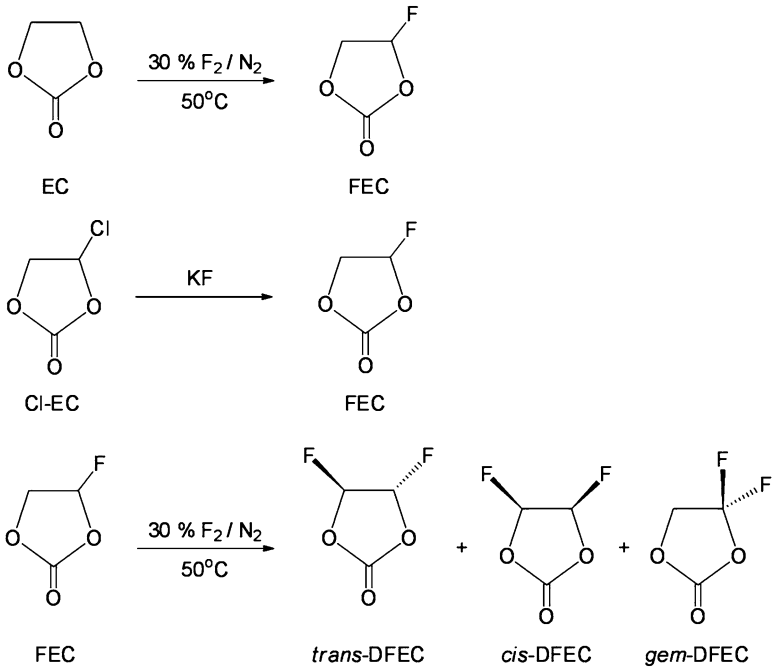

Scheme 2.3 Preparation methods of fluorinated ethylene carbonates

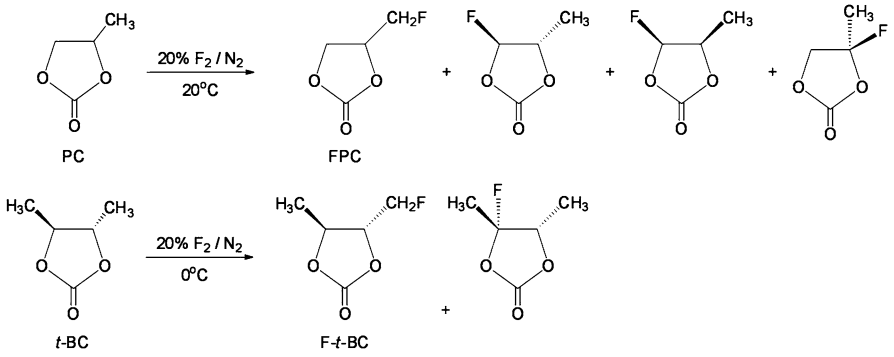

Scheme 2.4 Preparation of fluorinated propylene carbonates and *trans*-butylene carbonates

The direct fluorination of PC and *trans*-butylene carbonate (*t*-BC) gave four and two mono-fluorinated derivatives, respectively as shown in Scheme 2.4 [5, 26]. 4-Fluoromethyl-1,3-dioxolan-2-one (fluoromethylethylene carbonate, FMEC; hereafter renamed as FPC for easy understanding), 4-fluoromethyl-5-methyl-1,3-dioxolan-2-one (fluormethylmethylethylene carbonate, FMMEC; hereafter renamed as F-*t*-BC for easy understanding) were obtained by fractional distillation of the fluorinated samples.

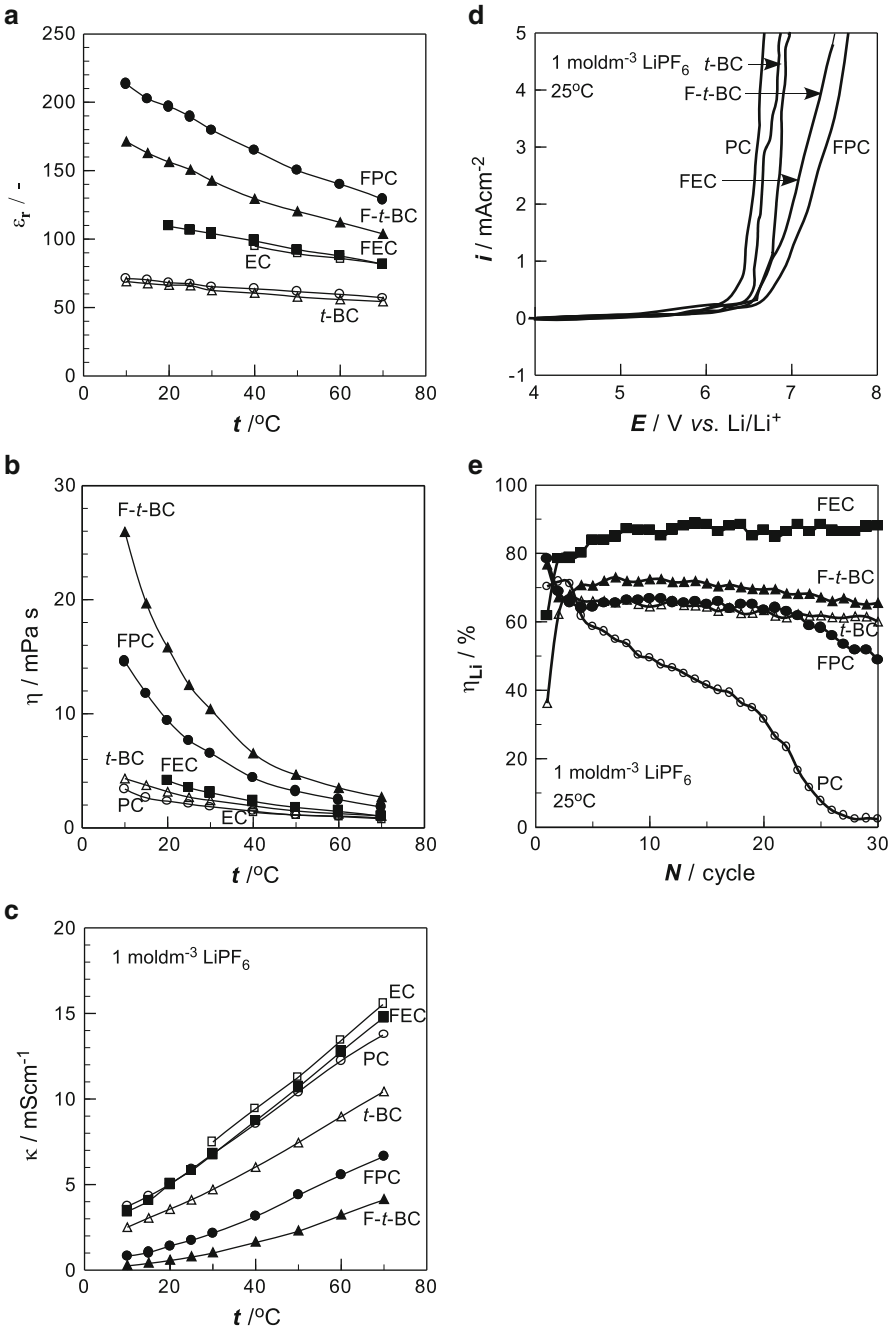

Fig. 2.4 Properties of cyclic carbonates and its mono-fluorinated derivatives. (**a**) relative permittivity (**b**) viscosity (**c**) electrolytic conductivity (**d**) oxidation potential (**e**) lithium cycling efficiency

The relative permittivities and viscosities of FPC and F-*t*-BC were higher than those of PC and *t*-BC, respectively (Fig. 2.4a, b) [27, 28]. The electrolytic conductivities of lithium salts in FPC and F-*t*-BC were always lower than those in PC and *t*-BC, respectively, due to their high viscosities (Fig. 2.4c) [4]. FPC and F-*t*-BC showed higher oxidation potentials on Pt than PC and *t*-BC, respectively (Fig. 2.4d). The lithium cycling efficiency in 1 moldm^{-3} $LiPF_6$/FPC and F-*t*-BC solutions was higher than those in PC and *t*-BC counterparts, respectively, but lower than FEC counterpart (Fig. 2.4e). The cycling efficiencies of Li/$LiCoO_2$ and graphite/$LiCoO_2$ cells containing 1 moldm^{-3} $LiPF_6$/FPC electrolyte were more than 95 % at a large cycle number. The cycling efficiency and discharge capacity of a graphite/$LiCoO_2$ cell containing 1 moldm^{-3} $LiPF_6$/FPC-EMC (1:3 in molar ratio) electrolyte was lower than those of EC-EMC counterpart at 25 °C; however, they were reversed at 60 °C [28].

As the novel fluorinated cyclic carbonates, the Li^+ intercalation of a graphite and SEI formation in 4-trifluoromethyl-1,3-dioxolan-2-one (trifluoromethylpropylene carbonate, TFPC) in Scheme 2.5 was investigated [29] and its 1 moldm^{-3} $LiPF_6$ binary mixed electrolytes with EC, PC, and ClEC were examined in graphite/Li and $LiMn_2O_4$/Li half cells [30]. The electrochemical behavior of 4-(2,2,3,3-tetrafluoropropoxymethyl)-1,3-dioxolan-2-one, 4-(2,3,3,3-tetrafluoro-2-trifluoromethylpropyl)-1,3-dioxolan-2-one, and 4,5-difluoro-4,5-dimethyl-1,3-dioxolan-2-one in Scheme 2.5 has been studied in EC-DEC and EC-DEC-PC mixtures [31, 32]. Electrochemical oxidation using a Pt microelectrode was largely suppressed by mixing these fluorinated derivatives with 0.67 moldm^{-3} $LiClO_4$/EC-DEC (1:1 in volume) or EC-DEC-PC (1:1:1 in volume). The oxidation current on a natural graphite was much smaller in 0.67 moldm^{-3} $LiClO_4$/EC-DEC-X (1:1:1 in volume) than in EC-DEC (1:1 in volume) or EC-DEC-PC (1:1:1 in volume) baseline solutions, and the reduction potentials of these fluorinated derivatives on the natural graphite were about 2 V vs. Li/Li^+, which were higher than those of EC, DEC, and PC. These fluorinated carbonates increased the first coulombic efficiencies on natural graphites due to the quick SEI formation in PC-containing solutions. Thermal stability was also increased by the use of these fluorinated derivatives. In addition, these fluorinated derivatives gave antioxidation ability to electrolyte solutions.

2.2.5 Fluorinated Linear Carbonates

Among the carbonate solvents used in practical lithium batteries, linear carbonates such as dimethyl carbonate (DMC), ethyl methyl carbonate (EMC), and diethyl carbonate (DEC) are well-known good co-solvents (thinner) for EC and PC. The direct fluorination of DMC gave fluorinated derivatives such as mono-fluorinated one, fluoromethyl methyl carbonate (FDMC), two di-fluorinated ones (bis(fluoromethyl) carbonate, DFDMC, and difluormethyl methyl carbonate, *gem*-DFDMC), and trifluorinated ones (difluoromethyl fluoromethyl carbonate, TFDMC) as shown in Scheme 2.6 [33]. Three kinds of partially fluorinated DMCs except *gem*-DFDMC were obtained by fractional distillation of the fluorinated sample.

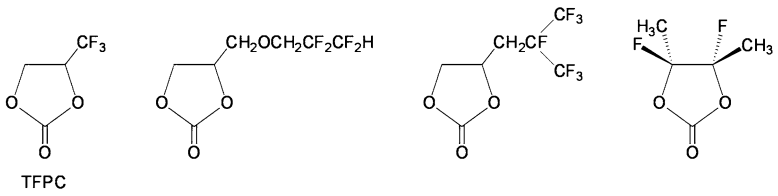

Scheme 2.5 Other fluorinated cyclic carbonates

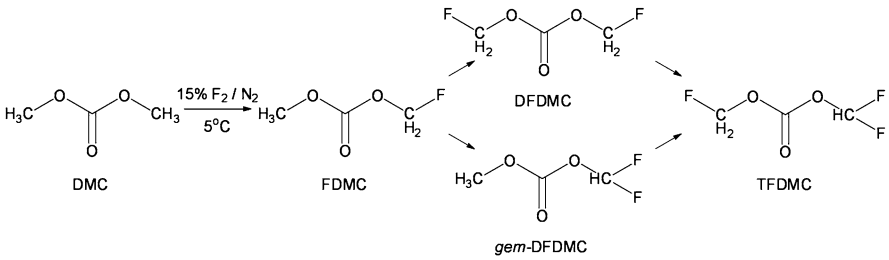

Scheme 2.6 Preparation of fluorinated dimethyl carbonates

The relative permittivity and viscosity of FDMC were higher than those of DMC (Fig. 2.5a, b) [34–36]. The electrolytic conductivities of 1 moldm^{-3} lithium salts ($LiClO_4$, $LiBF_4$, $LiPF_6$) in FDMC or EC-FDMC at 25 °C were always lower than those in DMC or EC-DMC counterparts due to their high viscosities (Fig. 2.5c). FDMC showed a higher oxidation potential on Pt than DMC (Fig. 2.5d). The lithium cycling efficiency in 1 moldm^{-3} $LiPF_6$/FDMC and EC-FDMC equimolar solution was higher than that in EC-DMC counterpart (Fig. 2.5e). The cycling efficiency of a Li/$LiCoO_2$ cell containing 1 moldm^{-3} $LiPF_6$/EC-FDMC equimolar electrolyte was higher than 95 % and the discharge capacity retentions of the cells were also higher than those of EC-DMC counterpart [36].

The relative permittivity and viscosity increased in the order; DMC < FDMC < TFDMC < DFDMC (Fig. 2.5a, b) [37, 38]. The electrolytic conductivities of 1 moldm^{-3} $LiPF_6$ solutions were in the order; DFDMC < FDMC < DMC over the concentration range from 0.5 to 2.0 moldm^{-3} (Fig. 2.5c). The electrolytic conductivities of 1 moldm^{-3} $LiPF_6$ in EC equimolar solutions were in the order; DFDMC < FDMC < DMC influenced by their viscosities. The oxidation potentials of these fluorinated DMC on Pt was in the order; DMC < FDMC < DFDMC as expected from HOMO energies (Fig. 2.5d). In general, the oxidation potential of the fluorinated organic solvents tends to increase with the increase in the number of fluorine atoms introduced to the solvent molecule; however, TFDMC with very poor solubility of $LiPF_6$ was excluded from the experiments. DFDMC and EC-DFDMC equimolar binary solutions containing 1 moldm^{-3} $LiPF_6$ showed higher lithium cycling efficiencies; especially, EC-DFDMC solution exhibited more than 80 % at the 100th cycle (Fig. 2.5e).

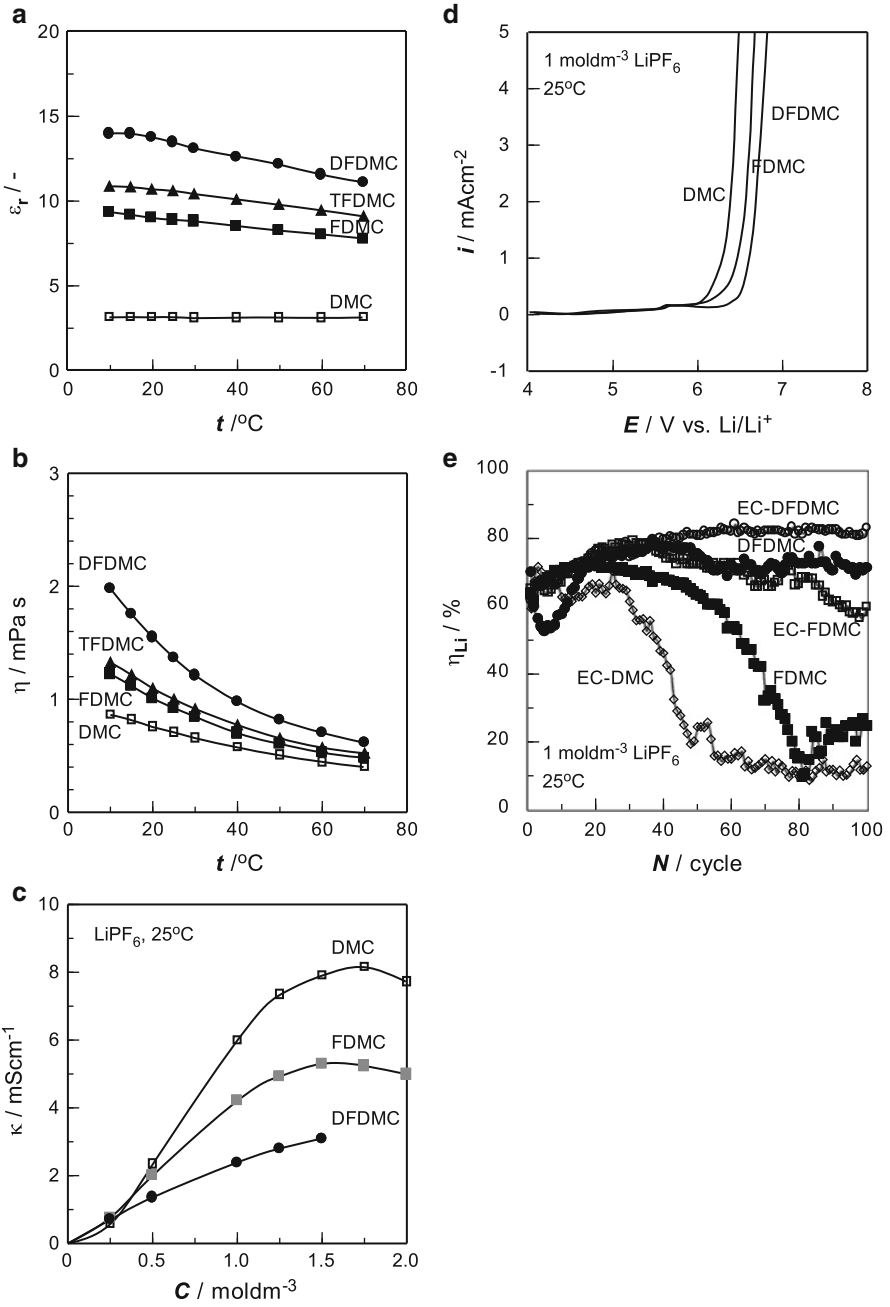

Fig 2.5 Properties of dimethyl carbonates and its fluorinated derivatives. (**a**) relative permittivity (**b**) viscosity (**c**) electrolytic conductivity (**d**) oxidation potential (**e**) lithium cycling efficiency

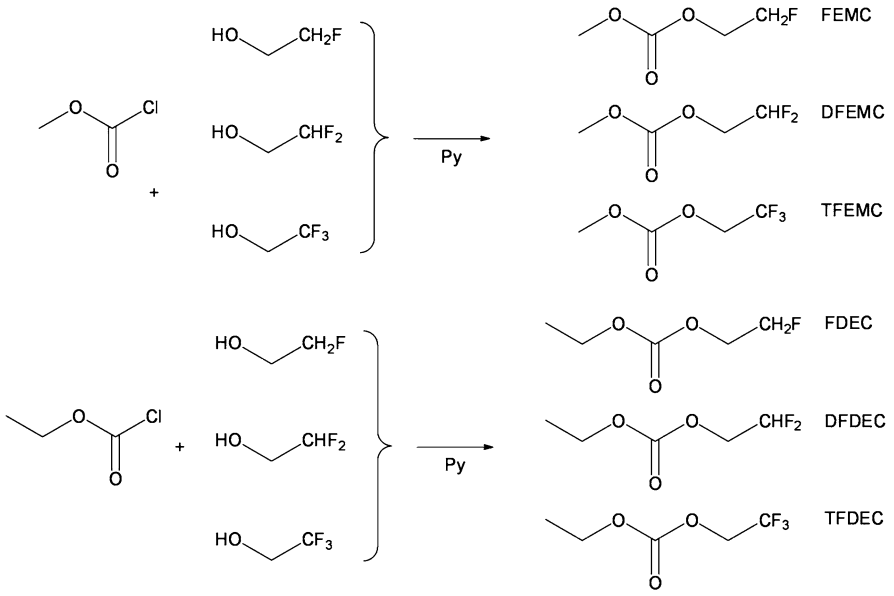

Scheme 2.7 Preparation of fluorinated ethyl methyl carbonates and diethyl carbonates

As partially fluorinated EMC and DEC derivatives, 2-fluoroethyl methyl carbonate (FEMC), 2,2-difluoroethyl methyl carbonate (DFEMC), methyl 2,2,2-trifluoroethyl carbonate (TFEMC), ethyl 2-fluoroethyl carbonate (FDEC), ethyl 2,2-difluoroethyl carbonate (DFDEC), and ethyl 2,2,2-trifluoroethyl carbonate (TFDEC) in Scheme 2.7 were examined [4, 5, 39, 40]. These fluorinated EMC and DEC derivatives were synthesized by use of the corresponding three kinds of fluoroethanols and methyl chlorocarbonate or ethyl chlorocarbonate in the presence of pyridine.

The relative permittivities and viscosities of these fluorinated linear carbonates were higher than those of EMC and DEC, respectively. The relative permittivity and viscosity were in the order; DEC < EMC << FDEC, DFDEC < TFEMC, TFDEC, FEMC << DFEMC and EMC < DEC < TFEMC < TFDEC << FEMC, FDEC, DFDEC << DFEMC, respectively, over the temperature range from 10 to 70 °C (Figs. 2.6a, b and 2.7a, b) [4]. The electrolytic conductivities of 1 moldm^{-3} $LiPF_6$ solutions at 25 °C were in the order; TFDEC < TFEMC, DFDEC < FDEC, DFEMC, DEC < FEMC < EMC (Figs. 2.6c and 2.7c) [4]. The electrolytic conductivities of lithium salts ($LiClO_4$, $LiBF_4$, $LiPF_6$) in FEMC or FDEC were not always lower than those of EMC or DEC counterparts, respectively, depending on the kind of lithium salts, its concentration, and temperature. For example, $LiPF_6$/FEMC or FDEC solutions showed higher conductivities than EMC or DEC counterparts at 25 °C and 0.5 moldm^{-3}, and 1 moldm^{-3} $LiPF_6$/FDEC showed higher conductivity than DEC counterpart above 40 °C [40, 41], which indicates the high degree of dissociation of $LiPF_6$ due to the increase of relative permittivity in spite of the increase of viscosity.

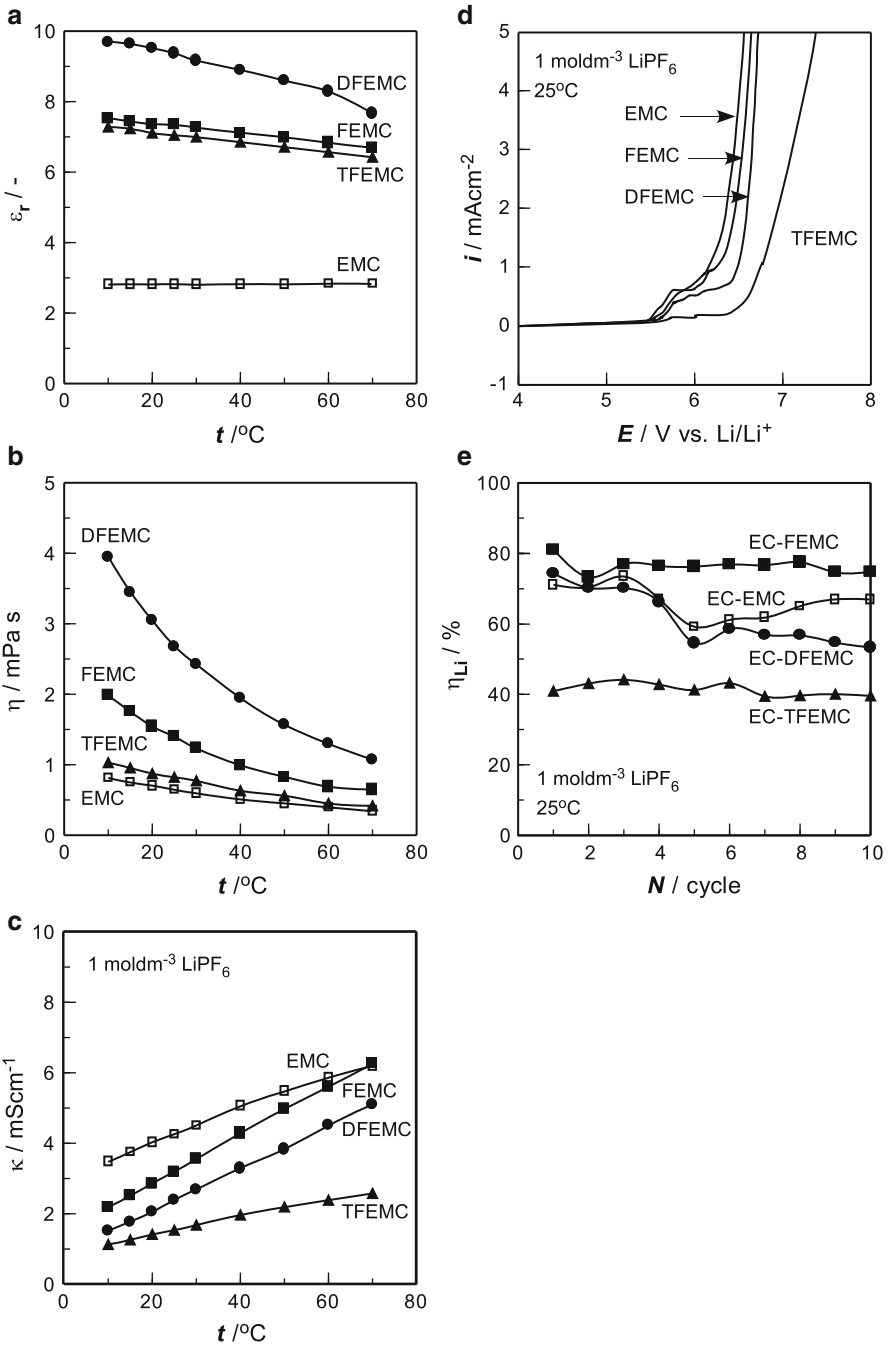

Fig. 2.6 Properties of ethyl methyl carbonates and its fluorinated derivatives. (**a**) relative permittivity (**b**) viscosity (**c**) electrolytic conductivity (**d**) oxidation potential (**e**) lithium cycling efficiency

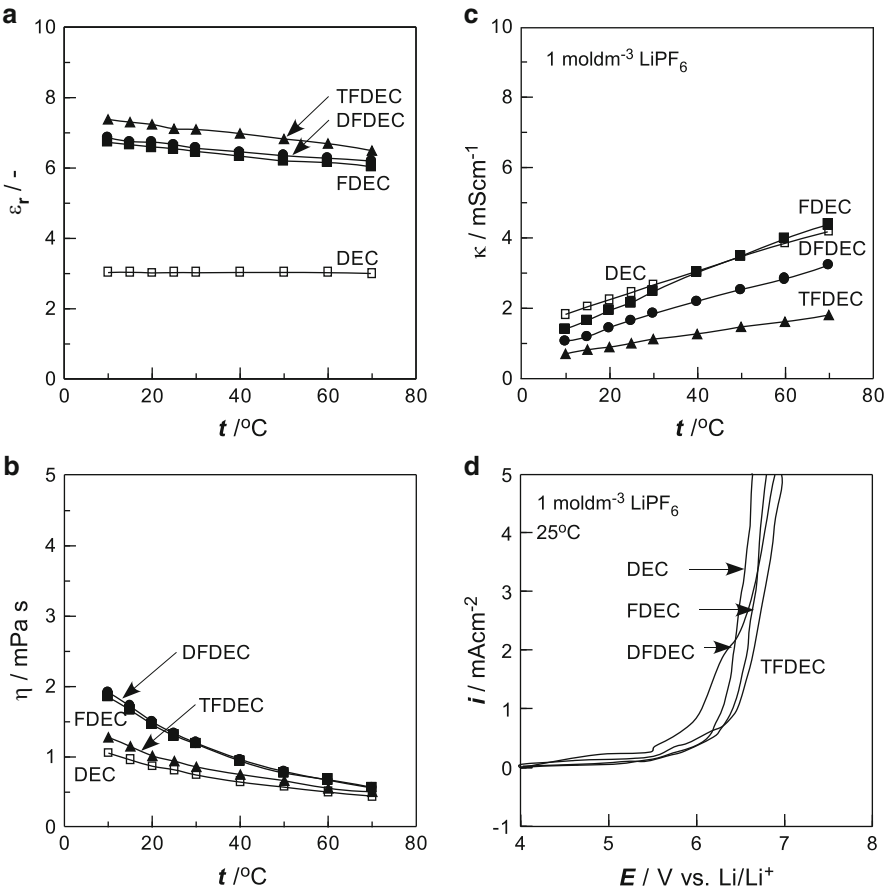

Fig. 2.7 Properties of diethyl carbonates and its fluorinated derivatives. (**a**) relative permittivity (**b**) viscosity (**c**) electrolytic conductivity (**d**) oxidation potential

The electrolytic conductivities of 1 moldm^{-3} $LiPF_6$/EC-FEMC or EC-FDEC equimolar solutions at 25 °C were always lower than those in EC-EMC or EC-DEC counterparts due to their high viscosities. The oxidation potentials on Pt were in the order; EMC, DEC < FEMC, FDEC < DFEMC, DFDEC < TFEMC, TFDEC with increasing the number of fluorine atom (Figs. 2.6d and 2.7d) [4, 5]. The lithium cycling efficiencies in 1 moldm^{-3} $LiPF_6$/EC-FEMC and EC-FDEC equimolar solutions were higher than those in EC-EMC and EC-DEC counterparts, whereas those in EC-DFEMC and EC-TFEMC equimolar electrolytes were lower (Fig. 2.6e). The cycling efficiencies and discharge capacity retentions of a Li/$LiCoO_2$ cell containing 1 moldm^{-3} $LiPF_6$/EC-FEMC and EC-FDEC equimolar electrolytes were higher than those of EC-EMC and EC-DEC counterparts. On the other hand, the cycling

efficiency and discharge capacity retention of a graphite/$LiCoO_2$ cell containing 1 moldm^{-3} $LiPF_6$/EC-FEMC equimolar electrolyte was lower than those of EC-EMC counterpart [4].

Methyl propyl carbonate (MPC) is a structural isomer of DEC. Physical and electrochemical properties of four kinds of partially fluorinated MPC derivatives, 3-fluoropropyl methyl carbonate (FPMC), methyl 3,3,3-trifluoropropyl carbonate (TrFPMC), methyl 2,2,3,3-tetrafluoropropyl carbonate (TeFPMC), and methyl 2,2,3,3,3-pentafluoropropyl carbonate (PeFPMC) in Scheme 2.8 were examined [42].

The relative permittivities and viscosities of these fluorinated MPC derivatives except PeFPMC with five fluorine atoms increased with increasing the number of fluorine atom. The relative permittivity and viscosity of FPMC were higher than those of MPC and lower than those of other fluorinated MPC derivatives. Donor numbers (DN) of these fluorinated solvents, which were estimated by ^{29}Si NMR chemical shifts of triphenylsilanol [42], decreased with increasing the number of fluorine atom except PeFPMC. The electrolytic conductivities of 1 moldm^{-3} $LiPF_6$ in the fluorinated MPC derivatives at 25 °C were in the order; MPC = FPMC > TrPMC > TePMC = MPC. However, the electrolytic conductivity of 1 moldm^{-3} $LiPF_6$/FPMC became higher than that of MPC counterpart above 25 °C. The oxidation potentials of the fluorinated MPC derivatives on Pt increased with increasing the number of fluorine atom. The lithium cycling efficiency in 1 moldm^{-3} $LiPF_6$/PC-FPMC equimolar solution was higher than those in PC and PC-MPC counterparts. In addition, the discharge capacity retention of a Li/$LiCoO_2$ cell containing 1 moldm^{-3} $LiPF_6$/PC-FPMC equimolar electrolyte was higher than those of PC and PC-MPC counterparts.

Electrochemical properties of many ternary and quaternary electrolyte formulations based upon a partially fluorinated carbonate solvent selected from methyl 2,2,2-trifluoroethyl carbonate (TFEMC), ethyl 2,2,2-trifluoroethyl carbonate (TFDEC), propyl 2,2,2-trifluoroethyl carbonate (TFEPC), 2,2,2,2′,2′,2′-hexafluoro-i-propyl methyl carbonate, ethyl 2,2,2,2′,2′,2′-hexafluoro-*i*-propyl carbonate, and bis(2,2,2-trifluoroethyl) carbonate in Scheme 2.9 were examined in detail [43]. A number of electrolyte formulations containing a partially fluorinated aliphatic carbonate showed excellent reversibility, with most of the formulations resulting in higher reversible capacity after the formation cycles compared to the baseline electrolyte formulations in experimental Li/MCMB carbon half cells. Good low temperature performance was observed in many cases, with TFDEC- and TFEPC-containing cells performing the best. The electrodes in contact with the novel electrolytes generally displayed low film resistance and low charge transfer resistance, especially at low temperature. In addition, when Tafel polarization measurements were performed, the novel electrolytes resulted in the least amount of electrode polarization and the highest limiting current densities implying facile lithium intercalation/de-intercalation kinetics. Similar results were reported on bis(2,2,3,3-tetrafluoropropyl) carbonate and bis(2,2,3,3,3-pentafluoropropyl) carbonate in Scheme 2.9 [31].

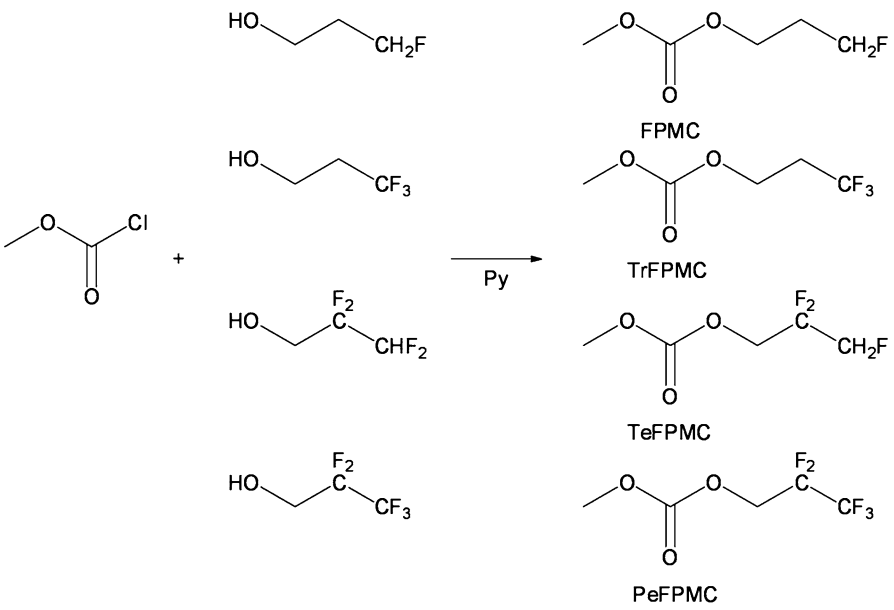

Scheme 2.8 Preparation of fluorinated methyl propyl carbonates

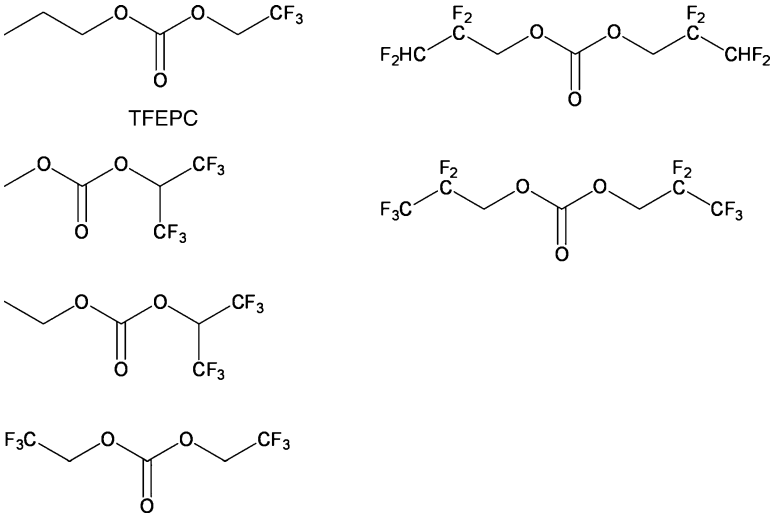

Scheme 2.9 Other fluorinated linear carbonates

2.2.6 *Fluorinated Monoethers*

The addition effect of the hydrofluoroethers such as $CF_3CF_2CH_2OCH_3$, $(CF_3)_2CHCF_2OCH_3$, $HCF_2CF_2CH_2OCHF_2$, $CF_3CHFCF_2OCH_2CH_3$, and $CHClFCF_2OCH_2CF_3$ in Scheme 2.10 to EC-DEC or EC-DEC-PC was investigated using graphite electrodes [12, 32]. The charge capacities higher than in EC/DEC were observed in these electrolytes when the reduction potentials of the fluoroethers are slightly higher than that of EC. The reduction potentials and irreversible capacities decreased with increasing LUMO energies of the fluoroethers. 1,1,2,2-Tetrafluoro-3-(1,1,2,2-tetrafluoroethoxy)-propane (TFTFEP) mixed with FEC was used for high voltage application. A Li/$LiCoO_2$ cell containing 1 moldm^{-3} $LiPF_6$/FEC-TFTFEP (1:1 in volume) exhibited high and stable discharge capacity in 30 cycles even with a high upper cutoff voltage of 4.5 V when compared with a cell containing 1 moldm^{-3} $LiPF_6$/EC-DMC (1:1 in volume). This electrolyte provided lower resistant SEI at the cathode before and after cycles [44].

Use of nonflammable hydrofluoroethers such as methyl nanofluorobutyl ether (MFE) and ethyl nanofluorobutyl ether (EFE) in Scheme 2.10 was studied in terms of the flammability, electrolytic conductivity, and charge–discharge cell performances of a graphite/$LiCoO_2$ and an amorphous carbon/$LiMn_2O_4$ cylindrical cells [45–47]. These fluorinated ethers have no flash point and are nonviscous; however, their low polarity and permittivity make difficult to dissolve lithium salts. By mixing appropriate amounts of MFE with linear carbonate co-solvents, the mixed solution showed no flash point. MFE-EMC (8:2 in volume) solution containing 0.94 moldm^{-3} $LiN(SO_2CF_3)_2$ (LiTFSA) showed a maximum conductivity of 0.97 mScm^{-1}. However, less than 0.2 moldm^{-3} $LiBF_4$ and $LiPF_6$ were dissolved in this mixed solvent. A graphite/$LiCoO_2$ cylindrical cell assembled with 1 moldm^{-3} $LiN(SO_2C_2F_5)_2$ (LiBETI)/MFE-EMC (8:2 in volume) discharged the designed capacity (1400 mAh) at a 0.1 C rate and sustained 80 % of their initial capacity up to 50 cycles. No thermal runaway was detected and cell surface temperature increased very slowly in the nailing test.

EFE was also tested as a co-solvent of nonflammable electrolyte for lithium ion batteries [48]. A typical composition satisfying both nonflammability and the rechargeability of a graphite electrode was 1 moldm^{-3} $LiPF_6$/EFE-DEC-EC (50:48:2 in volume), whose electrolytic conductivity is 1.7 mScm^{-1} at 25 °C. High reversible capacity was obtained for the graphite negative electrode but less rechargeability of the metal oxide positive electrode ($LiCr_{0.1}Mn_{1.9}O_4$) was observed in this EFE-based electrolyte, which was improved by the SEI modification by the addition of a small amount of biphenyl.

Another nonflammable hydrofluoroethers such as 2-trifluoromethyl-3-methoxyperfluoropentane (TMMP) and 2-(trifluoro-2-fluoro-3-difluoropropxy)-3-difluoro-4-fluoro-5-trifluoropentane (TPTP) in Scheme 2.10 were studied in terms of the flammability, electrolytic conductivity, and charge–discharge cell performances of a MCMB/$LiCoO_2$ cells [49, 50]. Effective nonflammability was achieved with adding 50 vol.% of TMMP or TPTP for the co-solvent of EC-DEC.

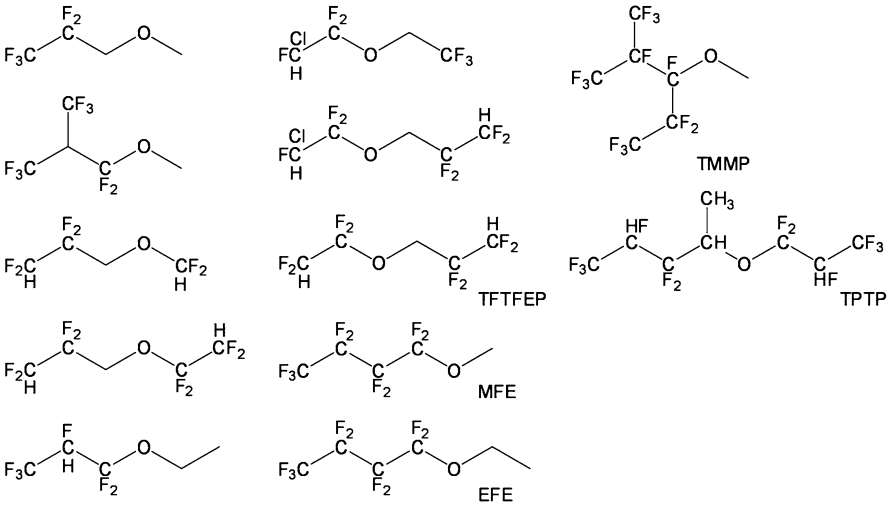

Scheme 2.10 Fluorinated monoethers

The cell containing 1 moldm^{-3} LiBETI/TMMP-EC-DEC (50:5:45 in volume) showed better discharge capacities than EC-DEC counterparts (5:95 and 50:50 in volume) as the discharge rate was increased from 0.2 to 12 C and the operation temperature was decreased from 25 to −20 °C, even though the electrolytic conductivity of 1 moldm^{-3} LiBETI/TMMP-EC-DEC is much lower than those of EC-DEC counterparts. TPTP showed better miscibility with 1 moldm^{-3} $LiPF_6$ in EC-DEC than that of TMMP, because TPTP was expected to show a higher intermolecular force due to lower F/H ratio (EFE = 1.8, TPTP = 2.0, MFE = 3.0, TMMP = 4.3). Similarly, 1 moldm^{-3} $LiPF_6$/TPTP-EC-DEC (50:5:45 in volume) showed better discharge capacities than EC-DEC counterparts (5:95 and 50:50 in volume) as the discharge rate was increased from 0.2 to 12 C and the operation temperature was decreased from 25 to −20 °C. This behavior was attributed to the decrement in the activation energy for the Li^+ desolvation process due to the decrease of solvation number of Li^+ by the addition of the hydrofluoroethers. Thus, the rate capability improvements by adding TMMP or TPTP are exerted by both enhancements of the intercalation kinetics and Li^+ diffusion at the $LiCoO_2$ interface, where the hydrofluoroethers preferentially exist by their affinity with the hydrophilic $LiCoO_2$ surface [50, 51].

2.2.7 Fluorinated Diethers

In addition to fluorinated linear diethers of 1,2-dimethoxyethane (DME) [6], fluorinated cyclic diethers such as 2,2-bis(trifluoromethyl)-1,3-dioxolane, 2,2-dimethyl-4,5-difluoro-1,3-dioxolane, and 2,2-dimethyl-4,4,5,5-tetrafluoro-1,3-dioxolane having low melting points were disclosed in a patent [52].

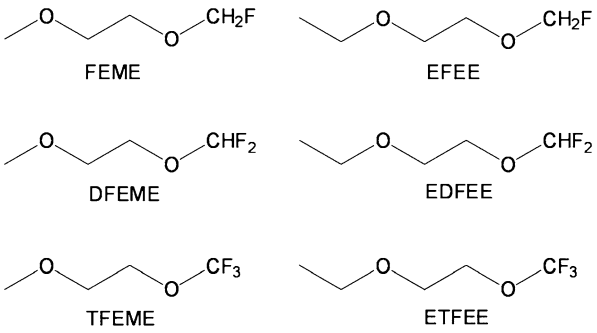

Scheme 2.11 Fluorinated dialkoxyethanes

Physical and electrochemical properties of partially fluorinated 1-ethoxy-2-methoxyethane (EME) and 1,2-diethoxyethane (DEE) derivatives such as 2-fluoroethoxymethoxyethane (FEME), 2,2-difluoroethoxymethoxyethane (DFEME), methoxy-2,2,2-trifluoroethoxyethane (TFEME), ethoxy-2-fluoroethoxyethane (EFEE), 2,2-difluoroethoxyethoxyethane (EDFEE), and ethoxy-2,2,2-trifluoroethoxyethane (ETFEE) in Scheme 2.11 were examined [53]. EME and DEE have higher relative permittivities and lower viscosities compared with those of EMC and DEC with similar molecular weights and boiling points. These fluorinated EME and DEE derivatives were obtained by reacting methoxyethanol or ethoxyethanol and each fluorinated ethyl p-toluenesulfonate synthesized with p-toluenesulfonyl chloride and each fluoroethanol. The relative permittivities and viscosities of these fluorinated EME and DEE derivatives were higher than those of EME and DEE (Figs. 2.8a, b and 2.9a, b). In addition, the relative permittivities of these fluorinated derivatives are almost independent on the number of fluorine atoms. The viscosities of TFEME and ETFEE with three fluorine atoms become smaller than those of mono- and di-fluorinated EME and DEE derivatives. The donar numbers (DNs) of the fluorinated EME and DEE derivatives decreased with increasing the number of fluorine atoms. The electrolytic conductivities of 1 moldm^{-3} $LiPF_6$ solutions decreased with increasing the number of fluorine atoms (Figs. 2.8c and 2.9c). The electrolytic conductivities of 1 moldm^{-3} $LiPF_6$/EC-equimolar binary solutions are always lower than those of EME and DEE counterparts (Figs. 2.8d and 2.9d). The oxidation potentials of the fluorinated derivatives on Pt increased with increasing the number of fluorine atoms (Figs. 2.8e and 2.9e). However, variation of the oxidative potentials among the fluorinated DEE derivatives is very small. The lithium cycling efficiencies in 1 moldm^{-3} $LiPF_6$/EC-TFEME and ETFEE solutions were higher than those in EC-EMC and EC-DEC counterparts, respectively (Figs. 2.8f and 2.9f). In general, the cycling efficiencies and discharge capacity retentions of a Li/$LiCoO_2$ cell containing 1 moldm^{-3} $LiPF_6$/EC-fluorinated EME and DEE derivative equimolar electrolytes were equivalent to those of EC-EME and EC-DEE counterparts.

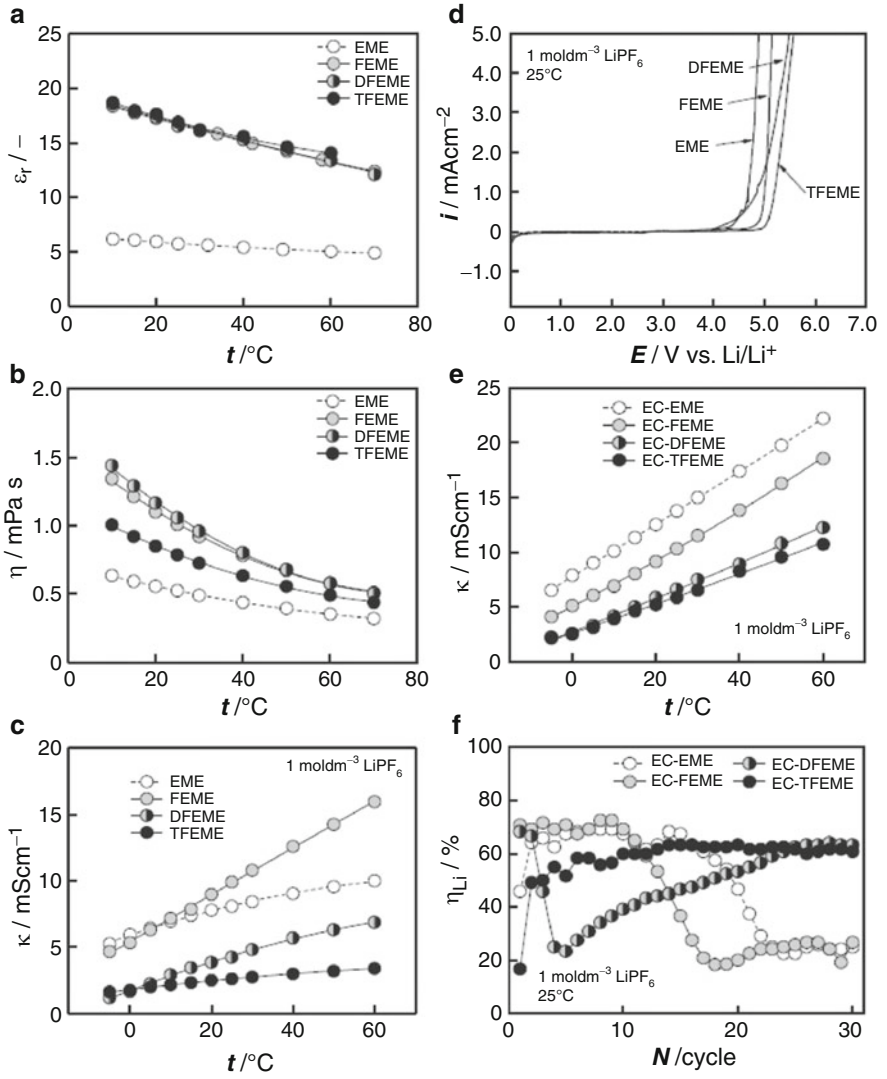

Fig. 2.8 Properties of ethoxymethoxyethane and its fluorinated derivatives. (**a**) relative permittivity (**b**) viscosity (**c**) electrolytic conductivity (**d**) oxidation potential (**e**) electrolytic conductivity (EC equimolar solution) (**f**) lithium cycling efficiency

2.2.8 Other Fluorinated Solvents

3-Methyl-2-oxazolidinone (NMO) is isostructural with EC with an N-CH_3 group substituted for one of the EC ring oxygen atoms. It is a highly polar solvent ($\varepsilon_r = 78$ at 25 °C) and was once used in primary lithium cells [54]. However, its oxidation potential on a glassy carbon is much lower than that of PC [55]. To increase its

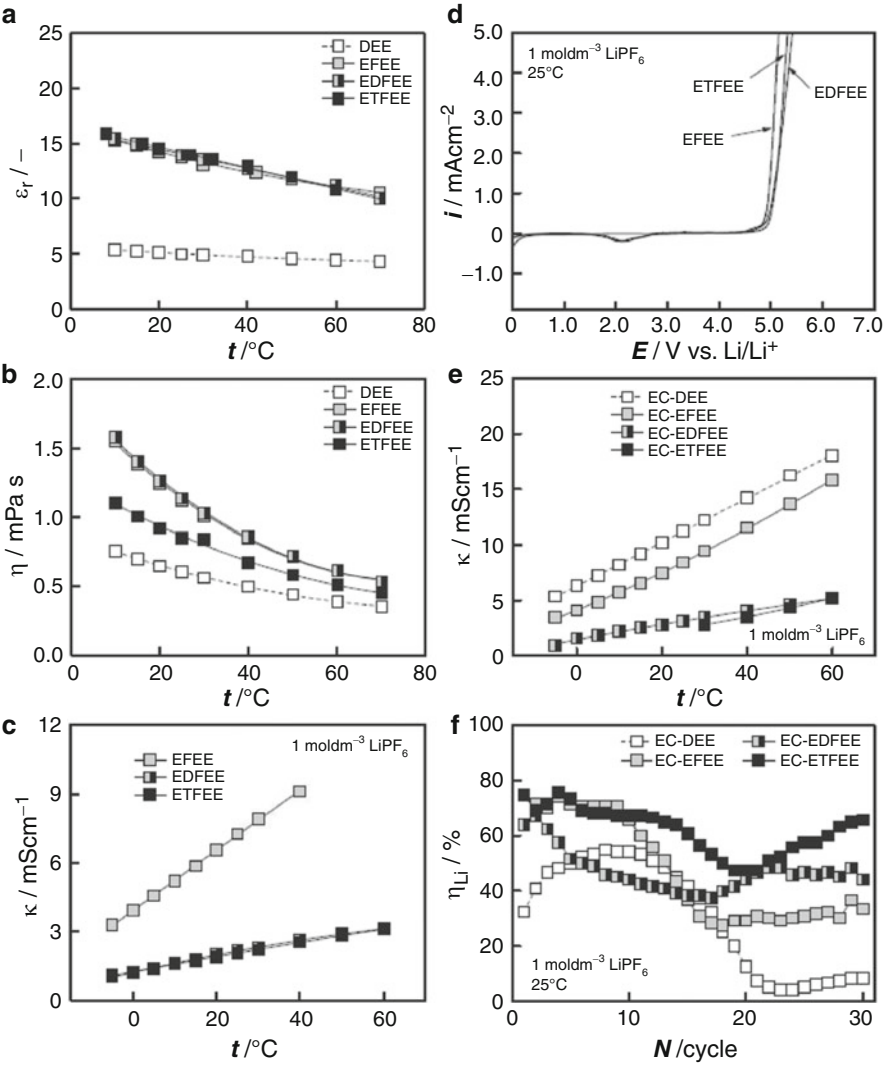

Fig. 2.9 Properties of diethoxyethane and its fluorinated derivatives. (**a**) relative permittivity (**b**) viscosity (**c**) electrolytic conductivity (**d**) oxidation potential (**e**) electrolytic conductivity (EC equimolar solution) (**f**) lithium cycling efficiency

oxidation potential, the direct fluorination of NMO was carried out, and an 3:7 isomeric mixture ($DFNMO_{mix}$) of 4,4-difluoro-3-methyl-2-oxazolidinone (4,4-DFNMO) and 4,5-difluoro-3-methyl-2-oxazolidinone (4,5-DFNMO) in Scheme 2.12 was obtained [56]. The relative permittivity of $DFNMO_{mix}$ was lower than that of NMO, although the viscosity of $DFNMO_{mix}$ was higher than that of NMO. This kind of opposite behavior was observed for fluoroacetonitrile [57].

Scheme 2.12 Fluorinated carbamates

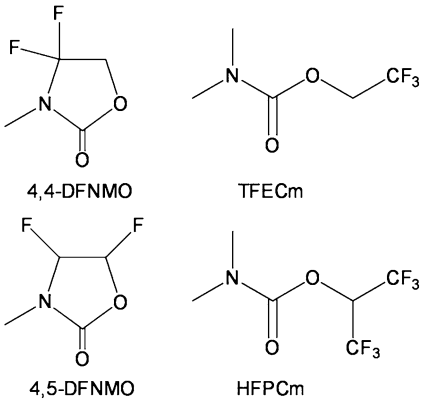

The electrolytic conductivity of 1 moldm^{-3} $LiPF_6$/$DFNMO_{mix}$ was much lower than that of NMO due to the high viscosity and low permittivity. The oxidation potential of $DFNMO_{mix}$ on Pt was increased but still lower than that of PC. The addition of $DFNMO_{mix}$ to 1 moldm^{-3} $LiPF_6$/EC-DEC equimolar binary solution suppressed discharge capacity fading in a Li/$LiCoO_2$ cell.

Partially fluorinated carbamates such as 2,2,2-trifluoroethyl *N*,*N*-dimethyl carbamate (TFECm) and hexafluoro-i-propyl *N*,*N*-dimethyl carbamate (HFPCm) in Scheme 2.12 were also applied to lithium cells, but no marked results were obtained [43].

The direct fluorination of *N*-methylpyrrolidinone (NMP) was also carried out to afford α-fluoro-*N*-methylpyrrolidinone (α-F-NMP). Its relative permittivity (70) and viscosity (3.6) were almost doubled those of NMP (32, 1.7), respectively. The electrolytic conductivity of 1 moldm^{-3} $LiPF_6$/α-F-NMP solution at 25 °C was 2.5 mScm^{-1}, less than half of that of NMP (6.1) [58].

2.2.9 Summary

Fluorinated organic solvents show very different physical and electrochemical properties. In particular, mono- or di-fluorinated organic solvents show very fairly high polarity, which generally results in the increases of relative permittivity, viscosity, and oxidation potential. Although the electrolytic conductivity of lithium salts decreases due to the increase of viscosity, the lithium cycling efficiency is always enhanced by the good SEI formation, and usually results in low capacity fading in a Li/$LiCoO_2$ cell. In addition, the nonflammability of solvents increases with increasing of the number of fluorine atoms; however, the solubility of lithium salts decreases.

The enhancement of both energy density and cell safety of rechargeable lithium(−ion) batteries is important for electric vehicle and power grid applications. Therefore, partially fluorinated organic compounds are expected as a good solvent

for rechargeable lithium(−ion) batteries. It is still necessary to study harder finding the novel fluorinated solvents giving not only high electrolytic conductivity, high oxidation potential, and nonflammability, but also good cell performances.

2.3 Boron-Containing Organic Solvents

2.3.1 Introduction

The urgent requirement for secondary batteries such as lithium-ion batteries for vehicle installation is that they be small and light. The indexes of the smallness and lightness are energy densities of per-unit volume (=V A h/dm^3) and mass (=V A h/kg). Thus, these numbers are expressed as a product of the capacity of electrodes and the operating voltage of the cell. Recently, cathodes possessing high capacity as well as high redox-potential have been developed to increase these numbers [59]. In contrast, the development of liquid electrolytes with a high oxidation potential falls far behind since organic compounds consisting of liquid electrolytes such as carbonate esters are generally being oxidized with facility (~4.3 V (Li/Li$^+$), Fig. 2.10a). Attention has thus been paid to seek or design an organic compound with a high oxidation potential as the electrolyte solvent. The organic compounds also come equipped with the following physical and electrochemical properties: high dielectric constant to dissociate the supporting electrolyte salt; high fluidity to acquire the enough ionic conductivity; low flammability to be absolutely secure; and low toxicity. During the last decade, some novel organic compounds have been proposed.

Organic sulfones exhibited high oxidation potential but low fluidity, eventually decreasing ionic conductivity (Fig. 2.10b) [60]. The sulfones also caused the abruption of carbon anodes. Nitriles such as adiponitrile also showed a high oxidation potential because the nitrile substituents in the strong electron withdrawing group resulted in high oxidation resistance (Fig. 2.10c) [61]. However the nitriles also lack enough fluidity. Fluorinated carbonate esters in which some hydrogen atoms in carbonate esters were substituted with fluorine atoms indicated a high oxidation potential due to the fluorine nature of electron withdrawing (Fig. 2.10d) [62]. The fluorine atoms substituted also created low flammability for the carbonate ester. Moreover, they maintained their intrinsic high fluidity, but were not a good solvent for supporting electrolyte salts. Synthetic complexity also remained.

When designing the electrolyte solvent and salt compounds one can consult the molecular orbital methods with some programs such as the Gaussian [63]. The molecular orbital method calculates the most stable conformation as well as the highest occupied molecular orbital (HOMO) and the lowest unoccupied molecular orbital (LUMO) levels of the compound concerned. Figure 2.11 indicates the relationship between molecular orbitals and their energy levels in a molecule. When the oxidation takes place an electron is removed from the HOMO. When the reduction occurs an electron is inserted into the LUMO. Therefore, the lower HOMO level

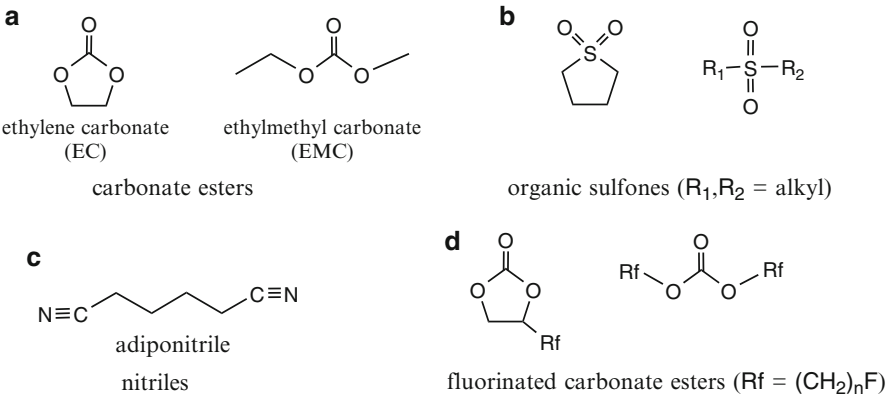

Fig. 2.10 Chemical structures of (**a**) carbonate esters, (**b**) organic sulfones, (**c**) nitriles, and (**d**) fluorinated carbonate esters

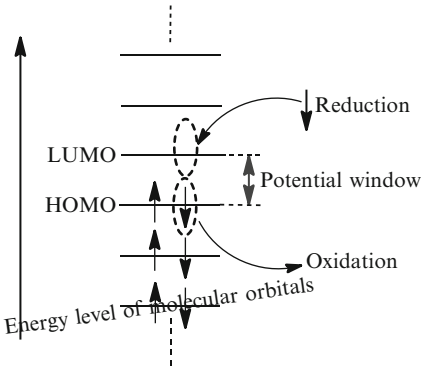

Fig. 2.11 The relationship between molecular orbitals and their energy levels. The *arrow* refers to an electron and its direction does the direction of electron spin

indicates the higher oxidation potential and the higher LUMO level does the lower reduction potential. Therefore the wider differential of HOMO-LUMO levels, i.e., the wider potential window, is preferable to the electrolyte. One can seek a compound with the molecular orbital methods in such a way before synthesizing. However, an organic compound generally has a quite narrow potential window.

2.3.2 Nature of Boron Compounds

According to some statistics, boron is an element with an abundance in the earth's crust of about 10–1,000 ppm and is thus a reasonably rich resource [64]. The output of boron compounds such as borax ($Na_2B_4O_5(OH)_4 \cdot 8H_2O$) is about one million tons a year. Therefore, it is easily supplied. Boric acid ($B(OH)_3$, Fig. 2.12, **1**) is prepared

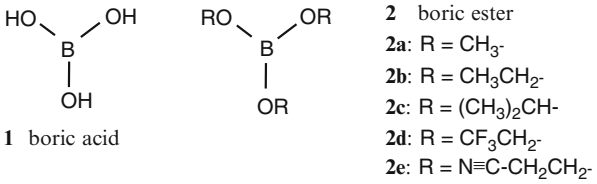

Fig. 2.12 Chemical structures of boric acid (**1**), methylborate (**2a**), ethylborate (**2b**), *iso*-propylborate (**2c**), trifluoroethylborate (**2d**), and 2-cyanoethylborate (**2e**)

from a reaction of $Na_2B_4O_7 \cdot 10H_2O$ with H_2SO_4. One use of boric acid is as an absorbent of neutrons at a nuclear power plant. Natural boron consists of 19.9 % ^{10}B and 80.1 % ^{11}B, where only ^{10}B absorbs neutrons. Boric acid is also used in mouse poison pellets and as an eyedrop ingredient. This means that boric acid has toxicity. However, the LD_{50} for mammals of boric acid is 5.14 g/kg while that of NaCl is 3.75 g/kg [65]. Thus, the toxicity is quite moderate. A further advantage of boron-containing compounds is their ability to reduce weight because the atomic weight of boron is only 10.8.

Both ^{10}B and ^{11}B nuclei are NMR (nuclear magnetic resonance) active. Because of the high content, high resonant frequency, and lower nuclear quadrupole moment, the NMR spectroscopy of the ^{11}B nucleus is generally observed [66]. Trivalent or quadrivalent boron can be comfortably differentiated by means of a chemical shift of ^{11}B: trivalent > 0 ppm > quadrivalent (*d* value). Thus, the electron density on the boron atom can also estimated with the chemical shift. In this way, ^{11}B NMR spectroscopy is a potent tool for structural analyses of boron-containing materials.

2.3.3 Boric Esters

Boric esters ($B(OR)_3$, Fig. 2.12, **2**) are esters prepared from a condensation of boric acid (**1**) and corresponding alcohols as in the case of carbonate esters that form carbonic acid (H_2CO_3) and alcohols (Fig. 2.13a, b). Physical and electrochemical properties of boric esters are tunable due to substituents R in **2**. Methyl, ethyl, *iso*-propyl, and trifluoroethylborates (**2a**, **2b**, **2c**, and **2d**) are transparent liquids, whereas a boric ester possessing nitrile substituent (R = $-CH_2CH_2CN$, **2e**) is solid at room temperature. Thus, **2a**, **2b**, **2c**, and **2d** are highly fluid; **2d** has nonflammability as well. Any lithium salts poorly dissolve in these boric esters. In contrast, **2e** is a good solvent of lithium salts. Once the salt dissolves, the solution in **2e** becomes a liquid. The electrolytes of lithium salts in **2e** exhibit the oxidation potential of over 6.0 V [Pt/(Li/Li^+)] [67]. When a boric ester was blended with the other boric ester, the substituent exchange reaction (ester exchange reaction) spontaneously took place to give mixed boric esters (Fig. 2.14). The reaction was in an equilibrium that largely shifted to right. The mixed boric esters obtained acquired all the preferable

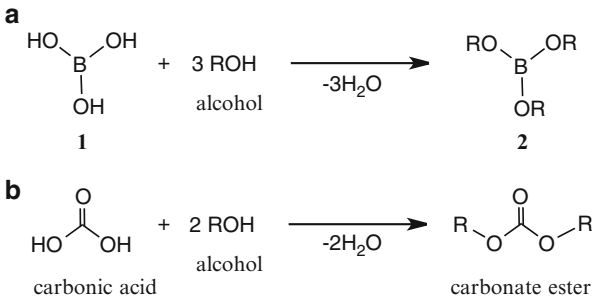

Fig. 2.13 Preparation of (**a**) boric ester (**2**) from boric acid (**1**) and alcohol and (**b**) carbonate ester from carbonic acid and alcohol

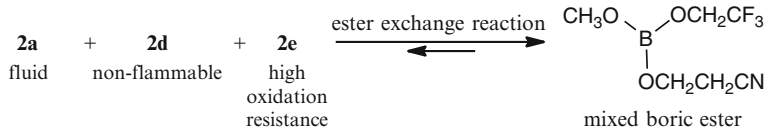

Fig. 2.14 Substituent exchange reaction (ester exchange reaction) among **2a**, **2d**, and **2e** giving the mixed boric ester

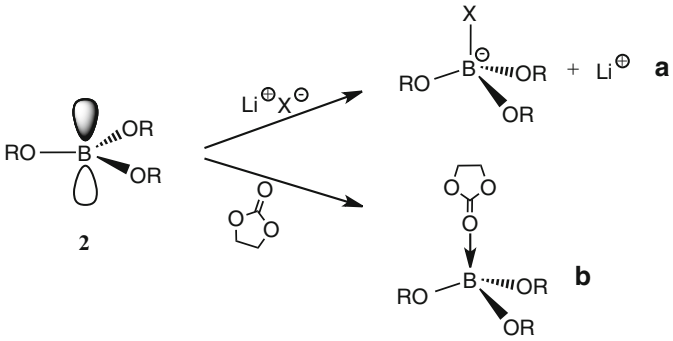

Fig. 2.15 Intermolecular interaction of boric ester (**a**) with lithium salt and (**b**) with carbonyl compound based on Lewis acid-base neutralization

properties that parent boric esters intrinsically bear. In particular, the mixed boric esters showed ionic conductivity of over 10^{-3} S cm^{-1} at room temperature and an oxidation potential of 5.5 V [Pt/(Li/Li^+)] [67]. A coin cell consisting of the $LiNi_{0.5}Mn_{1.5}O_4$ cathode, Li metal anode, and electrolyte of 0.7 mol/kg $LiBF_4$ in **2c** and **2e** (1/2 mol) exhibited stable charge–discharge cycles.

The trivalent boron compounds, including boric esters, are Lewis acids because of the vacant *p*-orbital on the boron atom capable of accepting an electron pair (Fig. 2.15). When the substituents bear electron-withdrawing groups such as nitrile,

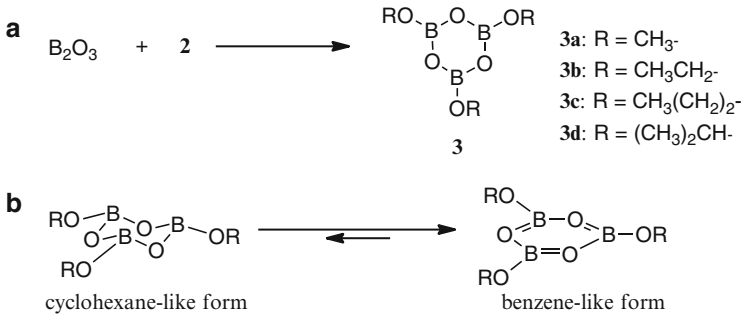

Fig. 2.16 (**a**) Preparation of trialkokyboroxine (**3**) from boric anhydride and boric ester (**2**) and (**b**) the most stable structure of trialkoxyboroxine

the acidity of the Lewis acid increases and then accelerates the dissociation of salts (Fig. 2.15a). In particular, lithium salts are soluble in **2e** but not in **2a**–**2d**. The interaction of boric ester with an anion also causes the lithium transference number to rise (t^{Li+} = Li^+ conductivity/ionic conductivity). In fact, the t^{Li+} is about 0.6 for the boric ester electrolyte, while that for the carbonate ester is about 0.3 [67]. This indicates that the boric esters are acting as an anion receptor. Moreover, a boric ester can bind another Lewis base such as carbonyl compound to decrease the electron density in the carbonyl compound to give it a high oxidation potential (Fig. 2.15b). For example, a blended electrolyte of 1.0 mol/kg $LiBF_4$ in **2e** and carbonate esters (1/1 mol) exhibited the oxidation potential of over 5.2 V [Pt/(Li/Li^+)] while the decomposition of absolute carbonate ester electrolyte commenced at 4.3 V.

2.3.4 Cyclic Boric Esters

Boric anhydride (boric oxide, B_2O_3) reacts with boric ester to give a cyclic boric ester of trialkoxyboroxine (**3**, Fig. 2.16a). The six-membered ring of the trialkoxyboroxine takes a planar benzenelike structure rather than the cyclohexanelike form where π-electrons of oxygen atoms are delocalized on the six-membered ring including vacant *p*-orbitals of three boron atoms to give a planar structure (Fig. 2.16b). When a small amount of **3** (0.2 wt%) is added to the carbonate ester electrolyte, the anodic reaction is stabilized [68]. The electric current at 5.0 V (vs. Li/Li^+) derived from decomposition of the carbonate ester largely decreased in the presence of **3d** when $LiMn_2O_4$, as a high-potential cathode, was utilized. A unique substituent effect was also observed: the trialkoxyboroxine (**3d**) possessing *isopropyl* moieties was most effective among the trialkokyboroxines (**3a**–**3d**). Presumably only **3d** has the preferable oxidation potential and thus is decomposed at around 4.0 V, resulting in formation of a solid electrolyte interface (SEI) containing boron atoms at the surface of the cathode to prevent further decomposition of the electrolyte.

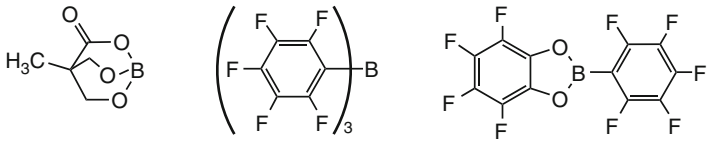

4
triol borate

5
TPFPB

6
PFPBDB

Fig. 2.17 Anion receptor molecules

Another cyclic boric ester of triol borate (**4**, Fig. 2.17) has a highly strained structure owing to the tricyclic skeleton which causes a strong Lewis acid nature [69]. **4** binds counter anions of LiF, Li_2O, and Li_2O_2 to dissociate them and to dissolve them into organic solvents. In addition to **3** and **4,** anion receptor molecules in battery electrolytes have recently received attention. As described above the required functions for an anion receptor are (a) to dissociate an insoluble salt into the cation and anion, (b) to dissolve the salt into a solvent, (c) to increase the lithium transference number (t^{Li+}) as the result of immobilizing anions, and (d) to interact with the solvent molecule to withdraw the electrons on the molecule to prevent the facile oxidation of it. Tris-(pentafluorophenyl)borane (TPFPB, **5**, Fig. 2.17) also functions as an anion receptor and combines the required functions above [70]. **5** also stabilizes the charge–discharge behavior when the electrolyte containing **5** constitutes a battery. 2-(2,3,4,5,6-pentafluorophenyl)-4,5,6,7-tetrafluoro-1,3,2-benzodioxaborole (PFPBDB, **6**, Fig. 2.17) also acts as an anion receptor [71]. **6** exhibits the reversible redox-potential at 4.43 V and is expected to behave as a redox shuttle molecule in the electrolyte. The redox shuttle molecule protects the electrodes from their overcharge with own redox-reaction.

2.3.5 Other Boron Compounds

Lithium tetrafluoroborate ($LiBF_4$) is thermally stable and is not extremely moisture sensitive when compared with lithium hexafluorophosphate ($LiPF_6$). $LiPF_6$ easily reacts with H_2O to exhaust HF and decomposes at 80 °C. However, the ionic conductivity of the $LiPF_6$ electrolyte is superior to that of the $LiBF_4$ electrolyte due to the difference in the degree of dissociation. Novel supporting salt molecules therefore are designed to be thermally stable, moisture insensitive, and have a high dissociation. Orthoborates in which the central boron atom has four B–O bonds are thermostable compounds and thus are suitable for anions of lithium salts. Although lithium bis(oxalate)borate (LiBOB, **7**, Fig. 2.18) initially commanded attention as a lithium salt and was well described in the literature [72], recently it has been viewed less as a support salt and more as an additive because of its low solubility in organic solvents, low fluidity in solution, and difficulty in purifying [73]. **7** stabilizes the cathodic reaction at the surface of the carbon anodes.

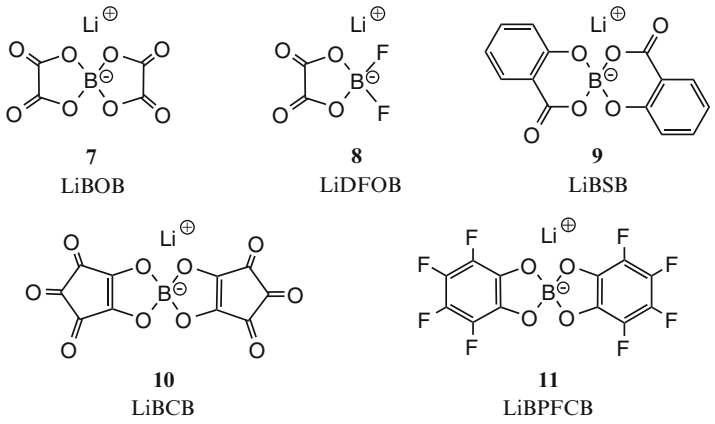

Fig. 2.18 Orthoborate lithium salt molecules

Lithium difluoro(oxalato)borate (LiDFOB, **8**, Fig. 2.18) also shows the same effect as the additive for an electrolyte [74]. Lithium bis[salicylato(2-)]-borate (LiBSB, **9**) [75], lithium bis[croconate]-borate (LiBCB, **10**) [76], and lithium bis[1,2-tetrafluorobenzenediolato(2-)-O,O′] borate (LiBPFCB, **11**) [77] have also been proposed as novel orthoborate lithium salts (Fig. 2.18).

2.3.6 Summary

Boron is a fascinating atom when designing the novel functional solvent, additive, or supporting salt molecules because of its intrinsic electronic structure, giving rise to unique physical and electrochemical properties for boron-containing molecules. The properties differ quite a lot from those of molecules involving carbon, nitrogen, and oxygen atoms even if B, C, N, and O share similar atomic weights. Therefore, the boron-containing molecules may give an initial clue to novel functions for battery materials.

2.4 Phosphorous-Containing Organic Solvents

2.4.1 Introduction

Lithium-ion batteries (LIBs) have been developed as advanced electric power sources for wide variety of portable electronics such as cellular phones, laptop comports, and camcorders. Larger-size LIBs are now considered fit to power systems such as electric vehicles (EV) and energy storage systems (ESS) due to their merits

Table 2.5 Classification of nonflammable electrolytes for lithium-ion batteries

Category	Composition	Example	Characteristics
Organic electrolyte solutions (with nonflammable components)	Nonflammable components as co-solvents or additives	Fluorinated esters Organic phosphorous compounds	High ionic conductivity; trade-off between nonflammability and electrode performances
Polymeric solid electrolytes	Polymer complexes with lithium salts (LiX)	LiX/Poly(ethylene oxide) (PEO) LiX/PEO-grafted polymer	Low ionic conductivity at lower temperature; low Li^+ transport number
Polymeric gel electrolytes	Polymer complexes swollen with organic solutions	LiX/alkylcarbonate/PEO with nonflammable component	High ionic conductivity; trade-off between nonflammability and electrode performances
Ionic liquids	Ionic liquids (IL) dissolving lithium salt (LiX)	LiX/IL, IL: 1-ethyl-3methylimidazolium fluorosulfonylamide (EMIFSA)	High ionic conductivity; low rate capability of electrode performances
Inorganic solid electrolytes	Li^+-containing oxides, sulfides, glass, ceramics	Li_2S-P_2S_5 glass, $Li_{10}GeP_2S_{12}$ crystal	High ionic conductivity; high Li^+ transport number; low interfacial properties

of high-energy density, high power, and long cycle life. Much attention has been focused on the safety issue of LIBs as battery sizes have increased and they have been more widely used [78]. The organic solvent-based electrolytes presently used in LIBs are highly flammable and can cause safety problems. Different approaches have so far been adopted to establish a safer electrolyte [79]. Some of these are: a polymeric solid electrolyte generally composed of lithium salt with a polyether-based polymer [80–82], room-temperature ionic liquids (RTIL) as nonflammable solvents [83–86], flame-retardant co-solvents or additives including phosphorous-containing organic esters or fluorinated esters/ethers [87–91]. Use of inorganic solid electrolytes that conduct lithium-ion (Li^+) at an ambient temperature is another option to construct nonflammable LIBs [92, 93]. Table 2.5 shows the classification and fundamental properties of nonflammable electrolyte systems so far proposed to build safer LIBs. Unfortunately, these approaches generally meet difficulties in compatibility when assessing the basic battery performance, and reliabilty of the system. That is, the use of a safer electrolyte system tends to decrease the charge–discharge performance including the rate capability of the cell and/or the reliability of the system. Thus, composite electrolyte systems consisting of several components have so far been proposed as the practical electrolytes of LIBs: e.g.,, polymeric gels composed of nonflammable organic solvents [94], inorganic glass--ceramic electrolytes dispersed in polymeric matrices [95], ionic liquids mixed with nonflammable, and low-viscosity organic solvents [96–99].

In the present chapter, the use of a phosphorous-containing organic compound, typically alkylphosphates and related compounds, has been reviewed as a

nonflammable component in LIB electrolytes. Generally, phosphorous-containing organic compounds are well known and practically used as fire-retardant materials that suppress the flammability of organic polymers [100, 101]. In the following sections, research papers on organic electrolyte solutions containing alkylphosphates and related compounds for LIBs are reviewed first, and then successful results on the development of polymeric gel electrolytes containing alkyl phosphates are described next.

2.4.2 Alkylphosphates and Related Compounds as Flame-Retardant Additives/Co-solvents

2.4.2.1 Alkylphosphates

The use of alkylphosphates as a nonflammable component in LIB electrolytes was first proposed by Wang and colleagues [87]. They reported that trimethylphosphate (TMP) works as a flame-retardant additive or co-solvent in a mixed alkylcarbonate-based electrolyte solution. The most alkylcarbonate solvents used in conventional LIB shows good compatibility with TMP. That is, the solubility of TMP is generally high in alkylcarbonates. Figure 2.19 shows the results of qualitative evaluation for nonflammability and a self-extinguishing property of TMP-containing mixed alkyl carbonate, ethylene carbonate (EC) and diethyl carbonate (DEC) [94]. In a binary system of EC+TMP, the amount of 20 vol.% of TMP is enough to suppress the flammability. However, more than 50 vol.% of TMP is needed to keep nonflammability in the DEC+TMP binary system. These results are consistent with those reported by other research groups [87, 102–104]. As clearly shown in Fig. 2.19, the flame-retardant ability of TMP depends on the composition of the base solution. In EC+DEC (2:1 by vol), addition of TMP with 20 vol.% or higher suppresses the flammability of the electrolyte solution. In a mixed system of EC with ethyl methyl carbonate in 1:1 mass (weight) ratio (EC+EMC, 1:1), however, greater amounts of TMP are needed to suppress the flammability of the solution. The nonflammability of the electrolyte solution was more quantitatively evaluated by a self-extinguish time (SET) [103, 105]. According to the SET examination, the minimum amount of TMP suppressing the combustion was 30 % (in mass) in a mixed EC+EMC (1:1 by mass) solvent system [103].

Changes in physicochemical properties of the electrolyte solution when adding TMP have also been reported by Morimoto et al. [106]. Because the viscosity of TMP is lower than ethylene carbonate (EC) but higher than linear alkylcarbonates such as dimethyl carbonate (DMC) and DEC, the viscosity of the solution slightly increases with the addition of TMP. In Fig. 2.20, ionic conductivity of 1.0 mol dm^{-3} (M) $LiPF_6$ and $LiBF_4$ in the mixed alkyl carbonates is shown as a function of the solvent composition [106]. The conductivity of $LiPF_6$ decreases with the TMP content. This is because the viscosity of the solution increases with the TMP content. However, in the $LiBF_4$ solution, the conductivity increases with the TMP blending,

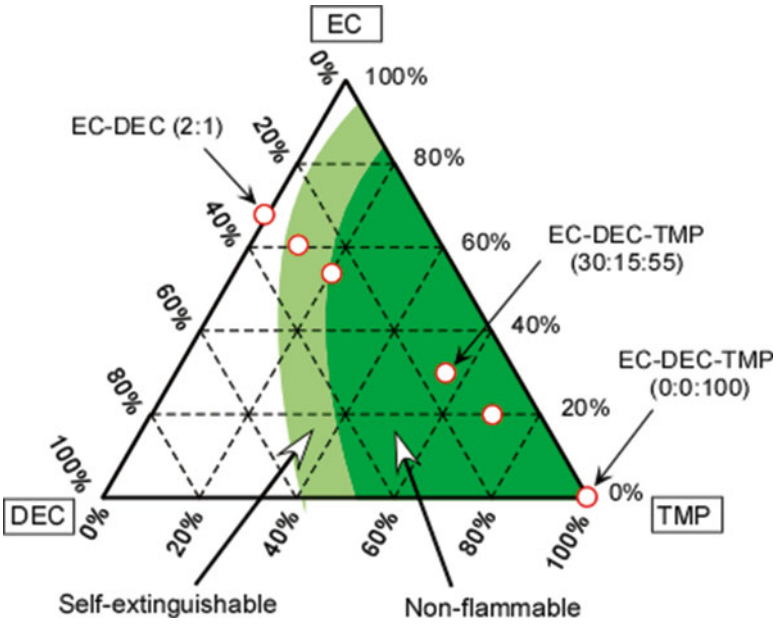

Fig. 2.19 Nonflammable and self-extinguishable compositions in $LiPF_6$/EC + DEC + TMP system

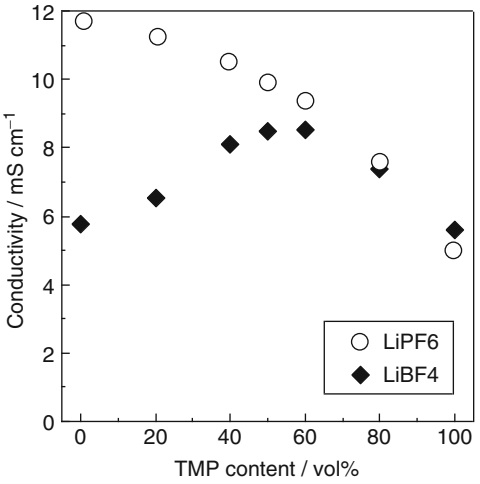

Fig. 2.20 Ionic conductivity of 1 mol dm^{-3} $LiPF_6$ and $LiBF_4$ solutions as a function of TMP content in EC + DMC (1:1 by vol.) at 25 °C

and then decreases in the solution containing higher TMP content than 80 %. Because the $LiBF_4$ salt has rather strong interaction between the cation (Li^+) and anion (BF_4^-), the degree of ionic association is rather high in the system containing a high concentration of $LiBF_4$. Thus, the increase in the conductivity with the addition of TMP up to 50 vol.% is attributable to the decrease in the ionic association caused by the introduction of the higher permittivity component TMP.

Besides nonflammability, the contribution of TMP to the thermal stability of the $LiPF_6$ solution with EC-based mixed solvents is significant [94]. It is well known that $LiPF_6$ is thermally decomposed at around 60 °C or higher. The addition of TMP with 20 vol.% or higher suppresses the decomposition of the PF_6 salt dissolved in the EC-based solvent. Possible reaction schemes have been proposed, in which radical propagation in the oxidation process of alkyl esters will be terminated by TMP [94]. The thermal decomposition of PF_6^- anion evolves an acid HF, which would assist the oxidative decomposition of alkyl esters. The component TMP would act as a scavenger of organic radicals in such oxidation processes. With respect to the fire-retardant ability of TMP, some reaction mechanisms have been proposed. One of the proposed schemes is shown in Fig. 2.21 [87], in which a phosphorous-containing radical, [P]•, evolved by partial decomposition of TMP traps the hydrogen radical, H•, being a main carrier in the oxidative chain reaction (i.e., combustion) of alkyl esters. This radical trapping by the phosphorous-containing radical can be effective for suppressing the thermal decomposition of mixed alkyl ester solutions containing the PF_6^- anion. The effects of TMP addition on the thermal stability of an LIB system are also examined in alkylcarbonate-based electrolytes in contact with fully charged graphite negative and $LiCoO_2$ positive electrodes [107]. The addition of TMP improves the thermal stability of the positive electrode side, while it does not suppress the highly exothermic reaction at the fully charged negative electrode. Thus, only a limited contribution of the flame-retardant component to the thermal stability of the LIB system is generally recognized.

The basic properties of the LIB electrode in the electrolyte solutions containing TMP have also been presented by Wang et al. [87, 103]. For the graphite negative electrode, the addition of considerable amounts of TMP causes the irreversibility of the charge--discharge process. This is because the surface process at the graphite in the electrolyte-containing TMP is different from the EC-based electrolyte [87]. As already discussed, the electrochemical Li-intercalation into graphite structure occurs through a thin layer, the so-called SEI (solid electrolyte interphase) formed at the graphite electrode [108–110]. In the EC-based electrolyte, the decomposition product of the EC component produces good SEI structure, while the electrochemical process in the solution containing TMP does not form compact SEI. The addition of an SEI-forming component, such as vinylene carbonate (VC), improves the rechargeability of the graphite electrode, as shown in Fig. 2.22 [111]. A small amount of the additive is effective in forming a film on the graphite surface. On the other hand, nongraphitizable carbon (hard carbon) shows rather good rechargeability as the negative electrode even in the solution containing TMP, because it does not need the formation of compact SEI that is required for the graphite electrode [103]. Also, common lithiated transition-metal oxides, such as $LiCoO_2$ and $LiMn_2O_4$, work well as positive electrodes in TMP-containing electrolytes [87, 106]. As shown in Fig. 2.23 [87], sufficiently high rechargeable capacity was reported for the $LiCoO_2$ positive electrode in a $LiPF_6$ solution dissolved in EC + DEC + TMP (35:35:30). Almost the same discharge capacity and cycle performance are reported for $LiMn_2O_4$ in $LiBF_4$/EC + DMC + TMP as those in the conventional electrolyte solutions without TMP [106].

1. Thermal decomposition of organic compounds

$RH \rightarrow R\cdot + H\cdot$ (1)

$H\cdot + O_2 \rightarrow HO\cdot + O\cdot$ (2)

$HO\cdot + H_2 \rightarrow H\cdot + H_2O$ (3)

$O\cdot + H_2 \rightarrow HO\cdot + H\cdot$

2. Evolution of P-containing radical from TMP

$TMP_{gas} \rightarrow [\,P\,]\cdot$

3. Trapping $H\cdot$ by radical $[\,P\,]\cdot$, suppressing the reaction of step (2)

$[\,P\,]\cdot + H\cdot \rightarrow [\,P\,]H$

$\rightarrow$Terminating the chain-reaction

Fig. 2.21 A proposed mechanism for suppressing the decomposition reaction by addition of a phosphorous-containing compound

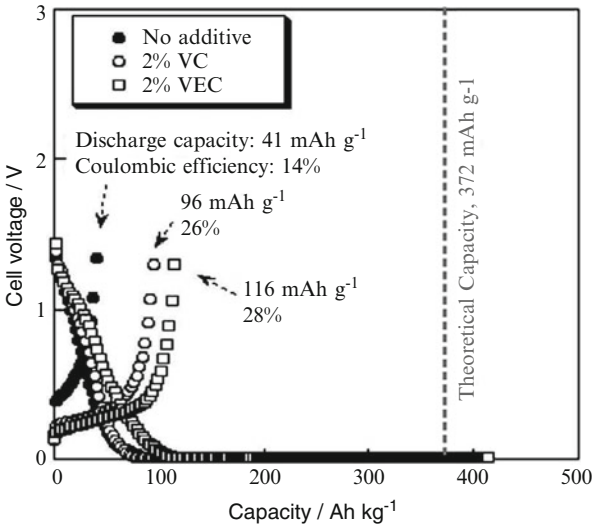

Fig. 2.22 First-cycle charge–discharge curves of Li/graphite (STG) half-cell using 1 mol dm^{-3} LiBETI/TMP electrolyte with and without additives

Other alkylphosphates have also been examined as fire-retardant additives or co-solvents in LIB electrolytes [112]. With respect to fire-retardant ability, the length of the alkyl chain in the phosphates is critical. The SET values of the solutions containing different alkylphosphates tend to be longer as the length of the alkyl chain when the systems contain the same mole fraction for different phosphates. That is, the P/C atomic ratio in the system determines SET. On the other hand, the reduction potential of alkylphosphate, which is strongly related to the SEI formation process at the graphite negative electrode, tends to shift to negative one when increasing the carbon in the alkyl group. Viscosity and dielectric properties are also influenced by the length of the alkyl chain in the phosphates.

Feng et al. [112] reported the use of dimethyl methyl phosphate (DMMP) as a nonflammable solvent. The basic properties of DMMP are between those of TMP

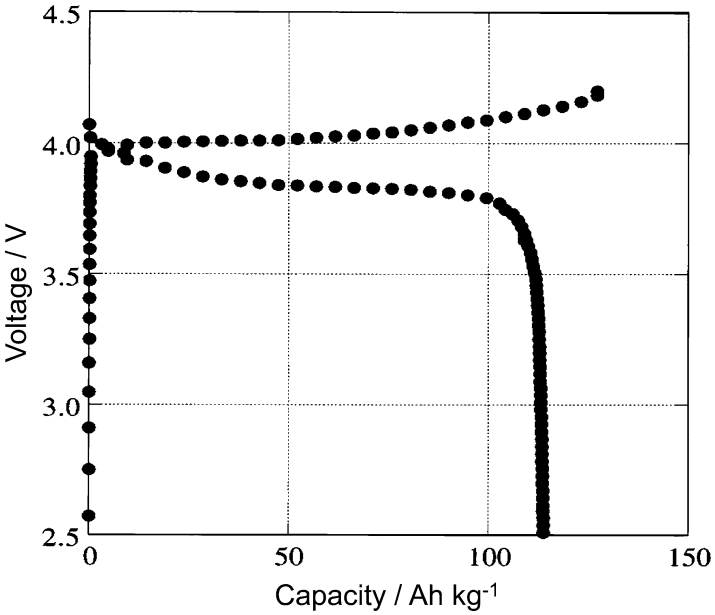

Fig. 2.23 First-cycle charge–discharge curves of Li/$LiCoO_2$ half-cell with1 mol dm^{-3} $LiPF_6$/EC + DEC + TMP (35:35:30)

and triethylphosphate (TEP). With respect to rechargeability of the graphite negative electrode, highly irreversible behavior was observed in the electrolyte ($LiClO_4$) solution using a DMMP solvent. However, reasonable cycling capacity was given by adding 10 vol.% of chloroethylene carbonate (Cl-EC) to the DMMP-based solution. Charge–discharge performances of a graphite/$LiCoO_2$ cell were also reported for the case using $LiClO_4$/DMMP + Cl-EC. Consequently, possible alkylphosphates as the co-solvents giving both sufficient nonflammability and electrochemical performances of the LIB electrolyte would be limited to such lower molecular weight compounds as TMP, TEP, and related compounds.

2.4.2.2 Fluoroalkylphosphates

Organic compounds that contain C–F bonds generally show nonflammability or fire-retardant property. Thus, fluoroalkyl-ethers and -esters have been attempted as nonflammable or flame-retardant solvents for LIB electrolytes [88, 89, 113]. Fluorinated alkylphosphates, or fluoroalkylphosphates, have higher flame-retardant properties than the corresponding alkylphosphates. Jow and co-workers [104, 114–116] reported a series of fluoroalkylphosphate, i.e., tris(2,2,2-trifluoroethyl) phosphate (TFP), bis(2,2,2-trifluoroethyl)-methyl phosphate (BMP) and (2,2,2-trifluoroethyl)-diethyl phosphate (TDP) (Fig. 2.24), as nonflammable additives or co-solvents of

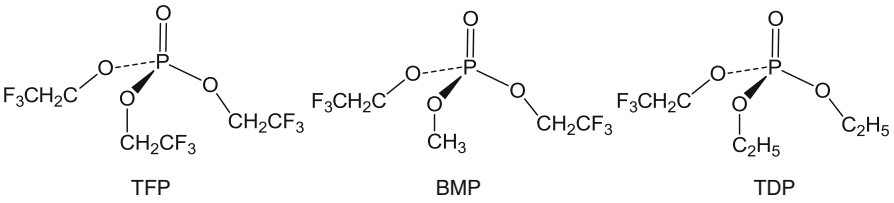

Fig. 2.24 Chemical structures of typical fluorinated alkylphosphates

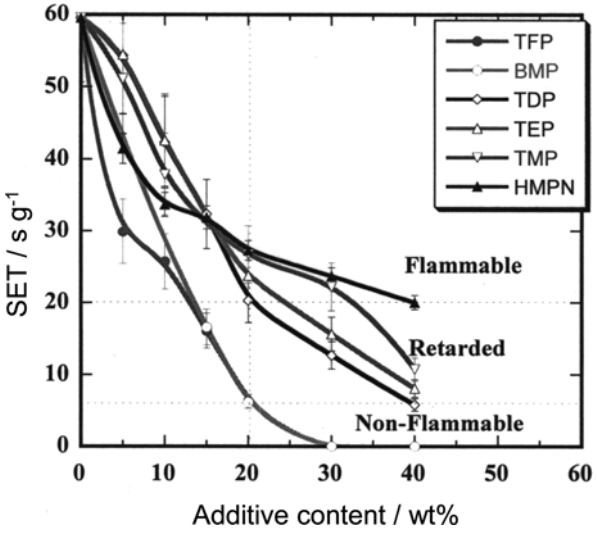

Fig. 2.25 Comparison in flammability of the electrolyte solutions with different fire-retardant additives. The base electrolyte: 1.0 mol dm^{-3} $LiPF_6$/EC + EMC (1:1)

LIBs. Among them, TFP shows high nonflammability of the electrolyte and good compatibility with the graphite-based negative electrode. Introduction of fluorine atoms to ethyl groups of TEP decreases its boiling point (bp) and viscosity. In Fig. 2.25 [115], SET values of the electrolytes containing fluoroalkylphosphates are compared with those of the solutions containing alkylphosphates. The results clearly imply that fluorinated alkylphosphates have higher nonflammability than that of TEP-containing solutions, with respect to the same amount (in mass%) of the flame-retardant components.

Because the dielectric constant (relative permittivity) of TFP is lower than that of EC (ε_r: 11 for TFP, 90 for EC), the ionic conductivity of $LiPF_6$ solution decreases when adding TFP to mixed EC + EMC solvent in the wide temperature range [115]. Also the higher concentration of TFP tends to decrease the rechargeability of the graphite-based negative electrode. Thus, about 40 % of the TFP component in the electrolyte satisfies both the nonflammability and the reversibility of the electrode in the LIB system.

2.4.2.3 Alkyl Phosphonates and Phosphites

The use of alkyl phosphonates as the co-solvent of EC-based electrolytes has been proposed by Xiang and co-workers [91, 117, 118]. Dimethyl methylphosphonate (DMMPp), a typical alkyl phosphonate, has low viscosity (η: 1.75 mPa s) and moderate permittivity (ε_r: 22.3) with a low melting point (−50 °C) and a high boiling point (180 °C). Nonflammability of DMMPp seems to be superior to or comparable with that of a corresponding alkyl phosphate [91]. That is, the addition of 10 mass% DMMPp to $LiPF_6$/EC + DEC showed a self-extinguishing property. However, sufficient nonflammability was observed for the system containing about 50 vol.% of DMMPp [117]. In those systems, a huge irreversible capacity was also observed for graphitic carbon, MCMB (mesocarbon microbead), as the negative electrode. Addition of such SEI-forming reagents as vinyl ethylene carbonate (VEC) improved the reversibility of the MCMB negative electrode (Fig. 2.26). Xiang et al. also reported that the DMMPp-based nonflammable electrolyte works for a cell consisting of $Li_4Ti_5O_{12}$ negative and $LiNi_{0.5}Mn_{1.5}O_4$ positive electrodes, in which about 3 V of the operation voltage is available [118]. The effects of DMMPp addition in the electrolyte consisting of lithium bis(oxalatoborate) (LiBOB) salt have been more recently reported [119]. Better compatibility between nonflammability and the electrode performances was obtained. Further, Wu et al. [120] reported dimethyl(2-methoxyethoxy)methylphosphonate (DMMEMPp) as a new flame-retardant solvent in a Li/$LiFePO_4$ system. They confirmed the nonflammability of the LiTFSA/DMMEMPp electrolyte system (TFSA: trifluoromethylsulfonyl amide) and good cycling performance of the $LiFePO_4$ positive electrode.

Alkylphosphites are another family of phosphorous-containing organic esters, in which the oxidation state of phosphorous is III. Chen et al. [121, 122] first reported the use of trimethylphosphite (TMPi) as a flame-retardant additive in $LiPF_6$/EC + DEC. The effect of TMPi on the nonflammability of the electrolyte is unclear, but some positive effects on the thermal stability of $LiCoO_2$ and $LiNiO_2$ electrodes have been demonstrated. The experimental results on thermal and FT-IR analyses gave a possible mechanism for improving the thermal stability and electrode performance in the electrolyte containing TMPi.

Jow and co-workers have reported fluorinated alkyl phosphites as the additive components in EC-based electrolytes. Among them, tris(2,2,2-trifluoroethyl) phosphite (TTFP) was first reported as a thermal stabilizer for $LiPF_6$-based electrolytes [90, 123].

2.4.2.4 Other Phosphorous-Containing Compounds

Arylphosphates are also possible candidates of flame-retardant additives. Wang et al. [124, 125] reported the effects of 4-isopropyl phenyl diphenyl phosphate (IPPP) addition on the thermal stability of $LiPF_6$/EC + DEC electrolyte. Addition of 5 mass% of IPPP showed positive effects on the decrease in the onset temperature and exothermic behavior of the electrolyte solution [125]. A flame-propagation test was also examined for the electrolyte containing IPPP. Addition of 15 wt% (% in

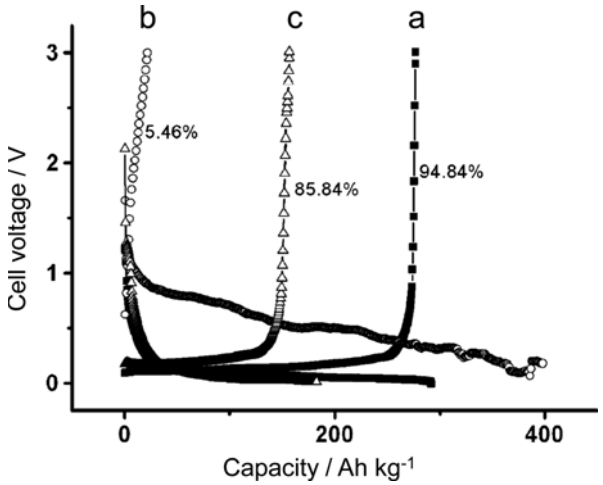

Fig. 2.26 First-cycle charge–discharge curves of Li/graphite (MCMB) half-cells with different electrolytes. (a): 1 M $LiPF_6$/EC + DEC(1:1), (b) 1 M $LiPF_6$/EC + DEC + DMMPp (1:1:2), (c) 1 M $LiPF_6$/EC + DEC + DMMPp (1:1:2) + 5 wt% VEC

mass) or more gave a good result for the nonflammability of the electrolyte, but decreased the discharge capacity and the cycleability of the $LiCoO_2$ positive electrode [124].

As another phosphate-based flame-retardant additive, cresyldiphenyl phosphate (CDP) has been examined in $LiPF_6$/EC + DEC (1:1) [126] and $LiPF_6$/EC + DMC + EMC (1:1:1) [127]. The addition of 5 % (in mass) CDP decreased SET, but its ability for nonflammability was not so high. The effect of CDP on the battery performance of the graphite/$LiCoO_2$ system was small when the addition to the electrolyte solution was limited to a lower level (~5 %). The effect of tris-(4-methoxyphenyl)phosphate (TMMP) on the overcharge protection is also reported in a graphite/$LiFePO_4$ system using [128]. The addition of TMMP in $LiClO_4$/EC + DMC electrolyte shows a decrease in the SET and shifts the oxidation potential of the electrolyte to a less positive one.

Phosphazenes have also been known as effective flame retardants for plastics [129]. Several research groups reported the utility of this family as the flame-retardant component in the LIB electrolytes. Lee et al. [130] examined hexamethoxycyclotriphosphazene $[NP(OCH_3)_2]_3$: HMPN, in $LiPF_6$/EC + DMC (1:1). The addition of HMPN delays the exothermal reaction of lithiated graphite with the electrolyte in a DSC measurement and decreased the self-heating rate in an ARC (accelerating rate calorimater) test [130]. A relatively small amount (1.5 wt%) of HMPN does not show a significant influence on the cycling performance of the $LiNi_{0.8}Co_{0.2}O_2$ positive electrode [130]. Xu et al. [103] reported that, in SET experiments, a considerable amount of HMPN (>40 wt%) is needed to establish sufficient nonflammability for the $LiPF_6$/EC + EMC electrolyte. In

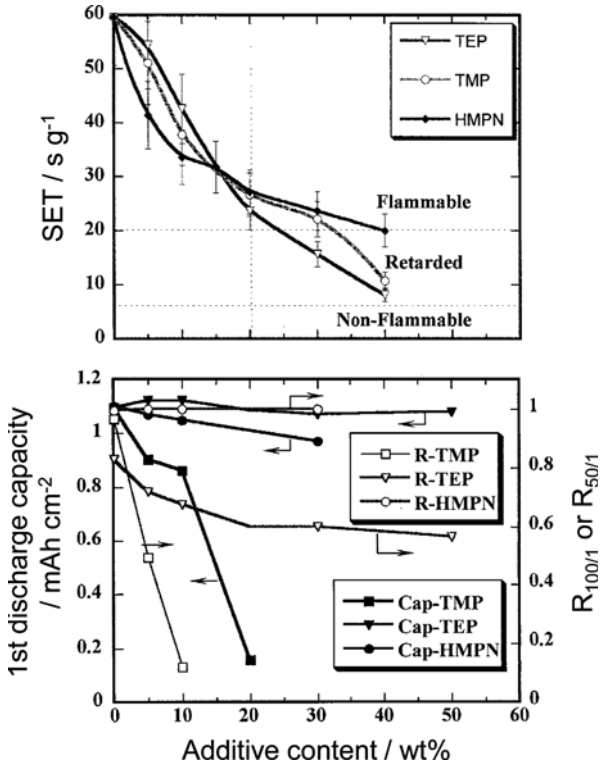

Fig. 2.27 Trade-off between low flammability and electrolyte performance. Capacity utilization of first cycle and retention at hundredth (for TMP, TEP) or fiftieth cycle (HMPN)

Fig. 2.27 [103], the SET value of the electrolyte solution and the discharge capacity of the graphite/$LiNiO_x$ cell using the additive-containing electrolytes are shown as a function of the flame-retardant content. We can see trade-off behavior between low flammability and the electrode performance for the HMPN-added electrolyte, which is commonly observed in the electrolyte systems containing organophosphorous compounds as the flame-retardant components. Sazhin et al. [131] synthesized two kinds of phosphazene compounds and evaluated the nonflammability in EC + EMC-based electrolyte. They observed a significant increase in the flash point of the electrolyte with the content of the additives.

Hu et al. reported a phosphonamidate, bis(*N*,*N*-diethyl) (2-methoxyethoxy) methylphosphonamidate (DEMEMPA), as a new P-N-containing organic flame-retardant additive [132]. Addition of 10 wt% of DEMEMPA to $LiPF_6$/EC + DMC decreases the SET value. The effects of DEMEMPA addition on the cycling performances are rather small for MCMB negative and $LiFePO_4$ positive electrodes.

2.4.3 *Polymeric Gel Electrolytes Containing Alkylphosphates*

Polymeric gel electrolytes that consist of polymer matrices swollen with organic electrolyte solutions are promising quasi-solid electrolytes that contribute to establishing safer and more reliable LIB systems for stationary and vehicle uses [94, 133]. The author's research group has proposed polymeric gel electrolytes containing nonflammable organic components [133, 134]. The key technology of such gel electrolytes is ensuring compatibility of the nonflammability with the cell performance. In this section, basic properties and LIB electrode characteristics of polymeric gel systems containing alkylphosphates are reviewed.

2.4.3.1 Gel Electrolytes Containing Trimethylphosphate

Nonflammable polymeric gel films can be obtained by swelling a polymer matrix with a lithium salt solution containing sufficient amount of nonflammable component. Typically, a polar polymer matrix such as poly(vinylidenefluoride-co-hexafluoropropylene) (PVdF-HFP) is chosen as the host polymer and mixed EC + DMC solution dissolving lithium salt ($LiPF_6$ or $LiBF_4$) is utilized as the liquid component. It is confirmed that nonflammability is established for the gel consisting of 20 vol.% or more of TMP in the liquid phase. Gelation of the flame-retardant EC + DMC + TMP solution decreases the ionic conductivity, but still maintains high values of over 10^{-3} S cm^{-1} at room temperature, as shown in Fig. 2.28 [135]. Similar to the case in liquid electrolyte solutions, addition of VC as an SEI modifier in the liquid phase of the gel is also effective for rechargeability of graphite-based negative electrode in TMP-containing gel electrolyte systems. Figure 2.29 shows the changes in the discharge capacity of the graphite (KS6, TIMICAL) electrode in the gels consisting of $LiPF_6$/EC + DEC + TMP (55:25:20) with and without VC (2 wt%), compared with that observed in conventional liquid electrolyte, $LiPF_6$/EC + DEC (2:1) [134]. For both gel electrolytes, several cycles were initially required to obtain stable capacity. During the initial cycles, the liquid component will be introduced into the pore structure of the electrode to form a good electrode/electrolyte interface. The addition of VC leads to high rechargeability of graphite in the gel containing the nonflammable component TMP.

On the rechargeability of the oxide-based positive electrode, the TMP-containing nonflammable gel electrolyte shows good compatibility with positive electrode materials. With respect to the electrolytic salt, however, $LiBF_4$ is better than $LiPF_6$ for the rechargeability of the $LiMn_2O_4$ positive electrode [135]. In the gel electrolyte dissolving $LiPF_6$, trace amounts of water in the system assist thermal decomposition of PF_6^- anion during the gelation with heat treatment. The resulting gel contains a small amount of HF that promotes the dissolution of Mn species in $LiMn_2O_4$, leading to the degradation of the cycleability of the positive electrode.

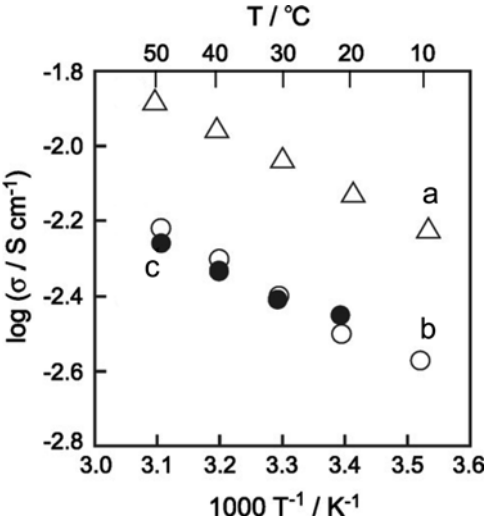

Fig. 2.28 Temperature dependence of ionic conductivity for (a) 0.8 M $LiPF_6$/EC + DEC + TMP (55:25:20) solution, (b) 0.8 M $LiPF_6$/EC + DEC + TMP (55:25:20) gel, and (c) 0.8 M $LiBF_4$/EC + DEC + TMP (55:25:20) gel

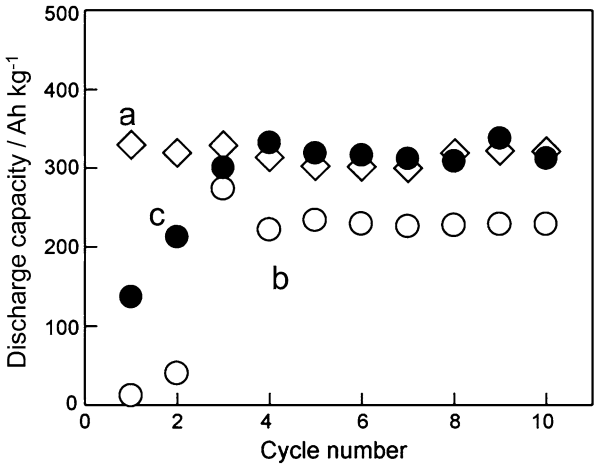

Fig. 2.29 Discharge capacity of a graphite (KS6) electrode in (a) 1 M $LiPF_6$/EC + DEC (2:1) solution, (b) 0.8 M $LiPF_6$/EC + DEC + TMP (55:25:20) gel, and (c) 0.8 M $LiPF_6$/EC + DEC + TMP (55:25:20) + VC (2 wt%) gel

2.4.3.2 Gel Electrolytes Containing Triethylphosphate

The fire-retardant ability of TEP itself is somewhat lower than that of TMP because of the lower P/C ratio in its chemical structure. However, the former would be superior to the latter with respect to compatibility with the graphite-based negative

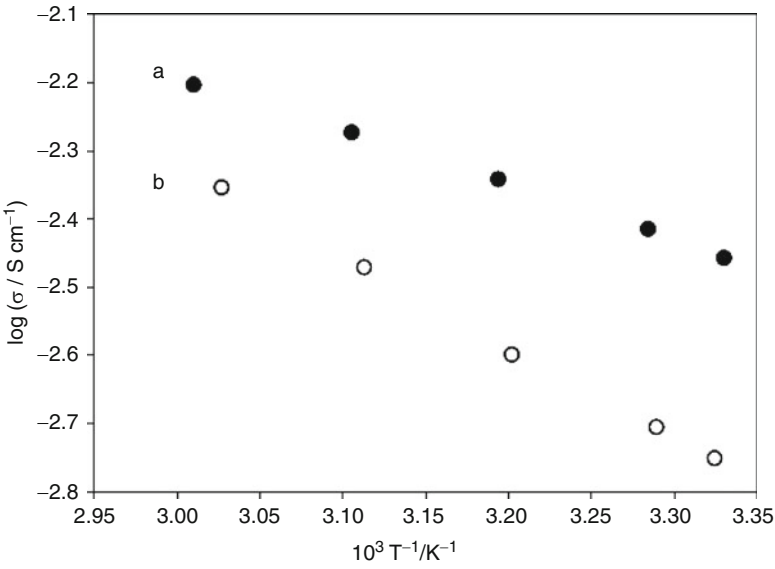

Fig. 2.30 Temperature dependence of ionic conductivity for (a) 1 M $LiBF_4$/EC + DEC + TEP (55:25:20) solution and (b) 1 M $LiBF_4$/EC + DEC + TEP (55:25:20) gel

electrode. Similar to the system containing TMP, an electrolyte solution of 1.0 M $LiBF_4$ in mixed EC + DEC + TEP (55:25:20 in volume) is easily solidified by PVdF-HFP to form transparent self-standing film with sufficient mechanical strength. From the experimental results of thermal analyses, the addition of TEP also shows higher on-set temperature for exothermic decomposition than that of the gel without TEP. Thus, a gel system containing TEP would be promising for practical LIB as nonflammable polymeric gel electrolyte (NPGE). In Fig. 2.30, ionic conductivity of NPGE is compared with that of the base solution electrolyte, $LiBF_4$ (1.0 M)/EC + DEC + TEP [136]. The gel system containing TEP shows a high ionic conductivity of ca. 2 mS cm^{-1} at room temperature, which is a value comparable to that of the gel consisting of TMP [94, 134].

The compatibility of NPGE containing TEP with LIB electrodes is examined for graphite (KS6) negative and $LiMn_2O_4$ positive electrodes by cyclic voltammetry and constant-current charge/discharge cycling. In Fig. 2.31 [136], a typical cyclic voltammetric response of the graphite electrode in the NPGE containing TEP is compared with that in the gel containing TMP. The voltammogram in the gel containing TEP shows reversible current response corresponding to Li-insertion/desertion, which is similar to that in the gel without TEP and completely different from the behavior in the gel containing TMP. This difference in the current responses among the gel composition would be caused by the difference in the interfacial properties between the graphite electrode and the gel electrolyte. That is, the chemistry and electrochemical properties of SEI formed at the graphite surface would depend much on the flame-retardant additives, TEP and TMP, as already discussed

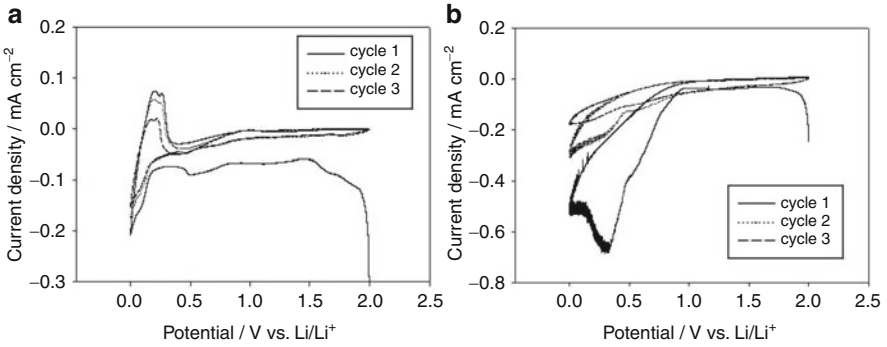

Fig. 2.31 Cyclic voltammograms of graphite (KS6) electrode in (a) 1 M $LiBF_4$/EC + DEC + TEP (55:25:20) gel and (b) 1 M $LiBF_4$/EC + DEC + TMP (55:25:20) gel electrolytes

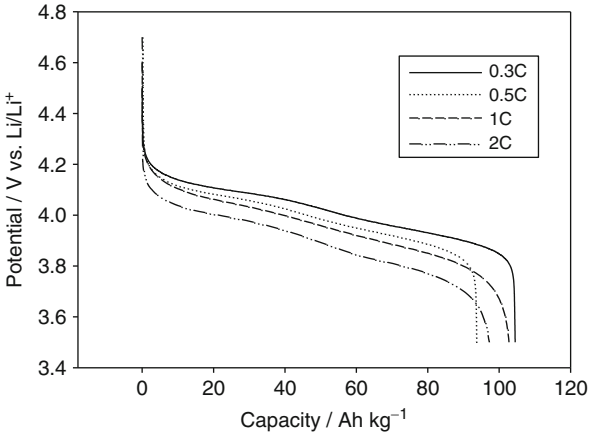

Fig. 2.32 Discharge capacity of a $LiMn_2O_4$ electrode in 1 M $LiBF_4$/EC + DEC + TEP (55:25:20) gel electrolyte (NPGE) at a different discharge rate

above. Figure 2.32 shows an example of the rate-capability of the $LiMn_2O_4$ positive electrode in NPGE containing TEP [136]. More than 90 % of the utility is obtained at a 2C-rate discharge under room temperature conditions.

In order to examine the general features of NPGE, alkylcarbonate-based electrolyte solutions containing different phosphorous-containing additives have been prepared. Free-standing polymeric gel films are easily obtained by a thermal casting method using a PVdF-HFP host polymer. In most cases, the gel films containing a sufficient amount of the fire-retardant additives show excellent nonflammability and ionic conductivity. However, the compatibility of NPGE with the electrode materials is strongly dependent on the sort of the additive component. For example, NPGE containing diphenylphosphite (DPP) as the fire-retardant additive shows excellent nonflammability but poor cycleability of the $LiMn_2O_4$ positive electrode. Anodic

oxidation of DPP inhibits the rechargeability of the positive electrode. If one uses electrode material having a lower redox potential, such as $LiFePO_4$, NPGE containing DPP shows a reversible electrode reaction with high coulombic efficiency [137].

2.4.3.3 Effects of Lewis-Acid Polymer in Gels Containing Triethylphosphate

In order to improve the mass-transport properties, especially at the interface of the solid electrode and the gel electrolyte, different attempts have been reported. The introduction of Lewis-acid polymers (LAPs) into gel electrolyte systems is effective to enhance the Li^+ ion mobility and compatibility of quasi-solid (gel) electrolytes with solid electrode materials [138–140]. With respect to the gel containing the flame-retardant additive, the authors' group reported the utility of LAP in a polymeric gel containing TEP [141]. Typical LAP is synthesized by dehydrated condensation of boron oxide (B_2O_3) with tri(ethylene glycol) monomethylether (TEGMME) and poly(ethylene glycol) (PEG) with a molecular weight of 300. The resulting polymer is blended in a PVdF-HFP-based polymeric gel electrolyte containing TEP (NPGE: PVdF-HFP/$LiBF_4$/EC + DEC + TEP). The effects of the addition of LAP on the ionic conductivity of NPGE are shown in Fig. 2.33 [141]. The addition of a small amount of LAP, with a molar ratio of $[Li^+]/B = 10/1$, improved the ionic conductivity across the whole temperature range examined (−20 to +60 °C). The excess amount of LAP added to NPGE is practically avoided because the higher content of LAP tends to deteriorate the mechanical strength of NPGE.

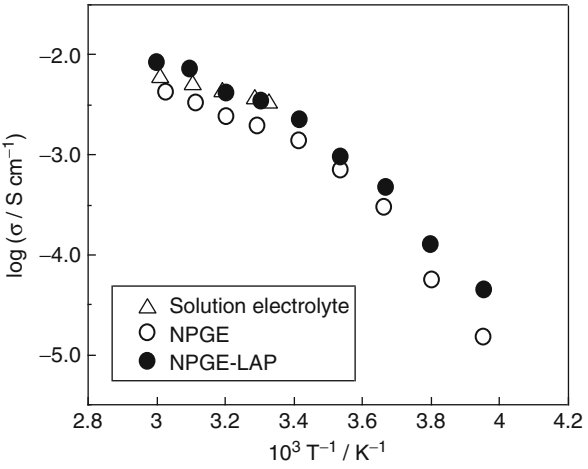

Fig. 2.33 Temperature dependence of ionic conductivity for 1 M $LiBF_4$/EC + DEC + TEP (55:25:20) solution (*open triangle*), 1 M $LiBF_4$/EC + DEC + TEP (55:25:20) gel (NPGE, *open circle*), and 1 M $LiBF_4$/EC + DEC + TEP (55:25:20) + LAP gel (NPGE-LAP, *filled circle*)

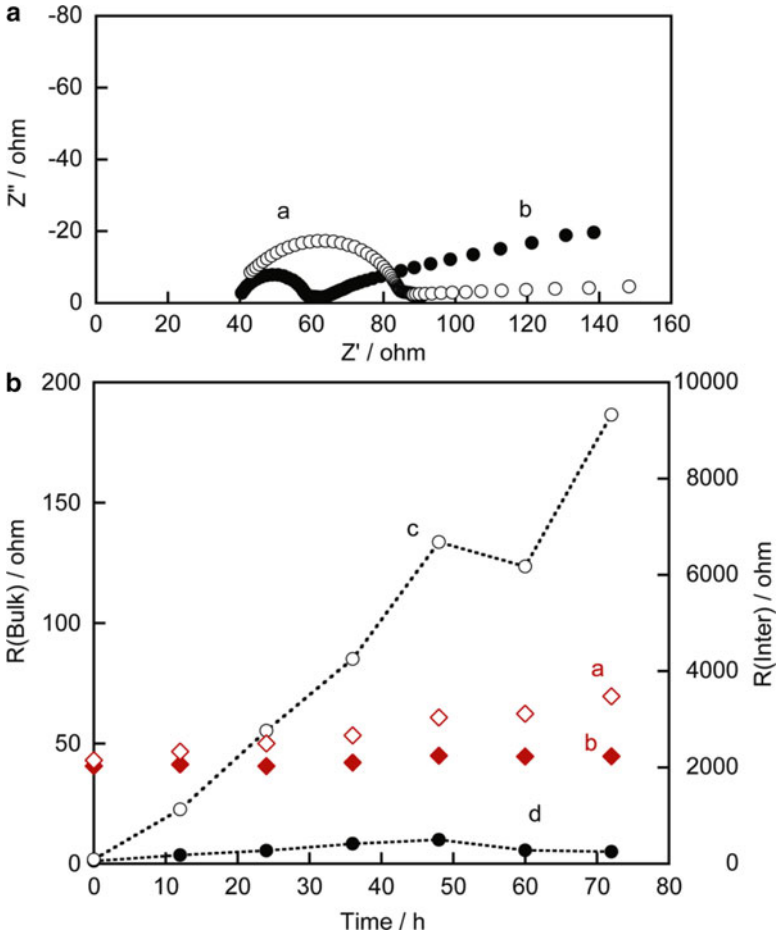

Fig. 2.34 AC impedance responses of Li/gel electrolyte/Li cells: (a) Nyquist plot (*a*: NPGE, *b*: NPGE-LAP), (b) time dependence of bulk resistance (R_{bulk}: *a* and *b*) and interfacial resistance (R_{int}: *c* and *d*), (*a* and *c*: for NPGE, *b* and *d*: for NPGE-LAP)

The improvement of the conductivity by adding LAP is considered to be mainly due to a decrease in the association between the Li^+ cation and the BF_4^- anion. The spectroscopic data of NPGEs with and without LAP prove that the Lewis-acid boron center interacts with the Lewis-base BF_4^-, and there is no ion-pair formation in the LAP-containing NPGE [141]. With respect to the ionic mobility itself, a high value of Li^+ with a transport number (~0.6) is demonstrated as the result of direct-current polarization measurements combined with an ac impedance technique. As smaller values than 0.5 have been usually obtained for conventional organic electrolyte solutions and poly(ethlene oxide)–based solid electrolytes, the above value for NPGE-LAP is regarded to be quite high for Li^+ ion conduction in this kind of gel electrolyte system.

In Fig. 2.34 [141], ac impedance responses of Li metal/NPGE (with and without LAP)/Li metal symmetric cells are shown as an example of the examination of

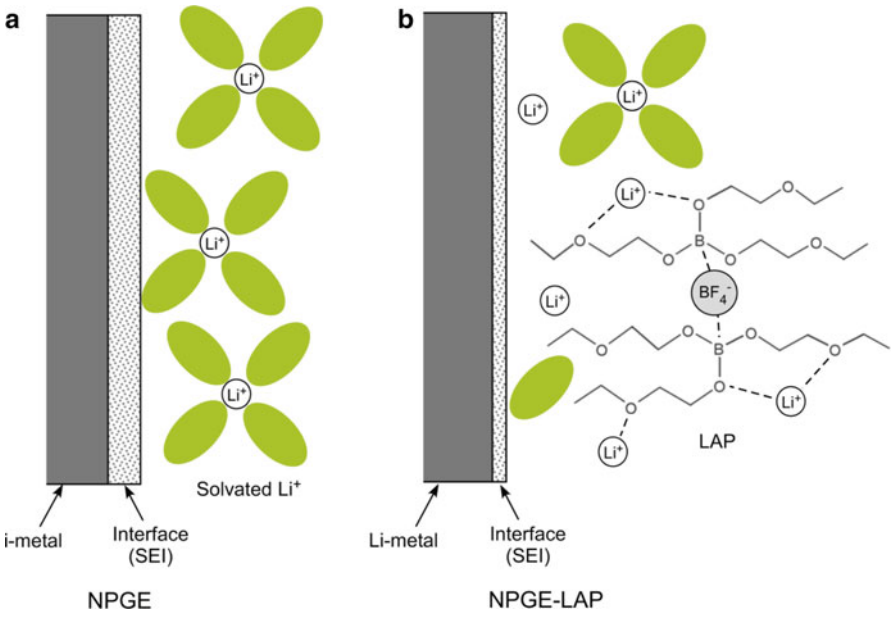

Fig. 2.35 A schematic model for an Li/gel electrolyte interface having interactions between ions and LAP in NPGE. (a) NPGE, (b) NPGE-LAP

influences of LAP on the interface behavior of NPGE. The interfacial resistance, R_{int}, between Li/NPGE (without LAP) increases with the time, while its bulk resistance, R_{bulk}, remains almost constant during the storage. The addition of LAP decreases R_{int} itself by one- to twofold, and reduces the increment during the storage. A model for the additional effects of LAP on the interfacial behavior is presented as shown in Fig. 2.35 [141]. Because Li metal is highly reactive toward organic compounds, it reacts with alkyl carbonate molecules that form Li^+ solvation at the vicinity of the interface between the Li electrode and the gel electrolyte. The decomposition of the organic solvent molecules produces a surface thin layer (SEI). The resistance of the resulting thin layer influences the Li^+ mobility at the interface. A thicker layer with high resistivity hinders the fast movement of Li^+ at the interface. The introduction of LAP in the NPGE leads to the anion trapping by the Lewis-acid interaction, providing free Li^+ at the interface. Thus, the number of Li^+ solvation decreases at the interface, and a thinner layer will be formed as compared to NPGE without LAP.

The results of thermal analyses demonstrated that the introduction of LAP into NPGE also reduces the exothermic heat for thermal decomposition of the liquid component dissolving the Li salt. The charge/discharge characteristics of $LiMn_2O_4$ positive electrode have also been reported. The addition of LAP to NPGE does not have a negative influence on the electrode behavior of $LiMn_2O_4$. There is a high rate capability of the oxide electrode in the present NPGE-LAP system: ca. 80 % or higher of utilization is achieved for the cycling under a 2C-rate at ambient

temperature [141]. We conclude that NPGE-LAP can be used for an LIB system for high-power-density applications with sufficient safety and reliability.

2.4.4 Summary

A variety of organophosphorous compounds, especially in the alkylphosphates family, have been examined as flame-retardant co-solvents or additives in LIB electrolyte systems. Polymeric gel electrolytes containing flame-retardant components would be another choice to produce a battery with a safer and more reliable cell performance. In both cases, nonflammability or the self-extinguishing property of the electrolyte system depends very much on the P/C atomic ratio in the resulting electrolyte. Thus, the higher P/C ratio tends to be effective in establishing nonflammability. However, battery performances, especially for graphite-based negative electrodes, have a tendency to decrease with an increasing P/C ratio. No clear solution has been found for this trade-off behavior. Utilization of an efficient SEI-forming reagent would be a condition to deliver sufficient cell performance for the system using completely nonflammable electrolyte systems.

2.5 Sulfur-Containing Organic Solvents

2.5.1 Introduction

Sulfur has been an important element used for the electrolyte solvents for lithium and lithium-ion batteries. Sulfur-containing organic solvents such as dimethyl sulfoxide and sulfolane are popular solvents for nonaqueous electrolytes [142]. Sulfur-containing inorganic solvents such as SO_2 and $SOCl_2$ have been used as catholytes for lithium cells as listed in Tables 2.6 and 2.7, where typical chemistries for primary and secondary cells are given, respectively [143, 144]. Although no sulfur-containing organic solvent is commercially used in lithium-ion cells, nonaqueous electrolytes containing sulfolane have already been commercially produced for aluminum electrolytic capacitors and double-layer capacitors [145, 146], and have been examined for lithium cells for high-temperature applications. The authors review the papers on lithium and lithium-ion cells using sulfur-containing organic solvents that were published after 1990.

2.5.2 Properties of Organo-Sulfur Compounds

Organo-sulfur compounds are classified into sulfide, sulfoxide, sulfone, sulfite, sulfonate, and sulfate depending on the number and kind of oxygen atoms. The physical properties of acyclic (dimethyl derivatives) and cyclic (five-membered derivatives)

Table 2.6 Primary lithium cells commercialized in the 1970s

Code	Positive electrode	Electrolyte	Voltage	Manufacturer	Year
B	$(CF)_n$	$LiBF_4$/GBL	2.6	Panasonic	1971
–	I_2-PVP	LiI	2.7	Wilson Greatbatch	1972
–	Ag_2CrO_4	$LiClO_4$/PC	3.0	SAFT	1973
–	SO_2	LiBr/AN-SO_2	2.6	(American Cyanamid)	1974
E	$SOCl_2$	$LiAlCl_4/SOCl_2$	3.5	GTE	1974
–	V_2O_5	$LiAsF_6$-$LiBF_4$/MF	2.8	Honeywell	1975
–	CuS	$LiClO_4$/DOL-DME	1.8	DuPont	1975
G	CuO	$LiClO_4$/DOL	1.5	SAFT	1975
F	FeS_2	$LiCF_3SO_3$/MOX-DOL-DME	1.6	Union Carbide	1976
C	MnO_2	$LiClO_4$/PC-DME	2.8	Sanyo Electric	1976

Table 2.7 Secondary lithium cells developed in the 1980s

Type	Negative electrode	Positive electrode	Electrolyte	Manufacturer	Year
Coin	Li-Al	TiS_2	$LiClO_4$/DOL	Exxon	1978
	Li-BiPbSnCd	C	$LiClO_4$/PC-DME	Panasonic	1985
	Li-Al	PAn	$LiBF_4$/PC-DME	Bridestone	1987
	Li-Al	TiS_2	$LiPF_6$/4MeDOL-HMPA	Hitachi Maxwell	1988
	Li-LGH	V_2O_5	$LiClO_4$/PC	Toshiba	1988
	Li-PAS	PAS	$LiBF_4$/PC	Kanebo	1989
	Li-AlMn	Li_xMnO_2	$LiCF_3SO_3$/EC-BC-DME	Sanyo Electric	1989
Cylidrical	Li	TiS_2	$LiAsF_6$/2MeTHF	EIC Lab.	1979
	Li	SO_2	$Li_2B_{10}Cl_{10}/SO_2$	Duracell	1981
	Li	MoS_2	$LiAsF_6$/EC-PC	Moli Energy	1987
	Li	TiS_2	$LiAsF_6$/2MeTHF	W. R. Grace	1987
	Li	$NbSe_3$	$LiAsF_6$/PC-2MeTHF	AT&T Bell Laboratories.	1988
	Li	$CuCl_2$, SO_2	$LiAlCl_4/SO_2$	Altus	1989
	Li	$LiMn_3O_6$	$LiAsF_6$/DOL-TBA	Tadiran	1989

compounds are listed in Table 2.8, where FW, d, mp, bp, fp, ε_r, η, E_{IP}, and E_{EA} are formula weight, density, melting point, boiling point, flash point, relative permittivity, viscosity, ionization potential, and electron affinity, respectively. The ionization potential (IP) and electron affinity (EA) in one-electron oxidation and reduction of a single molecule was calculated by B3LYP/6−311+G(2d,p) without changing the atomic coordinates during the electron transition [147]. The values for DMC and EC are also given for reference. Generally, the ionization potential increases and the electron affinity decreases as the number of oxygen atoms increases.

(a) Sulfides
Sulfides contain a bivalent sulfur atom. Their strong, unpleasant odor is a problem for use. Since lone-pair electrons on the sulfur atoms are easy to oxidize (low IP), there are no recent uses for use in batteries.

Table 2.8 Physical properties of organosulfur compounds at 25 °C

Name	FW	d (g cm^{-3})	mp (°C)	bp (°C)	fp (°C)	ε_r	η (m Pa s)	E_{IP} (eV)	E_{EA} (eV)
Acyclic									
Dimethyl sulfide	62.13	0.85	−98	38	−37			8.65	1.24
Dimethyl sulfoxide (DMSO)	78.13	1.10	18	189	85	46.5	1.99	8.93	1.17
Dimethyl sulfone	94.13	1.16	108	238	143	47.4	1.37	10.60	0.75
Dimethyl sulfite	110.13	1.29	−141	127	41	(110°C)		9.97	0.95
						22.5	0.87		
Methyl methanesulfonate	110.13	1.30	20	203	104			10.64	0.92
Dimethyl sulfate	126.13	1.33	−32	188	83			10.72	0.92
Dimethyl carbonate (DMC)	90.08	1.07	5	90	18	3.2	0.59	10.91	1.09
Cyclic									
Tetramethylene sulfide	88.17	1.00	−96	119	13			8.36	1.09
Tetramethylene sulfoxide (TMSO)	104.17	1.17	−41	236	110	42.9	5.25	8.63	0.90
Tetramethylene sulfone (TMS)	120.17	1.26	28	287	166	43.3	10.28	10.06	0.75
Ethylene sulfite (ES)	108.12	1.43	−17	159	79	(30°C)		10.56	0.88
						39.6	2.06		
Propane sultone (PS)	122.14	1.39	31	295	110			10.69	0.78
Ethylene sulfate	124.12	1.60	96	231	94			11.09	0.74
Ethylene carbonate (EC)	88.06	1.32	37	238	160	90.4	1.93	11.15	0.88
						(40°C)			

(b) Sulfoxides
Dimethyl sulfoxide (DMSO) is a very popular solvent, because it has strong solvating power with a high relative permittivity and an optimum liquid temperature range. Tetramethylene sulfoxide (TMSO) seems to have similar properties with a wider liquid temperature range. Since sulfoxides contain a tetra-valent sulfur atom, they are not as stable toward oxidation as carbonates are due to the existence of lone-pair electrons on the sulfur atoms (low IP). Conductivity and viscosity of $LiClO_4$ in DMSO-ether (THF, DME, DOL) mixtures were extensively studied [148]. Both $LiCF_3SO_3$ and $LiPhSO_3$-DMSO electrolytes were tested for Li/$LiMn_2O_4$ and Li/V_2O_5 cells [149].

(c) Sulfones
Sulfolane (TMS) is the most studied sulfur-containing organic solvent for lithium [150] and lithium-ion [151] cells. Since sulfolane is a solid at room temperature, like EC, it is often mixed with low-viscosity solvents to make electrolyte solutions. Dimethyl sulfone has a high melting point of 108 °C, and it is not easy to handle as a solvent, although it was used for lithium cells in high-temperature operation above 150 °C [152, 153]. Unsymmetrical ethyl methyl sulfone has a relatively low melting point of 37 °C, and it was studied extensively as an electrolyte solvent [154].

(d) Sulfites
Because of the similarity in the structures of sulfites with those of carbonates, the properties of cyclic and acyclic sulfites such as ethylene sulfite [155], propylene sulfite [156], dimethyl sulfite [157], and diethyl sulfite [157] were studied in comparison with EC, PC, DMC, and DEC as an electrolyte additive or co-solvent. Among these, ethylene sulfite (ES) is one of the practical anode SEI-forming additives [158], and dimethyl sulfite is a promising candidate as a co-solvent that improves low-temperature performance of graphite/$LiCoO_2$ cells [159].

(e) Sulfonates
Due to the high chemical reactivity of sulfonates, they are not easy to use as electrolyte solvents. Among sulfonates, 1,3-propane sultone (PS) is one of the practical additives that work as both an anode SEI-forming agent [160–162] and as a cathode protection agent [158, 161].

(f) Sulfates
Due to the high chemical reactivity and toxicity of sulfates, they cannot be used as electrolyte solvents and have been tested only as additives. Among these, ethylene sulfate was tested as an anode SEI-forming agent [163–165].

2.5.3 Electrolyte Formulation and Cell Performance

The oxidation process of electrolyte solutions is complicated. Although electrolyte solutes (lithium salts) are involved, solvents are believed to be the major component responsible for the catalytic decomposition on the cathodes [147, 166]. Angell's

Table 2.9 Electrolytic conductivity of lithium salts in $EMSO_2$

Salt	κ (mS cm^{-1})
$LiN(CF_3SO_2)_2$	5.3
$LiPF_6$	3.2
$LiClO_4$	1.2
$LiCF_3SO_3$	1.0

1 mol dm^{-3}, 25 °C

group in Arizona State University has conducted systematic studies on sulfone solvents in order to increase the anodic stability of the electrolyte solution, which is a recent R&D trend to obtain high-voltage cells. As described in the previous section, sulfones are promising electrolyte solvents for lithium and lithium-ion batteries among sulfur-containing organic solvents. Angell's group introduced an unsymmetrical sulfone, ethyl methyl sulfone ($EMSO_2$), which lowers the melting point (108 °C) of dimethyl sulfone ($DMSO_2$) down to 37 °C by breaking the molecular symmetry [154].

$EMSO_2$ liquefies spontaneously in the presence of lithium salts and the resultant solutions are stable over wide ranges of temperatures from ca.10 °C (when salts or solvate precipitate or $EMSO_2$ crystallizes, depending on lithium salt and concentration) to ca. 220 °C (when $EMSO_2$ begins to evaporate). $EMSO_2$ dissolves various lithium salts readily and it seems to have a special affinity for $LiN(CF_3SO_2)_2$. The electrolytic conductivity of 1 mol dm^{-3} solutions of various lithium salts are given in Table 2.9. A 3:1 mixture of $EMSO_2$ and $DMSO_2$ has an eutectic temperature of 23 °C, and its solution containing $LiN(CF_3SO_2)_2$ is stable to below 0 °C. The anodic stability of $EMSO_2$-based electrolytes was announced to be higher than EC-based electrolytes. It has been confirmed by the successful intercalation of PF_6^- into graphite in $EMSO_2$ up to 5.5 V vs. Li/Li$^+$, whereas EC-based electrolytes are strongly oxidized above 5.2 V, preventing complete loading of graphite with PF_6^- [167], and by the attempt to completely remove lithium ion from $Li_{2/3}Ni_{1/3}Mn_{2/3}O_2$ around 5.4 V [168]. However, its relatively high melting point essentially eliminates the possibility of $EMSO_2$ as a single solvent. Therefore, it must be mixed with a cosolvent to lower the melting point and viscosity for practical use [151].

The studies of Angell's group were extended to other sulfone derivatives as listed in Table 2.10 [151]. The high boiling points of the sulfones correlate reliably with their viscosities at room temperature, and these are high enough to seriously limit the ionic mobilities. The concentration and temperature dependence of electrolytic conductivity of $LiN(CF_3SO_2)_2$ in $EMSO_2$, TMS, and ethyl sec-butyl sulfone (E^sBSO_2) are given in Figs. 2.36 and 2.37, respectively. All sulfones demonstrated a rather uniform high anodic stability toward a $LiMn_2O_4$ cathode despite their different chemical structures. In contrast with the stability on the cathode surface, which is invariant for all sulfones, the ability to form an effective SEI film on the graphite anode is found to be critically sensitive to the sulfone structure. The reductive decomposition of $EMSO_2$ occurred at ca. 0.7 V vs. Li/Li$^+$ without forming an effective SEI on the graphite. Similarly, the coulombic efficiencies for the oxidation-reduction of

Table 2.10 Physical properties of sulfones and their electrolytes

Name	mp (°C)	bp (°C)	ε_r	η (mPa s)	Solubility, m ($LiN(CF_3SO_2)_2$/ $LiPF_6$)	κ^b (mS cm^{-1})
Acyclic						
Dimethyl sulfone	108	238				
Ethyl methyl sulfone	37	239	95 (20˚C)		3.8/2.7	5.3
Diethyl sulfone	74	246				
Ethyl iso-propyl sulfone	<−20	265[a]			2.3/1.0	2.3
Ethyl iso-butyl sulfone	<−20	280[a]				2.5
Ethyl sec-butyl sulfone	−60	290[a]	48 (20˚C)		1.5/0.8	1.5
Dipropyl sulfone	31	266	33 (30˚C)	5.4 (30˚C)		
Dibutyl sulfone	45	295	26 (50˚C)	4.7 (50˚C)		
Cyclic						
Trimethylene sulfone	75	290[a]				
2-Methyltrimethylene sulfone	<−20	270[a]			3.3/–	2.3
Tetramethylene sulfone	28	287	43.3 (30˚C)	10.3 (30˚C)	3.5/2.0	3.1
3-Methyltetramethylene sulfone	6	276	29.4 (25˚C)	11.8 (25˚C)		
2,4-Dimethyltetramethylene sulfone	−3	281	29.7 (25˚C)	9.1 (25˚C)		

[a]Value extrapolated by nomograph
[b]1 mol dm^{-3} $LiN(CF_3SO_2)_2$, 25 °C

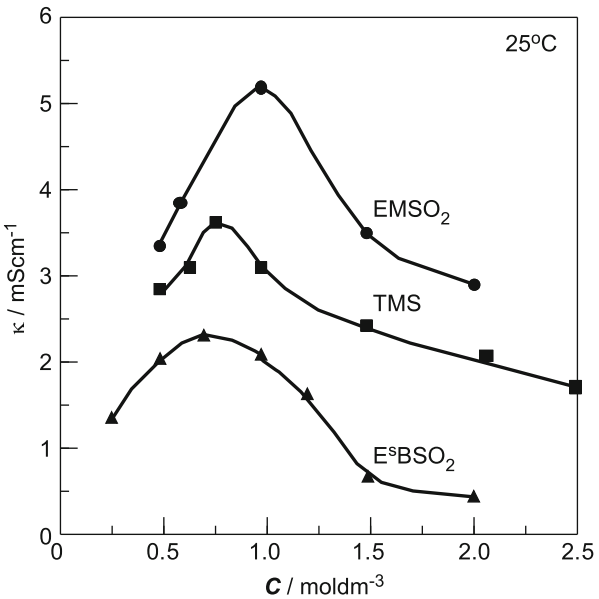

Fig. 2.36 Concentration dependence of electrolytic conductivity of $LiN(CF_3SO_2)_2$ in sulfone solvents

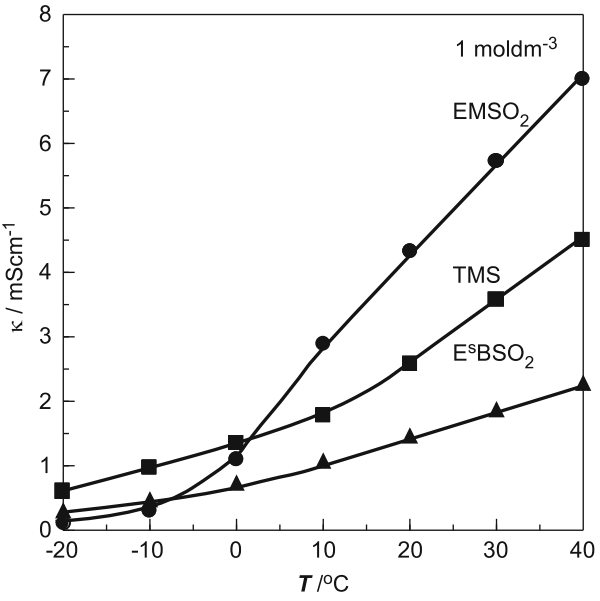

Fig. 2.37 Temperature dependence of electrolytic conductivity of $LiN(CF_3SO_2)_2$ in sulfone solvents

lithium on Pt and Al were low in $EMSO_2$ solvent [169]. Therefore, 1 mol dm^{-3} $LiN(CF_3SO_2)_2$ in $EMSO_2$ or TMS were tested using a $Li_4Ti_5O_{12}$ anode, which does not need a SEI layer to operate [170]. 2.5 V $Li_4Ti_5O_{12}/LiMn_2O_4$ cells containing 1 mol dm^{-3} $LiN(CF_3SO_2)_2$ in $EMSO_2$ or TMS were operated at C/3 rate for 100 cycles with 99 % capacity retention and 100 % coulombic efficiency. Furthermore, a 3 V $Li_4Ti_5O_{12}/LiNi_{1/2}Mn_{3/2}O_4$ cell containing 1 mol dm^{-3} $LiPF_6$ in TMS cycled fairly well at C/12 rate, although a separator wettability problem occurred at the initial cycles.

To lower the melting points of $EMSO_2$, oligoether-containing sulfones [171] and cycloalkyl group-containing sulfones [172] were synthesized and characterized as in Table 2.11. Although these new sulfones showed lower melting points, the electrolytic conductivity of lithium salts in these solvents were always lower than in $EMSO_2$, due to the increased viscosity. The anodic stability decreased by the incorporation of oligoether segments, which was proved by quantum-mechanical calculations [173].

1 mol dm^{-3} $LiPF_6$ in EMES was tested in graphite (MCMB25-28)/Li and $LiCr_{0.015}Mn_{1.985}O_4$/Li half-cells, respectively [171]. The capacity of the first half-cell decreased rapidly with cycling at 0.013 mA cm^{-2} (C/78), presumably due to the ineffective SEI formation, whereas that of the second half-cell decreased gradually with cycling at 0.092 mA cm^{-2} (C/11). A discharge capacity of more than 50 mA h g^{-1} was maintained after 200 cycles with a stable coulombic efficiency around 0.86. Similarly, 1 mol dm^{-3} $LiN(CF_3SO_2)_2$ in ESCP was also tested in graphite (MCMB25-28)/Li and $LiCr_{0.015}Mn_{1.985}O_4$/Li half-cells, respectively [172]. The capacity of the first half-cell decreased rapidly with cycling at 0.068 mA cm^{-2}

Table 2.11 Physical properties of sulfone derivatives and their electrolytes

Name	mp (°C)	bp[a] (°C)	T_g (°C)	T_g[b] (°C)	κ[b](mS cm^{-1})
$CH_3SO_2C_2H_5$ ($EMSO_2$)	37	240	–	–96	5.3
$CH_3OCH_2CH_2SO_2CH_3$ (MEMS)	15	275	–90	–81	1.5
$CH_3OCH_2CH_2SO_2C_2H_5$ (EMES)	2	286	–91	–83	1.4
$CH_3(OCH_2CH_2)_2SO_2C_2H_5$ (EMEES)	<0	>290	–88	–73	0.8
$CH_3(OCH_2CH_2)_3SO_2C_2H_5$ (EMEEES)	<0	>290	–83	–72	0.6
$(CH_3OCH_2CH_2)_2SO_2$ (DMES)	47	>290	–91	–84	1.0
$CH_3SO_2C_5H_9$ (MSCP)	–20	320	–92	–86	0.6
$C_2H_5SO_2C_5H_9$ (ESCP)	38	328	–93	–85	0.6
$CH_3SO_2CH_2C_5H_9$ (MSMCP)	19	325	–87	–80	0.5
$C_2H_5SO_2C_6H_{11}$ (ESCH)	21	337	–76	–72	0.1
$C_2H_5SO_2CH_2C_6H_{11}$ (ESMCH)	9	345	–89	–65	0.1

[a]Value extrapolated by nomograph
[b]1 mol dm^{-3} $LiN(CF_3SO_2)_2$, 25 °C

(C/4.4) due to the incompatibility of the conductivity with the charge/discharge rate, whereas that of the second half-cell decreased gradually with cycling at 0.15 mA cm^{-2} (C/2). A discharged capacity of more than 60 mA h g^{-1} was maintained after 120 cycles with a stable coulombic efficiency around 0.86.

Because these sulfone derivatives have no ability to form an effective SEI, 2 wt% of vinylene carbonate (VC) was added in 1 mol dm^{-3} $LiPF_6$ in EMES or MEMS for graphite/$LiCoO_2$ full cells [174]. 1 mol dm^{-3} $LiPF_6$ in EMES + 2 wt% VC showed a capacity drop, when the rate was raised to 0.50 mA cm^{-2} (C/4.6), whereas 1 mol dm^{-3} $LiPF_6$ in MEMS + 2 wt% VC exhibited almost the same performance as the reference electrolyte, 1 mol dm^{-3} $LiPF_6$ in EC-DMC (50–50 vol.%), at 0.46 mA cm^{-2} (C/5). These results indicated that more fluid versions of the sulfone-based electrolytes are necessary.

To circumvent the low separator wettability and low electrolytic conductivity of single-solvent systems based on sulfone solvents as mentioned before, blending with a low-viscosity solvent such as EMC is a practical approach [170]. Based on this guideline, 1 mol dm^{-3} $LiBF_4$ in TMS-ethyl acetate (50–50 vol.%) + 2 vol.% VC was tested for Li/$LiNi_{1/2}Mn_{3/2}O_4$ cells.

Although sulfone solvents such as $EMSO_2$ and TMS give better performance than EC for high-voltage cells using $LiNi_{0.5}Mn_{1.5}O_4$ cathodes, there is a controversy about the electrochemical stability of sulfone solvents. Xu pointed out that open-chain alkyl sulfones such as $EMSO_2$ are more stable against chemical oxidation and reduction than cyclic sulfones such as TMS [154]. However, their difference seems to be small according to experimental results [170] and IP calculated by density functional theory (cf. Table 2.8). There exists ambiguity in determining the limiting redox potentials because there is always a possibility to include the effect of passivation on the electrode surface by reacted products.

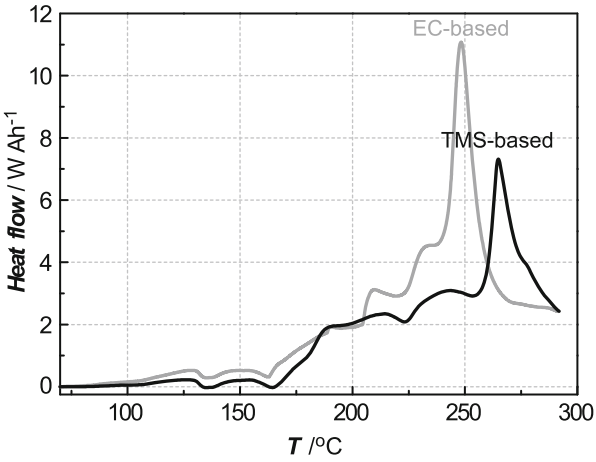

Fig. 2.38 Thermal behavior of 4.4 V graphite/$LiNi_{1/3}Mn_{1/3}Co_{1/3}O_2$ pouch cells

The research on high-voltage cells is going on over the world to meet the requirements for automotive applications, because the utilization of high-voltage cathodes enables is to increase the energy density by enhancing operational voltage such as $LiNi_{0.5}Mn_{1.5}O_4$ and $LiCoPO_4$, or increasing capacity such as $LiNi_xMn_yCo_zO_2$ and Li_2MnO_3-$LiNi_xMn_yCo_zO_2$ ($x+y+z=1$). However, lithium-ion cells intrinsically have serious safety problems, and the cell safety becomes still more severe for the high-voltage cells. Ue's group at Mitsubishi Chemical Corporation have developed high safety electrolytes including a TMS solvent for hybrid electric vehicle applications. One of the ways to avoid the thermal runaway is to apply materials that generate less heat even at elevated temperatures. They have found that the major source of heat generation in conventional electrolytes was EC, and a partial replacement of EC with TMS decreased the heat generation, when graphite/$LiNi_{1/3}Mn_{1/3}Co_{1/3}O_2$ pouch cells (4.1 V, 20 mA h) and 18,650 cylindrical cells (4.1 V, 1.2 A h) were heated up [175]. Encouraged by this result, the charging voltage was raised from 4.1 to 4.4 V and the thermal behavior and cell performance of these cells were examined [176, 177]. A TMS-based electrolyte [1 mol dm^{-3} $LiPF_6$/EC–FEC–SLF–DMC–EMC (5–5–20–40–30 vol.%)] showed lower heat generation rate than the conventional EC-based counterpart [1 mol dm^{-3} $LiPF_6$/EC–EMC (30–70 vol.%)] as shown in Fig. 2.38. A nail penetration test (0.0025 mφ, 0.35 ms^{-1}) of the 18,650 cylindrical cells at room temperature proved that the TMS-based electrolyte is safer than the conventional EC-based counterpart, because the former showed no event, whereas the latter exploded. Although cycle performances of the cells using TMS-based electrolytes are almost equivalent to that of the conventional EC-based counterparts, their output performances were inferior, as shown in Fig. 2.39.

Ue's group have also found that TMS-based electrolytes suppress the crystal change of $LiNi_{1/3}Mn_{1/3}Co_{1/3}O_2$ (layered) to spinel M_3O_4 at elevated temperatures over 280 °C due to passivation on the cathode by sulfur compounds such as Li_2SO_4. Contrary to experimental observations, TMS has lower IP and EA than EC. If it is

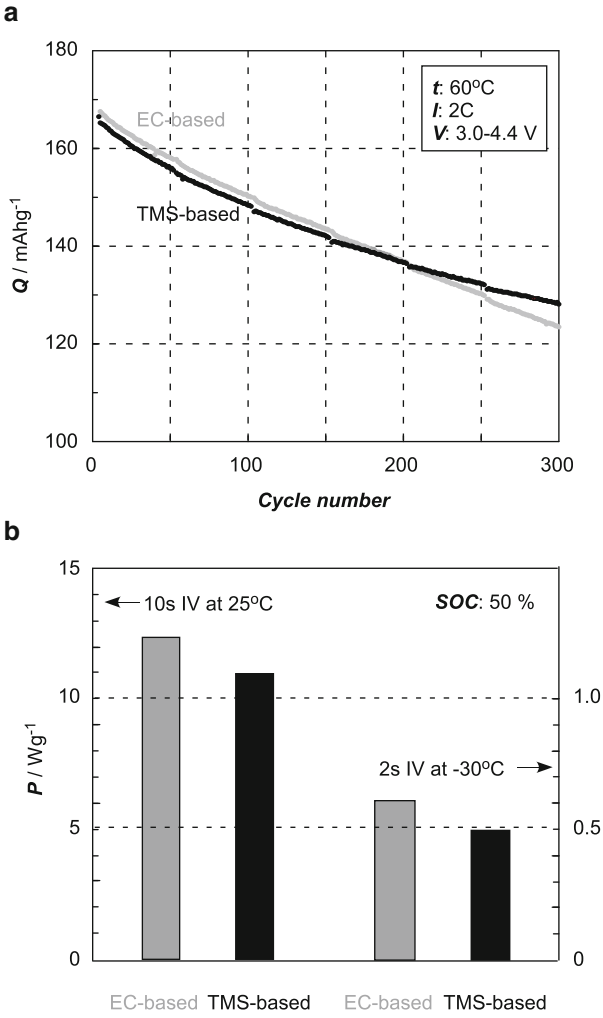

Fig. 2.39 Cell performances of graphite/$LiNi_{1/3}Mn_{1/3}Co_{1/3}O_2$ pouch cells. (**a**) Cycle test and (**b**) output test

true, the observed higher anodic and cathodic stability of sulfones can be explained by the formation of SEI on the electrodes, which must be examined in detail.

2.5.4 Summary

Sulfur-containing organic solvents, particularly sulfones such as $EMSO_2$ and TMS, were examined as electrolyte solvents for high-voltage cells. As single solvents, they have a few disadvantages such as low-anode SEI film–forming ability, and low

electrolytic conductivity, particularly at low temperatures. However, these disadvantages are mitigated by the aids of SEI-forming additives and low-viscosity carbonate co-solvents. Further progress is expected by introducing new sulfone derivatives. For example, a computational study to examine the effect of multiple functionalization with fluorine, cyano, ester, and carbonate groups has recently been reported as a key to achieving high oxidation potentials [178].

References

1. Ue, M., Electrolytes: nonaqueous, In *Encyclopedia of electrochemical power sources*; Garche, J.; Dyer, C.; Moseley, P.; Ogumi, Z.; Rand, D.; Scrosati, B., Eds.; Elsevier: Amsterdam, Netherlands, 2009; Vol. 5; 71–84.
2. Ding, M. S., Liquid-solid phase diagrams of ternary and quaternary organic carbonates, *J. Electrochem. Soc.* **2004**, *151*, A731–A738.
3. Ding, M. S.; Xu, K.; Zhang, S. S.; Amine, K.; Henriksen, G. L.; Jow, T. R., Change of conductivity with salt content, solvent composition, and temperature for electrolytes of $LiPF_6$ in ethylene carbonate-ethyl methyl carbonate, *J. Electrochem. Soc.* **2001**, *148*, A1196–A1204.
4. Sasaki, Y., The status and view for fluorine-containing organic solvents, In *Advanced battery technologies-2011*; *the Electrochemical Society of Japan*: Tokyo, Japan, 2011; 17–30.
5. Sasaki, Y., Organic electrolytes of secondary lithium batteries, *Electrochemistry* **2008**, *76*, 2–15.
6. Prager, J. H., *Cyclic fluorocarbonates*, US Patent 3,455,954: 1969.
7. Adcock, J. L.; Lagow, R. J., The synthesis of the perfluoroethers, "perfluoroglyme" and "perfluorodiglyme" by direct fluorination, *J. Org. Chem.* **1973**, *38*, 3617–3618.
8. Sasaki, Y.; Ebara, R.; Nanbu, N.; Takehara, M.; Ue, M., Direct fluorination of γ-butyrolactone, *J. Fluorine Chem.* **2001**,*108*, 117–120.
9. Hasegawa, M; Ishi, H.; Fuchigami, T., Electroorganic synthesis under solvent-free conditions. Highly regioselective anodic monofluorination of cyclic ethers, lactones and a cyclic carbonate, *Tetrahedron Lett*. **2002**, *43*, 1503–1505.
10. Takehara, M.; Ebara, R.; Nanbu, N.; Ue, M.; Sasaki, Y., Electrochemical properties of fluoro-γ-butyrolactone and its application to lithium rechargeable cells, *Electrochemistry* **2003**, *71*, 1172–1176.
11. Nakajima, T.; Dan, K.; Koh, M., Effect of fluoroesters on the low temperature electrochemical characteristics of graphite electrode, *J. Fluorine Chem.* **1998**, *87*, 221–227.
12. Nakajima, T.; Dan, K.; Koh, M; Ino, T.; Shimizu, T., Effect of addition of fluoroethers to organic solvents for lithium ion secondary batteries, *J. Fluorine Chem.* **2001**, *111*, 167–174.
13. Chandrasekaran, R.; Koh, M; Ozhawa, Y.; Aoyama, H; Nakajima, T., Electrochemical cell studies on fluorinated natural graphite in propylene carbonate electrolyte with difluoromethyl acetate (MFA) additive for low temperature lithium battery application *J. Chem. Sci.* **2009**, *121*, 339–346.
14. Yamaki, J.; Yamazaki, I.; Egashira, M.; Okada, S., Thermal studies of fluorinated ester as a novel candidate for electrolyte solvent of lithium metal anode rechargeable cells, *J. Power Sources* **2001**, *102*, 288–293.
15. Sato, K.; Yamazaki, I.; Okada, S.; Yamaki, J., Mixed solvent electrolytes containing fluorinated carboxylic acid esters to improve the thermal stability of lithium metal anode cells, *Solid State Ionics* **2002**, *148*, 463–466.
16. Yamaki, J.; Tanaka, T.; Ihara, M.; Sato, K.; Egashira, M.; Watanabe, I.; Okada, S., Thermal stability of methyl difluoroacetate as a novel electrolyte solvent for lithium batteries electrolytes, *Electrochemistry* **2003**, *71*, 1154.

17. Ihara, M.; Hang, B. T.; Sato, K.; Egashira, M.; Okada, S.; Yamaki, J., Properties of carbon anodes and thermal stability in $LiPF_6$/methyl difluoroacetate electrolyte, *J. Electrochem. Soc.* **2003**, *150*, A1476–A1483.
18. Nanbu, N.; Suzuki, Y.; Ohtsuki, K.; Meguro, T.; Takehara, M.; Ue, M.; Sasaki, Y., Physical and electrochemical properties of monofluorinated ethyl acetates for lithium rechargeable batteries, *Electrochemistry* **2010**, *78*, 446–449.
19. Sato, K.; Zhao, L.; Okada, S.; Yamaki, J., $LiPF_6$/methyl difluoroacetate electrolyte with vinylene carbonate additive for Li-ion batteries, *J. Power Sources* **2011**, *196*, 5617–5622.
20. Kobayashi, M.; Inoguchi, T.; Iida, T.; Tanioka, T.; Kumase, H.; Fukai, Y., Development of direct fluorination technology for application to materials for lithium battery, *J. Fluorine Chem.* **2003**, *120*, 105–110.
21. McMillan, R.; Slegr, H.; Shu, Z. X.; Wang, W., Fluoroethylene carbonate electrolyte and its use in lithium ion batteries with graphite anodes, *J. Power Sources* **1999**, *81–82*, 20–26.
22. Mogi, R.; Inaba, M.; Jeong, S.-K.; Iriyama, Y.; Abe, T.; Ogumi, Z., Effects of some organic additives on lithium deposition in propylene carbonate, *J. Electrochem. Soc.* **2002**, *149*, A1578–A1583.
23. Choi, N.-S.; Yew, K. H.; Lee, K. Y.; Sung, M.; Kim, H.; Kim, S.-S., Effect of fluoroethylene carbonate additive on interfacial properties of silicon thin-film electrode, *J. Power Sources* **2006**, *161*, 1254–1259.
24. Profatilova, I. A.; Kim, S.-S.; Choi, N.-S., Enhanced thermal properties of the solid electrolyte interphase formed on graphite in an electrolyte with fluoroethylene carbonate, *Electrochim. Acta* **2009**, *54*, 4445–4450.
25. Hagiyama, K.; Suzuki, K.; Ohtake, M.; Shimada, M.; Nanbu, N.; Takehara, M.; Ue, M.; Sasaki, Y., Physical properties of substituted 1,3-dioxolan-2-ones, *Chem. Lett.* **2008**, *37*, 210–211.
26. Sasaki, Y.; Takimoto, K.; Nanbu, N.; Takehara, M.; Ue, M., Direct fluorination of propylene carbonate, In *Meeting abstracts of the 6th Japan-France joint seminar on lithium ion batteries*; Kohu, Yamanashi, Japan, 2006; 24.
27. Nanbu, N.; Takimoto, K.; Suzuki, K.; Ohtake, M.; Hagiyama, K.; Takehara, M.; Ue, M.; Sasaki, Y., Temperature dependence of physical constants of monofluororinated propylene carbonate as highly polar liquid, *Chem. Lett.* **2008**, *37*, 476–477.
28. Nanbu, N.; Takimoto, K.; Takehara, M.; Ue, M.; Sasaki, Y., Electrochemical properties of fluoropropylene carbonate and its application to lithium-ion batteries, *Electrochem. Commun.* **2008**, *10*, 783–786.
29. Inaba, M.; Kawatate, Y.; Funabiki, A.; Jeong, S.-K.; Abe, T.; Ogumi, Z., STM study on graphite/electrolyte interface in lithium-ion batteries: solid electrolyte interface formation in trifluoropropylene carbonate solution, *Electrochim. Acta* **1999**, *45*, 99–105.
30. Arai, J.; Katayama, H.; Akahoshi, H., Binary mixed solvent electrolytes containing trifluoropropylene carbonate for lithium secondary batteries, *J. Electrochem. Soc.* **2002**, *149*, A217–A226.
31. Achiha, T.; Nakajima, T.; Ohzawa, Y.; Koh, M.; Yamauchi, A.; Kagawa, M.; Aoyama, H., Electrochemical behavior of nonflammable organo-fluorine compounds for lithium ion batteries, *J. Electrochem. Soc.* **2009**, *156*, A483–A488.
32. Achiha, T.; Nakajima, T.; Ohzawa, Y.; Koh, M.; Yamauchi, A.; Kagawa, M.; Aoyama, H., Thermal stability and electrochemical properties of fluorine compounds as nonflammable solvents for lithium-ion batteries, *J. Electrochem. Soc.* **2010**, *157*, A707–A712.
33. Takehara, M.; Watanabe, S.; Nanbu, N.; Ue, M.; Sasaki, Y., Synthesis of fluorinated dimethyl carbonates by direct fluorination, *Synth. Commun.* **2004**, *34*, 1367–1375.
34. Takehara, M.; Watanabe, S.; Nanbu, N.; Ue, M.; Sasaki, Y., Physical properties of monofluorodimethyl carbonate, *Chem. Lett.* **2004**, *33*, 338–339.
35. Sasaki, Y.; Takehara, M.; Watanabe, S.; Oshima, M.; Nanbu, N.; Ue, M., Electrolytic behavior and application to lithium batteries of monofluorinated dimethyl carbonate, *Solid State Ionics* **2006**, *177*, 299–303.

36. Nanbu, N.; Watanabe, S.; Takehara, M.; Ue, M.; Sasaki, Y., Electrolytic characteristics of fluoromethyl methyl carbonate for lithium rechargeable batteries, *J. Electroanal. Chem.* **2009**, *625*, 7–15.
37. Nanbu, N.; Takehara, M.; Watanabe, S.; Ue, M.; Sasaki, Y., Polar effect of successive fluorination of dimethyl carbonate on physical properties, *Bull. Chem. Soc. Jpn.* **2007**, *80*, 1302–1306.
38. Sasaki, Y.; Takehara, M.; Watanabe, S.; Nanbu, N.; Ue, M., Physical and electrolytic properties of difluorinated dimethyl carbonate, *J. Fluorine Chem.* **2004**, *125*, 1205–1209.
39. Takehara, M., Tsukimori, N.; Nanbu, N.; Ue, M.; Sasaki, Y., Physical and electrolytic properties of fluoroethyl methyl carbonate, *Electrochemistry* **2003**, *71*, 1201–1204.
40. Handa, M.; Kataoka, M.; Watanabe, M.; Sasaki, Y., Physical and donor–acceptor properties of 3-propyl-4-ethylsydnone, *Bull. Chem. Soc. Jpn.* **1997**, *70*, 315–320.
41. Tsukimori, N.; Nanbu, N.; Takehara, M.; Ue, M.; Sasaki, Y., Electrolytic properties of ethyl fluoroethyl carbonate and its application to lithium battery, *Chem. Lett.* **2008**, *37*, 368–369.
42. Sasaki, Y.; Satake, H.; Tsukimori, N.; Nanbu, N.; Takehara, M.; Ue, M., Physical and electrolytic properties of partially fluorinated methyl propyl carbonate and its application to lithium batteries, *Electrochemistry* **2010**, *78*, 467–470.
43. Smart, M. C.; Ratnakumar, B. V.; Ryan-Mowrey, V. S.; Surampudi, S.; Prakash, G. K. S.; Hu, J.; Cheung, I., Improved performance of lithium-ion cells with the use of fluorinated carbonate-based electrolytes, *J. Power Sources* **2003**, *119–121*, 359–367.
44. Kitagawa, T; Azuma, K.; Koh, M.; Yamaguchi, A.; Kagawa, M.; Sakata, H.; Miyawaki, H.; Nakazono, A.; Arima, H.; Yamagata, M.; Ishikawa, M., Application of fluorine-containing solvents to $LiCoO_2$ cathode in high voltage operation, *Electrochemistry* **2010**, *78*, 345–348.
45. Arai, J., A novel non-flammable electrolyte containing methyl nonafluorobutyl ether for lithium secondary batteries, *J. Appl. Electrochem.* **2002**, *32*, 1071–1079.
46. Arai, J., Nonflammable methyl nonafluorobutyl ether for electrolyte used in lithium secondary batteries, *J. Electrochem. Soc.* **2003**, *150*, A219–A228.
47. Arai, J., No-flash-point electrolytes applied to amorphous carbon/$Li_{1+x}Mn_2O_4$ cells for EV use, *J. Power Sources* **2003**, *119–121*, 388–392.
48. Morita, M.; Kawasaki, T.; Yoshimoto, N.; Ishikawa, M., Nonflammable organic electrolyte solution based on perfluoro-ether solvent for lithium ion batteries, *Electrochemistry* **2003**, *71*, 1067–1069.
49. Naoi, K.; Iwama, E.; Ogihara, N.; Nakamura, Y.; Segawa, H.; Ino, Y., Nonflammable hydrofluoroether for lithium-ion batteries: enhanced rate capability, cyclability, and low-temperature performance, *J. Electrochem. Soc.* **2009**, *156*, A272–A276.
50. Naoi, K.; Iwama, E.; Honda, Y.; Shimodate, F., Discharge behavior and rate performances of lithium-ion batteries in nonflammable hydrofluoroethers(II), *J. Electrochem. Soc.* **2010**, *157*, A190–A195.
51. Iwama, E.; Shimodate, F.; Oki, Y.; Naoi, K., Super-enhanced lithium-ion transport by an effective shift of solvation shell structure in branched hydrofluoroether electrolyte, *Electrochemistry* **2010**, *78*, 266–272.
52. Ikeda, K.; Kawasato, T.; Hiratsuka, K.; Morimoto, T., *Nonaqueous electrolytic secondary battery*; JP 3,557,724 (B2): 2004.
53. Sasaki, Y.; Shimazaki, G.; Nanbu, N.; Takehara, M.; Ue, M., Physical and electrolytic properties of partially fluorinated organic solvents and its application to secondary lithium batteries: partially fluorinated dialkoxyethanes, *ECS Trans.* **2009**, *16(35)*, 23–31.
54. Blomgren, G. E., Properties, structures and conductivity of organic and inorganic electrolytes for lithium battery systems, In *Lithium batteries*; Gabano, J.-P., Ed.; Academic Press: London, United Kingdom, 1983; Ch. 2; 13–41.
55. Ue, M.; Ida, K.; Mori, S., Electrochemical properties of organic liquid electrolytes based on quaternary onium salts for electrical double-layer capacitors, *J. Electrochem. Soc.* **1994**, *141*, 2989–2996.
56. Nanbu, N.; Hagiyama, K.; Takehara, M.; Ue, M.; Sasaki, Y., Physical and electrolytic properties of difluorinated 3-methyl-2-oxazolidinones and their application to lithium rechargeable batteries, *Electrochemistry* **2010**, *78*, 450–453.

57. Suzuki, K.; Shin-Ya, M.; Ono, Y.; Matsumoto, T., Nanbu, N.; Takehara, M.; Ue, M.; Sasaki, Y., Physical and electrochemical properties of fluoroacetonitrile and its application to electric double-layer capacitors, *Electrochemistry* **2007**, *75*, 611–614.
58. Hagiyama, K.; Nanbu, N.; Takehara, M.; Ue, M.; Sasaki, Y., Electrolytic properties of α-fluorinated 1-methyl-2-pyrrolidinone, In *Meeting abstracts of the 2002 fall meeting of the Electrochemical Society of Japan*; Atsugi, Kanagawa, Japan, 2002; 99.
59. (a) Lu, Z.; MacNeil, D. D.; Dahn, J. R., Layered cathode materials $Li[Ni_xLi_{(1/3-2x/3)}Mn_{(2/3-x/3)}]O_2$ for lithium-ion batteries, *Electrochem. Solid-State Lett.* **2001**, *4*, A191–A194; (b) Ohzuku, T.; Makimura, Y., Layered lithium insertion material of $LiCo_{1/3}Ni_{1/3}Mn_{1/3}O_2$ for lithium-ion batteries, *Chem. Lett*. **2001**, *(7)*, 642–643; (c) Ohzuku, T.; Makimura, Y., Layered lithium insertion material of $LiNi_{1/2}Mn_{1/2}O_2$: a possible alternative to $LiCoO_2$ for advanced lithium-ion batteries, *Chem. Lett*. **2001**, *(8)*, 744–745; (d) Ohzuku, T.; Ariyoshi, K.; Yamamoto, S.; Makimura, Y., A 3-volt lithium-ion cell with $Li[Ni_{1/2}Mn_{3/2}]O_4$ and $Li[Li_{1/3}Ti_{5/3}]O_4$: a method to prepare stable positive-electrode material of highly crystallized $Li[Ni_{1/2}Mn_{3/2}]O_4$, *Chem. Lett.* **2001**, *(12)*, 1270–1271; (e) Lu, Z. H.; Beaulieu, L. Y.; Donaberger, R. A.; Thomas, C. L.; Dahn, J. R., Synthesis, structure, and electrochemical behavior of $Li[NixLi_{1/3-2x/3}Mn_{2/3-x/3}]O_2$, *J. Electrochem. Soc*. **2002**, *149*, A778–A791; (f) Lu, Z. H.; Chen, Z. H.; Dahn, J. R., Lack of cation clustering in $Li[Ni_xLi_{1/3-2x/3}Mn_{2/3-x/3}]O_2$ ($0 < x \leq 1/2$) and $Li[Cr_xLi_{(1-x)/3}Mn_{(2-2x)/3}]O_2$ ($0 < x < 1$), *Chem. Mater.* **2003**, *15*, 3214–3220; (g) Makimura, Y.; Ohzuku, T., Lithium insertion material of $LiNi_{1/2}Mn_{1/2}O_2$ for advanced lithium-ion batteries, *J. Power Sources* **2003**, *119–121*, 156–160.
60. (a) Xu, K.; Angell, C. A., High anodic stability of a new electrolyte solvent: unsymmetric noncyclic aliphatic sulfone, *J. Electrochem. Soc.* **1998**, *145*, L70–L72; (b) Xu, K.; Angell, C. A., Sulfone-based electrolytes for lithium-ion batteries, *J. Electrochem. Soc.* **2002**, *149*, A920–A926; (c) Abouimrane, A.; Belharouak, I.; Amine, K., Sulfone-based electrolytes for high-voltage Li-ion batteries, *Electrochem. Commun.* **2009**, *11*, 1073–1076; (d) Sun, X,; Angell, C. A., Doped sulfone electrolytes for high voltage Li-ion cell applications, *Electrochem.Commun.* **2009**, *11*, 1418–1421.
61. Abu-Lebdeh, Y.; Davidson, I., New electrolytes based on glutaronitrile for high energy/power Li-ion batteries, *J. Power Sources* **2009**, *189*, 576–579.
62. (a) Sasaki, Y.; Takehara, M.; Watanabe, S.; Oshima, M.; Nanbu, N.; Ue, M., Electrolytic behavior and application to lithium batteries of monofluorinated dimethyl carbonate, *Solid State Ionics* **2006**, *177*, 299–303; (b) Nanbu, N.; Takimoto, K.; Takehara, M.; Ue, M.; Sasaki, Y., Electrochemical properties of fluoropropylene carbonate and its application to lithium-ion batteries, *Electrochem. Commun.* **2008**, *10*, 783–786.
63. Gaussian 09 is the current integrated program including several molecular orbital methods, see Gaussian Inc. http://www.gaussian.com/
64. For example, *Minerals yearbook*, *Volume I. Metals and minerals*, USGS: 2009.
65. *Merck Index*, 13th Edition, 2001.
66. (a) Kidd, R. G., In *NMR of newly accessible nuclei, Vol. 2*; Laszlo, P., Ed.; Academic Press: New York, NY, 1983; (b) Noeth, H.; Wrackmeyer, B., In *Nuclear magnetic resonance spectroscopy of boron compounds*; Springer: Berlin, 1987; (c) Kennedy, J. D., In *Multinuclear NMR*; Mason, J., Ed.; Plenum Press: New York, NY, 1987.
67. Tanaka, Y.; Kaneko, J.; Minoshima, M.; Iriyama, Y.; Fujinami, T., Electrochemical properties of a mixed boric ester as a novel electrolyte solvent, *Electrochemistry* **2010**, *78*, 397–399.
68. Hirono, T.; Tamada, H.; Kishimoto, A.; Kaneko, J.; Iriyama, Y.; Tanaka, Y.; Fujinami, T., High voltage stability of interfacial reaction at the $LiMn_2O_4$ thin-film electrodes/liquid electrolytes with boroxine compounds, *J. Electrochem. Soc.* **2010**, *157*, A667–A681.
69. Shanmukaraj, D.; Grugeon, S.; Gachot, G.; Laruelle, S.; Mathiron, D.; Tarascon, J.-M.; Armand, M., Boron esters as tunable anion carriers for non-aqueous batteries electrochemistry, *J. Am. Chem. Soc.* **2010**, *132*, 3055–3062.
70. (a) Lee, H. S.; Yang, X. Q.; Sun, X.; McBreen, J., Synthesis of a new family of fluorinated boronate compounds as anion receptors and studies of their use as additives in lithium battery electrolytes, *J. Power Sources* **2001**, *97–98*, 566–569; (b) Sun, X.; Lee, H. S.; Yang, X. Q.;

McBreen, J., A new additive for lithium battery electrolytes based on an alkyl borate compound, *J. Electrochem. Soc.* **2002**, *149*, A355–A359; (c) Li, L. F.; Lee, H. S.; Lee, H.; Yang, X. Q.; Nam, K. W.; Yoon, W. S.; McBreen, J.; Huang, X. J., New electrolytes for lithium ion batteries using LiF salt and boron based anion receptors, *J. Power Sources* **2008**, *184*, 517–521.

71. (a) Lee, H. S.; Sun, X.; Yang, X. Q.; McBreen, J., Synthesis and study of new cyclic boronate additives for lithium battery electrolytes, *J. Electrochem. Soc.* **2002**, *149*, A1460–A1465; (b) Lee, H. S.; Ma, X. Z. F.; Yang, X. Q.; Sun, X.; McBreen, J., Synthesis of a series of fluorinated boronate compounds and their use as additives in lithium battery electrolytes, *J. Electrochem. Soc.* **2004**, *151*, A1429–A1435; (c) Chen, Z.; Amine, K., Bifunctional electrolyte additive for lithium-ion batteries, *Electrochem. Commun.* **2007**, *9*, 703–707; (d) Chen, Z.; Amine, K., Computational estimates of fluoride affinity of boron-based anion receptors, *J. Electrochem. Soc.* **2009**, *156*, A672–A676; (e) Weng, W.; Zang, Z.; Schlueter, J. A.; Redfern, P. C.; Curtiss, L. A.; Amine, K., Improved synthesis of a highly fluorinated boronicester as dual functional electrolyte additive for lithium-ion batteries, *J. Power Sources,* **2011**, *196*, 2171–2178.
72. (a) Xu, W.; Angell, C. A., LiBOB and its derivatives. Weakly coordinating anions, and the exceptional conductivity of their nonaqueous solutions, *Electrochem. Solid-State Lett.* **2001**, *4*, E1–E4; (b) Xu, W.; Shusterman, A. J.; Videa, M.; Velikov, V.; Marzke, R.; Angell, C. A., Structures of orthoborate anions and physical properties of their lithium salts in nonaqueous solutions, *J. Electrochem. Soc.* **2003**, *150*, E74–E80.
73. (a) Xu, K.; Lee, U.; Zhang, S. S.; Alen, J. L.; Jow, T. R., Graphite/electrolyte interface formed in LiBOB-based electrolytes, *Electrochem.Solid-State Lett.* **2004**, *7*, A273–A277; (b) Xu, K.; Lee, U.; Zhang, S. S.; Jow, T. R., Graphite/electrolyte interface formed in LiBOB-based electrolytes, *J. Electrochem. Soc.* **2004**, *151*, A2106–A2112.
74. (a) Zhang, S. S., An unique lithium salt for the improved electrolyte of Li-ion battery, *Electrochem. Commun.* **2006**, *8*, 1423–1428; (b) Zhang, S. S., Electrochemical study of the formation of a solid electrolyte interface on graphite in a $LiBC_2O_4F_2$-based electrolyte, *J. Power Sources* **2007**, *163*, 713–718.
75. (a) Barthel, J.; Buestrich, R.; Gores, H. J.; Schmidt, M.; Wuhr, M., A new class of electrochemically and thermally stable lithium salts for lithium battery electrolytes, *J. Electrochem. Soc*. **1997**, *144*, 3866–3870; (b) Sasaki, Y.; Handa, M.; Kurashima, K.; Tonuma, T.; Usami, K., Application of lithium organoborate with salicylic ligand to lithium battery electrolyte, *J. Electrochem. Soc*. **2001**, *148*, A999–A1003; (c) Sasaki, Y.; Handa, M.; Sekiya, S.; Kurashima, K.; Usami, K., Application to lithium battery electrolyte of lithium chelate compound with boron, *J. Power Sources* **2001**, *97–98*, 561–565; (d) Xue, Z.-M.; Ding, Y.-Z.; Chen, C.-H., A DFT study of electronic structures, energies, and molecular properties of lithium bis[croconate]borate and its derivatives, *Electrochim. Acta* **2007**, *53*, 990–997.
76. (a) Nanbu, N.; Shibazaki, T.; Sasaki, Y., Thermal and electrolytic behavior of lithium chelatoborates and application to lithium batteries, *Electrochemistry* **2003**, *71*, 1205–1213; (b) Xue, Z.-M.; Wu, K.-N.; Liu, B.; Chen, C.-H., New lithium salts with croconato-complexes of boron for lithium battery electrolytes, *J. Power Sources* **2007**, *171*, 944–947.
77. (a) Barthel, J.; Buestrich, R.; Carl, E.; Gores, H. J., A new class of electrochemically and thermally stable lithium salts for lithium battery electrolytes. III. Synthesis and properties of some lithium organo borates *J. Electrochem. Soc*. **1996**, *143*, 3572–3575; (b) Barthel, J.; Buestrich, R.; Gores, H. J.; Schmidt, M.; Wuhr, M., A new class of electrochemically and thermally stable lithium salts for lithium battery electrolytes, *J. Electrochem. Soc*. **1997**, *144*, 3866–3870; (c) Xue, Z.-M.; Chen, C.-H., Density functional theory study on lithium bis[1,2-benzenediolato (2-)-O,O′] borate and its derivatives: electronic structures, energies, and molecular properties, *Electrochim. Acta* **2004**, *49*, 5167–5175; (d) Aurbach, D.; Gnanaraj, J. S.; Geissler, W.; Schmidt, M., Vinylene Carbonate and Li salicylatoborate as additives in $LiPF_3(CF_2CF_3)_3$ solutions for rechargeable Li-ion batteries, *J. Electrochem. Soc*. **2004**, *151*, A23–A30.

78. Lisbona, D.; Snee, T., A review of hazards associated with primary lithium and lithium-ion batteries, *Process Safety and Environmental Protection* **2011**, *89*, 434–442.
79. Scrosati, B.; Garch, J., Lithium batteries: status, prospects and future, *J. Power Sources* **2010**, *195*, 2419–2430.
80. Murata, K.; Izuchi, S; Yoshihisa, Y., An overview of the research and development of solid polymer electrolyte batteries, *Electrochim. Acta* **2000,** *45*, 1501–1508.
81. Aihara, Y.; Kuratomi, J.; Bando, T.; Iguchi, T.; Yoshida, H.; Ono, T.; Kuwana, K., Investigation on solvent-free solid polymer electrolytes for advanced lithium batteries and their performance, *J. Power Sources* **2003**, *114*, 96–104.
82. Rodrigues, L. C.; Barbosa, P. C.; Silva, M. M.; Smith, M. J., Electrochemical and thermal properties of polymer electrolytes based on poly(epichlorohydrin-co-ethylene oxide-co-allyl glycidyl ether), *Electrochim. Acta* **2007**, *53*, 1427–1431.
83. Koura, N.; Iizuka, K.; Idemoto, Y., Ui, K., Li and Li-Al negative electrode characteristics for the lithium secondary battery with a nonflammable $SOCl_2$, Li added, LiCl saturated $AlCl_3$-EMIC molten salt electrolyte, *Electrochemistry* **1999**, *67*, 706–712.
84. Nakagawa, H.; Izuchi, S.; Kuwana, K.; Nukuda, T.; Aihara, Y., Liquid and polymer gel electrolytes for lithium batteries composed of room-temperature molten salt doped by lithium salt, *J. Electrochem. Soc.* **2003**, *150*, A695–A700.
85. Seki, S.; Kobayashi, Y.; Miyashiro, H.; Ohno, Y.; Usami, A.; Mita, Y.; Kihira, N.; Watanabe, M.; Terada, N., Lithium secondary batteries using modified-imidazolium room temperature ionic liquids, *J. Phys. Chem. B* **2006**, *110*, 10228–10230.
86. Ui, K.; Yamamoto, K.; Ishikawa, K.; Minami, T.; Takeuchi, K.; Itagaki, M.; Watanabe, K.; Koura, N., Development of non-flammable lithium secondary battery with room-temperature ionic liquid electrolyte: performance of electroplated Al film negative electrode, *J. Power Sources* **2008**, *183*, 347–350.
87. Wang, X. M.; Yasukawa, E.; Kasuya, S., Nonflammable trimethyl phosphate solvent-containing electrolytes for lithium-ion batteries, I. Fundamental properties, *J. Electrochem. Soc.* **2001**, *148*, A1058–A1065.
88. Arai, J., A novel non-flammable electrolytes containing methyl nonafluorobutyl ether for lithium secondary batteries, *J. Appl. Electrochem.* **2002**, *32*, 1071–1079.
89. Morita, M.; Kawasaki, T.; Yoshimoto, N.; Ishikawa, M., Nonflammable organic electrolyte solution based on perfluoro-ether solvent for lithium ion batteries, *Electrochemistry* **2003**, *71*, 1067–1069.
90. Zhang, S. S.; Xu, K.; Jow, T. R., Tris(2,2,2-trifluoroethyl)phosphate as a co-solvent for non-flammable electrolytes in Li-ion batteries, *J. Power Sources* **2003**, *113*, 166–172.
91. Xiang, H. F.; Xu, H. Y.; Wang, Z. Z.; Chen, C. H., Dimethylmethylphosphonate (DMMP) as an efficient flame retardant additives for the lithium-ion battery electrolytes, *J. Power Sources* **2007**, *173*, 562–564.
92. Murayama, M.; Sonoyama, N.; Yamada, A.; Kanno, R., Material design of new lithium ionic conductor, thio-LISICON, in the Li_2S-P_2S_5 system, *Solid State Ionics* **2004**, *170*, 173–180.
93. Nagao, M.; Hayashi, A.; Tatsumisago, M., All-solid-state lithium secondary batteries with high capacity using black phosphorus negative electrode, *J. Power Sources* **2011**, *196*, 6902–6905.
94. Morita, M.; Niida, Y.; Yoshimoto, N.; Adachi, K., Polymeric gel electrolyte containing alkylphosphate for lithium ion batteries, *J. Power Sources* **2005**, *146*, 427–430.
95. Hayashi, A.; Harayama, T.; Mizuno, F.; Tatsumisago, M., Mechanochemical synthesis of hybrid electrolytes from the Li_2S-P_2S_5 glasses and polyethers, *J. Power Sources* **2006**, *163*, 289–293.
96. Noda A.; Watanabe, M., Highly conductive polymer electrolytes prepared by in situ polymerization of vinyl monomers in room temperature molten salts, *Electrochim. Acta* **2000**, *45*, 1265–1270.
97. Shin, J.-H.; Henderson, W. A.; Passerini, S., Ionic liquids to rescue? Overcoming the ionic conductivity limitations of polymer electrolytes, *Electrochem. Commun.* **2003**, *5*, 1016–1020.

98. Egashira, M.; Todo, H.; Yoshimoto, N.; Morita, M., Lithium ion conduction in ionic liquid-based gel polymer electrolyte, *J. Power Sources* **2008**, *178*, 729–735.
99. Lalia, B. S.; Yoshimoto, N.; Egashira, M.; Morita, M., A mixture of triethylphosphate and ethylene carbonate as a safe additives for ionic liquid-based electrolytes of lithium ion batteries, *J. Power Sources* **2010**, *195*, 7426–7431.
100. Annakutty, K. S.; Kishore, K., A novel approach to structure-flammability correlation in polyphosphate esters, *Polymer* **1988**, *29*, 1273–1276.
101. Wang, X.; Yasukawa, E.; Kasuya, S., Nonflammable trimethyl phosphate solvent-containing electrolytes for lithium-ion batteries, II. The use of amorphous carbon anode, *J. Electrochem. Soc.* **2001**, *148*, A1066–A1071.
102. Wang, C. S.; Shieh, J. Y.; Sun, Y. M., Synthesis and properties of phosphorus containing PET and PEN (I), *J. Applied Polymer Science* **1998**, *70*, 1959–1964.
103. Xu, K.; Ding, M. S.; Zhang, S.; Allen, J. L.; Jow, T. R., An attempt to formulate nonflammable lithium ion electrolytes with alkyl phosphates and phosphazenes, *J. Electrochem. Soc.* **2002**, *149*, A622–A626.
104. Ota, H.; Kominato, A.; Chun, W. J.; Yasukawa, E.; Kasuya, S., Effect of cyclic phosphate additive in non-flammable electrolyte, *J. Power Sources* **2003**, *119–121*, 393–398.
105. Xu, K.; Zhang, S.; Allen, J. L.; Jow, T. R., Nonflammable electrolytes for Li-ion batteries based on a fluorinated phosphate, *J. Electrochem. Soc.* **2002**, *149*, A1079–A1082.
106. Morimoto, E.; Yoshimoto, N.; Egashira, M.; Morita, M., Cathode performance of $LiMn_2O_4$ in nonflammable organic electrolyte solutions containing alkylphosphate, In *Extended abstract of 56th annual meeting of international society of electrochemistry (56th ISE), Busan, Korea*, 2005; 1132.
107. Shigematsu, Y.; Ue, M.; Yamaki, J.-I., Thermal behavior of charged graphite and Li_xCoO_2 in electrolytes containing alkylphosphates for lithium-ion cell, *J. Electrochem. Soc.* **2009**, *156*, A176–A180.
108. Aurbach, D.; Ein-Eli, Y., The study of Li-graphite intercalation process in several electrolyte systems using *in situ* X-ray diffraction, *J. Electrochem. Soc.* **1995**, *142*, 1746–1752.
109. Ein-Eli, Y.; McDevitt, S. F.; Aurbach, D.; Markovsky, B.; Schecheter, A., Methyl propyl carbonate: A promising single solvent for Li-ion battery, *J. Electrochem. Soc.* **1997**, *144*, L180–L184.
110. Zhang, S. S., A review on electrolyte additives for lithium-ion batteries, *J. Power Sources* **2006**, *162*, 1379–1394.
111. Wang, X.; Yamada, C.; Naito, H.; Segami, G.; Kibe, K., High-concentration trimethyl phosphate-based nonflammable electrolytes with improved charge-discharge performance of a graphite anode for lithium-ion cells, *J. Electrochem. Soc.* **2006**, *153,* A135–A139.
112. Feng, J. K.; Sun, X. J.; Ai, X. P.; Cao, Y. L.; Yang, H. X., Dimethyl methyl phosphate: a new nonflammable electrolyte solvent for lithium-ion batteries, *J. Power Sources* **2008**, *184*, 570–573.
113. Yamaki, J.; Yamazaki, I.; Egashira, M.; Okada, S., Thermal studies of fluorinated ester as a novel candidate for electrolyte solvent of lithium metal anode rechargeable cells, *J. Power Sources* **2001**, *102*, 288–293.
114. Ding, M. S.; Xu, K.; Jow, T. R., Effects of tris(2,2,2-trifluoroethyl) phosphate as a flame-retarding cosolvent on physicochemical properties of electrolytes of $LiPF_6$ in EC-PC-EMC of 3:3:4 weight ratios, *J. Electrochem. Soc.* **2001**, *149*, A1489–1498.
115. Xu, K.; Ding, M. S.; Zhang, S.; Allen, J. L.; Jow, T. R., Evaluation of fluorinated alkylphosphates as flame retardants in electrolytes for Li-ion batteries I. Physical and electrochemical properties, *J. Electrochem. Soc.* **2003**, *150*, A161–A169.
116. Xu, K.; Zhang, S.; Allen, J. L.; Jow, T. R., Evaluation of fluorinated alkylphosphates as flame retardants in electrolytes for Li-ion batteries II. Performance in cell. *J. Electrochem. Soc.* **2003**, *150*, A170–A175.
117. Xiang, H. F.; Jin, Q. Y.; Chen, C. H.; Ge, X. W.; Guo, S.; Sun, J. H., Dimethyl methylphosphonate-based nonflammable electrolyte and high safety lithium-ion batteries, *J. Power Sources* **2007**, *174*, 335–341.

118. Xiang, H. F.; Jin, Q. Y.; Wang, R.; Chen, C. H.; Ge, X. W., Nonflammable electrolyte for 3-V lithium-ion battery with spinel materials $LiNi_{0.5}Mn_{1.5}O_4$ and $Li_4Ti_5O_{12}$, *J. Power Sources* **2008**, *179*, 351–356.
119. Dalavi, S.; Xu, M.; Ravdel, B.; Zhou, L.; Lucht, B. L., Nonflammable electrolytes for lithium-ion batteries containing dimethyl methylphosphonate, *J. Electrochem. Soc.* **2010**, *157*, A1113–A1120.
120. Wu, L.; Song, Z.; Liu, L.; Guo, X.; Kong, L.; Zhan, H.; Zhou, Y.; Li, Z., A new phosphate-based nonflammable electrolyte solvent for Li-ion batteries, *J. Power Sources* **2009**, *188*, 570–573.
121. Yao, X. L.; Xie, S.; Chen, C. H.; Wang, Q. S.; Sun, J. H.; Li, Y. L.; Lu, S. X., Comparative study of trimethyl phosphite as electrolyte additives in lithium ion batteries, *J. Power Sources* **2005**, *144*, 170–175.
122. Xu, H. Y.; Xie, S.; Wang, Q. Y.; Yao, X. L.; Wang, Q. S.; Chen, C. H., Electrolyte additive trimethyl phosphite for improving electrochemical performance and thermal stability of $LiCoO_2$ cathode, *Electrochim. Acta* **2006**, *52*, 636–642.
123. Zhang, S. S.; Xu, K.; Jow, T. R., A thermal stabilizer for $LiPF_6$-based electrolytes of Li-ion cells, *Electrochem. Solid-State Lett,* **2002**, *5*, A206–A208.
124. Wang, Q.; Sun, J.; Yao, X.; Chen, C., 4-isopropyl phenyl diphenyl phosphate as flame-retardant additive for lithium-ion battery electrolyte, *Electrochem. Solid-State Lett.* **2005**, *8*, A467–A470.
125. Wang, Q.; Sun, J.; Chen, C., Enhancing the thermal stability of $LiCoO_2$ electrode by 4-isopropyl phenyl diphenyl phosphate in lithium ion batteries, *J. Power Sources* **2006**, *162*, 1363–1366.
126. Wang, Q.; Ping, P.; Sun, J.; Chen, C., Improved thermal stability of lithium ion battery by using cresyl diphenyl phosphate as an electrolyte additive, *J. Power Sources* **2010**, 195, 7457–7461.
127. Zhou, D.; Li, W.; Tan, C.; Zuo, X.; Huang, Y., Cresyl diphenyl phosphate as flame retardant additive for lithium-ion batteries, *J. Power Sources* **2008**, *184*, 589–592.
128. Feng, J. K.; Yao, Y. L.; Ai, X. P.; Yang, H. X., Tri-(4-methokythphenyl) phosphate: a new electrolyte additive with both fire-retardancy and overcharge protection for Li-ion batteries, *Electrochim. Acta* **2008**, *53*, 8265–8268.
129. Tsujikawa, T.; Yabuta, K.; Matsushita, T.; Matsushima, T.; Hayashi, K.; Arakawa, M., Characteristics of lithium-ion battery with non-flammable electrolyte, *J. Power Sources* **2009**, *189*, 429–434.
130. Lee, C. W.; Venkatachalapathy, R.; Prakash, J., A novel flame-retardant additive for lithium batteries, *Electrochem. Solid-State Lett,* **2000**, *3*, 63–65.
131. Sazhin, S. V.; Harrup, M. K.; Gering, K. L., Characterization of low flammability electrolytes for lithium-ion batteries, *J. Power Sources* **2011**, *196*, 3433–3438.
132. Hu, J.; Jin, Z.; Zhong, H.; Zhan, H.; Zhou, Y.; Li, Z., A new phosphonamidate as flame retardant additive in electrolytes for lithium ion batteries, *J. Power Sources* **2012**, *197*, 297–300.
133. Morford, R. V.; Kellam III, E. C.; Hofmann, M. A.; Allcock, H. R., A fire-retardant organophosphorus gel polymer electrolyte additive for use in rechargeable lithium batteries, *Solid State Ionics* **2000**, *133*, 171–177.
134. Yoshimoto, N.; Niida, Y.; Egashira, M.; Morita, M., Nonflammable gel electrolyte containing alkyl phosphate for rechargeable lithium batteries, *J. Power Sources* **2006**, *163*, 238–242.
135. Yoshimoto, N.; Goto, D.; Egashira, M.; Morita, M., Alkylphosphate-based nonflammable gel electrolyte for $LiMn_2O_4$ positive electrode in lithium-ion battery, *J. Power Sources* **2008**, *185*, 1425–1428.
136. Lalia, B. S.; Fujita, T; Yoshimoto, N.; Egashira, M.; Morita, M., Electrochemical performance of nonflammable gel electrolyte containing triethylphosphate, *J. Power Sources* **2009**, *186*, 211–215.
137. Lalia, B. S.; Yoshimoto, N.; Egashira, M.; Morita, M., Electrochemical performances of nonflammable gel electrolyte for lithium ion battery using $LiFePO_4$ positive electrode, *Electrochemistry* **2010**, *78*, 332–335.

138. McBreen, J.; Lee, H. S.; Yang, X. Q.; Sun, X., New approaches to the design of polymer and liquid electrolytes for lithium batteries, *J. Power Sources* **2000**, *89*, 163–167.
139. Tabata, S.; Hirakimoto, T.; Nishimura, M.; Watanabe, M., Synthesis of Lewis-acid boric acid ester monomer and effect of its addition to electrolyte solutions and polymer gel electrolytes on their ion transport properties, *Electrochim. Acta* **2003**, *48*, 2105–2112.
140. Xu, W.; Sun, X. G.; Angell, C. A., Anion-trapping and polyanion electrolytes based on acid-in-chain borate polymers, *Electrochim. Acta* **2003**, *48*, 2255–2266.
141. Lalia, B. S.; Yoshimoto, N.; Egashira, M.; Morita, M., Effects of Lewis-acid polymer on the electrochemical properties of alkylphosphate-based non-flammable gel electrolyte, *J. Power Sources* **2009**, *194*, 531–535.
142. Blomgren, G. E., Properties, structures and conductivity of organic and inorganic electrolytes for lithium battery systems, In *Lithium batteries*; Gabano, J.-P., Ed.; Academic Press: London, United Kingdom, 1983; Ch. 2; 13–41.
143. Ue, M., Thinking way in electrolyte materials, In *50th Electrochemistry seminar*; Kansai branch of the Electrochemical Society of Japan: Osaka, Japan, 2010.
144. Ue, M., Electrolyte technologies supporting the progress of lithium batteries, In *2012 Taipei forum on large format lithium batteries*; Taipei, Taiwan, 2012.
145. Tamamitsu, K., Aluminum electrolytic capacitors using sulfolane as an electrolyte solvent, *J. Technology and Education* **2003**, *10*, 115–120.
146. Ue, M.; Takehara, M.; Takeda, M., Triethylmethylammonium tetrafluoroborate as a highly soluble supporting electrolyte salt for electrochemical capacitors, *Denki Kagaku* **1997**, *65*, 969–971.
147. Ue, M.; Murakami, A.; Nakamura, S., Anodic stability of several anions examined by ab initio molecular orbital and density functional theories, *J. Electrochem. Soc.* **2002**, *149*, A1572–A1577.
148. Kumar, T. P.; Prabhu, P. V. S. S.; Srivastava, A. K.; Kumar, U. B.; Ranganathan, R.; Gangadharan, R., Conductivity and viscosity studies of dimethyl sulfoxide (DMSO)-based electrolyte solutions at 25°C, *J. Power Sources* **1994**, *50*, 283–294.
149. Prisyazhnii, V. D.; Sirenko, V. I.; Potapenko, O. V.; Zmievs'ka, T. A., Solutions of lithium benzenesulfonate in dimethyl sulfoxide as electrolytes for lithium-based batteries, *Dopov. Nats. Akad. Nauk Ukr.* **2007**, 136–141.
150. Fouache-Ayoub, S.; Garreau, M.; Prabhu, P. V. S. S.; Thevenin, J., Mass-transport properties of lithium surface layers formed in sulfolane-based electrolytes, *J. Electrochem. Soc.* **1990**, *137*, 1659–1665.
151. Xu, K.; Angell, C. A., Sulfone-based electrolytes for lithium-ion batteries, *J. Electrochem. Soc.* **2002**, *149*, A920–A926.
152. Giwa, C. O., Feasibility study of sulfone-based electrolytes for a medium-temperature reserve cell concept, *J. Power Sources* **1993**, *42*, 389–397.
153. Bach, S.; Baffier, N.; Pereira-Ramos, J. P.; Messina, R., Rechargeable γ-MnO_2 for lithium batteries using a sulfone-based electrolyte at 150°C, *J. Power Sources* **1993**, *43–44*, 569–575.
154. Xu, K.; Angell, C. A., High anodic stability of a new electrolyte solvent: unsymmetric non-cyclic aliphatic sulfone, *J. Electrochem. Soc.* **1998**, *145*, L70–L72.
155. Wrodnigg, G. H.; Besenhard, J. O.; Winter, M., Ethylene sulfite as electrolyte additive for lithium-ion cells with graphitic anodes, *J. Electrochem. Soc.* **1999**, *146*, 470–472.
156. Wrodnigg, G. H.; Wrodnigg, T. M.; Besenhard, J. O.; Winter, M., Propylene sulfite as film-forming electrolyte additive in lithium ion batteries, *Electrochem. Commun.* **1999**, *1(3), 148–150*,
157. Wrodnigg, G. H.; Besenhard, J. O.; Winter, M., Cyclic and acyclic sulfites: new solvents and electrolyte additives for lithium ion batteries with graphitic anodes?, *J. Power Sources* **2001**, *97–98*, 592–594.
158. Ue, M., Role-assigned electrolytes: additives, In *Lithium-ion batteries*; Yoshio, M.; Brodd, R. J.; Kozawa, A., Eds.; Springer: New York, NY, 2009; Ch. 4; 75–115.
159. Yu, B. T.; Qiu, W. H.; Li, F. S.; Cheng, L., A study on sulfites for lithium-ion battery electrolytes, *J. Power Sources* **2006**, *158*, 1373–1378.

160. Park, G.; Nakamura, H.; Lee, Y.; Yoshio, M., The importance role of additives for improved lithium ion battery safety, *J. Power Sources* **2009**, *189*, 602–606.
161. Xu, M.; Li, W.; Lucht, B. L., Effect of propane sultone on elevated temperature performance of anode and cathode materials in lithium-ion batteries, *J. Power Sources* **2009**, *193*, 804–809.
162. Jeong, S. K.; Lee, H. N.; Kim, Y. S., Thermal stability of surface film formed on a graphite negative electrode in lithium secondary batteries, *J. Korean Electrochem. Soc.* **2011**, *14*, 157–162.
163. Han, Y. K.; Lee, S. U.; Ok, J. H.; Cho, J. J.; Kim, H. J., Theoretical studies of the solvent decomposition by lithium atoms in lithium-ion battery electrolyte, *Chem. Phys. Lett.* **2002**, *360*, 359–366.
164. Sano, A.; Maruyama, S., Decreasing the initial irreversible capacity loss by addition of cyclic sulfate as electrolyte additives, *J. Power Sources* **2009**, *192*, 714–718.
165. Yao, Y. W.; Xu, J.; Yao, W. H.; Wang, Z. C.; Yang, Y., Effect of ethylene sulfate as electrolyte additive on performance of Li-ion batteries, *Yingyong Huaxue* **2010**, *27*, 823–828.
166. Guyomard, D.; Tarascon, J. M., Rechargeable $Li_{1+x}Mn_2O_4$/carbon cells with a new electrolyte composition: potentiostatic studies and application to practical cells, *J. Electrochem. Soc.* **1993**, *140*, 3071–3081.
167. Seel, J. A.; Dahn, J. R., Electrochemical intercalation of PF_6 into graphite, *J. Electrochem. Soc.* **2000**, *147*, 892–898.
168. Lu, Z. H.; Dahn, J. R., Can all the lithium be removed from T/2 $Li_{2/3}[Ni_{1/3}Mn_{2/3}]O_2$?, *J. Electrochem. Soc.* **2001**, *148*, A710–A715.
169. Park, S. H.; Winnick, J.; Kohl, P. A., Investigation of the lithium couple on Pt, Al, and Hg electrodes in lithium imide-ethyl methyl sulfone, *J. Electrochem. Soc.* **2002**, *149*, A1196–A1200.
170. Abouimrane, A.; Belharouak, I.; Amine, K., Sulfone-based electrolytes for high-voltage Li-ion batteries, *Electrochem. Commun.* **2009**, *11*, 1073–1076.
171. Sun, X. G.; Angell, C. A., New sulfone electrolytes for rechargeable lithium batteries. part I. oligoether-containing sulfones, *Electrochem. Commun.* **2005**, *7*, 261–266.
172. Sun, X. G.; Angell, C. A., New sulfone electrolytes, *Solid State Ionics* **2004**, *175*, 257–260.
173. Shao, N.; Sun, X. G.; Dai, S.; Jiang, D. E., Electrochemical windows of sulfone-based electrolytes for high-voltage Li-ion batteries, *J. Phys. Chem. B* **2011**, *115*, 12120–12125.
174. Sun, X. G.; Angell, C. A., Doped sulfone electrolytes for high voltage Li-ion cell applications, *Electrochem. Commun.* **2009**, *11*, 1418–1421.
175. Watarai, A.; Tokuda, H.; Kawai, T.; Ue, M., Development of electrolytes for highly safe lithium-ion batteries, In *216th Electrochemical society meeting*; Vienna, Austria, 2009.
176. Ue, M.; Kagimoto, J.; Tokuda, H.; Kawai, T., Sulfolane-based LIB electrolytes for HEV applications, In *5th International conference on polymer batteries and fuel cells*; Argonne, IL, 2011.
177. Ue, M.; Kagimoto, J.; Tokuda, H.; Kawai, T., High-safety LIB electrolytes for HEV applications, In *6th Asian conference on electrochemical power sources*; Chennai, India, 2012.
178. Shao, N.; Sun, X. G.; Dai, S.; Jiang, D. E., Oxidation potentials of functionalized sulfone solvents for high-voltage Li-ion batteries: a computational study, *J. Phys. Chem. B* **2012**, *116*, 3235–3238.

Chapter 3
Nonaqueous Electrolytes and Advances in Additives

Koji Abe

3.1 General Theory

3.1.1 Background of This Chapter

In retrospect, development of additives for Li-ion battery electrolyte has made significant progress in recent 15 years. Therefore, it is getting difficult to learn rapidly and systematically about this subject from past to present. Today, it is totally impossible to satisfy all the required battery properties by single additive in the electrolyte, and the mainstream of electrolyte development is equal to "quest for multiple combinations of additives." Under current situation, the author's top priority for this chapter is to select additives that are practically utilized as "long seller items" or try to replace those (so far not successful) and organize them chronologically. So references for those additives are mainly patents, but the author picked up so many interesting (including not well known but important) additives not previously reported anywhere.

As the author selected additives based on the policy above, about 50 % of the additives are developed by Ube Industries, Ltd. (UBE), so, if the author reveals concepts or evaluation data for these UBE additives, the author feels that it is not fair and it might be deemed as selfish advertisement. In addition, it is commonly accepted in Li-ion battery that the performance data varies according to testing conditions and materials utilized in the battery, so the author regards that it is not

K. Abe (✉)
Advanced Energy Materials R&D Center, UBE Industries, Ltd.,
1978-10, Kogushi, Ube, Yamaguchi 755-8633, Japan

Advanced Electrolyte Technologies LLC, Tory, MI, USA
e-mail: 29405u@ube-ind.co.jp

T.R. Jow et al. (eds.), *Electrolytes for Lithium and Lithium-Ion Batteries*,
Modern Aspects of Electrochemistry 58, DOI 10.1007/978-1-4939-0302-3_3,

fair to pick up, compare, and evaluate performance data based on particular electrode materials and conditions, so the author intentionally did not include performance data.

Concerning concepts, chemistry, and mechanism for each additive, the author kept his comments at minimum, as they are shown in the references, so the author strongly recommends readers to look up the reference patent, and just for introduction, the author would like to suggest the following journal articles, for anode additives by Winter [1], for cathode additives by himself [2], and for safety additives by Ue [3]. The author intends this chapter to be utilized as a library for readers who develop electrolyte additives or evaluate batteries containing them and not familiar with organic chemistry. So, from enormous number of patents, the author basically tried his best to pick up important patents starting from the 1990s (especially US patents after the year of 2000) and organized additives chronologically, separated paragraphs according to chemical structures and functional groups, and clearly showed molecular structures.

It is his great pleasure that this chapter with fulfilling and unprecedented volume of references contributes to the "quest for multiple combination of additives" by readers in their own battery systems.

3.1.2 Introduction

The basic concept of the currently popular lithium-ion batteries (LIBs) was developed in 1985 by Yoshino et al. from Asahi Kasei Corporation [4–6]. LIBs were first marketed by Sony Corporation in 1991, after which Sanyo Electric Company's batteries with graphite anodes were marketed in 1994 [7]. The capacity of LIBs around 1997 was more than 1.5-fold that when they were launched, and from the point of view of battery design, increasing the capacity further was considered difficult.

3.1.3 Functional Electrolytes

Although reports following the initial marketing of Sony Corporation's batteries focused not only on metallic lithium anodes and graphite anodes but also on the solid electrolyte interphase (SEI), which forms on the anode as a result of electrolyte decomposition, intentional control of SEI was not considered in sufficient depth. The concept of SEI was advocated by Peled from Tel-Aviv University and Aurbach from Bar-Ilan University [8–10]. Nevertheless, upon entering the industry in 1997, Ube Industries, Ltd. started adding small amounts of additives to the electrolyte, which allowed for the undesirable thick SEI to be controlled by deliberately causing additive decomposition in order to form a controlled thin layer (CTL).

In 1999, the concept of "functional electrolytes" was coined and developed [11, 12] on the basis of the idea of intentionally controlling thick SEI and improving

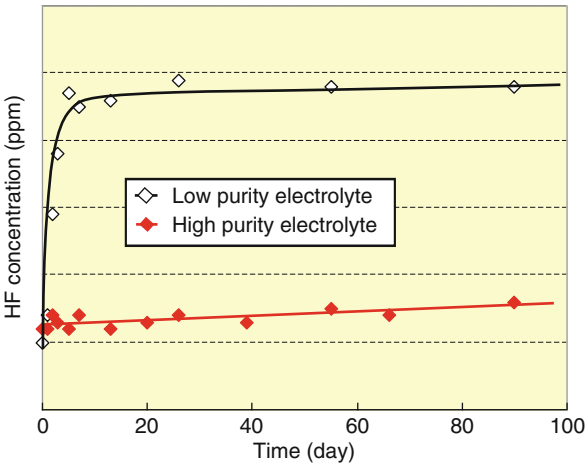

Fig. 3.1 Chemical stability of electrolyte storage

battery performance by adding miniscule amounts of various additives, such as anode additives, cathode additives, and overcharge prevention additives, to high-purity electrolytes. This suddenly inspired considerable interest in research on additives, leading to the coining of the term "role-assigned electrolytes" by Ue from Mitsubishi Chemical Corporation 4 years later in 2003 [13–15]. Such electrolytes are now commonly considered to be a core technology in the development of batteries, and it would not be an exaggeration to say that research on additives is a key to research on electrolytes.

3.1.4 Highly Purified Electrolytes

The standard composition of an electrolyte in LIBs is a mixture of cyclic carbonates (such as ethylene carbonate (EC) and propylene carbonate (PC)) and chain carbonates (such as dimethyl carbonate (DMC), ethyl methyl carbonate (EMC; abbreviated as MEC below), and diethyl carbonate (DEC)), to which about 1 mol/L of a lithium salt (such as lithium hexafluorophosphate ($LiPF_6$)) is added. Ube Industries, Ltd. discovered that if small amounts of impurities exist in the electrolyte, decomposition current generated from the impurities begins to flow, which leads to the formation of undesirable thick SEI. This spurred the development of a pioneering high-grade purification process for the base electrolyte in 1997 [16]. High purity is a key feature of functional electrolytes developed by Ube Industries, Ltd. and enables production of transparent and chemically stable electrolytes, in contrast to the conventional electrolytes which were less stable and brown owing to its low purity (Fig. 3.1).

One year later, researchers from Merck KGaA also discovered the same technique for high-grade purification as the one used by Ube Industries, Ltd. [17] and published a paper entitled "Challenge in manufacturing electrolyte solutions for lithium

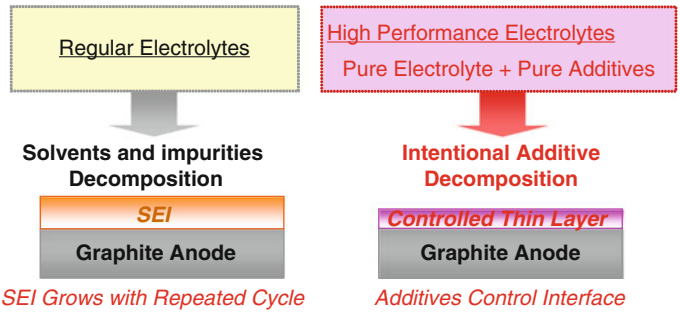

Fig. 3.2 Conceptual figure of graphite anode surface

and lithium ion batteries quality control and minimizing contamination level" [18], which is indicative of the strong impetus for developing highly pure electrolytes [19, 20] since the quality of electrolytes in those days was not satisfactory.

3.1.5 Classification of Additives

3.1.5.1 Function-Improving Additives

In LIBs, part of the impurities in the electrolyte decomposes naturally during charging, and the phenomenon of thick SEI formation at the surface of graphite anodes was reported in numerous studies, starting with a report by Aurbach. One disadvantage of conventional electrolytes was that small quantities of impurities originating from carbonate and $LiPF_6$ solvents gradually decomposed and accumulated as a coating on the graphite anode as the number of recharges increased, which introduced resistance and lowered the battery performance. It was common knowledge that electrolytes using conventional PC as a solvent could not be used with graphite electrodes; however, in 1995 Ube Industries, Ltd. found phenylene carbonates, which allow for PC-based electrolytes to be used even with graphite electrodes [21].

This was followed by the discovery of a number of unique additives which suppress the decomposition of PC through the formation of CTL (Fig. 3.2) [12] by causing the additive to undergo reductive decomposition before the main carbonate solvent decomposes. In particular, this encompasses not only compounds with unsaturated carbon–carbon bond structures, such as alkenes and alkynes [22–28], but also a large number of sulfur-containing compounds, halogen-containing compounds, phosphorus-containing compounds, and nitrogen-containing compounds, which are reported later in Sect. 3.2.

Following the recent improvements in capacity and advances toward higher voltage, electrolyte decomposition on the surface of cathodes has become evident (Fig. 3.3). Reports concerning the cathode/electrolyte interface were first published in 1985 by Goodenough from the University of Texas at Austin [29], and an analysis of coatings on cathodes was reported in 2001 by Wang from the City University of

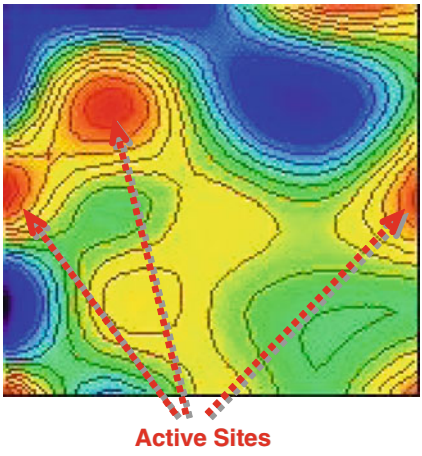

Fig. 3.3 Image for voltage distribution of cathode surface in charging

New York and by Amine from Argonne National Laboratory [30]. Consequently, the concept of controlling the cathode surface with additives for cathodes which further improve the life-span and increase the voltage of the battery [1, 31–33] is presented later in Sect. 3.3.

3.1.5.2 Additives for Safety Improvement

With the intensification of competition for increasing battery capacity, the requirements for ensuring that batteries are safe are becoming proportionally stricter. In particular, when a battery is overcharged, both the cathode and the anode become thermally unstable, which results in a sudden exothermic reaction accompanied by internal shorting and the release of gas, and there is a possibility of thermal runaway occurring in the battery. Although devices such as protective elements and circuits are used as a measure for ensuring the stability of the battery, following the increase in battery capacity, there has been a wide-spreading move toward choosing appropriate materials for the electrodes and applying coating procedures to ensure that battery materials themselves are inherently safe.

In this context, regarding the approach to electrolytes, Sect. 3.4 presents an examination of anisole compounds, biphenyl compounds, halogenobenzene compounds, and alkylbenzene compounds as additives for overcharge prevention as well as phosphate compounds [34] and phosphazene compounds [35] as additives for non-flammability.

3.1.5.3 Miscellaneous Additives

Research on additives involves numerous other additives separate from those mentioned above, for example, additives for wettability improvement [36] and corrosion inhibition [37] as well as new lithium salts which can be used as substitutes for $LiPF_6$ and $LiBF_4$ [38]. Relevant case studies are also reported.

3.2 Additives for Anodes

Additives for anodes reported in this section are categorized into (1) compounds containing unsaturated carbon–carbon bond, (2) carboxylic acid anhydrides, (3) oxalates, (4) sulfur-containing compounds, (5) halogen-containing compounds, (6) phosphorus-containing compounds, and (7) nitrogen-containing compounds.

3.2.1 Compounds Containing Unsaturated Carbon–Carbon Bond

In 1992, Sanyo Electric Company found that vinylene carbonate (VC) (**1**), the most well-known additive at present, can be used as a solvent in lithium secondary batteries [39].

Subsequently, in 1994, Saft discovered that small quantities of VC, which is reducible at the graphite anode at a potential higher than 1 V with respect to lithium, can be added to solvents characterized by high dielectric constant and low viscosity. As described in the relevant report, "a rechargeable lithium electrochemical cell comprising: a cathode, an anode containing a carbon-containing material with a degree of crystallinity which is greater than 0.8, and an electrolyte comprising a lithium salt and a mixture of at least two aprotic saturated organic solvents wherein at least one of the two solvents contains a carbonate, of which the first solvent has a high dielectric constant and the second solvent has low viscosity and is selected from the group consisting of ether, DEC, DMC, dioxolane, dioxolane derivatives, tetrahydrofuran, tetrahydrofuran derivatives, and propylene oxide, characterized in that the electrolyte further contains a soluble compound which is a carbonate containing at least one unsaturated carbon–carbon bond, and which can be reduced at the anode at a potential of more than 1 V with respect to lithium to form a passivation layer" [40]. In addition, a paper on this topic was presented by Mitsubishi Chemical Corporation in 2004 [41].

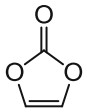

1

In 1997, Ube Industries, Ltd. discovered that small quantities of VC can be added for the purpose of suppressing PC decomposition at the graphite anode [42], and in 1998 the same company first became aware of the yellow to brown color of conventional VC and recognized that such colored VC contained considerable amounts of chlorine-based impurities. As a consequence, the same company developed electrolytes containing colorless and highly pure VC with chlorine

content of 100 ppm or less as well as methods for manufacturing such highly pure VC [43]. As a result, research activities on additives suddenly intensified in the field of electrolyte development.

With regard to research on suppression of PC decomposition, in 1993, Shu et al. from the National Research Council of Canada reported that by adding large quantities (0.5 M) of 12-crown-4 ether (**2**), the formation of complexes of 12-crown-4 ether with Li occurs preferentially to the solvation of Li in PC, which allows for intercalation by suppressing co-intercalation into the graphite layer [44].

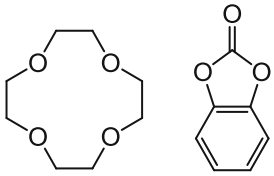

2 **3**

As described in the report on this work, "crown ethers are good chelating reagents for lithium ions. They will compete with electrolyte solvents for lithium ion coordination sites. Furthermore, because of the size of crown ethers, they are too big to be co-intercalated into the graphite layers thus preventing excessive amounts of electrolyte decomposition" [44]. However, this concerned complex formation did not necessarily control the SEI.

Although Ube Industries, Ltd. discovered in 1995 that phenylene carbonate (**3**) can be used as an additive in small quantities, which allowed for PC-based electrolytes to be used even with graphite anodes [20, 45], at that time the general consensus was that graphite anodes could not be used due to PC decomposition. Around 1997, when Ube Industries, Ltd. began the addition of highly pure VC [42] and largely expanded toward the use of various compounds with unsaturated carbon–carbon bond for the purpose of suppressing PC decomposition, the concept of "suppressing PC decomposition by controlling the anode/electrolyte interface with additives" was firmly established and became standard in the LIB industry.

Furthermore, with regard to graphite anodes, in 1998 Mitsubishi Chemical Corporation discovered PC-based electrolytes with chloroethylene carbonate (**4**) and VC [46], and in 1999 the same company discovered that VC containing 33 wt% chloroethylene carbonate can be used as an additive to achieve a the VC/PC weight ratio of 1:9 in the PC-based electrolyte [47]. According to the description, ordinary VC contains chloroethylene carbonate as a residual starting material. The percentage content of such organic halogenides in VC is typically between 1 ppm and 50 wt%. As noted above, around 1999, researchers clearly had to utilize VC with rather high chlorine content for this reason.

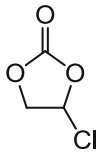

4

In 1998, Mitsui Chemicals discovered that PC can be used even with graphite anodes in the presence of 4,4-dimethyl-5-methylene-1,3-dioxolan-2-one (**5**) [48], and in 1998 the same company discovered that vinylethylene carbonate (**6**) [49] can also be used for the same purpose.

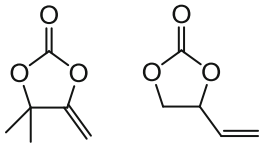

5 **6**

Moreover, in 1998 Ube Industries, Ltd. discovered that PC decomposition is suppressed by small quantities of additives (carboxylic acid vinyl esters, such as vinyl acetate (**7**) and divinyl adipate (**8**); vinyl carbonates, such as methyl vinyl carbonate (**9**) [50]; carboxylic acid allyl esters, such as allyl acetate (**10**); allyl carbonates, such as allyl methyl carbonate (**11**) [51]; and cyclic vinyl esters, such as α-angelica lactone (**12**) [52]).

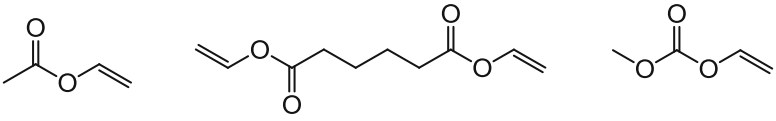

7 **8** **9**

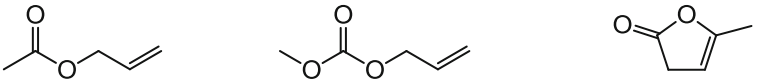

10 **11** **12**

Furthermore, in 1998 Ube Industries, Ltd. expanded their research from double-bond compounds to triple-bond compounds and discovered that alkyne compounds such as methyl propargyl carbonate (**13**), propargyl acetate (**14**), and 2-butyne-1,4-diol dimethyl dicarbonate (**15**) suppress the decomposition of PC [53]. In 1999, the same company discovered that a mixture of methyl propargyl carbonate (**13**) and VC is capable of improving battery performance even further [27, 54].

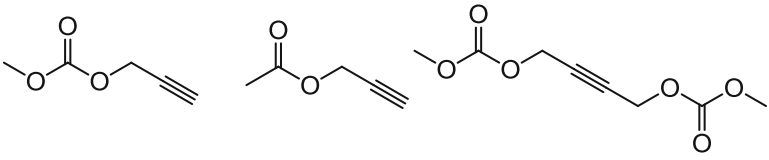

13 **14** **15**

3.2.2 Carboxylic Acid Anhydrides

In 1991, Panasonic found that small quantities of additives such as acetic anhydride (**16**) and benzoic anhydride (**17**) can suppress the temperature-dependent increase in resistance, which is considered to be caused by water inside the battery or residual alkali mixed into the active material of the cathode [55].

As described in the relevant report, "Consequently, by having acid anhydride included in positive electrodes, reduction of the water content or the residual alkali within batteries is made possible with a resultant prevention of the battery performance deterioration occurring at high temperature storage and assumedly caused by the existence of water or residual alkali" [55].

Also, in 1999, Mitsubishi Chemical Corporation discovered that the addition of cyclic carboxylic acid anhydrides, such as succinic anhydride (**18**) and maleic anhydride (**19**), suppresses the decomposition of PC even when graphite anodes are used [56].

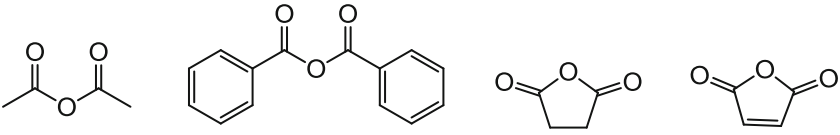

16 **17** **18** **19**

3.2.3 Oxalates

In 2000, Ube Industries, Ltd. discovered that oxalates such as dipropargyl oxalate (**20**) and methyl propargyl oxalate (**21**) can be used as additives in small quantities [57]. Furthermore, in 2001, Mitsubishi Chemical Corporation discovered that oxalates such as diethyl oxalate (**22**) can be used as additives in small quantities for LIBs [58]. In 2003, Ube Industries, Ltd. discovered that asymmetrical oxalates, such as ethyl methyl oxalate (**23**), can be combined with VC (**1**) [59].

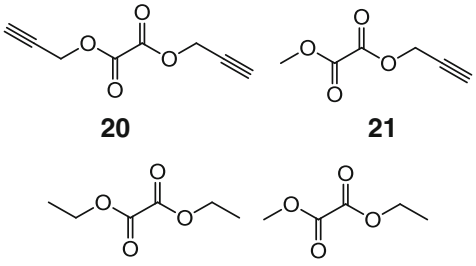

20 **21**

22 **23**

3.2.4 Sulfur-Containing Compounds

3.2.4.1 Cyclic Sulfonates (Sultones)

In 1996, Sony Corporation found that 1,4-butane sultone (**24**) (5–50 wt%) can be substituted for EC as a solvent [60]; in 1997, Ube Industries, Ltd. discovered that the addition of small quantities of cyclic monosulfonic acid esters (sultones), such as 1,3-propane sultone (PS) (**25**), suppresses PC decomposition [61]. Furthermore, in 1999, researchers at Ube Industries, Ltd. found that 3-hydroxypropanesulfonic acid (**26**), which is present as an impurity in PS, decomposes at the electrode before PS decomposition and thus adversely affects battery performance by inhibiting the formation of SEI of PS [62] and consequently developed highly pure PS containing little 3-hydroxypropanesulfonic acid (**26**) [62]. In the same year, Ube Industries found that the combination of small amount of PS (**25**) and VC (**1**) can be used as additives [54].

Since then, there has been intensive research on combinations of VC (**1**) and PS (**25**).

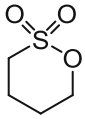

24

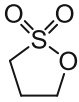

25

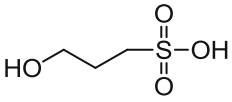

26

Concerning properties of PS (**25**), it is registered as CMR (carcinogenic, mutagenic, or toxic for reproduction) substance in REACH regulation and attracts attention for its mutagenicity, but *N*-methylpyrrolidone (NMP) is also registered substance. Risk of vapor inhalation of PS is lower than NMP since PS is solid at room temperature. In addition, PS is quickly transformed to AMES-negative compound (**26**) by atmospheric moisture. Furthermore, amount of PS utilized in 18,650 cells is very small compared with NMP for cell fabrication process and there is no exposure during this process. Therefore the handling risk of PS is equivalent to normal electrolytes.

In 2001, Mitsui Chemicals discovered that cyclic monosulfonic acid esters containing unsaturated bonds, such as 1,3-propene sultone (PRS) (**27**) [63], can be used as additives in small quantities; however, in 2010, the same company mentioned, "PRS which is a comparative unsaturated sultone compound was added, an increase in the initial resistance was confirmed" [64].

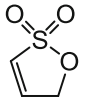

27

In 2002, NEC Corporation discovered that cyclic alkylenedisulfonic acid esters, such as methylene methanedisulfonate (**28**), ethylene methanedisulfonate (**29**), and

1,5-dioxa-2,4-dithian-6-one-2,2,4,4-tetraoxide (**30**), can be used as additives in small quantities [65].

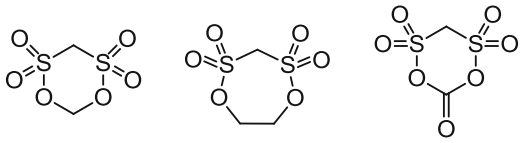

28 **29** **30**

3.2.4.2 Chain Sulfonates

In 1996, Mitsubishi Chemical Corporation discovered that chain sulfonates, such as ethyl methanesulfonate (**31**), can be used as additives in small quantities [66]. Furthermore, Ube Industries, Ltd. discovered the applicability of chain diol disulfonates, such as 1,4-butanediol dimethanesulfonate (**32**) [67], in 1998, as well as chain diol sulfonates with a branched structure, such as 1,3-butanediol dimethanesulfonate (**33**) in 2000 [68].

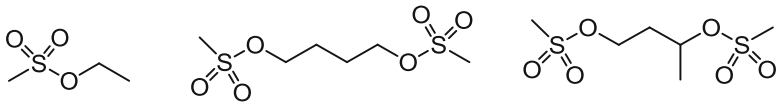

31 **32** **33**

In addition, in 1998, the same company discovered chain monosulfonates containing triple bonds, such as propargyl methanesulfonate (**34**), as well as monosulfonates containing triple bonds in the main chain, such as 2-butyne-1,4-diol dimethanesulfonate (**35**) [53].

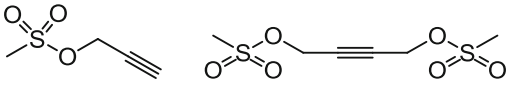

34 **35**

Subsequently, research on disulfonates intensified considerably. For example, in 2002 Mitsubishi Chemical Corporation discovered fluorine-substituted chain disulfonates, such as 1,4-butanediol bis(trifluoromethanesulfonate) (**36**) [69], as well as chain triol trisulfonates, such as 1,2,4-butanetriol trimethanesulfonate (**37**) [70].

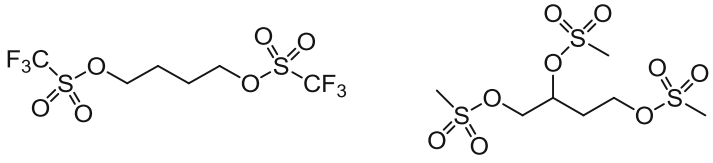

36 **37**

In 2003, NEC Corporation found that chain alkyne disulfonates, such as dimethyl methanedisulfonate (**38**), diethyl methanedisulfonate (**39**), and diphenyl methanedisulfonate (**40**) [71], can be used as additives in small quantities.

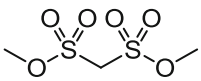

38

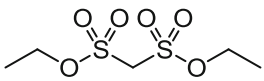

39

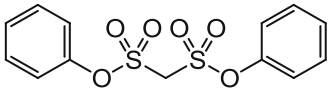

40

3.2.4.3 Sulfites

In 1993, Panasonic found that the cyclic sulfites such as ethylene sulfite (**41**) can be used as a solvent (with a volume ratio of 1/3–5/7) [72], and in 1995, Sony Corporation found that ethylene sulfite (**41**) can be used as an additive in small quantities [73]. Subsequently, Winter et al. from the University of Münster reported these findings in a paper in 1999 [1].

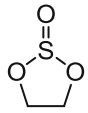

41

In 2000 Ube Industries, Ltd. found that sulfites with triple bond, such as dipropargyl sulfite (**42**), can also be used as additives in small quantities [57].

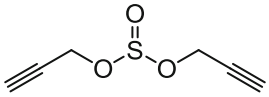

42

3.2.4.4 Sulfates

In 1996, Mitsubishi Chemical Corporation found that cyclic sulfates, such as ethylene sulfate (**43**), can be used as additives in small quantities [74], and in 1998 Ube Industries, Ltd. discovered that cyclic sulfates with unsaturated bonds, such as vinylene sulfate (**44**), can be used as additives in small quantities [75].

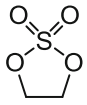

43

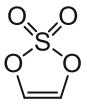

44

In 1998, Wilson Greatbatch Technologies found that chain sulfates, such as diallyl sulfate (**45**) and benzyl methyl sulfate (**46**), as well as chain sulfates including silyl groups, such as bis(trimethylsilyl) sulfate (**47**), can be used as additives in small quantities [76].

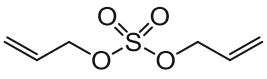

45

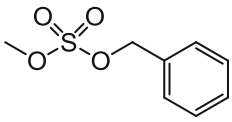

46

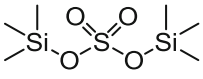

47

In 2000 Ube Industries, Ltd. found that sulfates with triple bonds, such as dipropargyl sulfate (**48**), can also be used as additives in small quantities [57].

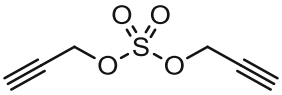

48

3.2.4.5 Acid Anhydrides

In 1996, Mitsubishi Chemical Corporation discovered that chain sulfonic acid anhydrides, such as methanesulfonic anhydride (**49**), can be used as additives in small quantities [77]. Furthermore, in 2002, NEC Corporation found that the cyclic sulfonic anhydride 1,2-ethanedisulfonic anhydride (**50**) can be used as an additive in small quantities [78].

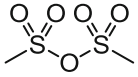

49

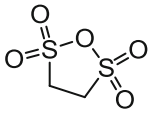

50

In 2000, Mitsui Chemicals found that anhydrides of the sulfonic and carboxylic acids, such as 3-sulfopropionic anhydride (**51**) and 2-sulfobenzoic anhydride (**52**), can be used as additives in small quantities [79].

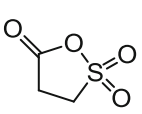

51

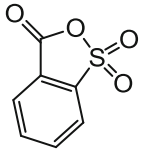

52

3.2.4.6 Sulfones

In 1994, Japan Storage Battery Company found that chain sulfones, such as dimethylsulfone (**53**) (50 vol.%), can be used as solvents [80].

53

In 1998, Ube Industries, Ltd. discovered that divinyl sulfone (**54**) can be used as an additive in small quantities [81]. In 2005, Yuasa Corporation found 1,2-bis(vinylsulfonyl)methane (**55**) [82], and in 2007, Ube Industries, Ltd. found bis(2-vinylsulfonylethyl) ether (**56**), dipropargyl sulfone (**57**), and 1,2-bis(propargylsulfonyl)ethane (**58**) [83].

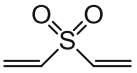

54

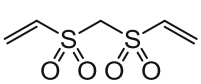

55

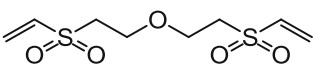

56

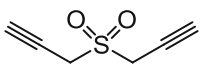

57

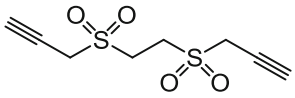

58

In 2010, Mitsui Chemical discovered 1,3-dithietane-1,1,3,3-tetraoxide (**59**) [64].

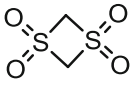

59

3.2.5 Halogen-Containing Compounds

In 1986, Sanyo Electric Company found that cyclic carbonates obtained by introducing halogens into EC can be used as solvents [84], which was followed by numerous reports on this topic [85–91]. In 1996, McMillan et al. from the National Research Council of Canada found an electrolyte that was compatible with graphite anode by utilizing fluoroethylene carbonate (**60**) [87] and propylene carbonate. The number of patent application for electrolytes consisting of fluoroethylene carbonate in combination with dinitrile compounds increased drastically around 2004. Details are described in Sect. 3.5.2 in the discussion of dinitriles.

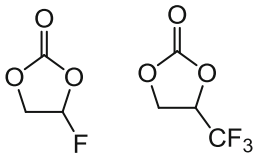

60 **61**

In 1999 Winter et al. from the University of Münster reported the results of analyzing SEI formed by chloroethylene carbonate (**4**) [89]. In addition, in 1999, Inaba et al. from Kyoto University and in 2002 Arai et al. from Hitachi Limited reported that trifluoromethyl ethylene carbonate (**61**) forms SEI [90, 91].

In 1998, Ube Industries, Ltd. discovered that pentafluorobenzoates, such as methyl pentafluorobenzoate (**62**), can be used as additives in small quantities [92]. Also, in 1999, Toyota Central R&D Labs found that fluorinated benzoates, such as methyl 2,6-difluorobenzoate (**63**), can be used as additives in small quantities [93], and in 2002, Ube Industries, Ltd. found that pentafluorophenol compounds, such as pentafluorophenyl methanesulfonate (**64**) and methyl pentafluorophenyl carbonate (**65**), can be used as additives in small quantities [94].

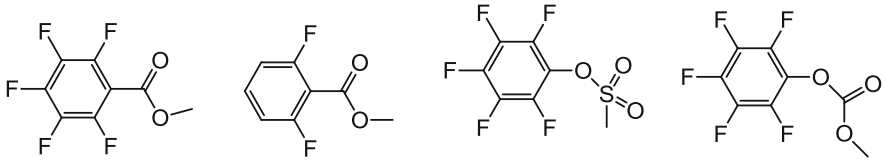

62 **63** **64** **65**

3.2.6 Phosphorus-Containing Compounds

The feasibility of using triethyl phosphate (**66**), whose flash point is extremely high, as a nonflammable solvent was discovered by Mitsui Chemicals and Sony Corporation in 1994 [95]. Details are presented later in the section concerning safety.

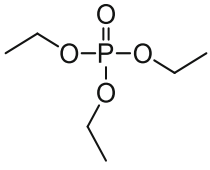

66

In 1998, Wilson Greatbatch Technologies discovered that phosphates with unsaturated bonds, such as triallyl phosphate (**67**) and tripropargyl phosphate (**68**),

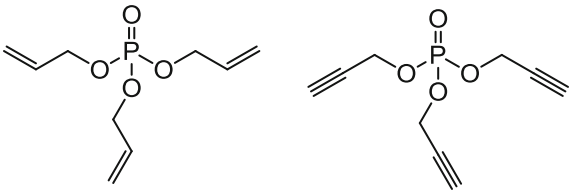

67 **68**

can be used as additives in small quantities [96]. Furthermore, in 2002, Mitsubishi Chemical Corporation found that phosphinates, such as ethyl diethylphosphinate (**69**), and diphosphinates, such as 1,4-butanediol bis(diethylphosphinate) (**70**), can be used as additives in small quantities [97].

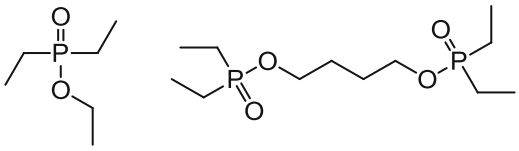

69 **70**

In 2003, Mitsubishi Chemical Corporation found that the cyclic phosphate 2-ethoxy-1,2-oxaphospholane 2-oxide (**71**) can be used as an additive in small quantities [98].

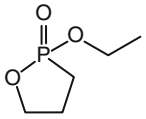

71

3.2.7 Nitrogen-Containing Compounds

In 1990, Sony Corporation found that the amides *N*-methylpyrrolidone (**72**) and *N*,*N*-dimethylacetamide (**73**) can be used as additives in small quantities [99], and in 1995, Wilson Greatbatch Technologies found that the imides bis(*N*-succinimidyl) carbonate (**74**) and benzyl *N*-succinimidyl carbonate (**75**) can be used as additives in small quantities [100]. In 1997, Fujitsu and Ube Industries, Ltd. found that *N*-hydroxysuccinimide (**76**) can be used as an additive in small quantities [101], and Sanyo Electric Company discovered that cyclic imides such as succinimide (**77**) and maleimide (**78**) can also be used as additives in small quantities in 1997 and 1998, respectively [102, 103].

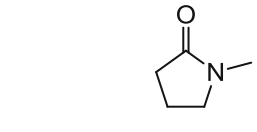

72

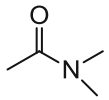

73

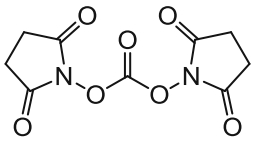

74

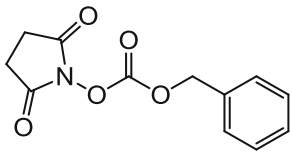

75

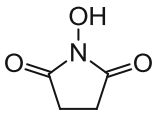

76

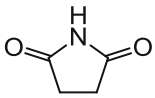

77

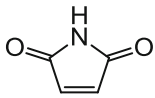

78

In 2003 Samsung SDI discovered that *N*-vinyl-ε-caprolactam (**79**) can be used as an additive in small quantities [104].

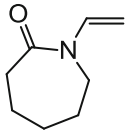

79

3.3 Additives for Cathodes

In this section, additives for cathodes are reported by categorizing them into (1) sulfur-containing compounds with active site poisoning function [105–107] and (2) aromatic compounds forming an electro-conducting membrane (ECM) [2, 109, 110].

3.3.1 Sulfur-Containing Compounds with Active Site Poisoning Function

In 1996, Fujifilm Corporation discovered that sulfides containing phenyl groups, such as diphenyl sulfide (**80**), 4,4′-dimethoxydiphenyl sulfide (**81**), and 1,2-bis (*p*-methoxyphenylthio)ethane (**82**), can be used as additives in small quantities [105]. In this regard, the first report on sulfur-containing additives for cathodes contains the following three descriptions. (1) Although the potential of the cathode increases gradually during charging, the potential at the surface of the cathode is not

necessarily uniform, and there are microscopic regions where the potential is excessively high (overvoltage regions), where strong oxidizing chemical species such as oxygen radicals are generated. For this reason, oxidative decomposition of organic solvents in the electrolyte can be expected to occur at such overvoltage regions. In such cases, if an additive with the desirable potential (appropriate reducing properties) is present, it is oxidized preferentially, and thus the decomposition of the organic solvent can be avoided. (2) The appropriate range for the oxidation potential was between +3.8 and +4.3 V when metallic lithium was taken as a reference electrode, with a more preferable range being between +3.9 and +4.2 V. (3) Some of the products of oxidation of these additives adhered to the cathode.

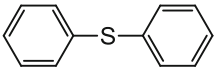

80

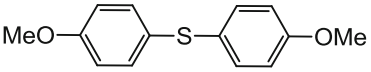

81

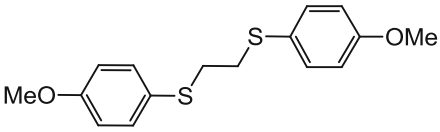

82

In 1998, Ube Industries, Ltd. discovered that compounds such as methyl oxo(phenylthio)acetate (**83**), *S*,*S*′-diphenyl dithiooxalate (**84**), *S*-phenyl *O*-methyl thiocarbonate (**85**), and *S*,*S*′-diphenyl dithiocarbonate (**86**) can be used as additives in small quantities [106].

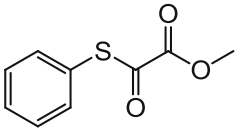

83

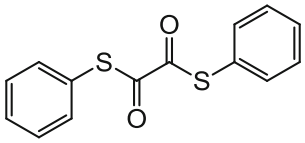

84

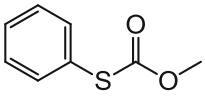

85

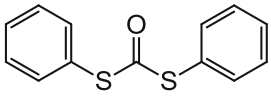

86

In 1998, that company found that disulfides such as diphenyl disulfide (**87**) and di-*p*-tolyl disulfide (**88**) can be used as additives in small quantities [107].

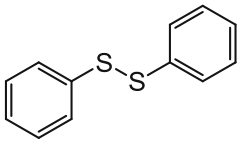

87

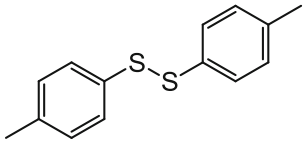

88

Moreover, in 1999, the same company found that bis(4-methoxyphenyl) disulfide (**89**) can be used as an additive in small quantities [108].

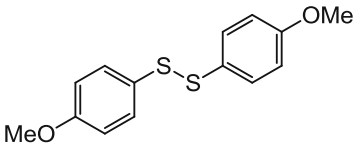

89

3.3.2 Aromatic Compounds Forming an Electro-Conducting Membrane

Around the same time in 2000, Ube Industries, Ltd. discovered that compounds such as biphenyl (**90**) can be used as additives in extremely small quantities of 0.03–0.5 wt% [109].

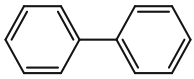

90

Later, in paper published in 2004 and 2006, a concept of ECM was proposed for the cathode and was distinguished from SEI, which was generally used in reference to anodes. Examples of additives that form an ECM are monomers of conducting polymers such as biphenyl (**90**) and compounds (**91**) through (**97**) [2, 110].

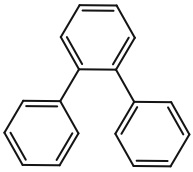

91

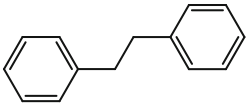

92

93

94

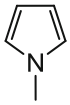

95

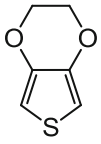

96

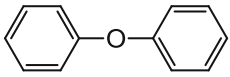

97

3.4 Additives for Safety Improvement

Following the increase in battery capacity, the safety of LIBs is becoming an increasingly important topic. Compounds for safety improvement presented in this section are grouped into (1) additives for overcharge prevention [3, 111–138], (2) nonflammable solvents and additives [139–141], and (3) others [142–146].

3.4.1 Additives for Overcharge Prevention

When LIBs are overcharged, excess lithium is extracted from the cathode, after which oxygen release from inside the crystal begins and the crystal structure becomes unstable. Moreover, excessive intercalation of lithium occurs at the anode, which results in the deposition of lithium metal. When the anode and the cathode become thermally unstable, they start to decompose organic solvents in the electrolyte. This results in a sudden exothermic reaction, and the battery begins to produce unusual amounts of heat, which compromises the safety of the battery (Figs. 3.4 and 3.5).

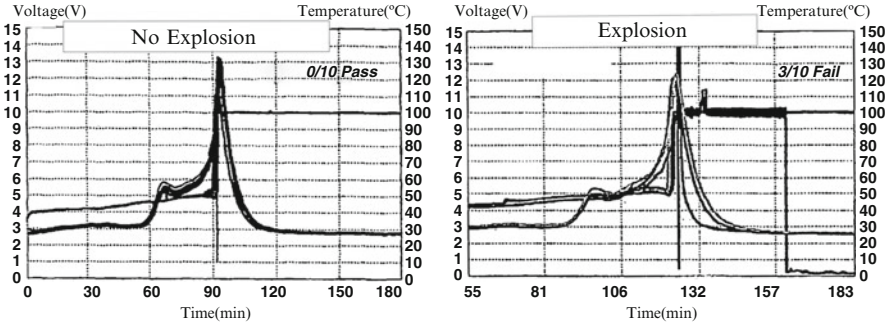

Fig. 3.4 Charging profiles of overcharged cell [111]

Fig 3.5 Overcharge test of the cell containing electrolyte without additives

Although there are safety measures such as shutdown methods based on the fusion of a separator and prevention methods using electronic circuits, various methods using additives for overcharge prevention mixed into the electrolyte have been reported since they are particularly effective.

3.4.1.1 Anisole Compounds

In 1994, Sony Corporation discovered that alkoxybenzenes, such as 1,3,5-trimethoxybenzene (**98**), 2,6-dimethoxytoluene (**99**), and 3,4,5-trimethoxytoluene (**100**), can be used as additives in small quantities [112]. These compounds are called "redox shuttle additives" as they suppress the increase in battery voltage by consuming electric current through a redox process.

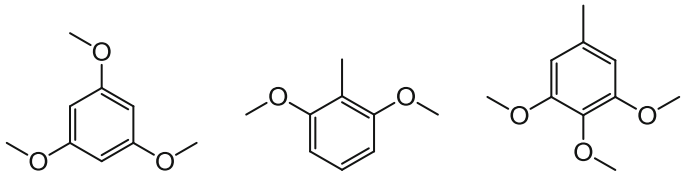

98 **99** **100**

Furthermore, in 1995, Sony Corporation found that halogen-containing alkoxybenzenes, such as 2-chloro-*p*-xylene (**101**), 4-chloroanisole (**102**), 2,4-difluoroanisole (**103**), 3,5-difluoroanisole (**104**), and 2,6-difluoroanisole (**105**) can be used as additives in small quantities [113].

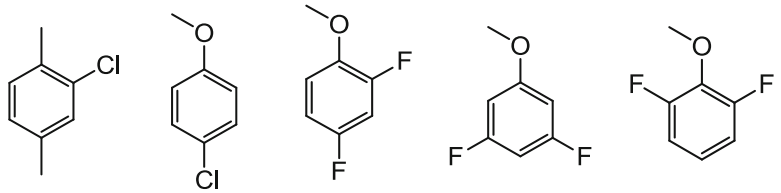

101 **102** **103** **104** **105**

3.4.1.2 Alkylbenzenes and Halogen-Containing Benzene Compounds

In 1995, NEC Moli Energy found that aromatic compounds such as biphenyl (**90**), 3-chlorothiophene (**106**), and furan (**107**) can be used as additives in small quantities [114]. According to the description in the relevant reference, the polymerization of the additive at the cathode produces an insulating layer of polymer: "polymerization of the additive is believed to occur at the cathode resulting in the formation of insulating polymer on the cathode surfaces" and "the aromatic additive polymerizes at voltages greater than the maximum operating voltage thereby increasing the internal resistance of the battery sufficiently for protection" [114].

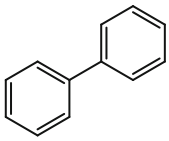

90 **106** **107**

In 1996, Fujifilm Corporation discovered that cumene (**108**) and cyclohexylbenzene (**109**) can be used as additives in small quantities [115].

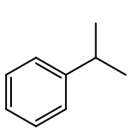

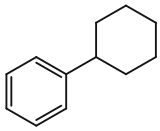

108 **109**

Furthermore, in 1996 Hitachi Maxell discovered that fluorobenzene compounds, such as fluorobenzene (**110**), 1,2-difluorobenzene (**111**), and 1,3,5-trifluorobenzene (**112**), can be used as additives in small quantities [116]. In 1997, the same company discovered that trimellitates, such as tris(2-ethylhexyl) trimellitate (**113**), can also be used as additives in small quantities [117].

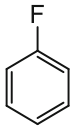

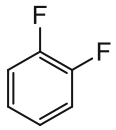

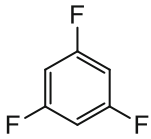

110 **111** **112**

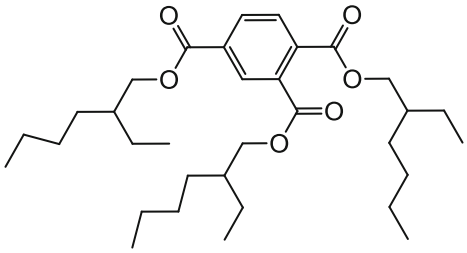

113

In 1997, NEC Moli Energy discovered that pyrrole (**114**) and *N*-methylpyrrole (**95**) can be used as additives in small quantities [118]. According to the description, "When the battery is overcharged, monomer additives begin to polymerize once the polymerization voltage is reached. Eventually, a sufficient amount of conductive polymer is created and a conductive frame is formed between the electrodes, thus shortening the battery internally and discharging it" [118].

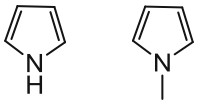

114 **95**

In the same year, the same company reported an electrolyte with biphenyl that "when cycle tested at 40 °C to an upper voltage limit of 4.3 V, the cycle life characteristics are progressively worse with increasing amounts of biphenyl additive present" [119]. The same report suggests that 2,2-diphenylpropane (**115**) and 2-fluorobiphenyl (**116**) can be used alternatively as additives in small quantities [119].

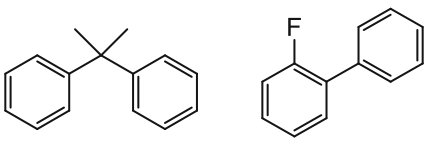

115 **116**

In 1999, Sanyo Electric Company and Ube Industries, Ltd. discovered that esters containing biphenyl groups, such as 4-acetoxybiphenyl (**117**) [120]; ethers containing aryl groups, such as diphenyl ether (**97**) [121]; ethylene glycol compounds containing phenyl groups, such as 1,2-diphenoxyethane (**118**) [122]; diphenoxybenzenes, such as 1,4-diphenoxybenzene (**119**) [123]; and terphenyl compounds, such as *o*-terphenyl (**91**), *m*-terphenyl (**120**), and *p*-terphenyl (**121**), can be used as additives in small quantities [124].

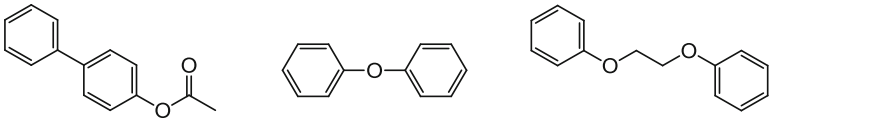

117 **97** **118**

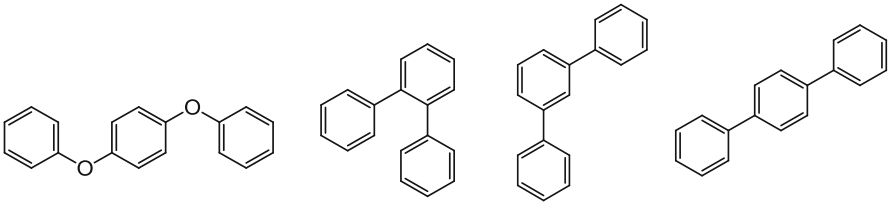

119 **91** **120** **121**

In 1998, Sanyo Electric Company and Ube Industries, Ltd. reported electrolytes containing aklylbenzene compounds having a tertiary carbon adjacent to the phenyl group, represented by compounds such as cumene (**108**) and cyclohexylbenzene (**109**). In combination with a battery cell casing equipped with a current interrupt

device, they effectively cut off the charge current of the battery when its internal gas pressure rises excessively [125]. As the hydrogen-tertiary carbon bond adjacent to the phenyl group is highly reactive, the hydrogen atom is easily extracted from the tertiary carbon in an overcharged battery condition. This causes rapid decomposition of the additive when the battery is overcharged. As a result, hydrogen gas is generated and the additive is polymerized [125].

On the same day, Panasonic discovered compounds such as hexaphenylbenzene (**122**), *p*-terphenyl (**121**), 1-phenylpiperazine (**123**), 1,2,3,4-tetrahydroisoquinoline (**124**), cyclohexylbenzene (**109**), 1,3,5-triphenylbenzene (**125**), dodecahydrotriphenylene (**126**), divinyl benzenze (**127**), and 1,4-dicyclohexylbenzene (**128**), for which the energy level of the highest occupied molecular orbital is between −8.5 and −11 eV and that of the lowest unoccupied molecular orbital is between −0.135 and 3.5 eV as calculated by using a semiempirical method for computation of molecular orbitals with the PM3 Hamiltonian [126].

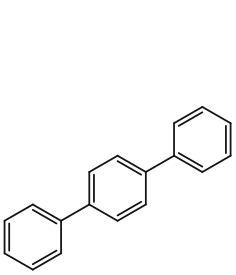

121

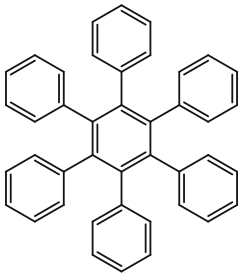

122

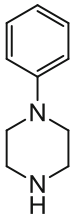

123

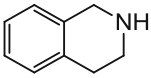

124

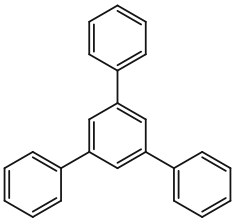

125

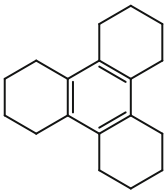

126

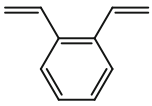

127

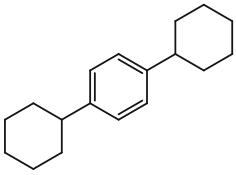

128

In 1999, Ube Industries, Ltd. discovered that *tert*-butylbenzene compounds, such as *tert*-butylbenzene (**129**), 4-*tert*-butyltoluene (**130**), and 1,3-di-*tert*-butylbenzene (**131**), can be used as additives in small quantities [127]. In 2000, the same company discovered that halogen-containing *tert*-butylbenzene compounds [128], such as 1-bromo-4-*tert*-butylbenzene (**132**), can be used as additives in small quantities, and in 2001 the same company discovered that *tert*-amylbenzene (**133**) as well can be used as an additive in small quantities [129].

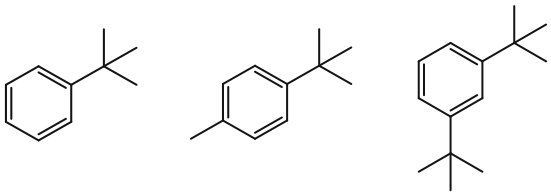

129 **130** **131**

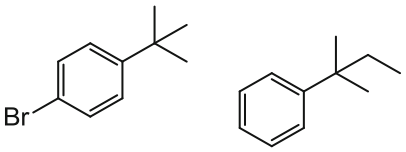

132 **133**

In 2003, Shima and Ue from Mitsubishi Chemical Corporation and Yamaki from Kyushu University presented the mechanism behind the overcharge prevention. According to the description in the relevant reference, "the aromatic compounds without hydrogen at the benzylic position (e.g., *tert*-butylbenzene) evolve mainly carbon dioxide (CO_2) gas, which is generated by the indirect decomposition of carbonate solvents. The CO_2 gas evolution reaction using a redox mediator is expected as a new overcharge protection method" [3].

3.4.1.3 Gear Change Concept

In 2000, Ube Industries, Ltd. reported that cyclohexylbenzene (**109**) and *tert*-alkylbenzene compounds, whose oxidation potentials are different, can be used as additives in small quantities and noted that "*tert*-butylbenzene is replaced with cyclohexylbenzene having a low oxidation potential, the prevention of overcharging is enhanced" [130].

In the same year, Panasonic and Ube Industries, Ltd. discovered that compounds such as *o*-terphenyl (**91**), triphenylene (**134**), cyclohexylbenzene (**109**), and biphenyl (**90**), whose oxidation potentials are different, can be used as mixed additives by combining small quantities of two or more such compounds [131, 132].

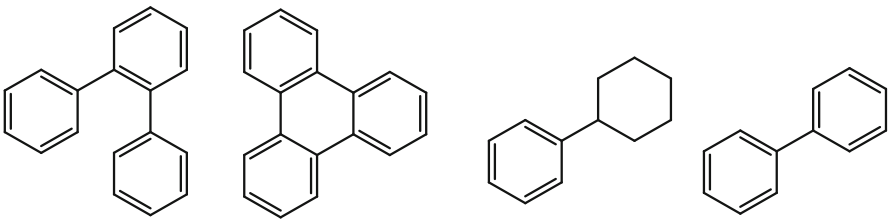

91 **134** **109** **90**

In 2001, Ube Industries, Ltd. discovered that mixtures of small quantities of *tert*-alkylbenzenes (such as *tert*-butylbenzene (**129**)) and biphenyl compounds (such as biphenyl (**90**)), whose oxidation potentials are different, can be used as additives [133].

As described in the relevant report, "the *tert*-alkylbenzene compound decomposes by oxidation at a potential of +4.6 to +5.0 V (relative value to that of lithium), and cobalt or nickel in the positive electrode rapidly dissolves and deposits on the negative electrode to inhibit a reaction of a carbonate in the non-aqueous electrolytic solution with a lithium metal deposited on the negative electrode. Further, in the invention, the internal short circuit may be formed in the battery by the deposition of cobalt and nickel, whereby the overcharge inhibitive effect can be attained and the safety of battery can be assured" [133].

In the same year, the same company discovered mixed additives of alkylbiphenyl compounds (e.g., 4-methylbiphenyl (**135**)) and cyclohexylbenzene (**109**), whose oxidative potentials are different and also found that such mixed additives can be combined with at least one species chosen from among biphenyl (**90**), *o*-terphenyl (**91**), and *tert*-butylbenzene (**129**). According to the description, additives whose oxidation polymerization potential is higher than that of alkylbiphenyl species continuously undergo oxidative polymerization, forming a thick polymer membrane at the cathode [3]. This is similar to the concept of engine braking in cars, where gears are shifted down in a stepwise manner, and the "gear change concept," which uses multiple overcharge prevention additives with different oxidation potentials, has recently become mainstream [134].

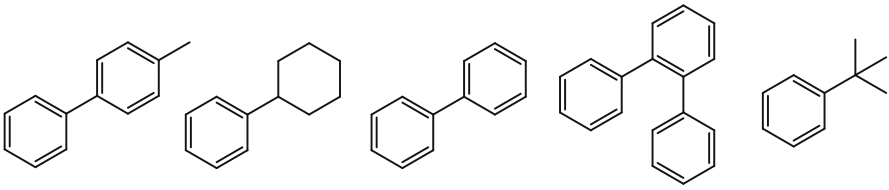

135 **109** **90** **91** **129**

In 2001, Mitsubishi Chemical Corporation discovered that "a mixture of two or more compounds of which one is diphenylcyclohexane that is present in an amount ranging from 10 to 65 wt% of the partially hydrogenated terphenyl" can be used as additives [144]. Partially hydrogenated *m*-terphenyl is used as a mixture of compounds such as hydrogenated *m*-terphenyl (**136**), 1,3-dicyclohexyl benzene (**137**), 3-phenyl-1,1′-bi(cyclohexane) (**138**), 1,3-diphenylcyclohexane (**139**), *m*-cyclohexybiphenyl (**140**), and *m*-terphenyl (**120**) [135].

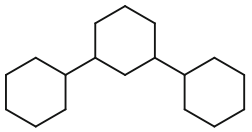

136

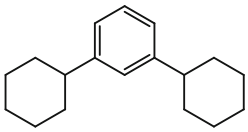

137

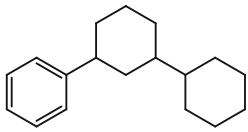

138

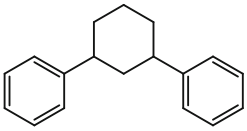

139

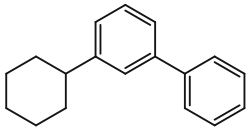

140

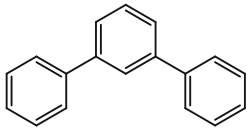

120

In 2002, Mitsubishi Chemical Corporation and Ube Industries, Ltd. found that fluorinated cyclohexylbenzens, such as 1-fluoro-2-cyclohexylbenzene (**141**), 1-fluoro-3-cyclohexylbenzene (**142**), and 1-fluoro-4-cyclohexylbenzene (**143**), can be used as additives in small quantities [136, 137].

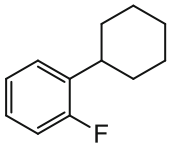

141

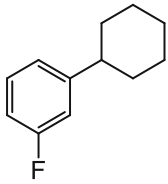

142

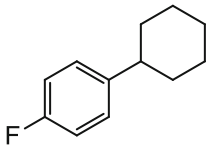

143

3.4.1.4 Miscellaneous Compounds

In 2005, Dahn et al. from Dalhousie University discovered that 2,5-di-*tert*-butyl-1,4-dimethoxybenzene (**144**) can be used as an additive in small quantities in batteries with $LiFePO_4$ cathodes [138]. Furthermore, in 2006, the same researchers discovered that phenothiazine compounds, such as 10-methylphenothiazine (**145**), can be used as additives in small quantities [139].

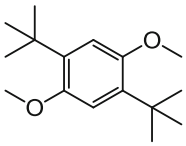

144

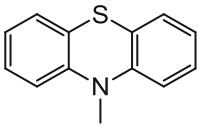

145

3.4.2 Nonflammable Solvents and Additives

With regard to nonflammable solvents, we focus on organic phosphates, phosphazenes, and other additives for safety improvement.

In 1990, Mitsubishi Chemical Corporation discovered solvents with unusually high flash point, such as triesters of phosphoric acid (triethyl phosphate (**66**) and others) as well as other esters of phosphoric acid (15 vol.% and above) [140]. This triggered prolific research on phosphate solvents.

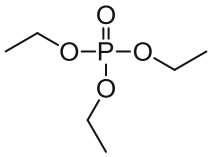

66

According to a paper by Wang et al. from the Japan Aerospace Exploration Agency (JAXA) published in 2006, "TMP exhibits excellent anode stability but poor cathode stability against a graphite anode" [141]. For this reason, they note the following: "The poor cathodic stability of the TMP solvent has led some authors to conclude that the goal of a TMP-based nonflammable electrolyte is impractical for lithium-ion cells" [141].

In 1992, Bridgestone discovered that cyclic phosphazenes, such as hexapropioxycyclotriphosphazene (**146**) and hexafuluoroethoxycyclotriphosphazene (**147**), can be used as additives [142].

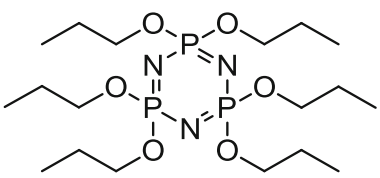

146

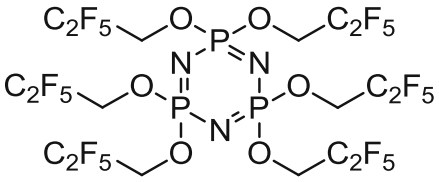

147

3.4.3 Others

In 1994, Tadiran, an Israeli company, made the discovery described as follows: "This cell comprises as main components a negative electrode which is Lithium or Lithium alloy, a positive cathode which includes MnO_2 and an electrolyte which is 1,3-Dioxolane (**148**) with Lithium hexafluoroarsenate ($LiAsF_6$) and a polymerization inhibitor" [143].

148

According to the report, in such batteries, "the solvents should be such that it polymerizes in the cell above 100 °C and at high voltages of above about 4 V" and "this polymerization is very effective in that it substantially increases the resistivity of the cell and thereby terminates its operation and precludes the possibility of further hazardous reactions between the lithium and the electrolyte itself" [143].

In 1999, Ube Industries Ltd. discovered that oxetane compounds, such as 3,3′-[oxybis(methylene)] bis(3-ethyl-oxetane) (**149**), can be used as additives in small quantities [144].

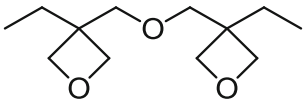

149

In 2001, Hitachi, Ltd. discovered that fluorinated alkyl esters, such as methyl perfluorobutyrate (**150**), can be used as additives in small quantities [145].

In 2003, Yamaki et al. from Kyushu University presented in a paper that methyl difluoroacetate (MFA) (**151**) can be used as an additive in small quantities and reported that MFA electrolyte is a good candidate to improve the thermal stability of the lithium ion and lithium metal anode battery [146].

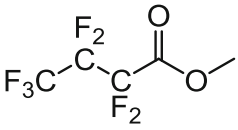

150

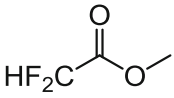

151

3.5 Miscellaneous

In this section, we present additives for wettability improvement, additives for corrosion inhibition, and lithium salts.

3.5.1 Additives for Wettability Improvement

In 1989, Asahi Kasei Corporation found phosphates containing long-chain aliphatics and aromatics, such as tris(2-ethylhexyl) phosphate (**152**) and triphenyl phosphite (**153**) [147].

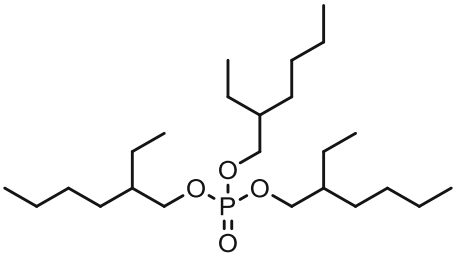

152

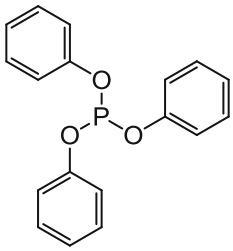

153

In 1995, Adeka Corporation discovered carbonates containing long-chain alkyl carbonates, such as dodecyl methyl carbonate (**154**) [148].

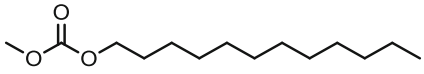

154

In 1999, Ube Industries, Ltd. discovered carbonates containing branched alkyl groups, such as methyl 1-methylpropyl carbonate (**155**) and methyl *sec*-butyl carbonate (**156**) [149].

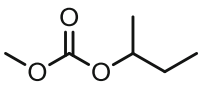

155

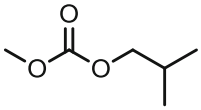

156

In 2000, Ube Industries, Ltd. discovered tertiary carboxylic acid esters, such as methyl 2,2-dimethylpropanoate (**157**), ethyl 2,2-dimethylpropanoate (**158**), butyl 2,2-dimethylpropanoate (**159**), and hexyl 2,2-dimethylpropanoate (**160**) [35].

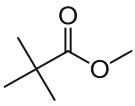

157

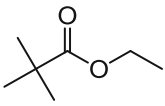

158

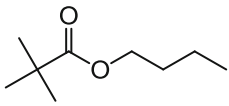

159

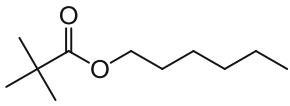

160

3.5.2 Additives for Corrosion Inhibition

In 2002, Ube Industries, Ltd. discovered that adding small quantities of dinitriles (such as adiponitrile (**161**)) to electrolytes reduces the corrosion of metal parts of the battery, such as the battery container and the electrodes [36].

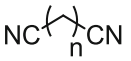

n=2~12

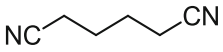

161

Subsequently, demand increased abruptly, and various electrolytes mixed with small quantities of dinitriles and other additives were discovered from 2004 onward. For example, in 2004, LG Chem Ltd. discovered that compounds such as succinonitrile (**162**) and sebaconitrile (**163**) can be combined with compounds such as 2-fluorotoluene (**164**) and 3-fluorotoluene (**165**) [150]. In the same year, Samsung SDI discovered that succinonitrile (**162**) is effective for protecting Cu current collector [151].

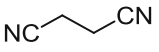

162

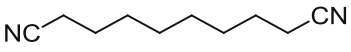

163

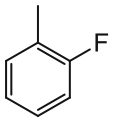

164

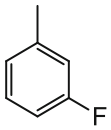

165

Also in 2006, LG Chem Ltd. discovered that dinitriles such as succinonitrile (**162**) can be combined with fluoroethylene carbonate (**60**) for use as additives [152].

Although various dinitrile compounds have been examined as additives, their chemical properties vary considerably depending on their structure. For example, while adiponitrile (**161**) is liquid at normal temperature since its melting point is 3 °C, succinonitrile (**162**) is in the form of waxy oil since its melting point is 57 °C. Therefore, using succinonitrile (**162**) at normal operating temperatures is problematic [153].

3.5.3 Lithium Salts

3.5.3.1 Nitrogen-Containing (Imide Anion) Lithium Salts

In 1986, Hydro-Quebec discovered lithium salts containing imide anions, such as lithium bis(trifluoromethanesulfonyl)imide (**166**) [154].

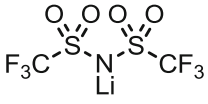

166

3.5.3.2 Boron-Containing Lithium Salts

In 1993, Wühr at the University of Regensburg discovered the utility of lithium organoborates containing aromatic rings, such as lithium bis(1,2-benzenediorate(2)-*O*,*O*′)borate (**167**) [155], and in 1996, Merck KGaA, together with Barthel et al. from the University of Regensburg, discovered other lithium organoborates containing aromatics, such as lithium bis(2, 3-naphthalenediolato) borate (**168**) and lithium bis[3-fluoro-1,2-benzenediolato(2-)-*O*,*O*′]borate (**169**) [156, 157].

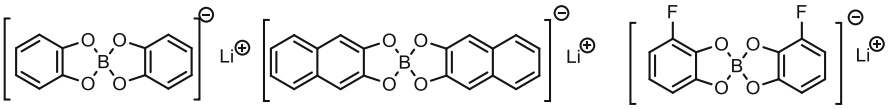

167 **168** **169**

In 1998, Chemetall GmbH found lithium bis(oxalato)borate (**170**) [158].

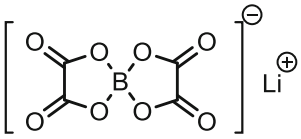

170

In 2000, Central Glass Co, Ltd. found lithium organoborates containing a structure of oxalic acid, such as lithium difluoro(oxalato)borate (**171**) [159].

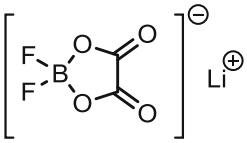

171

In 2004, Air Products found polyhalogenated lithium borates, such as dilithium dodecafluorododecaborate ($Li_2B_{12}F_{12}$) [160].

3.5.3.3 Phosphorus-Containing Lithium Salts

In 1996, Merck KGaA discovered lithium fluorophosphate containing fluorinated alkyl groups, such as lithium tris(pentafluoroethyl)trifluorophosphate (**172**) [161].

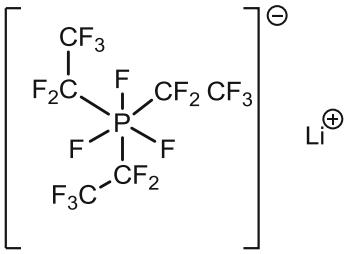

172

In 1997, Sanyo Electric Company discovered that lithium salts such as lithium fluorophosphate (Li_2PO_3F) (**173**) and lithium difluorophosphate ($LiPO_2F_2$) (**174**) can be used as additives in small quantities [162]. Furthermore, in 2003, Mitsubishi Chemical Corporation discovered a method for manufacturing lithium difluorophosphate (**174**) [163].

173 **174**

In 2000, Central Glass Co, Ltd. discovered lithium salts containing a structure of oxalic acid, such as lithium tetrafluoro(oxalato)phosphate (**175**) and lithium difluorobis(oxalato)phosphate (**176**) [159].

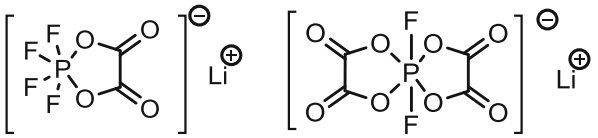

175 **176**

3.6 Future Prospects

In recent years, the role played by the electrolyte has become increasingly versatile due to the adoption of various cathodes, anodes, and separators as a result of the intensification of technological development in the field of LIB materials. Electrolytes and additives are key materials for optimizing the performance of materials used in cathodes, anodes, and separators and strongly affect critical parts governing battery performance parameters such as the cycle life characteristics, preservation characteristics, and output characteristics.

When intensive research and development of additives is conducted on a daily basis, some compounds might be serendipitously found and industrialized as additives.

However, such development has produced only a handful of additives that have truly established themselves as commercialized additives. The reason why additive development is difficult is that additives always have side effects. Thus, the key to developing new additives is to control the side effects, like in pharmaceutical development, in order to achieve good overall battery performance. Careful consideration of the phenomenon inside the batteries is essential in the development of novel additives.

The aim of this chapter is to present information from papers and patents in functional and historical order, as well as to provide numerous examples of additives, with the hope that it would be of assistance in future research on additives.

References

1. Wrodnigg, G.; Besenhard, J.; Winter, M., Ethylene sulfite as electrolyte additive for lithium-ion cells with graphitic anodes, *J. Electrochem. Soc.,* **1999**, *146* (2), 470-472.
2. Abe, K.; Ushigoe, Y.; Yoshitake H.; Yoshio, M., Functional electrolytes: Novel type additives for cathode materials, providing high cycleability performance, *J. Power Sources*, **2006**, *153* (2), 328-335.
3. Shima, K., Ue, M., Yamaki, J., Redox mediator as an overcharge protection agent for 4 V class lithium-ion rechargeable cells, *Electrochemistry*, **2003**, *71*, 1231-1235.
4. Yoshino, A.; Sanechika, K.; Nakajima, T., *Secondary battery*; US Patent 4,668,595, (Asahi Kasei Corporation): **1987** (applied in 1985).
5. Yoshino, A.; Sanechika, K.; Yamamoto, K., *Non-aqueous secondary battery*; JP Patent 2,128,922 (H4-52592) (Asahi Kasei Corporation): **1985** (applied in 1983).
6. Yoshino, A.; Nakanishi, K.; Ono, A., *Explosion-proof secondary battery*; JP Patent 2,642,206, (Asahi Kasei Corporation): **1991** (applied in 1989).
7. Ikeda, H.; Narukawa, K.; Nakajima, H., *Rechargeable lithium battery*; JP Patent 1,769,661 (Sanyo Electric Co., Ltd.): **1982** (applied in 1981).
8. Peled, E., The electrochemical behavior of alkali and alkaline earth metals in non-aqueous battery systems-The solid electrolyte interphase model, *J. Electrochem. Soc.,* **1979**, *126* (12), 2047-2051.
9. Aurbach, D.; Ein-Eli, Y.; Chusid (Youngman), O.; Carmeli, Y.; Babai, M.; Yamin, H., The correlation between the surface chemistry and the performance of Li-carbon intercalation anodes for rechargeable "rocking-chair" type batteries, *J. Electrochem. Soc.*, **1994**, *141*, 603-611.
10. Chusid, O.; Ein Ely, Y.; Aubach, D.; Babai M.; Carmelli, Y., Electrochemical and spectroscopic studies of carbon electrodes in lithium battery electrolyte systems, *J. Power Sources*, **1993**, *43*, 47-64.
11. Yoshitake, H., Recent trends in electrolyte for lithium battery, *Battery and Power Supply in Techno-Frontier Symposium*, Makuhari, Chiba, **1999**, 14-16 Apr.
12. Abe, K.; Yoshitake, H., Development of functional electrolytes, *Electrochemistry*, **2004**, *72*, 519.
13. Ue, M., Development trend of electrolyte materials for lithium ion battery, *Battery and Power Supply in Techno-Frontier Symposium*, Makuhari, Chiba, **2003**, 16-18 Apr.
14. Ue, M., Battery technology award address: "Role assigned electrolytes", *ECS 206th Meeting Abs*., **2004**, 308.
15. Ue, M., Role-assigned electrolytes: Additives, In *Lithium-ion batteries,* Yoshio, M., Bradd, R. J. and Kozawa, A., Ed.; Springer Science + Business Media, LLC: New York, USA, **2009**; 75-115.

16. Hamamoto, T; Hitaka, A.; Abe, K.; Ueno, Y.; Ohira, N.; Watanabe, M., *Electrolyte solution for lithium secondary battery*; US Patent 6,045,945 (Ube Industries, Ltd.): **1998** (applied in 1997).
17. Jungnitz, M., *Purification of battery electrolytes by means of physical adsorption*; WO99/67844 (Merck KGaA): **1999** (applied in 1998).
18. Heider, U.; Oesten, R.; Jungnitz, M., Challenge in manufacturing electrolyte solutions for lithium and lithium ion batteries quality control and minimizing contamination level, *J. Power Sources*, **1999**, *81-82*, 119-122.
19. Yoshitake, H., Functional Electrolytes, In *Lithium-ion secondary batteries 2nd Edition*; Yoshio, M. and Kozawa, A., Ed.; Nikkan Kogyo Shimbun Ltd.: Tokyo, Japan, **2001**; 73-82.
20. Yoshitake, H., Functional electrolytes specially designed for lithium-ion batteries, In *Lithium-ion batteries,* Yoshio, M., Bradd, R. J. and Kozawa, A., Ed.; Springer Science + Business Media, LLC: New York, USA, **2009**; 343-366.
21. Yoshio, M.; Nakamura, H.; Yoshitake, H.; Tanaka S., *Electrolyte for lithium secondary battery*; US Patent 5,681,669 (Ube Industries, Ltd.): **1996** (applied in 1995).
22. Yoshitake, H.; Abe, K.; Kitakura, T.; Gong, J.; Lee, Y.; Nakamura H.; Yoshio, M., The effect of nano-sized SEI film formed by vinyl acetate additive for Li-ion batteries, *Chem. Lett.*, **2003**, *32*, 134-135.
23. Abe, K.; Yoshitake, H.; Kitakura, T.; Hattori, T.; Wang, C.; Yoshio, M., Additives-containing functional electrolytes for suppressing electrolyte decomposition in lithium-ion batteries, *Electrochim. Acta*, **2004**, *49*, 4613-4622.
24. Ghimire, P.; Nakamura, H.; Yoshio, M.; Yoshitake, H.; Abe, K., Suppression of electrochemical decomposition of electrolyte in lithium ion batteries using electrolyte containing vinyl group compounds, *Electrochemistry*, **2003**, *71*, 1084-1086.
25. Ghimire, P.; Nakamura, H.; Yoshio, M.; Yoshitake, H.; Abe, K., *Chem. Lett.*, Suppression of electrochemical decomposition of electrolyte in lithium ion batteries: An electrolyte containing acetate group, **2005**, *34* (7), 1052-1053.
26. Ghimire, P.; Nakamura, H.; Isono, K.; Yoshio, M.; Abe, K.; Yoshitake, H., Suppression of electrochemical decomposition of electrolyte in lithium ion batteries using electrolyte containing acetate group compounds, *Electrochemistry*, **2005**, *73* (9) 788-790.
27. Abe, K., Hattori, T.; Kawabe, K.; Ushigoe, Y.; Yoshitake, H., Functional electrolytes: Triple-bonded compound as an additive for negative electrode, *J. Electrochem. Soc.*, **2007**, *154* (8), A810-815.
28. Abe, K.; Miyoshi, K.; Hattori, T.; Ushigoe, Y.; Yoshitake, H., Functional electrolytes: Synergetic effect of electrolyte additives for lithium-ion battery, *J. Power Sources*, **2008**, *184*, 449-455.
29. Thomas, M. G. S. R.; Bruce, P. G.; Goodenough, J. B., AC impedance analysis of polycrystalline insertion electrodes: Application to $Li_{1-x}CoO_2$, *J. Electrochem. Soc.*, **1985**, 132, 1521-1528.
30. Wang, Y.; Guo, X.; Greenbaum, S.; Liu, J.; Amine, K., Solid electrolyte interphase formation on lithium-ion electrodes, *Electrochem. Solid-State Lett.*, **2001**, 4, A68-A70.
31. Ota, H.; Sakata, Y.; Otake, Y.; Shima, K.; Ue, M.; Yamaki, J., Structural and functional analysis of surface film on Li anode in vinylene carbonate-containing electrolyte, *J. Electrochem. Soc.*, **2004**, *151* (11), A1778-A1788.
32. Abe, K.; Takaya, T.; Yoshitake, H.; Ushigoe, Y.; Yoshio, M.; Wang, H.; Functional electrolyte: Additives for improving the cyclability of cathode materials, *Electrochem. Solid-State Lett.*, **2004**, *7*, A462-A465.
33. Abe, K.; Yoshitake, H.; Takaya, T.; Nakamura H.; Yoshio, M., Development of additives on cathode performance improvement for lithium ion batteries, *Electrochemistry*, **2005**, *73*, 199-201.
34. Ue, M., *Flame-retardant for lithium battery electrolyte*; JP Patent 3,131,905 (Mistubishi Chemical Co.): **1992** (applied in 1990).
35. Kajiwara, M.; Ogino, T.; Miyazaki, T.; Kawagoe, T., *Non-aqueous electrolyte battery*; JP Patent 3,055,358 (Bridgestone Co.): **1994** (applied in 1993).

36. Hamamoto, T.; Abe, K.; Ushigoe, Y.; Matsumori, *Non-aqueous electrolytic solution and lithium secondary battery*; Y., US Patent 6,881,522 (Ube Industries, Ltd.): **2002** (applied in 2000)
37. Abe, K., Hattori, T.; Matsumori, Y., *Lithium secondary battery*; JP Patent 4,609,751(Ube Industries, Ltd): **2004** (applied in 2002).
38. Heider, U.; Schmidt, M.; Amann, A.; Niemann, M.; Kuhner A., *Use of additives in electrolyte for electrochemical cells*; US Patent 6,548,212 (Merck KGaA): **2000** (applied in 1999).
39. Fujimoto, M.; Takahashi, M.; Nishio, K., *Secondary battery*; US Patent 5,352,548 (Sanyo Electric Co, Ltd.): **1994** (applied in 1992).
40. Simon, B.; Boeuve, *J.*, *Rechargeable lithium electrochemical cell*; US Patent 5,626,981 (Saft Romainville.): **1995** (applied in 1994).
41. Ota, H.; Sakata, Y.; Inoue, A.; Yamaguchi, S., Analysis of vinylene carbonate derived SEI layers on graphite anode, *J. Electrochem. Soc.,* **2004**, *151* (10), A1659-A1669.
42. Hamamoto, T.; Hitaka, A.; Nakata, Y.; Abe, K., *Electrolyte for lithium secondary battery and lithium secondary battery using the same*; JP Patent 3,627,754 (Ube Industries, Ltd.): **1999** (applied in 1997).
43. Hamamoto, T.; Ueki, A.; Abe, K.; Takai, T., *Non-aqueous electrolyte and lithium secondary battery using the same*; US Patent 6,413,678 (Ube Industries, Ltd.): **2000** (applied in 1998).
44. Shu, Z. X.; McMillan, R. S.; Murray, J. J., Effect of 12 crown 4 on the electrochemical intercalation of lithium into graphite, *J. Electrochem. Soc.,* **1993**, *140* (6), L101-L103.
45. Wang, C.; Nakamura, H.; Komatsu, H.; Yoshio, M.; Yoshitake, H., Electrochemical behavior of a graphite electrode in propylene carbonate and 1,3-benzodioxol-2-one based electrolyte system, *J. Power Sources.,* **1998**, *74*, 142-145.
46. Suzuki, H.; Suzuki, H., *Non-aqueous electrolyte for secondary battery and Non aqueous electrolyte secondary battery*; JP Patent 4,197,785 (Mitsubishi Chemical Co.): **2000** (applied in 1998).
47. Suzuki, H.; Suzuki, H., *Non-aqueous electrolyte secondary battery and non-aqueous electrolyte utilized for the same*; JP Patent 4,568,920 (Mitsubishi Chemical Co.): **2000** (applied in 1999).
48. Toriida, M.; Ishida, T.; Mita, S.; Tan, H., *Non-aqueous electrolyte for secondary battery and non-aqueous electrolyte secondary battery*; JP Patent 4,149,042 (Mitsui Chemicals Co.): **2000** (applied in 1998).
49. Toriida, M.; Tan, H.; Mita, S.; Ishida, T.; Ishitoku, T., *Non-aqueous electrolyte for secondary battery and non-aqueous electrolyte secondary battery*; JP Patent 4,489,207 (Mitsui Chemical Co.): **2000** (applied in 1998).
50. Hamamoto, T.; Abe, K.; Takai, T., *Electrolyte for lithium secondary battery and lithium secondary battery using the same*; JP Patent 3,633,269 (Ube Industries, Ltd.): **1999** (applied in 1998).
51. Hamamoto, T.; Abe, K.; Takai, T., *Electrolyte for lithium secondary battery and lithium secondary battery using the same*; JP Patent 3,663,897 (Ube Industries, Ltd.): **1999** (applied in 1998).
52. Hamamoto, T.; Abe, K.; Takai, T., *Electrolyte for lithium secondary battery and lithium secondary battery using the same*; JP Patent 3,633,268 (Ube Industries, Ltd.): **1999** (applied in 1998).
53. Hamamoto, T.; Abe, K.; Takai, T.; Matsumori, Y.; Ito, A., *Electrolyte having alkyne derivative and lithium secondary battery using the same*; US Patent 6,479,191 (Ube Industries, Ltd.): **2000** (applied in 1998).
54. Hamamoto, T.; Ueki, A.; Abe, K.; Matsumori, Y., *Non-aqueous electrolytic solution and lithium secondary battery*; US Patent 6,927,001 (Ube Industries, Ltd.): **2001** (applied in 1999).
55. Bito, Y.; Hasegawa, M.; Ito, S.; Murai, S.; Toyoguchi, Y.; *Non-aqueous electrolyte secondary battery*; US Patent 5,296,319 (Matsushita Electric Co, Ltd.): **1992** (applied in 1991).
56. Suzuki, H.; Kotato, M., *Non-aqueous electrolyte secondary battery*; JP Patent 3,658,517 (Mitsubishi Chemical Co.): **2000** (applied in 1999).

57. Hamamoto, T.; Abe, K.; Yuguchi, M., Non aqueous electrolytes and lithi *Non-aqueous electrolytic solution and lithium secondary battery utilizing the same*; JP Patent 3,823,712 (Ube Industries, Ltd.): **2002** (applied in 2000).
58. Shizuka, K.; Okahara, K.; Shima, K., *Electrolyte and secondary battery*; JP Patent 4,934,912 (Mitsubishi Chemical Co.): **2002** (applied in 2001).
59. Abe, K.; Miyoshi, K.; Kuwata, K.; Matsumori, Y., *Lithium secondary cell and its non-aqueous electrolyte*; US Patent 7,781,106 (Ube Industries, Ltd.): **2005** (applied in 2003).
60. Yamadaira, T., *Non-aqueous electrolyte secondary battery*; JP Patent 3,669,064 (Sony Co.): **1998** (applied in 1996).
61. Hamamoto, T.; Hitaka, A.; Nakada, Y.; Abe, K.; *Lithium secondary battery and electrolyte thereof*; US Patent 6,033,809 (Ube Industries, Ltd.): **2000** (applied in 1997).
62. Hamamoto, T.; Abe, K.; Takai, T.; Ohhira, N.; Ito, A., *Non-aqueous electrolytic solution and lithium secondary battery utilizing the same*; JP Patent 3,815,180 (Ube Industries, Ltd.): **2001** (applied in 1999).
63. Hiwara, A.; Hayashi, T.; Ishida, T.; Hirano, T., *Non-aqueous electrolyte, secondary battery utilizing them and additive for electrolyte*; JP Patent 4,190,162 (Mitsui Chemical Co.): **2002** (applied in 2001).
64. Mio, S.; Nakamura, M.; Nogi, H.; Hayashi, T.; Kobayashi, T., *Non-aqueous electrolyte solution containing cyclic sulfone compound, and lithium secondary battery*; WO2011/136189 (Mitsui Chemical Co.): **2011** (applied in 2010).
65. Utsuki, K.; Kusaji, Y.; Yamazaki, I., *Electrolyte for secondary battery and secondary battery utilizing the same*; JP Patent 4,033,074 (NEC Co.): **2004** (applied in 2002).
66. Shima, K.; Kominato, A.; Yasukawa, E.; Mori, S., *Electrolyte for lithium secondary battery*; JP Patent 3,728,791 (Mitsubishi Chemical Co.): **1997** (applied in 1996).
67. Hamamoto, T.; Abe, K.; Takai, T.; Matsumori, Y., *Non-aqueous electrolyte and lithium secondary battery using the same*; US Patent 6,436,582 (Ube Industries, Ltd.): **2000** (applied in 1998).
68. Hamamoto, T.; Abe, K.; Takai, T.; Matsumori, Y., *Non-aqueous electrolyte and lithium secondary battery utilizing the same*; JP Patent 4,320,914 (Ube Industries, Ltd.): **2001** (applied in 2000).
69. Onuki, M., *Non-aqueous electrolyte and secondary battery utilizing the same*; JP Patent 4,283,565 (Mitsubishi Chemical Co.): **2003** (applied in 2002).
70. Onuki, M., *Non-aqueous electrolyte and secondary battery utilizing the same*; JP Patent 4,283,566 (Mitsubishi Chemical Co.): **2003** (applied in 2002).
71. Kawasaki, D.; Kusachi, Y.; Numata, T.; Utsugi, K., *Secondary battery*; US Patent 8,227,116 (NEC Co.): **2005** (applied in 2003).
72. Matsui, T.; Takeyama, K., *Non-aqueous electrolyte secondary battery*; JP Patent 3,287,927 (Matsushita Electric Co, Ltd.): **1995** (applied in 1993).
73. Naruse, Y.; Fujita, S.; Komaru, A., *Non-aqueous electrolyte secondary battery*; JP Patent 3,546,566 (Sony Co.): **1997** (applied in 1995).
74. Shima, K.; Yasukawa, E.; Mori, S.; *Electrolyte for lithium secondary battery*; JP Patent 3,760,540 (Mitsubishi Chemical Co.): **1998** (applied in 1996).
75. Hamamoto, T.; Abe, K.; Takai, T.; Matsumori, Y., *Non-aqueous electrolyte and lithium secondary battery using the same*; JP Patent 4,016,497 (Ube Industries, Ltd.): **2000** (applied in 1998).
76. Gan, H.; Takeuchi, E., *Sulfate additives for Non-aqueous Electrolyte Rechargeable Cells;* US Patent 6,350,546 (Wilson Greatbatch Ltd.): **2000** (applied in 1998).
77. Shima, K.; Akawa, S.; Mori, S., *Electrolyte for lithium secondary battery*; JP Patent 3,760,539 (Mitsubishi Chemical Co.): **1998** (applied in 1996).
78. Utsuki, K.; Mori, M., *Electrolyte for secondary battery and secondary battery utilizing the same*; JP Patent 4,379,567 (NEC Co.): **2004** (applied in 2002).
79. Hiwara, A., *Non-aqueous electrolyte and secondary battery utilizing the same*; JP Patent 4,557,381 (Mitsui Chemicals Co.): **2002** (applied in 2000).
80. Yoshida, H., *Non-aqueous electrolyte battery*; JP Patent 2,734,978 (Japan Storage Battery Co, Ltd.): **1995** (applied in 1994).

81. Hamamoto, T.; Abe, K.; Takai, T., *Non-aqueous electrolyte and lithium secondary battery using the same*; US Patent 7,976,988 (Ube Industries, Ltd.): **1999** (applied in 1998).
82. Mori, S., *Non-aqueous electrolyte secondary battery*; JP Patent 5,098,171 (GS Yuasa Co.): **2007** (applied in 2005).
83. Abe, K.; Miyoshi, K.; Ushigoe, Y.; Takase, M.; Kawabe, K., *Non-aqueous electrolyte solution for lithium secondary battery and lithium secondary battery using the same*; WO2008/133112 (Ube Industries, Ltd.): **2008** (applied in 2007).
84. Furukawa, O.; Yoshimura, S.; Takahashi, M., *Non-aqueous electrolyte battery*; JP Patent 1,990,335(H7-11967) (Sanyo Electric Co, Ltd.): **1987** (applied in 1986).
85. Shoji, Y.; Uehara M.; Kita Y., *Lithium secondary battery*; JP Patent 3,244,389 (Sanyo Electric Co, Ltd.): **1996** (applied in 1994).
86. Shu, Z. X.; McMillan, R. S.; Murray, J. J.; Davidson, I. J., Use of chloroethylene carbonate as an electrolyte solvent for a graphite anode in a lithium-ion battery, *J. Electrochem. Soc.,* **1996**, *143* (7), 2230-2235.
87. McMillan, R. S.; Worsfold, D. J.; Murray, J. J.; Davidson, I. J.; Shu, Z. X., *Electrolyte comprising fluoro-ethylene carbonate and propylene carbonate, for alkali metal-ion secondary battery*; US Patent 6,506,524 (National Research Council of Canada): **1998** (applied in 1996).
88. McMillan, R. S.; Slegr, H.; Shu, Z. X.; Wang, W., Fluoroethylene carbonate electrolyte and its use in lithium ion batteries with graphite anodes, *J. Power Sources.,* **1999**, *81-82*, 20-26.
89. Winter, M.; Imhof, R.; Joho, F.; Novák, P., FTIR and DEMS investigations on the electroreduction of chloroethylene carbonate-based electrolyte solutions for lithium-ion cells, *J. Power Sources.,* **1999**, *81-82*, 818-823.
90. Inaba, M.; Kawatate, Y.; Funabiki, A.; Jeong, S.; Abe, T.; Ogumi, Z., STM study on graphite/electrolyte interface in lithium-ion batteries: solid electrolyte interface formation in trifluoropropylene carbonate solution, *Electrochim. Acta* **1999**, *45*, 99-105.
91. Arai, J.; Katayama, H.; Akahoshi, H., Binary mixed solvent electrolytes containing trifluoropropylene carbonate for lithium secondary batteries, *J Electrochem. Soc.,* **2002**, *149* (2), A217-A226.
92. Hamamoto, T.; Abe, K.; Takai, T.; *Electrolyte for lithium secondary battery and lithium secondary battery utilizing the same*; JP Patent 4,045,644 (Ube Industries, Ltd.): **1999** (applied in 1998).
93. Igawa, Y., Shiga, T., *Lithium secondary battery*; JP Patent 4,253,921 (Toyota Central R&D Labs, Inc.): **2000** (applied in 1999).
94. Abe, K.; Kuwata, T.; Hattori, T.; Matsumori, Y., *Non-aqueous electrolytic solution and lithium secondary battery employing the same*; US Patent 7,297,442 (Ube Industries, Ltd.): **2003** (applied in 2002).
95. Hiwara, A.; Yokoyama, K.; Fujita, S.; Naruse, Y.; Omaru, A., *Non-aqueous electrolyte and non-aqueous electrolyte battery*; JP Patent 3,821,495 (Mitsui Chemical Co. & Sony Co.): **1996** (applied in 1994).
96. Gan, H.; Takeuchi, E.; Rubino, R., *Phosphate additives for non-aqueous electrolyte rechargeable electrochemical cells*; US Patent 6,919,141 (Wilson Greatbatch Technologies, Inc.): **1999** (applied in 1998).
97. Noda, D.; Oonuki, M.; Shima, K., *Non-aqueous electrolyte solution and non-aqueous electrolyte solution secondary battery employing the same*; US Patent 7,169,511 (Mitsubishi Chemical Co): **2004** (applied in 2002).
98. Ota, H.; Kominato, A.; Chun, W.; Yasukawa, E.; Kasuya, S., Effect of cyclic phosphate additive in non-flammable electrolyte, *J. Power Sources.,* **2003**, *119-121*, 393-398.
99. Kanno, N., *Non-aqueous electrolyte secondary battery*; JP Patent 3,060,505 (Sony Co.): **1992** (applied in 1990).
100. Gan, H.; Takeuchi, E., *Organic carbonate additives for non-aqueous electrolyte in alkali metal electrochemical cells*; US Patent 5,753,389 (Wilson Greatbatch Ltd.): **1996** (applied in 1995).
101. Tsutsumi, M.; Horiuchi, H.; Miyashita, T.; Yoshio, M; Yoshitake, S., *Ionic conductor for lithium secondary battery and lithium secondary battery utilizing the same*; JP Patent 3,416,016 (Fujitsu Ltd. & Ube Industries, Ltd.): **1998** (applied in 1997).

102. Kusumoto, Y.; Yoshimura, S.; Nouma, T.; Nishio, K., *Non-aqueous electrolyte battery*; JP Patent 3,439,079 (Sanyo Electric Co, Ltd.): **1999** (applied in 1997).
103. Kusumoto, Y.; Oshita, R.; Nouma, T., *Non-aqueous electrolyte battery*; JP Patent 3,369,947 (Sanyo Electric Co, Ltd.): **1999** (applied in 1998).
104. H, Noh.; E, Song., *Electrolyte for rechargeable lithium battery and rechargeable lithium battery comprising same*; US Patent 7,226,703 (Samsung SDI Co., Ltd.): **2004** (applied in 2003).
105. Tsukahara, J.; Negoro, M.; Okazaki, M.; Ishizuka, H., *Non-aqueous electrolyte secondary battery*; JP Patent 3,937,482 (Ube Industries, Ltd): **1998** (applied in 1996).
106. Hamamoto, T.; Abe, K.; Takai, T.; Matsumori, Y.; Miyoshi, K.; Ueki, A., *Lithium secondary battery electrolyte and lithium secondary battery using the same*; US Patent 6,413,677(Ube Industries, Ltd): **2000** (applied in 1998).
107. Hamamoto, T.; Abe, K.; Takai, T.; Matsumori, Y., *Non-aqueous secondary battery having increased discharge capacity retention*; US Patent 7,691,539 (Ube Industries, Ltd): **2000** (applied in 1998).
108. Hamamoto, T.; Abe, K.; Takai, T,; Matsumori, Y.; Miyoshi, K.; Ueki, A.; *Non-aqueous secondary battery having enhanced discharge capacity retention*; US Patent US 6,866,966 (UBE Industries, Ltd): **2001** (applied in 1999).
109. Hamamoto, T.; Abe, K.; Ueki, A., *Non-aqueous electrolytic solution and lithium secondary battery*; US Patent US 7,968,220 (Ube Industries, Ltd): **2001** (applied in 2000).
110. Abe, K.; Takaya, T.; Yoshitake, H.; Ushigoe, Y.; Yoshio, M.; Wang, H., Functional electrolyte: Additives for improving the cyclability of cathode materials, *Electrochem. Solid-State Lett.,* **2004**, *7*(12), A462-A465.
111. Kang, E.; Kang, K.; Lee, H.; Woo, *J.*, *Electrolyte of high temperature property and overcharge-prevention property and secondary battery employed with the same*; EP Patent 2,089,931 (LG Chem Ltd.): **2007** (applied in 2006).
112. Shimizu, R.; Adachi, M., *Non-aqueous electrolyte secondary battery*; JP Patent 3,809,657 (Sony Co.): **1995** (applied in 1994).
113. Shimizu, R., *Non-aqueous electrolyte secondary battery*; US Patent 5,709,968 (Sony Co.): **1997** (applied in 1995).
114. Huanyu, M., *Polymerizable aromatic additives for overcharge protection in non-aqueous rechargeable lithium batteries*; US patent 5,879,834 (NEC Moli Energy (Canada) Ltd.): **1997** (applied in 1995).
115. Tsukahara, J; Neku, M.; Tanaka, M., *Non-aqueous electrolyte secondary battery*; JP Patent 4,210,956 (Fujifilm Co.): **1998** (applied in 1996).
116. Kita, K.; Yumiba, H.; Toguchi M.; Matsumoto, K., *Organic electrolyte secondary battery*; JP Patent 3,354,057 (Hitachi Maxell Co.): **1998** (applied in 1996).
117. Kita, K.; Yumiba, H.; Matsumoto, K., *Organic electrolyte secondary battery*; JP Patent 3,275,998 (Hitachi Maxell Co.): **1998** (applied in 1997).
118. Huanyu, M.; Stanlay, D., *Non-aqueous rechargeable lithium battery*; JP Patent 3,575,735 (NEC Moli Energy (Canada) Ltd.): **1998** (applied in 1997).
119. Reimers, J.; Way, M., *Additives for overcharge protection in non-aqueous rechargeable lithium batteries*; US Patent 6,074,777 (NEC Moli Energy (Canada) Ltd.): **1998** (applied in 1997).
120. Takahashi, M.; Yamaguchi, H.; Abe, K.; Ueki, A.; Takai, T., *Electrolyte for non-aqueous battery and secondary battery utilizing the same*; JP Patent 2,963,898 (Sanyo Electric Co. Ltd. & Ube Industries Ltd.): **1999** (applied in 1998).
121. Takahashi, M.; Yasutake, Y.; Abe, K.; Ueki, A.; Takai, T., *Non-aqueous secondary battery*; JP Patent 2,983,205 (Sanyo Electric Co. Ltd. & Ube Industries Ltd.): **1999** (applied in 1998).
122. Takahashi, M.; Yasutake, Y.; Abe, K.; Ueki, A.; Takai, T., *Electrolyte for non-aqueous battery and secondary battery utilizing the same*; JP Patent 2,939,468 (Sanyo Electric Co. Ltd. & Ube Industries Ltd.): **1999** (applied in 1998).

123. Takahashi, M.; Yamaguchi, H.; Abe, K.; Ueki, A.; Takai, T., *Electrolyte for non-aqueous battery and secondary battery utilizing the same*; JP Patent 2,928,779 (Sanyo Electric Co. Ltd. & Ube Industries Ltd.): **1999** (applied in 1998).
124. Takahashi, M.; Ito, K.; Yasutake, Y.; Yamaguchi, N.; Abe, K.; Ueki, A.; Takai, T., *Electrolyte for non-aqueous battery and secondary battery utilizing the same*; JP Patent 2,939,469 (Sanyo Electric Co. Ltd. & Ube Industries Ltd.): **1999** (applied in 1998).
125. Takahashi, M.; Yasutake, Z.; Abe, K.; Ueki, A.; Hamamoto, T., *Lithium secondary battery*; US Patent 6,632,572 (Sanyo Electric Co. & Ube Industries Ltd): **2000** (applied in 1999).
126. Watanabe, S.; Iwamoto, K.; Ueda, A.; Nunome, J.; Koena, S., *Non-aqueous electrolyte secondary cell and device using the same*; WO 2001-03226 (Panasonic Co.): **2001** (applied in 1999).
127. Hamamoto, T.; Abe, K.; Matshumori, Y., *Non-aqueous electrolyte and lithium secondary battery using the same*; US Patent 6,503,662 (Ube industries Ltd.): **2001** (applied in 1999).
128. Hamamoto, T.; Abe, K.; Yuguchi, M.; Matsumori, Y., *Non-aqueous electrolyte and lithium secondary battery utilizing the same*; JP Patent 3,610,898 (Ube Industries Ltd.): **2002** (applied in 2000).
129. Abe, K.; Matsumori, Y.; Ueki, A., *Non-aqueous electrolytic solution and lithium secondary batteries*; US Patent 7,294,436 (Ube Industries Ltd.): **2002** (applied in 2001).
130. Hamamoto, T.; Ueki, A.; Abe, K.; Miyoshi, K., *Lithium secondary battery and non-aqueous electrolytic solution*; US Patent 7,981,552 (Ube Industries Ltd.): **2002** (applied in 2000).
131. Watanabe, S.; Goto, S.; Ishida, S.; Takagi, S.; Hamamoto, T.; Ueki, A.; Abe, K., *Electrolyte for non-aqueous cell and non-aqueous secondary cell*; US Patent 7,824,809 (Panasonic Co. & Ube Industries Ltd.): **2002** (applied in 2000).
132. Watanabe, S.; Goto, S.; Ishida, S.; Takagi, S.; Hamamoto, T.; Ueki, A.; Abe, K., *Electrolyte for non-aqueous cell and non-aqueous secondary cell*; US Patent 7,867,657 (Panasonic Co. & Ube Industries Ltd.): **2002** (applied in 2000).
133. Abe, K.; Matsumori, Y.; Ueki, A., *Non-aqueous electrolytic solution and lithium secondary batteries*; US Patent 7,615,316 (Ube Industries Ltd.): **2002** (applied in 2001).
134. Ueki, A.; Abe, K.; *Non-aqueous electrolyte and lithium secondary battery utilizing the same*; JP Patent 4,352,622 (Ube Industries Ltd.): **2002** (applied in 2001).
135. Shima, K.; Shiduka, K., *Non-aqueous electrolyte solution and non-aqueous electrolyte solution secondary battery using the same*; US Patent 7,144,660 (Mitsubishi Chemical Co.): **2002** (applied in 2001).
136. Takehara, M.; Shima, K.; *Non-aqueous electrolyte and lithium secondary battery utilizing the same*; JP Patent 4,337,359 (Mitsubishi Chemical Co.): **2003** (applied in 2002).
137. Abe, K.; Hattori, T.; Kuwata, T.; Matsumori, Y., *Lithium secondary battery employing fluorine-substituted cyclohexylbenzene containing electrolytic solution*; US Patent 7, 537,861 (Ube Industries Ltd.): **2004** (applied in 2002).
138. Buhrmester, C.; Chen, J.; Moshurchak, L.; Jiang, J.; Wang, R.; Dahn, J. R.; Studies of aromatic redox shuttle additives for LiFePO4-based Li-ion cells, *J. Electrochem. Soc.,* **2005**, *152*, A2390-A2399.
139. Buhrmester, C.; Moshurchak, L.; Wang, R.; Dahn, J., Phenothiazine molecules: Possible redox shuttle additives for chemical overcharge and overdischarge protection for lithium-ion batteries, *J. Electrochem. Soc.,* **2006**, *153*, A288-A294.
140. Ue, M., *Nonflammable electrolyte for lithium battery*; JP Patent 3,274,102 (Mitsubishi Chemical Co.): **1999** (applied in 1990).
141. Wang, X.; Yamada, C.; Naito, H.; Segami, G.; Kibe, K., High-concentration trimethyl phosphate-based nonflammable electrolytes with improved charge–discharge performance of a graphite anode for lithium-ion cells, *J. Electrochem. Soc.,* **2006**, *153*(1), A135-A139.
142. Kajiwara, N.; Ogino, T.; Miyazaki, T.; Kawagoe, T., *Non-aqueous electrolyte battery*; JP Patent 3,055,358 (Bridgestone Ltd.): **1994** (applied in 1992).
143. Dan, P.; Geronov, J.; Luski, S.; Emil, M.; Aurbach, D., *Non-aqueous safe secondary cell*; US Patent 5, 506,068 (Tadiran Ltd.): **1995** (applied in 1994).

144. Hamamoto, T.; Abe, K.; Takai, T., *Non-aqueous electrolyte and lithium secondary battery utilizing the same*; JP Patent 4,192,367 (Ube Industries Ltd.): **2001** (applied in 1999).
145. Arai, J.; Yamauchi, S.; Kobayashi, M., *Lithium secondary battery*; US Patent 7,074,523 (Hitachi, Ltd.): **2002** (applied in 2001).
146. Ihara, M.; Hang, B.; Sato, K..; Egashira, M.; Okada, S.; Yamaki, J., Properties of carbon anodes and thermal stability in $LiPF_6$/Methyl difluoroacetate electrolyte, *J. Electrochem. Soc.,* **2003**, *150*(11), A1476-A1483.
147. Ono, A.; Yoshino, A., *Non-aqueous battery*; JP Patent 2,110,644(H5-86032) (Asahi Kasei Co.): **1990** (applied in 1989).
148. Akutsu, M.; Kubota, N.; Mashita, S., *Non-aqueous battery*; JP Patent 3,583,193 (ADEKA Co.): **1997** (applied in 1995).
149. Hamamoto, T.; Abe, K.; Takai, T.; Matsumori, Y., *Non-aqueous electrolyte and lithium secondary battery utilizing the same*; JP Patent 4,147,691 (Ube Industries, Ltd.): **2001** (applied in 1999).
150. Kim, D.; Yoon, J.; Kim, Y.; Cho, B.; Jeong, J.; Jeong, D.; Bae, *Additive for lithium secondary battery*; JP Patent 4,543,085 (LG Chem Ltd.): **2005** (applied in 2004).
151. Shimizu, R.; Yamaguchi, T.; Jung, C.; Chung, H.; Chang, Y., *Lithium rechargeable battery and lithium rechargeable battery pack*; US Patent 7,776,475 (Samsung SDI Co., Ltd.): **2006** (applied in 2004).
152. Kim, Y.; Ahn, S.; Bae, J.; Ku, C.; Ha, S; Ryu, D; Yoon, S., *Non-aqueous electrolyte and electrochemical device with an improved safety*; WO2007/081169 (LG Chem Ltd.): **2007** (applied in 2006).
153. The Condensed Chemical Dictionary: 7th Ed.; Rose, A.; Rose, E., *Reinhold publishing Corporation*: New York, 1968.
154. Armand, M.; Gauthier, M.; Muller, D., *New ion conductive material composed of a salt in solution in a liquid electrolyte*; US Patent 5,021,308 (Hydro-Quebec): **1988** (applied in 1986).
155. Wühr, M. *Electrolyte for use in a galvanic cell*; US Patent 5,660,947 (University of Regensburg): **1996** (applied in 1993).
156. Barthel, J.; Buestrich, R.; Gores, H. J.; Schmidt, M.; Wühr, M. *Process for preparing lithium-borate complexes*; DE Patent 59,704,609 (Merck Patent GmbH): **1998** (applied in 1996).
157. Barthel, J.; Buestrich, R.; Carl, E.; Gores, H. J., A new class of electrochemically and thermally stable lithium salts for lithium battery electrolytes, *J. Electrochem. Soc.,* **1996**, *143*, 3565-3571.
158. Wietelmann, U.; Lischka, U.; Wegner, M., *Lithium bisoxalatoborate, the production thereof and its use as a conducting salt*; US Patent 6,506,516 (Metallgesellschaft Aktiengesellschaft): **2000** (applied in 1998).
159. Tsujioka, S.; Takase, H.; Takahashi, M.; Sugimoto H.; Koide, M., *Electrolyte for electrochemical device*; US Patent 6,783,896 (Central Glass Co., Ltd.): **2002** (applied in 2000).
160. Ivanov, S.; Casteel, W.; Bayley, W., *Process for the purification of lithium salts*; US Patent 7,981,388 (Air Products): **2006** (applied in 2004).
161. Sartori, P.; Ignatyev, N., *Lithium fluorophosphates and their use as a conducting salts*; US Patent 6,210,830 (Merck Patent GmbH): **1998** (applied in 1996).
162. Oshita, R.; Fujimoto, M.; Nouma, T.; Nishio, K., *Non-aqueous electrolyte secondary battery*; JP Patent 3,439,085 (Sanyo Electric Co., Ltd.): **1999** (applied in 1997).
163. Kato, R.; Suzuki, H., *Production method of difluoro phosphate salt*; JP Patent 4,483,221 (Mitsubishi Chemical Co): **2005** (applied in 2003).

Chapter 4
Recent Advances in Ionic Liquids for Lithium Secondary Batteries

Hajime Matsumoto

4.1 Introduction

Ionic liquids (ILs) composed only of ionic species without any organic molecules possess various unique properties such as reduced flammability, reduced volatility, and a relatively high ionic conductivity at ambient temperature. The existence of ILs has become especially popular in various fields during the past two decades due to the discovery of moisture-insensitive ILs based on perfluoroanions—such as tetrafluoroborate $[BF_4]^-$, and bis(trifluoromethylsulfonyl)amide $[(CF_3SO_2)_2N]^-$, denoted as Tf_2N^-—which are easy to prepare and handle under atmospheric conditions [1]. At the same time, these perfluoroanions have attracted attention as a nonflammable electrolyte for various electrochemical energy devices, especially for lithium secondary batteries, because these perfluoroanions have already been examined as a counter anion for lithium salts [2]. The number of papers about battery applications using these ILs has increased during the past decade since early reports indicated their compatibility with conventional composite electrodes such as lithium cobalt dioxide, $LiCoO_2$ [3–5]. Although various cathodes and anodes, and almost all composite electrodes, have been investigated, except for one carbon-based anode found to be compatible with these ILs, their performance, especially their rate performance, was found to be quite deficient compared to a conventional organic electrolyte. During the past decade, only a few anionic species have been developed to solve various defects derived from the conventional ILs. In particular, one of these new anions, bis(fluorosulfonyl)amide, denoted as $[(FSO_2)_2N]^-$, dramatically reverses the poor impression of ILs as a lithium battery electrolyte [6–9]. Recent research on the thermal stability of ILs, which have been seriously investigated since the appearance of new ILs composed of $[(FSO_2)_2N]^-$, revealed that the ILs are

H. Matsumoto (✉)
Institute for Ubiquitous Energy, Devices National Institute of Advanced Industrial Science and Technology (AIST), 1-8-31 Midorigaoka, Ikeda, Osaka 563-8577, Japan
e-mail: h-matsumoto@aist.go.jp

T.R. Jow et al. (eds.), *Electrolytes for Lithium and Lithium-Ion Batteries*,
Modern Aspects of Electrochemistry 58, DOI 10.1007/978-1-4939-0302-3_4,

indeed harder to ignite; however, once ignited by an external source of energy, significantly high heat release occurs when the ILs burn under forced conditions [10]. Furthermore, not all ILs exhibited an expected safety feature as a nonflammable electrolyte under severe conditions such as the charged state [11, 12]. However, such facts have not reduced motivation for studying ILs as a battery electrolyte because various new results on next-generation batteries, which do not operate well in a conventional organic electrolyte, are beginning to be published, for example, Li-Air [13, 14], Li-S [15], and sodium secondary batteries [16]. In this chapter, the recent progress regarding the study of ILs for a lithium battery system will be briefly described. Especially, the course of development of new anionic species during the past decade will be the focus in order to demonstrate the difference between these new anions and a conventional anion, such as $[(CF_3SO_2)_2N]^-$ or $[BF_4]^-$. Since there are many reports on the ILs for use as a battery electrolyte and also their basic electrochemical properties, all the reports could not be referred in this chapter, but several books and reviews are recommended [17–21].

4.2 Research and Development of Ionic Liquids for Battery Electrolytes During the Past Decade

4.2.1 Conventional Ionic Liquids Composed of $[Tf_2N]^-$ and $[BF_4]^-$

The explosive research and development of ionic liquids (ILs) and their applications started with the discovery of moisture-insensitive ILs composed of perfluoroanions, tetrafluoroborate, $[BF_4]^-$ [22], and bis(trifluoromethylsulfonyl)amide, $[(CF_3SO_2)_2N]^-$, denoted as Tf_2N^- [23, 24]. Various features pointed out for ILs, such as a lower volatility, a lower combustibility, and high thermal stability have been realized by the ILs composed of the two representative anions, and not all the ILs [25]. At the same time, these unique features also attracted attention as a safe lithium battery electrolyte, which is not obtained using conventional organic electrolytes. Figure 4.1 shows that the number of articles searched in Thomson Reuters' *Web of Science* using the keywords "("ionic liquid*" or "molten salt*") and batter*," was over 1,800 as of March 27, 2013. Most of the papers were published after 2003, and the number significantly increased with each passing year of the decade. Fundamental results on the use of these conventional ILs for typical lithium battery systems were reported around 2003 [3–5]. Except for cell performance, a 4-V class half-cell using a lithium cobalt oxide cathode [3] and a 2.5-V class full-cell using the same cathode and a lithium titanate anode ($Li_4Ti_5O_{12}$) [4, 5] operated using only the ILs without any organic additives such as vinylenecarbonate. These early studies developed a conventional composite electrode suitable for an organic electrolyte that could also be used by ILs. Furthermore, it seems fortunate that these two fundamental perfluoroanions $[Tf_2N]^-$ and $[BF_4]^-$, have already been practically used as a counter anion of their lithium salt before they were employed as a component of representative

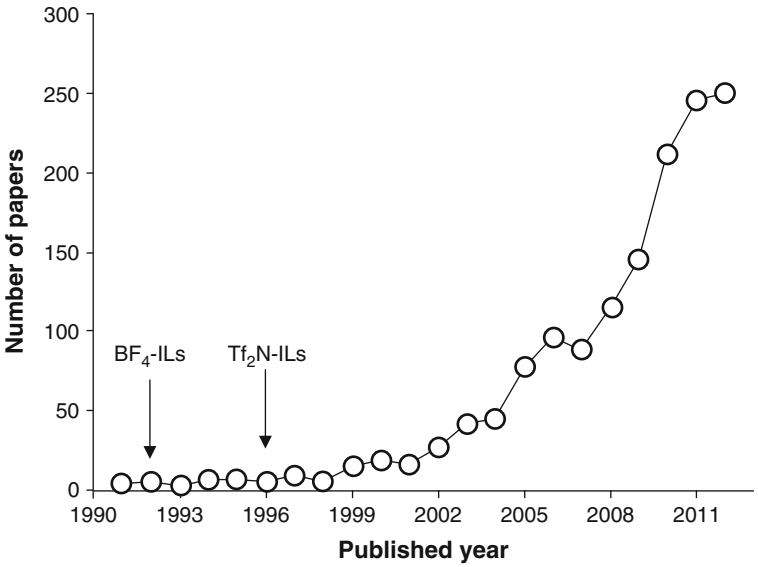

Fig. 4.1 Number of papers searched by Thomson Reuters' *Web of Science* as of March 27, 2013. Keywords: *Ionic liquid** and *battery*

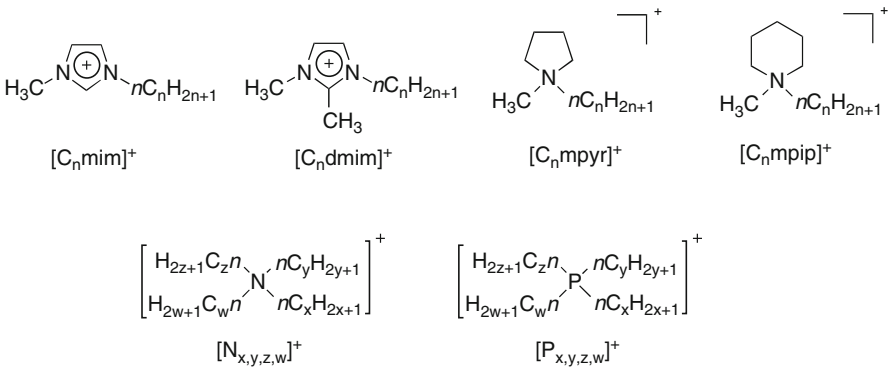

Fig. 4.2 Structure of typical cations used in lithium battery research

ILs, which means that the good availability of these anions as a lithium salt with high purity has promoted further investigations.

Both conventional anions form ILs not only with the most typical aromatic cation, such as 1-ethyl-3-methylimidazolium, which is denoted as $[C_2mim]^+$, but also a aliphatic quaternary ammonium as shown in Fig. 4.2; however, almost all the studies on the ILs for battery applications adopted ILs containing $[Tf_2N]^-$ not $[BF_4]^-$ due to significant differences between the two. The amide-based ILs are immiscible in water, and the borate-based ILs are miscible. The residual raw materials such as alkali metal salts in the immiscible ILs can be removed by washing with water;

however, the miscible ILs cannot use such a cleaning process. Except for this impurity problem, amide anions such as $[Tf_2N]^-$ can form ILs with many aliphatic onium cations.

Although quite a few examples of aliphatic quaternary ammonium ILs composed of $[BF_4]^-$, such as *N*,*N*-diethyl-*N*-methyl-*N*-(2-methoxyethyl)ammonium tetrafluoroborate, which is denoted as $[N_{2,2,1,2O1}][BF_4]$ [26], were reported, their viscosity was much higher (ca. over 300 mPa s at r.t.) than the corresponding Tf_2N salts (69 mPa s at r.t.) [27]. Furthermore, it was quite important that the $[Tf_2N]^-$ forms relatively low viscosity ILs with a cyclic quaternary ammonium such as C_3mpyr^+ (*N*-methyl-*N*-propylpyrrolidinium) [24], which shows a slightly higher viscosity (53 mPa s at r.t.) than the lowest $[C_2mim][Tf_2N]$ (35 mPa s at r.t.). Such ILs composed of an aliphatic quaternary ammonium (AQA) exhibit a much wider electrochemical window toward both the cathodic and anodic region than that for the ILs composed of the $[C_2mim]^+$ [20]. In the AQA-ILs, lithium metal plating and stripping could be observed without any organic additives such as a carbonate molecule [28–30], which guaranteed the possibility of constructing a 4-V class half-cell using $LiCoO_2$ as stated above. Indeed, the electrochemical stability of the ILs should be considered for stable charge and discharge cycling; however, the electrochemical stability, especially in the cathodic region, is known to be apparently expanded in the negative direction with the presence of a certain amount of a lithium salt [6, 31].

Though the phenomena are not clearly understood, various possibilities have been discussed. The decomposition of $[Tf_2N]^-$ in the cathodic region due to the coexisting of Li^+ would initiate a SEI (solid electrolyte interphase) formation on the surface of the negative electrode, which blocks the further decomposition of the component ions [32]. On the other hand, recent fundamental surface analysis of a metal electrode–ILs interface revealed that a unique layer structure composed of an ionic species was formed above the electrode surface [33]. If the first layer near the electrode surface consists of ionic species, such as Li^+, $[Tf_2N]^-$ or $[Li(Tf_2N)_2]^-$ [34], the surface ionic layer would act like a SEI, preventing the electrochemical reduction of the cationic species. However, considering the fact that a carbon anode has been known to be unsuccessfully operated in the ILs composed of $[Tf_2N]^-$ due to the co-intercalation of the cationic species [35], the conceivable surface structure or SEI might not exist on the surface of a carbon anode, or if it existed, it might not prevent the cation intercalation. The addition of carbonate molecules such as ethylenecarbonate and vinylenecarbonate as additives could solve these problems [36]; however, the co-existing volatile organic molecule in the ILs must negate the unique features of the ILs. In addition to these negative points for constructing a full-cell using $[Tf_2N]^-$-based ILs, a significant viscosity increase with the addition of a certain amount of $Li[Tf_2N]$ has known to be a major drawback. There is no doubt that the $[Tf_2N]^-$ contributes to the possibility of ILs being a unique electrolyte for a lithium secondary battery; however, the limitation for actual application has become apparent. In the next section we will describe the development of new anionic species to provide better results not only for the basic physical properties, but also for the performance of a lithium secondary battery using these new ILs.

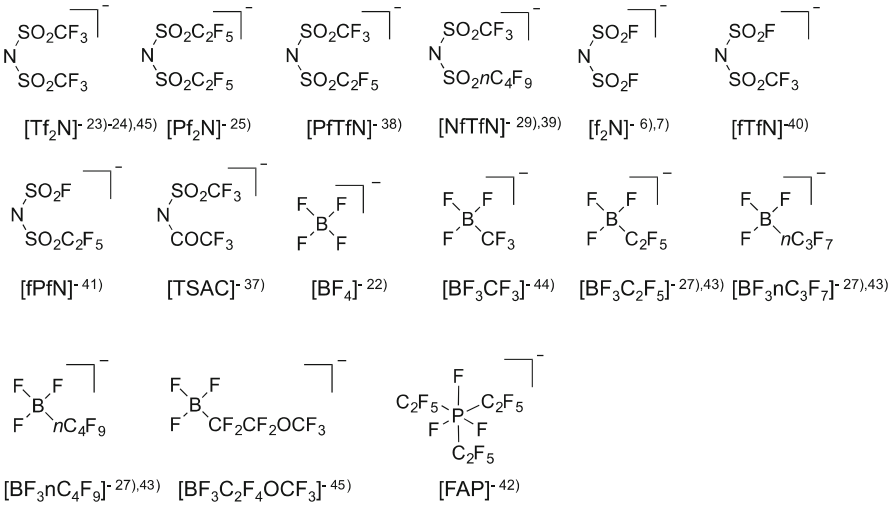

Fig. 4.3 Structure of typical anions used in lithium battery research and recently developed anions

4.2.2 New Ionic Liquids Composed of New Anions Developed During the Past Decade

Over the past decade, only a few anionic species have appeared, and the ILs composed of these new anions have played an important role in overcoming the defects of the commonly used ILs composed of $[Tf_2N]^-$ and $[BF_4]^-$, as stated in the previous section. New typical perfluoroanions are shown in Fig. 4.3. The concept of preparing these new anions is structural modification of the conventional anions, such as $[Tf_2N]^-$ and $[BF_4]^-$. In case of amide anions, various asymmetric amide anions were reported, such as $[TSAC]^-$ [37], $[PfTfN]^-$ [38], $[NfTfN]^-$ [39], $[fTfN]^-$ [40] and $[fPfN]^-$ [41]. On the other hand, in case of borate and phosphate anions, a perfluoroalkyl substitution of a fluorine atom in the $[BF_4]^-$ and $[PF_6]^-$ were also reported, such as $[FAP]^-$ [42], $[BF_3nC_4F_9]^-$ [43], $[BF_3nC_3F_7]^-$ [44], $[BF_3C_2F_4OCF_3]^-$ [45]. As stated above, the ILs composed of $[BF_4]^-$ have various drawbacks compared to ILs composed of $[Tf_2N]^-$. However, when one fluorine atom in $[BF_4]^-$ was replaced by a perfluoroalkyl group ($-R_F$), the resulting anions $[BF_3R_F]^-$, form water-immiscible ILs with various cations, such as $[N_{4,2,2,1}]^+$ (*N*-butyl-*N*,diethyl-*N*-butylammonium) [27] and $[C_4mpyr]^+$ (*N*-butyl-*N*-methylpyrrolidinium) [46], the salts of which are composed of $[BF_4]^-$ and exhibit very high melting points ($[N_{4,2,2,1}][BF_4]$: 165 °C, $[C_4mpyr][BF_4]$:150 °C). Furthermore, the viscosity of the ILs composed of $[BF_3R_F]^-$ significantly decreased as compared to the corresponding $[BF_4]$ melt (ex. $[N_{2,2,1,2O1}][BF_3CF_3]$ (trifluoromethyltrifluoroborate, $[BF_3CF_3]^-$): 108 mPa s at r.t. $[N_{2,2,1,2O1}][BF_4]$: 426 mPa s at r.t.) [27]. In connection with the effect of the substitution of a fluorine atom by an R_F- group, tris(pentafluoroethyl)trifluorophosphate ($[(C_2F_5)_3F_3P]^-$, which is denoted as FAP^-) was another important example [42].

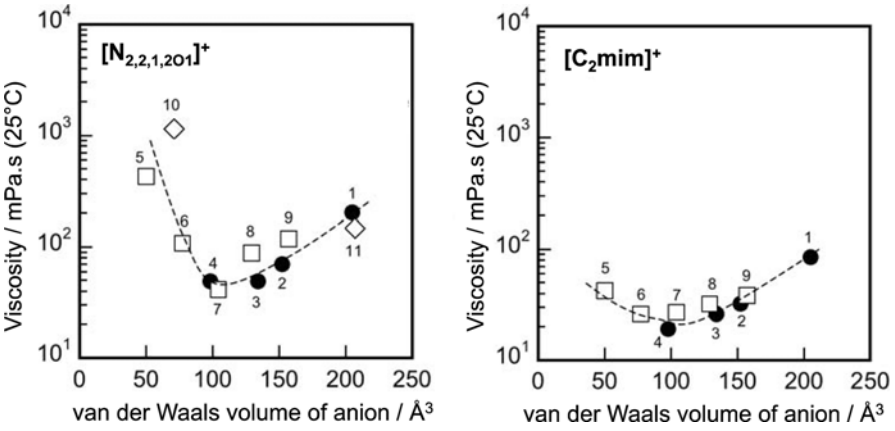

Fig. 4.4 Anion size dependence of viscosity of ILs. (*1*) $[Pf_2N]^-$, (*2*) $[Tf_2N]^-$, (*3*) $[TSAC]^-$, (*4*) $[f_2N]^-$, (*5*) $[BF_4]^-$, (*6*) $[BF_3CF_3]^-$, (*7*) $[BF_3C_2F_5]^-$, (*8*) $[BF_3nC_3F_7]^-$, (*9*) $[BF_3nC_4F_9]^-$, (*10*) $[PF_6]^-$, (*11*) $[FAP]^-$

The anions were reported as a counter anion for new a lithium salt [47] and also ILs [42], which improved the well-known defects of $[PF_6]^-$ such as a hydrolyzability.

Contrary to the fact that a $[PF_6]^-$ has been practically used as the counter anion of a supporting electrolyte for a conventional organic electrolyte, there have been few reports about ILs based on $[PF_6]^-$ because of their poor physical properties. The viscosity of ILs composed of $[PF_6]^-$ are much higher than that of corresponding amides and borates. For example, $[N_{2,2,1,2O1}][PF_6]$ has over 1×10^3 mPa s at r.t. [48], which is about 14 times greater than the corresponding amides, such as $[N_{2,2,1,2O1}][Tf_2N]$ (69 mPa s at r.t.) [27], which means that the diffusivity of Li^+ in the $[N_{2,2,1,2O1}][PF_6]$ was over ten times lower than that in $[N_{2,2,1,2O1}][Tf_2N]$ according to the Stokes–Einstein equation. The modified phosphate anion $[FAP]^-$, decreases the viscosity of the ILs about one-seventh as compared to the corresponding $[PF_6]^-$ melts ($[N_{2,2,1,2O1}][FAP]$: 146 mPa s at r.t.) [48]. The melting point of the ILs composed of $[FAP]^-$ also decreased due to the existence of an electron withdrawing group ($-R_F$) as in the case of $[BF_3R_F]^-$, which increase the dispersibility of a negative charge in order to reduce the electrostatic interactions between the cations and anions. The mobility and flexibility of the $-R_F$ group might disturb the close packing between an anion and a cation. The effect of the $-R_F$ group on the diffusivity of ions in the ILs was well reproduced by molecular dynamics simulations [49].

The favorable effect of the substitution of an $-R_F$ group on the physical properties of ILs as stated above was not established in perfluorosulfonylamide. Contrary to the above-mentioned borate anions and phosphate anions, the longer was the length of the perfluoroalkyl group in a perfluorosulfonylamide, the higher was the viscosity. For example, the viscosity of *N*,*N*,*N*-trimethyl-*N*-propylammonium bis(trifluoromethylsulfonyl)mide ($[N_{3,1,1,1}][Tf_2N]$) (72 mPa s at r.t.), which is the smallest aliphatic quaternary ammonium cation forming ILs with $[Tf_2N]^-$ [50], significantly increased by changing the anion from $[Tf_2N]^-$ to pentafluoroethyl(trifluor

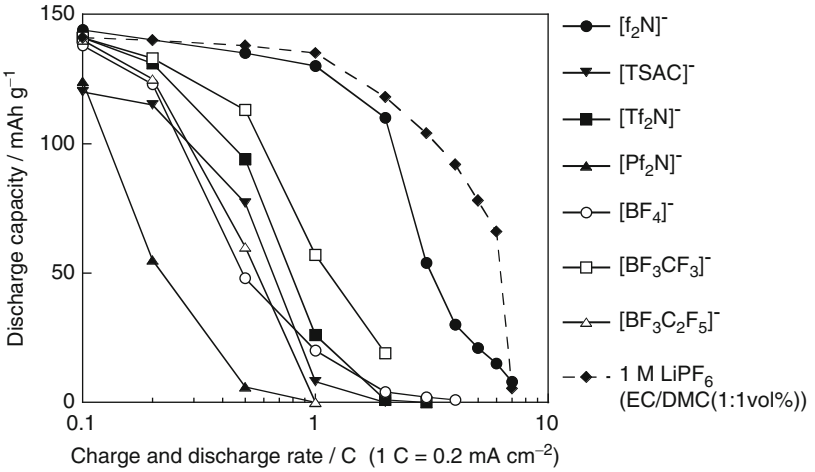

Fig. 4.5 Charge–discharge rate property of Li/$LiCoO_2$ cell using ILs composed of $[N_{2.2.1.2O1}]^+$. Lithium salt concentration: ca. 0.5 mol dm^{-3}. $T = 25$ °C

omethylsulfonyl)amide ($[C_1C_2]^-$) ($[N_{3,1,1,1}][C_1C_2]$:174 mPa s at r.t.) [38]. In the perfluoroamide, the molecular size should be reduced to decrease the viscosity.

Figure 4.4 shows the viscosity of various ILs composed of $[N_{2,2,1,2O1}]^+$, which suggest that the viscosity of the ILs composed of perfluoroanions depends on the size of the anions and there exists a lower minimum at about 100 Å^3 [48]. Within the range of the molecular size shown in Fig. 4.4, ILs composed of bis(fluorosulfonyl) amide ($[f_2N]^-$), ($[N_{2,2,1,2O1}][f_2N]$) exhibited the lowest viscosity. The fact that not only $[N_{2,2,1,2O1}]^+$, but also $[C_2mim]^+$, gave the same tendency implies that $[f_2N]^-$ provides the lowest viscosity ILs composed of perfluoroanions. However, the most remarkable fact about $[f_2N]^-$ was their uncommon abilities to overcome various unavoidable defects observed when using ILs composed of $[Tf_2N]^-$. For example, a carbon anode could operate without any additives even in $[C_2mim][f_2N]$ [7]. Also, the deposition and redissolution of lithium could be observed in the same ILs and under the same condition [6].

Furthermore, as shown in Fig. 4.5, the rate property of the $LiCoO_2$ half-cell using $[f_2N]^-$-based ILs was much better than the other various ILs [48]. This result was derived from their low viscosity that increased with the addition of a lithium salt and low interfacial charge transfer resistance on the lithium metal anode and $LiCoO_2$ composite cathode [48]. Not only theoretical studies on the $[f_2N]^-$ in ab initio calculations [51, 52], but also the solution chemistry [53], imply that a significant difference was present between the $[f_2N]^-$ and the other perfluoroamide, such as $[Tf_2N]^-$, regarding the interaction between Li^+ and $[f_2N]^-$ and also between $[f_2N]^-$ and a lithium metal and the complex structure around a Li^+. These differences must be attributed to the existence of the FSO_2- group.

Recent studies of a hybrid amide, such as $[fTfN]^-$ containing both the FSO_2^- and $CF_3SO_2^-$ moiety, revealed that the ILs composed of fluorosulfonyl(trifluorosulfon

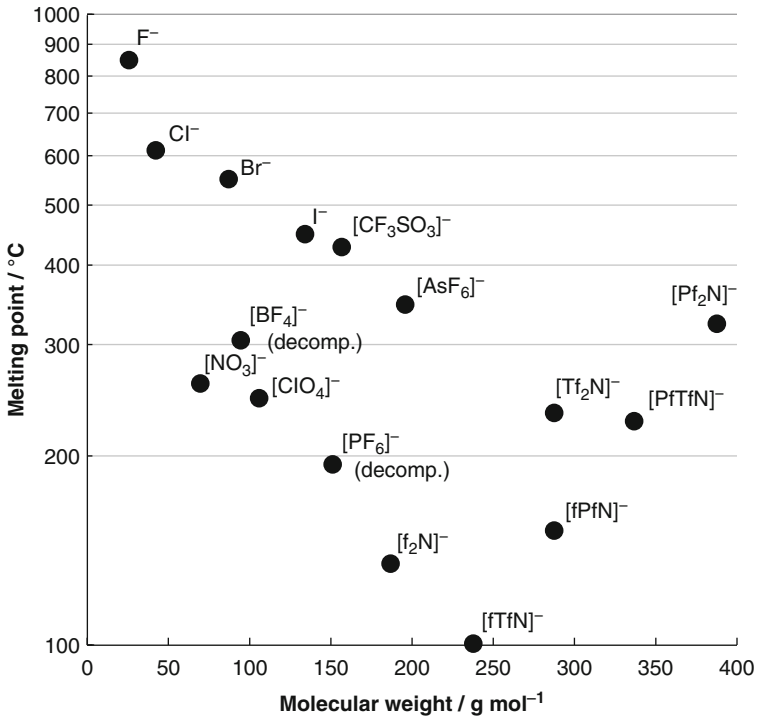

Fig. 4.6 Melting point of lithium salt composed of various anions

yl)amide, denoted as $[fTfN]^-$, behaved like $[f_2N]^-$ [54]. Although both the physical properties and the rate property using the $[fTfN]^-$ were much better than $[Tf_2N]^-$, but slightly less than $[f_2N]^-$, such asymmetric amides indicate a remarkable potential to reduce the melting point of their onium salts [40]. The $[fTfN]^-$ forms ILs with highly symmetrical cations such as tetraethylammonium, azoniaspiro-[4.4.]-nonane, and phosphoniaspiro-[4.4.]-nonane, which did not melt at room temperature when combining with symmetric anions, such as $[f_2N]^-$and $[Tf_2N]^-$, and also asymmetric but larger anions such as $[C_1C_2]^-$ [55]. The *N*-(trifluoromethanesulfonyl) trifluoroacetamide, which is denoted as $[TSAC]^-$, also has the ability to reduce the melting point, but the electrochemical stability of the anion was poor [37]. However a very interesting point is that the $[fTfN]^-$ also forms a low melting alkali metal salt [56, 57].

As shown in Fig. 4.6, the melting point of various lithium salts depends on the size of counter anions like the viscosity of the ILs as shown in Fig. 4.4. In the figure, the results for $[BF_3R_F]^-$ were omitted due to their low decomposition temperature (ca. 150 °C) [58]. It was quite interesting that both the melting point and viscosity have the same tendency toward the size of the anion. The Li[fTfN] can be used as a onium-free lithium single molten salt from 100 °C to the decomposition temperature (300 °C) [57]. Such an onium-free lithium single salt will be useful to focus on

the latent potential and also the limitation of perfluoroanions for battery applications. It should be emphasized again that developing new anionic species, not cationic species, causes such a dramatic and fundamental improvement as stated in this section. At the same time, the fact that the basic physical properties, such as the melting point and viscosity of the salts composed of perfluoroanions, have a lower limit for the size of the perfluoroanion, suggests that new anions with a fundamentally different system, such as tetracyanoborate $[B(CN)_4]^-$ [59], will be necessary to further improve the physical properties.

4.3 Application of ILs in Lithium Battery Systems During the Past Decade

4.3.1 Conventional ILs Composed of $[Tf_2N]^-$ and $[BF_4]^-$

Since early research revealed the compatibility of conventional ILs with composite electrodes, such as $LiCoO_2$ [3–5], the operation of other transition metal cathodes, such as $LiMn_2O_4$ [60], and $LiNi_{1/3}Mn_{1/3}Co_{1/3}O_2$ [61], have been reported using $[Tf_2N]^-$-based ILs containing aliphatic quaternary ammonium cations (AQAs). These results were appropriate considering almost the same operating voltage among these cathodes. However, it was interesting that a 5-V class cathode, such as $LiNi_{0.5}Mn_{1.5}O_4$ [62], could also operate in the ILs composed of the aliphatic quaternary ammonium cation (AQAs). At the same time, imidazolium-based ILs and also AQAs containing ether oxygen, such as $[N_{2,2,1,2O1}]^+$, could not be used due to the poor oxidation stability of these ILs [27, 50]. These results correspond to the difference in the oxidation limit potential of these ILs, that is, the oxidation potential of the imidazolium and also the AQAs with ether oxygen were less positive than that of the AQAs without an ether oxygen [20]. However, strictly speaking, capacity fading during a long cycle was observed to a greater or lesser degree even in the AQA-ILs due to the high catalytic activity of $LiCoO_2$. Such a capacity fading could be suppressed by a surface coating with Al_2O_3 and ZrO_2 on the cathode surface, which was developed for improving the cycling stability in an organic electrolyte [63]. If such a surface modification layer perfectly prevented from contacting any kind of ionic species on the catalytically active surface, low viscosity ILs without an electrochemical stability would also be re-evaluated as a lithium battery electrolyte. Not only the transition metal cathode as stated above, but also the thermally more stable $LiFePO_4$, has also been investigated. The combination of the $LiFePO_4$ cathode and a thermally stable lithium titanate (LTO) anode has been investigated as a full-cell application [64].

On the other hand, the number of reports on a carbon anode in neat ILs is much smaller than that of cathodes because the conventional ILs composed of $[Tf_2N]^-$ is incompatible with a carbon anode without any additives, as stated in the previous section. Contrary to the carbon anode, a silicon anode material with a much higher

theoretical capacity (ca. 4,000 mA h g^{-1}) than a conventional carbon anode was found to be operative in the $[Tf_2N]^-$-based ILs without any additives [65]. This result suggests a new direction for the research and development of ILs based on the following points. (1) The silicon anode was not stable in a conventional organic electrolyte. (2) The ILs composed of $[Tf_2N]^-$ with various drawbacks for use as a conventional battery material was valid for the next-generation battery materials. As will be stated in the next section, the high thermal stability of the ILs was not always expected inside a battery in a charged state especially at high temperatures [11, 12]' however, even conventional ILs have the possibility to be an essential electrolyte as a new battery material, as pointed out in a recent review [17]. The number of papers on the application of ILs for next-generation batteries has been gradually increasing, for example, a lithium-air battery [13, 14], and a lithium-sulfur battery [15].

The reports on $[BF_4]^-$-ILs for battery applications were much fewer than those for $[Tf_2N]^-$; however, a few notable findings have recently been reported for the low viscosity $[C_2mim][BF_4]$. For example, Li[BOB] (BOB^-: bis(oxalate)borate), which has been reported to form a good SEI at the anode in an organic electrolyte, also easily dissolved in $[C_2mim][BF_4]$ and also acted as an additive for protecting against cathodic decomposition of the $[C_2mim]^+$. Such a good SEI on the lithium metal allowed making a 3-V class Li/MnO_2 cell that exhibited a high discharge capacity (235 mA h g^{-1}). However, the viscosity increase with the addition of Li[BOB] was unfortunately much higher than that for $Li[BF_4]$ [66].

This chapter focuses on the use of neat ILs to clearly describe the unique features of this less-flammable electrolyte. However, the unique application of these ILs as flame-retardant additives for a conventional organic electrolyte should be noted. The flame retardency of an organic electrolyte was achieved by the addition of a relatively large amount of these ILs. In spite of the addition of viscous ILs, a relatively good battery performance was reported [67–69]. On the other hand, the recent unique studies as a synthesis media for an ionothermal process must also be mentioned [70]. The use of $[C_2mim]$-based ILs have known to play an important role in the synthesis of cathode materials such as $LiMPO_4$, $LiMPO_4F$ (M = Fe, Mn, Ni, Co) [70]. Furthermore, one of the $[BF_4]^-$-based ILs $[C_4mim][BF_4]$, also serves to prepare the nanostructured FeF_3 via a one-step synthesis under mild conditions [71]. The conventional ILs composed of $[Tf_2N]^-$ and $[BF_4]^-$ are expected to support research and development in the secondary battery field.

4.3.2 New ILs Composed of New Anions

Indeed, conventional ILs composed of $[Tf_2N]^-$ and $[BF_4]^-$ have played an important role in determining the possibility of unique liquids as not only an electrolyte, but also as a synthetic media, as stated in the previous section; however, two major defects, such as their incompatibility with a carbon anode and their poor rate performance, have been inevitable. However, these unavoidable defects were thoroughly alleviated by a new perfluoroamide, such as $[f_2N]^-$ [6–8]. As already described in

Sect. 2.2, this anion forms low-melting and low-viscosity ILs with various cations, and also the low internal resistance is comparable to an organic solvent electrolyte [48], however, the most surprising fact is that the $[C_2mim][f_2N]$ with a low viscosity is compatible with not only the carbon anode but also the lithium metal anode without any additives [6, 8]. The reports on the full-cell operation using $[f_2N]^-$-based ILs have gradually increased [8, 72]. In particular, a relatively large-scale laminate type cell (ca. 0.7 A h) using a $LiFePO_4$ cathode and a LTO anode was constructed using $[f_2N]^-$-based ILs, and a nail penetration test of the cell was also completed [73]. It should be noted that these studies used $Li[Tf_2N]$ as the lithium salts and not $Li[f_2N]$, probably due to the difficulty of obtaining a high-quality sample and also handling without water contamination. The thermal stability of $Li[f_2N]$ was quite sensitive to the existence of a trace amount of water [74]. These problems may also apply to other newly developed ILs composed of new anions. It is no exaggeration to say that the further extension of the ILs as a battery electrolyte significantly depends on the possibility of a high-quality and low-cost abundant supply. Anyway, the existence of $[Tf_2N]^-$ in the $[f_2N]^-$-based ILs has not significantly affected the performance of each full-cell operation [8, 72]. Contrary to these reports, a full-cell containing the $LiCo_{1/3}Mn_{1/3}Ni_{1/3}O_2$ cathode and a graphite anode also exhibited a good reversible cycling in $[C_3pip][Tf_2N]$ (C_3pip^+: *N*-methyl-*N*-propyl-piperidinium) with the addition of $Li[f_2N]$ [75]. These results suggest that the $[f_2N]^-$ must play an important role not only regarding the physical properties of the ILs, but also the possibility of the ILs as a lithium battery electrolyte. The good performance comparable to a conventional organic electrolyte clarified that the $[f_2N]^-$ will have been the one and only perfluoroanion to be considered as a counter anion of ILs for current lithium battery systems [76].

4.4 Thermal Stability of ILs

Recent studies have revealed that the features of ILs believed to be true for a long time are not always true. For example, the most common $[Tf_2N]^-$-based ILs can be distilled under high vacuum [77]. Also, conventional ILs are indeed harder to ignite; however, such ILs can be burned with the addition of external energy from an infrared heater (over 900 °C) in the presence of oxygen [10]. This means that ILs should not be categorized as "nonflammable" and "nonvolatile" liquids. However, these suggestions do not reduce our interest in the ILs as a potential electrolyte because these ILs are still "less-flammable" and "less-volatile" liquids, which are not realized by a conventional organic solvent. Indeed, assessment of the thermal stability of ILs coexisting with various battery components such as a charged cathode, an anode, and lithium metal by differential scanning calorimetry (DSC) [11, 78–82] or accelerated rate calorimetry (ARC) [12] revealed that not all the ILs exhibited thermal stabilities very different from those of an organic solvent electrolyte. However, these reports did not investigate all the cathodes and anodes that have been successively developed. As a matter of fact, of the ILs composed of $[f_2N]^-$,

only the [C_2mim][f_2N] may have a chance to compete with conventional organic electrolytes. Therefore, it is very important to find new cathodes and anodes that can combine with the [f_2N]$^-$-based ILs that exhibit both high performance and thermal stability. Such a really good battery system has not yet been developed. However, for the ILs electrolyte, [C_2mim][f_2N] is the most promising IL; it was discovered because early reports opened up the possibility of using ILs as a lithium battery electrolyte [5–7]. The ILs should be used as a reference IL for future studies concerning the ILs in a battery system.

4.5 Summary

In this chapter, the research and development progress of IL electrolytes for use in a lithium secondary battery during the past decade was briefly described back to the early reports on compatibility with a conventional composite electrode [3–5]. Many fundamentally important research studies such as the phase transition property [83], lithium metal plating and stripping and dendrite formation and suppression [84], the corrosion of the current collector [85], and development of new battery component such as a binder for the carbon anode [86] were not well described. Please see the reference papers for more details. In particular, it seems to suggest the incompatibility of [Tf_2N]$^-$-based ILs for a carbon anode has been much improved with the use of a new binder. From this result and also from the surface modification of the cathode as introduced in Sect. 3.1, the development of battery components is also important for the practical use of an IL electrolyte. The main purpose of this review was to indicate the importance of developing anionic species because the interaction between Li^+ and an anion must govern not only the transport of Li^+ through the bulk ILs, but also the electrochemical reactions at an electrode surface analogous to the solvation and desolvation of Li^+ in an organic solvent electrolyte [87]. To further develop new anions, it is very important to establish the molecular design with the aid of theoretical calculations [49, 51, 52, 88].

References

1. Clare B.; Sirwardana A.; MacFarlane D.R., Synthesis, Purification and Characterization, In *Ionic Liquids, Topics in Current Chemistry*; Kirchner B., Ed.; Springer-Verlag, Berlin, Heidelberg, 2009; Vol. 290; 1-40.
2. *Electrochemical Aspects of Ionic Liquids second edition*; Ohno H., Ed.; John Wiley & Sons, Hoboken, New Jersey, 2011.
3. Sakaebe H.; Matsumoto, H., N-Methyl-N-propylpiperidinium bis(trifluoromethanesulfonyl) imide (PP13-TFSI) - novel electrolyte base for Li battery, *Electrochem. Commun.*, 2003, 5, 594-598.
4. Nakagawa H.; Izuchi S.; Kuwana K.; Nukuda T.; Aihara Y., Liquid and Polymer Gel Electrolytes for Lithium Batteries Composed of Room-Temperature Molten Salt Doped by Lithium Salt, *J. Electrochem. Soc.,* 2003, 150, A695-A700.

5. Garcia B.; Lavallee S.; Perron G.; Michot C.; Armand M., Room temperature molten salts as lithium battery electrolyte, *Electrochim. Acta,* 2004, 49 4583-4588.
6. Matsumoto, H.; Sakaebe H.; Tatsumi K.; Kikuta M.; Ishiko E.; Kono M., Fast cycling of Li/$LiCoO_2$ cell with low-viscosity ionic liquids based on bis(fluorosulfonyl)imide $[FSI]^-$, *J. Power Sources*, 2006, 160, 1308-1313.
7. Ishikawa, M.; Sugimoto T.; Kikuta M.; Ishiko E.; Kono M., Pure ionic liquid electrolytes compatible with a graphitized carbon negative electrode in rechargeable lithium-ion batteries, *J. Power Sources*, 2006, 162, 658-662.
8. Guerfi, A.; Duchesne, S.; Kobayashi, Y.; Vijh A.; Zaghib, K., $LiFePO_4$ and graphite electrodes with ionic liquids based on bis(fluorosulfonyl)imide (FSI^-) for Li-ion batteries, *J. Power Sources*, 2008, 175, 866-873.
9. Zhou, Q.; Henderson, W.A.; Appetecchi, G.B.; Montanino, M.; Passerini, S.; Physical and Electrochemical Properties of N-Alkyl-N-methylpyrrolidinium Bis(fluorosulfonyl)imide Ionic Liquids: PY13FSI and PY14FSI, *J. Phys. Chem.,* 2008, 112, 13577-13580.
10. Diallo, A-O.; Morgan, A.B.; Len, C.; Marlair G., An innovative experimental approach aiming to understand and quantify the actual fire hazards of ionic liquids, *Energy & Environ. Sci.*, 2013, 6, 699-710.
11. Wang, Y.D.; Zaghib, K.; Guerfi, A.; Bazito, F.F.C.; Torresi, R.M.; Dahn, J.R., *Electrochim. Acta.*, 2007, 52, 6346-6352.
12. Ue, M.; Tokuda, H.; Kawai, T.; Yanagidate, M., Otake Y., Thermal Behavior of Ionic Liquid Electrolytes in Lithium-ion Cells, *ECS Trans.*, 2009, 16(35), 1731-181.
13. Kuboki, T; Okuyama, T; Ohsaki, T; Takami, N, Lithium-air batteries using hydrophobic room temperature ionic liquid electrolyte, *J. Power Sources*, 2004, 146, 766-769.
14. Mizuno, F.; Nakanishi, S.; Kotani, Y.; Yokoishi, S.; Iba, H., Rechargeable Li–air batteries with carbonate-based liquid electrolytes., *Electrochemistry*, 2010, 78, 403–405.
15. Wang, J.; Chew, S.Y.; Zhao, Z.W.; Ashraf, S.; Wexler, D.; Chen, J.; Ng, S.H.; Chou, S.L.; Liu, H.K., Sulfur-mesoporous carbon composites in conjunction with a novel ionic liquid electrolyte for lithium rechargeable batteries, *Carbon*, 2008, 46, 229-235.
16. Nohira, T.; Kuroda, K.; Hagiwara, R.; Fukunaga, A.; Sakai, S.; Nitta, K.; Inazawa, S. NaFSA-C_1C_3pyrFSA ionic liquids for sodium secondary battery operating over a wide temperature range, *J. Power Sorces*, 2013, 238, 296-300.
17. Armand, M; Endres, F.; MacFarlane D.R.; Ohno H.; Scrosati B., Ionic-liquid materials for the electrochemical challenges of the future, *Nature Mat*., 2009, 8, 621-629.
18. Lewandowski A.; Świderska-Mocek A., Ionic liquids as electrolytes for Li-ion batteries—An overview of electrochemical studies, *J. Power Sorces*, 2009, 194, 601-609.
19. Trulove P. C.; Mantz R.A., Electrochemical Properties of Ionic Liquids, In *Ionic Liquids in Synthesis, Topics Second, Completely Revised and Enlarged Edition*; Wasserscheid P.; Welton T., Ed.; Wiley-VCH: Weinheim, Germany, 2008; 141-174.
20. Matsumoto H., Electrochemical Windows of Room-Temperature Ionic Liquids (RTILs), In *Electrochemical Aspects of Ionic Liquids second edition*; Ohno H., Ed.; John Wiley & Sons: Hoboken, New Jersey, 2011; 43-63.
21. Sakaebe H.; Matsumoto H., Li Batteries, In *Electrochemical Aspects of Ionic Liquids second edition*; Ohno H., Ed.; John Wiley & Sons: Hoboken, New Jersey, 2011; 205-220.
22. Wilkes, J.S.; Zaworotko, M.J., Air and water stable 1-methyl-3-ethylimidazolium based ionic liquids, *J. Chem. Soc., Chem. Comm.*, 1992, 965-967.
23. Bônhote, P.; Dias, A.P.; Papageorgiou, N.; Kalyanasundaram, K.; Grätzel, M., Hydrophobic, highly conductive ambient-temperature molten salts, *Inorg. Chem.*, 1996, 35, 1168-1178.
24. MacFarlane, D.R.; Meakin, P.; Sun, J.; Amini, N.; Forsyth, M., Pyrrolidinium imides: A new family of molten salts and conductive plastic crystal phases, *J. Phys. Chem. B*, 1999, 103, 4164-4170.
25. Ngo, H. L.; LeCompte, K.; Hargens, L.; McEwen, A.B., Thermal properties of imidazolium ionic liquids, *Thermochimica Acta*,2000, 357-358, 97-102.
26. Sato, T.; Masuda, G.; Takagi, K., Electrochemical properties of novel ionic liquids for electric double layer capacitor applications, *Electochim. Acta*, 2004, 49, 3606-3611.

27. Zhou, Z-B., Matsumoto, H., Tatsumi, K., Low-melting, low-viscous, hydrophobic ionic liquids: Aliphatic quaternary ammonium salts with perfluoroalkyltrifluoroborates, *Chem. Eur. J.*, 2005, 11, 752-766.
28. Matsumoto, H.; Miyazaki, Y.; Ishikawa, H., Japan Patent Kokai 1999-297355: 1999.
29. Matsumoto, H.; Yanagida, Y.; Tanimoto, T.; Kojima, Y.; Tamiya, Y.; Miyazaki, Y., Improvement of ionic conductivity of room temperature molten salt based on quaternary ammonium cation and imide anion, In *Molten Salts XII Proceedings of the International Symposium,* Trulove, P.C.; De Long, H. C.;, Stafford, G. R.; Deki, S., Ed.; The Electrochemical Society Proceeding Series, The Electrochemical Society, Pennington, NJ, 2000; PV99-41, 186-192.
30. Howlett, P. C.; MacFarlane, D. R.; Hollenkamp, A. F., High lithium metal cycling efficiency in a room-temperature ionic liquid, *Electochem. Solid-State Lett.*, 2004, 7, A97-A101.
31. Matsumoto, H.; Kageyama, H.; Miyazaki, Y., Effect of ionic additives on the limiting cathodic potential of EMI-based room temperature ionic liquids, *Electrochemistry*, 2005, 71, 1058-1060.
32. Howlett, P. C.; Izgorodina, E. I.; Forsyth, M.; MacFarlane, D. R., Electrochemistry at negative potentials in bis(trifluoromethanesulfonyl)amide ionic liquids, *Z. Phys. Chem.,* 2006, 220, 1483-1498.
33. Endres, F.; Borisenko, N.; El Abedin, S.Z.; Hayes, R.; Atkin, R., The interface ionic liquid(s)/ electrode(s): In situ STM and AFM measurements, *Faraday Dsicuss*., 2012, 154, 221-233.
34. Lassègues, J.-C.; Grondin, J.; Talaga, D., Lithium solvation in bis(trifluoromethanesulfonyl) imide-based ionic liquids, *Phys. Chem. Chem. Phys.,* 2006, 8, 5629-5632.
35. Katayama, Y.; Yukumoto, M.; Miura, T.; *Electrochem. Solid-State Lett.,* 2003, 6, A96-A97.
36. Holzapfel, M.; Jost, C.; Prodi-Schwab, A.; Krumeich, F.; Wursig, A.; Buqa, H.; Novak, P., Stabilisation of lithiated graphite in an electrolyte based on ionic liquids: an electrochemical and scanning electron microscopy study, *Carbon*, 2005, 43, 1488-1498.
37. Matsumoto, H.; Kageyama H.; Miyazaki Y., Room temperature ionic liquids based on small aliphatic ammonium cations and asymmetric amide anions, *Chem. Commun.*, 2002, 16, 1726-1727.
38. Matsumoto, H.; Sakaebe, H.; Tatsumi, K., Preparation of room temperature ionic liquids based on aliphatic onium cations and asymmetric amide anions and their electrochemical properties as a lithium battery electrolyte, *J. Power Source.*, 2005, 146, 45-50.
39. Appecchi, G.B.; Scaccia, S.; Tizzani, C.; Alessandrini, F.; Passerini, S., Synthesis of Hydrophobic Ionic Liquids for Electrochemical Applications, *J. Electrochem. Soc.*, 2006, 153, A1685-A1691.
40. Matsumoto, H.; Terasawa, N.; Umecky, T.; Tsuzuki, S.; Sakaebe, H.; Asaka, K.; Tatsumi, K., Low Melting and Electrochemically Stable Ionic Liquids Based on Asymmetric Fluorosulfon yl(trifluoromethylsulfonyl)amide *Chem. Lett.*, 2008, 37, 1020-1021.
41. Liu, K.; Zhou, Y-X.; Han, H-B.; Zhou, S-S.; Feng, W-F.; Nie, J.; Li, H.; Huang, X-J.; Armand, M., Ionic liquids based on (fluorosulfonyl)(pentafluoroethanesulfonyl)imide with various oniums, *Electrochim. Acta.*, 2010, 55, 7145-7151.
42. Ignat'ev, N.V.; Welz-Biermann, U.; Kucheryna, A.; Bissky, G.; Willner, H., New ionic liquids with tris(perfluoroalkyl)trifluorophosphate (FAP) anions, *J. Fluorine Chem.*, 2005, 126, 1150-1169.
43. Zhou, Z-B.; Takeda, M.; Ue, M., New hydrophobic ionic liquids based on perfluoroalkyltrifluoroborate anions, *J. Fluorine Chem.*, 2003, 125, 471-476.
44. Zhou, Z-B.; Matsumoto, H.; Tatsumi, K., Low-viscous, low-melting, hydrophobic ionic liquids: 1-alkyl-3-methylimidazolium trifluoromethyltrifluoroborate, *Chem. Lett.,* 2004, 33, 680-681.
45. Terasawa, N.; Tsuzuki, S.; Umecky, T.; Saito, Y.; Matsumoto, H., Alkoxy chains in ionic liquid anions; effect of introducing ether oxygen into perfluoroalkylborate on physical and thermal properties, *Chem. Commun.,* 2010, 46, 1730-1732.
46. Zhou, Z-B.; Matsumoto, H.; Tatsumi, K., Cyclic quaternary ammonium ionic liquids with perfluoroalkyltrifluoroborates: Synthesis, characterization, and properties, *Chem. Eur. J.,* 2006, 12, 2196-2212.

47. Schmidt, M.; Heider, U.; Kuehner, A.; Oesten, R.; Jungnitz, M.; Ignat'ev, N.; Saroti, P., Lithium fluoroalkylphosphates: a new class of conducting salts for electrolytes for high energy lithium-ion batteries, *J. Power Sources*, 2001, 97, 557-560.
48. Matsumoto, H.; Sakaebe, H.; Tatsumi, K., Li/$LiCoO_2$ Cell Performance Using Ionic Liquids Composed of N,N-Diethyl-N-methyl-N-(2-methoxyethyl)ammonium - Effect of Anionic Structure, *ECS Trans.*, 2009, 16(35), 59-66.
49. Tsuzuki, S.; Umecky, T.; Matsumoto, H.; Shinoda, W.; Mikami, M., Interactions of Perfluoroalkyltrifluoroborate Anions with Li Ion and Imidazolium Cation: Effects of Perfluoroalkyl Chain on Motion of Ions in Ionic Liquids, *J. Phys. Chem. B*, 2010, 114, 11390-11396.
50. Matsumoto, H., Yanagida, M.; Tanimoto, K.; Nomura, K.; Kitagawa, Y.; Miyazaki, Y., Highly conductive room temperature molten salts based on small trimethylalkylammonium cations and bis(trifluoromethylsulfonyl)imide, *Chem. Lett.*, 2000, 29, 922-923.
51. Tsuzuki, S.; Hayamizu, K.; Seki, S., Origin of the Low-Viscosity of [emim][$(FSO_2)_2N$] Ionic Liquid and Its Lithium Salt Mixture: Experimental and Theoretical Study of Self-Diffusion Coefficients, Conductivities, and Intermolecular Interactions, *J. Phys. Chem. B*, 2010, 114, 16329-16336.
52. Valencia, H.; Kohyama, M.; Tanaka, S.; Matsumoto, H., First-Principles Study of EMIM-FAFSA Molecule Adsorption on a Li(100) Surface as a Model for Li-Ion Battery Electrodes, *J. Phys. Chem. C*, 2012, 116, 8493-8509.
53. Hayamizu, K.; Tsuzuki S.; Seki, S.; Umebayashi, Y., Nuclear magnetic resonance studies on the rotational and translational motions of ionic liquids composed of 1-ethyl-3-methylimidazolium cation and bis(trifluoromethanesulfonyl)amide and bis(fluorosulfonyl)amide anions and their binary systems including lithium salts, *J. Chem. Phys.,* 2011, 135, 084505.
54. Matsumoto, H.; Terasawa N.; Tsuzuki S.; Sakaebe H., Charge and Discharge Property of Li/$LiCoO_2$ Cell Using Ionic Liquids Composed of N,N-Diethyl-N-Methyl-N-(2-Methoxyethyl) Ammonium and Fluorosulfonyl (Trifluoromethylsulfonyl) Amide, *ECS Trans*., 2011, 33(28), 37-42.
55. Matsumoto, H.; Terasawa N.; Tsuzuki S.; Sakaebe H., Ionic liquids; WO 2009/136608 A1: 2009.
56. Kubota, K; Matsumoto, H., Melting and Crystallization Behaviors of Alkali Metal (Fluorosulfonyl)(trifluoromethylsulfonyl)amides, *Chem. Lett.,* 2011, 40, 1105-1106.
57. Kubota, K.; Matsumoto, H., Investigation of an Intermediate Temperature Molten Lithium Salt Based on Fluorosulfonyl(trifluoromethylsulfonyl)amide as a Solvent-Free Lithium Battery Electrolyte, *J. Phys. Chem. C*, 2013, 117, 18829-18836.
58. Zhou, Z-B.; Takeda, M.; Ue, M., Novel electrolyte salts based on perfluoroalkyltrifluoroborate anions: 1. Synthesis and characterization, *J. Fluorine Chem.,* 2003, 123, 127-131.
59. Kuang, D.; Wang, P.; Ito, S.; Zakeeruddin, S.M.; Grätzel, M., Stable Mesoscopic Dye-Sensitized Solar Cells Based on Tetracyanoborate Ionic Liquid Electrolyte, *J. Am. Chem. Soc.*, 2006, 128, 7732-7733.
60. Zheng, H.; Zhang, H.; Fu, Y.; Abe, T.; Ogumi, Z., Temperature Effects on the Electrochemical Behavior of Spinel LiMn2O4 in Quaternary Ammonium-Based Ionic Liquid Electrolyte, *J. Phys. Chem. B*, 2005, 109, 13676-13684.
61. Tsunashima, K.; Yonekawa, F.; Sugiya, M., Lithium Secondary Batteries Using a Lithium Nickelate-Based Cathode and Phosphonium Ionic Liquid Electrolytes, *Electochem. Solid-State Lett.*, 2009, 12, A54-A57.
62. Borgel, V.; Markevich, E.; Aurbach, D.; Semrau, G.; Schmidt, On the application of ionic liquids for rechargeable Li batteries: High voltage systems, *J. Power Sources*, 2009, 189, 331-336.
63. Seki, S.; Kobayashi, Y.; Miyashiro, H.; Ohno, Y.; Usami, A.; Mita Y.; Watanabe, M.; Terada, N., Highly reversible lithium metal secondary battery using a room temperature ionic liquid/lithium salt mixture and a surface-coated cathode active material, *Chem. Commun.*, 2006, 544-545.
64. Reale, P.; Femicola, A.; Scrosati, B., Compatibility of the Py24TFSI-LiTFSI ionic liquid solution with Li4Ti5O12 and LiFePO4 lithium ion battery electrodes, *J. Power Sources*, 2009, 194, 182-189.

65. Usui, H.; Yamamoto, Y.; Yoshiyama, K.; Itoh, T.; Sakaguchi, H., Application of electrolyte using novel ionic liquid to Si thick film anode of Li-ion battery, *J. Power Sources*, 2011, 196, 3911-3915.
66. Saruwatari, H.; Kuboki, T.; Kishi T.; Mikoshiba, S.; Takami, N., Imidazolium ionic liquids containing LiBOB electrolyte for lithium battery, *J. Power Sources*, 2010, 195, 1495-1499.
67. Nakagawa, H.; Fujino, Y.; Kozono, S.; Katayama, Y.; Nukuda, T.; Sakaebe, H.; Matsumoto, H.; Tatsumi, K., Application of nonflammable electrolyte with room temperature ionic liquids (RTILs) for lithium-ion cells, *J. Power Sources*, 2007, 174, 1021-1026.
68. Guerfi, A.; Dontigny, M.; Charest, P.; Petitclerc, M.; Lagacé, M.; Vijh, A.; Zaghib, K., Improved electrolytes for Li-ion batteries: Mixtures of ionic liquid and organic electrolyte with enhanced safety and electrochemical performance, *J. Power Sources*, 2010, 195, 845-852.
69. Lombardo, L.; Brutti, S.; Navarra, M.A.;Panero, S.; Reale, P., Mixtures of ionic liquid – Alkylcarbonates as electrolytes for safe lithium-ion batteries, *J. Power Sources*, 2013, 227, 8-14.
70. Tarascon, J-M.; Recham, N.; Armand, M.; Chotard, J-N.; Barpanda, P.; Walker, W.; Dupont, L., Hunting for Better Li-Based Electrode Materials via Low Temperature Inorganic Synthesis, *Chem. Matter.*, 2010, 22, 724-739.
71. Li, C.; Gu, L.; Tsukamoto S.; van Aken, P.A.; Maier J., Low-Temperature Ionic-Liquid-Based Synthesis of Nanostructured Iron-Based Fluoride Cathodes for Lithium Batteries, *Adv, Mater.*, 2010, 22, 3650-3654.
72. Kim, G.-T.; Jeong, S. S.; Xue, M.-Z.; Balducci, A.; Winter, M.; Passerini, S.; Alessandrini, F.; Appetecchi, G. B., Development of ionic liquid-based lithium battery prototypes, *J. Power Sources.*, 2012, 199, 239-246.
73. Balducci, A.; Jeong, S. S.; Kim, G.-T.; Passerini, S.; Winter, M.; Schmuck, M.; Appetecchi, G. B.; Marcilla, R.; Mecerreyes, D.; Barsukov, V.; Khomenko, V.; Cantero, I.; De Meatza, I.; Holzapfgel, M.; Tran, N., Development of safe, green and high performance ionic liquids-based batteries (ILLIBATT project), *J. Power Sources.*, 2011, 196, 9719-9730.
74. Huang, J.; Hollenkamp, A. F., Thermal Behavior of Ionic Liquids Containing the FSI Anion and the Li^+ Cation, *J. Phys. Chem. C*, 2010, 114, 21840-21847.
75. Reiter, J.; Nádherná, M.; Dominko, R., Graphite and $LiCo_{1/3}Mn_{1/3}Ni_{1/3}O_2$ electrodes with piperidinium ionic liquid and lithium bis(fluorosulfonyl)imide for Li-ion batteries, *J. Power Sources.*, 2012, 205, 402-407.
76. Yamagata, M.; Matsui, Y.; Sugimoto, T.; Kikuta, M.; Higashizaki, T.; Kono, M.; Ishikawa, M., High-performance graphite negative electrode in a bis(fluorosulfonyl)imide-based ionic liquid, *J. Power Sources.*, 2013, 227, 60-64.
77. Earle, M. J.; Esperança, J. M. S. S.; Gilea, M. A.; Canongia Lopes, J. N.; Rebelo, L. P. N.; Magee, J. W.; Seddon, K. R.; Widegren, J. A., The distillation and volatility of ionic liquids, *Nature*, 2006, 439, 831-834.
78. Egashira, M.; Tanaka-Nakagawa, M.; Watanabe, I.; Okada, S.; Yamaki, J., Charge–discharge and high temperature reaction of $LiCoO_2$ in ionic liquid electrolytes based on cyano-substituted quaternary ammonium cation, *J. Power Sources.*, 2006, 160, 1387-1390.
79. Sakaebe, H.; Matsumoto, H.; Tatsumi, K., Application of room temperature ionic liquids to Li batteries, *Electrochim. Acta*, 2007, 53, 1048-1054.
80. Larush, L.; Borgel, V.; Markevich, E.; Haik, O.; Zinigrad, E.; Aurbach, D.; Semrau, G.; Schmidt, M., On the thermal behavior of model Li–$LixCoO_2$ systems containing ionic liquids in standard electrolyte solutions, *J. Power Sources.*, 2009, 189, 217-223.
81. Profatilova, I. A.; Choi, N-S.; Roh, S. W.; Kim, S. S., Electrochemical and thermal properties of graphite electrodes with imidazolium- and piperidinium-based ionic liquids, *J. Power Sources.*, 2009, 192, 636-643.
82. Plashnitsa, L.; Kobayashi, E.; Okada, S.; Yamaki, J., Symmetric lithium-ion cell based on lithium vanadium fluorophosphate with ionic liquid electrolyte, *Electrochim. Acta*, 2011, 56, 1344-1351.
83. Henderson, W.A.; Passerini, S., Phase Behavior of Ionic Liquid–LiX Mixtures: Pyrrolidinium Cations and TFSI-Anions, *Chem. Mater.,* 2004, 16, 2881-2885.
84. MacFarlane D.R.; Forsyth, M.; Howlett, P. C.; Pringle, J. M.; Sun, J.; Annat, G.; Neil, W., Izgorodina, E. I., Ionic Liquids in Electrochemical Devices and Processes: Managing Interfacial Electrochemistry, *Acc. Chem. Res.*, 2007, 40, 1165-1173.

85. Peng, C.X.; Yang, L.; Zhang, Z.X.; Tachibana, K.; Yang, Y., Anodic behavior of Al current collector in 1-alkyl-3-methylimidazolium bis[(trifluoromethyl)sulfonyl] amide ionic liquid electrolytes, *J. Power Sources.*, 2007, 173, 510-517.
86. Komaba, S.; Yabuuchi, N.; Ozeki, T.; Okushi, K.; Yui, H.; Konno, K.; Katayama, Y.; Miura, T., Functional binders for reversible lithium intercalation into graphite in propylene carbonate and ionic liquid media, *J. Power Sources.*, 2010, 195, 6069-6074.
87. Abe, T.; Fukuda, H.; Iriyama, Y.; Ogumi, Z., Solvated Li-Ion Transfer at Interface Between Graphite and Electrolyte, *J. Electrochem. Soc.,* 2004, 151, A1120-A1123.
88. Borodin, O.; Smith, G.D., Henderson, W., Li^+ Cation Environment, Transport, and Mechanical Properties of the LiTFSI Doped N-Methyl-N-alkylpyrrolidinium + TFSI-Ionic Liquids, *J. Phys. Chem. B*, 2006, 110, 16879-16886.

Chapter 5
Interphases Between Electrolytes and Anodes in Li-Ion Battery

Mengqing Xu, Lidan Xing, and Weishan Li

Abstract The successful application of lithium-ion batteries depends to a great extent on the existence of interphases at anodes. In this chapter, the role and the significance of interphases in lithium-ion batteries are introduced firstly, then the theories proposed before 2005 are outlined, and the latest research progresses are reviewed at last, mainly focused on the formation processes, chemistries, and properties of the interphases on graphite.

5.1 Background

5.1.1 Introduction: Significance in Understanding of Interphases and Challenges

Interface, called boundary as well, results from the contact of two different phases. The electrode/electrolyte interface is necessary for an electrochemical system, because it provides valid locations where electron exchange is participating and the

M. Xu
School of Chemistry and Environment, South China Normal University, Guangzhou 510006, China
e-mail: mqxu@scnu.edu.cn

L. Xing
Key Laboratory of Electrochemical Technology on Energy Storage and Power Generation of Guangdong Higher Education Institutes, South China Normal University, Guangzhou 510006, China
e-mail: xingld@scnu.edu.cn

W. Li (✉)
Engineering Research Center of Materials and Technology for Electrochemical Energy Storage (Ministry of Education), South China Normal University, Guangzhou 510006, China
e-mail: liwsh@scnu.edu.cn

T.R. Jow et al. (eds.), *Electrolytes for Lithium and Lithium-Ion Batteries*, Modern Aspects of Electrochemistry 58, DOI 10.1007/978-1-4939-0302-3_5,

electrochemical redox reactions are taking place [1]. Interphases grow in some electrode/electrolyte interface accompanying the electrochemical redox reactions and provide the interface new properties and new structures.

Typically, an electrochemical reaction could be classified into two types: spontaneous, such as in a primary battery or a rechargeable battery during the discharge process: of course, in this case, an external energy is not needed; the other one, nonspontaneous, such as in an electrolytic reaction or a rechargeable battery during the charging process: in this case, an external energy is definitely needed to drive the energy-consuming reactions taking place [2]. Since all the electrochemical reactions are related to electron transfer and the electron exchanges can only happen at electrode/electrolyte interfaces, the interphases always control the cell reaction kinetics, which refers to the charge–discharge rate for a rechargeable battery system. In addition, for a rechargeable battery, an interphase also participates in determining whether the cell reactions are reversible or not, and with what columbic and energy efficiencies if the reaction is reversible, which represents the reversibility and the cycle life of the rechargeable device. Moreover, the interphase could even affect the working voltage range, which directly determines the energy density of the devices [3].

5.1.2 Significance of Interphase in Li-Ion Batteries

Li-ion batteries have the best gravimetric and volumetric energy density of commercially produced rechargeable batteries. The high energy density is due to a large potential difference between the electrodes (3–5 V per cell) and high-capacity electrode materials enabled by the use of nonaqueous electrolytes. Due to the high energy density, lithium-ion batteries are being intensively pursued for transportation applications, including hybrid electric vehicles (HEV), plug-in hybrid electric vehicles (PHEV), and electric vehicles (EV). However, cost, safety, cycle and calendar life, and energy and power density are some of the major obstacles in successfully adopting lithium-ion technology for vehicle applications. One of the leading contributors to many of these obstacles is the interactions and reactions of the electrolytes with the electrode materials [4].

Figure 5.1 illustrates the operating principles involved in a lithium-ion battery. Basically, the structure of a lithium-ion battery is similar with a sandwich, with two insertion lithium hosts (anode and cathode), and electrolyte. Metallic lithium was firstly used as an anode material over five decades based on its special advantages: (1) its lowest atomic weight as a metal providing the largest theoretical specific capacity of 3,860 m Ah g^{-1}; (2) the most negative electrochemical potential (−3.07 vs. SHE) providing the highest possible cell operation voltage when coupled with given cathode material; and (3) its smallest density (5.4×10^2 kg m^{-3}) providing the possible highest gravimetric energy density [3]. However, the catastrophe arising from lithium dendrite growth happened in 1989 forced people to find the substitutes. In such case, the graphite intercalation compound (GIC) of Li^+ was proposed to substitute for the lithium metal as anode material. However, the GIC anode

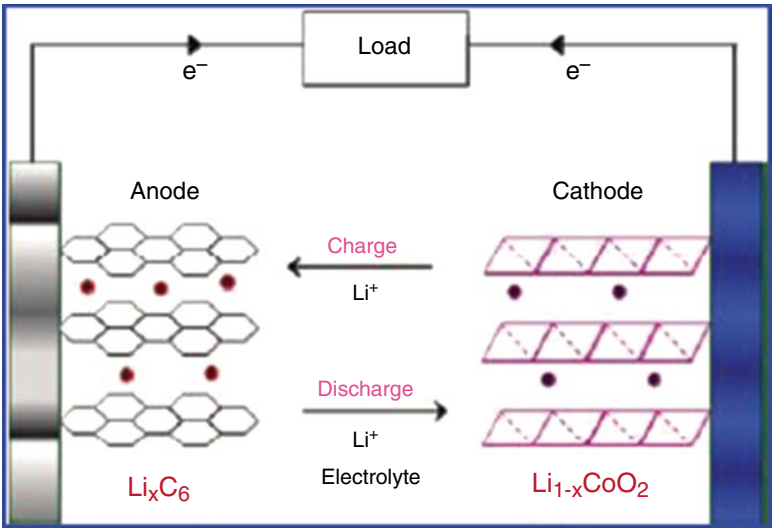

Fig. 5.1 Illustration of the charge/discharge process involved in a lithium-ion cell consisting of graphite as anode and layered $LiCoO_2$ as the cathode (reproduced with permission by the American Chemical Society from [4])

material results in a loss of 0.2–0.3 V cell voltage and more than 90 % original capacity [5]. Nevertheless, when the GIC anode material is coupled with a given cathode material, ranging from 3.0 to 5.0 V, around 100–200 W h kg^{-1} of energy density can be achieved, which is still the highest energy density in the rechargeable battery systems.

It has been established that nonaqueous electrolytes are not thermodynamically stable on the surface of lithium metal or lithiated graphite resulting in the reductive decomposition of electrolyte. Electrolyte decomposition products deposit on the electrode surface during the initial formation cycling and prevent further electrolyte reduction while allowing Li^+ conduction [6]. The interfacial deposition layers have been termed "solid electrolyte interphase (SEI)" [7]. An understanding of this complex component of Li-ion batteries has been of significant interest since the inception of Li-ion battery technology [8–11]. The effects of different factors, including graphite structure, electrolyte composition, and Li^+ solvation sphere, on the chemistry and formation mechanism of the SEI have been extensively explored [12].

5.1.3 Symbolic Significance: PC–EC Disparity

The best example to highlight the importance of interphase is the EC–PC disparity and its impact on the history of Li-ion battery, as shown in Fig. 5.2 [13]. Lithium ion-graphite intercalation compound (Li^+-GIC) was firstly discovered in early 1950s by Hérold via the reacting graphite with either molten lithium metal or lithium

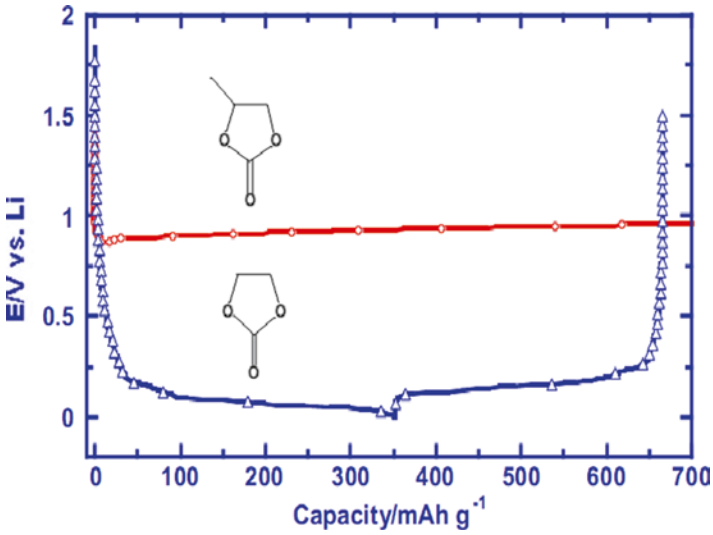

Fig. 5.2 The difference in interphasial chemistry caused by a methyl group might be responsible for the four-decade postponement of Li-ion technology: voltage profiles of graphic anodes in $LiPF_6$/EC and $LiPF_6$/PC during polarization to 0.002 V vs. Li (reproduced with the permission from the Electrochemical Society, [13])

vapor [14]. Even today, the chemical approach has still been adopted to prepare intercalation compounds. Maluangnont and co-workers prepared new ternary GICs including M $(Ic3)_{0.4}C_{15–18}$ (M = Li, Na; Ic3 = iso-propylamine) and Li(1,2-diaminopropane)$_x$C$_y$ [15, 16]. Since the first discovery of Li^+-GIC via chemical approach, many efforts had been addressed to prepare the Li^+-GIC via electrochemical approaches, with the purpose to develop a new anode material. However in the four decades, not a single progress was obtained. The primary reason for the above failure is that the nonaqueous electrolytes during that period were almost exclusively based on propylene carbonate (PC), which cointercalates and subsequently decomposes at 0.7 V vs. Li, leading to physical disintegration of the graphite anode [13]. It was once believed that it is impossible to prepare the Li^+-GIC via electrochemical approaches. However during 1990s, successful lithiation of graphite was achieved by using ethylene carbonate (EC) as the primary solvent to substitute the PC solvent. Eventually the interphasial chemistry based on EC solvent drives the birth of Li-ion battery in today's configuration. It is hard to image that only a single methyl group caused the delay of Li-ion technology over four decades.

As we mentioned the importance of classic interphases above, SEI in Li-ion batteries also plays crucial roles on the performances of the battery, such as controlling the kinetics of cell reaction (charge–discharge rate or power density of the device); determining the reversibility of the cell chemistry and cycle life of the device; and affecting the capacity or the energy density and safety performance of device.

5.2 State of the History (Before 2005)

5.2.1 2-D vs. 3-D Formation Mechanism

The original SEI concept was firstly proposed by Peled derived from the passivation phenomenon of alkali metal electrode, which possesses a non-intercalating surface [7, 17]. The alkali metals in nonaqueous electrolyte are inevitably covered by a surface layer which is immediately formed by the reaction of the metal with the electrolyte since the potential of the alkali metal is lower far beyond the decomposition potential of the solvents or the salt. The reduction of electrolyte components on a lithium metal electrode, a flat surface, stops once the surface layer builds up to a thickness while preventing electron tunneling across it. Since the reduction and the surface layer growing on a simple flat surface, this formation mechanism was referred to as "2D formation model" of SEI. Considering the similar potential of a fully lithiated graphite and lithium metal, it has been suggested that the chemical nature of the SEIs in both cases should be similar. Dahn adapted Peled's model for lithium's surface and extended it to carbonaceous electrode [18].

With regard to the formation mechanism on graphite, people realized that simply the 2D formation model of SEI for lithium metal could not be adopted to carbonaceous anode because not only the potential of graphite is around 3.0 V vs. Li, but also the intrinsic structure of graphite is not a simple 2D flat surface like that of lithium metal. Therefore, the former factor offers a preferential reduction of the electrolyte components, not liking the instantaneous reaction occurring on lithium metal, because the potential of graphite is gradually brought down to the lithiation region (~0.2 V vs. Li/Li^+), which allows some electrolyte components to be preferentially reduced before others. While the latter factor, the intrinsic structure of graphite, provides an electrode surface with different "active sites," since we know that the solvated Li^+ could only intercalate at the edge sites of the graphite, it is expected that the chemical ingredients of SEI would appear at edge sites instead of basal planes. This graphic-specific mechanism was first discovered by Chu and co-workers using atomic force microscopy (AFM), illustrating the growth of SEI during the first charging process: at the voltage higher than 2 V, the highly oriented pyrolytic graphite (HOPG) surface is clean and smooth; below 1.6 V, surface species appear on steps or edge surface; and below 0.8 V, species deposit on both edge and basal plane surface, as shown in Fig. 5.3 [19].

The early studies have identified that the solvents could cointercalate into graphene layers before they decompose. On the basis of the knowledge about intercalation compounds and their reactions, a mechanism for SEI formation was proposed by Besenhard which involves the formation of ternary GIC $[Li(solvent)_xC_y]$ and its subsequent decomposition on the edge site of the graphite to form SEI [20], as shown in Fig. 5.4.

One decade later, based on their previous research work, Besenhard and co-workers studied the reduction of PC-based electrolyte on graphite via combination of in situ XRD with cyclic voltammetry. Their results confirmed the formation of the ternary GIC: $Li^+(PC)_yC_n^-$ ($y \geq 4$) with a 3-dimensional, tetrahedral solvate shell

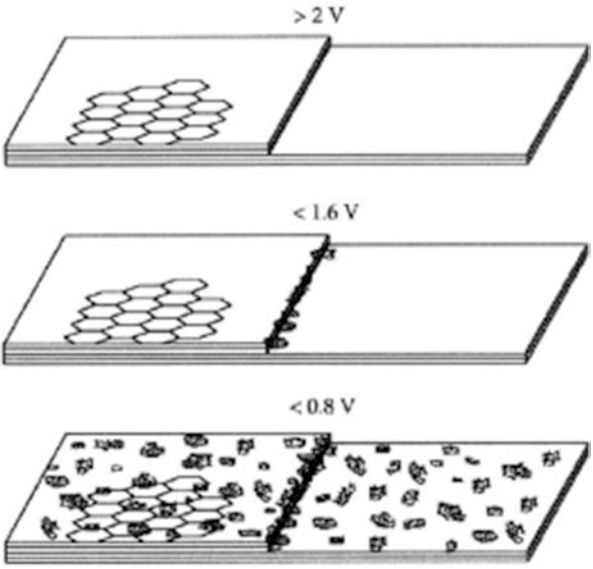

Fig. 5.3 Schematic diagrams of the stepwise formation of SEI on graphite surface based on AFM results (reproduced with permission by the Electrochemical Society from [19])

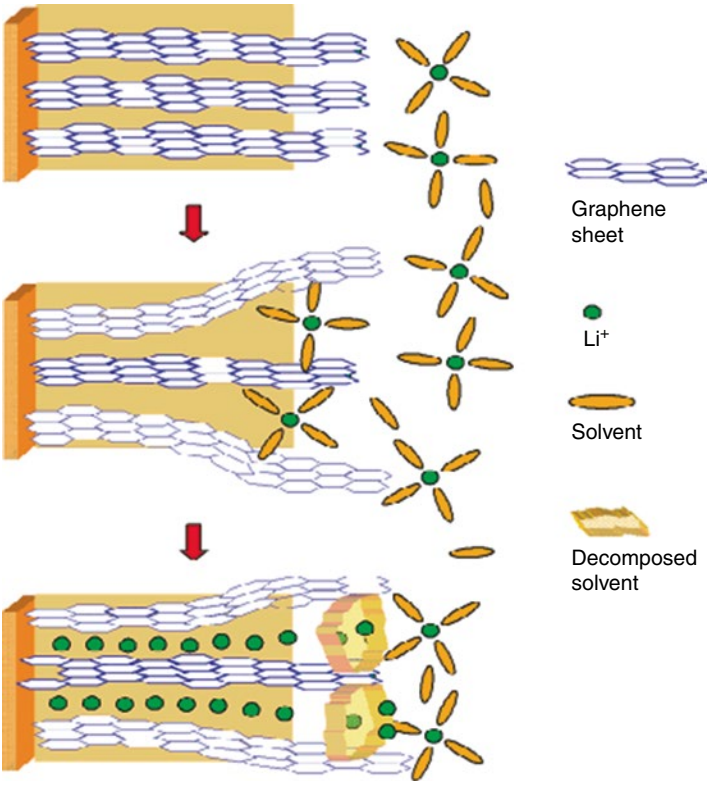

Fig. 5.4 Schematic illustration of the SEI formation mechanism via the decomposition of $Li(solv)_xC_y$ (reproduction with permission from the American Chemical Society from [12])

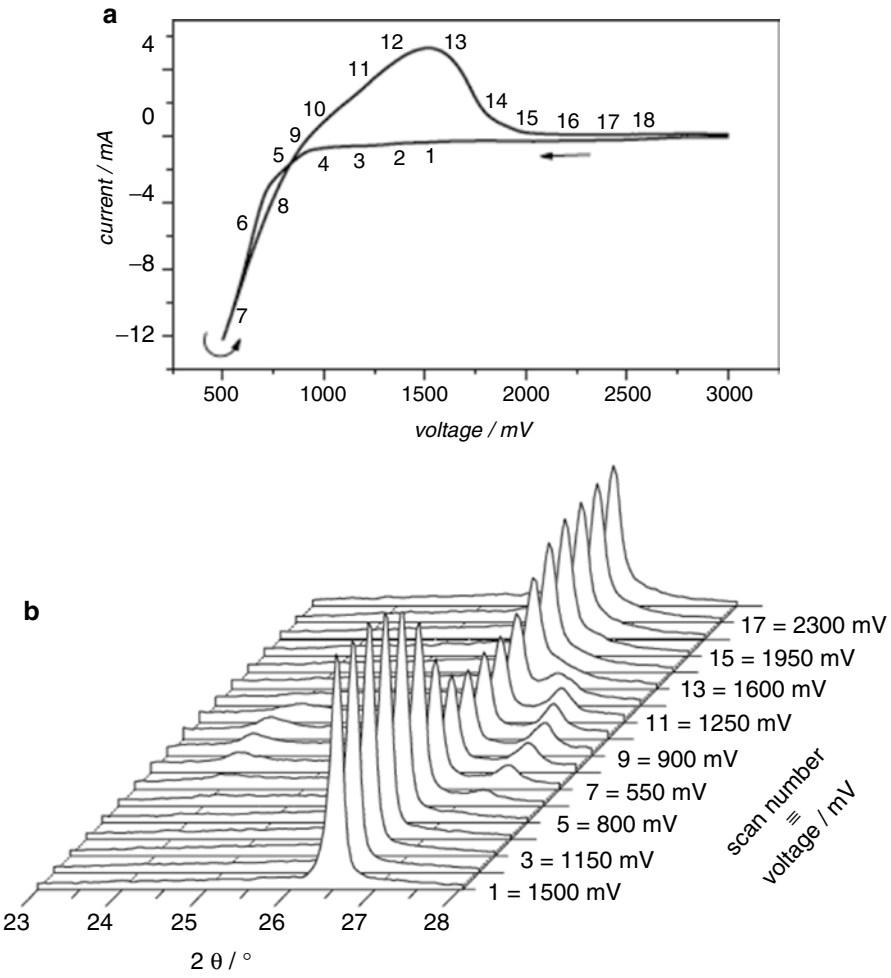

Fig. 5.5 (**a**) CV of SFG 44 graphite electrodes in 1 M $LiClO_4$/PC electrolyte, scan rate 10 mV s^{-1}; (**b**) in situ XRD evidence of the ternary GIC composed of $Li(PC)_4$-graphite (reproduced with permission by Elsevier from [21])

involving in over 374 % expansion of the basal plane spacing in c-direction of the graphite structure [21], as schematically shown in Fig. 5.5. This formation mechanism is thus known as "3-D model of SEI."

5.2.2 Extension from Li Metal

Aurbach and co-workers developed another model of SEI formation from the original Peled's concept for lithium electrode passivation, in which the surface reaction is the major process, and concerns were placed upon the composition and structure

Scheme 5.1 Proposed two-electron mechanism for the reduction of PC

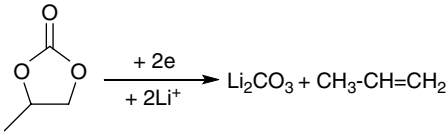

of graphite material and components of the electrolyte as well. They used various electrolytes, solvents, salts, and graphite electrodes with different structures and morphologies and attempted to correlate the SEI effectiveness with these parameters [22, 23]. Their extensive studies led to the conclusions that the failure of SEI formation on graphite is closely related to the structure and morphology of graphite as well as the components and conditions of the electrolytes. They suggested that the key fact is the structure of facets, perpendicular to the basal planes of graphite, through which Li insertion takes place; another important factor is the existence of some degree of disorder and distortion in the graphite structure. As respect to the electrolyte solvents, they found that the failure of SEI formation occurred in ester-based electrolyte because no effective surface film was observed above 0.3 V, and the solvents, coordinating with lithium ions, cointercalated into graphene and caused completely exfoliation. On the basis of their conclusions, Aurbach and co-workers proposed a model for SEI formation that makes a compromise between solvent intercalation and surface reaction mechanism. According to the model, they suggested that the graphite electrode was covered by surface film in the carbonate electrolytes, even including PC-based electrolyte. The formation of precipitation of highly cohesive surface films and the overall surface reactions producing gaseous products are competitive, and the success or the failure of stabilizing of graphite depends on the balance between the kinetics of the two competitive reactions.

5.2.3 Chemical Ingredients

5.2.3.1 Lithium Metal Electrode

Organic carbonates with cyclic structures, such as EC, PC, and acyclic structures, including dimethyl carbonate (DMC), diethyl carbonate (DEC), and ethylmethyl carbonate (EMC), sever as the main ingredients as electrolyte solvents in state-of-the-art Li-ion batteries mainly because they can form stable interphase on graphite and transition metal oxide [12]. It was believed that the chemical composition of SEI is closely related to the electrolyte components. For example, the SEI is proposed to be mainly composed of Li_2O in ether-based electrolyte [24]. After performing microscopic observations of lithium surface treated with PC-based electrolytes, Dey believed that the major component of the surface film is Li_2CO_3, which is the decomposition product of PC through a two-electron mechanism [25], Scheme 5.1.

This conclusion was furthered supported by the results from Auger electron spectroscopy (AES) and X-ray photoelectron spectroscopy (XPS) [26, 27].

However Aurbach and co-workers argued that the main component in the SEI on lithium is not Li_2CO_3 but the lithium salt of alkyl carbonate, which formed via a one-electron mechanism followed by the radical termination paths as shown in Scheme 5.2 [28].

The direct evidence of this reaction mechanism is the observation of carbonyl stretching signature at ~1,650 cm^{-1} in FTIR spectrum. The decomposition products from lithium salt were also found through the XPS surface analysis, such as alkoxides or oxides, a competition reaction between solvents and salts. However, the formation of alkyl carbonate seems to be predominant when EC is the component of electrolyte because of the more reactive nature of EC toward cathodic reductions [28]. The formation of lithium alkyl carbonate was also confirmed in an independent work, where the reduction products of EC in a supporting electrolyte were hydrolyzed by D_2O and then subject to NMR analysis, which identified ethylene glycol as the major products formed, as indicated by the singlet at ^1H spectrum [29]. Therefore, Aurbach and co-workers concluded the reduction products of EC and PC, lithium ethylene dicarbonate (LEDC) and lithium propylene dicarbonate (LPDC), respectively:

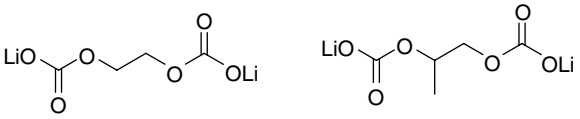

In addition, they pointed out that the lithium alkyl carbonate is very sensitive to moisture in the electrolyte, which is most likely the reason that early work identified Li_2CO_3 as the main component in the SEI [25, 26].

However, when the salt anion is susceptible to hydrolysis by trace moisture, like PF_6^- and BF_4^-, the generated HF may further react with the alkyl carbonate, and LiF is the overwhelming surface component [28]. Further studies suggest that alkyl carbonate is not stable upon storage or cycling on the lithium electrode, probably due to its continuous electrochemical reduction [30]. Thus, Aurbach first proposed that the SEI might have a multilayer structure within which the simple inorganic species such as Li_2CO_3 and Li_2O are more stable and closer to lithium, while alkyl carbonate is more likely to be distributed in the outer layers [28, 30, 31].

Kanamura et al. studied the SEI components in various electrolyte solutions, $LiBF_4$/PC, $LiBF_4$/γ-GBL, and $LiBF_4$/THF, via the combination of XPS and FTIR [32, 33]. By sputtering the surface of lithium metal electrode, they were able to record the depth profile of the related chemical species. Their conclusions are in good agreement with the hypothesis by Aurbach et al. as discussed above, that is, the alkyl carbonate is in the outer layers of the SEI, as indicated by its signature binding energy of 289.0 eV at the C 1s spectrum, and its abundance rapidly decreases with sputtering time. In addition, the O 1s and Li 1s spectra clearly reveal the increasing abundance of Li_2O species and deceasing of LiOH or Li_2CO_3 with sputtering time. LiF was detected throughout the SEI and was found relatively independent of sputtering. The generation of LiF was believed to have two possible reasons: (1) the reaction between

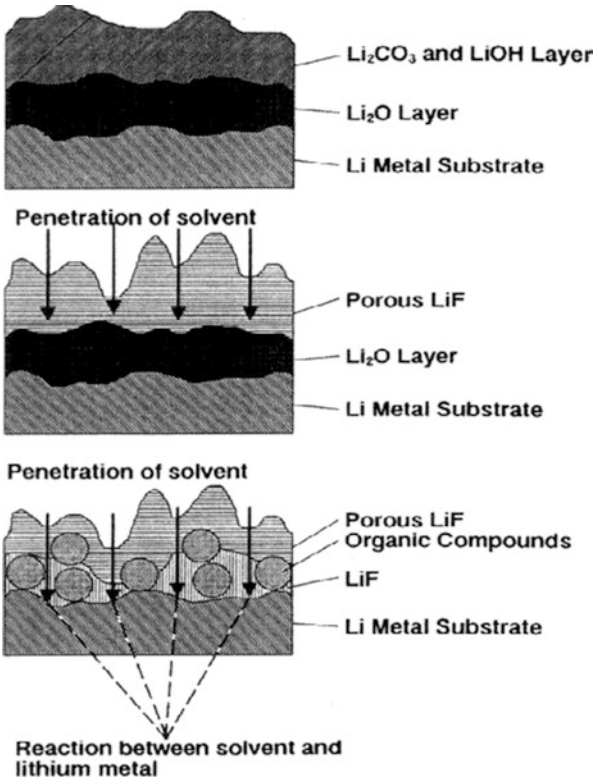

Fig. 5.6 Schematic illustrations of the surface film formed on lithium in nonaqueous electrolyte based on $LiBF_4$ solutions and the subsequent reactions (reproduced with the permission from Electrochemical Society from [32])

HF and alkyl carbonate or Li_2CO_3 and (2) direct reduction of BF_4^- anion by lithium. Additional reactions between solvents with lithium seem to be also possible after the initial formation of SEI, since the abundance of organic species increases in the inner layer with storage time, as supported by XPS C 1s spectrum. The increase in organic abundance of SEI component is most likely due to the permeation of solvent through the SEI and its subsequent reaction with lithium electrode. Figure 5.6 schematically shows the lithium surface structure and these subsequent reactions of the SEI.

5.2.3.2 Graphite Carbon Electrode

The earlier study on graphite exfoliation by PC has led to a simple two-electron reduction process, producing Li_2CO_3 and propylene as the major product, the same as PC reduction on lithium electrode, Scheme 5.1. As we mentioned above, this proposed mechanism was challenged by Aurbach and co-workers. They believed that the solvent preferentially formed a radical anion during the first cathodic process and then subsequently underwent intermolecular electron transfer between the two radical anions, as shown in Scheme 5.3:

Since only one electron is involved in this reduction process, this mechanism is called "single-electron" reduction pathway. Apparently, in this single-electron

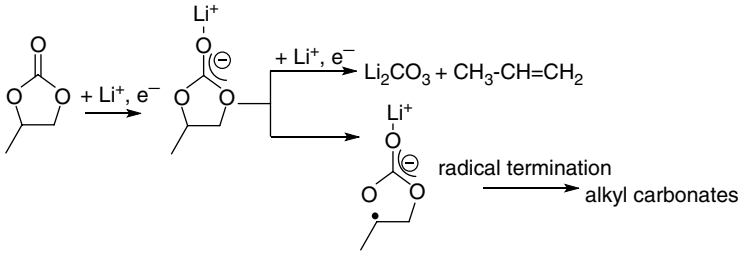

Scheme 5.2 Proposed one-electron mechanism for the reduction of PC

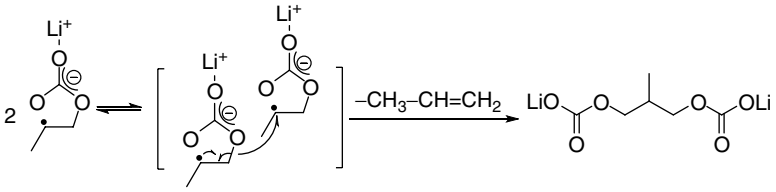

Scheme 5.3 Intermolecular electron transfer between the two radical anions

mechanism only half of organic moiety is lost in the form of gas, while the rest remained as SEI ingredient, known as either alkyl carbonate or semi-carbonate. The alkyl carbonate and semi-carbonate are extremely sensitive to moisture and instantaneous conversion to Li_2CO_3 upon exposure to even trace amount of moisture. This is probably explained by the fact that the earlier analysis only found Li_2CO_3 as the major species on anode surface.

Recently, an interesting work has been done by Edström and co-workers using XPS [34]. The results revealed how moisture control affects ex situ surface analysis, which might be able to reveal the source of Li_2CO_3. Basically, the binding energy for C 1s electron in carbonyl of alkyl carbonate is lower than its full carbonate counterpart, such as Li_2CO_3, due to the increases of electron-withdrawing functional group, and the signal at 289 eV has been used as the chemical signature of the alkyl carbonate; however, many XPS data reported in previous literature often showed conspicuous peak at >290.0 eV for cycled graphite anode. To support this chemical shift of alkyl carbonate to Li_2CO_3, Edström and co-workers conducted the XPS experiments without employing a vacuum transporter that ensures the moisture exclusion during the sample loading, instead exposure of the sample to ambient for a little bit while. They found that the carbonyl C 1s signals shift from 289 to 290 eV, which convincingly confirmed that the overwhelming presence of Li_2CO_3 on the anode surface is due to the exposure of moisture.

Based on the work of PC reduction on graphite, Aurbach et al. proposed the similar reaction mechanism for EC based on single-electron process, that is, LEDC. Considering that EC is an essential cosolvent of commercial electrolyte, therefore, LEDC is a key composition of SEI on anode surface in current Li-ion batteries.

Besides alkyl carbonates, several other species were also identified as possible SEI ingredients on graphite anode, including inorganic species such as the partially

$$H_2O + e^- + Li^+ \longrightarrow LiOH + 1/2\ H_2$$

$$LiOH + e^- + Li^+ \longrightarrow Li_2O + 1/2\ H_2$$

$$H_2O + (CH_2OCO_2Li)_2 \longrightarrow Li_2CO_3 + CO_2 + (CH_2OH)_2$$

$$2CO_2 + 2e^- + 2Li^+ \longrightarrow Li_2CO_3 + CO$$

$$LiPF_6 + H_2O \longrightarrow LiF + 2HF + PF_3O$$

$$PF_6^- + ne^- + nLi^+ \longrightarrow LiF + Li_xPF_y$$

$$PF_3O + ne^- + nLi^+ \longrightarrow LiF + Li_xPOF_y$$

$$HF + (CH_2OCO_2Li)_2,\ Li_2CO_3 \longrightarrow LiF + (CH_2COCO_2H)_2,\ H_2CO_3$$

Scheme 5.4 Possible inorganic species on the graphite anode surface (reproduced with permission Elsevier from [35])

reduced products from lithium salt anions, such as LiF or Li_xPF_y in $LiPF_6$-based electrolyte, as well as some dissociation products from lithium salts, such as $Li_xPO_yF_z$ in $LiPF_6$-based electrolyte due to the thermal dissociation or the prolonged cycling or aging [35], as described in Scheme 5.4, and organic species such as alkoxides as well as possibly polymeric moieties [36].

5.3 New Insights Achieved Since 2005

5.3.1 Chemistry

The well-established mechanism of the surface reduction for cyclic carbonates has been the single-electron reduction pathway proposed by Aurbach et al. (Scheme 5.3), which leads to the commonly named alkyl carbonates or semi-carbonates. Thereafter, Aurbach et al. further proposed that the presence of LEDC from EC reduction passivates graphite carbonaceous materials, which allows the intercalation/de-intercalation of lithium ions. This seminal notion addressed the fact that EC is the indispensable cosolvent in all electrolyte compositions and hence has been well accepted by the electrochemical community. Few years later, Ein-Eli found that electrolytes based on DMC and EMC were also able to support reversible Li-ion chemistry with graphite anodes, and the above single-electron pathway was extended to these linear carbonates, Scheme 5.5 [37].

In an effort to gain fundamental understanding on those key ingredients in the SEI, Xu et al. from the US Army Research Laboratory (ARL) synthesized a series of model lithium alkyl carbonate compounds to simulate the proposed chemical species on the anode surface, including lithium methyl carbonate (LMC), lithium ethyl carbonate (LEC), LEDC, and LPDC, as summarized in Scheme 5.6 [38].

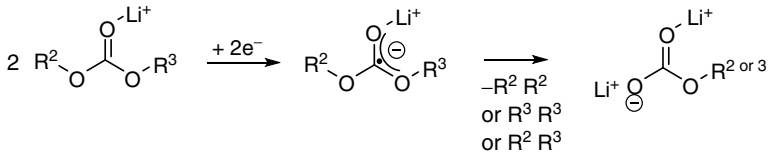

Scheme 5.5 Single-electron mechanism extended to reduction of linear carbonates

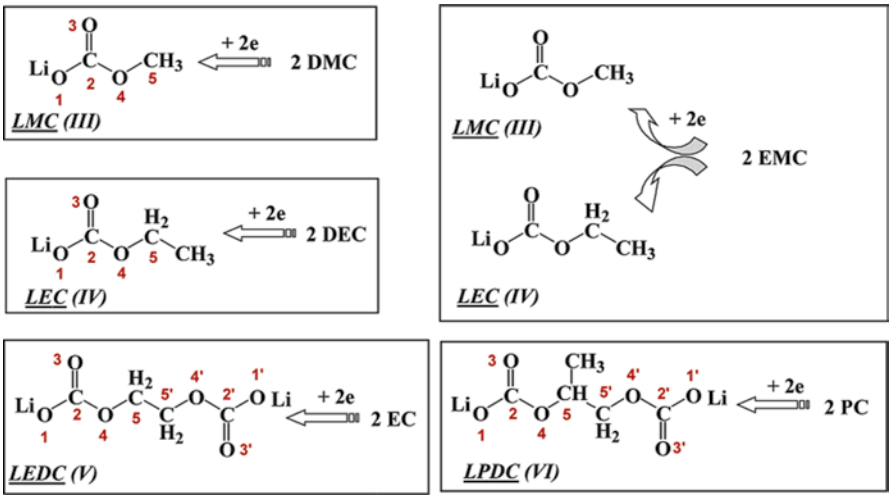

Scheme 5.6 Model compounds LMC, LEC, LEDC, and LPDC, as postulated reduction products from DMC, EMC, DEC, EC, and PC, respectively, via the single-electron reduction pathway on the graphite anode surface (reproduced with permission by the American Chemical Society from [38])

The selected NMR spectra of these synthesized lithium alkyl ethylene dicarbonate and lithium alkyl propylene dicarbonate are shown in Fig. 5.7.

The highly symmetric structure of LEDC results in simple spectra for both ^{1}H and ^{13}C nuclei. The NMR spectra of LEDC are in good agreement with the structure: only one ^{1}H signals at 3.53 ppm (for –O–**C**H_2–**C**H_2–O–), while only two ^{13}C signals at 62.9 ppm (for –O–**C**H_2–**C**H_2–O–) and 157 pm for (–O–**C**O_2–). As for the LPDC, the ^{1}H NMR spectrum characterized three chemical shifts; the doublet at 1.10 ppm for CH_3– indicates a **C**H_3–CH– substructure, while the multiplets between 3.37 and 3.81 ppm represent a characteristic split pattern of the –O–**C**H(CH_3)–**C**H_2–O–. ^{13}C NMR detected four nonisotropic ^{13}C nuclei, which are located at 17.87 ppm (for **C**H_3–), 66.50 ppm (for –O–**C**H_2–), 67.8 ppm (for O–**C**H(CH_3)–), and 160.50 ppm (for –**C**(=O)–).

Zhuang et al. compared the FTIR spectra of pure LEDC on Ni surface after cyclic voltammetry in1.2 M $LiPF_6$ EC/EMC electrolyte, and metallic lithium cleaved the same electrolyte, as shown in Fig. 5.8 [39]. By comparison of IR spectra, they established that LEDC is the predominant surface species on a Ni electrode after lithium deposition in $LiPF_6$/EC:EMC electrolyte, confirming that at the lithiation potential the

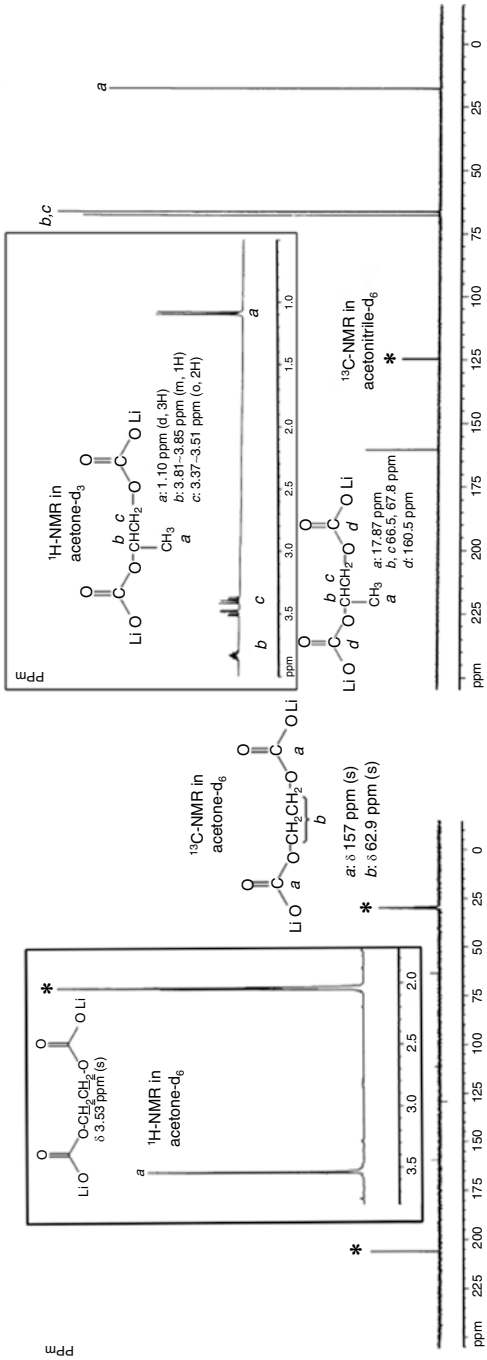

Fig. 5.7 The ^{1}H- and ^{13}C-NMR of the synthesized lithium ethylene dicarbonate (LEDC, *left*) and lithium propylene dicarbonate (LPDC, *right*), and the proposed reduction of EC and PC through single-electron pathway, respectively (reproduced with permission by the American Chemical Society from [38])

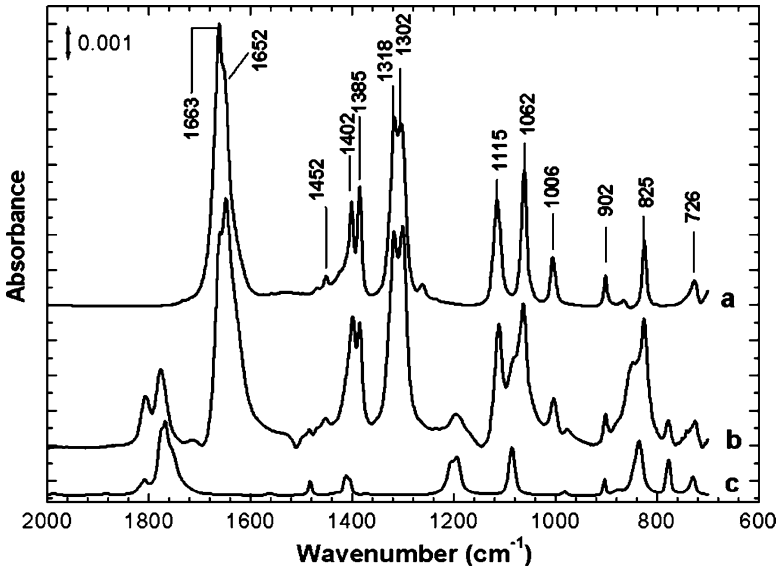

Fig. 5.8 FTIR spectra of (*a*) synthetic lithium ethylene dicarbonate; (*b*) surface species on the Ni electrode after Li deposition cycling between −0.5 and +2.5 V; (*c*) EC:$LiPF_6$ solvate (reproduced with permission by American Chemical Society from [39])

single-electron reduction indeed is the major process. Even below the fingerprint region, the spectra of pure LEDC and Ni surface match well and LDEC is the only species detected on the electrode, despite the major population of linear carbonate solvent in the electrolyte composition. In addition, they also employed Hartree–Fock method calculations to better interpret the IR spectra, indicating that intermolecular association through O–Li^+–O interactions is also occurring, which is not observed for LPDC although the latter is also a dilithium salt. It is very likely that LEDC is more prone to form a network instead of remaining a monomer in the SEI as well [3]. This finding led to the later investigation of relative competiveness of cyclic and linear carbonate for Li^+ solvation shell and its implication in the eventual interphasial chemistry.

The reduction process on graphite anode is more complicated than what was detected on nickel electrode. In addition to LEDC that dominates the SEI component, other species including lithium oxalate ($Li_2C_2O_4$), lithium carboxylate (RCOOLi), and lithium methoxide ($LiOCH_3$) were also identified through FTIR approaches and soft X-ray spectroscopy [40, 41]. The formed oxalate resulted from CO_2, but its source is still unclear. Upon the reductive process, CO_2 is reduced immediately and the resultant radical anion possesses lifetime long enough for a bimolecular recombination reaction, as shown in Scheme 5.7:

The lithium alkoxide is probably formed in a new two-electron pathway that involves acyl-oxygen cleavage instead of the alkyl-oxygen cleavage as proposed by Aurbach et al., as shown in Scheme 5.8:

Scheme 5.7 SEI formation from reduction of CO_2

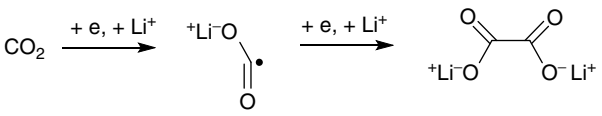

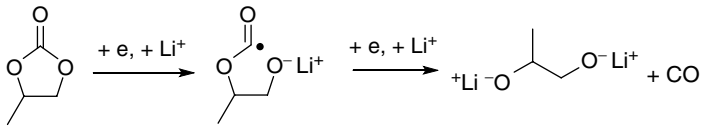

Scheme 5.8 SEI formation from two-electron reduction reaction

5.3.2 Formation Mechanism

5.3.2.1 Graphene Specific: Role of Li-Solvation Sheath

During the past decade, people already established the 3D model for the SEI formation mechanism, as proved by Chu, Winter, and Besenhard [19–21]. Few years later, Xu et al. adopted AC impedance to analyze the "charge-transfer" resistance and the associated activation energy [42]. The results improve the "3D interphase" mechanism, as illustrated in Fig. 5.9.

In this improved model, they believed that the solvated lithium ion would access the graphene structure during the first charge/lithiation process and then force the graphene layer to open up till the bulky $Li^+(solv)_x$ is accommodated in the 1.59 nm interstitial, which corresponds to the formation of intermediate ternary Li-GIC at potential ~1.5 V vs. Li. While the potential is bringing down below 1.0 V, the graphene interlayers turn into very reductive and solvent molecules in the solvated sheath subsequently are reduced by accepting electrons from the p-bands from sp2 carbon. The graphene interlayer distance is back to 0.35 nm during this reduction process and remains in the consecutive lithiation/delithiation cycles. The formed SEI, thus, partially penetrating graphene edge sites, acts as "binder" that prevents the graphene layers from expanding and also as "filter" that forces solvated Li^+ to de-solvate before lithiation.

In addition, they also established the characteristic correlations between the activation energies (E_{AC}) for Li^+ transfer measured at electrolyte/graphite interface and the electrolyte composition such as solvent ratio and salt concentration through the study of impedance [43]. To further confirm that the correlation is valid not only for the electrolyte system investigated therein but also for the typical electrolyte system, they expanded the EIS studies to an electrolyte system considered more suitable for low-temperature application, which is $LiPF_6$/EC/EMC with EC/EMC ratio at 10:90, 20:80, 30:70, 40:60, and 50:50, respectively. Within the frequency range, two partially merged semicircles were observed; typically, these two semicircles were attributed to the Li^+ migration processes corresponding to diffusion of naked Li^+ through SEI layer at middle frequencies and charge transfer at low frequencies.

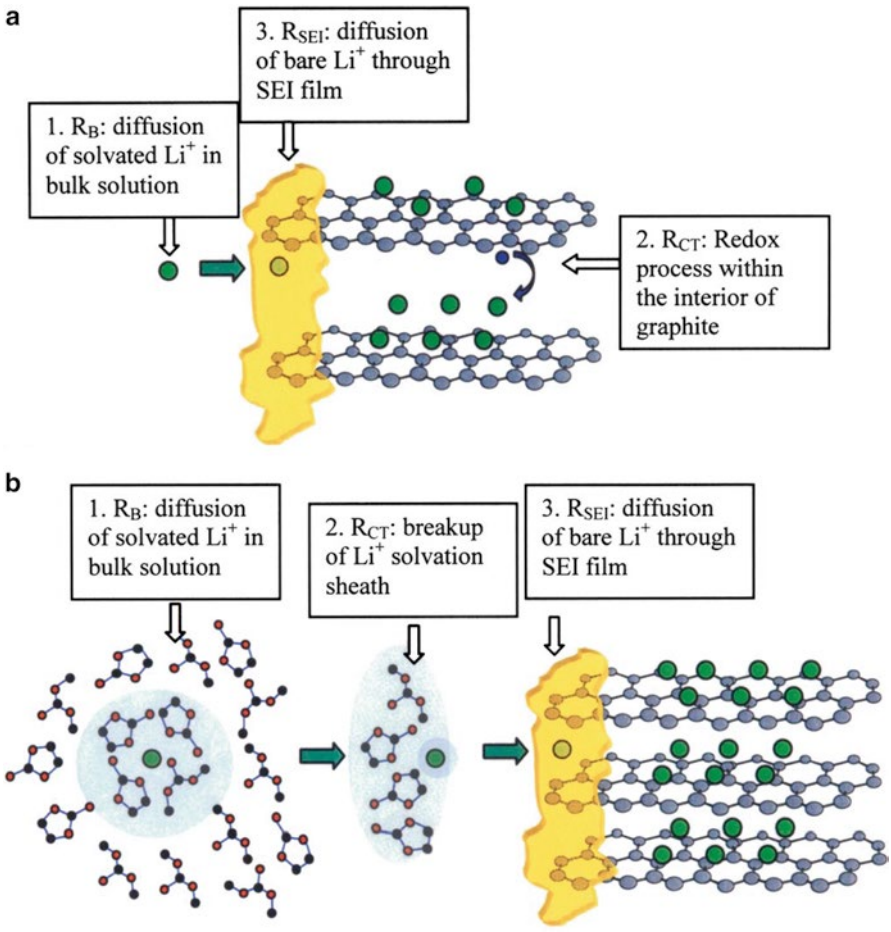

Fig. 5.9 Schematic description of a solvated lithium ion's journey from solution bulk to graphene interior, and the impedance components associated with these steps. (**a**) Assignment by convention where the process occurring at low AC frequencies was assigned to charge transfer after Li-ion diffusion across the interface film. (**b**) Rationale by Abe and Ogumi et al., where the desolvation process of Li-(solvent)$_x$ complex is identified as responsible for the above impedance components (reproduced with the permission by Electrochemical Society from [42])

The corresponding reciprocal resistances of the two semicircles, $1/R_{\text{int}}$ and $1/R_{\text{ct}}$, should be viewed as the measures of Li^+ transport though these two components SEI and charge transfer, thus, following equation are addressed, $\dfrac{1}{R(ct,\text{int})} = A_0 e^{-Ea/RT}$.

Excellent Arrhenius behaviors were obtained for both R_{ct} and R_{int}, as indicated by the near-unity values of the linearity indices (R) [44]. The activation energies were expected to be 20–25 kJ mol^{-1} for the interfacial component and 50–70 kJ mol^{-1} for the charge-transfer component, respectively, for the anode/electrolyte interfaces

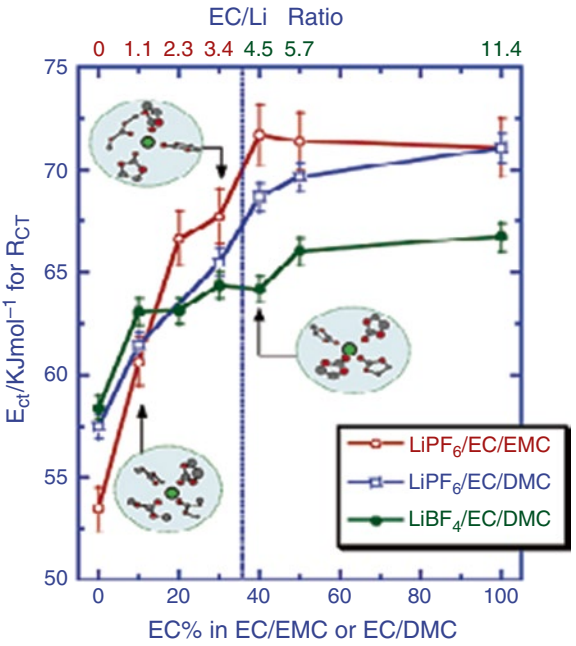

Fig. 5.10 The correlation between the activation energies corresponding to the charge-transfer process and the ratio of cyclic to linear carbonate molecules in the bulk electrolyte solution (reproduced with the permission by American Chemical Society from [43])

formed at different electrolyte compositions. This suggested that breakup of its salvation sheath experienced a much higher energy barrier during an intercalation process of solvated Li^+. Thus, to better view the correlation between electrolyte composition and E_{ct}, they also plotted the E_{ct} values derived for all these interfaces against the electrolyte compositions, as shown in Fig. 5.10. The E_{ct} remained almost a constant when EC/Li is above 4, while it dramatically decreased when EC/Li is below 3. That is, an all-EC salvation sheath should be expected in the solution with EC content >30 % (equivalent to EC/Li ≈ 3.5), while linear carbonate solvents DMC and EMC will be recruited in the sheath in solution when EC content is below 20 % (or EC/Li < 2.3).

On the basis of the identification of correlation between Li^+-solvation sheath with electrolyte composition, it is not hard to image the close relationship between interfacial chemistries with the Li^+-solvation sheath. One can imagine that the SEI ingredients are dominated by EC-based reduction products with EC content over 30 % in the electrolyte, while the degradation products from linear carbonate solvents should also be observed in the SEI components with EC content below 20 %. To further confirm that the correlation holds true, Xu et al. employed NMR technique to distinguish the interfacial products in various electrolytes [43].

In their previous work, they already synthesized the pure semi-carbonates, including LEDC, LMC, and LEC as well, corresponding to the reductions of EC, DMC, and DEC, respectively, as summarized in scheme 5.6 [38]. The NMR spectra of these pure compounds provide the authors a powerful reference to assign the signals with binary or ternary electrolyte system. Two series of electrolytes were

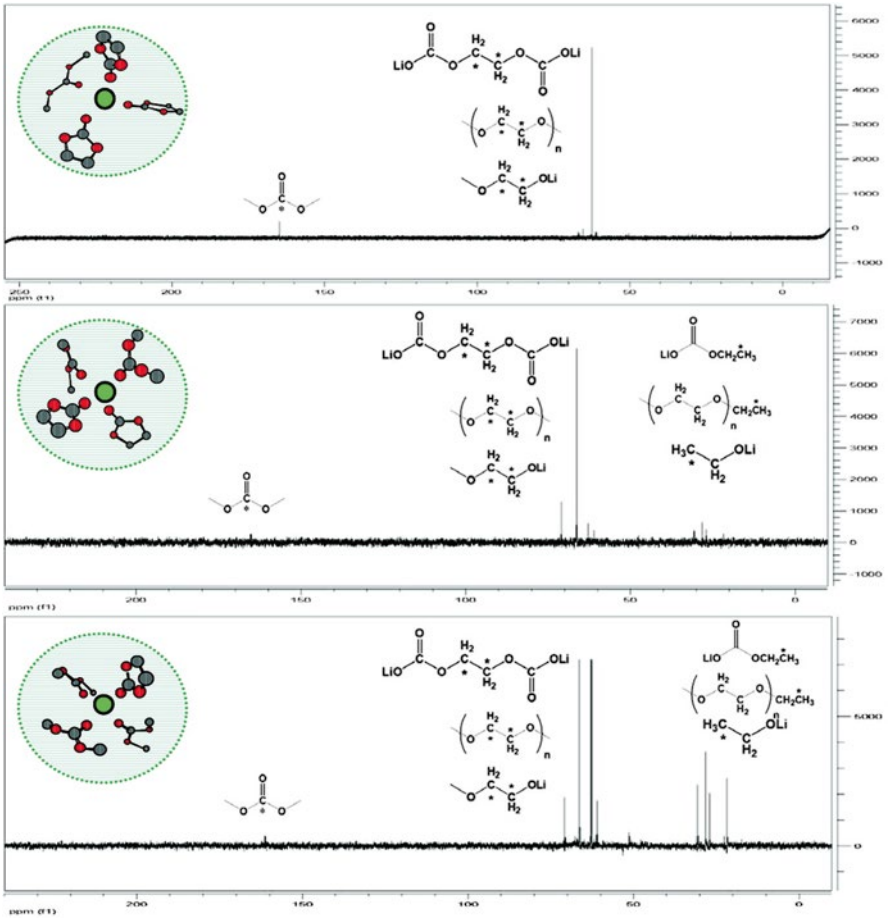

Fig. 5.11 ^{13}C NMR of surface species collected from graphitic anodes cycled in $LiPF_6$/EC/EMC 30:70 (*upper*), 20:80 (*middle*), and 10:90 (*below*) (reproduced with the permission by American Chemical Society from [43])

investigated, $LiPF_6$ in EC/DMC (50:50, 10:90) and $LiPF_6$ in EC/EMC (30:70, 20:80, 10:90). For the EC/DMC (50:50) electrolyte system, they found that the surface species seemed to predominantly consist of the EC-originated product LEDC, while with EC/DMC ratio at 10:90, the reduction product from DMC is identified because of its presence in the Li^+ salvation sheath. With regard to the EC/EMC system, the reduction product from EMC is present on the graphite anode surface until the EC/EMC ratio is lower than 20:80 (EC/Li $\approx$ 2.3, or averagely two EMC molecules in each salvation sheath), as shown in Fig. 5.11. One year later, similar conclusion was made by Onuki et al. using ^{13}C-labeled solvents. They fabricated carbon-$LiNi_xCo_yAl_{1-x-y}O_2$ cells employing 1.0 M $LiPF_6$ ^{13}C-labeled ethylene carbonate (^{13}C-EC) and diethyl carbonate (^{13}C-DEC) (3:7, v/v) electrolyte system and then

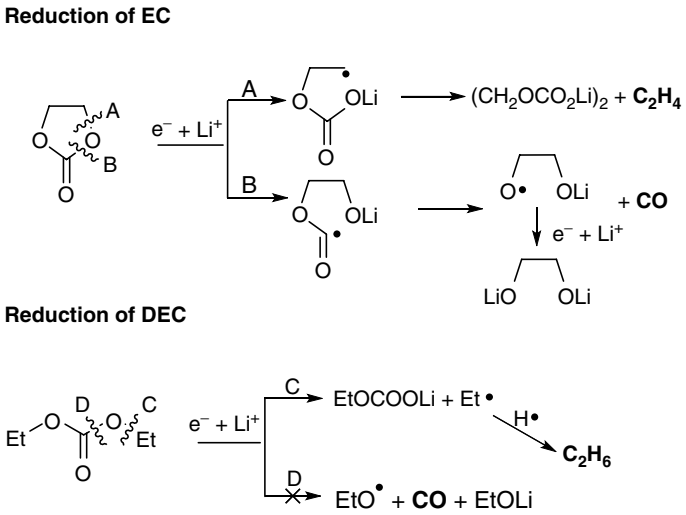

Scheme 5.9 Proposed gas evolution mechanism during storage and initial charge (reproduced with the permission by the Electrochemical Society from [45])

stored the cells at 85 °C. The gas species evolved during storage were analyzed by gas chromatography/atomic emission detector [45]. They found the gas evolution including CO_2, CO, H_2, and C_2H_4 during the thermal storage, and initial charge process was from EC reduction instead of linear carbonates; even though DEC dominates the electrolyte composition, related reduction mechanisms were proposed in Scheme 5.9.

Typically, the electrolytes currently used by the Li-ion battery industry as well as the research community are composed of lithium salt dissolved in a mixture of high dielectric constant molecules, such as cyclic carbonate solvents, EC or PC, and low-viscosity molecules, such as linear carbonate solvents, which include DMC, DEC, and EMC. We already knew that cyclic carbonate (EC) possesses an unsymmetrical precedence in participating surface reductions, despite its relatively low population in most electrolyte formulations [39]. Recent studies suggested that the solvents recruited by Li^+ into its primary solvation sheath are the precursors of interphasial chemistry, and most researchers believe that Li^+ prefers to solvate to solvent molecules with higher dielectric constant [46, 47] and also believe that the donicity (donor number) prevails [48].

In order to confirm the hypothesis that Li^+ prefers to coordinate with cyclic solvents other than acyclic carbonates, Cresce et al. employed a nondestructive mass spectrum (MS) technique to map the distribution of cyclic and acyclic carbonate molecules within a Li^+-solvation sheath [49]. Figure 5.12 shows the MS spectra of a few selected electrolyte compositions consisting of varying ratios of cyclic EC and acyclic EMC. In the absence of EC (Fig. 5.12, top), Li^+ is solvated by the only solvent, and the spectrum looks rather clean, with Li(EMC) and $Li(EMC)_2$ being the major solvates.

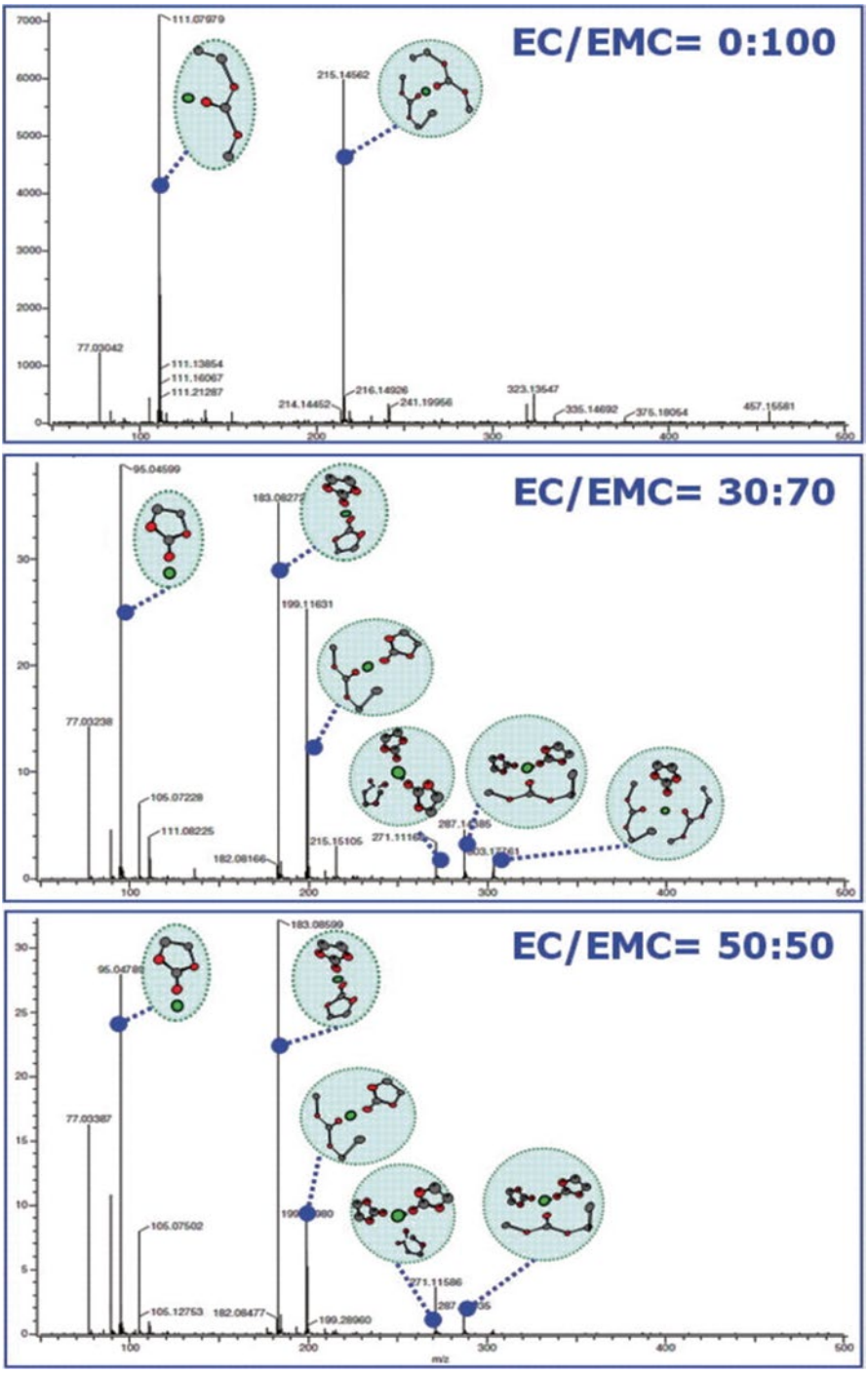

Fig. 5.12 Mass spectra of 1.2 M $LiPF_6$ in EC/EMC solutions with three typical cyclic/acyclic carbonate ratios: EC/EMC 0:100, EC/EMC 30:70, and EC/EMC 50:50. The peak at $m/e = 77$ corresponding to complex of AN-$(H_2O)_2$, caused by contamination of environmental moisture and trace amount of AN remaining in the chamber after nozzle cleaning (reproduced with permission by Electrochemical Society from [49])

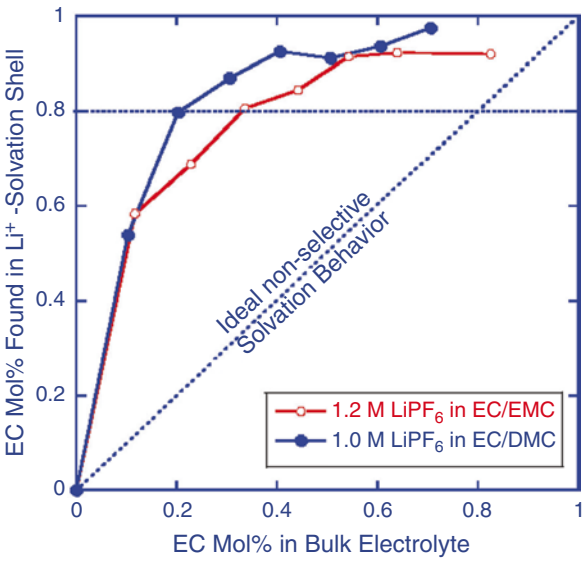

Fig. 5.13 Distribution of cyclic carbonate EC population within Li^+-solvation sheath against bulk electrolyte solution (reproduced with permission by Electrochemical Society from [49])

For the EC/EMC = 30:70 (or 34.1 mol %), which is the most typical composition adopted in Li-ion battery research community, the presence of Li^+-solvation sheath has already become predominant (Fig. 5.12, middle), with the most populous species being Li(EC) and $Li(EC)_2$. Considering that EMC is still the dominant ingredient in the bulk electrolyte, apparently, Li^+ exhibits a strong preference in recruiting EC as its solvation sheath. When the concentration of EC increases to 50 % (or 56.7 % mol %), EMC has essentially disappeared from the solvation sheath, while EC nearly becomes the exclusive sheath member, despite the fact the EMC presence in the bulk electrolyte is approximate half ratio.

Based on the abundances of each species, Cresce et al. quantitatively calculated the statistic distribution of cyclic and acyclic carbonate molecules within the Li^+-solvation sheath, as shown in Fig. 5.13. If there is no preferential solvation by Li^+, then EC and EMC should have the same opportunity to enter the sheath, and the relation between EC-sheath population and EC-bulk composition should ideally follow the dotted diagonal straight line in Fig. 5.13. However, a very positive deviation toward EC content occurs in all the electrolyte composition investigated, revealing this favorite between EC and Li^+.

Based on the above discussion, in the current electrolytes used by Li-ion battery industries and research communities the wt.% of EC is normally above 20 %, in which each individual Li^+ almost exclusively coordinated with EC molecules; that is why the interphasial chemistry on graphite anode almost exclusively consists of EC-reduction products.

The Li^+ solvation factor might also play an important role in the reduction kinetics of solvents molecules. This was also supported by the computation results. According to the Wang et al. calculation results, the reduction of a neat-solvent molecule is thermodynamically forbidden with a higher energy barrier for the initial

ring-opening process, while the energy barrier is dramatically decreased with the formation of Li^+-solvation sheath [11].

5.3.2.2 Simulations: From Quantum Mechanics and Molecular Dynamic

Most of the available SEI formation mechanisms were proposed based on the experiment phenomena, such as decomposition products and surface resistance. Hence, these mechanisms are somewhat limited by the artifact of measurement and processing techniques, and it is difficult to give detailed and high certainty information of the SEI formation and growth. Nowadays, quantum mechanics and molecular dynamic simulations using chemically accurate methods show good advantage of providing detailed information on electron transfer between electrode and electrolyte and decomposition reaction pathways and predicting reaction products and spatial distribution of reaction products in the SEI film.

Reduction Mechanism of Solvent and Additives in Gas and Solution

One- and two-electron reduction decomposition reaction of isolated EC and supermolecules as $Li^+(EC)_n$ ($n = 1–5$) were studied by using density functional calculations, both in gas phase and in solvent [11]. The coordination with Li^+ was found to significantly lower the reduction stability of EC and stabilized the reduction intermediates of EC. Surprisingly, the excess electron was found to be more energetic favorable to distribute on EC, instead of Li^+. Different with the effect from Li^+, the reduction stability of $Li^+(EC)_n$ complex increased with the increasing of solvent number. However, the decomposition activation energy and products showed weak dependence on the solvent number. As shown in their results, formation of Li_2CO_3 is slightly favorable in the complex with smaller EC number, and $(CH_2OCO_2Li)_2$ is favored in higher EC number complex. One year later, the calculations on a reduction reaction of $(EC)_nLi^+(VC)$ complexes were also carried out to elucidate the role of SEI film additive vinylene carbonate (VC) in EC solvent [50]. Similar with $Li^+(EC)_n$ complex, the reduction stability of $(EC)_nLi^+(VC)$ was found to increase with the increasing of solvent number. As expected, the reduction stability of $Li^+(VC)$ is lower than $Li^+(EC)$ and leads to a previous reduction of VC than EC in electrolyte, which is in agreement with most of the experimental results. The reduction mechanism of $(EC)Li^+(VC)$ is given in Fig. 5.14, which shows that it is more energetically favorable for giving the excess electron on VC instead of EC in (EC) $Li^+(VC)$ complex. However, the subsequent decomposition reaction is more likely to happen via a ring opening on EC, which is about 7 kcal mol^{-1} lower than on VC. In addition, the former forms a more stable radical anion than the latter by 12.4 kcal mol^{-1}.

Taking into account thermodynamic as well as kinetic aspects of the reduction decomposition of $(EC)Li^+(VC)$, the optimal reaction path is initially reduced to the most stable intermediate by VC reduction (17 in Fig. 5.14) and then proceeds through a hemolytic ring-opening reaction of EC (23 and 22 in Fig. 5.14) to

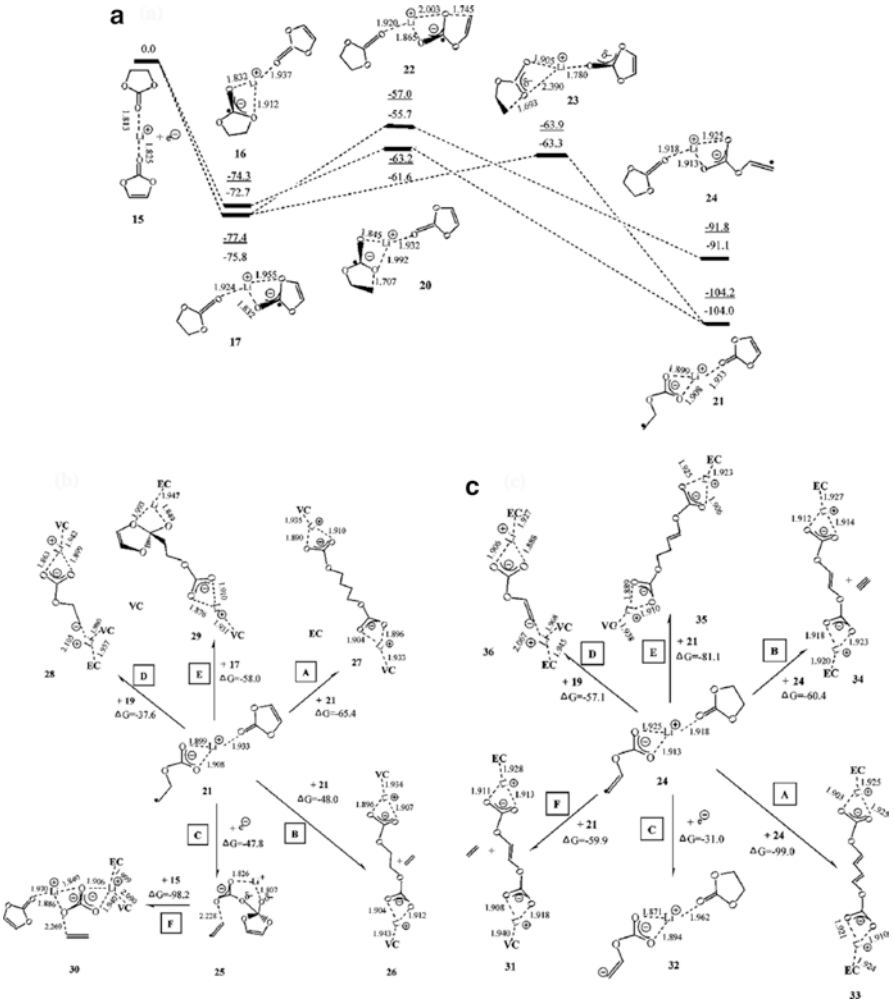

Fig. 5.14 (**a**) Potential energy (*underlined data*) and Gibbs free energy profile at 298.15 K for the reductive decomposition process of (EC)Li^+(VC) calculated with B3PW91/6-311++G(d,p)// B3PW91/6-31G(d). (**b**) Termination paths for the radical anion from the EC reductive dissociation in (EC)Li^+(VC) calculated with B3PW91/6-311++G(d,p)//B3PW91/6-31G(d) method. (**c**) Termination paths for the radical anion from the VC reductive dissociation in (EC)Li^+(VC) calculated with the B3PW91/6-311++G(d,p)//B3PW91/6-31G(d) method (reproduced with permission by the American Chemical Society from [50])

generate a more stable initial decomposition product (21 in Fig. 5.14). So far, the role of VC as an SEI film additive was understood by catalyzing the decomposition of EC. The major calculated reduction decomposition products from this electrolyte system are organic products that would build up an effective SEI film, such as lithium dicarbonates and lithium carbonate. The reduction products from VC are expected to improve the SEI film by further polymerizing on the electrode surface.

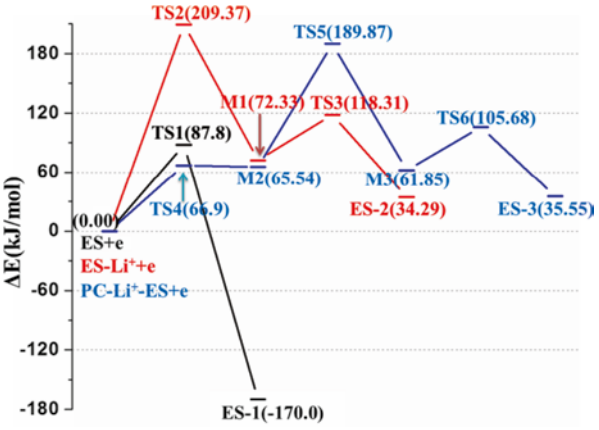

Fig. 5.15 Potential energy profile for the decomposition process of ES in the forms of isolated ES, ES-Li^+, and ES-Li^+-PC (reproduced with permission by Elsevier from [54])

Reduction decomposition of clusters of $(PC)_nLi^+$($n=2$, 3) and $(PC)_nLi^+(VC)$ ($n=1$, 2) was studied in the same year [51]. The results revealed that the cointercalation of PC with Li^+ into graphite layers (due to the strong interaction of PC with Li^+) and the nature of the reduction products of PC may be responsible for its disability to passivate the graphite surface. VC plays a similar role in PC-based system with EC, that is, weakening the co-interaction of PC, stabilizing the initial reduction products, and generating more proper film-forming agents. On the contrary, a decomposition of VC near a Li cluster surface was found to be smaller than EC and PC, while its reaction enthalpy is only moderately different from that of EC and PC [52]. And this lower activation energy of VC is explained by the somewhat stronger binding between the carbonyl group and the Li cluster surface, generating Li-organic product. This indicates that the nature of the electrode would change the reaction mechanism of the solvent and the formation of SEI.

Reduction decomposition reactions of two SEI film additives, 1,3-benzodioxol-2-one and ethylene sulfite (ES), were investigated with density functional theoretical calculation in gas phase [53, 54]. Both of these additives were found to have lower reduction stability than PC. Hence, preferable reductions of these additives are expected. Coordinating with Li^+ was found to lower the reduction stability of ES but increase the decomposition activation energy, as shown in Fig. 5.15. A cluster of ES-Li^+-PC was also investigated to understand the effect of coordinated solvent. Reduction stability of this cluster was found to be higher than ES-Li^+ and lower than ES. Interestingly, the structure and charge distribution of PC changed very slightly during the reduction decomposition of ES-Li^+-PC, which means that PC is not involved in this decomposition and film formation.

Based on these above calculation results, a conclusion can be drawn that an ideal candidate SEI film additive should at least have lower reduction stability than the cosolvent, so that it would reduce before the solvent. Also, it is necessary that the final decomposition products of these additive–solvent–salt complexes could incorporate into the SEI film.

Most components of the SEI film, such as LMC, LEC, LEDC, LPDC, and Li_2CO_3, have been identified by recent advanced techniques [9, 22, 38, 40]; the structure,

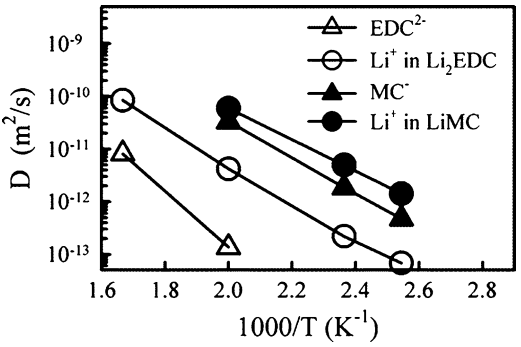

Fig. 5.16 Alkyl carbonate and EC/$LiTFSI_{16}$ conductivity from MD simulations (reproduced with permission by the American Chemical Society from [56])

aggregation energy, and electrochemical properties of these film components were also understood by simulation. Lithium alkyl carbonates associated through intermolecular O–Li^+–O were proposed by Want et al., based on density functional theoretical studies in gas phase [55]. The interaction of O–Li^+ is ionic. The calculated IR spectra of the associated lithium alkyl dicarbonates are in agreement with the experimental data, indicating that lithium alkyl dicarbonate exits on the anode surface as dimmers, trimers, tetramers, and even higher order *n*-mers rather than monomers. A more detailed and precise studies on the properties of LMC and LEDC were carried out later by using molecular dynamic simulation with quantum chemistry-based many-body polarizable force field [56]. It was found that the intermolecular bridging via one Li^+ dominates and each Li^+ is coordinated by approximately four oxygen atoms that come primarily from different alkyl carbonate molecular. Based on the results from the calculated ion self-diffusion and conductivity of LMC and LEDC system, they predicted that SEI comprising primarily LEDC with a typical width of about 10 nm would give rise to significant SEI layer resistance, the order of 10^{-10} S cm^{-1} at the simulated temperature of −30 °C, as shown in Fig. 5.16. Charge transport in LEDC was found to be almost entirely due to Li^+, based on the results that the cages formed by carbonate groups around Li^+ lived longer than the residence time of one Li^+ near these carbonate groups. The conductivity of LMC was up to an order of magnitude higher than LEDC, and the lifetime of Li cation was comparable to the residence time of Li^+ complexation of carbonate groups.

Interstitial positions and migration barriers of Li^+ diffusion mechanisms in Li_2CO_3 have been studied recently by using density functional methods [57]. They found that the most probable path of Li^+ diffusion in bulk monoclinic Li_2CO_3 crystal is along the open 010 channel, which has the lowest barrier, about 0.3 eV. The diffusion mechanism of Li^+ involves a continuous making and breaking O–Li^+ bonds while maintaining a high coordination with O during the process and resulting in low migration barrier. These results predict that a thin layer of the graphite surface with the proper orientation will provide good ion conductivity and enhance the stability of the battery. Chen et al. using density functional theory confirmed that SEI composed of Li_2CO_3, Li_2O, and LiF is prohibitive to electronic conduction. Specifically, from the calculation, the electronic structures of these three species are all insulated with large forbidden band gap. The calculated barrier for Li^+ diffusion in Li_2CO_3 ranges from 0.227 to 0.491 eV, which is quite close to the previous

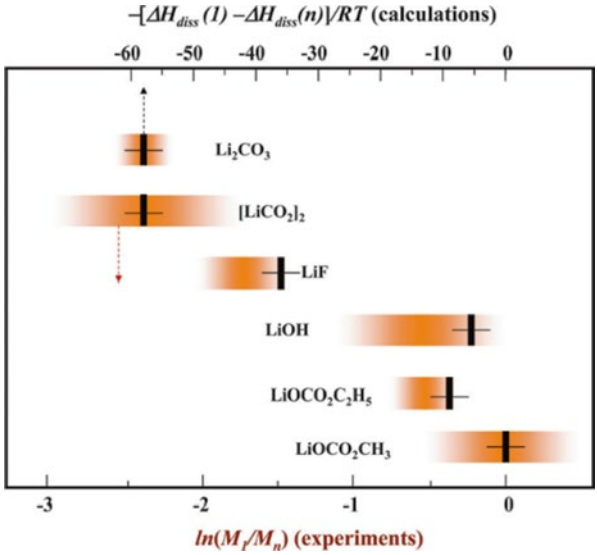

Fig. 5.17 The natural logarithm of M_1/M_n ($\ln(M_1/M_n)$), the lower axis, plotted against $-[\Delta H_{diss}/(1) - \Delta H_{diss}/(n)]/RT$, the upper axis, for the salts for which 1 and n refer to $LiOCO_2CH_3$ and any other salt, respectively. The *wide bar* represents $\ln(M_1/M_n)$ with the experimental error; the *perpendicular line* shows $-[\Delta H_{diss}/(1) - \Delta H_{diss}/(n)]/RT$, with the statistical error shown by a *thin horizontal line*. The solvent was DMC (reproduced with permission by the Electrochemical Society from [58])

simulation results [57]. Li^+ diffusion in Li_2CO_3 and Li_2O was found to be as fast as in graphite, but more difficult in LiF, since the calculated barrier in LiF is as high as 0.729 eV. Based on these simulations, better ion conductivity of the SEI film could be achieved by increasing LMC, Li_2CO_3, and Li_2O and reducing LiF.

Solubility of several well-known organic and inorganic salts that form the SEI, such as lithium oxide(Li_2O), lithium carbonate (Li_2CO_3), lithium oxalate ($[LiCO_2]_2$), lithium fluoride (LiF), lithium hydroxide (LiOH), lithium methoxide ($LiOCH_3$), LMC, LEDC, and dilithium ethylene glycol dicarbonate (LEGC), has been studied in DMC and EC solvents by using molecular dynamic simulation [58]. The calculated heat generation from the dissolution of investigated salts in DMC was found to range from exothermic for organic salts to endothermic for inorganic salts, in the order as $LEGC < LMC < LiOH < LEDC < LiOCH_3 < LiF < [LiCO_2]_2 < Li_2CO_3 < Li_2O$ (the value went from more negative in the left to more positive in the right), which is in good agreement with their previously experimental results [59], as shown in Fig. 5.17. The solubility order of these salts was found to be almost the same, while a overall higher solubility was found in EC compared with DMC. Polarity, size, and shape of the solvent molecular were found to play important roles in dissolved salts. On the other hand, the larger the size of the salt is, the more soluble it will be. Having a linear or a planar molecular shape will promote an enhanced molecular packing in crystal lattice and tend to dissolve less easily than the one having bulky groups or flexible chains.

Reduction Mechanism of the Solvent on Electrode Surface

More recently, people started to look into the reduction reaction/SEI film formation of solvent on the electrode surface. On the other hand, the developments of

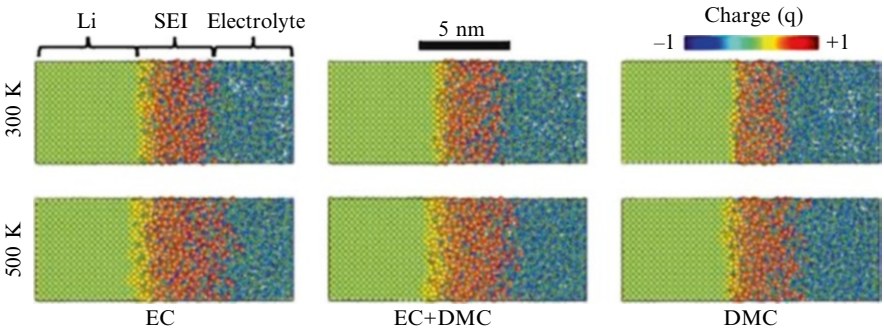

Fig. 5.18 Atomic configuration in the SEI formed between Li metal and electrolytes (EC, EC+DMC, and DMC) at different temperatures (300 and 500 K). Snapshots in the figure are obtained after 40 ps of NVT MD simulations. The atoms are color coded according to their charge state (green is neutral) (reproduced with permission by Elsevier from [61])

high-performance computers enable researchers to have both electrode and electrolyte in the simulated systems. Initial stages of SEI formation of EC on graphitic surface with different terminated groups were investigated by using ab initio molecular simulation [60]. On pristine graphite electrode surface and before the formation of SEI, fast EC decomposition was found to initiate at the graphite edge regions, which is in good agreement with the previous experimental reports [24, 37]. Decomposition products CO_3^- and $(CH_2CO_3Li)_2$ would coordinate to the carbon edges with Li^+ and other ionic products, forming SEI film. In this stage, termination groups of carbon edge strongly affect the decomposition of EC. Termination group C=O gives stronger driving force to the decomposition of EC than C–OH and C–H groups, generating both C_2H_4 and CO gas and ionic products. However, once the SEI film was formed on the graphite surface, the decomposition mechanism of EC would change due to the slower electron transfer from the electrode to the solvent, which may also change the composition of the later stages of SEI formation. Later on, the electron transfer on the lithium electrode/EC interface was investigated, showing that there are two regimes for the electron transfers to the adsorbed EC. EC is coupled strongly with the pristine Li (100) electrode surface and accepts electron undergoing decomposition in picosecond time scale. However, on the electrode coated with oxide layer, electron transfer to absorbed EC is significantly slowed down due to the reorganization energy of the adsorbed EC. These simulation results were confirmed by gravimetric measurements.

Besides electrode surface structure, the nature of the electrode and solvent also affect the evolution of the SEI. An interesting and detailed simulation of formation and growth of SEI on Li metal surface in EC, DMC, and EC mixed with DMC electrolyte was done by Kim et al., using reactive force field (ReaxFF) molecular simulations [61]. The SEI film was found to grow faster in EC-based electrolyte compared to DMC, generating thicker SEI film, and EC mixed with DMC electrolyte came in between, as shown in Fig. 5.18. This simulation result agrees with the

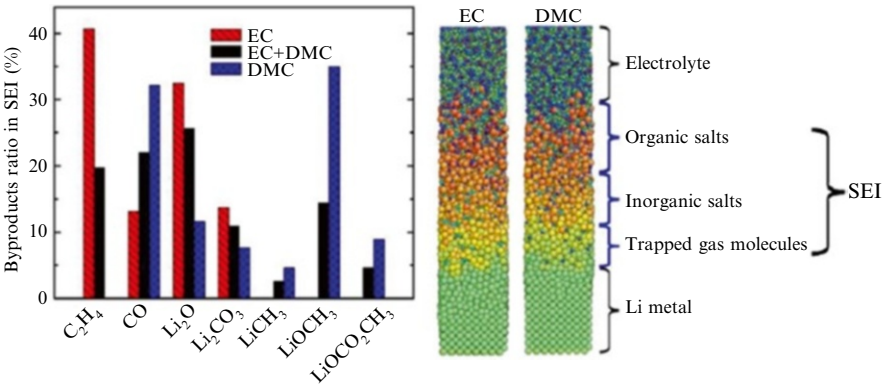

Fig. 5.19 Distribution of the SEI components for different electrolytes (*left*). Atomic configurations from MD simulations; the components of the SEI are identified (*right*) (reproduced with permission by Elsevier from [61])

experiment observations that EC is more reactive than DMC [62, 63]. On the other hand, the SEI film grew with the increase of temperature. The components of the SEI were shown to be highly dependent on the type of solvent as well as the electrode. For example, on Li electrode surface, the SEI is composed largely of Li_2O and Li_2CO_3 in EC-based electrolyte and Li_2O, Li_2CO_3, $LiOCO_2CH_3$, $LiCH_3$, and $LiOCH_3$ in DMC-based electrolyte. The absence of LEDC in SEI film on lithium electrode surface found from the recent experiment work [64] was well understood from this simulation. LEDC formed in the early stages of the SEI formation decomposed into inorganic salts and hydrocarbon molecules in lithium-rich environment, while in Li-poor environment, such as graphite electrode; LEDC stayed as the major component with the growth of SEI film. Figure 5.19 shows the multilayer SEI formed in the SEI growth simulation. Inorganic salts are found closer to the electrode surface, while the organic salts are near the electrolyte–SEI interphase. The SEI formation potential predicted from this simulation is between 0.9 and 1.0 V vs. Li/Li^+, which is also in agreement with experimental results [65, 66].

5.3.2.3 Possibility of Manipulation

The surface SEI layer formed on electrode prevents the sustaining decomposition of electrolyte but slows down the mass/charge transfer rates across the interface, which degrades the battery performance, especially in the application of sub-ambient temperature discharge or high rate charge–discharge. To minimize this negative effect, numerous studies were addressed to manipulate the SEI in the past two decades.

In order to tailor an interphase which allows higher rate or low-temperature discharge capability, researchers have been adopting the strategy of forming a thinner

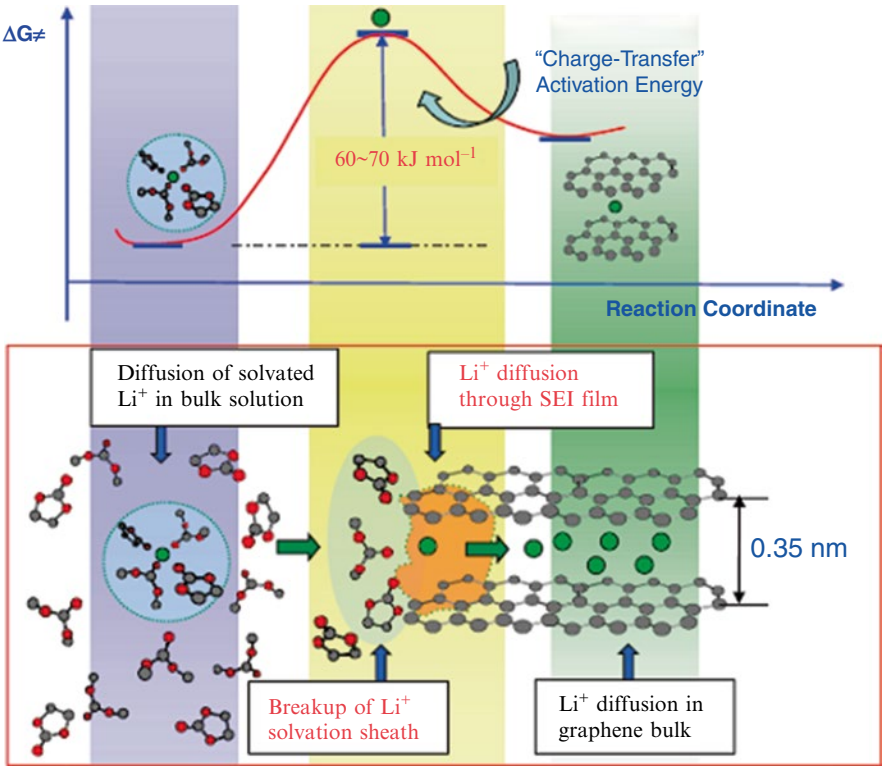

Fig. 5.20 The energy barrier during the journey of a Li^+ from bulk electrolyte into graphite anode and its two contributing sources: (1) Li^+ desolvation and (2) Li^+ migration through interphase (reproduced with permission by the American Chemical Society from [67])

SEI to achieve maximum of Li^+ conductance. So far, series of electrolyte additives have been designed, modeled, and synthesized to meet the purpose. However two restrictions should be taken into account when we manipulate the interphase: (1) the minimal thickness of SEI cannot be thinner than 2 nm, below which electron tunnel occurs and sustaining decomposition of electrolyte inevitably takes place, and (2) no matter how thin the SEI is, Li^+ desolvation cannot be avoided at graphite/electrolyte interface during charging process. The overall energy barrier of Li^+ desolvation can be estimated from $Li_4Ti_5O_{12}$(LTO)/electrolyte interface, on which it is believed to be free of any interphase because the reversible intercalation of Li^+ occurs at ~1.5 V vs. Li/Li^+. The pure contribution from Li^+ desolvation process to the lithiation of LTO ranges around 50 kJ mol^{-1} [67]. On the basis of Ogumi [68] and Xu's work, the so-called charge-transfer component on graphitic anode/electrolyte is usually characterized by an activation energy of 50–70 kJ mol^{-1}, as shown in Fig. 5.20. Therefore, the Li^+ desolvation controls the kinetics of lithiation process of intercalation anode materials, such as graphite and LTO.

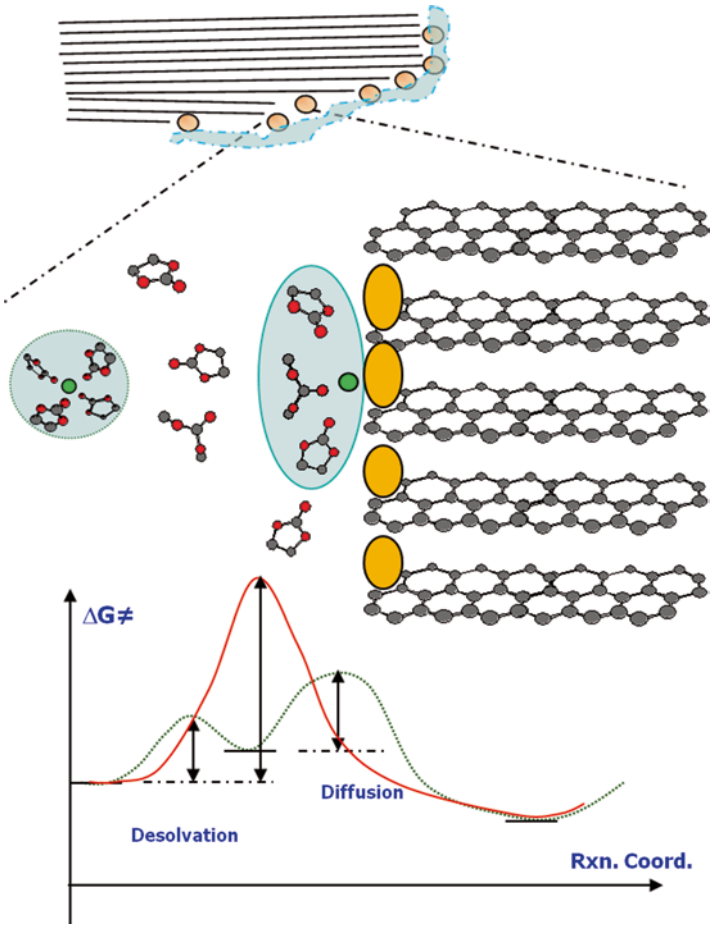

Fig. 5.21 New strategy is needed to target the interphasial chemistry at graphitic edge sites in order to "catalyze" the disruption of Li^+-solvation sheath (reproduced with permission by the American Electrochemical Society from [69])

Considering that the Li^+ desolvation dominates the energy consuming during the entire lithiation process, one can imagine that an ideal interphase should not be just thin in physical thickness but be chemically desirable in a way that can catalyze the breaking up of Li^+-solvation sheath, as illustrated in Fig. 5.21 [69]. Specifically, since we know that lithium intercalation only occurs at the edge sites of graphite, a new strategy of manipulating SEI chemistry should directly target these active sites by designing new electrolyte additives that can modify the physicochemical properties there. This new direction that has been under exploration in the past could result in breakthroughs in new power-intense graphic anode materials.

5.3.3 *Properties of Interphases*

5.3.3.1 Growth

SEI thickness on composite electrodes cannot be accurately measured or even reasonably defined in some cases because of the porous surface of graphite electrode and the uneven distribution of the surface ingredients. Estimates based on spectroscopic data identified the average value ranging from 3.0 to 7.0 nm, comparable to the estimates for an interphase on lithium metal. Scanning tunnel microscope (STM) also confirmed that the minimal thickness of SEI should be >2 nm, which is the maximum electron tunneling distance.

The thickness of the interphase is proportional to the amount of electrolytes consumed during its formation cycles; the irreversible capacity in the initial cycles was often used to quantify the thickness as a measure for the quality of the SEI. Based on the correlation between the thickness of interphase and irreversible capacity, Dahn et al. developed a high-precision coulometry method to study the growth of interphase formed on graphite surface [70]. Their experimental results showed that time and temperature, while not cycle count, are the dominant contributors to the growth of the SEI. They also addressed the equations (5.1–5.3) to describe the SEI growth rate and consumption of Li on graphite electrode:

$$\frac{\mathrm{d}x}{\mathrm{d}t} = \frac{k}{x} \tag{5.1}$$

$$x = \left(2kt\right)^{\frac{1}{2}} \tag{5.2}$$

$$\frac{\mathrm{d}x}{\mathrm{d}t} = \left(1/2k\right)\frac{1}{2}t - \frac{1}{2} \tag{5.3}$$

Herein, x represents the thickness of the passivating layer, k is a proportional constant, and t is time. Therefore, the SEI thickness increases approximately with time$^{1/2}$ consistent with a process where the temperature-dependent SEI growth is inversely proportional to the SEI thickness.

Not long after Dahn's work, Shenoy et al. employed molecular dynamics simulations to study the formation and growth of solid electrolyte interphase for the case of EC, DMC, and mixtures of these two solvent on lithium metallic electrode [61]. In their work, they investigated the constitutes and structures of SEI on lithium metal electrode with the dependence of electrolyte composition and temperature change. The results show that the SEI films grow faster in the case of EC compared to DMC, with EC + DMC mixtures falling in between, as shown in Fig. 5.22.

The density of Li consumed in the SEI tends to be of asymptotic limit, which depends on the electrolyte composition but weakly on the temperature. In addition, the Li density in SEI formed in EC-based electrolyte is slightly higher than that in DMC and EC + DMC mixtures, suggesting that EC is more reactive compared to

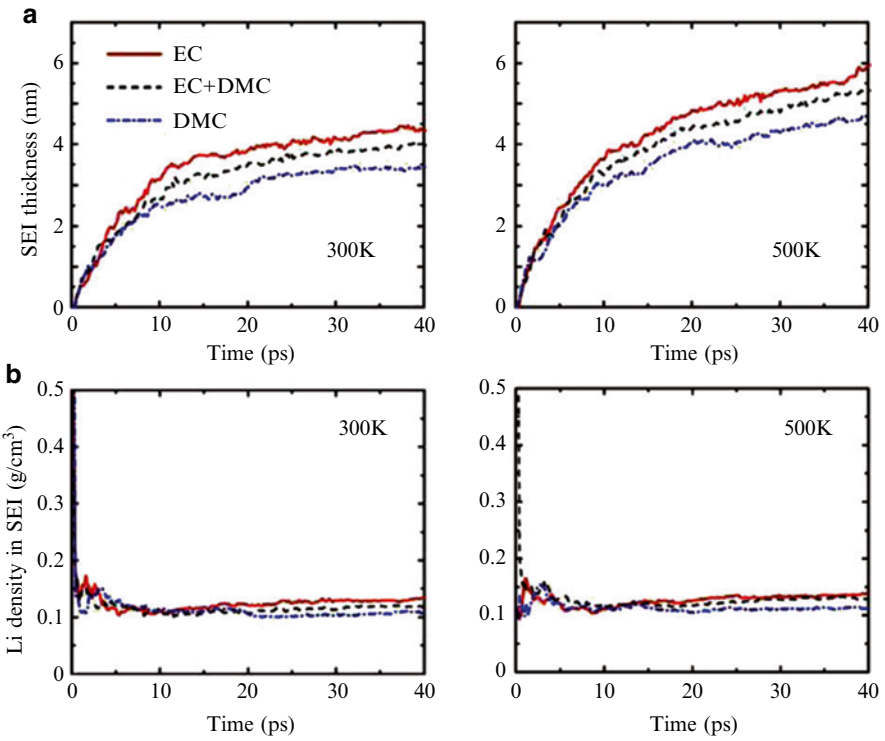

Fig. 5.22 Evolution of the thickness of the SEI (**a**) and Li density in the SEI (**b**) formed between Li metal and electrolyte (EC, EC+DMC, and DMC) at different temperatures (300 and 500 K) (reproduced with the permission by Elsevier from [61])

DMC. And they also found that SEI films formed in EC electrolyte are rich in Li_2CO_3 and Li_2O, accompanying with gas molecules, C_2H_4 and CO, while $LiOCH_3$ is the primary constituent of DMC electrolyte. While LEDC is formed in the presence of EC at low Li surface densities, it quickly decomposes to inorganic salts during subsequent growth in Li-rich environments. As the growth of SEI progresses, the quantity of Li_2CO_3 keeps increasing. The amount of Li_2O in the SEI increases at the expense of LEDC, as shown in Fig. 5.23. Moreover, they also concluded that the multilayer structure of SEI with regions rich in inorganic salts is located closely to the anode surface, while organic ingredients are located near the electrolyte interface.

5.3.3.2 Ion Transport

Compared to the studies on the chemistry composition, structure, and formation mechanisms of SEI, not too much attention has been paid to understanding the ion transport mechanism by which Li^+ passes through the SEI during the charging and

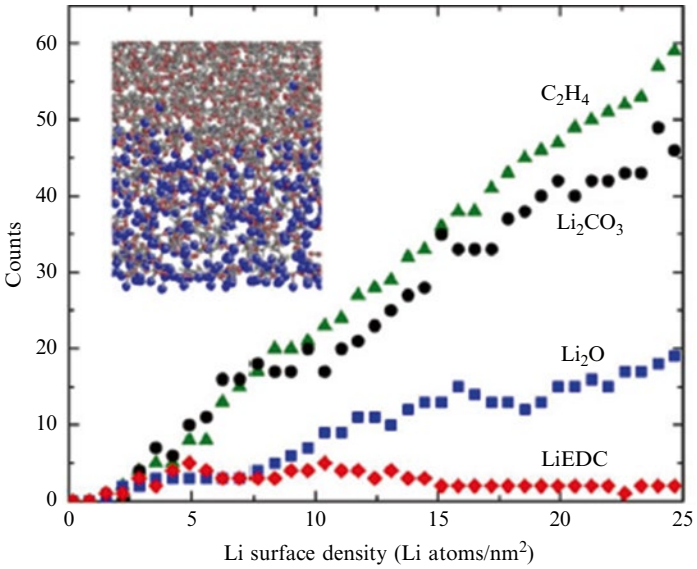

Fig. 5.23 The evolutions of EC-based SEI components with increasing Li density (reproduced with the permission by Elsevier from [61])

discharging steps. Some reports or experiments had been done by Peled et al. to understand the ionic conductivity in SEI films [6, 7, 17]. Aurbach proposed that some of Li^+ in SEI is exchanged with Li^+ in the electrolyte based on the observation of dynamic precipitation and dissolution of the salt in SEI [36].

Transportation of Li^+ in the electrolyte through the SEI may occur via several different mechanisms. One possible mechanism is that Li^+ after desolvation directly passes through pores since SEI is porous; the other possibility is that Li^+ after desolvation exchanges with Li^+ in the SEI. Recently, Harris et al. provided a more detailed description of ion transport mechanisms in SEI film by using isotope-labeled electrolyte approach [71]. They immersed three copper electrodes which were preformed SEI in $LiClO_4$ EC/DEC electrolyte into 1 M $^6LiBF_4$ EC/DEC electrolyte for 30 s, 3 min, and 15 min. After immersion, the electrodes were rinsed with DMC solvent and then transferred under Ar to a time-of-flight secondary ion mass spectrometer (TOF-MS); the results are shown in Fig. 5.24.

After immersion in $^6LiBF_4$ electrolyte, the increase of $^6Li^+$:$^7Li^+$ ratio suggested that electrolyte $^6Li^+$ appeared within the $^7LiClO_4$ SEI. For the samples experienced 30-s and 3-min immersion, the $^6Li^+$:$^7Li^+$ ration peaked near surface and then decreased to a nearly constant value beyond a depth of 5 nm.

5.3.3.3 Thermal Stability

Since we know that buildup of SEI prevents continuous electrolyte reduction, the SEI in a working Li-ion battery should maintain its physical integrity on a graphite

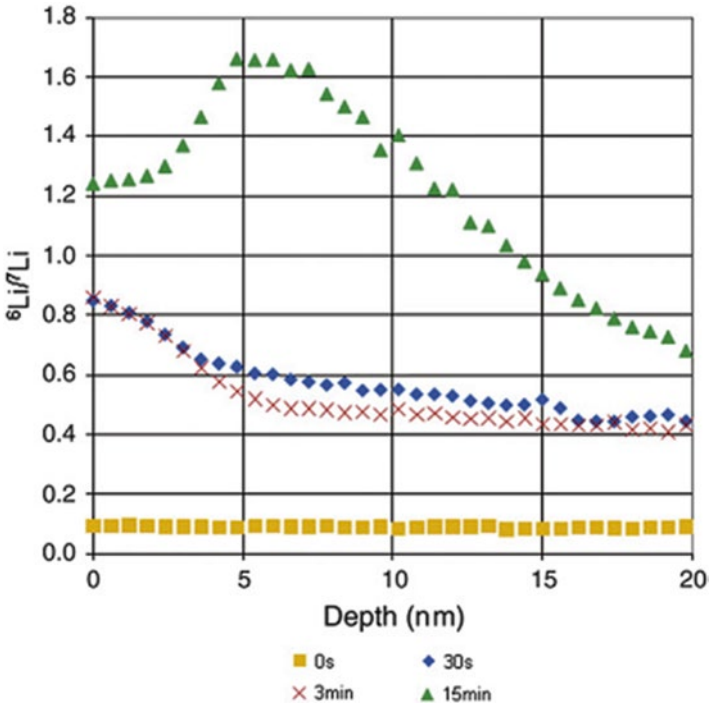

Fig. 5.24 SIMS depth profile of $^{6}Li^{+}$:$^{7}Li^{+}$ isotope ratio for $^{7}LiClO_4$ SEI after immersion in $^{6}LiBF_4$ electrolyte for 30 s, 3 min, and 15 min (reproduced with the permission of Elsevier from [71])

anode against both dissolution and chemical erosion from the acidic electrolyte solution. In the real application case, Li-ion batteries inevitably work at elevated temperatures. Therefore, the thermal stability of SEI formed on graphite electrode at elevated temperature should be evaluated.

Wan et al. investigated the thermal stability of SEI formed in $LiPF_6$ and $LiClO_4$ EC/DEC electrolyte via the combination of electrochemical impedance spectroscopy (EIS) and in-line FTIR-DSC [72]. The SEI formed in $LiPF_6$ EC/DEC electrolyte suffered periodical damage/reformation after storage at 85 °C, resulting in an oscillating impedance pattern. The source of thermal instability has been identified to be the strong Lewis acid PF_5, which is the thermal decomposition product of $LiPF_6$ salt. However the SEI formed in $LiClO_4$ EC/DEC electrolyte showed significant thermal stability after exposure to elevated temperature due to the absence of Lewis acid PF_5. Their results showed that the type of the conductive salt has a great impact on the thermal stability of the SEI when the cell experienced aging.

A few years later, Zhao et al. also studied the thermal stability and chemical structure of SEI formed on a natural graphite electrode in $LiPF_6$ EC/DMC electrolyte by thermogravimetry-differential thermal analysis combined with mass

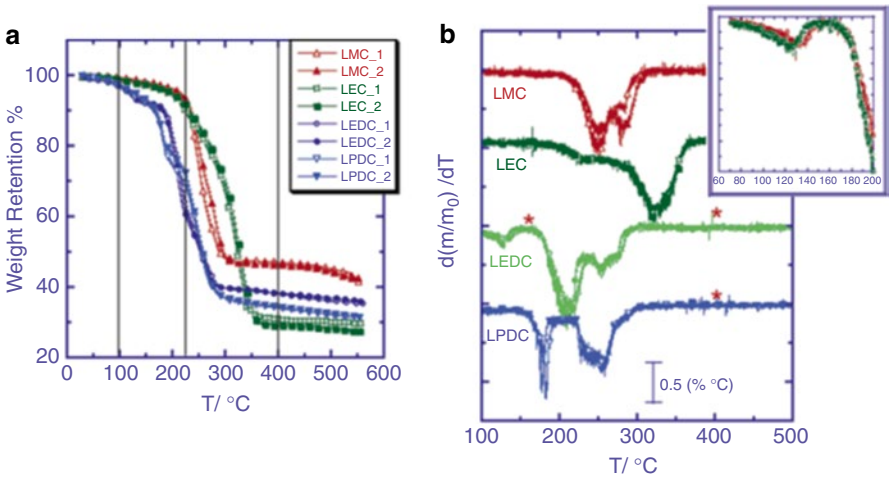

Fig. 5.25 Thermal instability of the lithium alkyl carbonate: (**a**) weight retention as function of temperature as recorded with TGA; (**b**) onset temperatures of the multistage thermal decomposition as demonstrated by DTG plots (reproduced with permission by the American Chemical Society from [38])

spectrometry (TG-DTA/MS) and XPS [73]. They found that the SEI formed on graphite electrode in discharged state was decomposed at around 330 and 430 °C and accompanied by CO_2 evolution. The evolution of CO_2 at 330 °C was not detected after the prolonged charge–discharge cycles, while the intensity of that at 430 °C increased. CO_2 evolution at 330 and 430 °C is believed to be mainly caused by the decomposition of lithium alkyl carbonate and lithium oxalate, respectively. The formation of lithium oxalate was attributed to the reduction of lithium alkyl carbonate during the intercalation of lithium ions.

However either Wan or Zhao was focusing on the SEI formed on graphite electrode with the presence of $LiPF_6$/carbonate electrolyte solution. The anions, solvents, or their dissociation products at elevated temperature may affect the thermal stability of SEI. Xu et al. extensively investigated the thermal stability of the pure SEI components, LEDC, LMC, LEC, and LPDC [38]. TGA had been done to monitor the weight loss of these lithium alkyl mono- and dicarbonates in the temperature range of 30–550 °C, as shown in Fig. 5.25a. The derivative thermogravimetric (DTG) quantity $d(m/m_0)/DT$ was also plotted to locate the onset temperatures of weight loss, as shown Fig. 5.25b.

The lithium alkyl monocarbonate, LMC and LEC, exhibits much higher thermal stability than the two dicarbonates, LEDC and LPDC. Either the mono- or dicarbonate has multiple thermal processes with different onset temperature. On the base of identification of chemical components of TGA remnants via XPS and NMR after the samples were heated to different temperatures, they proposed the following competitive decomposition mechanisms (Scheme 5.10).

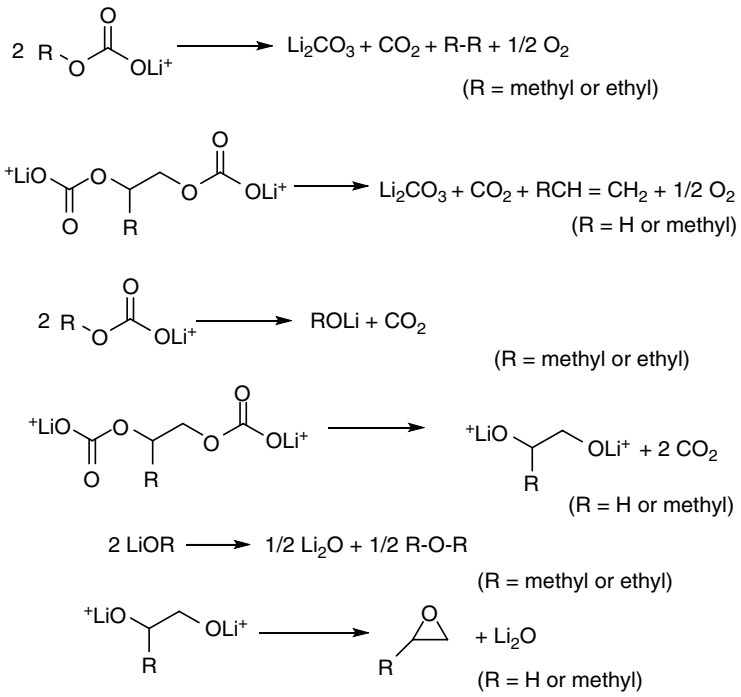

Scheme 5.10 Formation mechanisms of lithium alkyl monocarbonate (reproduced with permission by the American Chemical Society from [38])

5.3.4 Tailoring a Desired Interphase

Since we know that the interphase on graphitic anode plays a leading factor to the cell impedance, in the past three decades, many efforts have been favoring a thinner interphase in order to minimize the impedance of interphase, resulting in accelerating Li^+ transport through the resistive barrier. The most common approach to design or create thinner interphase is through introducing selected additives in the electrolyte, whose sacrificial decomposition prior to any other electrolyte components would form an interphase with different chemistry. Because the thickness of SEI on composite electrode is hard to measure or even define in some cases, basically, people like to calculate the irreversible capacity loss at initial cycle to quantify the thickness as a measure for the effectiveness of these additives.

5.3.4.1 Additives

As described above, computation approaches were usually employed to estimate the reduction or the oxidation potentials of candidate molecules, which are related to

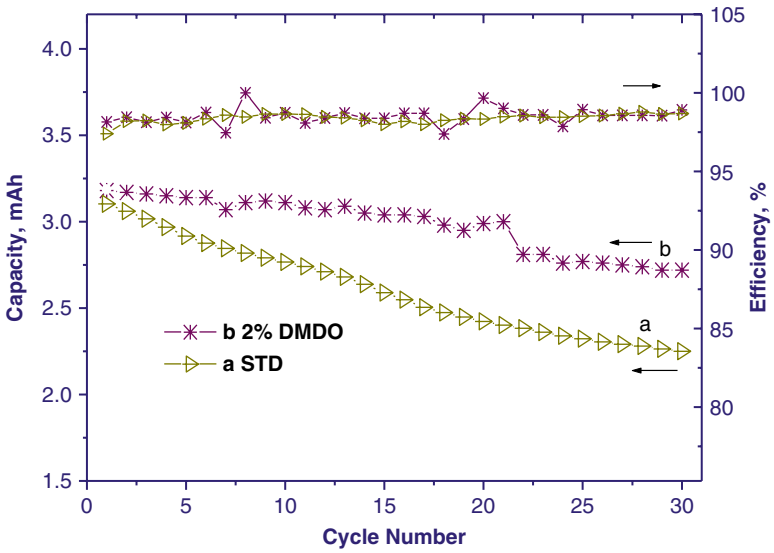

Fig. 5.26 Cycling performance of the cells with STD (*a*) and with STD+2 % DMDO (*b*) electrolytes (reproduced with permission by Elsevier from [80])

the energy levels of lowest unoccupied molecular orbit (LUMO) and highest occupied molecular orbit (HOMO), respectively. During the past two decades, the research field of seeking novel additives favoring thinner SEI on graphite anode is overwhelming through the computation approaches. Numerous additives have been developed to assist in the SEI formation, such as the type of polymerization monomer which is featured by one or more carbon–carbon double bonds in the molecules, VC [74–78], vinyl ethylene carbonate (VEC) [76, 79], and 4,5-dimethyl-[1,3] dioxol-2-one (DMDO) [80]. The mechanism of the polymerizable additives in facilitating SEI formation is based on an electrochemically induced polymerization [81], which can be described by a general equation:

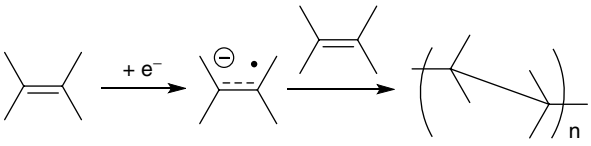

where the radical anion can be terminated by the solvent molecules to form insoluble and stable product as the preliminary SEI nuclei. Take DMDO as the example; its reduction on graphite anode at the first cycle is about 1.35 V. Figure 5.26 shows cyclic performances of $LiNi_{0.8}Co_{0.2}O_2$/MCMB cells in the standard (STD) and STD with 2 % DMDO electrolytes. Cells containing STD electrolyte experience a discharge capacity drop from 3.1 mA h on the first cycle to 2.25 mA h on the 30th cycle. The capacity retention is about 73 %. When STD with 2 % DMDO electrolyte is

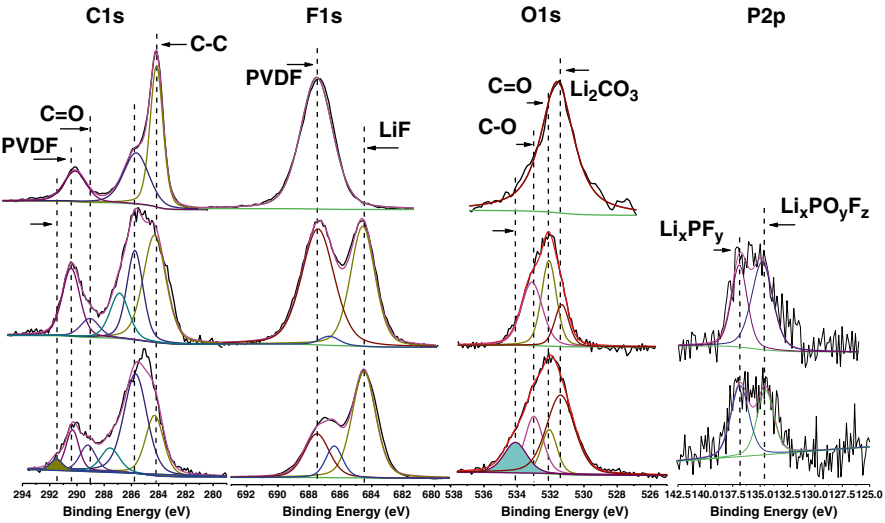

Fig. 5.27 C 1s, F 1s, O 1s, and P 2p XPS spectra of fresh MCMB anode (*top*) and cycled with STD (*middle*) and with STD + 2 % DMDO (wt.) (*bottom*) electrolytes (reproduced with permission by Elsevier from [80])

used the capacity drops from 3.18 mA h on the first cycle to 2.72 mA h on the 30th cycle, or about 85.5 % retention of the original capacity, which suggests that addition of 2 % DMDO can significantly improve the cycling stability at room temperature.

Analyses of the anode reveal significant differences in the surface species (Fig. 5.27). The C 1s spectrum of the anode cycled with the STD electrolyte contains peaks characteristic of PVDF (290.4 and 285.7 eV), C=O bonds in lithium alkyl carbonates and polycarbonates (290 eV), C–O bonds in ethers and carbonates (286–287 eV), and graphite (284.3 eV). The C 1s spectrum of the anode cycled with DMDO electrolyte contains peaks at 286–288 eV, consistent with the presence of C–O bonds in esters and carbonates, PVDF binder (290.4 and 285.7 eV), C=O bonds in lithium alkyl carbonates and polycarbonates (290 eV), as well as graphite (284.3 eV). In addition, a broad shoulder appears at about 291.5 eV at C1s spectrum of the anode with DMDO electrolyte. This peak could be ascribed to the product of decomposition of DMDO. Similar C 1s binding energies are reported for graphite anodes cycled in the presence of VC. The O 1s spectrum of the anode cycled with the STD electrolyte contains a broad peak characteristic of C–O and C=O containing components at 532–533.5 eV. This suggests the deposition of carbonate salts (Li_2CO_3 or lithium alkyl carbonates $ROCO_2Li$) on the surface of the electrode, resulting from the decomposition of the solvents. Several formation mechanisms of the carbonate species can be found in the literature.

Other oxygen-containing compounds may also be present in the SEI. The O 1s spectrum of the anode cycled containing STD with 2 % DMDO electrolyte is slightly different from that of the anode containing STD electrolyte. In addition to the C–O and C=O peaks observed with the STD electrolyte, a new peak at ~534.3 eV is

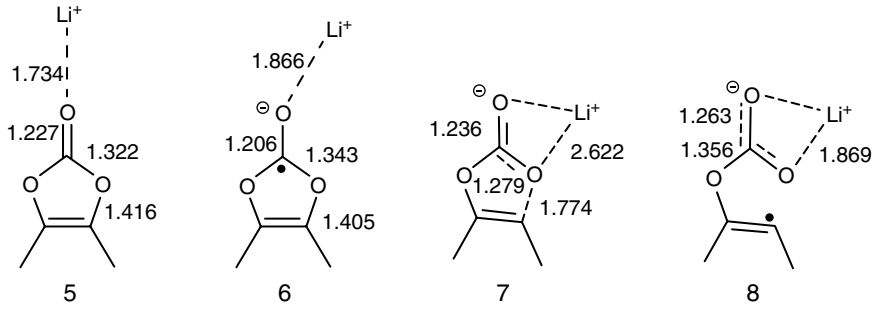

Fig. 5.28 Geometries of DMDO optimized at B3LYP/6-311++G(d,p) of the Li^+ effect in gas phase (reproduced with permission by Elsevier from [80])

observed. The additional peak suggests the presence of additional oxygenated degradation compounds in the SEI. Similar O 1s peaks are observed with VC containing electrolytes and are correlated to the new C 1s peak at 291.5 eV, as discussed above. The binding energy of 534.3 eV is a very high value for an O 1s peak and is assigned to the degradation products of DMDO. The F 1s spectrum of the anode cycled with STD electrolyte shows three main peaks. The peak at 687.6 eV is assigned to PVDF binder, while the peaks at 684.5 and 686.5 eV are attributed to LiF and $Li_xPO_yF_z$, respectively, the decomposition products of $LiPF_6$ commonly observed at electrode/electrolyte interface. The F 1s spectrum of the anode extracted from a cell containing STD with 2 % DMDO is similar, but the intensity of the peak corresponding to $Li_xPO_yF_z$ is greater. The intensity of PVDF binder of the anode cycled with STD electrolyte is much greater than that of the anode cycled with the STD with 2 % DMDO electrolyte, which suggests that the SEI film formed on the anode with STD is thinner than STD with 2 % DMDO electrolyte. The P2p spectra of the two samples are very similar, showing two peaks at about 134.5 and 137 eV; the peak at 134.5 eV is characteristic of $Li_xPO_yF_z$, and the peak at 137 eV could be assigned to Li_xPF_y.

Interestingly, ex situ XPS spectra after cycling with electrolyte containing the additive suggest that the electrode can be detected by the polymerization products of DMDO. Selected bond lengths of DMDO (1), the cyclic radical anion of DMDO (2), transition state for ring opening of the radical anion of DMDO (3), and acyclic radical anion of DMDO (4) are provided in Fig. 5.28. In the gas phase, the DMDO reductive decomposition is thermodynamically forbidden as supported by the positive ΔG (+20.7 kJ/mol) between DMDO and its reductive intermediate as well as the associated negative adiabatic electron affinity (EA ≈ −(ΔE + ΔZPE), −22.3 kJ/mol). The ring-opening reaction of the cyclic intermediate proceeds via the transition state (DMDO + e···ts); the energy barrier is approximately 67.7 kJ/mol in the gas phase. Frequency analysis shows only one imaginary frequency (−850) corresponding to the transition state. The results from intrinsic reaction coordinate (IRC) analysis also support that the DMDO + e···ts is connected with DMDO + e-cyclic and DMDO + e-acyclic. The formation of DMDO + e-acyclic is 3.4 kJ/mol more stable than the intermediate DMDO + e-cyclic.

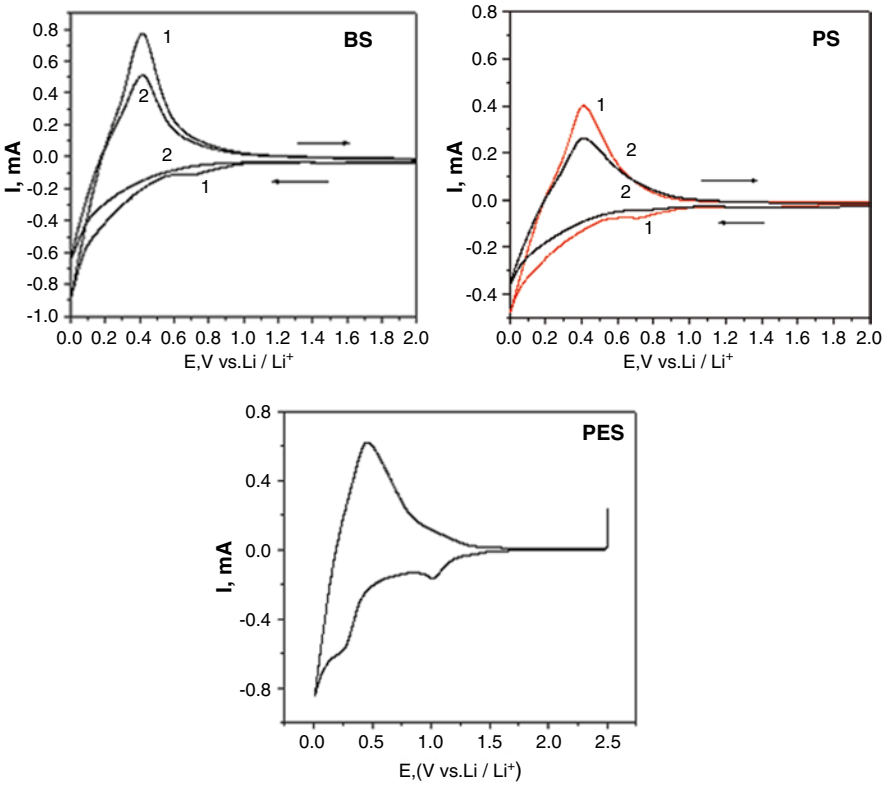

Fig. 5.29 Cyclic voltammograms of graphite electrodes in the electrolytes with and without BS, PS, and PES (reproduced with permission by Elsevier from [83], [85], and [86])

Based on the computation results we concluded that DMDO preferably reduced on the anode surface forming linear polymer as opposed to cyclic polymer:

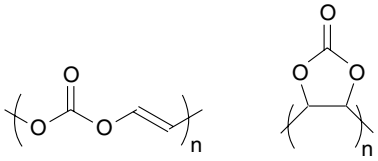

While the formation of DMDO-based species on cathode is not clear yet, the authors believed that the migration of the reduction products of DMDO on graphite anode surface to cathode side might be the possible reason.

Besides the above-described polymerizable monomer additives, sulfur-based compounds were proposed in our group as additives for forming anode SEI, including butyl sultone (BS) [82, 83], propane sultone (PS) [84, 85], prop-1-ene-1,3-sulton (PES) [86], as well as ES [54, 87]. These sulfur family additives have higher reduction potentials than the electrolyte solvents, as shown in Fig. 5.29.

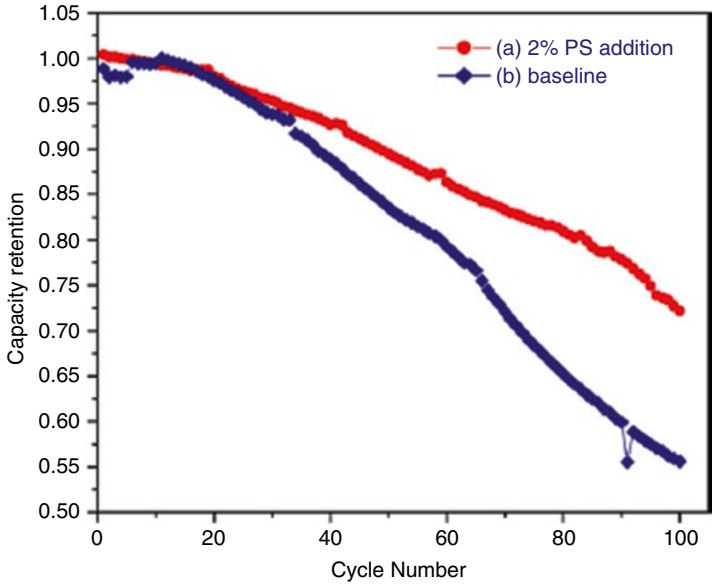

Fig. 5.30 Cycling performance of lithium-ion batteries after storage at 75 °C for 15 days (*a*) with 2 % PS and (*b*) blank electrolyte (reproduced with permission by Elsevier from [85])

Incorporation of low concentration of BS, PS, or PES can dramatically improve the cycling performance at room temperature due to the modification of surface interphase. In addition, addition of PS to the electrolyte can significantly improve the cycling performance of the cells after thermal aging. Cell containing ternary electrolyte retained only 56 % of their initial reversible capacity after the storage period, while cells with added PS retained 70 % of their initial storage capacity. Continued cycling of the cells after storage at 75 °C for 15 days is depicted in Fig. 5.30. The normalized capacity retention after thermal storage is improved significantly via incorporation of PS. The capacity retention during the first 100 charge/discharge cycles after thermal storage is much higher for the cell containing PS (72 %) than the cell without PS (56 %).

Ex situ spectroscopy results clearly show that the sulfur-based additives participate in the SEI formation and change the SEI chemistry on the graphite anode surface, as supported by the EDS and XPS data, Figs. 5.31 and 5.32. The surface compositions in the SEI layer of the anode cycled in 1 M $LiPF_6$ EC:DEC:DMC (1:1:1) and in 1 M $LiPF_6$ EC:DEC:DMC (1:1:1) + 2 % PS (wt %) were investigated by XPS (Fig. 5.32). Analysis of the C 1s spectrum reveals that the intensity of the peak located at 284.3 eV, assigned to graphite, and the peaks located at 285.7 and 290.4 eV, corresponding to PVDF binder, are diminished compared to the fresh anode as expected from the formation of the anode SEI. The surface of MCMB anode contains many species characteristic of electrolyte decomposition products. New peaks are observed in the 287.5–290 eV

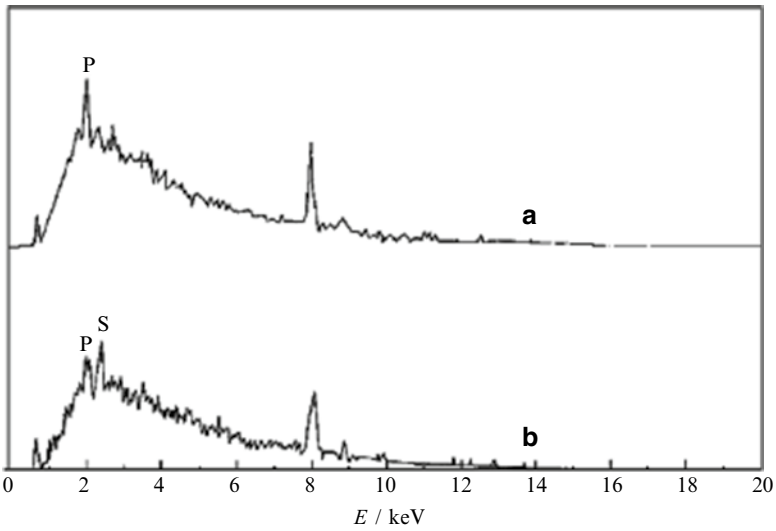

Fig. 5.31 EDS of graphite electrodes after the first cycle in 1 M $LiPF_6$ EC:PC:EMC electrolyte without (*A*) and with (*B*) 1 % BS (reproduced with permission by Elsevier from [83])

range suggesting the presence of Li_2CO_3 (290 eV), lithium alkyl carbonates (R–$\underline{C}H_2OCO_2Li$, 287.5 eV and R–$CH_2O\underline{C}O_2Li$, 288.5 eV), alkanes (285 eV), and ethers (286 eV). The major peaks in O 1s spectra at 531.6 eV and 532.5–533.5 eV correspond to Li_2CO_3 and lithium alkyl carbonates R–$CH_2\underline{O}$ (C=O)OLi (532.5 eV) and R–$CH_2O(C=\underline{O})OLi$ (533.5 eV), respectively. Analysis of the F 1s spectrum suggests that three main peaks are consistent with the presence of LiF (684.5 eV) and PVDF (687.6 eV). Examination of P 2p spectrum supports the presence of low concentrations of $Li_xPO_yF_z$ (134.5 eV) and residual $LiPF_6$ (136.2 eV).

Analysis of an MCMB composite anode extracted from a cell containing 2 % PS addition suggests the changes in surface compositions compared to anodes without PS. The C and F concentrations increase, while O concentration decreases and S is present. This indicates that the presence of PS modifies the anode SEI-forming reactions. The peak at 168.5 eV in the S 2p spectrum confirms that PS participates in formation of the SEI film on MCMB anode. This peak can be assigned to R–SO_3Li moieties, related to sodium benzenesulfonate (168 eV, S 2p).

The surface composition of an MCMB composite anode extracted from a cell cycled with the baseline ternary electrolyte and then stored at 75 °C for 15 days was investigated by XPS. The surface composition is modified significantly upon thermal storage; the concentration of O decreases while the concentration of P increases, consistent with a greater concentration of decomposition products of the $LiPF_6$. Analysis of the C 1s spectrum suggests that there is a relative decrease in the concentration of Li_2CO_3 (290 eV) and increase in the concentrations of alkyl carbonates (287–288.5 eV) and ethers including polyethylene oxide (286 eV). The F 1s

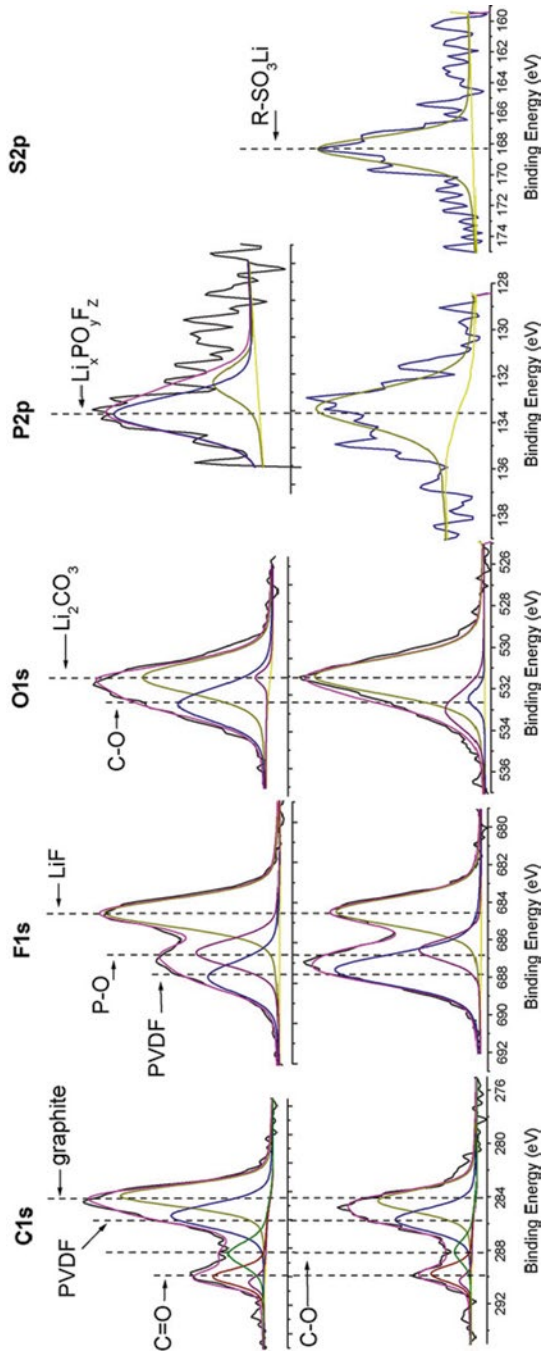

Fig. 5.32 C 1s, F 1s, O 1s, P 2p, and S 2p XPS spectra of MCMB anode cycled in 1 M $LiPF_6$ EC:DEC:DMC (*top*) and in 1 M $LiPF_6$ EC:DEC:DMC + 2 % PS (*bottom*) (reproduced with permission by Elsevier from [85])

spectrum reveals a relative decrease in the concentration of LiF (684.5 eV) and increase in the concentration of $Li_xPO_yF_z$ (686.5–688 eV), which is consistent with the significant increase in the concentration of P. Analysis of P 2p spectrum supports the presence of $Li_xPO_yF_z$ (134.5 eV), while the O 1s spectra contains a broad peak centered at ~532 eV consistent with a mixture of alkyl carbonates, ethers, and $Li_xPO_yF_z$. The MCMB anode extracted from the cell containing ternary electrolyte with 2 % PS addition after storage at 75 °C was investigated by XPS providing very similar results to the sample without PS. The decrease in S concentration, similarity of the elemental concentrations, and similarity of individual element spectra suggest that the anode surface modifications that were present after initial cycling with PS are lost upon storage at 75 °C for 15 days.

The PS reduction is thermodynamically disfavored in gas phase as suggested by the positive ΔG (4.47 kcal/mol) between PS and its reduction intermediate as well as the associated negative adiabatic electron affinity (EA ≈ ΔE0, −4.99 kcal/mol). The ring-opening reaction of intermediate 2 proceeds via the transition state 3, the energy barrier of which is approximately 12.1 kcal mol^{-1} in gas phase. Frequency analysis shows only one imaginary frequency (−1,456) corresponding to the transition state. The results from IRC analysis also support that the PS-1-TS is connected with PS-1 and PS-1. The charge distribution and bond orders of PS, PS anion, PS-TS, and PS-radical anion were also analyzed by the natural bond orbital (NBO) theory. The bond length of S_5–O_6 increases during the reduction process changing from 1.451 to 1.489 Å; the bond length of S_5–O_4 decreases from 1.662 to 1.490 Å. The bond lengths of S5 with O_4, O_6, and O_7 of radical anion are equivalent (difference less than 0.002 Å) to 1.490, 1.489, and 1.490 Å, respectively, which can also support the formation of –SO_3– anion, and most of the atomic spin density is located on C_3 consistent with a localized radical at C_3.

Figure 5.33 presents the potential energy surface and Gibbs free energy surface profiles together with some selected structure data. Li^+(PS) reductive decomposition proceeds via a similar mechanism to that of an isolated PS molecular. However, Li^+(PS) becomes much more easily reduced to the (Li^+)PS-1 reduction intermediate 7 with a remarkable EA decrease (−93.4 kcal/mol vs. 4.99 kcal/mol) The reductive decomposition of (Li^+)PS initially encounters the ion-pair intermediates 6 and 7. An electron was transferred to Li^+ to form the intermediate 6 and to PS in Li^+(PS) to form the intermediate 7, respectively. Then, the O_4–C_3 bond cleavage occurs to intermediate 7, leading to transition state 8 with a barrier of 5 kcal/mol. The structure of transition state 8 between species 7 and 9 was confirmed by primary IRC calculation and frequency analysis with the sole imaginary frequency −934 cm^{-1}. Formation of the radical anion 9 results in a significant loss in energy, −132.5 kcal mol^{-1}.

Due to the participation in SEI formation, the thermal stability of SEI containing sulfur-based components is dramatically enhanced. Cells with BS or PS addition show better capacity retention after storage at elevated temperature and also show smaller impedance increase after storage at elevated temperature.

However, although numerous additives were developed through this theoretical approach during the past two decades, the HOMO/LUMO method is still empirical in natural, because there is no necessary connection between the reduction potential

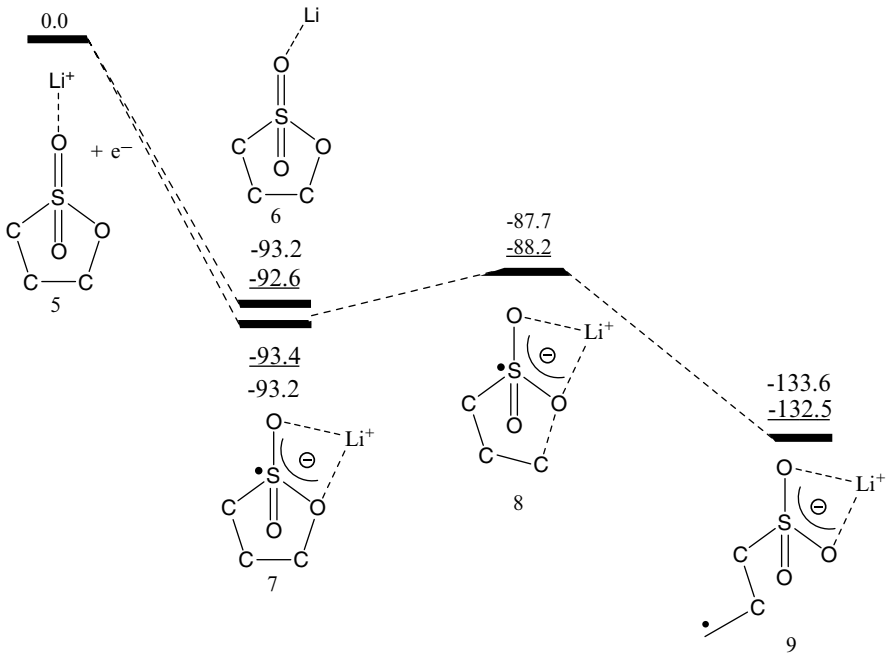

Fig. 5.33 Potential energy (*underlined data*) and Gibbs free energy profile (in kcal mol^{-1}) at 298.15 K for the reductive decomposition process of Li^+(PS) calculated at B3PW91/6-311++G (d,p) level

and the effectiveness of the SEI, and the properties of resultant SEI are not merely determined by the thermodynamics of the additives and, to some extent, the kinetics of the additives also need to be considered.

5.3.4.2 Artificial Coating

Additives sacrificially reduced to form desired SEI is indeed chemical coating an organic film onto the surface of graphite, which is the similar way as surface modification is nature. Early researchers used stable chemicals as alternative interphasial building blocks. Various metal oxides or phosphates, such as Al_2O_3, ZrO_2, and $AlPO_4$, have been thus applied directly on graphite particles through surface coating methods [88–92], with improvements in either reversible capacity in the initial cycle, cycling life, and elevated temperature performance or safety issues.

Similar works have been done by Zhang's research group; they soaked the graphite electrode in Li_2CO_3 aqueous solution, which forms a thin coating over the composite electrode upon drying [93]. The results showed that Li_2CO_3 coating can effectively increase reversibility of the initial forming cycle of Li/graphite half cell. Moreover, the Li_2CO_3 coating significantly suppresses self-dilithiation of the

lithiated graphite, which enhances storage performance of the Li-ion battery. One year later, the same research group reported the surface coating by employing a mixed solution of H_3BO_3 and $H_2C_2O_4$, followed by condensation at around 100 °C under vacuum condition, which forms oxalatoborate on the graphite surface [94]. It is shown that the resultant coating can also effectively increase reversibility of the initial forming cycles of Li/graphite half cell and also increases the storage performance of Li-ion battery at elevated temperature.

5.3.5 *Other Anodes: New Challenges from Alloy Anodes (Si, Sn)*

In pursuit of higher energy density for lithium-ion batteries, metal anode materials or alloy materials have been developing during the past decades due to its low discharge potential and much higher theoretical discharge capacity, such as Si and Sn; however, silicon anodes have limited applications because silicon's volume changes by 400 % upon insertion and extraction of lithium, which results in pulverization and loss of electrical contact between the active material and the current collector, as shown in Fig. 5.34 [95]. Meanwhile, both formation and chemistry of SEI are always accompanied during the abovementioned process since fresh metal surfaces are created repeatedly in each cycle. This continuous process builds up interphasial resistance, consumes the limited sources Li^+, and would eventually disable the cell. Thus, one of the key points of the successful application of Si or other alloy as Li-ion battery anode material is that the SEI formed on those alloys' surfaces must withstand a higher mechanical stress.

The 3D formation mechanism of interphase for graphic anode material is not suitable for the Si or the Sn alloy anode material, since they do not possess a structure for intercalation/de-intercalation; therefore, a simple 2D surface reaction is

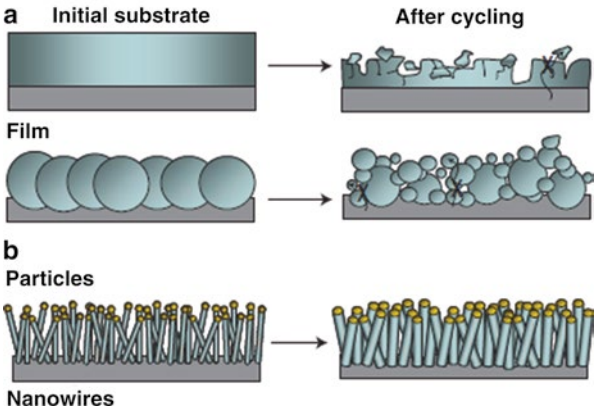

Fig. 5.34 Schematic illustration of (**a**) bulk and (**b**) nanostructured Si during the electrochemical lithiation/delithiation (reproduced with permission by the Nature Publishing Corp. from [95])

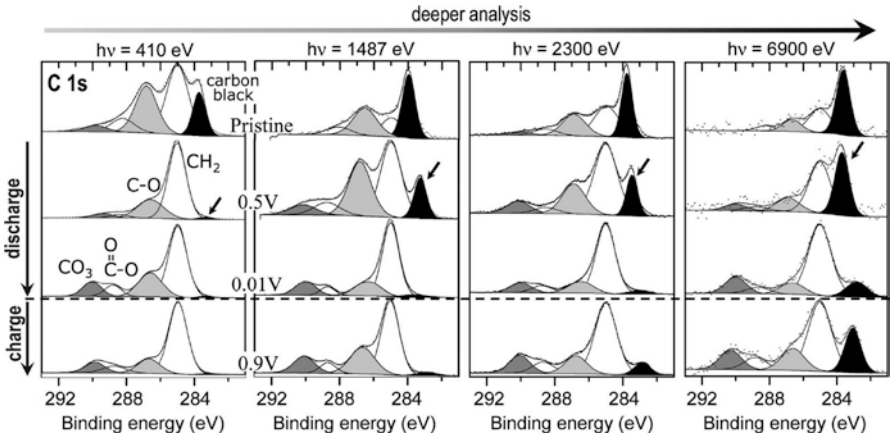

Fig. 5.35 C 1s spectra of the Si/C/CMS composite electrodes upon the first discharge/charge cycle (reproduced with permission by the American Chemical Society from [102])

more likely to be responsible for the formation of an interphase, which is similar with the formation mechanism on metallic lithium electrode.

To solve the problem caused by volume change during insertion/extraction process, researches have been working on synthesis of nanostructure or thin-film silicon anode materials [96–100]. Those nanoparticle materials have several advantages compared to the Si bulk films and micrometer-sized particles. First, the smaller diameter allows for better accommodation of the large volume changes without the initiation of fracture that occurs in bulk or micron-sized materials. Second, the nanoparticles have shorter diffusion pathway allowing for efficient charge transport. However the thin solid electrolyte interphase (SEI) is inevitably formed at the silicon anode. In a previous article, Chan et al. analyzed the composition and morphology of the SEI formed on nanowires by XPS and scanning electron microscopy (SEM). The morphology of the SEI was reported to be voltage dependent with a thicker SEI at a low potential and a partial dissolution and cracking during the delithiation [101]. After the first lithiation below 0.1 V vs. Li/Li^+ the SEI was found to be thicker than the XPS analysis depth (~10 nm), and consequently, the Si 2p signal was not observed.

Most recently, Dedryvere and Edstrom et al. conducted the extensive research work on the interfacial mechanisms of Si anode, as shown in Fig. 5.35, including reaction of surface oxide, Li–Si alloying process, and passivation layer formation by XPS [102]. To reveal more depth information of SEI ingredients, they conducted a thorough nondestructive depth-resolved analysis by using both soft X-rays (100–800 eV) and hard X-rays (2,000–7,000 eV) from two different synchrotron facilities compared with in-house XPS (1,487 eV). The formation of SEI starts from 0.5 V vs. Li/Li^+. At the end of discharge (0.01 V vs. Li/Li^+), a thick SEI layer has formed, and carbon black (284 eV, black shadows) can be observed only at 2,300 and 6,900 eV. New carbonaceous species have been identified at the surface, C–O

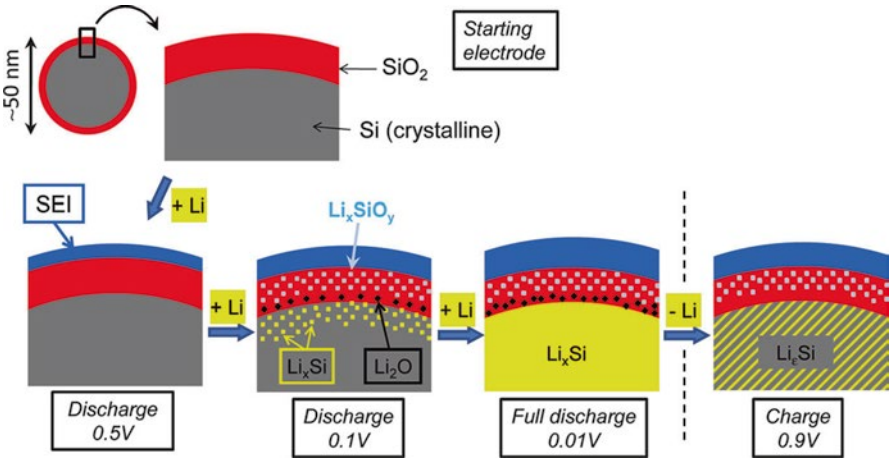

Fig. 5.36 Schematic view of the mechanisms occurring at the surface of the silicon nanoparticles. Formation of the SEI at the beginning of discharge. Formation of the Li–Si alloy upon further discharge, together with Li_2O and Li_xSiO_y interfacial phases (reproduced with permission by the American Chemical Society from [102])

(286.5 eV), O=C–O (288.5 eV), and Li_2CO_3 (290 eV). The overall shape of C 1s spectra, and thus the composition of carbonaceous species, is similar to the composition of the SEI formed on the surface of graphite electrodes or tin- and antimony-based intermetallic negative electrodes. In addition, at a given photo energy, there is no major change in components of the C 1s spectra from the beginning of discharge (0.5 V vs. Li/Li^+) to the end of the first cycle (0.9 V vs. Li/Li^+), which suggests that the overall composition of the SEI formed at the surface of the composite silicon electrodes is rather stable over the first discharge/charge cycle. Further F 1s XPS spectra show two components, residual $LiPF_6$ and LiF.

Based on the SEI components identified above, they proposed a schematic view of the mechanisms occurring at the surface of the silicon nanoparticles upon charge and discharge as presented in Fig. 5.36. At the beginning of discharge (0.5 V vs. Li/Li^+), lithium has not reacted with silicon but a thin SEI layer has already formed. The composition of SEI formed on silicon surface is very similar with the SEI formed at the surface of carbonaceous electrodes or Sn- or Sb-based intermetallic electrodes. After further discharge, at the beginning of 0.1 V vs. Li/Li^+, the thickness of SEI is increased but its composition does not change significantly. Meanwhile, lithium has started to react with the silicon nanoparticles, forming Li–Si alloying. After fully charged, lithium has been almost extracted from the core of particle, and the thickness of SEI is slightly decreased.

By the inspiration utilization of additive to improve the interfacial properties on graphite anode, researchers have also attempted to manipulate interfacial chemistry on Si by using electrolyte additives. Lithium bis (oxalatoborate) (LiBOB) was reported to maintain the spectroscopic presence of semi-carbonate species in the

SEI through reductive decomposition of the bis (oxalate) borate anion [103, 104]. Monofluoroethylene carbonate (FEC) can improve the cycling performance of Si-based anode material due to the generation of a more fluorinated SEI layer and inhibition of LiF production [104, 105]. Tris (pentafluorophenyl) borane (TPFPB) also was reported as an electrolyte additive for silicon thin-film electrode due to the formation of stable SEI, which therefore suppresses the surface pulverization [106]. The same research group also disclosed another additive, succinic anhydride (SA), as an electrolyte additive for silicon thin-film electrode. Similar mechanism was proposed by the authors that addition SA can prevent the decomposition of $LiPF_6$ salt the Si surface and an SEI layer with higher hydrocarbon and Li_2CO_3 contents is formed on the Si surface [107].

As regard to the bulk Sn or other alloy anodes, the buildup of interphase is also identified. Similar with carbonaceous or Si anode material, the major SEI ingredients are constituted of Li_2CO_3, $ROCO_2Li$, $Li_2C_2O_4$, and/or ROLi, whose balance is not markedly modified upon cycling [108]. So far, no efficient SEI is achieved to inhibit the volume change during the charge/discharge process for the alloy anode materials. Further studies are definitely needed to understand the failure modes of interphase on these alloy host electrodes, and interphases with unique chemistry and morphology should be tailored to the new requirements.

5.4 Summary

The SEI between the electrodes and electrolyte plays important roles in the Li-ion battery, whose key performances, such as cyclability, temperature dependence, power density, and safety, are close to the nature of the SEI properties. Chemistry, structure, thermodynamics, and formation mechanisms of the interphase between anode and electrolyte are well established via multi-analytical techniques and combination with computational method during the past few decades.

Based on the understanding of the formation mechanisms of SEI on graphite anode, it is possible to improve performance of lithium-ion battery by tailoring the structure and chemistry of an SEI. The application of additives is the most successful tailoring SEI. Numerous additives which assist in SEI formation process have been extensively explored, and a few of them have been widely utilized in commercial lithium-ion battery. The successful utilization of SEI formation additives boosts the applications of lithium-ion battery technology in our daily life and, the ultimate goal in future, electric vehicles.

The successful understanding of the SEI nature on graphite is inspiring the intensive interests on the SEI formation and manipulation for other anode materials or even cathode materials. Although the mechanism of SEI formation on these materials has not been well understood yet, it can be expected that tailoring SEIs on these materials will help solve the problems we are facing when using these electrode materials, such as the pulverization of Si or Sn anode materials and Mn dissolution of spinel cathode materials.

Acknowledgement This work is supported by the National Natural Science Foundation of China (No. 21003054, No. 21273084, and No. 21373092), the Joint Project of National Natural Science Foundation of China and Natural Science Foundation of Guangdong (No. U1134002), the Natural Science Foundation of Guangdong Province (No. 10351063101000001 and No. S2011040001731), and Specialized Research Fund for the Doctoral Program of Higher Education (No. 20104407120008).

References

1. *Modern electrochemistry*; vol. 2; Bockris, J.O'M.; Reddy, A. K. N., Plenum press: New York, NY, 1970.
2. Whittingham, M. S.; Savinell, R. F.; Zawodzinski T., Introduction: batteries and full cells, *Chem. Rev.,* **2004**, *104*, 4243-4244.
3. Xu, K.; Cresce, A. v., Interfacing electrolytes with electrodes in Li ion batteries, *J. Mater. Chem.,* **2011**, *21*, 9849-9864.
4. Manthiram, A., Materials challenges and opportunities of lithium ion batteries, *J. Phys. Chem. Lett.,* **2011**, *2*, 176-184.
5. Dahn, J. R., Phase diagram of Li_xC_6, *Phys. Rev. B: Condens. Matter and Mater. Phys.,* **1991**, *44*, 9170-9177.
6. Peled, E.; Straze, H., The kinetics of the magnesium electrode in thionyl chloride solution, *J. Electrochem. Soc.,* **1977**, *124*, 1030-1035.
7. Peled, E., The electrochemical behavior of alkali and alkaline earth metals in nonaqueous battery systems-The solid electrolyte interphase model, *J. Electrochem. Soc.,* **1979**, *126*, 2047-2051.
8. Aurbach, D.; Weissman, I.; Schechter, A.; Cohen, H. X-ray photoelectron spectroscopy studies of lithium surface prepared in several important electrolyte solutions. A comparison with previous studies by fourier transform infrared spectroscopy, *Langmuir* **1996**, *12*, 3991-4007.
9. Schechter, A.; Aurbach, D.; Cohen, H. X-ray photoelectron spectroscopy study of surface films formed on Li electrodes freshly prepared in alkyl carbonate solutions, *Langmuir* **1999**, *15*, 3334-3342.
10. Larush, L.; Zinigrad, E.; Goffer, Y.; Aurbach, D. Following the growth of surface films on lithium and their thermal behaviors in standard $LiPF_6$ solutions using differential scanning calorimetry, *Langmuir* **2007**, *23*, 12910-12914.
11. Wang, Y.; Nakamura, S.; Ue, M.; Balbuena, P. B. Theoretical studies to understand surface chemistry on carbon anodes for lithium-ion batteries: reduction mechanisms of ethylene carbonate, *J. Am. Chem. Soc.,* **2001**, *123*, 11708-11718.
12. Xu, K., Nonaqueous liquid electrolytes for lithium-based rechargeable batteries, *Chem. Rev.,* **2004**, *104*, 4304-4417.
13. Xu, K., Whether EC and PC differ in interphasial chemistry on graphitic anode and how, *J. Electrochem. Soc.,* **2009**, *156,* A751-755.
14. Hérold, A., Recherches sur les composés d'insertion du graphite, *Bull. Soc. Chim. Fr.* **1955**, *187*, 999-1012.
15. Maluangnont, T.; Sirisaksoontorn, W.; Lerner, M. M. A comparative structure study of ternary graphite intercalation compounds containing alkali metals and linear or branched amines, *Carbon*, **2012**, *50*, 597-602.
16. Maluangnont, T.; Gotoh, K.; Fujiwara, K.; Lerner, M. M. Cation-directed orientation of amines in ternary graphite intercalation compounds, *Carbon*, **2011**, *49*, 1033-1051.
17. Peled, E.; Golodnitsky, D.; Ardel G. Advanced model for solid electrolyte interphase electrodes in liquid and polymer electrolytes, *J. Electrochem Soc.* **1997**, *144*, L208-L210.
18. Fong, R.; Sacken, U. v.; Dahn, J. R. Studies of lithium intercalation into carbons using nonaqueous electrochemical cells, *J. Electrochem. Soc.,* **1990**, *137*, 2009-2013.

19. Chu, A. C.; Josefowicz, J. Y.; Farrington, G. C. Electrochemistry of highly ordered pyrolytic graphite surface film formation observed by atomic force microscopy. *J. Electrochem. Soc.,* **1997**, *144*, 4164-4169.
20. Besenhard, J. O.; Winter, M.; Yang, J.; Biberacher, W. Filming mechanism of lithium-carbon anodes in organic and inorganic electrolytes, *J. Power Sources*, **1995**, *54*, 228-231.
21. Wagner, M. R.; Albering, J. H.; Moeller, K.-C.; Besenhard, J. O.; Winter, M. XRD evidence for the electrochemical formation of $Li^+(PC)_yC_n^-$ in PC-based electrolytes, *Electrochem. Commun.,* **2005**, *7*, 947-952.
22. Aurbach, D.; Markovsky, B.; Weissamn, I.; Levi, E.; Ein-Eli, Y. On the correlation between surface chemistry and performance of graphite negative electrodes for Li ion batteries, *Electrochim. Acta* **1999**, *45*, 67-86.
23. Aurbach, D.; Levi, M. D.; Levi, E.; Schechter, A. Failure and stabilization mechanism of graphite electrodes, *J. Phys. Chem. B* **1997**, *101*, 2195-2206.
24. Aurbach, D.; Teller, H.; Levi, E. Morphology/behavior relationship in reversible electrochemical lithium insertion into graphite materials, *J. Electrochem. Soc.,* **2002**, *149*, A1255-A1266.
25. Dey, A. N. Lithium anode film and organic and inorganic electrolyte batteries, *Thin Solid Films* **1977**, *43*, 131-171.
26. Dousek, F. P.; Jansta, J.; Riha, J. Electrochemical system for galvanic cells in organic aprotic solvents. IV. Decomposition of propylene carbonate on lithium, *J. Electroanal. Chem.,* **1973**, *46*, 281-287.
27. Nazri, G.; Muller, R. H. In situ X-ray diffraction of surface layers on lithium in nonaqueous electrolyte, *J. Electrochem. Soc.,* **1985**, *132*, 1385-1387.
28. Aurbach, D.; Daroux, M. L.; Faguy, P. W.; Yeager, E., Identification of surface films formed on lithium in propylene carbonate solution, *J. Electrochem. Soc.,* **1987**, *134*, 1611-1620.
29. Aurbach, D.; Zaban, A.; Schechter, A.; Ein-Eli, Y.; Zinigrad, E.; Markovsky, B. The study of electrolyte solutions based on ethylene and diethyl carbonates for rechargeable Li Batteries, I. Li metal anodes, *J. Electrochem. Soc.,* **1995**, *142*, 2873-2882.
30. Aurbach, D.; Gofer, Y.; Ben-Zion, M.; Aped, P. The behavior of lithium electrodes in propylene and ethylene carbonate: The major factors that influence Li cycling efficiency, *J. Electroanl. Chem.,* **1992**, *339*, 451-471.
31. Aurbach, D.; Ein-Ely, Y.; Zaban, A. The surface chemistry of lithium electrodes in alkyl carbonate solutions, *J. Electrochem. Soc.,* **1994**, *141*, L1-L3.
32. Kanamura, K.; Tamura, H.; Shiraishi, S.; Takehara, Z.-i. XPS analysis of lithium surfaces following immersion in various solvents containing $LiBF_4$, *J. Electrochem. Soc.,* **1995**, *142*, 340-347.
33. Kanamura, K.; Shiraishi, S.; Takehara, Z.-i. Electrochemical deposition of very smooth lithium using nonaqueous electrolytes containing HF, *J. Electrochem. Soc.,* **1996**, *143*, 2187-2197.
34. Malmgren, S.; Rensmo, H.; Gustafsson, T.; Gorgoi, M.; Edström, K. Non-destructive depth profiling of the solid electrolyte interphase on $LiFePO_4$ and graphite electrodes, *ECS Tran.* **2010**, *25*, 201-210.
35. Aurbach, D.; Zinigrad, E.; Cohen, Y.; Teller, H. A short review of failure mechanisms of lithium metal and lithiated graphite anodes in liquid electrolyte solutions, *Solid State Ionics*, **2002**, *128*, 405-416.
36. Aurbach, D. Review of selected electrode-solution interactions which determine the performance of Li and Li ion batteries, *J. Power Sources* **2000**, *89*, 206-218.
37. Ein-Eli, Y. A new perspective on the formation and structure of the solid electrolyte interface at the graphite anode of Li-ion cells, *Electrochem. Solid-State Lett.,* **1999**, *2*, 212-214.
38. Xu, K.; Zhuang, G. V.; Allen, J. L.; Lee, U.; Zhang, S. S.; Ross, Jr. P. N.; Jow, T. R., Syntheses and characterization of lithium alkyl mono- and dicarbonates as components of surface films in Li-ion batteries, *J. Phys. Chem. B* **2006**, *110*, 7708-7719.
39. Zhuang, G.; Xu, K.; Yang, H.; Jow, T. R.; Ross, Jr. P. N. Lithium ethylene dicarbonate identified as the primary product of chemical and electrochemical reduction of EC in 1.2 M $LiPF_6$/EC:EMC electrolyte, *J. Phys. Chem. B* **2005**, *109*, 17567-17537.

40. Zhuang, G. V.; Ross, Jr. P. N. Analysis of the chemical composition of the passive film on Li-ion battery anodes using attenuated total reflection infrared spectroscopy, *Electrochem. Solid-State Lett.,* **2003**, *6*, A136-A139.
41. Augustsson, A.; Herstedt, M.; Guo, J.-H.; Edström, K.; Zhuang, G. V.; Ross, Jr. P. N.; Rubensson, J.-E.; Nordgren, J. Solid electrolyte interphase on graphite Li-ion battery anodes studied by soft X-ray spectroscopy, *Phys. Chem. Chem. Phys.* **2004**, *6*, 4185-4189.
42. Xu, K. "Change-transfer" process at graphite/electrolyte interface and the solvation sheath structure of Li^+ in nonaqueous electrolytes, *J. Electrochem. Soc.,* **2007**, *154*, A162-A167.
43. Xu, K.; Lam, Y.; Zhang, S. S.; Jow, T. R.; Curtis, T. B. Solvation sheath of Li^+ in nonaqueous electrolytes and its implication of graphite/electrolyte interface chemistry, *J. Phys. Chem. C* **2007**, *111*, 7411-7421.
44. Onuki, M.; Kinoshita, S.; Sakata, Y.; Yanagidate, M.; Otake, Y.; Ue, M.; Deguchi, M. Identification of the source of evolved gas in Li-ion batteries using ^{13}C-labling solvents, *J. Electrochem. Soc.,* **2008**, *155*, A794-A797.
45. Fukushima, T.; Matsuda, Y.; Hashimoto, H.; Arakawa, R. Studies on salvation of lithium ions in organic electrolyte solutions by electrospray ionization-mass spectroscopy, *Electrochem. Solid-State Lett.,* **2001**, *4*, A127-A128.
46. Matsuda, Y.; Fukushima, T.; Hashimoto, H.; Arakawa, R. Solvation of lithium ions in mixed organic electrolyte solution by electrospray ionization mass spectroscopy, *J. Electrochem. Soc.,* **2002**, 149, A1045-A1048.
47. von Cresce A.; Borodin, O.; Xu, K. Correlating Li^+ solvation sheath structure with interphasial chemistry on graphite, *J. Phys. Chem. C* **2012**, 116, 26111-26117.
48. Borodin, O.; Smith, G. Quantum chemistry and molecular dynamics simulation study of dimethyl carbonate: ethylene carbonate electrolytes doped with $LiPF_6$, *J. Phys. Chem. B* **2009**, *113*, 1763-1776.
49. **von Cresce A.**; Xu, K. Preferential solvation of Li^+ directs formation of interphase on graphite anode, *Electrochem. Solid-State Lett.,* **2011**, *14*, A154-A156.
50. Wang, Y.; Nakamura, S.; Tasaki, K.; Balbuena, P.B. Theoretical studies to understand surface chemistry on carbon anodes for lithium-ion batteries: how does vinylene carbonate play its role as an electrolyte additive? *J. Am. Chem. Soc.,* **2002**, *124*, 4408-4421.
51. Wang, Y.; Balbuena, P.B. Theoretical insights into the reductive decompositions of propylene carbonate and vinylene carbonate: density functional theory studies, *J. Chem. Phys. B.* **2002**, *106*,4486-4495
52. Tasaki, K.; Kanda, K.; Kobayashi, T.; Nakamura, S.; Ue, M. Theoretical studies on the reductive decompositions of solvents and additives for lithium-ion batteries near lithium anodes, *J. Electrochem. Soc.,* **2006**, *153*, A2192-A2197.
53. Xing, L.D.; Wang, C.Y.; Xu, M.Q.; Li, W.S.; Cai, Z.P. Theoretical study on reduction mechanism of 1,3-benzodioxol-2-one for the formation of solid electrolyte interface on anode of lithium ion battery, *J. Power Sources* **2009**, *189*, 689-692.
54. Xing, L.D.; Li, W.S.; Xu, M.Q.; Li, T.T.; Zhou, L., The reductive mechanism of ethylene sulfite as solid electrolyte interphase film-forming additive for lithium ion battery, *J. Power Sources*, **2011**, *196*, 7044-7047.
55. Borodin, O.; Smith, G.D.; Fan, P., Molecular dynamics simulations of lithium alkyl carbonates, *J. Phys. Chem. B* **2006**, *110*, 22773-22779.
56. Iddir, H.; Curtiss, L.A. Li ion diffusion mechanisms in bulk monoclinic Li_2CO_3 crystals from density functional studies, *J. Phys. Chem. C* **2010**, *114*, 20903–20906.
57. Tasaki, K. Harris, S.J. Computational study on the solubility of lithium salts formed on lithium ion battery negative electrode in organic solvents, *J. Phys. Chem. C* **2010**, *114*, 8076–8083.
58. Tasaki, K.; Goldberg, A.; Lian, J.J.; Walker, M.; Timmons, A.; Harrisc, S.J. Solubility of lithium salts formed on the lithium-ion battery negative electrode surface in organic solvents, *J. Electrochem. Soc.,* **2009**, *156*, A1019-A1027.
59. Leung, K.; Budzien, J.L. Ab initio molecular dynamics simulations of initial stages of solid-electrolyte interface formation on lithium ion battery graphitic anodes, *Phys. Chem. Chem. Phys.* **2010**, *12*, 6583-6586.

60. Leung, K.; Zavadil, K.R.; Jung, Y.S.; Dillon, A.C.; Cavanagh, A.S.; Lee, S.H.; George, S.M. Using atomic layer deposition to hinder solvent decomposition in lithium ion batteries: first-principles modeling and experimental studies, *J. Am. Chem. Soc.,* **2011**, *133*, 1471-14754.
61. Kim, S.P.; van Duin A.C.T.; Shenoy, V.B. Effect of electrolytes on the structure and evolution of the solid electrolyte interphase (SEI) in Li-ion batteries: A molecular dynamics study, *J. Power Sources*, **2011**, *196*, 8590-8597.
62. Clements, J. H. Reactive applications of cyclic alkylene carbonates, *Ind. Eng. Chem. Res.,* **2003**, 42, 663-674.
63. Ein-Eli, Y.; Markovsky, B.; Aurbach, D.; Carmeli, Y.; Yamin, H.; Luski, S. The dependence of the performance of Li-C intercalation anodes for Li-ion secondary batteries on the electrolyte solution composition, *Electrochim. Acta* **1994**, *39*, 2559-2569.
64. Momma, T.; Nara, H.; Yamagami, S.; Tatsumi, C.; Osaka, T. Effect of the atmosphere on chemical composition and electrochemical properties of solid electrolyte interface on electrodeposited Li metal, *J. Power Sources* **2011**, *196*, 6483-6487.
65. Gnanaraj, J.S.; Thompson, R.W.; Iaconatti, S.N.; DiCarlo, J.F.; Abraham, K.M. Formation and growth of surface films on graphitic anode materials for li-Ion batteries, *Electrochem. Solid-State Lett.,* **2005**, *8*, A128–A132.
66. Bryngelsson, H.; Stjerndahl, M. Gustafsson, T. Edstrom, K. How dynamic is the SEI? *J. Power Sources* **2007**, *174*, 970- 975.
67. Xu, K.; Cresce, A. v.; Lee, U. Differentiating contributions to "ion transfer" barrier from interphasial resistance and Li^+ desolvation at electrolyte/graphite interface, *Langmuir* **2010**, *26*, 11538-11543.
68. Yamada, Y.; Iriyama, Y.; Abe, T.; Ogumi, Z. Kinetics of lithium ion transfer at the interface between graphite and liquid electrolyte: effects of solvent and surface film, *Langmuir* **2009**, *25*, 12766-12770.
69. Ho, J.; Cresce, A. v.; Xu, K. Metalizing graphite/electrolyte interface for faster Li + -transport, Abstract #527, 221st ECS Meeting.
70. Smith, A. J.; Burns, J. C.; Zhao, X.; Xiong, D.; Dahn, J. R. A high precision coulometry study of the SEI growth in Li/graphite cells, *J. Electrochem. Soc.,* **2011**, *158*, A447-A452.
71. Lu, P.; Harris, S. J. Lithium transport within the solid electrolyte interphase, *Electrochem. Commun.,* **2011**, *13*, 1035-1037.
72. Lee, H. H.; Wan, C. C.; Wang, Y. Y. Thermal stability of the solid electrolyte interface on carbon electrodes of lithium batteries, *J. Electrochem. Soc.,* **2004**, *151*, A542-A547.
73. Zhao, L.; Watanabe, I.; Doi, T.; Okada, S.; Yamaki, J.-i. TG-MS analysis of solid electrolyte interphase (SEI) on graphite negative-electrode in lithium-ion batteries, *J. Power Sources*, **2006**, *161*, 1275-1280.
74. Aurbach, D.; Gamolsky, K.; Markovsky, B.; Gofer, Y.; Schimidt, M.; Heider U. On the use of vinylene carbonate (VC) as an additive to electrolyte solutions for Li-ion batteries, *Electrochim. Acta* **2002**, *47*, 1423-1439.
75. Contestabile, M.; Morselli, M.; Paraventi, R.; Neat, R. J. A comparative study on the effect of electrolyte/additives on the performance of ICP383562 Li-ion polymer (soft-pack) cells, *J. Power Sources* **2003**, *119-121*, 943-947.
76. Chen, G.; Zhuang, G. V.; Richardson, T. J.; Liu, G.; Ross, P. N. J. Anodic polymerization of vinyl ethylene carbonate in Li-ion battery electrolyte, *Electrochem. Solid-State Lett.*, **2005**, *8*, A344-A347.
77. Aurbach, D.; Gnanaraj, J. S.; Geissler, W.; Schmidt, M. Vinylene carbonate and Li salicylatoborate as additive in $LiPF_3(CF_2CF_3)_3$ solution for rechargeable Li-ion batteries, *J. Electrochem. Soc.*, **2004**, *151*, A23-A30.
78. Sasaki, T.; Abe T.; Iriyama, Y.; Inaba, M.; Ogumi, Z. Suppression of an alkyl dicarbonate formation in Li-ion cells, *J. Electrochem. Soc.,* **2005**, *152*, A2046-A2050.
79. Hu, Y. S.; Kong, W. H.; Wang, Z. X.; Li, H.; Huang, X. J.; Chen, L. Q. Effect of morphology and current density on the electrochemical behavior of graphite electrodes in PC-based electrolyte containing VEC additive, *Electrochem. Solid-State Lett.,* **2004**, *7*, A442-A446.

80. Xu, M. Q.; Zhou, L.; Xing, L. D.; Li, W. S.; Lucht, B. L. Experimental and theoretical investigations on 4,5-dimethyl-[1,3]dioxol-2-one as solid electrolyte interface forming additive for lithium-ion batteries, *Electrochim. Acta 2010*, 55, 6743-6748.
81. Zhang, S. S. A review on electrolyte additives for lithium-ion batteries, *J. Power Sources* **2006**, *162*, 1379-1394.
82. Xu, M. Q.; Zuo, X. X.; Li, W. S.; Zhou, H. J.; Liu, J. S.; Yuan, Z. Z. Effect of butyl sultone on the Li-ion battery performance of graphite electrode, *Acta Phys.-Chim. Sin.* **2006**, *22*, 335-340.
83. Xu, M. Q.; Li, W. S.; Zuo, X. X.; Liu, J. S.; Xu, X. Performance improvement of lithium ion battery using PC as a solvent component and BS as an SEI forming additive, *J. Power Sources* **2007**, *174*, 705-710.
84. Zuo, X. X.; Xu, M. Q.; Li, W. S.; Su, D. G.; Liu, J. S. Electrochemical reduction of 1,3-propane sultone on graphite electrodes and its application in Li-ion batteries, *Electrochem. Solid-State Lett.,* **2006**, *9*, A196-A199.
85. Xu, M. Q.; Li, W. S.; Lucht, B. L. Effect of propane sultone on elevated temperature performance of anode and cathode materials in lithium-ion batteries, *J. Power Sources*, **2009**, *193*, 804-809.
86. Li, B.; Xu, M. Q.; Li, T. T.; Li, W. S.; Hu, S. J. Prop-1-ene-1,3-sultone as SEI formation additive in propylene carbonate-based electrolyte for lithium ion batteries, *Electrochem. Commun.,* **2012**, *17*, 92-95.
87. Wrodnigg, G. H.; Besenhard, J. O.; Winter, M. Ethylene sulfite as electrolyte additive for lithium-ion cells with graphitic anodes, *J. Electrochem. Soc.,* **1999**, *146*, 470-472.
88. Cho, J.; Kim, Y. J.; Kim, T.-J.; Park, B. Zero-strain intercalation cathode for rechargeable Li-ion cell, *Angew. Chem. Int. Ed.,* **2001**, *40*, 3367-3369.
89. Cho, J.; Kim, Y.-W.; Kim, B.; Lee, J.-G.; Park, B. A breakthrough in the safety of lithium secondary batteries by coating the cathode material with $AlPO_4$ nanoparticles, *Angew. Chem. Int. Ed.,* **2003**, *42*, 1618-1621.
90. Kim, S.-S.; Kadoma, Y.; Ikuta, H.; Uchimoto, Y.; Wakihara, M. Electrochemical performance of natural graphite by surface modification using aluminum, *Electrochem. Solid-State Lett.,* **2001**, *4*, A109-A112.
91. Koggegoda, I. R. M.; Kadoma, Y.; Ikuta, H.; Uchimoto, Y.; Wakihara, M. Enhancement of rate capability in graphite anode by surface modification with zirconia, *Electrochem. Solid-State Lett.,* **2002**, *5*, A275-A278.
92. Lee, S.-E.; Kim, E.; Cho, J. Improvement of electrochemical properties of natural graphite anode materials with an ovoid morphology by $AlPO_4$ coating, *Electrochem. Solid-State Lett.,* **2007**, *10*, A1- A4.
93. Zhang, S. S.; Xu, K.; Jow, T. R. Effect of Li_2CO_3-coating on the performance of natural graphite in Li-ion batteries, *Electrochem. Commun.,* **2003**, *5*, 979-982.
94. Zhang, S. S.; Xu, K.; Jow, T. R. Enhanced performance of natural graphite in Li-ion battery by oxalatoborate coating, *J. Power Sources* **2004**, *129*, 275-279.
95. Chan, C. K.; Peng, H. L.; Liu, G.; McIlwarth, K.; Zhang, X. F.; Huggins, R. A.; Cui, Y. High-performance lithium battery anodes using silicon nanowires, *Nat. Nanotechnol.* **2008**, *3*, 31-35.
96. He, Y.; Yang, B.; Yang, K.; Brown, C.; Ramasamy, R.; Wang, H.; Lundgren, C.; Zhao, Y. Designing Si-based nanowall arrays by dynamics shadowing growth to tailor the performance of Li-ion battery anodes, *J. Mater. Chem.,* **2012**, *22*, 8294-8303.
97. Yang, H.; Huang, S.; Huang, X.; Fan, F.; Liang, W.; Liu, X. H.; Chen, L.-Q.; Huang, J. Y.; Li, J.; Zhu, T.; Zhang, S. Orientation-dependent interfacial mobility governs the anisotropic swelling in lithiated silicon nanowires, *Nano Lett.* **2012**, *12*, 1953-1958.
98. Murugesan, S.; Harris, J. T.; Korgel, B. A.; Stevenson, K. J. Copper-coated amorphous silicon particles as an anode material for lithium-ion batteries, *Chem. Mater.,* **2012**, *24*, 1306-1315.
99. Wang, C.-M.; Li, X.; Wang, Z.; Xu, W.; Liu, J.; Gao, F.; Kovarik, L; Zhang, J.-G.; Howe, J.; Burton, D. J.; Liu, Z.; Xiao, X.; Thevuthasan, S.; Baer, D. R. In situ TEM investigation of

congruent phase transition and structural evolution of nanostructured silicon/carbon anode for lithium ion, *Nano. Lett.* **2012**, *12*, 1624-1632.
100. Abel, P. R.; Lin, Y.-M.; Celio, H.; Heller, A.; Mullins, C. B. Improving the stability of nanostructured silicon thin film lithium-ion battery anodes through their controlled oxidation, *ACS Nano* **2012**, *6*, 2506-2516.
101. Chan, C. K.; Ruffo, R.; Hong, S. S.; Huggins, R. A.; Cui, Y. Structural and electrochemical study of the reaction of lithium with silicon nanowires, *J. Power Sources* **2009**, *189*, 34-39.
102. Philippe, B.; Dedryvere, R.; Allouche, J.; Lindgren, F.; Gorgoi, M.; Rensmo, H.; Gonbeau, D.; Edstrom, K. Nanosilicon electrodes for lithium-ion batteries: interfacial mechanisms studied by hard and soft X-ray photoelectron spectroscopy, *Chem. Mater.,* **2012**, *24*, 1107-1115.
103. Choi, N. S.; Yew, K. H.; Kim, H.; Kim, S. S.; Choi, W. U. Surface layer formed on silicon thin-film electrode in lithium bis (oxalate) borate-based electrolyte, *J. Power Sources* **2007**, *172*, 404-409.
104. Dalavi, S.; Guduru, P.; Lucht, B. L. Performance enhancing electrolyte additives for lithium ion batteries with silicon anodes, *J. Electrochem. Soc.,* **2012**, *159*, A642-A646.
105. Choi, N.S.; Yew, K. H.; Lee, K. Y.; Sung, M.; Kim, H.; Kim, S. S. Effect of fluoroethylene carbonate additive on interfacial properties of silicon thin-film electrode, *J. Power Sources* **2006**, *161*, 1254-1259.
106. Han, G. B.; Lee, J. N.; Choi, J. W.; Park, J. K. Tri (pentafluorophenyl) borane as an electrolyte additive for high performance silicon thin film electrodes in lithium ion batteries, *Electrochim. Acta* **2011** *56*, 8997-9003.
107. Han, G. B.; Ryou, M. H.; Cho, K. Y.; Lee, Y. M.; Park, J. K. Effect of succinic anhydride as an electrolyte additive on electrochemical characteristics of silicon thin-film electrode, *J. Power Sources* **2010**, *195*, 3709-3714.
108. Li, J. T.; Swiatowska, J.; Maurice, V.; Seyeux, A.; Huang, L.; Sun, S. G.; Marcus, P. XPS and ToF-SIMS study of electrode process on Sn-Ni alloy anodes for Li-ion batteries, *J. Phys. Chem. C* **2011**, *115*, 7012-7018.

Chapter 6
On the Surface Chemistry of Cathode Materials in Li-Ion Batteries

Susai Francis Amalraj, Ronit Sharabi, Hadar Sclar, and Doron Aurbach

Abstract The main cathode materials for Li batteries include the following systems: transition metal oxides and sulfides (MO_x, MS_x), lithiated transition metal oxides and sulfides (Li_xMO_y, Li_xMS_y), and $LiMPO_4$ olivine compounds. There are also oxygen- and sulfur-based cathodes whose main solid components are carbonaceous materials. Most of these cathodes develop very rich surface chemistry that affects very strongly their electrochemical performance. The main reactions are acid–base reactions (with acidic solution species, HF, PF_5, PF_3O, etc.); nucleophilic reactions between the basic compounds and the electrophilic alkyl carbonate solvents; polymerization; possible oxidation of solution species; and dissolution of transition metal ions. The behavior of many cathodes in Li-ion batteries is controlled by surface-film formation, passivation phenomena, and Li-ion migration through solid electrolyte interphases formed on the active mass by spontaneous reactions. We describe herein major surface processes, techniques that can address and analyze them, as well as means to improve the performance of cathodes in Li-ion batteries by controlling their surface phenomena.

Keywords Li-ion batteries • Li-insertion cathodes • Surface films • Passivation phenomena • Surface-sensitive techniques • SEI

6.1 Introduction

The cathode used in Li batteries includes the following main families of compounds:

1. Transition metal oxides, MO_x (e.g., V_2O_5) [1].
2. Transition metal sulfides, MS_x (e.g., TiS_2) [2].

S.F. Amalraj • R. Sharabi • H. Sclar • D. Aurbach (✉)
Department of Chemistry, Bar-Ilan University, Ramat Gan 52900, Israel
e-mail: sfaj1@yahoo.com; Doron.Aurbach@biu.ac.il

T.R. Jow et al. (eds.), *Electrolytes for Lithium and Lithium-Ion Batteries*,
Modern Aspects of Electrochemistry 58, DOI 10.1007/978-1-4939-0302-3_6,

3. Lithiated transition metal oxides: These compounds can be classified via their structure: layered compounds (e.g., $LiCoO_2$, $Li[MnNiCo]O_2$) and spinel (e.g., $LiMn_2O_4$, $LiNi_{0.5}Mn_{1.5}O_4$) [3].
4. Olivine compounds, $LiMPO_4$, including $LiFePO_4$, $LiMnPO_4$, and $LiCoPO_4$ as major cathode materials and doped $LiM_1M_2PO_4$ or mixed metal olivines (e.g., $Li[MnFe]PO_4$) [4].
5. Transition metal fluorides such as FeF_3 that undergo reversible conversion reactions with Li ions [5].
6. Liquid cathodes such as SO_2 and $SOCl_2$: These relate to primary Li batteries and are reduced irreversibly in the presence of Li ions to Li–S–O compounds, LiCl and Li–S–O–Cl moieties [6].
7. Sulfur cathodes that undergo reversible stepwise reduction in the presence of Li ions from S to Li_2S via a series of Li_2S_n (Li sulfides) moieties: The main substrates for sulfur cathodes are carbonaceous materials (usually on Al foil current collectors) [7].
8. Oxygen reduction cathodes for Li-air batteries: The main cathode material for Li-air batteries is carbon, which serves as the substrate on which the main oxygen reduction product (in the presence of Li ions), Li_2O_2, precipitates. The carbonaceous materials used for Li-air batteries may be decorated with particles of catalysts, e.g., MnO_2 [8].

Figure 6.1 shows typical voltage profiles of various representative cathodes that belong to all the above eight families. The aim of this chapter is to discuss the surface chemistry of cathodes in Li batteries as a topic by itself, and thereby, not all the above families of cathodes belong in this discussion.

The liquid (sulfur-based compounds) and solid sulfur cathodes (items 6 and 7) do not develop surface chemistry that can be separated from their main electrochemical redox reactions. Hence, when the reduction of sulfur SO_2 or $SOCl_2$ produces insoluble species such as LiCl, Li_2S, and Li_2O, they precipitate on the current collector [9]. When formed, Li_2S can be reoxidized, up to elemental sulfur, via various Li_xS intermediate compounds [10]. Hence, the current collector, which may be aluminum (Al) plus carbon in the case of sulfur cathodes or carbon in the case of $SOCl_2$ cathodes, does not develop intrinsic surface chemistry beyond the precipitation of the reduction products of the active mass.

FeF_3 cathodes also do not develop interesting surface chemistry, because their redox potential falls well within the electrochemical window of the most relevant electrolyte solutions. Neither FeF_3 nor LiF is basic or nucleophilic, and thereby, there are no reactions between them and the solution species. Hence, FeF_3, which may be considered as an interesting high-capacity cathode material, does not belong to the discussions developed in this chapter.

The case of air cathodes is complicated, as is presented later, and definitely deserves a separate discussion in this chapter. Therefore, the most interesting and important discussion on the surface chemistry of the positive electrodes in Li batteries relates to lithiated transition metal oxides and Li olivine compounds.

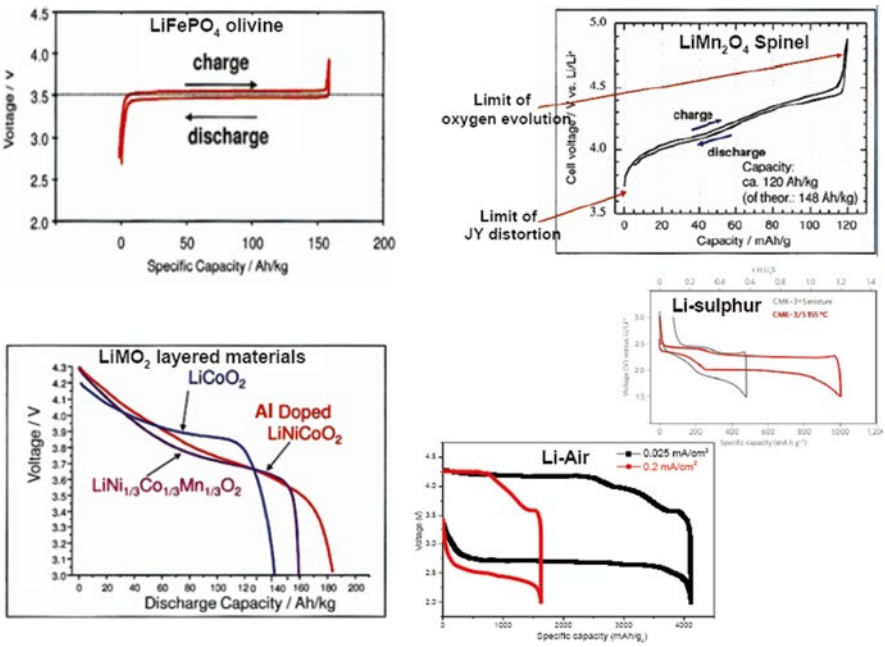

Fig. 6.1 Voltage profiles of various representative cathodes in lithium-ion batteries

These compounds have negatively charged oxygen atoms that may act as nucleophiles towards electrophilic solvents such as alkyl carbonates. In addition, in their lithiated state, these compounds may be basic, thus reacting with all kinds of acidic species in solutions (both Lewis acids such as PF_5, PF_3O, and protic contaminants such as trace HF and H_2O).

The following aspects are especially important, and they are discussed in this chapter:

1. The type of reactions of the various cathode materials.
2. The anodic stability of relevant electrolyte solutions. What happens? On what does this depend?
3. The contribution of the current collectors and commonly used additives to the anodic reactions of cathode solution systems: catalysis vs. inhibition.
4. The effect of the size of the particle on their surface reactivity.
5. How to measure correctly the surface chemical aspects of cathodes: which experiments are important and what techniques are relevant for measurements.
6. A review of various aspects of the cathodes' surface chemistry, presented individually for each type of cathode material.

This chapter deals systematically with the main surface chemical aspects related to cathodes for Li batteries. The first step includes a discussion on the types of

cathode reactions, after which the anodic stability of cathode/solution systems is discussed. Next, some experimental aspects related to surface chemical measurements are discussed. After these introductory sections, a general presentation on various cathode surface chemical aspects is presented, demonstrating the importance of electrode's surface chemistry and related complications. Finally, three types of electrodes are discussed: Li_xMO_y (lithiated transition metal oxides); $LiMPO_4$ olivine compounds, and O_2 cathodes for Li-air batteries.

6.2 On the Type of Cathode Reactions and the General Effect of the Nature of Cathode Material on Its Surface Chemistry

We can classify the cathode reactions into three types:

1. Li-ion insertion via a first-order phase transition:
   Example: $LiMPO_4 \leftrightarrow xLi^+ + xe^- + Li_{1-x}MPO_4$.
   Such reactions exhibit a flat potential profile [11].
2. Li-ion insertion that forms a solid solution.
   Example: $Li[MnNiCo]O_2 \leftrightarrow xLi^+ + xe^- + Li_{1-x}[MnNiCo]O_2$
   Such reactions exhibit sloping potential profiles [12]. The above two types of cathode reactions do not change the basic lattice structure of the compounds. Li ions are inserted reversibly into the empty sites in the compound's crystals.
3. Conversion reactions that change completely the cathode's material.
   Example: $Nano\text{-}FeF_3 + 3Li^+ + 3e^- \leftrightarrow nano\text{-}Fe^0 + 3LiF$ [5]

It should be noted that the type of cathode reaction has no direct effect on its surface chemistry. The most important aspects are the redox potentials, the particle size, and the level of reactivity of the surface oxygen atoms. Another important aspect relates to the ease of transition metal ion dissolution from the cathode material to the solution phase. In general, as the redox potential is lower, the cathode material is less reactive with the solution species. However, the redox potential is not the main important factor. The nucleophilicity and basicity of the oxygen atoms of the cathode compounds are also highly important. Li_xMO_y compounds are much more basic and nucleophilic than $LiMPO_4$ compounds [13]. The phosphorous atoms at the 5+ oxidation state in the olivine compounds moderate the basic nature of the oxygen atoms. Thereby, olivine compounds are much less reactive to solution species than Li_xMO_y compounds [14]. Consequently, they can be used as nanoparticles, which help to overcome their poor transport properties. The fluorine atoms in FeF_3 and its reduction product, LiF, are neither basic nor nucleophilic, and thereby this cathode material does not develop surface chemistry in conventional electrolyte solutions. Finally, as the particle size of cathode materials is smaller, they are supposed to be more surface reactive.

6.3 On the Anodic Stability of the Electrolyte Solutions, the Contribution of the Current Collectors and Carbon Black

The main components of the relevant electrolyte solutions for Li-ion batteries are nonaqueous polar aprotic solvents and Li salts. The main families of solvents are ethers, esters, and alkyl carbonates. This is the order of their anodic stability. Alkyl carbonates are the preferred solvents for Li-ion batteries because their anodic stability seems to be high enough for high-voltage cathodes, even up to 5 V vs. Li/Li (apparently!) due to the high oxidation state induced by the carbonate groups. As the anodic stability of a solvent is higher, its cathodic stability is lower. Indeed, alkyl carbonate suffers from relatively low cathodic stability. They can be reduced in the presence of Li ions to species such as $ROCO_2Li$ below 1.5 V vs. Li/Li^+ [15]. Note that the thermodynamic properties of the reduction reactions depend very strongly on the cation [16]. Ethylene and dimethyl carbonates (EC–DMC) can be considered as the basic solvent system for Li-ion batteries. Their anodic stability should be high because of the carbonate group and the relatively small number of C–H bonds in these molecules ($–CH_2–$ and $CH_3–$ are electron-donating groups). While their cathodic stability is low, their reduction products in the presence of Li ions, e.g., $(CH_2OCO_2Li)_2$, CH_3OCO_2Li, $(CH_2OLi)_2$, and CH_3OLi form effective passivating surface films on graphite that behave as a solid electrolyte interphase for Li-ion transport [17] but block electron transfer from lithiated graphite to the solution. Consequently, graphite anodes behave very reversibly in EC–DMC-based solutions. $LiPF_6$ was chosen as the preferred electrolyte in standard solutions for Li-ion batteries, because this salt forms highly conductive solutions, its reduction does not interfere adversely with the formation of passivating surface films, and its intrinsic stability is very high [18].

The most important fact is that the anodic stability of standard electrolyte solutions such as EC–DMC/$LiPF_6$ cannot be easily defined. There are indications that such solutions can be oxidized on noble metal electrodes (Pt, Au) around 4 V vs. Li [19]. In general, it can be said that the oxidation of alkyl carbonate solutions are inhibited with many practical cathodes for Li-ion batteries. The most important aspect regarding the anodic stability of these electrolyte solutions seems to be the nature of the substrate—the current collector and the presence of conductive additives such as carbon black. Examining the arsenal of materials that can be used as current collectors for Li-ion battery cathodes, aluminum (Al) seems to be the best choice. It is cheap; can be easily fabricated as thin, flexible, and strong sheets; and can reach excellent passivation that prevents its corrosion but allows fast electron transport from the Al metal foil to any adjacent phase (e.g., active cathode material, carbon black additive, electrolyte solution). The corrosion and passivation of Al (which is an active metal) depend very strongly on the electrolyte solution. Figure 6.2 shows the potentio-dynamic response of Al foil electrodes in different electrolyte solutions at 30 and 60 °C, as indicated [20]. The insert shows the morphology of

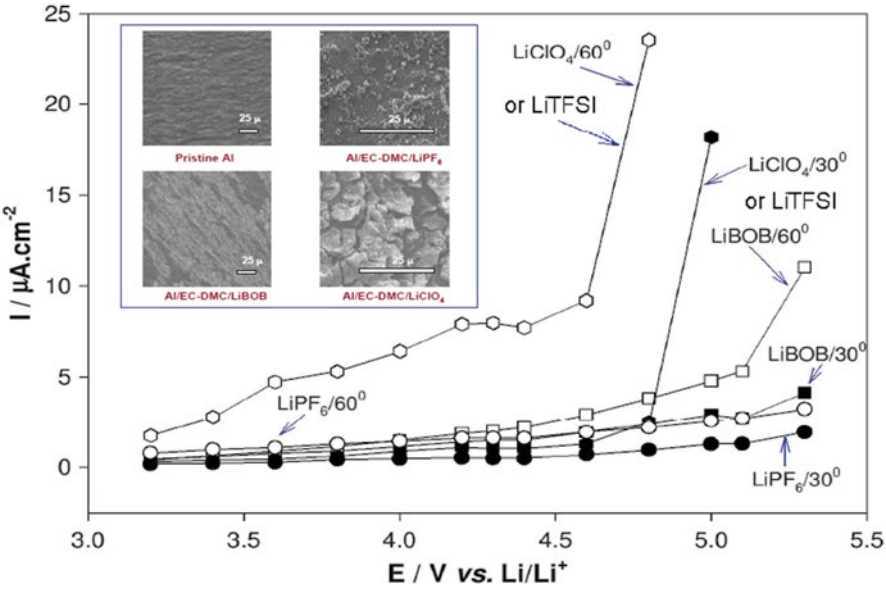

Fig. 6.2 Residual currents measured at 30 and at 60 °C from chronoamperograms of aluminum electrodes as a function of the applied potential. The *inset* shows the SEM images of the pristine aluminum electrode and aluminum electrodes tested by chronoamperometry and polarized at 5.30 V in various electrolyte solutions like EC–DMC/1 M $LiPF_6$, EC–DMC/1 M LiBOB, and EC–DMC/1 M $LiClO_4$ solutions at 60 °C. Reproduced with permission from [20], copyright (2010) The Electrochemical Society

these electrodes after polarization to 5 V vs. Li. It is clear that the Al foils undergo corrosion that affects their morphology on their way to reach passivation. It was found that the best passivation of Al is obtained in EC–DMC–$LiPF_6$ solutions, and the presence of this specific Li salt is critical for that [20]. However, it should be noted that Al reaches passivation after a certain consumption of charge that is needed to build the necessary surface film. The process adds an irreversible charge to the first cycle of any cathode. Our systematic measurements revealed that the oxidation of alkyl carbonate solvents is inhibited on Al electrodes when containing $LiPF_6$ (even as a co-electrolyte with a salt such as $LiClO_4$) [21]. The presence of carbon black worsens this inhibition. Hence, the irreversible charge measured with composite cathodes (comprising aluminum current collector (Al CC), active mass, and carbon black) depends strongly on the nature and amount of the carbon black additive in the composite electrode [22]. Consequently, it is hard to determine clearly the anodic stability threshold of standard electrolyte solutions in contact with various positive electrodes, because it depends on four factors that affect each other, namely, (1) the electrolyte solution composition, (2) the Al CC, (3) the nature, and (4) the amount of conductive additive in the composite electrodes (mostly carbon black) and the nature of the active mass (in terms of composition, structure, and morphology).

In conclusion, the oxidation of solution species can contribute significantly to the surface chemistry developed on composite cathodes in Li-ion battery systems. However, each system has to be examined and discussed separately.

6.4 How to Measure Surface Reactions of Cathode Materials and Relevant Composite Electrodes

The surface chemistry developed on cathodes for Li-ion batteries can be measured directly and indirectly by a variety of techniques that are described systematically below.

6.4.1 FTIR Spectroscopy

FTIR spectroscopy can be used in diffuse reflectance, specular reflectance, and external reflectance in grazing angle reflectance mode [23]. It enables the analysis of functional group and specific bonds of surface species. Particles can be measured separately (diffuse reflectance mode) after being scraped from composite electrodes [24].

6.4.2 Raman Spectroscopy

In general, this is a bulk technique with the capability of measuring surface species as well. The information is parallel and complementary to that obtained by FTIR spectroscopy, providing information on functional groups and specific bonds [25, 26].

6.4.3 X-Ray Photoelectron Spectroscopy

X-ray photoelectron spectroscopy (XPS) provides surface element analysis, including information on the oxidation states of the elements. It should be noted that XPS can be used in conjunction with sputtering the techniques, thus providing depth profiling of the composition of surface films [27, 28].

6.4.4 ICP

It is highly important to monitor and control the dissolution of transition metal cations to solution phase from the cathodes' active mass. It is important to measure solutions in which electrodes were cycled and solutions in which pristine

cathode powders were stored at different temperatures. The best technique that measures precisely elements in solutions is inductively coupled plasma (ICP) spectroscopy [29].

6.4.5 Electron Microscopy

High-resolution scanning and transmission electron microscopy (HRSEM, HRTEM) can provide very specific information about surface films on any kind of particles. A comparison between pristine particles and particles scraped from cycled electrodes can provide very comprehensive information. Using element analysis, STEM techniques, and selected area electron diffraction (SAED), it is possible to map surface species in a nanometric scale [30].

6.4.6 Solid-State NMR Spectroscopy

Li NMR spectroscopy can distinguish between bulk Li, related to the lattice and related to surface species. There are enough references on such measurements that provide all the relevant experimental details (e.g., the need of a low magnetic field, type of probes, measurements, conditions, and spectra identification) [30, 31].

6.4.7 Electrochemical Impedance Spectroscopy

Electrochemical impedance spectroscopy (EIS) provides indirect information about the surface phenomena of all kinds of electrodes [32]. The high-frequency part of impedance spectra of electrodes is usually attributed to surface phenomena such as Li-ion migration through surface films, surface film capacitance, and interfacial charge transfer [33]. However, it should be noted that EIS provides very ambiguous information. A special skill, as well as experience, is needed for a reliable assignment of spectral features to the time constants of a complicated electrochemical system such as that of composite electrodes [34].

Before measuring the active mass itself and the composite electrodes, the intrinsic surface chemistry related to the Al CC, carbon black, and the chosen electrolyte solution can be measured by polarizing Al foil electrodes to high potentials, following *ex situ* measurements by surface-sensitive techniques (FTIR, Raman, XPS). In fact, the intrinsic surface chemistry of Al/solution systems can be measured in situ by FTIR and Raman spectroscopic methods. In order to understand the surface chemistry of composite cathodes, the following experimental steps are recommended:

1. Pristine particles of the active mass of interest should be stored at several temperatures (e.g., 30 °C, 60 °C) in the chosen electrolyte solutions. The solution

phase should be measured systematically (as a function of storage time) by ICP in order to follow transition metal cation dissolution. The aged particles can be measured by XPS, Raman, and FTIR spectroscopic methods (for the latter technique, the diffuse reflectance mode should be used).
2. It is recommended to prepare electrodes comprising only Al foil and the active mass—particles embedded by light pressure into soft Al foil electrodes. Such electrodes can be polarized, cycled, and then measured by FTIR spectroscopy (reflectance modes such as grazing angle reflectance or specular reflectance modes in which there are commercial accessories available), Raman, and XPS.
3. Finally, composite electrodes can be measured after cycling. Particles scraped from cycled electrodes can be measured by FTIR spectroscopy (diffuse reflectance mode), Raman, XPS, and high-resolution electron microscopy. Changes in the surface chemistry due to cycling, aging, and different temperatures can be measured by impedance spectroscopy.

6.5 A General Presentation of Various Surface Chemical Aspects and Their Demonstration

This section aims at demonstrating the importance and relevance of the surface chemistry developed on cathodes for Li-ion battery systems to their performance. The topics selected for discussion are the effect of nano-size, surface chemical aspects of lithiated transition metal oxide cathodes and a comparison with the surface chemistry of $LiMPO_4$ olivine-type cathodes.

6.5.1 The Effect of Nano-Size

There is a clear incentive to use nanoparticles in composite electrodes based on Li-insertion materials. Nanoparticles have a short diffusion length and a high surface area, which may facilitate remarkably the kinetics of Li-insertion cathode materials, both due to the fast solid-state diffusion of Li ions and the fast interfacial charge transfer. However, the use of nanoparticles may have several drawbacks: a high surface area means high surface reactivity and pronounced passivation in phenomena that can interfere badly with the particles' electrical contacts. In addition, composite electrodes comprising nanoparticles may suffer from problems of active mass integration (both mechanical and electrical) and low specific density. Lithiated transition metal oxides are highly surface reactive, and thereby, it seems that using them as nanoparticles is very problematic, as demonstrated in the following study.

Figure 6.3 presents a summary of the results obtained in a study of $LiMn_{1/3}Ni_{1/3}Co_{1/3}O_2$ electrodes [35]. The active mass was prepared by a self-combustion reaction (SCR) that initially forms nanoparticles [36]. Thus, by annealing at high temperatures >700 °C during different periods of time, it is possible to

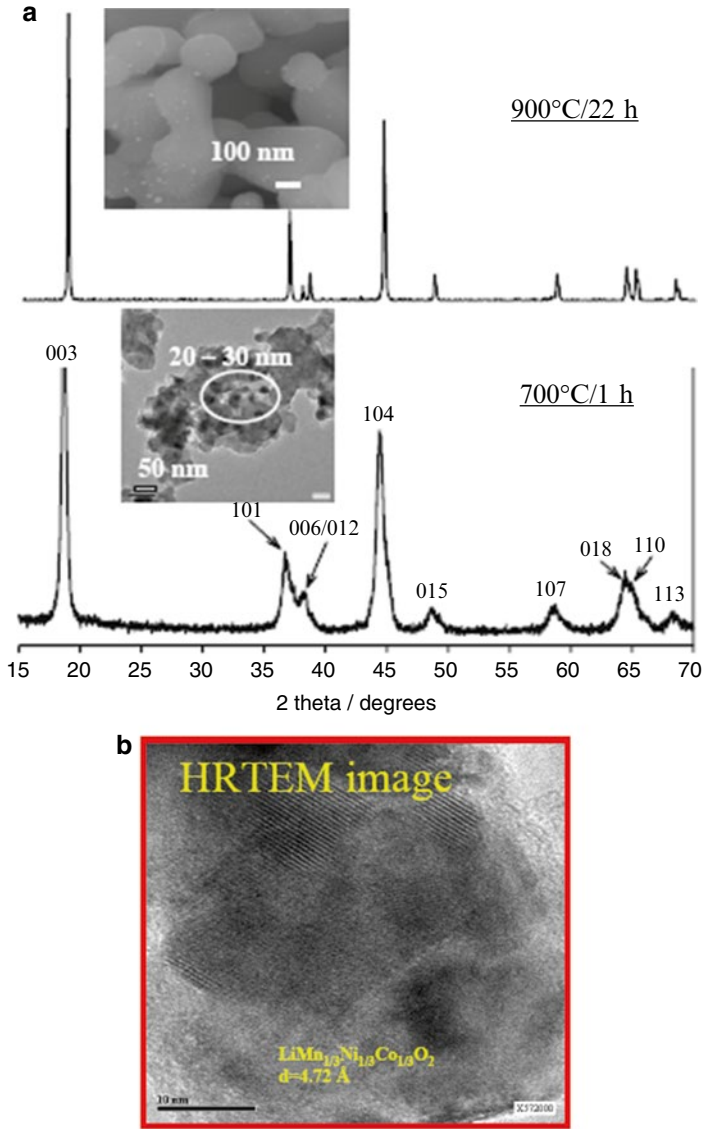

Fig. 6.3 (continued)

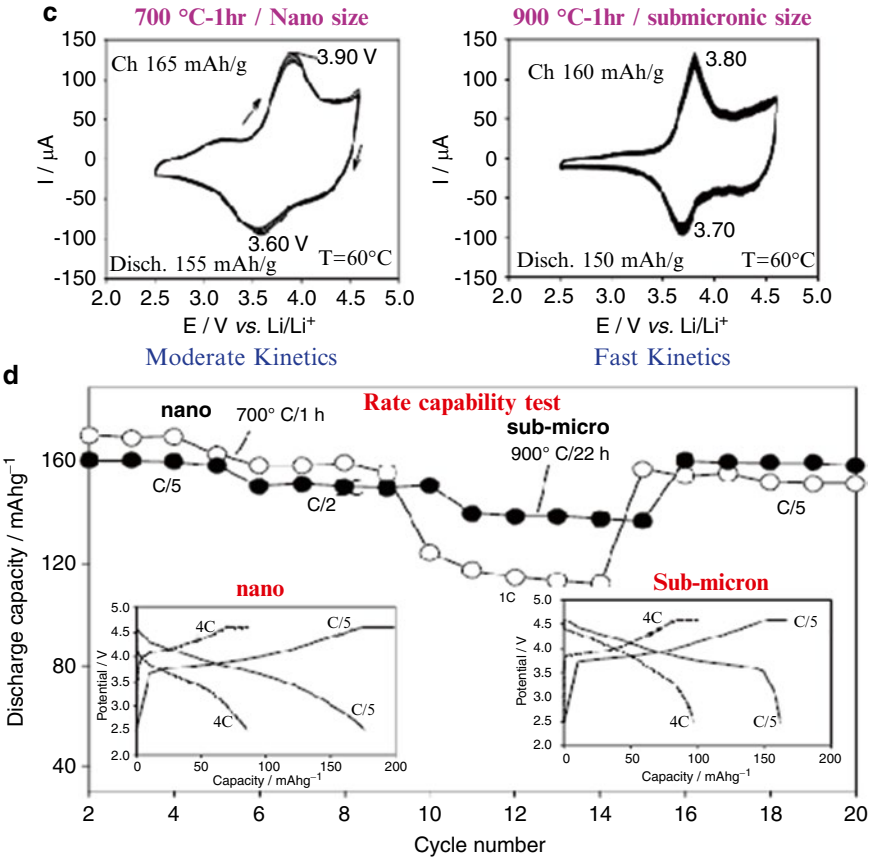

Fig. 6.3 The structural and electrochemical characteristics of nano- and sub-micrometric size $LiMn_{1/3}Ni_{1/3}Co_{1/3}O_2$ particles synthesized by SCR and further calcined in air at 700 °C/1 h and 900 °C/22 h, respectively. (**a**) The XRD patterns of nano- and submicronic $LiMn_{1/3}Ni_{1/3}Co_{1/3}O_2$ particles, (**b**) HRTEM image of nanoparticle annealed at 700 °C/1 h, (**c**) slow-scan-rate CVs, and (**d**) rate capabilities (*inset* shows the voltage profiles) measured from electrodes comprising $LiMn_{1/3}Ni_{1/3}Co_{1/3}O_2$ nano- and submicrometric particles in EC–DMC (1:2)/1.5 M $LiPF_6$ solution. Reproduced with permission from [35], copyright (2009) The Electrochemical Society

determine the particle size. In this study, nanoparticles and sub-micrometric particles of the same active mass, prepared by the same basic synthesis, were measured in parallel experiments. The XRD and SEM data shown in Fig. 6.3a, b confirms the difference in the particle size (the particle size calculated from the full width at half maximum XRD peaks matches with the values in SEM images), the right layered structure and composition. The electrochemical response provided in Fig. 6.3c, d shows steady-state, slow-scan cyclic voltammograms measured at 60 °C after aging, cycling data at different rates (C/5 h, C/2 h 1C), and typical voltage profiles measured at C/5 and 4C rates. The solution was EC–DMC/$LiPF_6$. The results are spectacular; the electrodes comprising nanoparticles show an inferior rate capability compared to

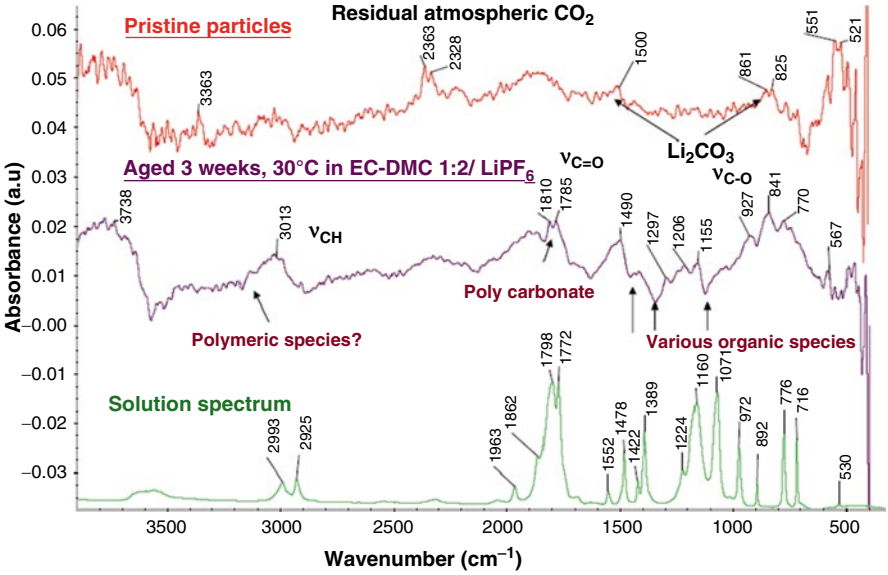

Fig. 6.4 FTIR spectrum of pristine $LiMn_{1/3}Ni_{1/3}Co_{1/3}O_2$ nanoparticles and spectrum of nanoparticles aged in an EC–DMC/$LiPF_6$ solution, at 30 °C for 3 weeks. IR spectrum of the electrolyte solution is also presented for comparison. Reprinted from [36], copyright (2009) with permission from Elsevier

those comprising sub-micrometric particles. The CV curves of the latter electrodes were sharper, and the capacity measured at a high rate is higher compared to electrodes comprising nanoparticles. It appears that the nanoparticles are more surface reactive and develop surface films that interfere badly with the kinetics of Li insertion into the active mass. This surface chemistry is discussed briefly in the next section.

6.5.2 *On the Surface Chemistry of Li_xMO_y, Lithiated Transition Metal Oxide Electrodes, and $LiMPO_4$ Olivine Cathodes; Some Examples and Introductory Remarks*

Figure 6.4 shows typical FTIR spectra of $LiMn_{1/3}Ni_{1/3}Co_{1/3}O_2$ particles measured by diffuse reflectance mode, pristine particles, and after aging in a standard solution (EC–DMC/$LiPF_6$) [37]. A solution transmission spectrum is provided for comparison. The spectrum of pristine particles usually shows Li_2CO_3 peaks due to the reaction of the active mass with CO_2 from the air. The spectrum of aged particles is rich in peaks of organic species that are not residual solution species. Different carbonate peaks ($ROCO_2Li$, polycarbonate) can be identified, as well as peaks of C–O and C–H stretching vibrations, plus many peaks of bending modes in the range of 1,300–600 cm^{-1}. Such spectra are typical to all kinds of Li_xMO_y particles aged in the same solutions (including $LiCoO_2$, $LiMn_{0.5}Ni_{0.5}O_2$, $LiMn_{1.5}Ni_{0.5}O_4$ spinel, $Li[CoNi]O_2$, and more).

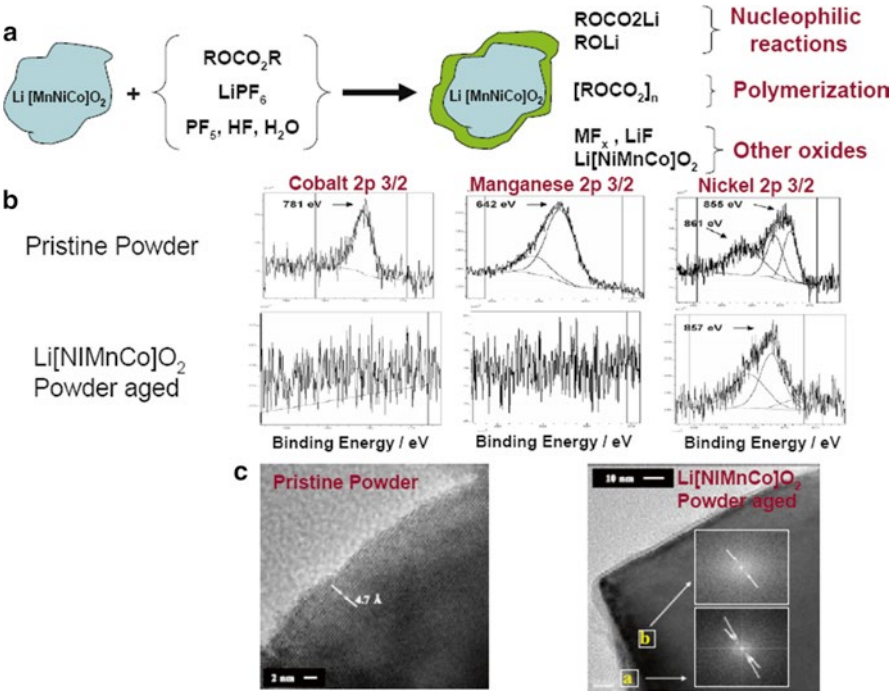

Fig. 6.5 (**a**) A schematic representation of the formation of the core–shell structure of the $Li[MnNiCo]O_2$ particles formed due to their surface reactions in solutions. (**b**) XPS spectra (Co 2p3/2, Mn 2p3/2, and Ni 2p3/2) [36] and (**c**) HRTEM images of pristine $LiMn_{1/3}Ni_{1/3}Co_{1/3}O_2$ particles and particles aged in ambient air, demonstrating surface reaction with CO_2 from air to form surface Li_2CO_3. Reproduced with permission from [37], copyright (2010) The Electrochemical Society

The conclusion from these surface measurements is exhibited in Fig. 6.5. All the Li_xMO_y materials react with solution species of standard electrolyte solutions and develop a core–shell structure, in which the shells comprise surface films that behave like SEI. The surface activity is more pronounced for nanoparticles. Figure 6.5 provides two more important pieces of information related to $Li[MnNiCo]O_2$ cathode material (and relevant to all other Li_xMO_y cathode compounds) [37]. XPS data of pristine particles shows, as expected, the peaks of Mn, Ni, and Co at similar intensity. After aging or cycling in standard solutions, XPS measurements show peaks of Ni but not peaks of Co and Mn. These results reflect the formation of surface films that cover the active mass, so that the X-ray beam cannot penetrate them. However, Ni is probably detected because Ni ions are involved in the formation of surface species while Mn and Co ions can more readily dissolve from the surface particles to the solution phase. The HRTEM images shown in Fig. 6.5c compare the pristine particle and the particle that was exposed during couple of years to ambient air [38]. The image and related analysis detect clearly the formation of a Li_2CO_3 surface layer that can be formed by two reactions:

1. $n\mathrm{Li[MnNiCo]O_2} + \mathrm{CO_2} \rightarrow \mathrm{Li_2CO_3} + n\mathrm{Li_{1-x}[MnNiCo]O_{2-y}}$
2. $n\mathrm{Li[MnNiCo]O_2} + 1/2\ \mathrm{O_2} + \mathrm{CO_2} \rightarrow \mathrm{Li_2CO_3} + n\mathrm{Li_{1-x}[MnNiCo]O_2}$

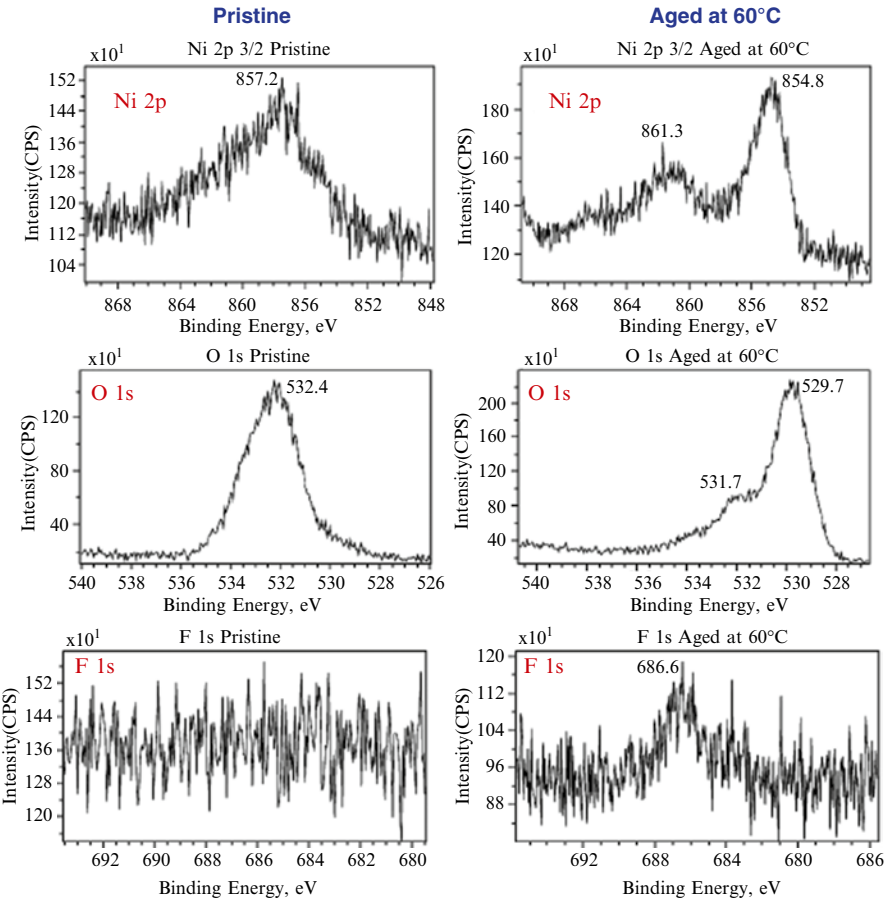

Fig. 6.6 XPS spectra of Ni 2p, O 1s, and F 1s measured from pristine and aged nano-$LiNi_{0.5}Mn_{0.5}O_2$ powders. Aging was carried out in an EC–DMC (1:2)/1.5 M $LiPF_6$ solution at 60 °C for 20 days. Reproduced with permission from [38], copyright (2006) The Electrochemical Society

The first reaction involves a structural and compositional change in the active mass (near the surface), while the second reaction involves only the delithiation (and Li_2CO_3 formation). It should be noted that Li_2CO_3 films formed on Li_xMO_y inhibit the kinetics of Li insertion and should be considered as a detrimental phenomenon.

Figure 6.6 presents XPS data related to the aging of $LiMn_{0.5}Ni_{0.5}O_2$ electrodes in standard electrolyte solutions at 60 °C [39]. An oxygen, fluorine, and nickel peak in the figure relates to pristine and aged nano-$LiNi_{0.5}Mn_{0.5}O_2$ electrodes. These spectral results are spectacular. They clearly show pronounced changes in the nickel and oxygen peaks, related to surface reactions with solution species, and the appearance of a new fluorine peak that can be attributed to Li and Ni fluorides. From these spectral studies, several conclusions can be drawn:

1. The nucleophilic oxygens of Li_xMO_y compounds can attack the alkyl carbonates to form surface species containing $ROCO_2LiM$ or ROM groups, M = Li, and/or transition metal.

2. There are obvious reactions between Li_xMO_y compounds and acidic species such as HF. These reactions form MF_x surface species, M = Li, or transition metal. Li_xMO_y compounds can also interact with trace PF_5 that can be formed by the thermal decomposition of $LiPF_6$ ($LiPF_6 \rightarrow LiF + PF_5$). The products should include MF_x species (always detected on the surface of lithiated transition metal oxides aged/cycled in standard electrolyte solutions).
3. There are indications of the formation of polycarbonate species on aged cathodes. These can be formed by anionic or cationic polymerization of ethylene carbonate.
4. We can add to it further information on $LiCoO_2$ electrodes obtained from our studies that show that the Co ions in 3.5+ oxidation state can oxidize alkyl carbonates to CO_2. Also the contact points of the particles with the binder (PVdF) are the most problematic for interactions with acidic species from $LiPF_6$ solutions. Interactions with trace HF drive to irreversible changes on the particle surface (see therein) [40].

Figure 6.7 shows typical impedance spectra of $LiMn_{0.5}Ni_{0.5}O_2$ electrodes, measured during very prolonged experiments at 60 °C in standard electrolyte solutions [39]. The spectra of composite electrodes comprising Li_xMO_y compounds always show a high-frequency semicircle and a low-frequency sloping line that resembles the response of a Warburg-type element. The assignment of the impedance spectra of composite electrodes to their relevant time constants is "mission impossible." Impedance data from these electrodes can serve mostly as a qualitative comparative tool. The most important information that can be extracted from the spectra is the stability of the electrode that they reflect. A typical spectrum of a composite Li_xMO_y electrode in standard electrolyte solutions depends strongly on the temperature and water contamination. The electrodes' impedance is developed with the first few cycles and then remains invariant during prolonged cycling and aging at constant temperature, even at 60 °C.

In contrast to the case of negative electrodes (Li, Li-graphite, Li-Si, etc.), where there is a continuous driving force for surface reactions (thermodynamic instability of the solution in potentials below 1.5 V vs. Li), for most of the pristine electrodes there is no thermodynamic driving force for continuous oxidation. The surface chemistry develops due to acid–base reactions, nucleophilic attacks, and probably some oxidation reactions that lead to the polymerization of EC. These surface reactions can be largely inhibited, even by the formation of monolayer thick surface film. However, the pronounced contamination of protic species in solutions (HF, H_2O) can lead to continuous surface reactions on cathodes, because H_2O or HF can percolate through all kinds of surface films and interact with the active mass. Other driving forces for instability may include too high potentials that lead to continuous oxidation of solution species in the absence of good passivation/inhibition. In addition, the continuous dissolution of transition metal cations to the solution phase can change the composition and the structure of the active mass, leading to the formation of thick shells around the contracting cores of the active mass particles [41]. Also highly detrimental are situations in which the dissolution of transition metal

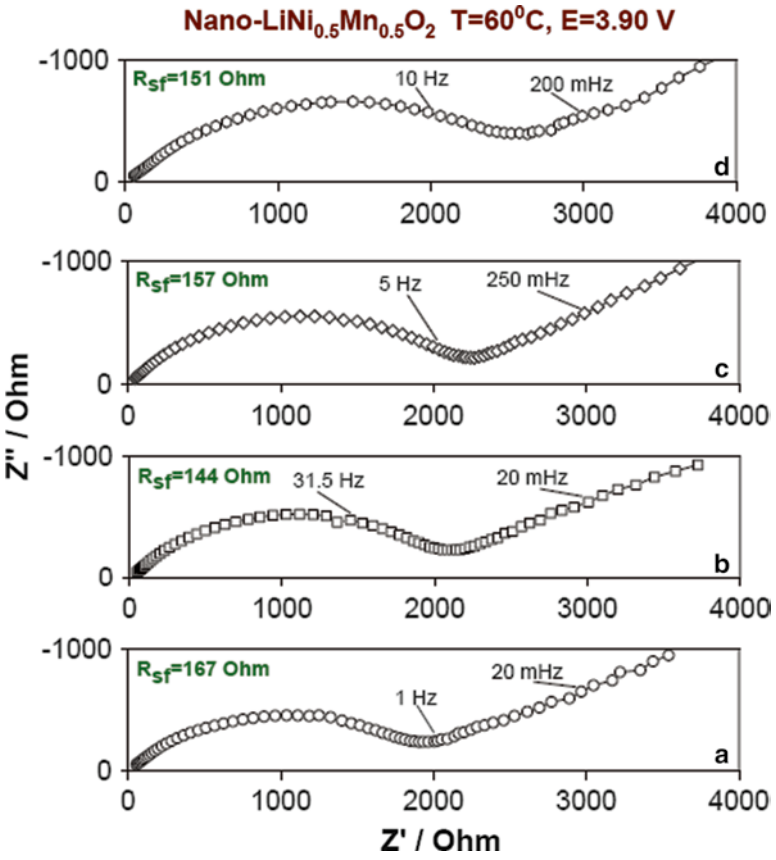

Fig. 6.7 Impedance spectra (Nyquist plots) measured from an electrode comprising $LiNi_{0.5}Mn_{0.5}O_2$ particles at $E = 3.90$ V under various conditions of cycling/aging: (**a**) initial steady state, after cycling the cell at 60 °C, (**b**) after 1-week aging at 60 °C, (**c**) after 2-week aging at 60 °C, and (**d**) after 50 days of cycling/aging at 60 °C in EC–DMC (1:2)/1.5 M $LiPF_6$ solution. Reproduced with permission from [38], copyright (2006) The Electrochemical Society

cations from Li_xMO_y-type cathodes never reaches the saturation point, because these cations are continuously depleted from the solution at the anode side. Lithiated graphite or silicon electrodes reduce M^{z+} cations in solutions to metallic clusters that precipitate on the anode side. Such clusters are detrimental to the effectiveness of the anodes' passivation [42].

Finally, as discussed in detail in the forthcoming chapters, $LiFePO_4$, $LiMnPO_4$, and $Li[MnFe]PO_4$ compounds are much less reactive towards standard electrolyte solutions compared to Li_xMO_y compounds. It can be concluded that different surface chemistry is developed on Li-olivine and Li-transition metal oxide compounds.

6.6 On the Surface Chemistry of Li_xMO_y-Type Cathodes

Formation mechanism of SEI layers on cathodes in Li-ion batteries, their thermal and electrochemical stability, and their roles in affecting the cycle life and safety characteristics are well documented by many researchers [43–46]. Here we present some recent data on identifying the surface layer generation and their composition on transition metal oxide cathodes like spinel and layered materials by various spectroscopic techniques. The structural changes and the reaction at the surface during the first delithiation process in Li-rich layered material are explained. The effects of additives and coatings on electrode materials to their electrochemical performance are also discussed at the end.

6.6.1 SEI-Like Surface Film Formation on Transition Metal Oxide Spinel Materials

All cathode materials of interest for Li-ion batteries are reactive with the commonly used electrolyte solutions, thus developing a rich surface chemistry. There is strong evidence that most of the lithiated transition metal oxides are covered by surface films in solutions due to spontaneous reactions with solution components [47]. Hence, the electrochemical behavior of most cathode materials may depend very strongly on their surface chemistry in electrolyte solutions. The surface-modified cathodes have better cyclability compared to the pristine cathode, suggesting that the coatings formed on the surface of the cathode give a stable passivation layer or a solid electrolyte interface (SEI). There are several investigations on the structure of cathode surface films formed under standard cycling 4.5 V vs. Li^+ and aging conditions [48, 49]. The remarkable stability of $LiNi_{0.5}Mn_{1.5}O_4$ electrodes under cycling and storage condition at elevated temperature in 1.5 M $LiPF_6$ solutions of alkyl carbonates was well demonstrated [50], despite the fact that their redox activity is high, around 4.5–4.9 V vs. Li/Li^+ due to the $Ni^{2+}/Ni^{3+}/Ni^{4+}$ couples.

Impedance spectra of $LiNi_{0.5}Mn_{1.5}O_4$ electrodes measured at 60 °C during cycling and aging at two different potentials are shown in Fig. 6.8. By studying the influence of temperature on the impedance of $LiNi_{0.5}Mn_{1.5}O_4$ electrodes, it can be concluded that surface films formed at high temperatures remain stable and do not change at lower temperatures, and hence, the impedance remains steady upon cycling and storage. It was also observed from XPS measurements that this surface chemistry involves the formation of LiF, C–F, and $P–F_x$ species as well as organic compounds (probably polyethers) on the aged $LiNi_{0.5}Mn_{1.5}O_4$ electrodes. It should also be noted that some Mn and Ni ion dissolution from these electrodes could be detected only after prolonged (several weeks) storage at 60 °C.

Li Yang et al. [51] have investigated the by-products formed during the storage of cells containing $LiNi_{0.5}Mn_{1.5}O_4$ material in contact with the electrolyte solutions containing 1 M $LiPF_6$ in ethylene carbonate/dimethyl carbonate/diethyl carbonate in the

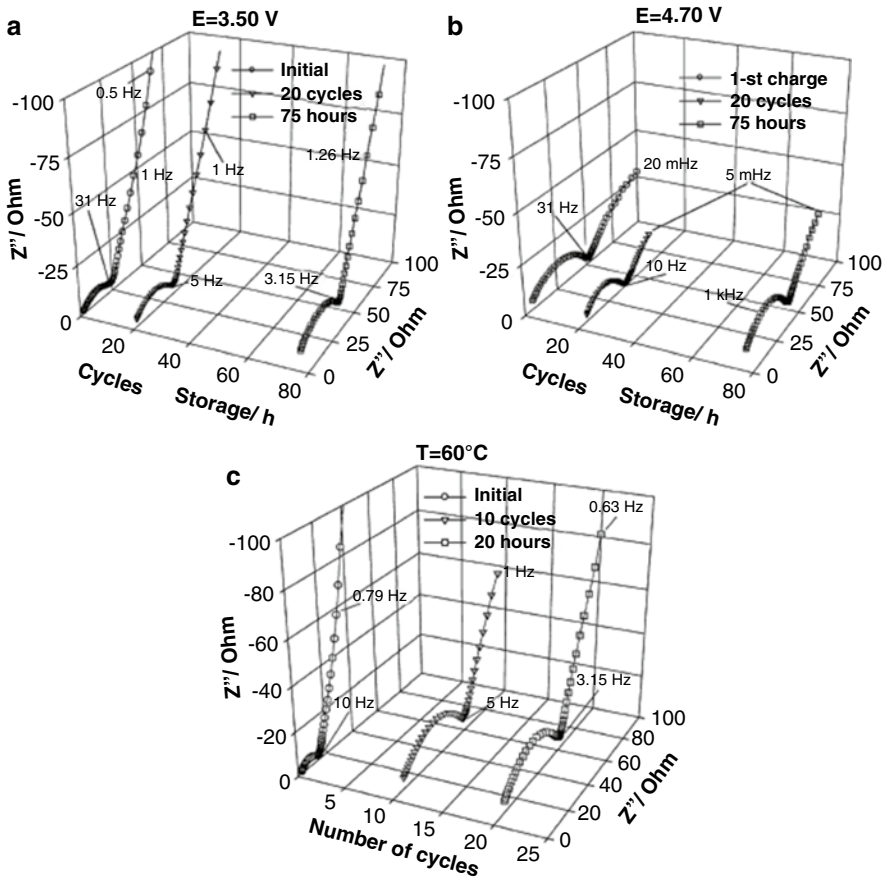

Fig. 6.8 Impedance spectra (Nyquist plots) of $LiMn_{1.5}Ni_{0.5}O_4$ electrodes measured at 60 °C during cycling and after aging at two different potentials as indicated. 1.5 M $LiPF_6$/EC–DMC solutions. Reprinted from [49], copyright (2006) with permission from Elsevier

ratio 1:1:1 at low and high voltage ranges. At low voltage ranges, low concentrations of decomposition products were observed along with low residual current. Upon storage at high voltage range 4.7–5.3 V vs. Li, the presence of polyethylene carbonate (PEC) species was identified by surface analysis (XPS and FTIR studies). The XPS and FTIR spectra showing the presence of PEC are presented in Fig. 6.9. By XPS it was observed that an increase in the voltage leads to the continuous increase in the C 1-s peaks characteristic of C–O (C 1 s, 286 eV) and C=O (C 1 s, 289 eV) bonds in approximately 2:1 ratio. This finding might indeed be related to the presence of surface PEC. The generation of PEC on the surface of these cathode materials was confirmed by other groups as well [52, 53]. Studies of the composition of the surface layer on $LiNi_{0.5}Mn_{1.5}O_4$ electrodes in half cell (vs. Li) and full cell vs. $Li_4Ti_5O_{12}$ anode were carried out by Duncan et al. in solutions comprising EC,

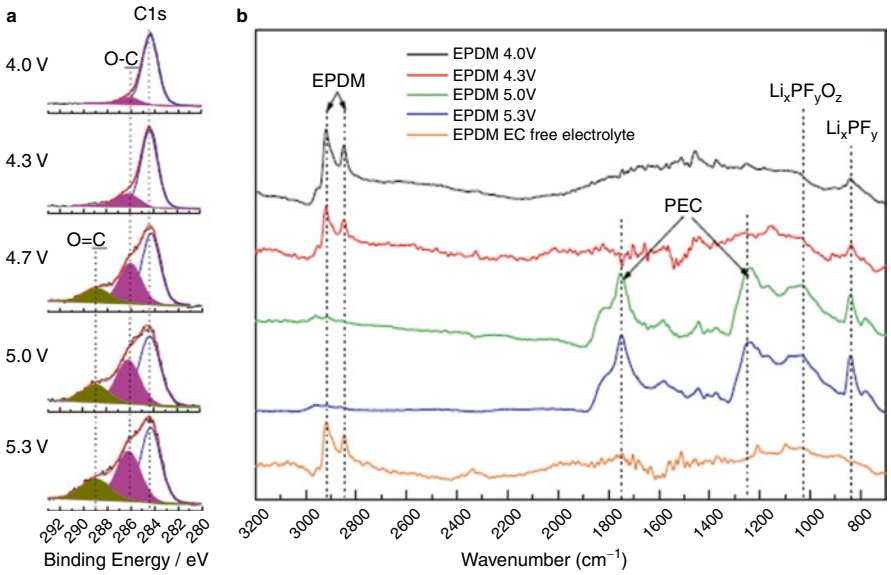

Fig. 6.9 The XPS, C 1s spectra (**a**) and FTIR spectra (**b**) measured after aging at different potentials showing the presence of polyethylene carbonate on $LiNi_{0.5}Mn_{1.5}O_4$ electrodes as mentioned therein. Reproduced with permission from [50], copyright (2010) The Electrochemical Society

DEC + $LiPF_6$, or $LiBF_4$ [54]. It was found that storage of cells at 60 °C deteriorated their capacity (upon cycling them after then at room temperature). XPS measurements revealed the presence of various surface species on $LiNi_{0.5}Mn_{1.5}O_4$ electrodes, as shown in Fig. 6.10. The surface species thus formed include lithium alkyl carbonates ($ROCO_2Li$), polycarbonates $–[OCO_2]_x–$, polyethers, Li_2CO_3, LiF, $Li_xPF_yO_z$, or $Li_xBF_yO_z$ (depending on the electrolyte). $LiMn_2O_4$ spinel is also considered as an important cathode material (cheap, fast, safe), despite relatively low capacity (120 mAh/g practical) and moderate voltage (4 V vs. Li). The performance and surface chemistry of this cathode material were also extensively explored by various methods [55, 56]. It is clear that as the temperature is higher, surface film formation in standard electrolyte solutions is more intensive, with a consequent increase in the electrodes' impedance (due to formation of surface LiF and MnF_3) and capacity fading. Extensive Mn ion dissolution from this material is the most detrimental phenomenon observed at elevated temperatures, leading to formation of inactive phases. It was found that the surface films formed on $LiMn_2O_4$ electrodes become thicker upon cycling [57]. Studies of $LiMn_2O_4$ electrodes in ionic liquid-based systems (e.g., LiTFSI/PMPyr-TFSI + LiTFSI) revealed much better stability of these systems at elevated temperatures compared to conventional solutions. Fortunately Al CC reach good passivation even in LiTFSI solutions when the solvents are quaternary ILs [56].

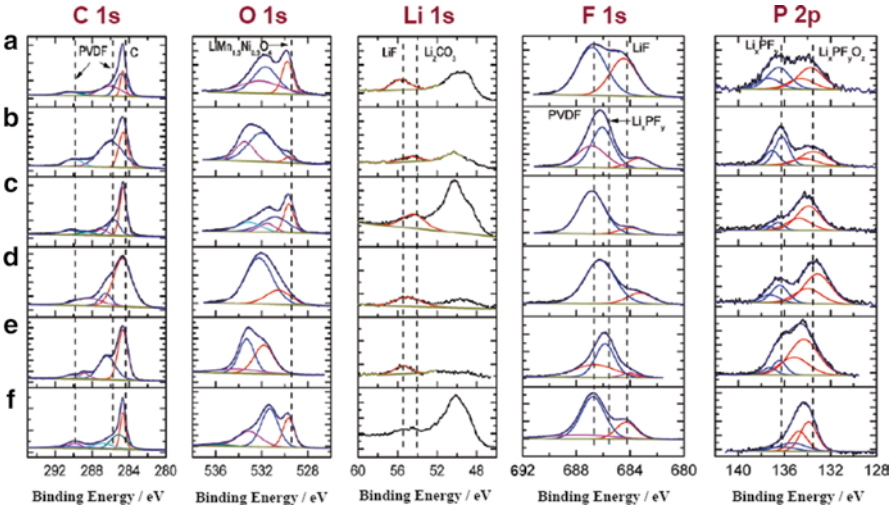

Fig. 6.10 The XPS O 1s, C 1s, Li 1s, F 1s, and P 2p spectra of as-synthesized $LiNi_{0.5}Mn_{1.5}O_4$ electrode in EC:DEC (3:7)/1 M $LiPF_6$ electrolyte, (**a**) stored for 24 h at 60 °C, (**b**) stored at 0 % SOC for 60 days at 60 °C, (**c**) stored at 100 % SOC for 60 days at 60 °C, (**d**) cycled 100 times at room temperature, (**e**) cycled 100 times at 60 °C, (**f**) cycled 100 times at room temperature, LTO-negative electrode. Reproduced with permission from [53], copyright (2011) The Electrochemical Society

6.6.2 SEI-Like Surface Film Formation on Transition Metal Oxide Layered Materials

It should be noted that the surface activity and possible formation of surface films depend strongly on the composition of the $LiMO_2$ compounds. The order of surface reactivity is $LiNiO_2 > LiCoO_2 > LiMn_2O_4$ [58]. Matsui et al. [59] reported on the possibility to have periodic surface film formation on $LiMn_2O_4$ and $LiNi_{0.5}Mn_{1.5}O_4$ electrodes, driven by the periodic redox activity of the transition metal upon cycling.

$LiMn_{0.33}Ni_{0.33}Co_{0.33}O_2$ (LMNC) can be considered as one of the most important currently available, commercial layered cathode materials for Li-ion batteries. This material is highly surface reactive in standard electrolyte solutions. The reactivity is higher as the particle size is smaller [35]. For example, Fig. 6.11 shows HRTEM images of pristine $LiMn_{0.33}Ni_{0.33}Co_{0.33}O_2$ nanoparticles which were aged in EC–DMC 1:2/1.5 M $LiPF_6$ solution at 60 °C for 3 weeks. It is easy to detect using HRTEM the surface layer formed on these particles upon aging (marked in Fig. 6.11b). In general, the electrochemical performance of electrodes comprising nano-LiMNC is worse than that of electrodes comprising sub-micrometric particles in terms of capacity, stability, and even rate capability due to the higher surface reactivity.

The commonly used $LiCoO_2$ electrodes are also highly surface reactive in standard electrolyte solutions used in Li-ion batteries (alkyl carbonates/$LiPF_6$).

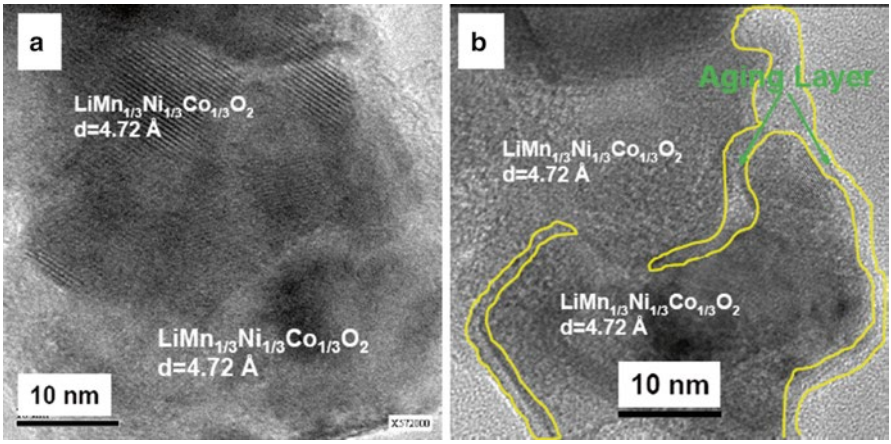

Fig. 6.11 HRTEM images of (**a**) pristine $LiMn_{0.33}Ni_{0.33}Co_{0.33}O_2$ nanoparticles annealed at 700 °C/1 h and (**b**) particles aged in an EC–DMC/1.5 M $LiPF_6$ solution at 60 °C for 3 weeks. Reproduced with permission from [34], copyright (2009) The Electrochemical Society

Their surface reactivity was extensively explored. Major surface phenomena are the following:

1. Formation of surface films comprising LiF, CoF_x, $ROCO_2M$ (M = Co, Li), and polycarbonates.
2. Disproportionation of surface Co^{3+} to Co^{2+} and Co^{4+}. The former ions dissolve to solution phase, and the latter ions oxidize alkyl carbonates to form Co_2.
3. Formation of surface Li-Co-O spinel phase was detected. Surface Co_3O_4 formation was also detected.
4. There are strong interactions between these cathode materials and H^+ moieties (trace HF).

Another important, now commercially available, family of cathode material is $Li[NiCo]O_2$ compounds. The most important one is the Al-doped $LiNi_{0.8}Co_{0.2}O_2$ compound. These compounds also develop very rich surface chemistry. For example, the formation of surface films formed on $LiNi_{0.85}Co_{0.15}O_2$ cathodes in lithium-ion cells was characterized using soft X-ray absorption spectroscopy (XAS) [60]. Surface LiF formation was clearly detected by surface studies of these electrodes. The surface reactivity increases and is accelerated as the temperature is higher [61].

Magic angle spinning (MAS) NMR has been proved to be an extremely powerful tool, able to probe both the bulk of the materials used as electrodes and the surface layers arising after contact with atmosphere or with the electrolyte of a lithium battery [62]. The amount of surface interphase formed on cathodes was proved to influence drastically the electrochemical performance. Either an excessive amount or an insufficient amount of surface species is detrimental to the performance, while there is optimal formation of surface films for each kind of electrodes in standard electrolyte solutions. The interphase formed as a function of

synthesis condition (combustion and coprecipitation techniques) and storage conditions (Argon and Air) for $LiNi_{0.5}Mn_{0.5}O_2$ sample has been studied extensively by Dupre [63]. They have shown that the same material has a different electrochemical behavior and a different evolution of the positive electrode/electrolyte interphase due to different pristine surface chemistry. The formation and the evolution of lithium-containing species during the electrochemical cycling have been followed using ^{7}Li MAS NMR and XPS on the surface of $LiNi_{0.5}Mn_{0.5}O_2$ layered material. ^{7}Li MAS NMR experiments performed upon cycling indicate the formation of interphase species in reduction and their partial removal in oxidation, indicating the dynamic character of the interphase upon cycling. In addition, XPS indicated the presence of Li_2CO_3 on the surface of grains of active material that have been stored in ambient atmosphere while Li_2CO_3 is absent from the surface of the materials stored in argon.

Another example: The spontaneous reactions occurring at the surface of $LiNi_{0.75}Co_{0.25}O_2$ electrodes in contact with solutions such as $LiPF_6$/EC–DMC and $LiClO_4$/PC were specially investigated by Raman and FTIR spectroscopy [64]. The formation of surface Li-carbonates, MF_x (M = Li, Co, or Ni), and P-O-F surface moieties (in $LiPF_6$ solutions) was clearly confirmed.

6.6.3 On Surface Structural Changes (Phase Transformation) in the Course of the First Delithiation of Lithiated Transition Metal Cathodes (First Charging Processes)

The first process which Li_xMO_y cathode materials undergo in Li-ion batteries is delithiation (charging) by application of high anodic voltages. Depending on the level of polarization (voltage), these processes lead to reversible Li-ion removal with no structural changes in the compound lattice. However, too high anodic polarization of Li_xMO_y electrodes may lead to pronounced structural changes at and near the material's surface due to oxygen evolution and/or disordering due to metal ion dislocations in the lattice. The judicious use of high-resolution electron microscopy in conjunction with electron and X-ray diffractometry revealed clearly the phenomena such as (1) formation of surface spinel phase on layered materials, (2) transition metal ion migration from their original sites to Li sites, (3) formation of surface films due to surface reactions with solution species, and (4) formation of core–shell structures due to the above-described structural changes, which may include formation of surface amorphous phases (due to a high anodic polarization) and related chemical changes [65]. The use of synchrotron-based techniques for the study of such structural surface transformations should also be mentioned [66].

In fact it is hard to measure the intrinsic anodic behavior of Li_xMO_y cathode materials in standard electrolyte solutions because at too high potentials the anodic reactions of solution species may dominate the potentio-dynamic response. However, ionic liquid solutions based on quaternary ammonium cations, TFSI anion, and LiTFSI salt demonstrate very high anodic stability. The passivation of Al current collector is excellent in these solutions. So, the anodic stability of Al

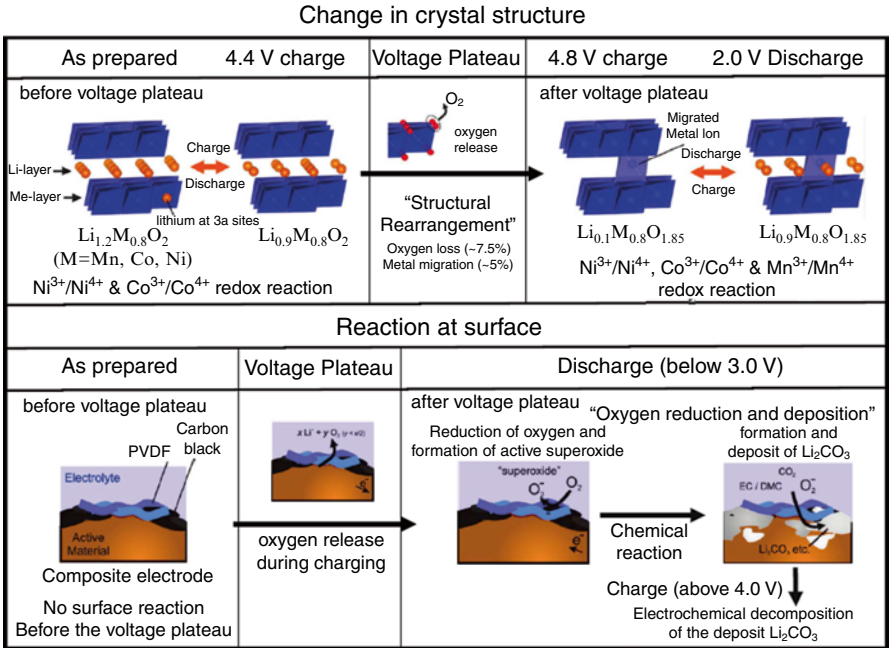

Fig. 6.12 *Upper chart*: Illustrations of the structural changes occurring in Li-rich layered $(Li_x[Mn_yNiCo]O_z$ cathode material upon delithiation to high potentials. *Lower chart*: illustration of the surface reactions occurring on Li rich layered $(Li_x[Mn_yNiCo]O_z$ cathode material upon de-lithiation to high potentials and then re-lithiation (the first cycles). Reproduced with permission from [65], copyright (2011) American Chemical Society

electrodes in ionic liquid (IL) solutions based on derivatives of piperidinium or pyrrolidinium TFSI (with LiTFSI as Li salt) may exceed 5.5 V vs. Li, which enables studying the intrinsic anodic behavior of Li_xMO_y cathode materials. Such studies with the important cathode material $LiNi_{0.8}Co_{0.15}Al_{0.05}O_2$ revealed that its polarization >4.5 V vs. Li leads to liberation of oxygen that readily reacts with carbon black in composite electrodes to form CO and CO_2 [67].

Highly important cathode materials that undergo extensive phase transformation during their first anodic polarization are the Li-rich high-capacity layered compounds with the formal initial stoichiometry and structure: $xLi_2MnO_3{\cdot}(1{-}x)$ $Li[MnNiCo]O_2$. Note that the first component (with Mn at 4+ oxidation state) is electrochemically inactive. During first anodic polarization, these materials are activated by simultaneous occurrence of some oxygen and lithium ion removal. It is not fully clear if the activation of these materials by high anodic polarization is a uniform bulk process or involve surface changes and formation of core–shell moieties. Figure 6.12, taken from reference [66], suggests mechanisms of surface reactions of Li_xMO_y compounds: structural changes due to oxygen evolution and transition metal cation exchange in the lattice (Fig. 6.12, upper chart) and surface reactions due to interactions of surface oxygen atoms with species in standard electrolyte solutions (Fig. 6.12, lower chart).

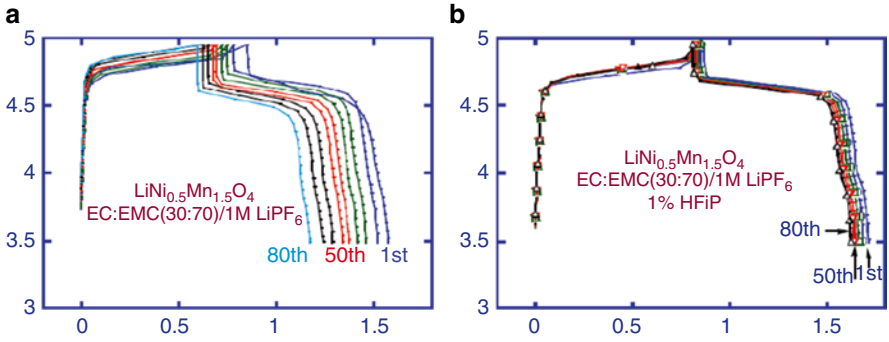

Fig. 6.13 The voltage profiles of cells containing $LiNi_{0.5}Mn_{1.5}O_4$ cathodes and 1 M $LiPF_6$/EC:EMC during prolonged cycling (**a**) no additive (**b**) solution containing 1 % HFiP. Reproduced with permission from [70], copyright (2011) The Electrochemical Society

6.6.4 The Effect of Additives on the Surface Chemistry of Li_xMO_y Cathode Materials

It was observed for a long time that commonly used nonaqueous electrolyte solutions based on organic carbonates may not be stable at potentials beyond 4.5 V vs. Li [51]. The use of surface-active and acid scavenger additives in standard electrolyte solutions serves as an effective approach to modify the surface chemistry of electrodes in Li-ion batteries towards higher stability. Additives are designed to form better surface films, to reduce flammability, and to provide overcharge protection [68]. Initially, surface-active additives were explored in connection to the anode side, mostly for improving the stability of graphite electrodes. It was found that some of the surface-active additives such as vinylene carbonate (VC) are surface active and that too at the positive side (high voltage) [69, 70].

Another important example for the use of surface-active additives for positive electrodes is the formulation of solution composition containing phosphate ester with highly fluorinated isopropyl moieties that dramatically improves the stability of the state-of-the-art electrolyte solutions [71]. The use of such additives in standard electrolyte solutions enables operation of 4.8 V Li-ion intercalation cathodes in full cells, in combination with graphitic anodes. It was nicely demonstrated that using 1 % of tris(hexafluoro-*iso*-propyl)phosphate $((CF_3)_2CHO)_3PO$ (denoted as) HFiP in EC–DMC/$LiPF_6$ (standard) solutions increased dramatically the performance of full cells comprising high-voltage $LiNi_{0.5}Mn_{1.5}O_4$ cathodes and graphite anodes. It is suggested that this HFiP additive is surface active on both positive and negative electrodes via polymerization that precipitate protective surface films. The effect of HFiP on the performance of cells containing high-voltage $LiNi_{0.5}Mn_{1.5}O_4$ cathodes is demonstrated in Fig. 6.13.

Another interesting example for surface-active additive that seems to have positive effect on both anode and cathode sides in Li-ion batteries is LiBOB (Li-bioxalato

borate, $LiBC_4O_8$). For instance it was found that the use of LiBOB as an additive to standard electrolyte solutions in cells containing $LiMn_2O_4$ cathodes suppresses Mn ion dissolution from this compound at elevated temperatures. It should be noted however that the mechanism of suppressing Mn dissolution from $LiMn_2O_4$ due to the presence of LiBOB in solutions is not yet clear.

6.6.5 Coating the Surface of Li–Ni–Co–Mn–O Cathodes in Order to Improve Electrochemical Performance and Stability

Dissolution of manganese ions or other transition metal cations from different cathode materials into the electrolyte solutions during prolonged cycling is believed to be one of the main reasons for capacity fading of full cells containing graphite anodes, especially at high temperatures. Transition metal ions in solution migrate towards the carbon anode and are reduced to metallic clusters that destroy the anode's passivation [72]. Several approaches were suggested to solve these problems, for instance by doping lithiated transition metal oxide cathode materials with active metal cations such as Al, Mg, and Ti [73] and the use of multi-transition metal oxides such as $Li[MnNiCo]O_2$ [37], thus enhancing the structural stability of these compounds [74]. However, doping is not sufficient to solve transition metal cation dissolution, because this process relates to surface interactions of the active cathode mass with acidic species in solutions (e.g., trace HF, PF_5, and trace water that react with $LiPF_6$ and release HF).

Another important approach to improve the surface stability of these cathode materials and avoid cation dissolution is their coating by thin layers that allows Li-ion migration through them and which provides a buffer zone that avoids detrimental interactions with solution species. Naturally, the best candidates for such coatings are basic oxides of active metals such as Al_2O_3, MgO, ZnO, ZrO_2, and Al compounds such as $AlPO_4$ and AlF_3. Many of such coatings demonstrated a good improvement in the stability and electrochemical performance of Li_xMO_y cathodes and considerable reduction of transition metal cation dissolution.

There are three main types of surface coatings, determined by the coating procedures:

1. The use of chemical means such as precipitation via pH changes or sol-gel reactions may lead to a rough coating based on deposition of small (sub-micrometric) particles on the surface of micrometric Li_xMO_y particles. With this approach there are many spots of bare area, and hence, the surface protection is limited.
2. The use of sonochemical methods [75, 76] leads to a core–shell structure, thus forming uniform coating comprising layers of nanoparticles. With this approach, a balance has to be well set because too thick surface layers impede Li-ion transport and thus lead to high electrodes' impedance.

3. Ultrathin film coating with tunable thickness can be achieved by atomic layer deposition (ALD) [77], chemical vapor deposition (CVD) [78], or pulse laser deposition (PLD) [79].

Coating should provide adequate chemical protection but should allow a smooth transport of Li ions. Thereby, either uniform thin films (as obtained by ALD) or particulate surface layers comprising nanoparticles (allowing transport of Li ions among them, in the grain boundaries) with high surface area facilitate effective scavenging of acidic species and are the appropriate approaches. It seems that for scavenging trace HF near Li_xMO_y particles' surface, their partial coverage by nanoparticles of basic active metal oxides (e.g., MgO) is sufficient [80]. We list below examples of references related to successful demonstration of cathode coating efforts, classified by the cathode materials and the coating material: $LiCoO_2$ [81], $LiMn_2O_4$ [76], $LiNi_{0.5}Mn_{1.5}O_4$ [75], and $LiFePO_4$ [82] coated with oxides such as MgO [75, 76], Al_2O_3 [81], $AlPO_4$ [83], SiO_2 [84], ZnO [85, 86], ZrO_2 [87], BiOF [88], and AlF_3 [89]. The method of using two types of coating for a single cathode material was also demonstrated [90].

In summary, coating the surface of Li_xMO_y cathode materials by appropriate thin functional layers that form buffer zone on their surface may provide the following advantages [91] (as exhibited in a recent review article):

1. Prevent the direct contact with the electrolyte solution.
2. Improve structural stability by suppressing detrimental phase transitions.
3. Decrease the disorder of cations in crystal sites near the surface.
4. Decrease side reactions and heat generation during cycling.
5. Avoid or suppress Mn^{2+}, Ni^{2+}, and Co^{2+} dissolution [75].
6. May increase the surface electrical conductivity. This is especially important of $LiMPO_4$ olivine compounds. Indeed, for $LiMPO_4$ cathode materials for which electronic conductivity is very low, the use of thin carbon coating is essential for their operation [92, 93].
7. Scavenge the trace HF from the electrolyte solutions near the surface of the active mass.

6.7 On the Surface Chemistry of $LiMPO_4$-Type Cathodes

Among many cathode materials, olivine compounds made great impact in recent years and became prominent positive electrodes in lithium-ion batteries. With many lithiated transition metal oxide cathode materials such as $LiCoO_2$ (which theoretical capacity can approach 300 mAh/g), the full intercalation capacity cannot be achieved due to limitations in structural changes and detrimental interaction with the electrolyte solutions at high charging potentials. On the other hand, $LiFePO_4$ can undergo complete lithiation–delithiation upon electrochemical cycling without any significant changes in its structure, which lead to the impressive stability of the $LiFePO_4$ cathodes during prolonged cycling. $LiFePO_4$ and other $LiMPO_4$ have very

poor electronic and ionic transport properties. However, due to relatively low basic and nucleophilic activity of the oxygen anions in these compounds (i.e., relatively low surface reactivity), it is possible to use them as nanoparticles. Composite $LiFePO_4$ cathodes comprising carbon-coated nanoparticles of the active mass demonstrate excellent performance (achieving practical capacity close to the theoretical value—170 mAh/g at excellent rate capability) [94]. Impressive performance was demonstrated with $LiMn_{0.8}Fe_{0.2}PO_4$ cathodes comprising carbon-coated nanoparticles [95]. However, these olivine cathodes have a serious problem of transition metal ion dissolution at elevated temperatures. As discussed earlier in this chapter, dissolved metal ions are reduced on the negative electrodes to metallic clusters, which affect very badly their passivation. These processes are the major reason of capacity loss in $LiFePO_4$/graphite cells at elevated temperatures [96, 97]. It was clearly demonstrated that dissolution of Fe ions from $LiFePO_4$ is pronounced only when the solutions contain acidic species (e.g., HF), especially at elevated temperatures. The impedance of $LiFePO_4$ electrodes in $LiPF_6$/alkyl carbonate solutions containing trace HF (a few tens ppm) can be higher by an order of magnitude than that of the same electrodes in $LiClO_4$/alkyl carbonate solutions, which do not contain any acidic moieties [98].

Surface studies (XPS) of $LiFePO_4$ electrodes that were stored in $LiPF_6$ solutions at elevated temperatures clearly proved the precipitation of LiF and $Li_xPO_yF_z$ surface species therein. Studies of the surface chemistry of $LiMnPO_4$ and $LiMn_{0.8}Fe_{0.2}PO_4$ electrodes also indicated formation of LiF and $Li_xPO_yF_z$ surface species during storage at elevated temperatures in standard ($LiPF_6$) electrolyte solutions [13, 99]. All our surface studies clearly demonstrated the much lower surface reactivity of $LiMPO_4$ compounds compared to Li_xMO_y cathode compounds [14, 17].

It was possible to suppress the dissolution of Fe^{2+} ions from $LiFePO_4$ electrodes in standard ($LiPF_6$) electrolyte solutions at elevated temperatures by the use of surface-active additives such as LiBOB [97] and acid scavenger additives [98] in solutions. $LiFePO_4$ is a hygroscopic material. Its exposure to humidity (in air or in solutions) leads to formation of LiOH and Li_2CO_3. It is important to note that exposure of $LiFePO_4$ to humid air or solutions is detrimental to its performance as a cathode material [100, 101].

The surface chemistry of $LiMnPO_4$ electrodes in EC:DMC(1:2)/1.5 M $LiPF_6$ solutions was thoroughly explored by various surface-sensitive spectroscopic techniques [13]. FTIR studies of pristine and aged C-$LiMnPO_4$ particles during 3 and 7 weeks at 60 °C show pronounced difference in the spectral range 450–650 cm^{-1} corresponding to the formation of oxygen- and fluorine-containing surface species which is in correlation with XPS spectra. The F1s spectra of aged particles show peaks around 685 eV (LiF) and 689 eV which corresponds to fluorine species at relatively higher oxidation state containing P–F or C–F bonds. The precipitation of these surface species increases the impedance of these electrodes during aging. It should be noted that $LiMnPO_4$ is always used as a carbon-coated particle. This coating further reduces the surface reactivity of this active mass [102]. HRTEM imaging of C–$LiMnPO_4$ particles aged during 3 weeks at 60 °C indicated that the carbon layer on the $LiMnPO_4$ particles remains undisturbed even after 3 weeks of aging in electrolyte solution.

Figure 6.14 shows FTIR and XPS spectra from pristine and aged (60 °C) $LiMn_{0.8}Fe_{0.2}PO_4$ electrodes in EC–DMC/$LiPF_6$ solutions [99]. In contrast to FTIR spectra of aged/cycled Li_xMO_y cathodes that reflect rich surface chemistry, FTIR spectra of aged $LiMPO_4$ (M = Fe, Mn) are very similar to those of pristine powder (see comparison in the figure). XPS measurements also show changes, mostly in the fluorine spectra. Figure 6.15 shows data from Raman and Mössbauer spectroscopic measurements and HRTEM imaging in which pristine and aged electrodes (60 °C, EC–DMC/$LiPF_6$) are compared [99]. The Raman spectra show the expected peaks of the carbon coating and the phosphate group underneath, while the Mössbauer spectra show iron peaks. The results presented in Fig. 6.15 from these three sources of spectral data reflect the high stability of these compounds. This stability is reflected well in the excellent performance demonstrated with $LiMn_{0.8}Fe_{0.2}PO_4$ electrodes.

In recent years great effort is being taken to understand the capacity fading and surface chemistry involved in $LiCoPO_4$ electrode material. Apart from possible irreversible structural transformation of the $LiCoPO_4$ material during cycling [103], and possible parasitic oxidation reactions' solution species, there is another important reason for possible instability of this cathode material in standard electrolyte solutions: detrimental reactions with trace HF which are unavoidably present in $LiPF_6$ solutions. The negative effect of HF in solutions on the stability of $LiCoPO_4$ electrodes was recently thoroughly investigated in EC–DMC (1:1) 1 M $LiPF_6$ [104, 105]. It was found that the presence of HF scavengers such as separators based on silicon–oxygen compounds such as quartz enables good cyclability of $LiCoPO_4$ electrodes in standard electrolyte solutions.

It was found that the main detrimental effect of the presence of HF in solutions on the performance of $LiCoPO_4$ electrodes is a nucleophilic attack of F^- anion on the P–O bonds of the phosphate anions, leading to the formation of a series of fluorophosphorous oxy compounds, namely, Li_2PO_3F, $LiPO_2F_2$, and POF_3 moieties in the electrolyte solution according to the following reactions:

$$\left(PO_4\right)^{3-} + HF + H^+ \leftrightarrow PO_3F^{2-} + H_2O$$
$$PO_3F^{2-} + HF + H^+ \leftrightarrow PO_2F_2^- + H_2O$$
$$PO_2F_2^- + HF + H^+ \leftrightarrow POF_3 + H_2O$$

Note the regenerative nature of these reactions, which makes them very detrimental for the stability of this cathode material. The presence of $PO_xF_y^{z-}$ species in solutions from cycled Li/$LiCoPO_4$ cells was confirmed by NMR spectroscopic studies [105]. ^{19}F and ^{31}P NMR spectra of standard electrolyte solution and of the electrolyte solution from cycled $LiCoPO_4$/Li cells are shown in Fig. 6.16. The electrolyte solution extracted from cycled cells showed a triplet and doublet at −18.7 and −86.2 ppm corresponding to the presence of $PO_2F_2^-$ species. The formation of these species is also supported by surface studies of cycled $LiCoPO_4$ electrodes by XPS [105]. The P2p spectra of pristine electrodes and electrodes cycled in the presence of HF scavenger (e.g., quartz-based separator) are dominated by the signal of the phosphate group (134.6 eV). In turn, the P2p spectra of electrodes cycled in

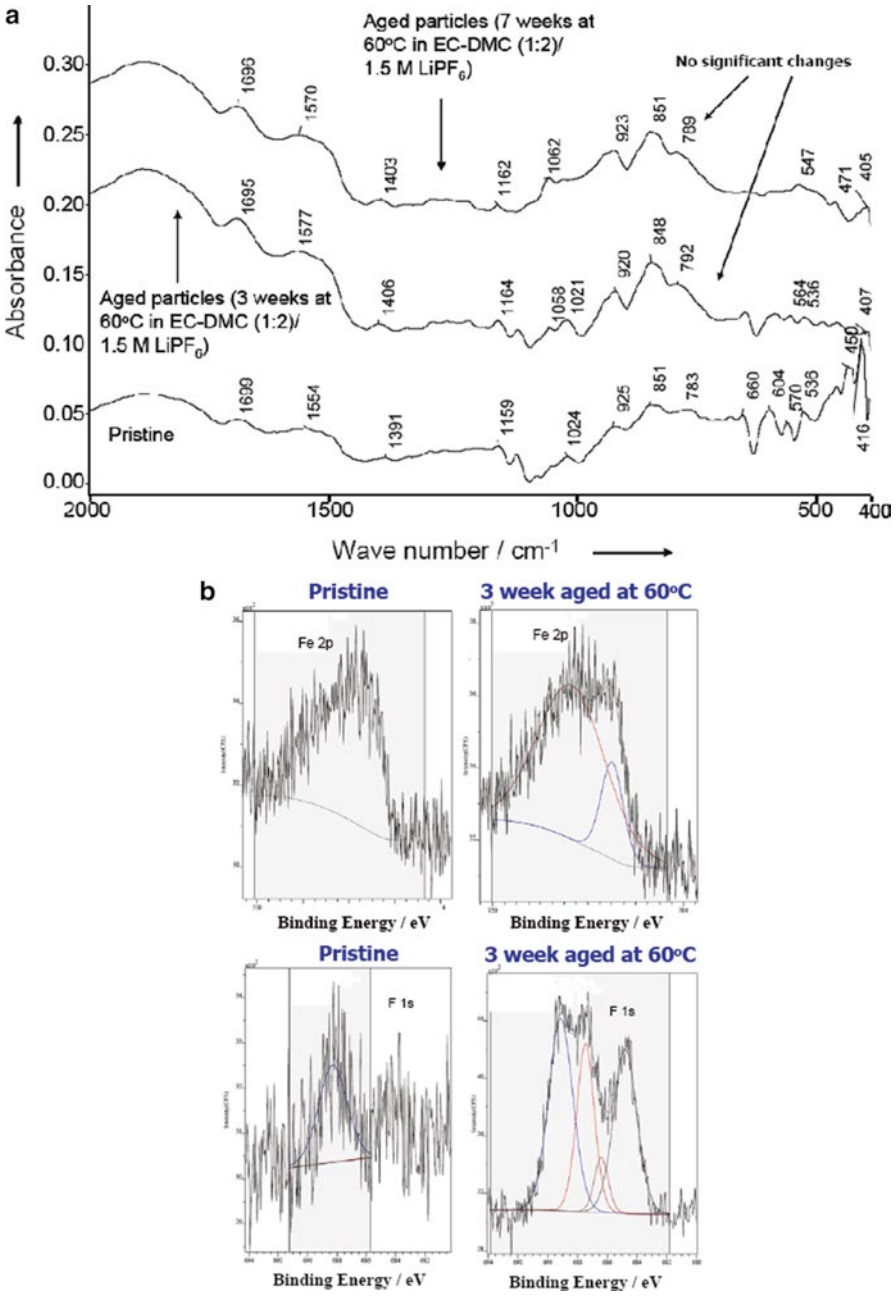

Fig. 6.14 (**a**) FTIR spectra of pristine and aged C- $LiMn_{0.8}Fe_{0.2}PO_4$ particles after 3 and 7 weeks (indicated) in EC–DMC 1:2/1.5 M $LiPF_6$ solution at 60 °C. (**b**) XPS spectra of Fe 2p and F 1s measured from pristine C-$LiMn_{0.8}Fe_{0.2}PO_4$ particles and particles aged during 3 weeks at 60 °C in EC–DMC 1:2/1.5 M $LiPF_6$ solutions. Reprinted from [98], copyright (2009) with permission from John Wiley and Sons

standard electrolytes without any scavenger (demonstrated indeed bad performance) showed peaks of $PO_xF_y^{x-}$ moieties (135.4 eV). It should be noted that this sensitivity to nucleophilic attacks by F^- moieties in standard electrolyte solutions is unique to $LiCoPO_4$. Other olivine cathode materials behave quite differently and demonstrate impressive stability in standard electrolyte solutions.

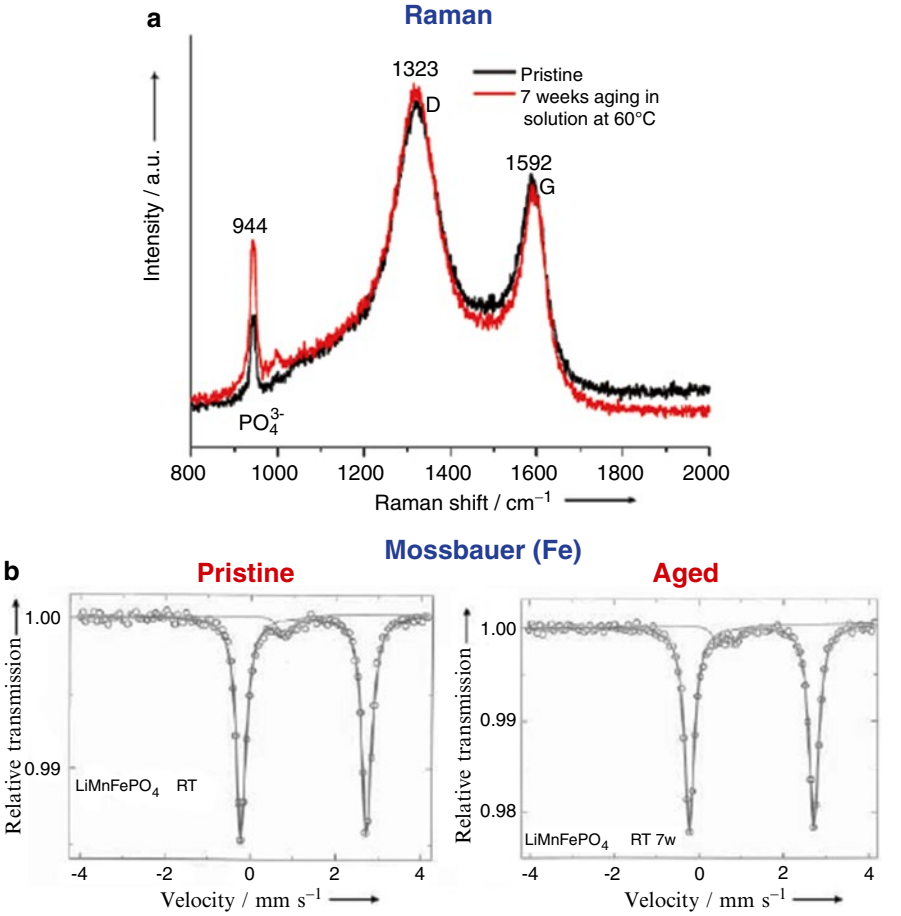

Fig. 6.15 (**a**) Raman spectra of pristine and aged C-$LiMn_{0.8}Fe_{0.2}PO_4$ particles (indicated). Aging was carried out during 7 weeks in EC–DMC 1:2/1.5 M $LiPF_6$ solution at 60 °C. (**b**) Mössbauer spectra measured at room temperature from C-$LiMn_{0.8}Fe_{0.2}PO_4$ pristine particles, particles aged during 7 weeks at 60 °C in EC–DMC 1:2/$LiPF_6$ 1.5 M solutions. (**c**) *Top*: HRTEM image of C-$LiMn_{0.8}Fe_{0.2}PO_4$ pristine particles showing their morphology, particle size, and thickness of the carbon layer. *Bottom*: HRTEM images of C-$LiMn_{0.8}Fe_{0.2}PO_4$ particles, after aging at 60 °C during 3 weeks in EC–DMC 1:2/$LiPF_6$ 1.5 M solutions. Reprinted from [98], copyright (2009) with permission from John Wiley and Sons

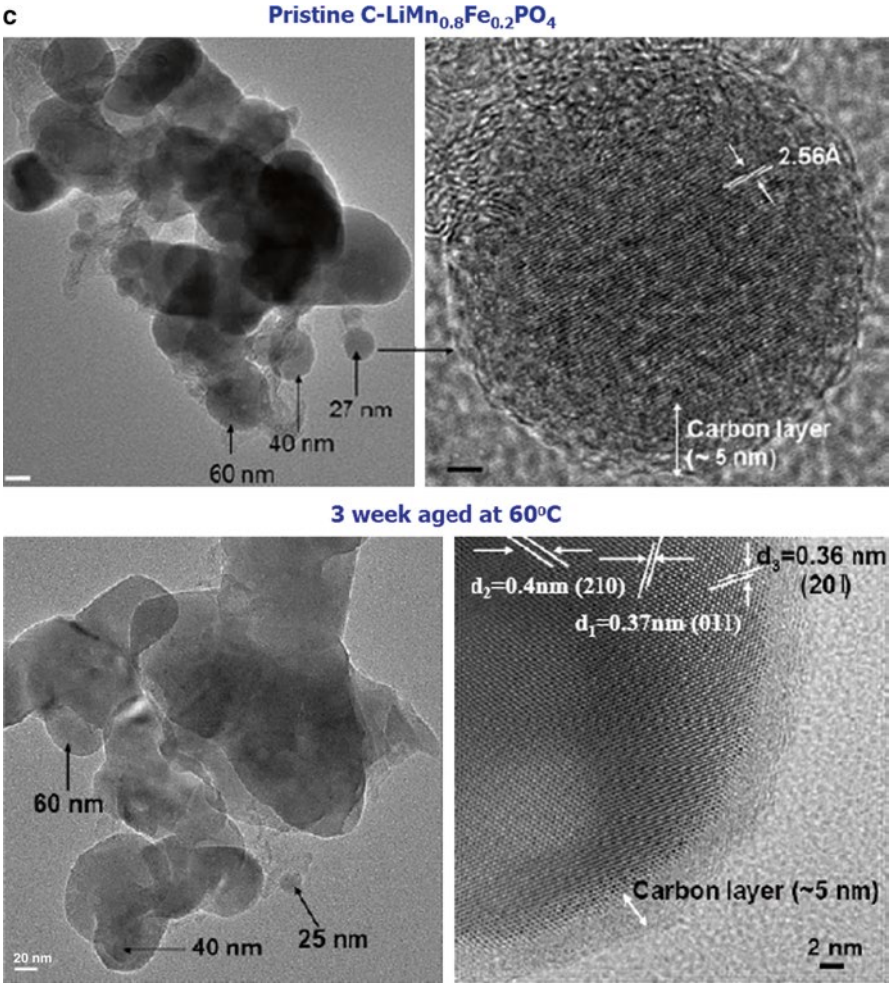

Fig. 6.15 (continued)

6.8 On the Surface Chemical Aspects of O_2 Cathodes

The most relevant substrates for oxygen cathodes in Li-air batteries are carbonaceous materials (nanotubes, graphene, activated carbon, and more) [106–108]. The electrolyte solutions relevant are those that cannot react with the highly reactive oxygen reduction products, LiO_2 (Li superoxide) and Li_2O_2 (Li peroxide). Most of the polar aprotic solvents, including alkyl carbonates, esters, sulfones, and nitriles, are irrelevant due to their electrophilicity. It seems that only ethereal solvents from the

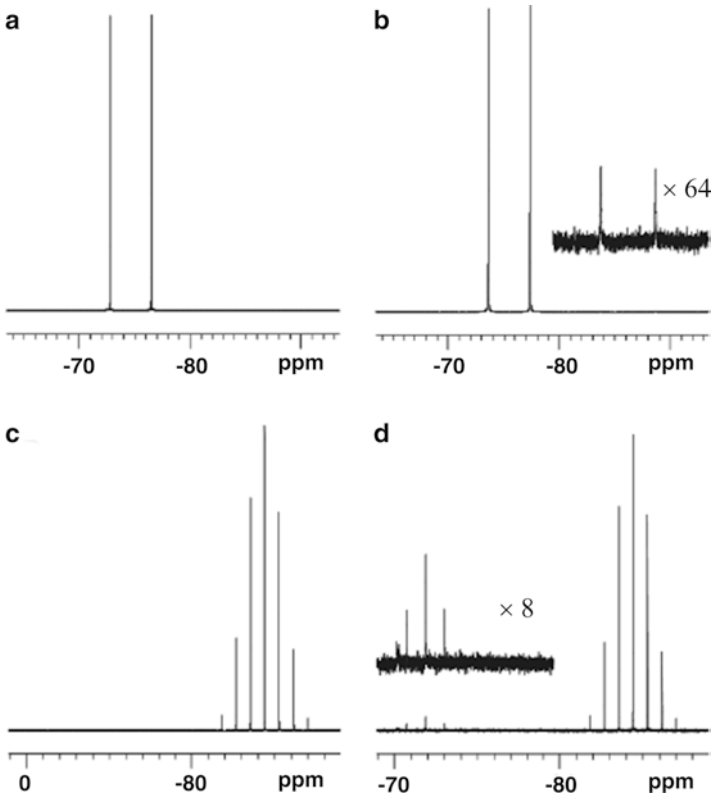

Fig. 6.16 ^{19}F (**a**, **b**) and ^{31}P (**c**, **d**) NMR spectra of a standard electrolyte solution (**a**, **c**) and electrolyte solution extracted from cells in which $LiCoPO_4$ electrodes were cycled (**b**, **d**). Reprinted from [104], copyright (2012) with permission from Elsevier

"glymes" family (these are nonvolatile enough so that they are suitable for gas electrodes) and some ionic liquid-based solutions may be relevant. The reduction of oxygen in the presence of Li ions forms as a main product and surface species Li_2O_2, which precipitates on the electrode's substrate until it is fully blocked (which stops the reduction). A complete re-oxidation of the Li_2O_2 that precipitates on carbonaceous electrodes is possible in several ethereal solutions [109]. However, there are signs confirming the presence of side reactions, even in the apparently inactive glyme-based solutions. The behavior of oxygen reduction electrodes in Li-salt solutions is currently being explored. So far, there are no clear conclusions and understanding regarding possible side reactions that occur in these systems. The carbonaceous substrates used for these electrodes may develop unique surface chemistry due to several possible reactions, including a partial oxidation of the carbon surfaces, reactions of LiO_2 and Li_2O_2 with solution species (solvent, salt anion) that form precipitants that cannot be removed within the electrochemical window of these systems.

It should be noted that without a full understanding of the surface chemistry of oxygen electrodes in aprotic Li-salt solutions, it will not be possible to advance R&D of Li-air battery technology towards any practical direction.

6.9 Summary

Li batteries of all kinds are thermodynamically unstable devices. Their apparent stability and successful operation are due to complicated passivation processes including surface film formation that brings the electrode–solution interfaces in Li batteries to an impressive metastability. From the beginning of the R&D efforts related to Li batteries, the formation of surface films on the negative electrodes that behave like an SEI was obvious. A lot of efforts were devoted over the last four decades to study these surface phenomena and to modify them for a better performance of Li batteries. Later on (during the late 1990s) it was discovered that the behavior of most relevant cathodes for Li batteries is also controlled by complicated surface phenomena. Specially surface reactive are lithiated transition metal oxide cathodes. The most preferred solvents for Li-ion batteries are alkyl carbonates, due to their relatively high anodic stability and unique reduction mechanisms at low potentials, that form (in the presence of Li ions) highly protecting, SEI-type surface films. These solvents are electrophilic. They can undergo reactions with the negatively charged surface oxygen atoms of the cathode materials and also polymerization (to form polycarbonate species). The basic cathode compounds interact strongly with acidic species in solutions (HF, PF_5, PF_3O). Highly challenging is the possibility of transition metal ion dissolutions, which is obviously accompanied by structural changes near the surface of the active mass. Due to their pronounced surface reactivity, Li_xMO_y cathode materials should not be used as nanoparticles. Olivine $LiMPO_4$ compounds are much less surface reactive than Li_xMO_y cathode materials. Thereby, they can be used as nanoparticles, thus gaining very good ionic transport properties. In recent years we see that more and more attention is given to the study and understanding of surface phenomena related to cathodes in Li-ion batteries. Surface modifications for the positive electrodes in Li batteries are developed via the introduction of surface-active additives and coatings.

References

1. K. H. Seng, J. Liu, Z. P. Guo, Z. X. Chen, D. Jia, H. K. Liu, Free-standing V2O5 electrode for flexible lithium ion batteries, Electrochem. Commun. 2011, 13, 383-386.
2. S. Surampudi, D. H. Shen, C. K. Huang, F. Deligiannis, A. Attia, G. Halpert, Advances in LiTiS2 cell technology, J. Power Sources 1991, 36, 395-402.
3. M. S. Whittingham, Lithium batteries and cathode materials, Chem. Rev. (Washington, DC, U. S.) 2004, 104, 4271-4301.

4. A. Yamada, M. Hosoya, S.-C. Chung, Y. Kudo, K. Hinokuma, K.-Y. Liu, Y. Nishi, Olivine-type cathodes: Achievements and problems, J. Power Sources 2003, 119–121, 232-238.
5. F. Badway, F. Cosandey, N. Pereira, G. G. Amatucci, Carbon metal fluoride nanocomposites - High-capacity reversible metal fluoride conversion materials as rechargeable positive electrodes for Li batteries, J. Electrochem. Soc. 2003, 150, A1318-A1327.
6. E. Peled, In: J.P. Gabano (ed) Lithium Batteries, Academic Press, London 1983, 43.
7. Y. V. Mikhaylik, J. R. Akridge, Polysulfide Shuttle Study in the Li/S Battery System, J. Electrochem. Soc. 2004, 151, A1969-A1976.
8. G. Girishkumar, B. McCloskey, A. C. Luntz, S. Swanson, W. Wilcke, Lithium−Air Battery: Promise and Challenges, The Journal of Physical Chemistry Letters 2010, 1, 2193-2203.
9. G. H. Boyle, F. Goebel, Development and Characterization of a High-Capacity Lithium Thionyl Chloride Battery, J. Power Sources 1995, 54, 186-191.
10. R. Elazari, G. Salitra, Y. Talyosef, J. Grinblat, C. Scordilis-Kelley, A. Xiao, J. Affinito, D. Aurbach, Morphological and Structural Studies of Composite Sulfur Electrodes upon Cycling by HRTEM, AFM and Raman Spectroscopy, J. Electrochem. Soc. 2010, 157, A1131-A1138.
11. C. W. Sun, S. Rajasekhara, J. B. Goodenough, F. Zhou, Monodisperse Porous LiFePO4 Microspheres for a High Power Li-Ion Battery Cathode, J. Am. Chem. Soc. 2011, 133, 2132-2135.
12. J. T. Son, E. J. Cairns, Preparation and Characterization of Li1.05 [Ni0.35Co0.25Mn0.4] O2 as a Cathode Material for Rechargeable Lithium Cells, Electrochem. Solid-State Lett. 2006, 9, A27-A30.
13. S. K. Martha, B. Markovsky, J. Grinblat, Y. Gofer, O. Haik, E. Zinigrad, D. Aurbach, T. Drezen, D. Wang, G. Deghenghi, I. Exnar, LiMnPO4 as an Advanced Cathode Material for Rechargeable Lithium Batteries, J. Electrochem. Soc. 2009, 156, A541-A552.
14. R. Marom, S. F. Amalraj, N. Leifer, D. Jacob, D. Aurbach, A review of advanced and practical lithium battery materials, J. Mater. Chem. 2011, 21, 9938-9954.
15. D. Aurbach, M. Daroux, P. Faguy, E. Yeager, The electrochemistry of noble metal electrodes in aprotic organic solvents containing lithium salts, Journal of Electroanalytical Chemistry and Interfacial Electrochemistry 1991, 297, 225-244.
16. D. Aurbach, H. Gottlieb, The electrochemical behavior of selected polar aprotic systems, Electrochim. Acta 1989, 34, 141-156.
17. V. Etacheri, R. Marom, R. Elazari, G. Salitra, D. Aurbach, Challenges in the development of advanced Li-ion batteries: a review, Energy & Environmental Science 2011, 4, 3243-3262.
18. J. M. Tarascon, D. Guyomard, New Electrolyte Compositions Stable Over The O-V To 5-V Voltage Range and Compatible With The Li1+XMn2O4 Carbon Li-Ion Cells, Solid State Ionics 1994, 69, 293-305.
19. M. Moshkovich, M. Cojocaru, H. E. Gottlieb, D. Aurbach, The study of the anodic stability of alkyl carbonate solutions by in situ FTIR spectroscopy, EQCM, NMR and MS J. Electroanal. Chem. 2001, 497, 84-96.
20. B. Markovsky, F. Amalraj, H. E. Gottlieb, Y. Gofer, S. K. Martha, D. Aurbach, On the Electrochemical Behavior of Aluminum Electrodes in Nonaqueous Electrolyte Solutions of Lithium Salts, J. Electrochem. Soc. 2010, 157, A423-A429.
21. R. Marom, O. Haik, D. Aurbach, I. C. Halalay, Revisiting LiClO4 as an Electrolyte for Rechargeable Lithium-Ion Batteries, J. Electrochem. Soc. 2010, 157, A972-A983.
22. M. L. Marcinek, J. W. Wilcox, M. M. Doeff, R. M. Kostecki, Microwave Plasma Chemical Vapor Deposition of Carbon Coatings on LiNi1/3Co1/3Mn1/3O2 for Li-Ion Battery Composite Cathodes, J. Electrochem. Soc. 2009, 156, A48-A51.
23. P. R. Griffiths, J. A. D. Haseth, Fourier Transform Infrared Spectrometry, Wiley-Interscience, New York, 2nd ed, 2007.
24. D. Aurbach, B. Markovsky, G. Salitra, E. Markevich, Y. Talyossef, M. Koltypin, L. Nazar, B. Ellis, D. Kovacheva, J Power Sources 2007, 165, 491.
25. C. M. Julien, M. Massot, Lattice vibrations of materials for lithium rechargeable batteries I. Lithium manganese oxide spinel, Materials Science and Engineering: B 2003, 97, 217-230.

26. R. Baddour-Hadjean, J.-P. Pereira-Ramos, Raman Microspectrometry Applied to the Study of Electrode Materials for Lithium Batteries, Chem. Rev. (Washington, DC, U. S.) 2009, 110, 1278-1319.
27. S. Leroy, H. Martinez, R. Dedryvere, D. Lemordant, D. Gonbeau, Influence of the lithium salt nature over the surface film formation on a graphite electrode in Li-ion batteries: An XPS study, Appl. Surf. Sci. 2007, 253, 4895-4905.
28. L. Castro, R. Dedryvère, J.-B. Ledeuil, J. Bréger, C. Tessier, D. Gonbeau, Aging Mechanisms of LiFePO4 // Graphite Cells Studied by XPS: Redox Reaction and Electrode/Electrolyte Interfaces, J. Electrochem. Soc. 2012, 159, A357-A363.
29. X. Hou, B. T. Jones, Inductively Coupled Plasma/Optical Emission Spectrometry, In Encyclopedia of Analytical Chemistry, R.A. Meyers Ed. 2000, John Wiley & Sons Ltd, Chichester, 9468–9485.
30. F. Amalraj, D. Kovacheva, M. Talianker, L. Zeiri, J. Grinblat, N. Leifer, G. Goobes, B. Markovsky, D. Aurbach, Synthesis of Integrated Cathode Materials xLi2MnO3· (1−x) LiMn1/3Ni1/3Co1/3O2 (x=0.3, 0.5, 0.7) and Studies of Their Electrochemical Behavior, J. Electrochem. Soc. 2010, 157, A1121-A1130.
31. M. Jiang, B. Key, Y. S. Meng, C. P. Grey, Electrochemical and Structural Study of the Layered, "Li-Excess" Lithium-Ion Battery Electrode Material Li[Li1/9Ni1/3Mn5/9]O2, Chem. Mater. 2009, 21, 2733-2745.
32. M. E. Orazem, B. Tribollet, Electrochemical Impedance Spectroscopy, John Wiley & Sons, New York, 2008.
33. D. Aurbach, M. D. Levi, E. Levi, H. Teller, B. Markovsky, G. Salitra, U. Heider, L. Heider, Common Electroanalytical Behavior of Li Intercalation Processes into Graphite and Transition Metal Oxides, J. Electrochem. Soc. 1998, 145, 3024-3034.
34. M. Gaberscek, R. Dominko, J. Jamnik, The meaning of impedance measurements of LiFePO4 cathodes: A linearity study, J. Power Sources 2007, 174, 944-948.
35. H. Sclar, D. Kovacheva, E. Zhecheva, R. Stoyanova, R. Lavi, G. Kimmel, J. Grinblat, O. Girshevitz, F. Amalraj, O. Haik, E. Zinigrad, B. Markovsky, D. Aurbach, On the Performance of LiNi1/3Mn1/3Co1/3O2 Nanoparticles as a Cathode Material for Lithium-Ion Batteries, J. Electrochem. Soc. 2009, 156, A938-A948.
36. O. Haik, S. K. Martha, H. Sclar, Z. Samuk-Fromovich, E. Zinigrad, B. Markovsky, D. Kovacheva, N. Saliyski, D. Aurbach, Characterizations of self-combustion reactions (SCR) for the production of nanomaterials used as advanced cathodes in Li-ion batteries, Thermochim. Acta 2009, 493, 96-104.
37. S. K. Martha, H. Sclar, Z. Szmuk Framowitz, D. Kovacheva, N. Saliyski, Y. Gofer, P. Sharon, E. Golik, B. Markovsky, D. Aurbach, A comparative study of electrodes comprising nanometric and submicron particles of LiNi0.50Mn0.50O2, LiNi0.33Mn0.33Co0.33O2, and LiNi0.40Mn0.40Co0.20O2 layered compounds, J. Power Sources 2009, 189, 248-255.
38. O. Haik, N. Leifer, H. Sclar, Z. Samuk-Fromovich, E. Zinigrad, B. Markovsky, L. Larush, Y. Goffer, G. Goobes, D. Aurbach, On the Surface Chemistry of $LiMO_2$ Cathode Materials (M=[MnNi] and [MnNiCo]): Electrochemical, Spectroscopic, and Calorimetric Studies, J. Electrochem. Soc. 2010, 157, A1099-A1107.
39. B. Markovsky, D. Kovacheva, Y. Talyosef, M. Gorova, J. Grinblat, D. Aurbach, Studies of Nanosized LiNi0.5Mn0.5O2-Layered Compounds Produced by Self-Combustion Reaction as Cathodes for Lithium-Ion Batteries, Electrochem. Solid-State Lett. 2006, 9, A449-A453.
40. E. Markevich, G. Salitra, D. Aurbach, Influence of the PVdF binder on the stability of LiCoO2 electrodes, Electrochem. Commun. 2005, 7, 1298-1304.
41. W. Choi, A. Manthiram, Comparison of metal ion dissolutions from lithium ion battery cathodes, J. Electrochem. Soc. 2006, 153, A1760-A1764.
42. B. Markovsky, A. Rodkin, G. Salitra, Y. Talyosef, D. Aurbach, H.-J. Kim, The Impact of Co2+ Ions in Solutions on the Performance of LiCoO2, Li, and Lithiated Graphite Electrodes, J. Electrochem. Soc. 2004, 151, A1068-A1076.
43. J. Lei, L. Li, R. Kostecki, R. Muller, F. McLarnon, Characterization of SEI Layers on LiMn2O4 Cathodes with In Situ Spectroscopic Ellipsometry, J. Electrochem. Soc. 2005, 152, A774-A777.

44. B. M. Meyer, N. Leifer, S. Sakamoto, S. G. Greenbaum, C. P. Grey, High Field Multinuclear NMR Investigation of the SEI Layer in Lithium Rechargeable Batteries, Electrochem. Solid-State Lett. 2005, 8, A145-A148.
45. S. Menkin, D. Golodnitsky, E. Peled, Artificial solid-electrolyte interphase (SEI) for improved cyclability and safety of lithium–ion cells for EV applications, Electrochem. Commun. 2009, 11, 1789-1791.
46. N. Liu, H. Li, Z. Wang, X. Huang, L. Chen, Origin of Solid Electrolyte Interphase on Nanosized LiCoO2, Electrochem. Solid-State Lett. 2006, 9, A328-A331.
47. D. Aurbach, B. Markovsky, M. D. Levi, E. Levi, A. Schechter, M. Moshkovich, Y. Cohen, New insights into the interactions between electrode materials and electrolyte solutions for advanced nonaqueous batteries, J. Power Sources 1999, 81–82, 95-111.
48. D. Aurbach, B. Markovsky, G. Salitra, E. Markevich, Y. Talyossef, M. Koltypin, L. Nazar, B. Ellis, D. Kovacheva, Review on electrode–electrolyte solution interactions, related to cathode materials for Li-ion batteries, J. Power Sources 2007, 165, 491-499.
49. S. S. Zhang, K. Xu, T. R. Jow, Understanding Formation of Solid Electrolyte Interface Film on LiMn2O4 Electrode, J. Electrochem. Soc. 2002, 149, A1521-A1526.
50. D. Aurbach, B. Markovsky, Y. Talyossef, G. Salitra, H.-J. Kim, S. Choi, Studies of cycling behavior, ageing, and interfacial reactions of LiNi0.5Mn1.5O4 and carbon electrodes for lithium-ion 5-V cells, J. Power Sources 2006, 162, 780-789.
51. L. Yang, B. Ravdel, B. L. Lucht, Electrolyte Reactions with the Surface of High Voltage LiNi0.5Mn1.5O4 Cathodes for Lithium-Ion Batteries, Electrochem. Solid-State Lett. 2010, 13, A95-A97.
52. H. Ota, Y. Sakata, A. Inoue, S. Yamaguchi, Analysis of Vinylene Carbonate Derived SEI Layers on Graphite Anode, J. Electrochem. Soc. 2004, 151, A1659-A1669.
53. L. Yang, T. Markmaitree, B. L. Lucht, Inorganic additives for passivation of high voltage cathode materials, J. Power Sources 2011, 196, 2251-2254.
54. H. Duncan, D. Duguay, Y. Abu-Lebdeh, I. J. Davidson, Study of the LiMn1.5Ni0.5O4/ Electrolyte Interface at Room Temperature and 60 °C, J. Electrochem. Soc. 2011, 158, A537-A545.
55. F. T. Quinlan, K. Sano, T. Willey, R. Vidu, K. Tasaki, P. Stroeve, Surface Characterization of the Spinel LixMn2O4 Cathode before and after Storage at Elevated Temperatures, Chem. Mater. 2001, 13, 4207-4212.
56. J. Mun, T. Yim, K. Park, J. H. Ryu, Y. G. Kim, S. M. Oh, Surface Film Formation on LiNi0.5Mn1.5O4 Electrode in an Ionic Liquid Solvent at Elevated Temperature, J. Electrochem. Soc. 2011, 158, A453-A457.
57. F. Simmen, A. Hintennach, M. Horisberger, T. Lippert, P. Novák, C. W. Schneider, A. Wokaun, Aspects of the Surface Layer Formation on Li1 + xMn2O4 – δ during Electrochemical Cycling, J. Electrochem. Soc. 2010, 157, A1026-A1029.
58. A. Würsig, H. Buqa, M. Holzapfel, F. Krumeich, P. Novák, Film Formation at Positive Electrodes in Lithium-Ion Batteries, Electrochem. Solid-State Lett. 2005, 8, A34-A37.
59. M. Matsui, K. Dokko, K. Kanamura, Surface Layer Formation and Stripping Process on LiMn2O4 and LiNi1⁄2Mn3⁄2O4 Thin Film Electrodes, J. Electrochem. Soc. 2010, 157, A121-A129.
60. M. Balasubramanian, H. S. Lee, X. Sun, X. Q. Yang, A. R. Moodenbaugh, J. McBreen, D. A. Fischer, Z. Fu, Formation of SEI on Cycled Lithium-Ion Battery Cathodes: Soft X-Ray Absorption Study, Electrochem. Solid-State Lett. 2002, 5, A22-A25.
61. S. E. Sloop, J. K. Pugh, S. Wang, J. B. Kerr, K. Kinoshita, Chemical Reactivity of PF 5 and LiPF6 in Ethylene Carbonate/Dimethyl Carbonate Solutions, Electrochem. Solid-State Lett. 2001, 4, A42-A44.
62. N. Dupre, J. F. Martin, D. Guyomard, A. Yamada, R. Kanno, Detection of surface layers using (7)Li MAS NMR, J. Mater. Chem. 2008, 18, 4266-4273.
63. N. Dupré, J.-F. Martin, J. Oliveri, P. Soudan, A. Yamada, R. Kanno, D. Guyomard, Relationship between surface chemistry and electrochemical behavior of LiNi1/2Mn1/2O2 positive electrode in a lithium-ion battery, J. Power Sources 2011, 196, 4791-4800.

64. D. Ostrovskii, F. Ronci, B. Scrosati, P. Jacobsson, A FTIR and Raman study of spontaneous reactions occurring at the LiNiyCo(1−y)O2 electrode/non-aqueous electrolyte interface, J. Power Sources 2001, 94, 183-188.
65. B. Xu, C. R. Fell, M. F. Chi, Y. S. Meng, Identifying surface structural changes in layered Li-excess nickel manganese oxides in high voltage lithium ion batteries: A joint experimental and theoretical study, Energy & Environmental Science 2011, 4, 2223-2233.
66. N. Yabuuchi, K. Yoshii, S. T. Myung, I. Nakai, S. Komaba, Detailed Studies of a High-Capacity Electrode Material for Rechargeable Batteries, Li2MnO3-LiCo1/3Ni1/3Mn1/3O2, J. Am. Chem. Soc. 2011, 133, 4404-4419.
67. R. Sharabi, E. Markevich, V. Borgel, G. Salitra, D. Aurbach, G. Semrau, M. A. Schmidt, In Situ FTIR Spectroscopy Study of Li/LiNi0.8Co0.15Al0.05O2 Cells with Ionic Liquid-Based Electrolytes in Overcharge Condition, Electrochem. Solid-State Lett. 2010, 13, A32-A35.
68. K. Xu, Nonaqueous Liquid Electrolytes for Lithium-Based Rechargeable Batteries, Chem. Rev. (Washington, DC, U. S.) 2004, 104, 4303-4418.
69. M. Contestabile, M. Morselli, R. Paraventi, R. J. Neat, A comparative study on the effect of electrolyte/additives on the performance of ICP383562 Li-ion polymer (soft-pack) cells, J. Power Sources 2003, 119–121, 943-947.
70. D. Aurbach, B. Markovsky, A. Rodkin, E. Levi, Y. S. Cohen, H. J. Kim, M. Schmidt, On the capacity fading of LiCoO2 intercalation electrodes:: the effect of cycling, storage, temperature, and surface film forming additives, Electrochim. Acta 2002, 47, 4291-4306.
71. A. von Cresce, K. Xu, Electrolyte Additive in Support of 5 V Li Ion Chemistry, J. Electrochem. Soc. 2011, 158, A337-A342.
72. S. Komaba, N. Kumagai, Y. Kataoka, Influence of manganese(II), cobalt(II), and nickel(II) additives in electrolyte on performance of graphite anode for lithium-ion batteries, Electrochim. Acta 2002, 47, 1229-1239.
73. M. C. Rao, O. M. Hussain, Synthesis and electrochemical properties of Ti doped LiCoO2 thin film cathodes, J. Alloys Compd. 2010, 491, 503-506.
74. T.-F. Yi, Y.-R. Zhu, X.-D. Zhu, J. Shu, C.-B. Yue, A.-N. Zhou, A review of recent developments in the surface modification of LiMn2O4 as cathode material of power lithium-ion battery, Ionics 2009, 15, 779-784.
75. H. Sclar, O. Haik, T. Menachem, J. Grinblat, N. Leifer, A. Meitav, S. Luski, D. Aurbach, The Effect of ZnO and MgO Coatings by a Sono-Chemical Method, on the Stability of LiMn1.5Ni0.5O4 as a Cathode Material for 5 V Li-Ion Batteries, J. Electrochem. Soc. 2012, 159, A228-A237.
76. J. S. Gnanaraj, V. G. Pol, A. Gedanken, D. Aurbach, Improving the high-temperature performance of LiMn2O4 spinel electrodes by coating the active mass with MgO via a sonochemical method, Electrochem. Commun. 2003, 5, 940-945.
77. L. A. Riley, S. Van Atta, A. S. Cavanagh, Y. Yan, S. M. George, P. Liu, A. C. Dillon, S.-H. Lee, Electrochemical effects of ALD surface modification on combustion synthesized LiNi1/3Mn1/3Co1/3O2 as a layered-cathode material, J. Power Sources 2011, 196, 3317-3324.
78. W. Chang, J.-W. Choi, J.-C. Im, J. K. Lee, Effects of ZnO coating on electrochemical performance and thermal stability of LiCoO2 as cathode material for lithium-ion batteries, J. Power Sources 2010, 195, 320-326.
79. Y. Iriyama, H. Kurita, I. Yamada, T. Abe, Z. Ogumi, Effects of surface modification by MgO on interfacial reactions of lithium cobalt oxide thin film electrode, J. Power Sources 2004, 137, 111-116.
80. Z. Chen, Y. Qin, K. Amine, Y. K. Sun, Role of surface coating on cathode materials for lithium-ion batteries, J. Mater. Chem. 2010, 20, 7606-7612.
81. J. Cho, T.-G. Kim, C. Kim, J.-G. Lee, Y.-W. Kim, B. Park, Comparison of Al2O3- and AlPO4-coated LiCoO2 cathode materials for a Li-ion cell, J. Power Sources 2005, 146, 58-64.
82. G.-M. Song, Y. Wu, G. Liu, Q. Xu, Influence of AlF3 coating on the electrochemical properties of LiFePO4/graphite Li-ion batteries, J. Alloys Compd. 2009, 487, 214-217.

83. K. S. Tan, M. V. Reddy, G. V. S. Rao, B. V. R. Chowdari, Effect of AlPO4-coating on cathodic behaviour of Li(Ni0.8Co0.2)O2, J. Power Sources 2005, 141, 129-142.
84. Y. Fan, J. Wang, Z. Tang, W. He, J. Zhang, Effects of the nanostructured SiO2 coating on the performance of LiNi0.5Mn1.5O4 cathode materials for high-voltage Li-ion batteries, Electrochim. Acta 2007, 52, 3870-3875.
85. D. Liu, X. Liu, Z. He, Surface modification by ZnO coating for improving the elevated temperature performance of LiMn2O4, J. Alloys Compd. 2007, 436, 387-391.
86. R. Alcantara, M. Jaraba, P. Lavela, J. L. Tirado, X-ray diffraction and electrochemical impedance spectroscopy study of zinc coated LiNi0.5Mn1.5O4 electrodes, J. Electroanal. Chem. 2004, 566, 187-192.
87. Y. Wu, A. Manthiram, Effect of surface modifications on the layered solid solution cathodes (1 − z) Li[Li1/3Mn2/3]O2 − (z) Li[Mn0.5–yNi0.5–yCo2y]O2, Solid State Ionics 2009, 180, 50-56.
88. H.-B. Kang, S.-T. Myung, K. Amine, S.-M. Lee, Y.-K. Sun, Improved electrochemical properties of BiOF-coated 5 V spinel Li[Ni0.5Mn1.5]O4 for rechargeable lithium batteries, J. Power Sources 2010, 195, 2023-2028.
89. B. C. Park, H. B. Kim, S. T. Myung, K. Amine, I. Belharouak, S. M. Lee, Y. K. Sun, Improvement of structural and electrochemical properties of AlF3-coated Li[Ni1/3Co1/3Mn1/3]O2 cathode materials on high voltage region, J. Power Sources 2008, 178, 826-831.
90. Q. Y. Wang, J. Liu, A. V. Murugan, A. Manthiram, High capacity double-layer surface modified Li[Li0.2Mn0.54Ni0.13Co0.13]O2 cathode with improved rate capability, J. Mater. Chem. 2009, 19, 4965-4972.
91. C. Li, H. P. Zhang, L. J. Fu, H. Liu, Y. P. Wu, E. Ram, R. Holze, H. Q. Wu, Cathode materials modified by surface coating for lithium ion batteries, Electrochim. Acta 2006, 51, 3872-3883.
92. Y. Zhou, C. D. Gu, J. P. Zhou, L. J. Cheng, W. L. Liu, Y. Q. Qiao, X. L. Wang, J. P. Tu, Effect of carbon coating on low temperature electrochemical performance of LiFePO4/C by using polystyrene sphere as carbon source, Electrochim. Acta 2011, 56, 5054-5059.
93. F. Wang, J. Yang, P. F. Gao, Y. N. NuLi, J. L. Wang, Morphology regulation and carbon coating of LiMnPO4 cathode material for enhanced electrochemical performance, J. Power Sources 2011, 196, 10258-10262.
94. Q.-B. Liu, S.-J. Liao, H.-Y. Song, Z.-X. Liang, High-performance LiFePO4/C materials: Effect of carbon source on microstructure and performance, J. Power Sources 2012, 211, 52-58.
95. H. L. Wang, Y. Yang, Y. Y. Liang, L. F. Cui, H. S. Casalongue, Y. G. Li, G. S. Hong, Y. Cui, H. J. Dai, LiMn1-xFexPO4 Nanorods Grown on Graphene Sheets for Ultrahigh-Rate-Performance Lithium Ion Batteries, Angew. Chem., Int. Ed. 2011, 50, 7364-7368.
96. N. Iltchev, Y. Chen, S. Okada, J.-i. Yamaki, LiFePO4 storage at room and elevated temperatures, J. Power Sources 2003, 119–121, 749-754.
97. K. Amine, J. Liu, I. Belharouak, High-temperature storage and cycling of C-LiFePO4/graphite Li-ion cells, Electrochem. Commun. 2005, 7, 669-673.
98. M. Koltypin, D. Aurbach, L. Nazar, B. Ellis, On the Stability of LiFePO4 Olivine Cathodes under Various Conditions (Electrolyte Solutions, Temperatures), Electrochem. Solid-State Lett. 2007, 10, A40-A44.
99. S. K. Martha, J. Grinblat, O. Haik, E. Zinigrad, T. Drezen, J. H. Miners, I. Exnar, A. Kay, B. Markovsky, D. Aurbach, LiMn0.8Fe0.2PO4: An Advanced Cathode Material for Rechargeable Lithium Batteries, Angew. Chem., Int. Ed. 2009, 48, 8559-8563.
100. C. M. Julien, A. Mauger, K. Zaghib, Surface effects on electrochemical properties of nanosized LiFePO4, J. Mater. Chem. 2011, 21, 9955-9968.
101. K. Zaghib, M. Dontigny, P. Charest, J. F. Labrecque, A. Guerfi, M. Kopec, A. Mauger, F. Gendron, C. M. Julien, Aging of LiFePO4 upon exposure to H2O, J. Power Sources 2008, 185, 698-710.

102. K. Edström, T. Gustafsson, J. O. Thomas, The cathode–electrolyte interface in the Li-ion battery, Electrochim. Acta 2004, 50, 397-403.
103. N. N. Bramnik, K. Nikolowski, D. M. Trots, H. Ehrenberg, Thermal Stability of LiCoPO4 Cathodes, Electrochem. Solid-State Lett. 2008, 11, A89-A93.
104. R. Sharabi, E. Markevich, V. Borgel, G. Salitra, D. Aurbach, G. Semrau, M. A. Schmidt, N. Schall, C. Stinner, Significantly improved cycling performance of LiCoPO4 cathodes, Electrochem. Commun. 2011, 13, 800-802.
105. E. Markevich, R. Sharabi, H. Gottlieb, V. Borgel, K. Fridman, G. Salitra, D. Aurbach, G. Semrau, M. A. Schmidt, N. Schall, C. Bruenig, Reasons for capacity fading of LiCoPO4 cathodes in LiPF6 containing electrolyte solutions, Electrochem. Commun. 2012, 15, 22-25.
106. J. Wu, H. W. Park, A. P. Yu, D. Higgins, Z. W. Chen, Facile Synthesis and Evaluation of Nanofibrous Iron-Carbon Based Non-Precious Oxygen Reduction Reaction Catalysts for Li-O2 Battery Applications, J. Phys. Chem. C 2012, 116, 9427-9432.
107. J. Xiao, D. Mei, X. Li, W. Xu, D. Wang, G. L. Graff, W. D. Bennett, Z. Nie, L. V. Saraf, I. A. Aksay, J. Liu, J.-G. Zhang, Hierarchically Porous Graphene as a Lithium–Air Battery Electrode, Nano Lett. 2011, 11, 5071-5078.
108. R. R. Mitchell, B. M. Gallant, C. V. Thompson, Y. Shao-Horn, All-carbon-nanofiber electrodes for high-energy rechargeable Li–O2 batteries, Energy & Environmental Science 2011, 4, 2952-2958.
109. S. A. Freunberger, Y. H. Chen, N. E. Drewett, L. J. Hardwick, F. Barde, P. G. Bruce, The Lithium-Oxygen Battery with Ether-Based Electrolytes, Angew. Chem., Int. Ed. 2011, 50, 8609-8613.

Chapter 7
Tools and Methodologies for the Characterization of Electrode–Electrolyte Interfaces

Jordi Cabana

7.1 Introduction

The preceding chapters have demonstrated the vast amount of insight gained over the years into how the electrolyte interacts with the electrodes in Li and Li-ion batteries. Such progress would not have been possible without a parallel development in experimental techniques that are capable of interrogating these interfaces with ever increasing level of chemical and spatial resolutions. The purpose of this chapter is to provide an overview of these tools, grouped by the kind of information they offer, through representative examples in the literature. A lot has been learned about the origin and result of undesired reactions at electrode–electrolyte interfaces (EEIs, hereafter), especially the solid electrolyte interphase (SEI) on graphite electrodes. In contrast, visualization of the microscopic phenomena that control the charge transfer across interfaces required for reversible energy storage remains largely elusive; in practice, it is mainly probed by macroscopic measurements such as impedance spectroscopy. As a result, the main focus of this discussion will be placed on how a suite of characterization tools can provide information on degradation processes. Nonetheless, some attention will also be devoted to experiments that are indirectly relevant to charge transfer chemistry, for instance, by probing ion solvation in bulk electrolytes. Because they are the most relevant to application, the discussion will be centered on liquid–solid EEIs. Much the same concepts can be applied to the study of solid electrolyte systems, although the experimental constraints are slightly different. For instance, the absence of liquids makes it easier to design setups for tools that require ultrahigh vacuum. It will become clear to

J. Cabana (✉)
Environmental Energy Technologies Division, Lawrence Berkeley National Laboratory, Berkeley, CA 94720, USA

Department of Chemistry, University of Illinois at Chicago, Chicago, IL 60607, USA
e-mail: jcabana@uic.edu

T.R. Jow et al. (eds.), *Electrolytes for Lithium and Lithium-Ion Batteries*, Modern Aspects of Electrochemistry 58, DOI 10.1007/978-1-4939-0302-3_7,

the reader that while the available toolbox offers extreme versatility, no single technique can currently provide the final answer to these complex interfacial phenomena. We will conclude the chapter with a look into the future, taking a glimpse into new capabilities which will soon push the boundaries of the current state-of-the-art, yet still keeping an eye on the general "lessons learned" from decades of work on this complex problem.

7.2 Electrical Characterization

Macroscopically, the most direct means of detecting the formation and growth of layers due to reactions between the electrode surface and the electrolyte is by monitoring the electrical resistance of the electrochemical cell [1, 2]. Since these layers are, in the best case scenario, somewhat ionically conductive, but always electronically insulating [3, 4], an increase in electrical resistance is an indication of their presence. However, many components in an electrochemical cell convolute into its macroscopic electrical resistance. A first level of discrimination between these components is afforded by using AC electrochemical impedance spectroscopy (EIS).

EIS relies on the principle that the dielectric properties of different components in the circuit formed by the electrochemical cell are frequency-dependent when an AC signal is applied. Thus, it measures the impedance of a system by following the response of the cell to electrical biasing over a range of frequencies. Data analysis involves the use of theoretical equivalent circuits to model the resulting spectra [6, 7], so that assignments of phenomena can be made. EIS is the basic tool to study the energetics of charge transfer at the electrolyte–electrode interface and how it depends on the nature of the electrode surface [8]. The deterioration of charge transport due to processes at the EEIs is often ascribed to the appearance of a semicircle in the mid-to-high frequency range of a Nyquist plot of the data (Fig. 7.1) [1, 5, 7]. Thus, monitoring its changes with experimental conditions can provide insight into the behavior of these layers. However, the results need to be analyzed with care, keeping in mind that phenomena associated with interparticle contacts in the electrode can also lead to signals at similar frequencies [9, 10]. For one, it is important to simplify the system of measurement so as to reduce the number of possible elements in the equivalent circuit. Preferably, reference electrodes will be introduced in the system so that only the working electrode contributions can be discriminated [10–12]. Even in these cases, significant complexity remains and the discussion is oftentimes kept qualitative and complemented by other techniques with chemical insight [13].

7.3 Electrochemical Quartz Crystal Microbalance

An electrochemical quartz crystal microbalance (EQCM) follows changes in frequency of a quartz crystal resonator, typically of disk form, during an electrochemical reaction. The frequency change is imposed through the piezoelectric effect, as two

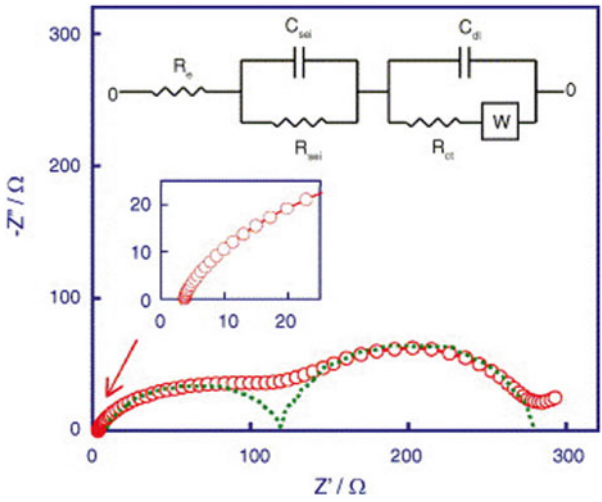

Fig. 7.1 Experimental data acquired by EIS and equivalent circuit for a Li/graphite cell. The shown EIS was recorded at 0.05 V. Reproduced with permission from [5]; copyright 2006, Elsevier

electrodes (normally, metallic) are deposited on both sides of the crystal and an alternating electric field is applied. For the purposes of electrolyte–electrode interfacial studies, one side of this quartz crystal can be covered with an additional thin film of the material to be studied (working electrode) [14]. The desired electrochemical reaction can be monitored by custom-designing a cell that contains the experimenter's choice of counter and, if desired, reference electrodes, as well as electrolyte system. The coated crystal is mounted in the cell in a manner that only the thin film working electrode is exposed to the electrolyte (Fig. 7.2) [15]. The electrochemical reaction is typically carried out using cyclic voltammetry (CV) [16], which allows the precise quantification of current at a given potential.

The principle of EQCM is based on the fact that frequency changes are directly related to changes in the mass deposited on the crystal by the Sauerbrey equation: $\Delta f = -C_f \Delta m$, where Δf is the change in frequency, Δm is the change in mass, and C_f is a sensitivity factor specific to the quartz crystal used [14]. In the context of electrode reactions, variations in Δm can both be due to electrolyte interactions and to the lithiation of the electrode itself. Thus, EQCM is a useful tool to determine the potentials at which electrolyte decomposition occurs, in real conditions, especially if lithiation conditions are avoided [15, 17, 18]. If both decomposition and lithiation occur, previous knowledge of the system assists in establishing a first level of correlation of the electrochemical signatures with Δm [19, 20]. A second layer of information is provided by calculating the mass per mol of electron transferred (mpe), by relating Δm with the charge measured in the CV during a process at a given potential. Processes corresponding to an mpe of 7 are typically associated with Li insertion/deposition processes [19–21]. In principle, values different from 7 could be pinpointed to a specific product of an electrolyte reaction, providing crude chemical insight. However, such conclusions can only be reached if only one reaction is known to be occurring, which is unlikely to be the case; concurrent reactions will

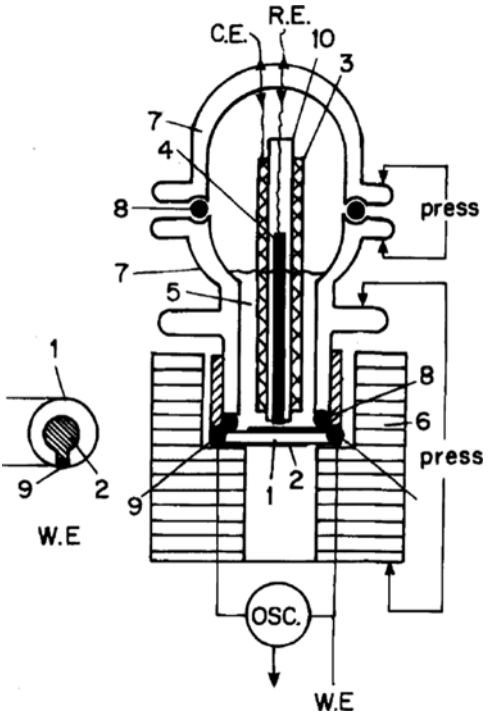

Fig. 7.2 Example of cell designed for EQCM measurements. 1, quartz crystal; 2, gold electrodes; 3, Li foil counter electrode; 4, Li wire reference electrode; 5, solution; 6, polyethylene body; 7, glass cell; 8, "O" rings; 9, electrical contacts; 10, glass tube. Reproduced with permission from [15]; copyright 1995, The Electrochemical Society

result in average mpe values, which can also be affected by the conditions of the electrochemical experiment [16]. There are a large variety of experimental effects that need to be considered to ensure that Δf is only affected by mass changes associated with electrochemical reactions; an extensive discussion can be found in the literature [14]. Of particular relevance to the study of liquid–solid interfaces are the possible changes of viscosity of the liquid in the vicinity of the electrode surface, especially if temperature gradients occur during the experiment, and regardless of whether a potential is applied. These should be taken into account during data analysis, by applying corrections based on viscosity data and blank experiments [22, 23]. When these experimental effects are considered, in general, passivation of the electrodes with cycling can easily be evaluated by EQCM, as it will result in stabilization of the total mass [23, 24]. Similarly, anodic dissolution of electrode–electrolyte reaction layers has also been uncovered using this tool [19].

7.4 Techniques of Compositional Analysis

This section will be devoted to the discussion of how techniques of widespread use in analytical chemistry for the determination of compositions have been applied to the study of EEIs. The formation of ionized particles or molecules is common to all

of them, but detection systems vary. The most popular detection system is mass spectrometry (MS) [25] due to its high sensitivity and precision. MS is based on the measurement of mass-to-charge ratios of the species resulting from ionization. Despite the undisputable power of MS, recent technical developments will be discussed where optical emission spectroscopy (OES) is used instead. OES measures the optical emission resulting from atomic processes that are characteristic of the elements in the sample. The choice of detector determines the ability of performing studies at atmospheric pressure; differential pumping in the experimental setup is required to keep mass spectrometers under the vacuum they need to operate. As a result, experiments where elemental analysis is performed on live interfaces would, in principle, be simpler and more versatile in an OES than a MS setup. It is also important to keep in mind that ionization can involve compound fragmentation, which bears consequences on the correlation between observations and the situation in the battery. Hence, it is typical to reconstruct molecules in the sample based on a specific and unique combination of ion fragments (spectra), as compared with available databases [26, 27].

The specifics of tools that have demonstrated value for the characterization of phenomena at EEIs are discussed below. The main difference among them lies on the method of analyte extraction, which has implications on how representative the final results are of the situation in vivo. These parameters should be carefully considered when designing an analytical experiment.

7.4.1 Thermal Extraction

Many of the products of deleterious electrolyte–electrode interactions in nonaqueous batteries are organic compounds and gases such as CO_2. A large part of the organic fraction can be introduced into the analytical equipment (e.g., MS) by simply heating up cell components such as the electrode or separator. This process will induce volatilization [28, 29] or thermal decomposition [30–32]. The latter phenomenon has been leveraged in studies of the stability of the SEI layer with temperature, which combined thermogravimetric analysis (TGA) with MS [33, 34]. The results can be contrasted [35] with studies specifically focused on thermal properties using more specialized calorimetric techniques [36–39].

Analyte separation is preferred when dealing with complex mixtures, as it enhances chemical resolution, especially when species of similar composition, but different chemical nature (e.g., polarity) are involved. Despite the vast variety of separation techniques available nowadays, gas chromatography is the most popular among scientists studying electrode–electrolyte interactions. A large variety of detectors can be employed in conjunction with GC [40], the most popular in this field being mass spectrometers. A comparative discussion of the possible detectors is beyond the scope of this overview; the reader is referred to general textbooks (see above) for extensive details. The most straightforward application of GC is to identify gases that may form during battery operation [32, 41–44] or thermal abuse after

cycling [35, 45, 46]. The critical step in these analyses is the extraction of the gas sample from the cell without contamination from the atmosphere. Protocols of extraction are proposed in the literature [42]. Extraction of liquid and solid analytes into the GC column is typically achieved using mild heat treatments, either directly from the cell components (in most cases, after light washing) [30, 31, 47–51] or after extraction using a different organic solvent with low boiling point as matrix [29, 42, 52]. The need for heat to ensure proper volatilization and separation of components in a GC experiment implies that some molecules in EEIs are typically not detected directly, but through the products of their thermal decay or reaction with water impurities. As a result, it is critical to carefully consider such decomposition reactions when ascertaining the origin of the species observed in the chromatograms [49, 51], especially if databases are not readily available or the observed fragments cannot be unambiguously traced back to a molecule.

7.4.2 Dissolution

In addition to being part of protocols of extraction of organic components in EEIs for MS or GC analysis (see above), dissolution has been used in the battery community in conjunction with classical tools of elemental analysis such as atomic absorption spectroscopy (AAS) and inductively coupled plasma (ICP), either with OES or MS. The protocols typically involve aqueous solutions in order to circumvent the challenges associated with organic matrices. These tools have been employed in the analysis of inorganic fractions in EEI layers [30]. However, their most common use is to explore metal dissolution from cathode materials in the presence of acidic impurities in the electrolyte [53–56]. The electrolyte portions in test cells are typically very small, and, thus, extremely difficult to extract reliably. Consequently, researchers typically opt for accelerated aging experiments in which the cathode powder (or composite electrode) is soaked in large amounts of electrolyte solution for extended periods of time, at controlled temperature. Comparison of the results with samples at different states of charge has shed light into the relationship between metal oxidation state and its tendency to dissolve [57].

7.4.3 Physical Extraction

The mechanism of physical extraction for analytical purposes always involves the bombardment or irradiation of a sample with an ion or laser beam, respectively [58, 59]. These processes are typically known as sputtering and ablation, respectively [60]. The interaction results in the volatilization of matter, in the form of solid fragments, neutral particles, or ions. While solid fragments need to be further divided before being introduced into an analyzer, neutral or charged particles can be detected directly with the appropriate technology. Nonetheless, post-extraction

ionization of neutrals is rather common. Analysis can be performed on OES signatures or by MS, the latter being the most popular. Sustained bombardment of the surface enables depth-resolved experiments. Further, in certain cases, the beam spot size on the sample is small, so that it can be rastered to yield 3D reconstructions of a layer at nanoscale spatial resolution [61]. The main precaution that needs to be considered is the interaction between the beams and the samples to be analyzed. As in GC/MS, the fragments that are observed are fingerprints of the species present in the sample. It is important to understand the physical phenomena of extraction, as different analytes can show significantly different sputtering or ablation rates. Of particular concern is the existence of matrix effects in some of these techniques [62]. These effects involve a different extraction mechanism of the same species depending on the matrix that contains it. They require a careful process of comparison of the data with accurately defined standards.

Many techniques that fall within this category have been used to characterize reaction layers at EEIs. Arguably the most popular is secondary ion mass spectrometry (SIMS), especially when coupled with a time-of-flight detector (ToF) [59]. SIMS is based on the extraction of ions from a sample surface through bombardment with energetic primary ions. This physical process results in sputtering from the very first atomic layers, making SIMS an extremely surface sensitive technique with very high depth resolution. Its sensitivity to trace constituents, combined with its resolution, renders it an attractive tool for the analysis of components at EEIs [64, 65] and their elemental profiles [63, 66–69]. Examples of lateral mapping of the SEI on graphite substrates are available as well [70, 71]. These profiles not only have compositional value but also provide a qualitative indication of the thickness of electrolyte decomposition layers and their variation with experimental conditions (Fig. 7.3) [63]. The powerful analytical capabilities of this tool include sensitivity to different isotopes of the same element. This feature recently enabled an elegant study of Li transport through SEI layers combining experiments with computational simulations [72].

Glow discharge (GD), whether combined with MS or OES detectors, is another compositional tool based on sputtering processes that has found application to the analysis of battery interfaces. The main difference between GD-MS/OES and SIMS lies on the mechanism and, thus, energy at which the extraction occurs [59]. GD also achieves very high depth sensitivity. In contrast, it suffers less from matrix effects than SIMS, but has much lower lateral resolution. As a result, it has been used only to produce composition profiles in a number of electrolyte–electrode systems [73–75]. In terms of enabling high sample throughput and even studies of live interfaces, it is important to consider that SIMS requires complete enclosing under ultrahigh vacuum, and GD does not, especially if OES detectors are used [76].

A couple of very recent examples are available in the literature of the use of laser-based extraction methodologies for the analysis of EEIs. The motivation for the use of lasers was different in both cases. In one case, matrix-assisted laser desorption/ionization (MALDI) coupled with MS was employed to collect evidence of solvent oligomerization during decomposition on metallic surfaces [24]. This technique is popular within the organic chemistry community for its sensitivity and

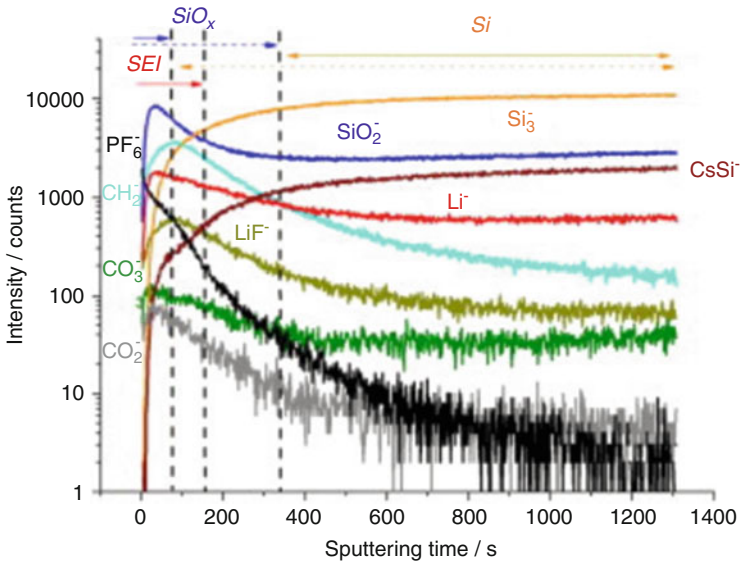

Fig. 7.3 ToF-SIMS depth profiles (negative ions) of Si nanowire electrodes, cycled in a Li metal cell with 1 M $LiPF_6$ in 1:1 EC:DMC. Reproduced with permission from [63]; copyright 2006, Elsevier

selectivity to high weight macromolecules [58]. In a separate report, using ultrafast lasers, the composition profiling of SEI components on graphite was achieved with depth resolutions comparable to those of sputtering tools [77]. The small spot sizes of the tool, together with the use of OES as detection method, opens the door for 3D analysis in the presence of liquids in atmospheric conditions [78], i.e., *operando* experiments.

7.4.4 Dynamic Analyses

While the tools discussed in the previous subsection provide powerful chemical insight, *operando* studies where electrochemical signatures can be directly related to reaction products still remain to be demonstrated. Such dynamic analyses would be of great interest to further uncover the mechanisms of electrolyte decomposition on electrode surfaces. Nonetheless, in the existence of gaseous product formation, detection can be performed *operando* through differential electrochemical mass spectrometry (DEMS). This technique is based on combining an electrochemical cell design that allows the extraction of these gases online, while the reaction is occurring, with the high sensitivity of MS to ultra-low concentrations of analyte. The key to a successful DEMS experiment is a membrane that separates the electrochemical cell, which operates in ambient conditions, in the presence of liquids, with

MS, which requires vacuum. This membrane needs to be impermeable to the liquid electrolyte, yet permit the transport of the generated gases [79]. In the case of polar solvents such as those in Li-based batteries, polytetrafluoroethylene (PTFE) is the most popular choice [80]. Typically, differential pumping systems are used to progressively approach the vacuum required by the MS. An extensive discussion of the specific modifications that enable different types of electrochemical experiments and the corresponding analytical sensitivities can be found in the literature [79].

DEMS has been used extensively for the study of gases formed during either the reductive or oxidative decomposition of battery electrolytes on electrode surfaces, as well as the dependence of their formation rates on the electrochemical potential. The results have been used to identify reaction mechanisms that lead to a better understanding of decomposition layers in various electrode materials [80–87], as well as modifications that alleviate or suppress undesired processes [88–95]. This analytical technique has been recently used to detect the efficiency of oxygen reduction and evolution reactions in nonaqueous solvents [96, 97], which is of interest in the assessment of the viability of the Li/air battery concept. By leveraging the sensitivity to isotopes of MS, it was possible to trace gas formation back to either electrolyte decomposition or oxygen electrochemical reactions [98, 99].

7.5 Vibrational Spectroscopy

7.5.1 Infrared (IR) Spectroscopy

IR light interacts with the spontaneous vibrations and rotations that happen in the different atomic bonds of a molecule, amorphous, or periodic solid. These vibrations are excited at discrete values of energy, leading to a spectrum that is composed of a collection of vibrational fingerprints. The energy of these fingerprints can be associated with a particular class of bond based on experimental knowledge; tables available in numerous monographs assist in the assignment to a specific chemical identity [100]. In simple samples, the envelope of signals can oftentimes be traced back to a specific compound, and even to its relative amount. Because it is especially sensitive to chemical bonds in organic compounds, IR spectroscopy is very commonly used in the field of analytical organic chemistry.

Modern spectrometers are all based on broad band IR light sources and interferometers that require Fourier transforming (FT) the data to produce usable spectra. Further, FTIR spectrometers have a notable degree of detection versatility, from the classical transmission (absorption) geometry to a suite of modalities based on reflectance of the IR beam [101]. The latter were specifically developed by surface scientists to study the physical chemistry of adsorbate molecules on ideal systems, especially of interest to catalysis [102]. As such, they are also highly suited for the study of interfaces in electrochemical systems [103], especially given that FTIR can operate under a variety of environments, including liquids. Reflectance-based tools can be divided according to their general mechanism. Attenuated total reflection

(ATR) is based on the use of an IR transparent, highly refractive crystal (e.g., Ge or ZnSe) through which the beam is transmitted to reach the sample at an angle that enables total internal reflectance within the crystal. The sample is placed on the side of the crystal that does not face the source. This phenomenon creates multiple interactions between sample and beam until it ultimately escapes the crystal, increasing the signal-to-noise ratio. Single internal reflectance is also used. The other subtype of surface-sensitive FTIR tools is based on external reflectance, meaning that they do not require a crystal, but a highly reflective material, typically a metal [102]. The canonical example is reflection–absorption IR spectroscopy (RAIRS or IRRAS) [104]. In this case, the signals from the species on the surface are detected after reflection from the metal.

When the ability of studying heterogeneous interfaces is taken together with its sensitivity to organic moieties, it comes as no surprise that FTIR is arguably the most popular tool in reports of the evolution of EEIs under electrochemical or aging conditions in systems relevant to batteries [13, 66, 105–114]. It was instrumental in the broad knowledge of the chemical composition of electrolyte decomposition layers, such as the SEI, that we have today, as described in other chapters of this book. However, several limitations need to be taken into account when applying this tool to the study of EEIs in nonaqueous systems. First, the picture that emerges is strongly skewed toward organic products, as compounds with ionic bonds are IR silent. Second, the decomposition products in EEIs share features with the solvents, but form a very thin layer compared to the bulk of the electrolyte. Consequently, the experiment must be designed so that the signal from the EEI is maximized over that of the bulk electrolyte. In some cases, the raw spectra can have interferences from species present in the electrode surface structure, for instance, when metal phosphates were characterized in the presence of fluorophosphate-based electrolytes [115]. While tracing the fate of a given molecule of interest could be partly achieved using redox-stable supporting electrolytes [111], in practice, washing the bulk electrolyte off the electrode surface is necessary in ex situ experiments. Obviously, this procedure generates considerable uncertainty over how representative the results are of the situation in vivo. Evidence exists that products formed during the electrochemical reaction can easily be washed away [116], so that the results can be highly misleading. Even in the presence of representative spectra, the chemical complexity of reaction layers formed at the EEI makes assignments somewhat challenging. Nonetheless, the appearance of new functional groups can be detected with a high degree of accuracy; these groups have been tracked back to the formation of specific compounds in numerous cases, especially when reference spectra are available for comparison [116–118].

The problem of signal selectivity of FTIR severely complicates the design and reduces the versatility of *operando* setups. A large number of cells for the study of liquid–solid EEIs has been built and demonstrated in different reflectance modes (Fig. 7.4) [105, 106, 109, 115, 119–122]. The material used as crystal (for internal reflection experiments) or transparent window (for external reflection experiments) needs to be carefully selected based on its chemical compatibility with the cell components. Insight into the formation of new products and the potentials at which

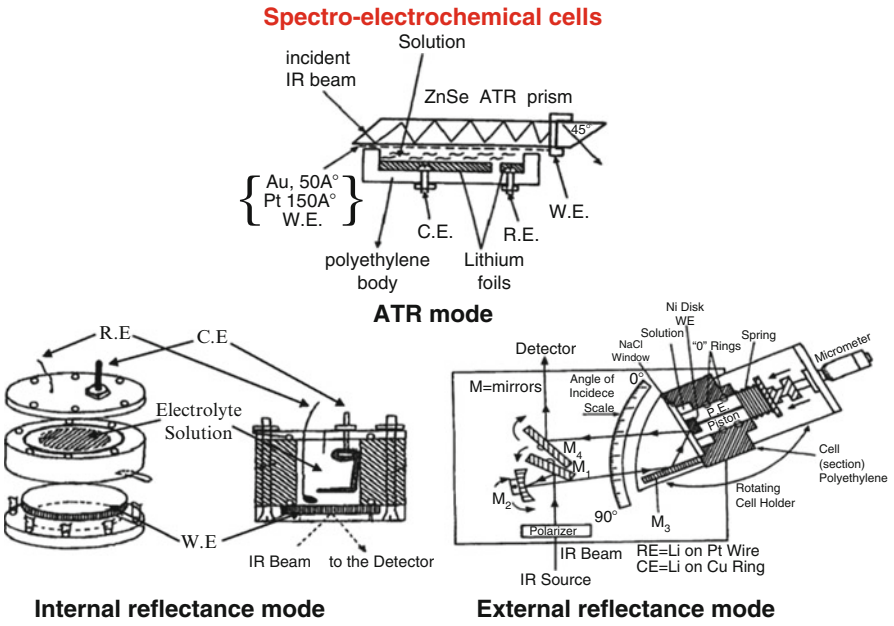

Fig. 7.4 Cells for three modes of operation for *operando* FTIR measurements: ATR, single internal reflectance mode and external reflectance mode. Reproduced with permission from [105, 119, 120]; copyright 1991 and 1993, The Electrochemical Society, 2001, Springer Science+Business Media

reactions occur can be obtained by subtracting the steady state spectrum of the pristine cell from all the spectra collected in working conditions. Some specificity can also be achieved by subtracting spectra obtained at different polarizations of the light source [123]. Thanks to such *operando* FTIR studies, it is now known that high potential side reactions between positive electrode and electrolyte are synchronized with the redox activity of the active material, and that the resulting layers can be highly dynamic (Fig. 7.5) [122]. However, these techniques result in highly distorted spectra so that valuable insight comes at the expense of chemical resolution of the species involved in these interactions. In principle, these experiments could be achieved by bringing the electrode surface in contact with the crystal (for internal reflection experiments) or a transparent window (for external reflection experiments). However, there are fundamental challenges to this approach. First, it is very difficult to control the amount of electrolyte between crystal/window and electrode. In the extreme case that no electrolyte is present, the electrochemical reaction will not proceed in that area. Second, when placed in contact, the crystal/window will experience the potential at the electrode, opening the door to possible parasitic reactions that will lead to damage if the crystal/window material is not stable at the working voltages. Given the interest of FTIR to answer questions pertaining to EEIs, it is expected that new and creative means to address these limitations will be proposed in the near future.

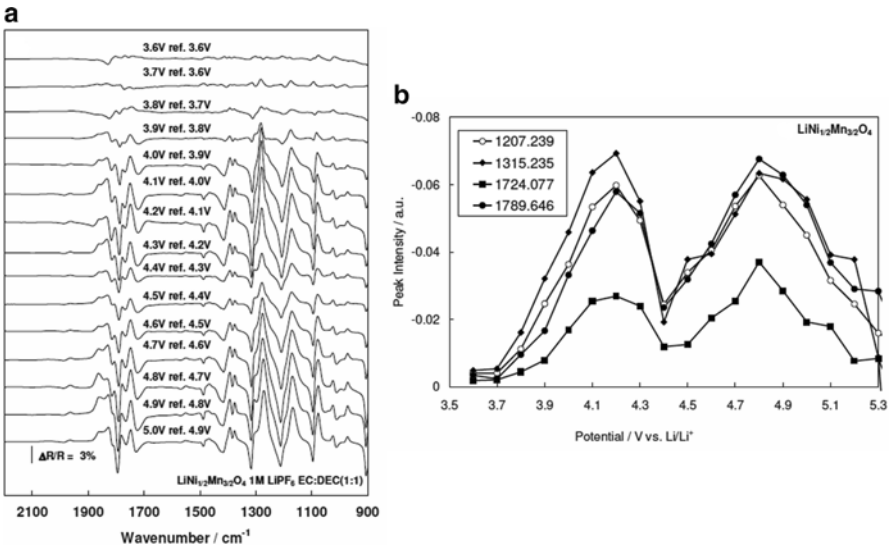

Fig. 7.5 (**a**) FTIR spectra collected during the anodic polarization of a $LiNi_{0.5}Mn_{1.5}O_4$ thin film in a Li metal cell; (**b**) evolution of the peak intensity, integrated from the data in (**a**), with electrochemical potential. Reproduced with permission from [122]; copyright 2010, The Electrochemical Society

7.5.2 Raman Spectroscopy

This kind of vibrational spectroscopy is based on the general Raman effect, which is a type of inelastic scattering of photons [124–126]. In this particular application, a monochromatic laser light, typically in the UV–Vis range, is shined onto a sample. At those energies, the laser interacts with the electronic structure of the material in a manner that results in deformation of polarizable bonds through the induction of an electric dipole. In this "deformed" (or virtual) state, bond vibrations occur at different frequencies as the initial state. These transitions happen mostly from the ground state, but, because of thermal excitation, a Boltzmann distribution of bonds will be in a slightly excited state. Relaxation from these new states occurs primarily through the release a photon of the same energy as the incident laser, thus leading to elastic (Rayleigh) scattering. However, if the molecule or crystal contains Raman active states, a very small fraction (in the order of ppm) of emitted photons could have either lower (Stokes) or higher (anti-Stokes) energy than the incident beam. Each Raman active state will lead to a characteristic energy loss or gain, controlled by symmetry rules. Since the exact nature of the inelastic scattering will depend on the initial state, Stokes scattering, which starts from a ground state, is more prominent than anti-Stokes. In order to be able to detect these photons, they must be discriminated from the much more intense Rayleigh scattering. Raman spectrometers contain hardware such as filters or stoppers that reduce the elastic signal.

Despite also being sensitive to vibrational and rotational interactions, the selection rules that operate in Raman spectroscopy are different from IR because it depends on bond polarizability instead of dipole interactions. As a result, both techniques are complementary. It also follows that a Raman spectrum can be uniquely traced to a particular chemical identity, just like IR. In conventional spectrometers, the penetration depth of the radiation and, thus, the sensitive sample volume, depends on the wavelength of the laser and the electronic conductivity of the compound, but is typically a few hundred nanometers [126]. Raman spectroscopy suffers from so-called skin effects on metallic samples, whose high electronic conductivity severely reduces the optical skin depth; in practice, severe signal loss is found for these materials [126]. While conventional Raman spectroscopy is generally considered a bulk technique, the scattering occurring on metal surfaces has been leveraged in the development of surface enhanced Raman spectroscopy (SERS) [127]. While the exact physical mechanisms of operation remain to be fully uncovered, suffice to say that SERS relies on the interactions between a metal surface and thin layers of compounds on it, so that it becomes a highly surface sensitive, albeit rather experimentally restrictive, tool. Performance of Raman spectroscopy in reflectance mode, much like FTIR spectroscopy, is also possible [128], but rather less common. Much the same shortcomings discussed above for IR spectroscopy apply to this experimental methodology. Finally, another attractive feature of the technique is that a number of confocal spectromicroscopes are available in the market that offer spatial resolutions in the order of 1 μm. This feature is of interest for the study of sample inhomogeneities. For instance, it revealed that one of the predominant mechanisms of interfacial impedance growth in layered oxide cathodes upon extensive cycling involved disconnection of individual particles or agglomerates at the electrode surface [9, 129–131]. Such disconnection was due to the loss of carbon additive fractions, and resulted in considerable microscopic variations in state of charge.

While Raman spectroscopy plays a central role in the characterization of battery phenomena [126], it is less used for the study of EEIs than FTIR, probably because it is generally considered bulk, not surface sensitive. Nonetheless, if the organic surface films are thick enough, features can be observed at wavenumbers that are rather specific to discrete molecular moieties [132, 133]. There are also a limited number of examples of the value of SERS on oxide electrodes for this purpose [134], but they are probably limited by experimental uncertainty and the need to modify surfaces to induce a metallic character for adequately enhanced signal. Nonetheless, SERS has proved of value to follow the formation of electrolyte decomposition layers on Li metal electrodes [135] or model metal systems [136–139]. Interestingly, the bulk sensitivity afforded by conventional Raman spectroscopy creates another point of synergy with FTIR spectroscopy, as it can be used to probe phenomena that occur on the electrode side of the interfaces. Indeed, it has been critical in our understanding of surface damage in graphite electrodes through exfoliation and formation of transition metal-based precipitates resulting from cathode dissolution in the electrolyte [140–148]. Cathode corrosion, especially at high temperature, can also be specifically probed by Raman spectroscopy, as it results in the formation of surface phases that are distinct from the pristine material [134, 149].

The involvement of solvent cointercalation in graphite surface exfoliation and how it can be avoided has been discussed based on the analysis of the solvates in the bulk electrolyte [150–152], which possess to distinct Raman active interactions [153, 154]. The knowledge of these solvate structures could also inform the rationalization of charge transfer reactions that occur at EEIs [155, 156].

The coupling of Raman spectroscopy and microscopy with electrochemical measurements has been extensively demonstrated in the literature; many reports are available that describe possible cell designs [105, 130, 135, 157–161]. A fortuitous finding derived from *operando* Raman spectroscopy studies was that certain electrolyte decomposition reactions lead to species that are fluorescent/phosphorescent. The onset of these species results in signals that significantly increase the background of the Raman spectra [162–164]. As will be discussed below, even though this effect compromises chemical resolution in the Raman spectroscopy experiment, these fluorescence signals carry information that can be leveraged with other tools. Finally, it is worth noting that the use of lasers as probes inherently carries the uncertainty of beam damage [163, 165], either through thermal or nonthermal effects. This risk is certainly higher than in FTIR when organic moieties are considered, so it needs to be carefully considered when evaluating the resulting data.

7.6 UV–Visible Techniques

7.6.1 UV–Vis Spectroscopy

UV–Visible light interacts with the electronic states of a given chemical species and promotes an excitation from the top of the valence band to the bottom of the conduction band. Measurement of the absorbance of a sample at different wavelengths results in a spectrum which is indicative of this optical band gap, and can be traced back to general families of molecular entities and compounds. In the case that electronic relaxations from the excited state after irradiation to a final state are preceded by a cascade of small vibrational transitions, fluorescence occurs that lowers the emitted photon energy. This signal can be detected with spectrometers different from those used for absorbance measurements. Fluorescence emission spectra are collected at constant incident wavelength, as the different vibrational and electronic transitions result in emission at different energies. These spectra are generally less specific and, thus, less straightforward to interpret than UV–Vis absorbance. Also, fluorescence occurs in only certain classes of molecules, which has traditionally made it relevant in biosciences or organometallic chemistry.

Despite the widespread use of UV–Visible spectroscopy in analytical chemistry, it has seen much more limited application to the study of electrochemical phenomena relevant to EEIs. However, the studies available are excellent representations of the kind of unique insight that could be gained from these tools. Absorption spectroscopy has been applied to the study of the electrochemical degradation of aromatic molecules on the surface of electrodes under working conditions [166].

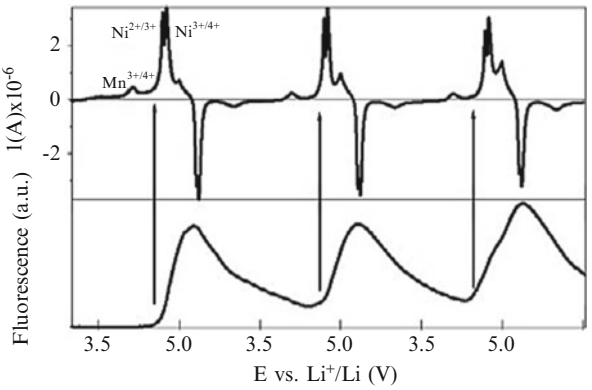

Fig. 7.6 Current (*top*) and integrated fluorescence intensity (*bottom*) variations during three CV sweeps between 3.5 and 5.0 V at 0.05 mV/s of a carbon- and binder-free $LiNi_{0.5}Mn_{1.5}O_4$ particulate electrode in a Li metal cell. Reproduced with permission from [164]; copyright 2013, Elsevier

The unexpected finding of fluorescence backgrounds during Raman spectroscopic studies of cathode surfaces (see above) was very recently leveraged to the analysis of the dynamics of interphase layers at EEIs [164]. Although the exact chemical origin of this fluorescence signals has not yet been ascertained, measurements of fluorescence intensity during the lithium (de)intercalation on high voltage $LiNi_{0.5}Mn_{1.5}O_4$ revealed that the appearance of the corresponding species is synchronized with the redox activity of Ni^{2+} (Fig. 7.6). Further, the fluorescence signal was found to strongly vary between oxidation and reduction of the electrode, suggesting that the layers resulting from electrolyte decomposition continue to evolve with cycling. This finding is still under investigation.

7.6.2 Ellipsometry

The basic principle of ellipsometry relies on the measurement of changes in polarization of light after it is reflected from a flat surface, conventionally in the specular direction (i.e., when reflected and incident angle are equal and coplanar). The polarization goes from linear to elliptical, a phenomenon that gives rise to the technique's nomenclature. It can be carried out either with a monochromatic or broad band source, typically at wavelengths from near UV to near IR, and mainly in the visible. Experiments employing broad band sources are typically grouped under the category of spectroscopic ellipsometry. The response at different wavelengths is correlated to the optical transitions possible in the electronic structure of the layer [168]. For this reason, ellipsometry was initially developed to probe the dielectric properties of thin films. However, this optical response, which depends on the complex refractive index, is also an indication of surface thickness, roughness, and density. The signal in an ellipsometry experiment is collected so that both its amplitude (Ψ) and phase (Δ) can be quantified (Fig. 7.7a). These values are extracted by measuring the ratio between the reflection coefficients of s- (parallel to the sample surface) and p- (normal) polarized light, which makes the tool rather robust against spurious scattering effects. The values of Ψ and Δ do not have direct optical meaning, so the data

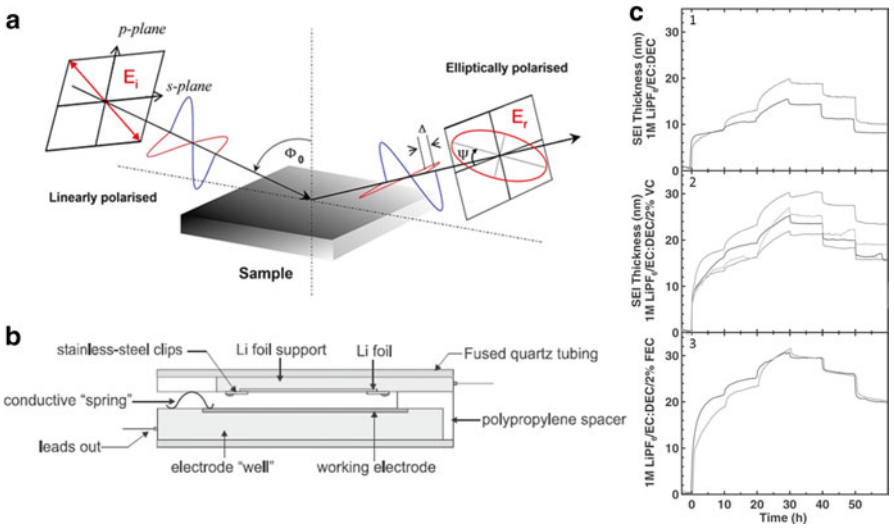

Fig. 7.7 (**a**) Schematics of the fundamentals of ellipsometry (see text for details); kindly provided by Christopher Smith, School of Physics, Trinity College Dublin (http://www.tcd.ie/Physics/Surfaces/ellipsometry2.php00); (**b**) working cell designed for ellipsometric studies coupled with electrochemistry; (**c**) SEI thickness determined ellipsometrically on TiN electrodes in Li metal cells using potentiostatic chronoamperometry. The electrolytes used were 1 M $LiPF_6$ in EC:DEC (1:2) (1), EC:DEC (1:2)/2 wt% VC (2), and EC:DEC (1:2)/2 wt% FEC (3). Reproduced with permission from [167]; copyright 2012, The Electrochemical Society

from ellipsometry needs to be modeled to extract values of layer thickness, index of refraction, and extinction coefficient. In the presence of chemically complex layers, building models is significantly complicated, and, in the case of success, the optical values are only considered formal.

The high accuracy, down to sub-nm in ideal cases, of ellipsometry in measuring the thickness of layers makes it valuable in the study of reaction interphases at EEIs [23, 167, 169]. The role of H_2O impurities on side reactions and formation of acidic species that can corrode an electrode has been evaluated with this tool [170, 171]. The design of cells that can be used for *operando* experiments has extensively been demonstrated (Fig. 7.7b) [23, 167, 172–175]. These time-resolved measurements have provided valuable insight into the dependence of reaction layers on electrochemical potential, their stability upon cycling and how their growth can be affected by the chemistry of the electrolyte (Fig. 7.7c), among others. It is common to use surface roughness data gathered by complementary tools (see below) as inputs for the models used to fit ellipsometry spectra [169, 174]. The most critical step for data interpretation is precisely the generation of these models, especially if quantification is desired. Given the extreme chemical complexity of these interfacial layers, some level of knowledge of the compounds present greatly improves the chances of accurate modeling of the signals [173]. Several references can be found that thoroughly discuss this step in the context of EEIs [167, 173], to which the reader is referred for further information.

7.7 X-Ray-Based Techniques

7.7.1 X-Ray Photoelectron Spectroscopy

The basic principle of X-ray photoelectron spectroscopy (XPS) relies on the ionization of a given compound by exciting a core level electron to the continuum using an X-ray beam (Fig. 7.8). The generated photoelectrons are detected by an analyzer that can measure their kinetic energy and intensity (i.e., number) [177]. The kinetic energy is characteristic of a particular element, and even light elements such as Li can be probed by XPS. Frequently, small variations in chemical shift can be observed depending on the specific chemical state (e.g., oxidation state). These chemical states need to be sufficiently different so as to alter the position of the core levels of the probed element within the energy resolution of the analyzer. In practice, this requirement involves noticeable changes in chemical bonding, although careful peak deconvolution can be used to resolve multiple signals under a broad peak. At any rate, qualitative identification of chemical states typically requires comparison with standard materials of known composition. XPS also demands careful experimental design to avoid charging effects when samples are non-electronically conductive; the result of these effects is typically a shift of the XPS peaks that can lead to misinterpretation. Such charging can be avoided by using conductive substrates, such as metal foils, and is typically a minor problem in carbon containing electrodes if the reaction layers are not too thick. Although integration of the photoelectron intensity at each energy value can be used for quantitative purposes [177], in practice, significant error is introduced by the experimental conditions, so that the accuracy is typically below 90 %. X-rays can excite depths of 10^2 nm, but the resulting photoelectrons are very easily absorbed by matter, so they have very short escape lengths. This phenomenon has two important consequences: (1) in general, the measurements need to be performed in ultra-high vacuum conditions, and (2) only electrons from

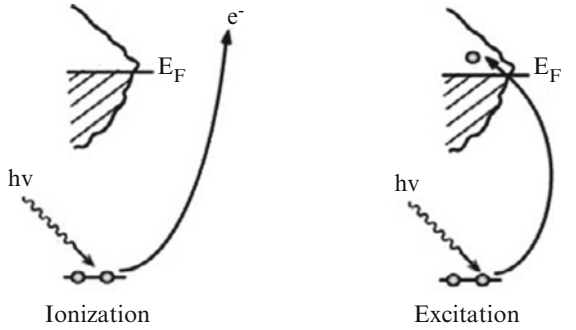

Fig. 7.8 Schematic illustration of processes of core level electron excitation by an X-ray beam. Reproduced with permission from [176]; copyright 2013, Elsevier

the first 10 nm of sample, at most, can be analyzed. These features turn XPS into a routine technique for surface characterization. Chemical information with depth can also be collected by changing the angle of X-ray incidence or sputtering a few layers of sample between data collection. In practice, the former has limited applicability due to limitations in escape length. In turn, differences in sputtering rates between species (see matrix effects discussed for SIMS above) and alterations to the sample that can subsequently be introduced during this process demand caution during data interpretation.

XPS has been widely used to characterize the products of electrolyte–electrode side reactions in a large variety of Li and Li-ion battery systems [1, 13, 178–180]. In this context, it is common for researchers to combine it with FTIR to obtain a notably complete chemical picture [108, 113]. Auger electron spectroscopy (AES), which is based on the detection of an outer shell electron generated when the core level hole is filled by an electron from an intermediate level, has a more testimonial role [30]. In general, the characterization efforts focus on the description of the chemical nature of these interfaces, not on the quantification of the species present. Because of escape length limitations, these studies are generally only possible post-mortem and require rinsing away the layers of bulk electrolyte that remain upon harvesting an electrode from a cell. As a result, and as already discussed in the context of FTIR spectroscopy, uncertainty prevails on the exact nature of the reaction film in vivo, as only the solid layer that remains attached to the electrode can be analyzed. Nonetheless, XPS has proved to be very effective in identifying both organic and inorganic species resulting from the decomposition of the electrolyte. Further, it has been employed to identify changes introduced on metal oxide surfaces as a result of the interactions with acidic and fluorinated species in the electrolyte [181]. Phase identification can be elusive especially in the case of organic species, as slightly different compounds with the same functional groups will have very similar spectra. Phases with metals in the same oxidation state and similar chemical bonding will also be difficult to resolve. Thus, signals are conventionally assigned to generic functional groups and oxidation states. The possibility of radiation damage and artificial chemical shifts due to sample charging also needs to be considered when interpreting the data [13]. This uncertainty, especially in the presence of the chemical complexity of EEIs, is alleviated by careful sample preparation and by leveraging the sensitivity of the tool to virtually all elements in the periodic system to build comprehensive pictures using the core levels of all the possible components. Additional insight can be gathered by collecting valence band XPS if equipment is available with sufficient energy resolution to collect data at very low kinetic energies [182]. This band is much more sensitive to chemical changes than the core levels, but the data collected is representative the total density of states (DOS) and, thus, convolutes contributions from all elements in the compound or sample. Consequently, while potentially affording rich information, high quality standards or computer simulations of the DOS are required.

A new dimension to XPS analysis has recently been provided by the application of synchrotron-based tools. The ability to tune the energy of the incident beam as well as the much higher fluxes compared to laboratory sources affords opportunities

to increase the depth resolution of the technique and even the design of experiments in partial pressures of gas and liquids, in semi-working conditions. Synchrotron XPS is now possible at incident energies from below 100 to almost 7,000 eV [184]. Using the hardest beams bypasses the need to significantly wash the samples to avoid signal flooding by the bulk of the electrolyte. Increasing the energy effectively probes layers at increasing depths. This feature is particularly attractive to scientists studying electrolyte–electrode interactions as it has long been known that the nature of the reaction layers changes with the distance from the electrode surface. Experimental validation using synchrotron XPS has already been provided for relevant oxide [185, 186] and Si-based systems (Fig. 7.9) [183, 184]. Using hard XPS, information can be collected on the chemistry as well as the thickness of the layers [186]. These reports are elegant examples of the possibilities opened by the use of this synchrotron-based tool.

7.7.2 X-Ray Absorption Spectroscopy (XAS)

Related to XPS, XAS is a spectroscopic technique based on the measurement of the energy at which X-ray photons are absorbed during the excitation of core level electrons to excited states in the electronic structure of a given compound (Fig. 7.8). It is also sensitive to virtually all elements in the Periodic System. Unlike XPS, the sample is not ionized, but electrons are excited to the valence bands of the probed compound. The interaction of the excited state with the core hole produces a unique fingerprint of the electronic structure. This fingerprint can be traced back to compounds containing a certain element with higher specificity than XPS, especially when the spectra can be compared to reference data and/or computational simulations [187]. While XPS can be performed using a laboratory X-ray source, high flux is required to produce measurable XAS signals. Because, the interaction between X-rays and matter scales with the atomic mass, a wide range of incident energies need to be available to produce information on the chemical state of a large variety of elements. All in all, XAS is almost exclusively performed using synchrotron beams. As the reaction layers formed after interaction between electrode and electrolyte are mostly composed of light elements, measurements are carried out at a soft X-ray beamline, which typically provides access to ~100 to ~1,200 eV, suitable to probe C (284 eV), O (543 eV), and F (697 eV) K edges and the L edges of all light transition metals [188]. These edges are suited for the analysis of EEIs, as they can probe both the electrode and the electrolyte [189]. The photons emitted by the sample after relaxation of an inner shell electron to the core hole can also be detected at the same beamlines as XAS; X-ray emission spectroscopy (XES) is highly chemically selective and can potentially provide unique insight [189]. There are also limited examples where XAS measurements have been carried out at the S K-edge (2,472 eV) in the case of sulfonated electrolytes [64, 190]. XAS measurements at the Li K edge (65 eV) are also possible [191], but normally demand a highly specialized beamline capable of reaching very low energies. X-ray beams at these

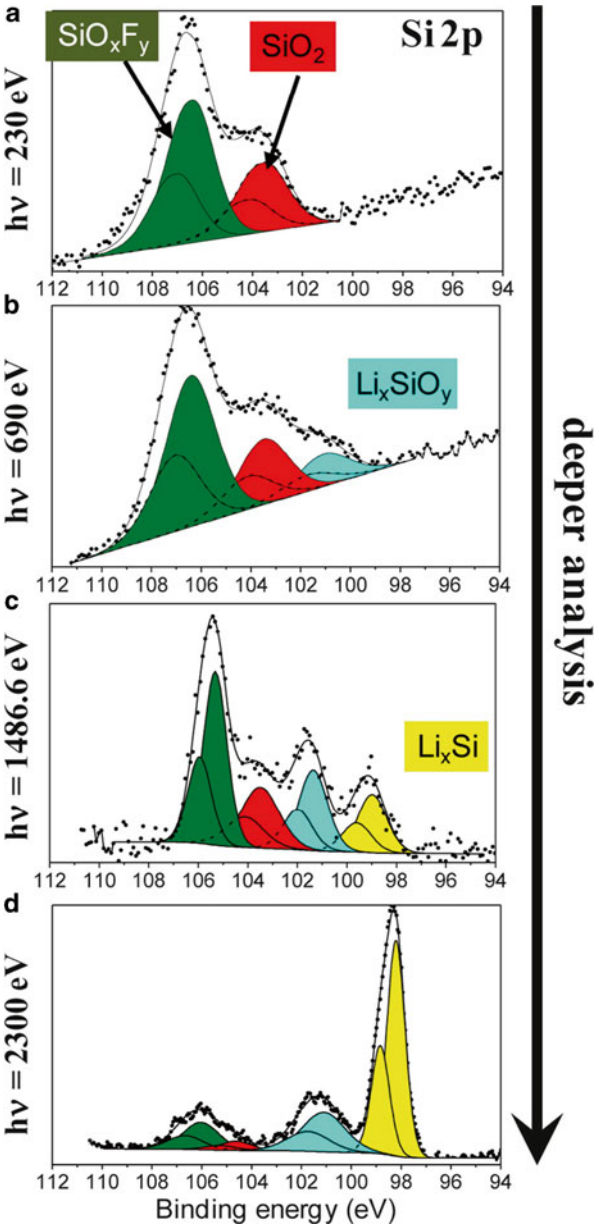

Fig. 7.9 Si 2p X-ray photoelectron spectra of a Si/C/CMC composite electrode after being cycled 100 times in a Li metal cell, as a function of the probing depth, i.e., incident energy: (**a**) 230 eV, (**b**) 690 eV, (**c**) 1486.6 eV, (**d**) 2,300 eV. Reproduced with permission from [183]; copyright 2013, American Chemical Society

energies are highly absorbed by matter, so that the detectors either analyze photoelectrons or fluorescent photons. These particles only escape the sample when produced at depths from a few angstroms to a few hundred nm, respectively, depending on the incident energy. Detected fluorescent photons are generated from deeper in the sample than detected photoelectrons. This difference provides an opportunity to gather information at different depths in the material of interest.

XAS has been applied to the study of electrolyte side reactions much less often than XPS. Nonetheless, a few examples exist in the literature of the kind of insight that can be gathered with this tool [189, 192, 193]. The possibility of collecting data with two different detectors with significantly different, "built-in" depth sensitivities affords an opportunity to compare the electrode surface with its bulk in a single experiment. Such measurements on layered transition metal oxides revealed a difference in the formal oxidation state of Ni with sample depth that pointed at the active participation of the transition metals in the decomposition of the electrolyte [194].

7.7.3 Grazing Incidence/Exit Spectroscopy and Diffraction

Instead of tuning the incident X-ray energy to gather insight from EEIs at different depths, measurements can be performed at a fixed energy by varying the incident angle instead. If high energy beams are used, the experiments can be performed at a very shallow angle, in what are known as grazing incidence experiments. An alternate setup is to direct the beam perpendicular to the sample surface while locating the detector at shallow angles with respect to the interface, in what are known as grazing exit experiments. In both cases, careful experimental design could generate information of pristine interfaces, bypassing the need to rinse the sample. Effectively, synchrotron sources are again required to achieve the necessary energy.

Many conventional techniques based on X-rays can be applied in grazing incidence/exit mode. While they have been developed for many years and their potential is obviously large, only a handful of reports exist of their application to the study of EEIs. They provided a unique insight into the reorganization of the electrode surface and EEI structure in numerous cathode materials [195–198], as well as evaluate the crystallinity of any reaction deposits [199]. This structural reorganization is of critical importance, as it can lead to increased activation barriers for the transfer of ions from the electrolyte to the electrode. Further, because hard X-rays, which penetrate deep into matter, were employed, setups have been proposed and demonstrated to carry out experiments in situ to probe live, electrified interfaces [196].

7.7.4 Reflectometry (or Reflectivity)

The basic principle of X-ray (or neutron, see below) reflectometry (XRR) is the same as ellipsometry. Yet instead of measuring changes in light polarization, it probes the profile of the momentum transfer resulting from the specular reflection of the beam, thus providing information about the structure of the surface and layers below, as well as an indication of density and roughness. The changes in scattering length density can be modeled using multilayers of different density as input; the results produce insight into chemical composition and morphological gradients. Just as in the case of ellipsometry, the modeling step is critical for a correct

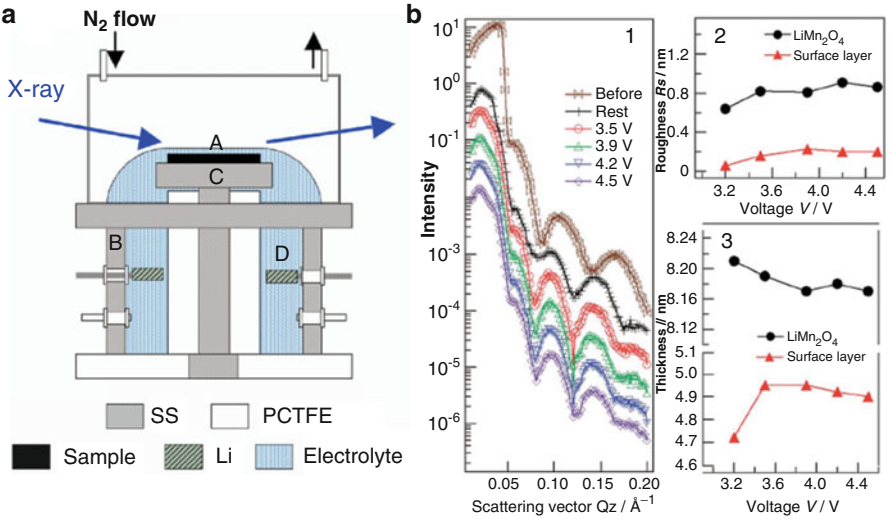

Fig. 7.10 (**a**) Electrochemical cell for *operando* XRR measurements; (**b**) XRR results collected during anodic polarization of a $LiMn_2O_4$ thin film in cell (**a**): (1) patterns, (2) potential dependence of surface roughness, and (3) potential dependence of film thickness. Reproduced with permission from [201]; copyright 2007, The Electrochemical Society

analysis [200]. Because of its sensitivity to roughness, successful reflectometry experiments require flat samples to minimize radiation scattering. As a result, they are carried out on model systems with a high degree of orientation. While this requirement limits its use in real systems, the data collected from such well-defined systems can contain a great degree of clean information. Furthermore, reflectometry experiments can be performed on samples with "live" interfaces, i.e., where the electrolyte is still on the electrode surface.

XRR has been applied to the study of EEIs on several systems [201–205]. The technique was found to be sensitive not only to the formation of reaction layers but also to mass loss at the electrode surface due to processes of corrosion (dissolution) [201]. Of particular interest is the application of high energy synchrotron beams as sources, as their deep penetration capabilities enables the design of *operando* cells (Fig. 7.10a) [203]. Therefore, uncertainty due to equilibration in the absence of an electrochemical potential is eliminated. The structural and chemical stability of EEIs during the lithium insertion/extraction processes have thus been evaluated (Fig. 7.10b) [201–204]. The dependence of these irreversible reactions on the crystal facet of the electrode material forming the EEI was established. It was found that electrolyte decomposition processes were coupled with the redox process occurring in the bulk of the electrode, which is a critical piece of information when designing materials that bypass such layer formation.

7.8 Neutron-Based Techniques

Much like X-rays, the interactions of neutrons with matter are atomic in nature. The difference is that neutrons are sensitive to nuclei directly, whereas X-rays interact with electrons. Hence, while X-rays are unsuitable to detect light elements because of the low atomic electron count, neutron scattering factors depend on the properties of the nucleus [206]. The most relevant consequence in the context of this discussion is that neutron-based tools are better suited for the detection of H and Li than X-rays, as ^{1}H and ^{6}Li are among the most highly neutron-absorbing atoms, and that they offer isotope resolution capability. In principle, they are also nondestructive.

The most obvious application of neutrons to the analysis of chemical processes in batteries is through the generation of concentration profiles. For instance, radiographic imaging can be carried out by measuring the attenuation of neutron beams after passing through a sample. It has been employed to locate the electrolyte (the richest component in H and Li) in full cells and trace changes after cycling back to its consumption during the formation of reaction layers at EEIs [207]. Increased analytical sensitivity has been achieved using neutron depth profiling. It is based on the measurement of charged particles resulting from the interaction between a neutron beam and nuclei in a certain material; in the case of ^{6}Li, such particles are α (^{4}He) and ^{3}H [208, 209]. As these particles escape toward the detector, their energy gets attenuated by their interaction with other atoms in the sample. The concentration profile with depth is the result of relating the measured energy spectrum of the charged particles to the stopping power function of the sample. Detecting both α and ^{3}H particles offers different probing power and depth resolution. The technique is sufficiently sensitive so that Li concentration profiles within the SEI on graphite electrodes and their dependence with cycling conditions and location within a rolled electrode have been reported [209]. Neutron depth profiling needs to be performed under vacuum to avoid spurious absorption of the charged particles by gas molecules. Together with the fact that thick cell casings can also significantly attenuate the intensity of the signal due to the charged particles, this requirement makes measurements during electrochemical cycling challenging, but not impossible. Indeed, they were recently demonstrated in thin film microbatteries containing solid state electrolytes [210].

Neutrons can penetrate through certain metallic components in batteries, such as the Al and Cu current collectors [207]. In contrast to depth profiling, experiments based on the measurement of scattered or attenuated neutrons are thus possible in real time, during the electrochemical reaction, and in closed cells. Indeed, neutron radiography was performed in commercial prismatic cells [207]. Small angle neutron scattering (SANS) data has also been collected in working coin cells [211]. SANS provides information on mesoscale structures, such as pore and/or coherent domain size and distribution. Data collected at different stages of lithiation in ordered mesoporous hard carbons revealed the sequence of phenomena that leads to the buildup of an SEI layer and the time dependence of its composition, with

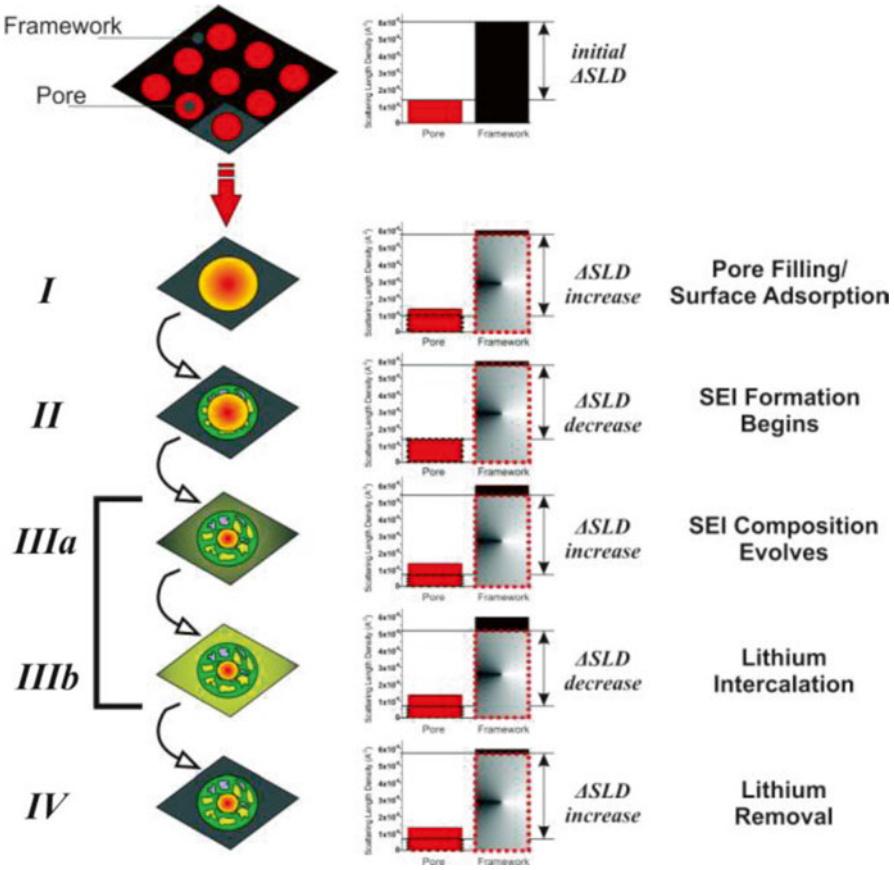

Fig. 7.11 (*Left*) Schematic illustration of the processes (*right*) occurring on mesoporous carbon electrodes during cycling in a Li metal cell, as probed by SANS. (*Middle*) Changes in contrast (**Δ**SLD) consistent with the observed peak intensity data for each stage. At each stage the dominant process affecting contrast is illustrated. Reproduced with permission from [211]; copyright 2013, American Chemical Society

carbonate species giving way to other lithium containing compounds in the early stages (Fig. 7.11). *Operando* experiments have also been demonstrated with neutron reflectometry (NR) [204, 212]. In these cases, cells were specially designed for NR, paying especial attention to building low roughness layers so as to enhance signal coherence. The SEI growth on copper under cathodic conditions was thus observed [212], revealing highly accurate information on the change in composition with potential and the increases in thickness with cycle number (from ~4 to ~9 nm). Interfacial phenomena occurring at the surface of $LiFePO_4$ electrodes have also been probed [204], although the results were less conclusive.

7.9 Nuclear Magnetic Resonance

The basic principle of Nuclear Magnetic Resonance (NMR) lies on the excitation of the magnetic spin of a nucleus of interest using a radio-frequency (rf) pulse, in the presence of an external magnetic field ($\vec{B}$). When the pulse ends, $\vec{B}$ induces the relaxation of the spins back to the equilibrium situation, in which they are all aligned with it. The relaxation generates an rf signal that can be measured by a spectrometer and is highly specific of the local chemical (and electronic) environment of the nucleus. The specificity is conferred by the many nuclear interactions (e.g., dipolar/quadrupolar couplings or Fermi contacts) [213] that can dominate the spin relaxation depending on the identity of the surrounding species. The result is a meaningful difference in both position and shape of the resulting signals. When the couplings between the probe nucleus and its environment are very strong, significant broadening of the NMR centerbands occur. Molecular tumbling, as occurs in liquids, is sufficient to average these interactions, and the final spectrum has narrow peaks. Such liquid phase spectra can be gathered from EEIs [214], but it requires the dissolution of the layers, which can induce undesired modifications. Nonetheless, significant and unique information can be gathered when these experimental limitations are considered. For instance, NMR has been used to analyze the correlation between solvation structure in bulk electrolytes and the interfacial chemistry on graphite electrodes [215]. In contrast to liquids, motion is limited in solids (such as the species at EEIs), leading to broad spectra where chemical resolution is compromised. The conventional solution to this issue is to spin the sample at an angle with respect to $\vec{B}$. The dipolar coupling, one of the most prominent interactions in solids, is angular dependent. At a specific value, called the magic angle, averaging occurs, leading to the decomposition of the broad static signal into an envelope that contains the centerband and spinning sidebands. In the presence of complete averaging, only the former is observed. As a result, magic angle spinning (MAS) is ubiquitous in the field of NMR of solids. Additional resolution can be gained by collecting data at different $\vec{B}$ or by designing pulse sequences where magnetization is transferred between nuclei, among others [216].

NMR requires the probe nuclei to be magnetically active, i.e., show a non-zero magnetic spin, *I*. In practice, virtually all elements in the Periodic System have isotopes that are magnetically active [217]. In some cases, several isotopes of the same element are accessible. More importantly, because the magnetic properties of different isotopes of the same element differ, the experimenter is able to choose the conditions that ensure the desired outcome. A suitable example for this discussion is Li, which exists as ^{6}Li and ^{7}Li with a natural abundance of ca. 7.6 and 92.4 %, respectively. NMR signals are directly proportional to the population of a given species in the sample. Thus, by proper calibration, quantitative ratios can be extracted from the data (Fig. 7.12) [218]. The highest sensitivities to a minority species are achieved when a high abundance isotope (e.g., ^{7}Li) is excited. This feature has been used by several authors to analyze the extent of electrolyte decomposition layer growth on a variety of electrode materials [219–221]. When coupled with the high specificity of

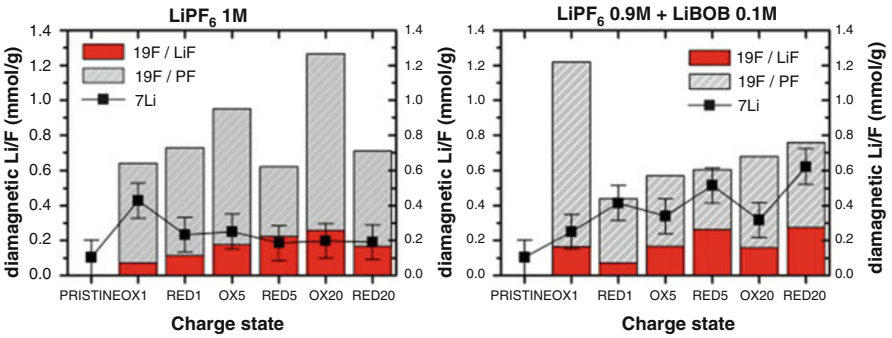

Fig. 7.12 Quantification, using ^{7}Li and ^{19}F MAS NMR spectroscopy, of inorganic species found in electrolyte decomposition layers formed on $LiMn_{0.5}Ni_{0.5}O_2$ electrodes during cycling in a Li metal cell, using $LiPF_6$– (*left*) and LiBOB-based electrolytes (*right*). Reproduced with permission from [218]; copyright 2012, Elsevier

the technique, a detailed picture of the nature of EEIs can be gathered [222], including insight into side reaction mechanisms [223].

Similar to XPS, collecting data from different excited nuclei, even at different $\vec{B}$, enhances the clarity of the results, particularly in Li-based systems. However, if this multidimensional level of chemical detail is desired, some challenges need to be considered and overcome. Typically, electrode materials contain transition metals, whose magnetization transfer mechanisms create shifts far away from the generally diamagnetic species of a surface reaction layer, so interferences from the electrode signal are not usually a serious problem. Nonetheless, the NMR chemical shift range of Li compounds that do not contain transition metals is narrow [217, 224], requiring stringent experimental conditions that cannot be completely fulfilled in complex samples. A similar situation applies to H [225], which also suffers from huge linewidths in the solid state due to the strong dipolar couplings of ^{1}H nuclei. The range of chemical shifts of C species is quite larger [225], but, unfortunately, the most abundant isotope (^{12}C, 98.9 %) is NMR silent. Thus, while gathering ^{13}C MAS NMR spectra in natural abundance samples is possible, it can require unrealistic amounts of time to get measurable signals. This technical barrier has now been extensively overcome by selectively enriching moieties in the electrolyte with ^{13}C. While this step complicates experimental design, it has produced unprecedented insight [226, 227]. The same limitation applies to O as it does to C, with the addition that ^{17}O enrichment is more cumbersome and less conventional than ^{13}C (although solutions to this problem may be around the corner [228]). Finally, F-containing species can be easily detected, as ^{19}F combines high abundance (100 %) with a high specificity, as defined by its broad chemical shift range [229].

A unique feature of NMR that applies to the phenomena of interest here is that the proximity to a diamagnetic solid of a paramagnetic surface alters the relaxation times of the nuclei in the latter. Thus, by following this magnitude with respect to reference data for pure phases, it is possible to probe the proximity of a given

species of interest to the electrode particles [230]. This contact can also be probed by leveraging the rich variety of pulse sequences designed at inducing transfer of magnetization between nuclei that are in close proximity, but may be on opposite sides of an interface [229].

7.10 Microscopy

7.10.1 Scanning Probe Microscopy

The ability to manufacture tips of a variety of materials with apices of decreasing dimensions, down to a single atom, brought about the advent of a class of microscopies based on the detection of different physical phenomena generated upon scanning the tips through a surface. The use of sharp tips as probes bypasses the diffraction limits on spatial resolution imposed by the use of light to create images. As a result, in the right conditions, scanning probe microscopy (SPM) can produce maps with sub-nanometer, atomic resolution. The specific phenomena being detected depends on the tip material (e.g., electronically conducting or not), the distance from the surface and the use of bias, among others [231]. The probe is mounted on a setup based on a piezoelectric mechanism, which controls the distance to the sample. The precision of the cantilever, as well as the existence of vibration, are as important in determining the ultimate spatial resolution of the images as the apex dimensions. Typically, SPM leads to maps of the topography of the sample, with color contrast depending on the physical phenomenon used to image (e.g., surface voltage). It can operate under a variety of environmental conditions, including air. As such, it is ideally suited for the imaging of surface processes and liquid–solid interfaces. It has thus become an important tool in the study of EEIs [232].

Scanning tunneling microscopy (STM), developed in the early 1980s, is the original SPM. The physical contrast is provided by establishing a bias between probe and sample, which are both conducting and at very close distance, but not in contact. The working distance is either kept constant or coupled to a desired current density. In this situation, quantum electron tunneling occurs and the local electron density can be imaged. The requirements of electronic conductivity of the sample limit the applicability of STM when applied to EEIs, as side reactions induce the formation of highly insulating layers on the electrode surface, which can be thick. Nonetheless, this tool has provided insight into morphological degradation at EEIs, such as graphite exfoliation, under operating conditions [233–237].

The sample limitations imposed by STM provided the motivation to continue to develop SPM with increased versatility. Under a decade after the first STM systems were assembled, atomic force microscopy (AFM) was demonstrated. In AFM, the tip is mounted on a cantilever, typically made of silicon, and brought in close proximity to the sample surface. The ensuing interaction (e.g., Van der Waals forces) pushes the tip back, creating a deflection of the cantilever that can be detected by

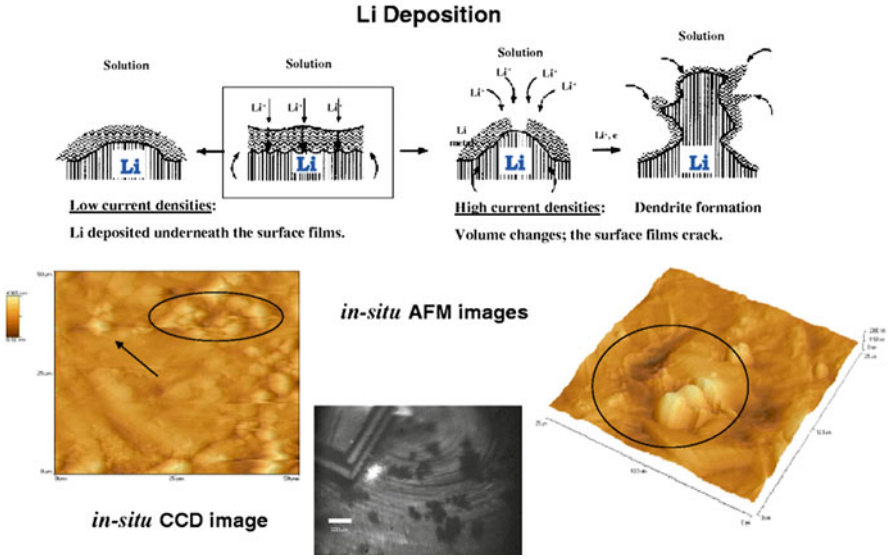

Fig. 7.13 Typical AFM images obtained from Li metal electrodes during anodic polarization. The scheme on *top* depicts the break-and-repair mechanism of the surface films during the course of dissolution of Li surfaces. The *left panel* in the scheme presents a hypothetical situation in which the surface films are flexible and accommodate morphological changes. Reproduced with permission from [105]; copyright 2011, Springer Science+Business Media

a variety of methods to produce a direct topographic image. Nowadays, AFM has evolved into a family of techniques depending on the forces involved and whether stimuli such as currents are sent through a metal-coated tip. In the latter mode, electrical signals can be decoupled from the movement of the tip, thereby creating the possibility of maps of electrical potential or conductance combined with high resolution topographic information [232]. AFM has been widely employed to obtain insight into the morphological changes occurring on a variety of electrode surfaces during electrochemical operation in liquid cells (Fig. 7.13) and upon aging [105, 238–246]. Cells that enable *operando* measurements have been designed by a number of groups [233], so that they have become rather commonplace. Achieving novel AFM capabilities continues to be the object of vigorous research. Further exploitation of existing and these new tools is bound to increase our understanding of phenomena at EEIs.

One last type of SPM that is finding emerging use to produce insight into the processes occurring at the EEI is scanning electrochemical microscopy (SECM). The tip in SECM is formed by an electrode of very small dimensions (known as ultramicroelectrode, UME); Pt wire inside a microcapillary is one of the most common UME configurations. Redox active species in the environment react at the UME surface, which generates a faradaic current that is detected by the probe. As a result, it has been used to detect transition metal ions resulting from the

corrosion of an electrode surface by the electrolyte [247]. The UME can be biased outside the window of redox stability of the Li^+–solvent complex in the electrolyte to probe the transport of ions out of an electrode, such as $LiCoO_2$, during an electrochemical reaction [248].

7.10.2 Electron Microscopy

This class of imaging tools relies on the illumination of a specimen using an electron beam that is focused by a set of electromagnetic lenses. Because electron beams possess a very short wavelength, the spatial resolution that can be achieved in electron microscopes is the highest of all comparable techniques and can reach subatomic scales. The downside is the requirement of sample preparation procedures of complexity that scales precisely with the desired spatial resolution [249]. Focused ion beam (FIB) slicing is often needed for good quality work in transmission mode. Indeed, electron microscopy imaging after sample slicing using an FIB has provided interesting insight into degradation processes at the electrode material and full cell level [250, 251]. Caution must be exercised when employing this method of sample preparation, as it can lead to questions about the representativity of the observations that need to be considered. In general, charge dissipation, especially when measuring poorly electronically conducting samples, requires the use of conductive supports and can result in irreversible sample alterations if it does not occur properly. It is also important to investigate and alleviate beam damage to the sample, which can be very severe when irradiating with electrons. Perhaps most importantly, electron microscopy operates in vacuum. All these effects introduce significant complications when observing liquid–solid interfaces and designing cells for *operando* studies. Nonetheless, solid state devices have been demonstrated and studied [252]. The advent of environmental microscopes, which operate at partial pressures of gas, and intense development in the design of sealed cells that can contain liquids has opened the door to simplification of experiments. However, to date, *operando* electron microscopy experiments are still in their infancy and limited to observing phenomena in solids even in cells containing liquids [253–255].

Scanning electron microscopes (SEM) detect the electrons emitted from the surface of a sample after irradiation by the primary beam that is rastered through a defined area. The highly focused nature of the electron beam affords topographic information even for extremely rough samples. As such, SEM is a powerful tool to evaluate sample morphology at nanoscale (down to 1 nm, in some cases) resolution. Most commonly, imaging relies on secondary electrons, which are generated by ionization of the sample (thus, in a process equivalent to XPS). Such type of imaging is extensively used to monitor changes in electrode surface morphology after exposure to liquid electrolytes under electrochemical potential and aging. The formation of decomposition layers [256–261], graphite exfoliation due to solvent cointercalation [91, 95, 258], corrosion of oxide surfaces [262–264], and shape changes

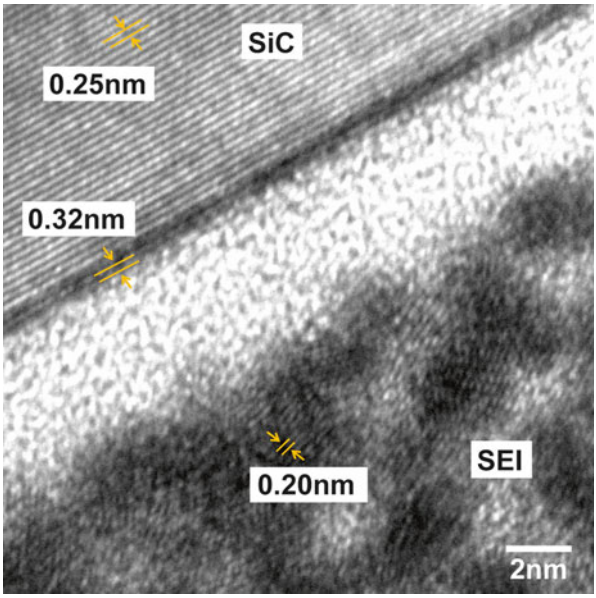

Fig. 7.14 Ex situ HRTEM near the surface of an epitaxial graphene film on a SiC [2 $1\bar{2}$ 0] substrate after cathodic polarization in a Li metal cell, showing the structure of the SiC, the graphene layers, and the solid electrolyte interphase (SEI) with LiF crystals. Reproduced with permission from [199]; copyright 2013, American Chemical Society

in lithium metal electrodes [252, 265] due to reactions with electrolyte components are representative examples of the kind of insight provided by SEM. Detection of backscattered electrons is possible in an SEM as well. Although no examples are available on this method of imaging of EEIs, it is worth noting that this method contains indirect elemental information, as backscattered electron intensity scales with the atomic number, *Z*.

Transmission electron microscopes (TEM) detect the electron beam scattered after crossing the sample. This beam carries structural as well as morphological information. For instance, direct atomic patterns can be related to a given crystal structure in some cases. As a result, TEM information is much richer than SEM. Detection technology has enabled imaging resolutions of several pm [266], although specimen requirements render this unattainable with the complex samples resulting from electrode–electrolyte interactions, especially when using liquid solvents. Consequently, and as stated above, TEM has so far been exclusively used in ex situ and postmortem analysis of EEIs. Nonetheless, very thin layers resulting from EEI interactions can be detected [267] and, in the right conditions, related to specific surface structure and chemistry of the electrode [196]. Its extremely high spatial resolution allows the observation of the morphology and the distribution of crystalline and amorphous components in electrode–electrolyte reaction layer; nanocrystals of LiF randomly embedded in a complex layer were thus directly observed (Fig. 7.14) [199].

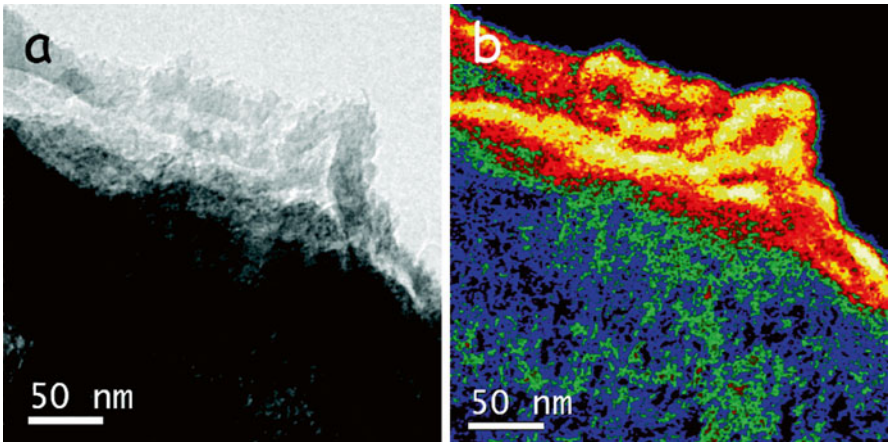

Fig. 7.15 Morphology of the solid electrolyte interphase formed on graphite particles discharged to 10 mV in a Li metal cell, and washed in the dimethyl carbonate; (**a**) bright field TEM image and (**b**) Li concentration map extracted from EELS data, viewed along the [0001] zone axis. Reproduced with permission from [271]; copyright 2011, American Chemical Society

7.10.3 Spectromicroscopy

Because the considerable compositional insight that can be obtained from both SEM and TEM imaging is not generally direct, coupling with spectroscopic information is desirable. The interaction of the primary electron beam with matter also leads to X-ray photoemission. Such X-ray photons are element specific, and can be collected at similar spatial resolutions to the imaging experiment, in what is referred to as electron dispersive X-ray spectroscopy (EDS, EDX, XEDS, depending on the manufacturer). The result of EDS imaging is an elemental map at the single particle (TEM) or ensemble (SEM) level. In the context of the characterization of EEIs, EDS is more commonly applied in SEM [251, 268–270] than TEM [198]. EDS can thus be viewed as a complement to the morphological information of secondary electron imaging.

Additional chemical information can be obtained in a TEM using electron energy loss spectroscopy (EELS). EELS results from measuring the energy lost by electrons after interaction with the sample. This energy value can be characteristic of the electronic processes, such as ionization, in a given element. Thus, like XAS, this tool directly probes the electronic structure around a given element, possessing both elemental and chemical specificity, combined with the very high spatial resolution of TEM. For instance, it has been used to locate specific compounds such as LiF in the complex layers that form the SEI on graphite (Fig. 7.15) [271, 272]. The main difficulty comes from sample preparation, as EELS demands even thinner samples than simple TEM imaging to lead to interpretable data that is not affected by multiple scattering effects.

7.11 Outlook

This chapter has made it apparent that the arsenal of tools available to electrochemists for the study of EEIs is immense. It is thanks to this arsenal that we possess the currently extensive knowledge of phenomena at these interfaces, especially in what refers to side reactions that affect the transfer of ionic charge. A lot less is known about the specific mechanisms that govern charge transfer, which involve the process of ion desolvation and creation of high energy intermediates between the stable states on each side of these heterogeneous interfaces, the specific timescales and, especially, how they are affected by the nature of the components and the interphase layers that may form. While the currently available tools should be suited to partly answer these questions, it is clear that more technical developments are still needed. There are frontiers in chemical and, particularly, space and time resolution that need to be crossed for the picture to be comprehensive. Chemical resolution will come from further improvements in specificity and selectivity of existing and new techniques. In the context of spatial resolution, exciting developments are in sight with the use of near field vibrational microscopy, which should combine the high chemical resolution of IR with spatial resolutions at the nanoscale [273]. Measuring in the near field, i.e., in close proximity to the sample, opens the door to truly specific measurements of near surface electrolyte species. Maps of reaction layers, potentially in all space dimensions, could thus be achieved. Continuous records in spatial resolution are reported in the field of X-ray microscopy [274], a tool that can be combined by XAS (see above) to produce pictures that include all components at the EEI, regardless of their nature. Increased insight into the dynamics of processes will be brought about by the continuous improvements in time resolution of our suite of tools. These are simply a few examples of the exciting future, but should not be considered by any means the only directions possible. The reader is challenged to design procedures to overcome the existing knowledge barriers.

While significant technical developments are in sight, it is important to keep in mind that, ultimately, truly representative data will come from careful experimental design. The experience of the last couple of decades has resulted in a large variety of methodologies. Given the complexity of EEIs, it is rather clear that a complete picture requires combining data from multiple tools [66, 275, 276], as, generally speaking, they are all sensitive to (slightly) different chemical moieties and physical phenomena. In this context, the generalization of multimodal techniques, where the sample is simultaneously analyzed by different tools, would be a welcome development in order to reduce uncertainty due to manipulation. It is worth noting the importance of interface preservation in ex situ measurements. Since most available tools are not specific to species at the interface, washing is required to remove the bulk electrolyte. This process needs to be carefully designed, as it has been shown to lead to misleading results [116], where irreversible changes are introduced by the time the data is collected. Ultimately, the best means to avoid uncertainty during sample manipulation is to perform *operando* studies, i.e., in working conditions. The supply of cell designs for simultaneous physico-chemical characterization and electrochemistry is sensational, as reviewed along this chapter. Researchers

continue to refine these designs in search for conditions that ensure that the data is representative of the conditions in a real battery. It is important to ensure that this condition is fulfilled. Some of these tools also require the preparation of model samples, where the surface morphological complexity is reduced. In this context, the emerging work with epitaxial films opens the door to very powerful measurements [196], which should continue to be pursued. Such highly oriented samples also help reduce chemical complexity and could be used to expand existing (but still too rare) systematic studies of the role of surface facets and defects on the electrolyte–electrode interactions [175], a series of research projects that could take lessons from the electrocatalysis field [277]. Given the large degree of understanding of water–solid interactions that this research generated, it is to be expected that much more information can still be collected of how nonaqueous systems operate.

Acknowledgements This overview was made possible by the support of the Assistant Secretary for Energy Efficiency and Renewable Energy, Office of Vehicle Technologies of the US Department of Energy, under Contract DE-AC02-05CH11231, as part of the Batteries for Advanced Transportation Technologies (BATT) Program. The program is managed by LBNL for the Department of Energy. Dr. Robert Kostecki is warmly acknowledged for his valuable insight into phenomena occurring at EEIs and for his mentorship.

References

1. Aurbach D. Review of selected electrode–solution interactions which determine the performance of Li and Li ion batteries, J. Power Sources 2000, 89, 206-218.
2. Broussely M., Biensan P., Bonhomme F., Blanchard P., Herreyre S., Nechev K., Staniewicz R. J. Main aging mechanisms in Li ion batteries, J. Power Sources 2005, 146, 90-96.
3. Xu K. Nonaqueous Liquid Electrolytes for Lithium-Based Rechargeable Batteries, Chem. Rev. 2004, 104, 4303-4418.
4. Andersson A. M., Abraham D. P., Haasch R., MacLaren S., Liu J., Amine K. Surface Characterization of Electrodes from High Power Lithium-Ion Batteries, J. Electrochem. Soc. 2002, 149, A1358-A1369.
5. Zhang S. S., Xu K., Jow T. R. EIS study on the formation of solid electrolyte interface in Li-ion battery, Electrochim. Acta 2006, 51, 1636-1640.
6. Paasch G., Micka K., Gersdorf P. Theory of the electrochemical impedance of macrohomogeneous porous electrodes, Electrochim. Acta 1993, 38, 2653-2662.
7. Zhuang Q.-C., Wei T., Du L.-L., Cui Y.-L., Fang L., Sun S.-G. An Electrochemical Impedance Spectroscopic Study of the Electronic and Ionic Transport Properties of Spinel $LiMn_2O_4$, J. Phys. Chem. C 2010, 114, 8614-8621.
8. Jow T. R., Marx M., Allen J. Distinguishing Li^+ Charge Transfer Kinetics at NCA/Electrolyte and Graphite/Electrolyte Interfaces, and NCA/Electrolyte and LFP/Electrolyte Interfaces in Li-Ion Cells, J. Electrochem. Soc. 2011, 159, A604-A612.
9. Kerlau M., Marcinek M., Srinivasan V., Kostecki R. M. Studies of local degradation phenomena in composite cathodes for lithium-ion batteries, Electrochim. Acta 2007, 52, 5422-5429.
10. Zheng H., Tan L., Liu G., Song X., Battaglia V. S. Calendering effects on the physical and electrochemical properties of $Li[Ni_{1/3}Mn_{1/3}Co_{1/3}]O_2$ cathode, J. Power Sources 2012, 208, 52-57.

11. Aurbach D., Zaban A. Impedance spectroscopy of lithium electrodes: Part 1. General behavior in propylene carbonate solutions and the correlation to surface chemistry and cycling efficiency, J. Electroanal. Chem. 1993, 348, 155-179.
12. Abraham D. P., Poppen S. D., Jansen A. N., Liu J., Dees D. W. Application of a lithium–tin reference electrode to determine electrode contributions to impedance rise in high-power lithium-ion cells, Electrochim. Acta 2004, 49, 4763-4775.
13. Verma P., Maire P., Novák P. A review of the features and analyses of the solid electrolyte interphase in Li-ion batteries, Electrochim. Acta 2010, 55, 6332-6341.
14. Buttry D. A., Ward M. D. Measurement of interfacial processes at electrode surfaces with the electrochemical quartz crystal microbalance, Chem. Rev. 1992, 92, 1355-1379.
15. Aurbach D., Zaban A. The Use of EQCM for the Study of Nonactive Metal Electrodes in Propylene Carbonate-$LiAsF_6$ Solutions: Significance of the Data Obtained, J. Electrochem. Soc. 1995, 142, L108-L111.
16. Kwon K., Evans J. W. Comparison between cyclic voltammetry and chronoamperometry when coupled with EQCM for the study of the SEI on a carbon film electrode, Electrochim. Acta 2004, 49, 867-872.
17. Larush-Asraf L., Biton M., Teller H., Zinigrad E., Aurbach D. On the electrochemical and thermal behavior of lithium bis(oxalato)borate (LiBOB) solutions, J. Power Sources 2007, 174, 400-407.
18. Wang F.-M., Shieh D.-T., Cheng J.-H., Yang C.-R. An investigation of the salt dissociation effects on solid electrolyte interface (SEI) formation using linear carbonate-based electrolytes in lithium ion batteries, Solid State Ionics 2010, 180, 1660-1666.
19. Ryu Y.-G., Lee S., Mah S., Lee D. J., Kwon K., Hwang S., Doo S. Electrochemical Behaviors of Silicon Electrode in Lithium Salt Solution Containing Alkoxy Silane Additives, J. Electrochem. Soc. 2008, 155, A583-A589.
20. Aurbach D., Moshkovich M. A Study of Lithium Deposition-Dissolution Processes in a Few Selected Electrolyte Solutions by Electrochemical Quartz Crystal Microbalance, J. Electrochem. Soc. 1998, 145, 2629-2639.
21. Li J.-T., Chen S.-R., Fan X.-Y., Huang L., Sun S.-G. Studies of the Interfacial Properties of an Electroplated Sn Thin Film Electrode/Electrolyte Using in Situ MFTIRS and EQCM, Langmuir 2007, 23, 13174-13180.
22. Kwon K., Evans J. W. Viscosity Changes of Li Battery Electrolytes and Their Long-Term Effect on the Frequency of EQCM Electrodes, Electrochem. Solid State Lett. 2002, 5, A59-A61.
23. Kwon K., Kong F., McLarnon F., Evans J. W. Characterization of the SEI on a Carbon Film Electrode by Combined EQCM and Spectroscopic Ellipsometry, J. Electrochem. Soc. 2003, 150, A229-A233.
24. Tavassol H., Buthker J. W., Ferguson G. A., Curtiss L. A., Gewirth A. A. Solvent Oligomerization during SEI Formation on Model Systems for Li-Ion Battery Anodes, J. Electrochem. Soc. 2012, 159, A730-A738.
25. Dass C. (2007) Fundamentals of contemporary mass spectrometry. 1st edn. John Wiley & Sons, Inc., Hoboken, NJ (USA).
26. NIST Mass Spectrometry Tools. http://chemdata.nist.gov/. Accessed August 2013
27. MassBank Project. http://www.massbank.jp/?lang=en. Accessed August 2013
28. Laruelle S., Pilard S., Guenot P., Grugeon S., Tarascon J.-M. Identification of Li-Based Electrolyte Degradation Products Through DEI and ESI High-Resolution Mass Spectrometry, J. Electrochem. Soc. 2004, 151, A1202-A1209.
29. Gireaud L., Grugeon S., Pilard S., Guenot P., Tarascon J.-M., Laruelle S. Mass Spectrometry Investigations on Electrolyte Degradation Products for the Development of Nanocomposite Electrodes in Lithium Ion Batteries, Anal. Chem. 2006, 78, 3688-3698.
30. Kominato A., Yasukawa E., Sato N., Ijuuin T., Asahina H., Mori S. Analysis of surface films on lithium in various organic electrolytes, J. Power Sources 1997, 68, 471-475.

31. Ota H., Sato T., Suzuki H., Usami T. TPD–GC/MS analysis of the solid electrolyte interface (SEI) on a graphite anode in the propylene carbonate/ethylene sulfite electrolyte system for lithium batteries, J. Power Sources 2001, 97–98, 107-113.
32. Ota H., Kominato A., Chun W.-J., Yasukawa E., Kasuya S. Effect of cyclic phosphate additive in non-flammable electrolyte, J. Power Sources 2003, 119–121, 393-398.
33. Zhao L., Watanabe I., Doi T., Okada S., Yamaki J.-i. TG-MS analysis of solid electrolyte interphase (SEI) on graphite negative-electrode in lithium-ion batteries, J. Power Sources 2006, 161, 1275-1280.
34. Doi T., Zhao L., Zhou M., Okada S., Yamaki J.-i. Quantitative studies on the thermal stability of the interface between graphite electrode and electrolyte, J. Power Sources 2008, 185, 1380-1385.
35. Doughty D. H., Roth E. P., Crafts C. C., Nagasubramanian G., Henriksen G., Amine K. Effects of additives on thermal stability of Li ion cells, J. Power Sources 2005, 146, 116-120.
36. von Sacken U., Nodwell E., Sundher A., Dahn J. R. Comparative thermal stability of carbon intercalation anodes and lithium metal anodes for rechargeable lithium batteries, J. Power Sources 1995, 54, 240-245.
37. Zhang Z., Fouchard D., Rea J. R. Differential scanning calorimetry material studies: implications for the safety of lithium-ion cells, J. Power Sources 1998, 70, 16-20.
38. Richard M. N., Dahn J. R. Accelerating Rate Calorimetry Study on the Thermal Stability of Lithium Intercalated Graphite in Electrolyte. I. Experimental, J. Electrochem. Soc. 1999, 146, 2068-2077.
39. Jiang J., Dahn J. R. Effects of solvents and salts on the thermal stability of LiC_6, Electrochim. Acta 2004, 49, 4599-4604.
40. McNair H. M., Miller J. M. (2009) Basic Gas Chromatography. 2nd edn. John Wiley & Sons, Inc., Hoboken, NJ (USA).
41. Yoshida H., Fukunaga T., Hazama T., Terasaki M., Mizutani M., Yamachi M. Degradation mechanism of alkyl carbonate solvents used in lithium-ion cells during initial charging, J. Power Sources 1997, 68, 311-315.
42. Kumai K., Miyashiro H., Kobayashi Y., Takei K., Ishikawa R. Gas generation mechanism due to electrolyte decomposition in commercial lithium-ion cell, J. Power Sources 1999, 81–82, 715-719.
43. Shin J.-S., Han C.-H., Jung U.-H., Lee S.-I., Kim H.-J., Kim K. Effect of Li_2CO_3 additive on gas generation in lithium-ion batteries, J. Power Sources 2002, 109, 47-52.
44. Kong W., Li H., Huang X., Chen L. Gas evolution behaviors for several cathode materials in lithium-ion batteries, J. Power Sources 2005, 142, 285-291.
45. Gachot G., Grugeon S., Eshetu G. G., Mathiron D., Ribière P., Armand M., Laruelle S. Thermal behaviour of the lithiated-graphite/electrolyte interface through GC/MS analysis, Electrochim. Acta 2012, 83, 402-409.
46. Eom J.-Y., Jung I.-H., Lee J.-H. Effects of vinylene carbonate on high temperature storage of high voltage Li-ion batteries, J. Power Sources 2011, 196, 9810-9814.
47. Ogumi Z., Sano A., Inaba M., Abe T. Pyrolysis/gas chromatography/mass spectroscopy analysis of the surface film formed on graphite negative electrode, J. Power Sources 2001, 97–98, 156-158.
48. Mogi R., Inaba M., Iriyama Y., Abe T., Ogumi Z. Study of the Decomposition of Propylene Carbonate on Lithium Metal Surface by Pyrolysis–Gas Chromatography–Mass Spectroscopy, Langmuir 2002, 19, 814-821.
49. Mogi R., Inaba M., Iriyama Y., Abe T., Ogumi Z. Study on the decomposition mechanism of alkyl carbonate on lithium metal by pyrolysis-gas chromatography-mass spectroscopy, J. Power Sources 2003, 119–121, 597-603.
50. Li W., Lucht B. L. Lithium-Ion Batteries: Thermal Reactions of Electrolyte with the Surface of Metal Oxide Cathode Particles, J. Electrochem. Soc. 2006, 153, A1617-A1625.
51. Gachot G., Ribière P., Mathiron D., Grugeon S., Armand M., Leriche J.-B., Pilard S., Laruelle S. Gas Chromatography/Mass Spectrometry As a Suitable Tool for the Li-Ion Battery Electrolyte Degradation Mechanisms Study, Anal. Chem. 2010, 83, 478-485.

52. Bazito F. F. C., Kawano Y., Torresi R. M. Synthesis and characterization of two ionic liquids with emphasis on their chemical stability towards metallic lithium, Electrochim. Acta 2007, 52, 6427-6437.
53. Amatucci G. G., Tarascon J. M., Klein L. C. Cobalt dissolution in $LiCoO_2$-based non-aqueous rechargeable batteries, Solid State Ionics 1996, 83, 167-173.
54. Blyr A., Sigala C., Amatucci G., Guyomard D., Chabre Y., Tarascon J. M. Self-Discharge of $LiMn_2O_4$/C Li-Ion Cells in Their Discharged State: Understanding by Means of Three-Electrode Measurements, J. Electrochem. Soc. 1998, 145, 194-209.
55. Zheng Z., Tang Z., Zhang Z., Shen W., Lin Y. Surface modification of $Li_{1.03}Mn_{1.97}O_4$ spinels for improved capacity retention, Solid State Ionics 2002, 148, 317-321.
56. Aurbach D., Markovsky B., Salitra G., Markevich E., Talyossef Y., Koltypin M., Nazar L., Ellis B., Kovacheva D. Review on electrode–electrolyte solution interactions, related to cathode materials for Li-ion batteries, J. Power Sources 2007, 165, 491-499.
57. Zheng H., Sun Q., Liu G., Song X., Battaglia V. S. Correlation between dissolution behavior and electrochemical cycling performance for $LiNi_{1/3}Co_{1/3}Mn_{1/3}O_2$-based cells, J. Power Sources 2012, 207, 134-140.
58. Hanton S. D. Mass Spectrometry of Polymers and Polymer Surfaces, Chem. Rev. 2001, 101, 527-570.
59. Pisonero J., Fernandez B., Gunther D. Critical revision of GD-MS, LA-ICP-MS and SIMS as inorganic mass spectrometric techniques for direct solid analysis, J. Anal. At. Spectrom. 2009, 24, 1145-1160.
60. Urbassek H. M. (2008) Sputtering and Laser Ablation. In: Hasselbrink E., Lundqvist B. I. (eds) Handbook of Surface Science, vol 3. Elsevier, Amsterdam (Netherlands), pp 871-913.
61. Yu B.-Y., Lin W.-C., Wang W.-B., Iida S.-i., Chen S.-Z., Liu C.-Y., Kuo C.-H., Lee S.-H., Kao W.-L., Yen G.-J., You Y.-W., Liu C.-P., Jou J.-H., Shyue J.-J. Effect of Fabrication Parameters on Three-Dimensional Nanostructures of Bulk Heterojunctions Imaged by High-Resolution Scanning ToF-SIMS, ACS Nano 2010, 4, 833-840.
62. Busch K. L., Hsu B. H., Xie Y. X., Cooks R. G. Matrix effects in secondary ion mass spectrometry, Anal. Chem. 1983, 55, 1157-1160.
63. Pereira-Nabais C., Światowska J., Chagnes A., Ozanam F., Gohier A., Tran-Van P., Cojocaru C.-S., Cassir M., Marcus P. Interphase chemistry of Si electrodes used as anodes in Li-ion batteries, Appl. Surf. Sci. 2013, 266, 5-16.
64. Ota H., Akai T., Namita H., Yamaguchi S., Nomura M. XAFS and TOF–SIMS analysis of SEI layers on electrodes, J. Power Sources 2003, 119–121, 567-571.
65. Wang J., Yang J., Tang Y., Li R., Liang G., Sham T.-K., Sun X. Surface aging at olivine $LiFePO_4$: a direct visual observation of iron dissolution and the protection role of nano-carbon coating, J. Mater. Chem. A 2013, 1, 1579-1586.
66. Li J.-T., Maurice V., Swiatowska-Mrowiecka J., Seyeux A., Zanna S., Klein L., Sun S.-G., Marcus P. XPS, time-of-flight-SIMS and polarization modulation IRRAS study of Cr_2O_3 thin film materials as anode for lithium ion battery, Electrochim. Acta 2009, 54, 3700-3707.
67. Li J.-T., Swiatowska J., Seyeux A., Huang L., Maurice V., Sun S.-G., Marcus P. XPS and ToF-SIMS study of Sn–Co alloy thin films as anode for lithium ion battery, J. Power Sources 2010, 195, 8251-8257.
68. Li J.-T., Światowska J., Maurice V., Seyeux A., Huang L., Sun S.-G., Marcus P. XPS and ToF-SIMS Study of Electrode Processes on Sn–Ni Alloy Anodes for Li-Ion Batteries, J. Phys. Chem. C 2011, 115, 7012-7018.
69. Walker E. K., Vanden Bout D. A., Stevenson K. J. Spectroelectrochemical Investigation of an Electrogenerated Graphitic Oxide Solid–Electrolyte Interphase, Anal. Chem. 2012, 84, 8190-8197.
70. Peled E., Bar Tow D., Merson A., Gladkich A., Burstein L., Golodnitsky D. Composition, depth profiles and lateral distribution of materials in the SEI built on HOPG: ToF-SIMS and XPS studies, J. Power Sources 2001, 97–98, 52-57.
71. Peled E., Golodnitsky D., Ulus A., Yufit V. Effect of carbon substrate on SEI composition and morphology, Electrochim. Acta 2004, 50, 391-395.

72. Shi S., Lu P., Liu Z., Qi Y., Hector L. G., Li H., Harris S. J. Direct Calculation of Li-Ion Transport in the Solid Electrolyte Interphase, J. Am. Chem. Soc. 2012, 134, 15476-15487.
73. Yin J., Wada M., Yamamoto K., Kitano Y., Tanase S., Sakai T. Micrometer-Scale Amorphous Si Thin-Film Electrodes Fabricated by Electron-Beam Deposition for Li-Ion Batteries, J. Electrochem. Soc. 2006, 153, A472-A477.
74. Saito Y., Rahman M. K. Investigation of positive electrodes after cycle testing of high-power Li-ion battery cells IV: An approach to the power fading mechanism by depth profile analysis of electrodes using glow discharge optical emission spectroscopy, J. Power Sources 2007, 174, 877-882.
75. Takahara H., Miyauchi H., Tabuchi M., Nakamura T. Elemental Distribution Analysis of $LiFePO_4$/Graphite Cells Studied with Glow Discharge Optical Emission Spectroscopy (GD-OES), J. Electrochem. Soc. 2013, 160, A272-A278.
76. Shimizu K., Habazaki H., Skeldon P., Thompson G. E. Radiofrequency GD-OES: a powerful technique for depth profiling analysis of thin films, Surf. Interface Anal. 2003, 35, 564-574.
77. Zorba V., Syzdek J., Mao X., Russo R. E., Kostecki R. Ultrafast laser induced breakdown spectroscopy of electrode/electrolyte interfaces, Appl. Phys. Lett. 2012, 100, 234101.
78. Nishi T., Sakka T., Oguchi H., Fukami K., Ogata Y. H. In Situ Electrode Surface Analysis by Laser-Induced Breakdown Spectroscopy, J. Electrochem. Soc. 2008, 155, F237-F240.
79. Baltruschat H. Differential electrochemical mass spectrometry, J. Am. Soc. Mass Spectrom. 2004, 15, 1693-1706.
80. Imhof R., Novák P. In Situ Investigation of the Electrochemical Reduction of Carbonate Electrolyte Solutions at Graphite Electrodes, J. Electrochem. Soc. 1998, 145, 1081-1087.
81. Hambitzer G., Joos M., Schriever U. Volatile products of electrode reactions in inorganic electrolyte, J. Power Sources 1993, 44, 727-732.
82. Imhof R., Novák P. Oxidative Electrolyte Solvent Degradation in Lithium-Ion Batteries: An In Situ Differential Electrochemical Mass Spectrometry Investigation, J. Electrochem. Soc. 1999, 146, 1702-1706.
83. Wagner M. R., Raimann P. R., Trifonova A., Moeller K.-C., Besenhard J. O., Winter M. Electrolyte Decomposition Reactions on Tin- and Graphite-Based Anodes are Different, Electrochem. Solid State Lett. 2004, 7, A201-A205.
84. Wagner M. R., Raimann P. R., Trifonova A., Möller K. C., Besenhard J. O., Winter M. Dilatometric and mass spectrometric investigations on lithium ion battery anode materials, Anal. Bioanal. Chem. 2004, 379, 272-276.
85. Ufheil J., Würsig A., Schneider O. D., Novák P. Acetone as oxidative decomposition product in propylene carbonate containing battery electrolyte, Electrochem. Commun. 2005, 7, 1380-1384.
86. Holzapfel M., Buqa H., Hardwick L. J., Hahn M., Würsig A., Scheifele W., Novák P., Kötz R., Veit C., Petrat F.-M. Nano silicon for lithium-ion batteries, Electrochim. Acta 2006, 52, 973-978.
87. La Mantia F., Novák P. Online Detection of Reductive CO_2 Development at Graphite Electrodes in the 1 M $LiPF_6$, EC:DMC Battery Electrolyte, Electrochem. Solid State Lett. 2008, 11, A84-A87.
88. Lanz M., Novák P. DEMS study of gas evolution at thick graphite electrodes for lithium-ion batteries: the effect of γ-butyrolactone, J. Power Sources 2001, 102, 277-282.
89. Spahr M. E., Palladino T., Wilhelm H., Würsig A., Goers D., Buqa H., Holzapfel M., Novák P. Exfoliation of Graphite during Electrochemical Lithium Insertion in Ethylene Carbonate-Containing Electrolytes, J. Electrochem. Soc. 2004, 151, A1383-A1395.
90. Ufheil J., Baertsch M. C., Würsig A., Novák P. Maleic anhydride as an additive to γ-butyrolactone solutions for Li-ion batteries, Electrochim. Acta 2005, 50, 1733-1738.
91. Buqa H., Würsig A., Vetter J., Spahr M. E., Krumeich F., Novák P. SEI film formation on highly crystalline graphitic materials in lithium-ion batteries, J. Power Sources 2006, 153, 385-390.
92. Vetter J., Holzapfel M., Wuersig A., Scheifele W., Ufheil J., Novák P. In situ study on CO_2 evolution at lithium-ion battery cathodes, J. Power Sources 2006, 159, 277-281.

93. Holzapfel M., Würsig A., Scheifele W., Vetter J., Novák P. Oxygen, hydrogen, ethylene and CO_2 development in lithium-ion batteries, J. Power Sources 2007, 174, 1156-1160.
94. Zheng J. M., Zhang Z. R., Wu X. B., Dong Z. X., Zhu Z., Yang Y. The Effects of AlF_3 Coating on the Performance of $Li[Li_{0.2}Mn_{0.54}Ni_{0.13}Co_{0.13}]O_2$ Positive Electrode Material for Lithium-Ion Battery, J. Electrochem. Soc. 2008, 155, A775-A782.
95. Märkle W., Lu C.-Y., Novák P. Morphology of the Solid Electrolyte Interphase on Graphite in Dependency on the Formation Current, J. Electrochem. Soc. 2011, 158, A1478-A1482.
96. McCloskey B. D., Bethune D. S., Shelby R. M., Girishkumar G., Luntz A. C. Solvents' Critical Role in Nonaqueous Lithium–Oxygen Battery Electrochemistry, J. Phys. Chem. Lett. 2011, 2, 1161-1166.
97. McCloskey B. D., Bethune D. S., Shelby R. M., Mori T., Scheffler R., Speidel A., Sherwood M., Luntz A. C. Limitations in Rechargeability of Li-O_2 Batteries and Possible Origins, J. Phys. Chem. Lett. 2012, 3, 3043-3047.
98. McCloskey B. D., Speidel A., Scheffler R., Miller D. C., Viswanathan V., Hummelshøj J. S., Nørskov J. K., Luntz A. C. Twin Problems of Interfacial Carbonate Formation in Nonaqueous Li–O_2 Batteries, J. Phys. Chem. Lett. 2012, 3, 997-1001.
99. McCloskey B. D., Scheffler R., Speidel A., Girishkumar G., Luntz A. C. On the Mechanism of Nonaqueous Li–O_2 Electrochemistry on C and Its Kinetic Overpotentials: Some Implications for Li–Air Batteries, J. Phys. Chem. C 2012, 116, 23897-23905.
100. Socrates G. (2004) Infrared and Raman Characteristic Group Frequencies: Tables and Charts. 3rd edn. John Wiley & Sons, Inc., Hoboken, NJ (USA).
101. Griffiths P., De Haseth J. A. (2007) Fourier Transform Infrared Spectrometry. 2nd edn. John Wiley & Sons, Inc., Hoboken, NJ (USA).
102. Chabal Y. J. Surface infrared spectroscopy, Surf. Sci. Rep. 1988, 8, 211-357.
103. Iwasita T., Nart F. C. In situ infrared spectroscopy at electrochemical interfaces, Prog. Surf. Sci. 1997, 55, 271-340.
104. Trenary M. Reflection absorption infrared spectroscopy and the structure of molecular adsorbates on metal surfaces, Annu. Rev. Phys. Chem. 2000, 51, 381-403.
105. Amalraj S. F., Aurbach D. The use of in situ techniques in R&D of Li and Mg rechargeable batteries, J. Solid State Electrochem. 2011, 15, 877-890.
106. Li J.-T., Zhou Z.-Y., Broadwell I., Sun S.-G. In-Situ Infrared Spectroscopic Studies of Electrochemical Energy Conversion and Storage, Acc. Chem. Res. 2012, 45, 485-494.
107. Aurbach D., Weissman I., Zaban A., Chusid O. Correlation between surface chemistry, morphology, cycling efficiency and interfacial properties of Li electrodes in solutions containing different Li salts, Electrochim. Acta 1994, 39, 51-71.
108. Yazami R. Surface chemistry and lithium storage capability of the graphite–lithium electrode, Electrochim. Acta 1999, 45, 87-97.
109. Winter M., Imhof R., Joho F., Novák P. FTIR and DEMS investigations on the electroreduction of chloroethylene carbonate-based electrolyte solutions for lithium-ion cells, J. Power Sources 1999, 81–82, 818-823.
110. Ostrovskii D., Ronci F., Scrosati B., Jacobsson P. A FTIR and Raman study of spontaneous reactions occurring at the $LiNi_yCo_{(1-y)}O_2$ electrode/non-aqueous electrolyte interface, J. Power Sources 2001, 94, 183-188.
111. Zhang X., Kostecki R., Richardson T. J., Pugh J. K., Ross P. N. Electrochemical and Infrared Studies of the Reduction of Organic Carbonates, J. Electrochem. Soc. 2001, 148, A1341-A1345.
112. Zhuang G. V., Ross P. N. Analysis of the Chemical Composition of the Passive Film on Li-Ion Battery Anodes Using Attentuated Total Reflection Infrared Spectroscopy, Electrochem. Solid State Lett. 2003, 6, A136-A139.
113. Kang S. H., Abraham D. P., Xiao A., Lucht B. L. Investigating the solid electrolyte interphase using binder-free graphite electrodes, J. Power Sources 2008, 175, 526-532.
114. Nguyen C. C., Song S.-W. Interfacial structural stabilization on amorphous silicon anode for improved cycling performance in lithium-ion batteries, Electrochim. Acta 2010, 55, 3026-3033.

115. Norberg N. S., Kostecki R. Interfacial Phenomena at a Composite $LiMnPO_4$ Cathode, J. Electrochem. Soc. 2012, 159, A1091-A1094.
116. Song S.-W., Zhuang G. V., Ross P. N. Surface Film Formation on $LiNi_{0.8}Co_{0.15}Al_{0.05}O_2$ Cathodes Using Attenuated Total Reflection IR Spectroscopy, J. Electrochem. Soc. 2004, 151, A1162-A1167.
117. Zhuang G. V., Xu K., Yang H., Jow T. R., Ross P. N. Lithium Ethylene Dicarbonate Identified as the Primary Product of Chemical and Electrochemical Reduction of EC in 1.2 M $LiPF_6$/EC:EMC Electrolyte, J. Phys. Chem. B 2005, 109, 17567-17573.
118. Zhuang G. V., Yang H., Ross P. N., Xu K., Jow T. R. Lithium Methyl Carbonate as a Reaction Product of Metallic Lithium and Dimethyl Carbonate, Electrochem. Solid State Lett. 2006, 9, A64-A68.
119. Goren E., Chusid O., Aurbach D. The Application of In Situ FTIR Spectroscopy to the Study of Surface Films Formed on Lithium and Noble Metals at Low Potentials in Li Battery Electrolytes, J. Electrochem. Soc. 1991, 138, L6-L9.
120. Aurbach D., Chusid O. In situ FTIR Spectroelectrochemical Studies of Surface Films Formed on Li and Nonactive Electrodes at Low Potentials in Li Salt Solutions Containing CO_2, J. Electrochem. Soc. 1993, 140, L155-L157.
121. Morigaki K.-i. In situ analysis of the interfacial reactions between MCMB electrode and organic electrolyte solutions, J. Power Sources 2002, 103, 253-264.
122. Matsui M., Dokko K., Kanamura K. Surface Layer Formation and Stripping Process on $LiMn_2O_4$ and $LiNi_{1/2}Mn_{3/2}O_4$ Thin Film Electrodes, J. Electrochem. Soc. 2010, 157, A121-A129.
123. Barusseau S., Beden B., Broussely M., Perton F. The use of polarized light in the infrared reflectance spectroscopic investigation of the lithium-organic electrolyte interface, J. Power Sources 1995, 54, 296-300.
124. Raman C. V. A new radiation, Ind. J. Phys. 1928, 2, 387-398.
125. Landsberg G., Mandelstam L. Eine neue Erscheinung bei der Lichtzerstreuung in Krystallen, Naturwissenschaften 1928, 16, 557-558.
126. Baddour-Hadjean R., Pereira-Ramos J.-P. Raman Microspectrometry Applied to the Study of Electrode Materials for Lithium Batteries, Chem. Rev. 2009, 110, 1278-1319.
127. Nie S., Emory S. R. Probing Single Molecules and Single Nanoparticles by Surface-Enhanced Raman Scattering, Science 1997, 275, 1102-1106.
128. Iwamoto R., Miya M., Ohta K., Mima S. Total internal reflection Raman spectroscopy, J. Chem. Phys. 1981, 74, 4780-4790.
129. Kostecki R., McLarnon F. Local-Probe Studies of Degradation of Composite $LiNi_{0.8}Co_{0.15}Al_{0.05}O_2$ Cathodes in High-Power Lithium-Ion Cells, Electrochem. Solid State Lett. 2004, 7, A380-A383.
130. Lei J., McLarnon F., Kostecki R. In Situ Raman Microscopy of Individual $LiNi_{0.8}Co_{0.15}Al_{0.05}O_2$ Particles in a Li-Ion Battery Composite Cathode, J. Phys. Chem. B 2004, 109, 952-957.
131. Kostecki R., Lei J., McLarnon F., Shim J., Striebel K. Diagnostic Evaluation of Detrimental Phenomena in High-Power Lithium-Ion Batteries, J. Electrochem. Soc. 2006, 153, A669-A672.
132. Eriksson T., Andersson A. M., Bishop A. G., Gejke C., Gustafsson T., Thomas J. O. Surface Analysis of $LiMn_2O_4$ Electrodes in Carbonate-Based Electrolytes, J. Electrochem. Soc. 2002, 149, A69-A78.
133. Abouimrane A., Odom S. A., Tavassol H., Schulmerich M. V., Wu H., Bhargava R., Gewirth A. A., Moore J. S., Amine K. 3-Hexylthiophene as a Stabilizing Additive for High Voltage Cathodes in Lithium-Ion Batteries, J. Electrochem. Soc. 2013, 160, A268-A271.
134. Matsuo Y., Kostecki R., McLarnon F. Surface Layer Formation on Thin-Film $LiMn_2O_4$ Electrodes at Elevated Temperatures, J. Electrochem. Soc. 2001, 148, A687-A692.
135. Schmitz R., Ansgar Müller R., Wilhelm Schmitz R., Schreiner C., Kunze M., Lex-Balducci A., Passerini S., Winter M. SEI investigations on copper electrodes after lithium plating with Raman spectroscopy and mass spectrometry, J. Power Sources 2013, 233, 110-114.
136. Irish D. E., Deng Z., Odziemkowski M. Raman spectroscopic and electrochemical studies of lithium battery components, J. Power Sources 1995, 54, 28-33.

137. Deng Z., Irish D. E. Surface-Enhanced Raman Scattering from Silver Electrode Surfaces in Contact with Solutions of $LiAsF_6$+Tetramethylammonium Bromide/Methyl Acetate, Langmuir 1994, 10, 586-591.
138. Li H., Mo Y., Pei N., Xu X., Huang X., Chen L. Surface-Enhanced Raman Scattering Study on Passivating Films of Ag Electrodes in Lithium Batteries†, J. Phys. Chem. B 2000, 104, 8477-8480.
139. Li G., Li H., Mo Y., Chen L., Huang X. Further identification to the SEI film on Ag electrode in lithium batteries by surface enhanced Raman scattering (SERS), J. Power Sources 2002, 104, 190-194.
140. Huang W., Frech R. In Situ Raman Studies of Graphite Surface Structures during Lithium Electrochemical Intercalation, J. Electrochem. Soc. 1998, 145, 765-770.
141. Kostecki R., McLarnon F. Microprobe study of the effect of Li intercalation on the structure of graphite, J. Power Sources 2003, 119–121, 550-554.
142. Hardwick L. J., Buqa H., Novák P. Graphite surface disorder detection using in situ Raman microscopy, Solid State Ionics 2006, 177, 2801-2806.
143. Markevich E., Baranchugov V., Salitra G., Aurbach D., Schmidt M. A. Behavior of Graphite Electrodes in Solutions Based on Ionic Liquids in In Situ Raman Studies, J. Electrochem. Soc. 2008, 155, A132-A137.
144. Baranchugov V., Markevich E., Salitra G., Aurbach D., Semrau G., Schmidt M. A. In Situ Raman Spectroscopy Study of Different Kinds of Graphite Electrodes in Ionic Liquid Electrolytes, J. Electrochem. Soc. 2008, 155, A217-A227.
145. Sethuraman V. A., Hardwick L. J., Srinivasan V., Kostecki R. Surface structural disordering in graphite upon lithium intercalation/deintercalation, J. Power Sources 2010, 195, 3655-3660.
146. Hintennach A., Novák P. A novel combinative Raman and SEM mapping method for the detection of exfoliation of graphite in electrodes at very positive potentials, J. Raman Spectrosc. 2011, 42, 1754-1760.
147. Nakagawa H., Domi Y., Doi T., Ochida M., Tsubouchi S., Yamanaka T., Abe T., Ogumi Z. In situ Raman study on degradation of edge plane graphite negative-electrodes and effects of film-forming additives, J. Power Sources 2012, 206, 320-324.
148. Lai Y., Cao Z., Song H., Zhang Z., Chen X., Lu H., Jia M., Li J. Influence of Fe (II) Species in Electrolyte on Performance of Graphite Anode for Lithium-Ion Batteries, J. Electrochem. Soc. 2012, 159, A1961-A1966.
149. Aurbach D., Markovsky B., Talyossef Y., Salitra G., Kim H.-J., Choi S. Studies of cycling behavior, ageing, and interfacial reactions of $LiNi_{0.5}Mn_{1.5}O_4$ and carbon electrodes for lithium-ion 5-V cells, J. Power Sources 2006, 162, 780-789.
150. Jeong S.-K., Inaba M., Iriyama Y., Abe T., Ogumi Z. Surface film formation on a graphite negative electrode in lithium-ion batteries: AFM study on the effects of co-solvents in ethylene carbonate-based solutions, Electrochim. Acta 2002, 47, 1975-1982.
151. Yamada Y., Koyama Y., Abe T., Ogumi Z. Correlation between Charge−Discharge Behavior of Graphite and Solvation Structure of the Lithium Ion in Propylene Carbonate-Containing Electrolytes, J. Phys. Chem. C 2009, 113, 8948-8953.
152. Zheng H., Liu G., Battaglia V. Film-Forming Properties of Propylene Carbonate in the Presence of a Quaternary Ammonium Ionic Liquid on Natural Graphite Anode, J. Phys. Chem. C 2010, 114, 6182-6189.
153. Yeager H. L., Fedyk J. D., Parker R. J. Spectroscopic studies of ionic solvation in propylene carbonate, J. Phys. Chem. 1973, 77, 2407-2410.
154. Morita M., Asai Y., Yoshimoto N., Ishikawa M. A Raman spectroscopic study of organic electrolyte solutions based on binary solvent systems of ethylene carbonate with low viscosity solvents which dissolve different lithium salts, J. Chem. Soc., Faraday Trans. 1998, 94, 3451-3456.
155. Ostrovskii D., Torell L. M., Battista Appetecchi G., Scrosati B. An electrochemical and Raman spectroscopical study of gel polymer electrolytes for lithium batteries, Solid State Ionics 1998, 106, 19-24.

156. Kato Y., Ishihara T., Uchimoto Y., Wakihara M. Charge-Transfer Reaction Rate of Li^+/Li Couple in Poly(ethylene glycol) Dimethyl Ether Based Electrolytes, J. Phys. Chem. B 2004, 108, 4794-4798.
157. Novák P., Panitz J. C., Joho F., Lanz M., Imhof R., Coluccia M. Advanced in situ methods for the characterization of practical electrodes in lithium-ion batteries, J. Power Sources 2000, 90, 52-58.
158. Panitz J.-C., Novák P., Haas O. Raman Microscopy Applied to Rechargeable Lithium-Ion Cells - Steps Towards in Situ Raman Imaging with Increased Optical Efficiency, Appl. Spectrosc. 2001, 55, 1131-1137.
159. Howlett P. C., MacFarlane D. R., Hollenkamp A. F. A sealed optical cell for the study of lithium-electrodelelectrolyte interfaces, J. Power Sources 2003, 114, 277-284.
160. Dokko K., Shi Q., Stefan I. C., Scherson D. A. In Situ Raman Spectroscopy of Single Microparticle Li^+−Intercalation Electrodes, J. Phys. Chem. B 2003, 107, 12549-12554.
161. Novák P., Goers D., Hardwick L., Holzapfel M., Scheifele W., Ufheil J., Würsig A. Advanced in situ characterization methods applied to carbonaceous materials, J. Power Sources 2005, 146, 15-20.
162. Itoh T., Anzue N., Mohamedi M., Hisamitsu Y., Umeda M., Uchida I. Spectroelectrochemical studies on highly polarized $LiCoO_2$ electrode in organic solutions, Electrochem. Commun. 2000, 2, 743-748.
163. Naudin C., Bruneel J. L., Chami M., Desbat B., Grondin J., Lassègues J. C., Servant L. Characterization of the lithium surface by infrared and Raman spectroscopies, J. Power Sources 2003, 124, 518-525.
164. Norberg N. S., Lux S. F., Kostecki R. Interfacial Side-Reactions at a $LiNi_{0.5}Mn_{1.5}O_4$ Electrode in Organic Carbonate-Based Electrolytes, Electrochem. Commun. 2013, 34, 29–32.
165. Odziemkowski M., Krell M., Irish D. E. A Raman Microprobe In Situ and Ex Situ Study of Film Formation at Lithium/Organic Electrolyte Interfaces, J. Electrochem. Soc. 1992, 139, 3052-3063.
166. Richardson T. J., Ross P. N. In situ UV–visible spectroscopy: characterization of overcharge protection additives for secondary lithium batteries, J. Power Sources 1999, 84, 1-5.
167. McArthur M. A., Trussler S., Dahn J. R. In Situ Investigations of SEI Layer Growth on Electrode Materials for Lithium-Ion Batteries Using Spectroscopic Ellipsometry, J. Electrochem. Soc. 2012, 159, A198-A207.
168. Kim K. J., Lee J. H. Effects of nickel doping on structural and optical properties of spinel lithium manganate thin films, Solid State Commun. 2007, 141, 99-103.
169. Kostecki R., Kong F., Matsuo Y., McLarnon F. Interfacial studies of a thin-film $Li_2Mn_4O_9$ electrode, Electrochim. Acta 1999, 45, 225-233.
170. Zhuang G., Ross P. N., Kong F., McLarnon F. The Reaction of Clean Li Surfaces with Small Molecules in Ultrahigh Vacuum: II. Water, J. Electrochem. Soc. 1998, 145, 159-164.
171. Lux S. F., Lucas I. T., Pollak E., Passerini S., Winter M., Kostecki R. The mechanism of HF formation in $LiPF_6$ based organic carbonate electrolytes, Electrochem. Commun. 2012, 14, 47-50.
172. Kong F., Kim J., Song X., Inaba M., Kinoshita K., McLarnon F. Exploratory Studies of the Carbon/Nonaqueous Electrolyte Interface by Electrochemical and In Situ Ellipsometry Measurements, Electrochem. Solid State Lett. 1998, 1, 39-41.
173. Kong F., McLarnon F. Spectroscopic ellipsometry of lithium/polymer electrolyte interfaces, J. Power Sources 2000, 89, 180-189.
174. Kong F., Kostecki R., Nadeau G., Song X., Zaghib K., Kinoshita K., McLarnon F. In situ studies of SEI formation, J. Power Sources 2001, 97–98, 58-66.
175. Lucas I. T., Syzdek J., Kostecki R. Interfacial processes at single-crystal β-Sn electrodes in organic carbonate electrolytes, Electrochem. Commun. 2011, 13, 1271-1275.
176. Nilsson A. Applications of core level spectroscopy to adsorbates, J. Electron. Spectrosc. 2002, 126, 3-42.
177. Hufner S. (2003) Photoelectron Spectroscopy. Advanced Texts in Physics, 3rd edn. Springer, Berlin.

178. Bryngelsson H., Stjerndahl M., Gustafsson T., Edström K. How dynamic is the SEI?, J. Power Sources 2007, 174, 970-975.
179. Martha S. K., Sclar H., Szmuk Framowitz Z., Kovacheva D., Saliyski N., Gofer Y., Sharon P., Golik E., Markovsky B., Aurbach D. A comparative study of electrodes comprising nanometric and submicron particles of $LiNi_{0.50}Mn_{0.50}O_2$, $LiNi_{0.33}Mn_{0.33}Co_{0.33}O_2$, and $LiNi_{0.40}Mn_{0.40}Co_{0.20}O_2$ layered compounds, J. Power Sources 2009, 189, 248-255.
180. Yang L., Ravdel B., Lucht B. L. Electrolyte Reactions with the Surface of High Voltage $LiNi_{0.5}Mn_{1.5}O_4$ Cathodes for Lithium-Ion Batteries, Electrochem. Solid State Lett. 2010, 13, A95-A97.
181. Lu Y.-C., Mansour A. N., Yabuuchi N., Shao-Horn Y. Probing the Origin of Enhanced Stability of "$AlPO_4$" Nanoparticle Coated $LiCoO_2$ during Cycling to High Voltages: Combined XRD and XPS Studies, Chem. Mater. 2009, 21, 4408-4424.
182. Dedryvère R., Martinez H., Leroy S., Lemordant D., Bonhomme F., Biensan P., Gonbeau D. Surface film formation on electrodes in a $LiCoO_2$/graphite cell: A step by step XPS study, J. Power Sources 2007, 174, 462-468.
183. Philippe B., Dedryvère R., Gorgoi M., Rensmo H., Gonbeau D., Edström K. Role of the $LiPF_6$ Salt for the Long-Term Stability of Silicon Electrodes in Li-Ion Batteries – A Photoelectron Spectroscopy Study, Chem. Mater. 2013, 25, 394-404.
184. Philippe B., Dedryvère R., Allouche J., Lindgren F., Gorgoi M., Rensmo H., Gonbeau D., Edström K. Nanosilicon Electrodes for Lithium-Ion Batteries: Interfacial Mechanisms Studied by Hard and Soft X-ray Photoelectron Spectroscopy, Chem. Mater. 2012, 24, 1107-1115.
185. Shikano M., Kobayashi H., Koike S., Sakaebe H., Ikenaga E., Kobayashi K., Tatsumi K. Investigation of positive electrodes after cycle testing of high-power Li-ion battery cells II: An approach to the power fading mechanism using hard X-ray photoemission spectroscopy, J. Power Sources 2007, 174, 795-799.
186. Takanashi Y., Orikasa Y., Mogi M., Oishi M., Murayama H., Sato K., Yamashige H., Takamatsu D., Fujimoto T., Tanida H., Arai H., Ohta T., Matsubara E., Uchimoto Y., Ogumi Z. Thickness estimation of interface films formed on $Li_{1-x}CoO_2$ electrodes by hard X-ray photoelectron spectroscopy, J. Power Sources 2011, 196, 10679-10685.
187. Fister T. T., Schmidt M., Fenter P., Johnson C. S., Slater M. D., Chan M. K. Y., Shirley E. L. Electronic structure of lithium battery interphase compounds: Comparison between inelastic x-ray scattering measurements and theory, J. Chem. Phys. 2011, 135, 224513-224515.
188. Thompson A. C., Attwood D. T., Gullikson E. M., Howells M. R., Kortright J. B., Robinson A. L., Underwood J. H., Kim K.-J., Kirz J., Lindau I., Pianetta P., Winick H., Williams G. P., Scofield J. H. (2009) X-ray data booklet. 3rd edn. Lawrence Berkeley National Laboratory, Berkeley, CA (USA).
189. Augustsson A., Herstedt M., Guo J. H., Edstrom K., Zhuang G. V., Ross J. P. N., Rubensson J. E., Nordgren J. Solid electrolyte interphase on graphite Li-ion battery anodes studied by soft X-ray spectroscopy, Phys. Chem. Chem. Phys. 2004, 6, 4185-4189.
190. Akai T., Ota H., Namita H., Yamaguchi S., Nomura M. XANES study on solid electrolyte interface of Li ion battery, Phys. Scr. 2005, 2005, 408-411.
191. Kobayashi H., Emura S., Arachi Y., Tatsumi K. Investigation of inorganic compounds on the surface of cathode materials using Li and O K-edge XANES, J. Power Sources 2007, 174, 774-778.
192. Balasubramanian M., Lee H. S., Sun X., Yang X. Q., Moodenbaugh A. R., McBreen J., Fischer D. A., Fu Z. Formation of SEI on Cycled Lithium-Ion Battery Cathodes: Soft X-Ray Absorption Study, Electrochem. Solid State Lett. 2002, 5, A22-A25.
193. Choi H. C., Kim S. B., Jung Y. M. Application of soft X-ray absorption spectroscopy and two-dimensional correlation spectroscopy to the electrochemical reaction in the $Li_{1+x}V_3O_8$/Li cell, J. Mol. Struct. 2006, 799, 91-95.
194. Yoon W.-S., Balasubramanian M., Chung K. Y., Yang X.-Q., McBreen J., Grey C. P., Fischer D. A. Investigation of the Charge Compensation Mechanism on the Electrochemically Li-Ion

Deintercalated $Li_{1-x}Co_{1/3}Ni_{1/3}Mn_{1/3}O_2$ Electrode System by Combination of Soft and Hard X-ray Absorption Spectroscopy, J. Am. Chem. Soc. 2005, 127, 17479-17487.
195. Sakamoto K., Hirayama M., Sonoyama N., Mori D., Yamada A., Tamura K., Mizuki J. i., Kanno R. Surface Structure of $LiNi_{0.8}Co_{0.2}O_2$: a New Experimental Technique Using in Situ X-ray Diffraction and Two-Dimensional Epitaxial Film Electrodes, Chem. Mater. 2009, 21, 2632-2640.
196. Hirayama M., Ido H., Kim K., Cho W., Tamura K., Mizuki J. i., Kanno R. Dynamic Structural Changes at $LiMn_2O_4$/Electrolyte Interface during Lithium Battery Reaction, J. Am. Chem. Soc. 2010, 132, 15268-15276.
197. Sakamoto K., Hirayama M., Konishi H., Sonoyama N., Dupre N., Guyomard D., Tamura K., Mizuki J. i., Kanno R. Structural changes in surface and bulk $LiNi_{0.5}Mn_{0.5}O_2$ during electrochemical reaction on epitaxial thin-film electrodes characterized by in situ X-ray scattering, Phys. Chem. Chem. Phys. 2010, 12, 3815-3823.
198. Okumura T., Nakatsutsumi T., Ina T., Orikasa Y., Arai H., Fukutsuka T., Iriyama Y., Uruga T., Tanida H., Uchimoto Y., Ogumi Z. Depth-resolved X-ray absorption spectroscopic study on nanoscale observation of the electrode-solid electrolyte interface for all solid state lithium ion batteries, J. Mater. Chem. 2011, 21, 10051-10060.
199. Chattopadhyay S., Lipson A. L., Karmel H. J., Emery J. D., Fister T. T., Fenter P. A., Hersam M. C., Bedzyk M. J. In Situ X-ray Study of the Solid Electrolyte Interphase (SEI) Formation on Graphene as a Model Li-ion Battery Anode, Chem. Mater. 2012, 24, 3038-3043.
200. X-ray and Neutron Reflectivity (2009), vol 770. Lecture Notes in Physics, 1st edn. Springer, Berlin (Germany).
201. Hirayama M., Sonoyama N., Ito M., Minoura M., Mori D., Yamada A., Tamura K., Mizuki J., Kanno R. Characterization of electrode/electrolyte interface with X-ray reflectometry and epitaxial-film $LiMn_2O_4$ electrode, J. Electrochem. Soc. 2007, 154, A1065-A1072.
202. Hirayama M., Sakamoto K., Hiraide T., Mori D., Yamada A., Kanno R., Sonoyama N., Tamura K., Mizuki J. Characterization of electrode/electrolyte interface using in situ X-ray reflectometry and $LiNi_{0.8}Co_{0.2}O_2$ epitaxial film electrode synthesized by pulsed laser deposition method, Electrochim. Acta 2007, 53, 871-881.
203. Hirayama M., Sonoyama N., Abe T., Minoura M., Ito M., Mori D., Yamada A., Kanno R., Terashima T., Takano M., Tamura K., Mizuki J. Characterization of electrode/electrolyte interface for lithium batteries using in situ synchrotron X-ray reflectometry - A new experimental technique for $LiCoO_2$ model electrode, J. Power Sources 2007, 168, 493-500.
204. Hirayama M., Yonemura M., Suzuki K., Torikai N., Smith H., Watkinsand E., Majewski J., Kanno R. Surface Characterization of $LiFePO_4$ Epitaxial Thin Films by X-ray/Neutron Reflectometry, Electrochemistry 2010, 78, 413-415.
205. Fister T. T., Long B. R., Gewirth A. A., Shi B., Assoufid L., Lee S. S., Fenter P. Real-Time Observations of Interfacial Lithiation in a Metal Silicide Thin Film, J. Phys. Chem. C 2012, 116, 22341-22345.
206. Sears V. F. Neutron scattering lengths and cross sections, Neutron News 1992, 3, 26-37.
207. Lanz M., Lehmann E., Imhof R., Exnar I., Novak P. In situ neutron radiography of lithium-ion batteries during charge/discharge cycling, J. Power Sources 2001, 101, 177-181.
208. Whitney S., Biegalski S. R., Huang Y. H., Goodenough J. B. Neutron Depth Profiling Applications to Lithium-Ion Cell Research, J. Electrochem. Soc. 2009, 156, A886-A890.
209. Nagpure S. C., Downing R. G., Bhushan B., Babu S. S., Cao L. Neutron depth profiling technique for studying aging in Li-ion batteries, Electrochim. Acta 2011, 56, 4735-4743.
210. Oudenhoven J. F. M., Labohm F., Mulder M., Niessen R. A. H., Mulder F. M., Notten P. H. L. In Situ Neutron Depth Profiling: A Powerful Method to Probe Lithium Transport in Micro-Batteries, Adv. Mater. 2011, 23, 4103-4106.
211. Bridges C. A., Sun X.-G., Zhao J., Paranthaman M. P., Dai S. In Situ Observation of Solid Electrolyte Interphase Formation in Ordered Mesoporous Hard Carbon by Small-Angle Neutron Scattering, J. Phys. Chem. C 2012, 116, 7701-7711.

212. Owejan J. E., Owejan J. P., DeCaluwe S. C., Dura J. A. Solid Electrolyte Interphase in Li-Ion Batteries: Evolving Structures Measured In situ by Neutron Reflectometry, Chem. Mater. 2012, 24, 2133-2140.
213. Grey C. P., Dupré N. NMR Studies of Cathode Materials for Lithium-Ion Rechargeable Batteries, Chem. Rev. 2004, 104, 4493-4512.
214. Nie M., Chalasani D., Abraham D. P., Chen Y., Bose A., Lucht B. L. Lithium Ion Battery Graphite Solid Electrolyte Interphase Revealed by Microscopy and Spectroscopy, J. Phys. Chem. C 2013, 117, 1257-1267.
215. Xu K., Lam Y., Zhang S. S., Jow T. R., Curtis T. B. Solvation Sheath of Li^+ in Nonaqueous Electrolytes and Its Implication of Graphite/Electrolyte Interface Chemistry, J. Phys. Chem. C 2007, 111, 7411-7421.
216. Duer M. (2005) Introduction to Solid-State NMR Spectroscopy. 1st edn. John Wiley & Sons, Inc., Hoboken, NJ (USA).
217. MacKenzie K. J. D., Smith M. E. (2002) Multinuclear Solid-State NMR of Inorganic Materials, vol 6. Pergamon Materials Series. Elsevier, Oxford (UK).
218. Cuisinier M., Martin J. F., Moreau P., Epicier T., Kanno R., Guyomard D., Dupré N. Quantitative MAS NMR characterization of the $LiMn_{1/2}Ni_{1/2}O_2$ electrode/electrolyte interphase, Solid State Nucl. Magn. Reson. 2012, 42, 51-61.
219. Smart M. C., Ratnakumar B. V., Surampudi S., Wang Y., Zhang X., Greenbaum S. G., Hightower A., Ahn C. C., Fultz B. Irreversible Capacities of Graphite in Low-Temperature Electrolytes for Lithium-Ion Batteries, J. Electrochem. Soc. 1999, 146, 3963-3969.
220. Wang Y., Guo X., Greenbaum S., Liu J., Amine K. Solid Electrolyte Interphase Formation on Lithium-Ion Electrodes: A ^{7}Li Nuclear Magnetic Resonance Study, Electrochem. Solid State Lett. 2001, 4, A68-A70.
221. Cuisinier M., Dupré N., Martin J.-F., Kanno R., Guyomard D. Evolution of the $LiFePO_4$ positive electrode interface along cycling monitored by MAS NMR, J. Power Sources 2013, 224, 50-58.
222. Dupré N., Cuisinier M., Guyomard D. Electrode/Electrolyte Interface Studies in Lithium Batteries Using NMR, Interface 2011, 20, 61-67.
223. Krämer E., Schmitz R., Niehoff P., Passerini S., Winter M. SEI-forming mechanism of 1-Fluoropropane-2-one in lithium-ion batteries Electrochim. Acta 2012, 81, 161-165.
224. Meyer B. M., Leifer N., Sakamoto S., Greenbaum S. G., Grey C. P. High Field Multinuclear NMR Investigation of the SEI Layer in Lithium Rechargeable Batteries, Electrochem. Solid State Lett. 2005, 8, A145-A148.
225. Fox M. A., Whitesell J. K. (2004) Organic Chemistry. 3rd edn. Jones & Bartlett Publishers, Oxford (UK).
226. Leifer N., Smart M. C., Prakash G. K. S., Gonzalez L., Sanchez L., Smith K. A., Bhalla P., Grey C. P., Greenbaum S. G. ^{13}C Solid State NMR Suggests Unusual Breakdown Products in SEI Formation on Lithium Ion Electrodes, J. Electrochem. Soc. 2011, 158, A471-A480.
227. Gmitter A. J., Halajko A., Sideris P. J., Greenbaum S. G., Amatucci G. G. Subsurface diffusion of oxide electrolyte decomposition products in metal fluoride nanocomposite electrodes, Electrochim. Acta 2013, 88, 735-744.
228. Blanc F., Sperrin L., Jefferson D. A., Pawsey S., Rosay M., Grey C. P. Dynamic Nuclear Polarization Enhanced Natural Abundance ^{17}O Spectroscopy, J. Am. Chem. Soc. 2013, 135, 2975-2978.
229. Murakami M., Yamashige H., Arai H., Uchimoto Y., Ogumi Z. Association of paramagnetic species with formation of LiF at the surface of $LiCoO_2$, Electrochim. Acta 2012, 78, 49-54.
230. Huo H., Chamas M., Lippens P.-E., Ménétrier M. Multinuclear NMR Study of the Solid Electrolyte Interface on the Li-$FeSn_2$ Negative Electrodes for Li-Ion Batteries, J. Phys. Chem. C 2012, 116, 2390-2398.
231. Kalinin S. V., Gruverman A. (2007) Scanning Probe Microscopy. 1st edn. Springer, New York, NY (USA).

232. Kalinin S. V., Balke N. Local Electrochemical Functionality in Energy Storage Materials and Devices by Scanning Probe Microscopies: Status and Perspectives, Adv. Mater. 2010, 22, E193-E209.
233. Cohen Y., Aurbach D. The use of a special work station for in situ measurements of highly reactive electrochemical systems by atomic force and scanning tunneling microscopes, Rev. Sci. Instr. 1999, 70, 4668-4675.
234. Inaba M., Siroma Z., Kawatate Y., Funabiki A., Ogumi Z. Electrochemical scanning tunneling microscopy analysis of the surface reactions on graphite basal plane in ethylene carbonate-based solvents and propylene carbonate, J. Power Sources 1997, 68, 221-226.
235. Inaba M., Siroma Z., Funabiki A., Ogumi Z., Abe T., Mizutani Y., Asano M. Electrochemical Scanning Tunneling Microscopy Observation of Highly Oriented Pyrolytic Graphite Surface Reactions in an Ethylene Carbonate-Based Electrolyte Solution, Langmuir 1996, 12, 1535-1540.
236. Inaba M., Kawatate Y., Funabiki A., Jeong S.-K., Abe T., Ogumi Z. STM study on graphite/electrolyte interface in lithium-ion batteries: solid electrolyte interface formation in trifluoropropylene carbonate solution, Electrochim. Acta 1999, 45, 99-105.
237. Wang L., Deng X., Dai P.-X., Guo Y.-G., Wang D., Wan L.-J. Initial solid electrolyte interphase formation process of graphite anode in $LiPF_6$ electrolyte: an in situ ECSTM investigation, Phys. Chem. Chem. Phys. 2012, 14, 7330-7336.
238. Alliata D., Kötz R., Novák P., Siegenthaler H. Electrochemical SPM investigation of the solid electrolyte interphase film formed on HOPG electrodes, Electrochem. Commun. 2000, 2, 436-440.
239. Le Granvalet-Mancini M., Hanrath T., Teeters D. Characterization of the passivation layer at the polymer electrolyte/lithium electrode interface, Solid State Ionics 2000, 135, 283-290.
240. Jeong S.-K., Inaba M., Mogi R., Iriyama Y., Abe T., Ogumi Z. Surface Film Formation on a Graphite Negative Electrode in Lithium-Ion Batteries: Atomic Force Microscopy Study on the Effects of Film-Forming Additives in Propylene Carbonate Solutions, Langmuir 2001, 17, 8281-8286.
241. Jeong S.-K., Inaba M., Iriyama Y., Abe T., Ogumi Z. AFM study of surface film formation on a composite graphite electrode in lithium-ion batteries, J. Power Sources 2003, 119–121, 555-560.
242. Inaba M., Tomiyasu H., Tasaka A., Jeong S.-K., Ogumi Z. Atomic Force Microscopy Study on the Stability of a Surface Film Formed on a Graphite Negative Electrode at Elevated Temperatures, Langmuir 2004, 20, 1348-1355.
243. Leroy S., Blanchard F., Dedryvère R., Martinez H., Carré B., Lemordant D., Gonbeau D. Surface film formation on a graphite electrode in Li-ion batteries: AFM and XPS study, Surf. Interface Anal. 2005, 37, 773-781.
244. Lucas I. T., Pollak E., Kostecki R. In situ AFM studies of SEI formation at a Sn electrode, Electrochem. Commun. 2009, 11, 2157-2160.
245. Kitta M., Akita T., Maeda Y., Kohyama M. Study of Surface Reaction of Spinel $Li_4Ti_5O_{12}$ during the First Lithium Insertion and Extraction Processes Using Atomic Force Microscopy and Analytical Transmission Electron Microscopy, Langmuir 2012, 28, 12384-12392.
246. Ochida M., Domi Y., Doi T., Tsubouchi S., Nakagawa H., Yamanaka T., Abe T., Ogumi Z. Influence of Manganese Dissolution on the Degradation of Surface Films on Edge Plane Graphite Negative-Electrodes in Lithium-Ion Batteries, J. Electrochem. Soc. 2012, 159, A961-A966.
247. Snook G. A., Huynh T. D., Hollenkamp A. F., Best A. S. Rapid SECM probing of dissolution of $LiCoO_2$ battery materials in an ionic liquid, J. Electroanal. Chem. 2012, 687, 30-34.
248. Xu F., Beak B., Jung C. In situ electrochemical studies for Li^+ ions dissociation from the $LiCoO_2$ electrode by the substrate-generation/tip-collection mode in SECM, J. Solid State Electrochem. 2012, 16, 305-311.

249. Williams D. B., Carter C. B. (2009) Specimen Preparation. In: Transmission Electron Microscopy. 2nd edn. Springer US, pp 173-193.
250. Brazier A., Dupont L., Dantras-Laffont L., Kuwata N., Kawamura J., Tarascon J. M. First Cross-Section Observation of an All Solid-State Lithium-Ion "Nanobattery" by Transmission Electron Microscopy, Chem. Mater. 2008, 20, 2352-2359.
251. Zhang H.-L., Li F., Liu C., Tan J., Cheng H.-M. New Insight into the Solid Electrolyte Interphase with Use of a Focused Ion Beam, J. Phys. Chem. B 2005, 109, 22205-22211.
252. Dollé M., Sannier L., Beaudoin B., Trentin M., Tarascon J.-M. Live Scanning Electron Microscope Observations of Dendritic Growth in Lithium/Polymer Cells, Electrochem. Solid State Lett. 2002, 5, A286-A289.
253. Morcrette M., Rozier P., Dupont L., Mugnier E., Sannier L., Galy J., Tarascon J. M. A reversible copper extrusion-insertion electrode for rechargeable Li batteries, Nat. Mater. 2003, 2, 755-761.
254. Huang J. Y., Zhong L., Wang C. M., Sullivan J. P., Xu W., Zhang L. Q., Mao S. X., Hudak N. S., Liu X. H., Subramanian A., Fan H., Qi L., Kushima A., Li J. In Situ Observation of the Electrochemical Lithiation of a Single SnO_2 Nanowire Electrode, Science 2010, 330, 1515-1520.
255. White E. R., Singer S. B., Augustyn V., Hubbard W. A., Mecklenburg M., Dunn B., Regan B. C. In Situ Transmission Electron Microscopy of Lead Dendrites and Lead Ions in Aqueous Solution, ACS Nano 2012, 6, 6308-6317.
256. Aurbach D., Markovsky B., Rodkin A., Levi E., Cohen Y. S., Kim H. J., Schmidt M. On the capacity fading of $LiCoO_2$ intercalation electrodes:: the effect of cycling, storage, temperature, and surface film forming additives, Electrochim. Acta 2002, 47, 4291-4306.
257. Araki K., Sato N. Chemical transformation of the electrode surface of lithium-ion battery after storing at high temperature, J. Power Sources 2003, 124, 124-132.
258. Abe K., Yoshitake H., Kitakura T., Hattori T., Wang H., Yoshio M. Additives-containing functional electrolytes for suppressing electrolyte decomposition in lithium-ion batteries, Electrochim. Acta 2004, 49, 4613-4622.
259. Chan C. K., Ruffo R., Hong S. S., Cui Y. Surface chemistry and morphology of the solid electrolyte interphase on silicon nanowire lithium-ion battery anodes, J. Power Sources 2009, 189, 1132-1140.
260. Wu H., Chan G., Choi J. W., Ryu I., Yao Y., McDowell M. T., Lee S. W., Jackson A., Yang Y., Hu L., Cui Y. Stable cycling of double-walled silicon nanotube battery anodes through solid-electrolyte interphase control, Nat. Nanotech. 2012, 7, 310-315.
261. Xu M., Lu D., Garsuch A., Lucht B. L. Improved Performance of $LiNi_{0.5}Mn_{1.5}O_4$ Cathodes with Electrolytes Containing Dimethylmethylphosphonate (DMMP), J. Electrochem. Soc. 2012, 159, A2130-A2134
262. Larcher D., Courjal P., Herrera Urbina R., Gérand B., Blyr A., du Pasquier A., Tarascon J. M. Synthesis of MnO_2 Phases from $LiMn_2O_4$ in Aqueous Acidic Media: Mechanisms of Phase Transformations, Reactivity, and Effect of Bi Species, J. Electrochem. Soc. 1998, 145, 3392-3400.
263. Talyosef Y., Markovsky B., Salitra G., Aurbach D., Kim H. J., Choi S. The study of $LiNi_{0.5}Mn_{1.5}O_4$ 5-V cathodes for Li-ion batteries, J. Power Sources 2005, 146, 664-669.
264. Yang Y., Xie C., Ruffo R., Peng H., Kim D. K., Cui Y. Single Nanorod Devices for Battery Diagnostics: A Case Study on $LiMn_2O_4$, Nano Lett. 2009, 9, 4109-4114.
265. López C. M., Vaughey J. T., Dees D. W. Morphological Transitions on Lithium Metal Anodes, J. Electrochem. Soc. 2009, 156, A726-A729.
266. Girit Ç. Ö., Meyer J. C., Erni R., Rossell M. D., Kisielowski C., Yang L., Park C.-H., Crommie M. F., Cohen M. L., Louie S. G., Zettl A. Graphene at the Edge: Stability and Dynamics, Science 2009, 323, 1705-1708.
267. Myung S.-T., Izumi K., Komaba S., Sun Y.-K., Yashiro H., Kumagai N. Role of Alumina Coating on Li–Ni–Co–Mn–O Particles as Positive Electrode Material for Lithium-Ion Batteries, Chem. Mater. 2005, 17, 3695-3704.

268. Choi Y.-K., Chung K.-i., Kim W.-S., Sung Y.-E., Park S.-M. Suppressive effect of Li_2CO_3 on initial irreversibility at carbon anode in Li-ion batteries, J. Power Sources 2002, 104, 132-139.
269. Fu L. J., Endo K., Sekine K., Takamura T., Wu Y. P., Wu H. Q. Studies on capacity fading mechanism of graphite anode for Li-ion battery, J. Power Sources 2006, 162, 663-666.
270. Kerlau M., Kostecki R. Interfacial Impedance Study of Li-Ion Composite Cathodes during Aging at Elevated Temperatures, J. Electrochem. Soc. 2006, 153, A1644-A1648.
271. Wang F., Graetz J., Moreno M. S., Ma C., Wu L., Volkov V., Zhu Y. Chemical Distribution and Bonding of Lithium in Intercalated Graphite: Identification with Optimized Electron Energy Loss Spectroscopy, ACS Nano 2011, 5, 1190-1197.
272. Cosandey F., Su D., Sina M., Pereira N., Amatucci G. G. Fe valence determination and Li elemental distribution in lithiated $FeO_{0.7}F_{1.3}$/C nanocomposite battery materials by electron energy loss spectroscopy (EELS), Micron 2012, 43, 22-29.
273. Knoll B., Keilmann F. Near-field probing of vibrational absorption for chemical microscopy, Nature 1999, 399, 134-137.
274. Falcone R., Jacobsen C., Kirz J., Marchesini S., Shapiro D., Spence J. New directions in X-ray microscopy, Contemp. Phys. 2011, 52, 293-318.
275. Novák P., Joho F., Lanz M., Rykart B., Panitz J.-C., Alliata D., Kötz R., Haas O. The complex electrochemistry of graphite electrodes in lithium-ion batteries, J. Power Sources 2001, 97–98, 39-46.
276. Zhang X., Ross P. N., Kostecki R., Kong F., Sloop S., Kerr J. B., Striebel K., Cairns E. J., McLarnon F. Diagnostic Characterization of High Power Lithium-Ion Batteries for Use in Hybrid Electric Vehicles, J. Electrochem. Soc. 2001, 148, A463-A470.
277. Stamenkovic V. R., Fowler B., Mun B. S., Wang G., Ross P. N., Lucas C. A., Marković N. M. Improved Oxygen Reduction Activity on $Pt_3Ni(111)$ via Increased Surface Site Availability, Science 2007, 315, 493-497.

Chapter 8
Molecular Modeling of Electrolytes

Oleg Borodin

Abstract Recent advances in molecular modeling provide significant insight into electrolyte electrochemical and transport properties. The first part of the chapter discusses applications of quantum chemistry methods to determine electrolyte oxidative stability and oxidation-induced decomposition reactions. A link between the oxidation stability of model electrolyte clusters and the kinetics of oxidation reactions is established and compared with the results of linear sweep voltammetry measurements. The second part of the chapter focuses on applying molecular dynamics (MD) simulations and density functional theory to predict the structural and transport properties of liquid electrolytes and solid electrolyte interphase (SEI) model compounds; the free energy profiles for lithium desolvation from electrolytes; and the behavior of electrolytes at charged electrodes and the electrolyte–SEI interface.

8.1 Introduction to Molecular Modeling Methodologies

Designing electrolyte for batteries is a multiphysics, multivariable problem because of a number of often conflicting requirements that should simultaneously be met. For example, a suitable electrolyte should possess high ionic conductivity, low viscosity, good wetting properties for the electrodes and separator, high thermal stability, low toxicity, etc. It also should either be electrochemically stable at the operating voltage of the electrodes or, if decomposed, able to form a stable passivation layer on the battery electrode surface, often called the solid electrolyte interphase (SEI). Most research efforts have focused on obtaining a fundamental understanding of the electrochemical stability and decomposition reactions of electrolyte components;

O. Borodin (✉)
Electrochemistry Branch, Sensors & Electron Devices Directorate, U. S. Army Research Laboratory, 2800 Powder Mill Rd., Adelphi, MD 20783, USA
e-mail: oleg.a.borodin.civ@mail.mil

T.R. Jow et al. (eds.), *Electrolytes for Lithium and Lithium-Ion Batteries*,
Modern Aspects of Electrochemistry 58, DOI 10.1007/978-1-4939-0302-3_8,

predicting the structural and transport properties of electrolytes in bulk and at interfaces; and understanding the influence of applied potential on the interfacial properties at electrodes.

A choice of the modeling technique is dictated by the problem of interest. Ab initio wavefunction and density functional theory (DFT) quantum chemical (QC) methods and reactive force fields such as ReaxFF [1, 2] are the methods of choice for examining electrochemical stability and decomposition reactions. In QC methods, the atomic centers, electrons orbits, or electron density are treated explicitly, allowing one to obtain binding energies, oxidation, and reduction energies, as well as the barriers for chemical reactions. QC methods are extremely powerful and accurate provided the proper level of theory or type of a density functional was used. However, DFT and especially accurate correlated wavefunction methods (coupled cluster [CCSD(T)], Møller–Plesset perturbation theory MP2, MP4, or composite Gn methods [3]) quickly become computationally prohibitive with increasing system size. Reactive force field methods such as ReaxFF do not provide an explicit treatment of electrons; instead, ReaxFF uses a concept of a bond order and is extensively trained to reproduce chemical reactions. Thus, ReaxFF has a significantly lower computational cost and could be used for simulations of large systems. Nonreactive force fields, however, are even less computationally expensive than ReaxFF and are often chosen when predicting electrolyte structural and transport properties in bulk and at charged interfaces. In such force fields, molecular interactions are represented by interaction between the permanent charges assigned to atoms, atomic or bond polarizabilities, and Lennard–Jones type of nonbonded interactions. Molecular force fields are often parameterized against QC data and reproduce molecular geometries, binding energies, electrostatic potential around molecules, dipole and higher moments, polarizabilities, conformational energies, and barriers.

Due to the importance of obtaining a fundamental understanding of electrolyte electrochemical stability and the electrolyte decomposition reactions related to battery operation, these topics are extensively discussed in this book. Scheers and Johansson give a historical prospective of the application of QC methods in determining redox stability of electrolyte components. In another chapter, Lau et al. discuss applying QC methods to understanding electrolyte stability and electrolyte–electrode interactions with a focus on lithium–air chemistry. This chapter concentrates on the fundamental aspects of extracting the oxidation and reduction stability of electrolytes and their decomposition reactions from QC calculations. Specifically, the connection of the absolute and electrochemical scales is discussed. Because QC calculations yield energies associated with the electron detachment (oxidation) from and the electron addition (reduction) to the molecular complex of interest relative to electron at rest, a fundamental question arises with regard to how to connect the absolute scale associated with the electron at rest with the commonly used electrochemical scale, such as the Li^+/Li couple. The second important question is how to choose a proper electrolyte model in order to establish a connection between the oxidation energies calculated for the electrolyte model systems and the oxidation and reduction stability extracted from linear sweep voltammetry (LSV) measurements. This discussion focuses on the relationship between the thermodynamic and kinetic

aspects of oxidation reductions. Finally, the oxidation-induced decomposition reactions are discussed. In the second part of this chapter, the application of molecular dynamics (MD) simulations to predict the structural and transport properties of electrolytes and SEI compounds in bulk and at electrified interfaces is reviewed.

8.2 Quantum Chemistry Studies of Electrolyte Oxidation Redox Stability and Reactions

8.2.1 Absolute and Electrochemical Scales of Electrolyte Redox Stability

In order to establish a connection between the quantities extracted from QC calculations and the measured oxidation stability, the energy cycle shown in Fig. 8.1 is commonly used. The absolute oxidation potential of a complex M relative to an electron at rest in vacuum [$E^{\circ}_{abs}(M)$], is given by (8.1):

$$E^{\circ}_{abs}(M) = \left[\Delta G_e + \Delta G^{\circ}_{S}(M^{+}) - \Delta G^{\circ}_{S}(M)\right]/F, \tag{8.1}$$

where ΔG_e is the ionization free energy in gas phase at 298.15 K; $\Delta G_S(M^+)$ and $\Delta G_S(M)$ are the free energies of solvation of the oxidized and initial complexes M^+ and M, respectively; and F is the Faraday constant. The ionization free energy ΔG_e has contributions from the ionization potential that include the adiabatic ionization energy and zero point vibrational correction as well as the entropic term $-T\Delta S$.

The predicted values from QC calculations of the absolute $E^{\circ}_{abs}(M)$ need to be converted to the commonly used standard hydrogen electrode (SHE) or Li^+/Li potential scale in order to compare them with experimental data. There are two main approaches for accomplishing this. In the first approach, well-established data for aqueous electrolytes are used to connect the absolute and electrochemical scales. This approach neglects the influence of the nature of a particular aprotic solvent on the lithium free energy of solvation. The International Union of Pure and Applied Chemistry (IUPAC)-recommended values [4] for the absolute SHE potential in

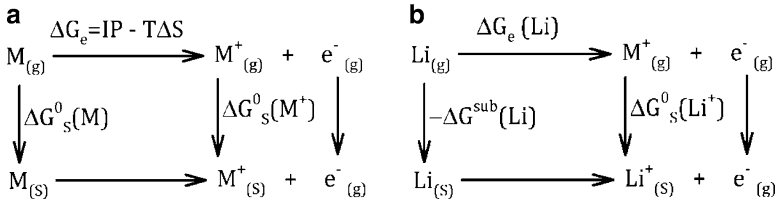

Fig. 8.1 Free-energy cycle for the redox reaction ($M \rightarrow M^+ + e^-$), where $M_{(g)}$ denotes molecule M in gas phase, $M_{(S)}$ denotes the solvated molecule, and IP denotes ionization potential

nonaqueous solvents are within a few tenths of a volt of the absolute SHE potential value in aqueous solutions, suggesting that an additional variation on the order of 0.1–0.3 V is expected for the conversion factor from the absolute scale to Li^+/Li in nonaqueous solvents. Indeed, the variation of the lithium free energy of solvation in water, methanol, acetonitrile, hydrazine, and ammonia was reported to be in this range [5]. IUPAC recommends a SHE value of 4.42–4.44 V in the absolute potential scale at room temperature [4]. A more recent work by Isse et al. [6] suggested that the SHE potential is 4.281 V. Using the Li^+/Li standard electrode potential of −3.05 V versus SHE [4] for aqueous solutions, the conversion factor is established by (8.2):

$$E^\circ\left(vs.Li^+/Li\right) = E^\circ_{abs} - 4.42 + 3.05\,\mathrm{V} = E^\circ_{abs} - 1.37\,\mathrm{V} \approx E^\circ_{abs} - 1.4\,\mathrm{V}, \quad (8.2)$$

where E°(vs. Li^+/Li) is the potential vs. Li^+/Li. If the SHE estimate from Isse et al. [6] is used, the relation is E°(vs. Li^+/Li) = E°_{abs} − 1.23 V.

In the second approach, an implicit solvent such as the polarized continuum method (PCM), an explicit solvent, or a combination of these methods is used in order to calculate the lithium free energy of solvation so that the conversion factor is specific for the electrolyte of interest needed for the cycle shown in Fig. 8.1b. A number of groups [7, 8] have used DFT calculations to relate the absolute and Li^+/Li potential scales using the thermodynamic cycles shown in Fig. 8.1a, b for the complex M oxidation and Li^+/Li reduction reactions $M_{(S)} - e \rightarrow M^+_{(S)}$, $Li^+_{(S)} + e \rightarrow Li_{(S)}$, as shown in (8.3):

$$E^\circ_{abs}\left(Li^+/Li\right) = -\left(\Delta G^{sub}\left(Li\right) + IP\left(Li\right) + \Delta G^\circ_s\left(Li^+\right)\right)/F, \quad (8.3)$$

where ΔG^{sub}(Li) is the heat of lithium evaporation (sublimation), IP is the free energy of Li ionization in gas phase, and $\Delta G^\circ_S(Li^+)$ is the free energy of Li^+ solvation in a solvent. The handbook [9] value of ΔG^{sub}(Li) at 298.15 K is 1.65 eV, IP(Li) = 5.39172 eV, recommended by the National Institute of Science and Technology's (NIST) webbook [10]. The experimentally determined Li^+ free energy of solvation in water of −529.4 kJ/mol = −5.49 eV was reported by Tissandier et al. [11], while $\Delta G^\circ_S(Li^+)$ for dimethylsulfoxide (DMSO) solvent was reported [12] to be −554.4 kJ/mol = −5.75 eV. The latter value was found to be in good agreement with the value of −5.88 eV from a theoretical ab initio and careful cluster-continuum model study [12]. Gomer et al. [5] reported in 1977 an estimate of $\Delta G^\circ_S(Li^+) = -5.25$ eV for acetonitrile solvent. Substituting these values in (8.3) yields $E^\circ_{abs}(Li^+/Li)$ of −1.56, −1.3, and −1.79 V for water, DMSO, and acetonitrile solvents, respectively. These values agree reasonably well with the value of −1.4 V [see (8.2)], in contrast to the values reported by Zhang et al. [7] and Shao et al. [8] who calculated IP(Li) and $\Delta G^\circ_S(Li^+)$ using a number of functional and the MP2 level in conjunction with a various implicit solvent solvation models. They used a value of 1.22 eV for the free energy of lithium vaporization instead of the value of 1.65 eV from the handbook [9]. Importantly, the application of the PCM model to a small Li^+ cation is problematic due to the high sensitivity of the solvation energy on the Li^+ cation radius that was used to build the molecular cavity

around it [13, 14]. Moreover, the recent cluster-continuum model study of lithium solvation [12] argued that it is important to explicitly consider the first solvation shell of the small cation such as Li^+. The implicit solvent models that are implemented in Gaussian g09 do not appear to have been parameterized for or tested on small atomic cations such as Li^+ [15]. To summarize, Shao et al. [8] reported $-E^{\circ}_{abs}(Li^+/Li)$ for a number of sulfones to be in the range of 2.75–3.35 V and 2.67–3.17 V using a B3LYP/6-31+G(d,p) level with SMD and PCM solvation models, respectively, which is significantly higher than our estimates in the range of 1.2–1.79 V discussed above [16]. Usage of (8.2) is recommended for fast screening.

8.2.2 Calculations of the Electrolyte Oxidation Stability

A number of QC studies have focused on understanding the oxidation stability of electrolyte nonionic and ionic solvents [7, 8, 17–24], redox shuttles [25–27], and anions [28–31]. The majority of the studies considered isolated solvents or anions that do not explicitly interact with the electrode; in situations where there is no specific interaction such as hydrogen bonding with other electrolyte components; and where the solvent effect is included via the PCM. A few studies went beyond to include the condensed-phase interactions present in ionic liquids [32], cation–anion interactions [33], or solvent–anion interactions [16, 34–37]. The most successful were DFT predictions of shuttle redox potentials [26, 38], which reported a close agreement with the experimental data showing a root mean square deviation of 0.08 V. Similarly, Wang, Buhrmester, and Dahn [38] reported excellent agreement between the calculated values for 17 redox shuttle additives, with a root mean square deviation between the calculated and measured oxidation potentials of 0.15 V and a maximum deviation of 0.25 V, indicating that DFT calculations at B3LYP/6-31G(d,p) could be effectively used for screening redox additives. Fu et al. [18] have shown that DFT calculations can predict redox potentials for a diverse set of hundreds of organic molecules and free radicals in acetonitrile when 0.25 eV was added to the DFT values, indicating that computational electrochemistry could become a powerful tool for the organic chemistry community.

While DFT calculations often reproduced experimentally observable trends for the oxidation stability of anions [17, 19] and solvents [7, 18, 21, 24, 39], they often failed to quantitatively relate the calculated oxidation potential for numerous electrolytes and experimentally measured data. For example, the intrinsic oxidation potentials of common electrolyte solvents or anions obtained from DFT and higher level correlated methods were significantly higher than experimentally determined values from LSV experiments, especially when LSV measurements were extrapolated to low scan rates [16, 34–36]. A step toward reconciling QC predictions and LSV measurements was made in recent DFT studies [16, 34–36], which focused on the oxidation stability of solvent–anion and solvent–solvent clusters. These studies showed that the oxidation stability of solvent–solvent and solvent–anion clusters is lower than stability of the isolated solvents and anions that comprise these clusters.

For example, oxidation of carbonate solvents such as EC, PC, and DMC complexed with anions such as PF_6^-, BF_4^-, and ClO_4^- resulted in an anion nucleophilic attack on the solvent upon oxidation (electron removal) and deprotonation of the carbonates [34, 35] that significantly reduced the oxidation stability of these solvent–anion complexes compared to values obtained for isolated solvents. Xing et al. [36] reported that the oxidation potentials of EC_2 and EC_4 clusters were significantly lower than the intrinsic oxidation potential of an isolated EC and even lower than the oxidation potential of the EC–BF_4^- complex. In these clusters, the exothermic proton abstraction from the ethylene group of EC by the carbonyl group of another EC was responsible for the decreased oxidative stability of EC_2 and EC_4 compared to EC. Radiolytic ionization experiments confirmed the H-abstraction reaction in oxidized EC complexes [40]. These studies [16, 34–37] indicated that the cluster approach to understanding electrolyte oxidation stability yields a distribution of oxidation stabilities associated with the cluster composition. Specifically, the oxidation stability of model electrolyte complexes follows the order $EC_4/BF_4^- < EC_n$ ($n = 2,4$) < EC/BF_4^- < EC/PF_6^- < isolated EC, as shown in Fig. 8.2 [16]. Examination of this figure suggests that the H-transfer from EC to BF_4^- and HF formation in the oxidized EC/BF_4^- complex reduced the oxidation stability by ~0.7 V compared to the isolated EC. The H-transfer from one EC to the carbonyl group of the other in the oxidized EC_2 complex resulted in an even lower oxidation stability for this complex, which is more than 1 V lower than the isolated EC. The same H-transfer reaction in the EC_4/BF_4^-(a) complex yields a similar oxidation stability to EC_2; however, the H-transfer from one EC to the carbonate group of a neighboring EC in the EC_4/BF_4^-(b) complex results in the lowest oxidation stability among the investigated EC_n–BF_4^- complexes [16]. Formation of an ion pair between the cation (EC+H) and BF_4 in the oxidized EC_4/BF_4^-(b) complex stabilized the oxidized state and made the oxidation stability of this complex lower. The ring opening reaction in the EC(–H) neutral radical is the next oxidation-induced reaction that is expected to occur in the complexes shown in Fig. 8.2. This reaction is exothermic with an energy of 1 eV calculated at G4MP2 level with PCM($\varepsilon = 20$).

In order to connect the oxidation stability of the model electrolyte complexes to LSV experimental data, one needs to consider the reaction rates for the oxidation reaction of each complex. Indeed, the H-transfer reaction in the solvent–solvent or solvent–anion complexes leads to a significant molecular rearrangement and distortion; thus, one expects a significant barrier for these oxidation reactions compared to the oxidation of an isolated EC. Rates for each electron transfer reaction can be estimated in a first approximation using Marcus theory of electron transfer, where the rate (k) of the activation-controlled reaction is proportional to

$$k \sim e^{-\Delta G_a / RT}, \tag{8.4}$$

where ΔG_a is the activation Gibbs free energy of the formation of the transition state. Using a parabolic approximation for the intersection yields

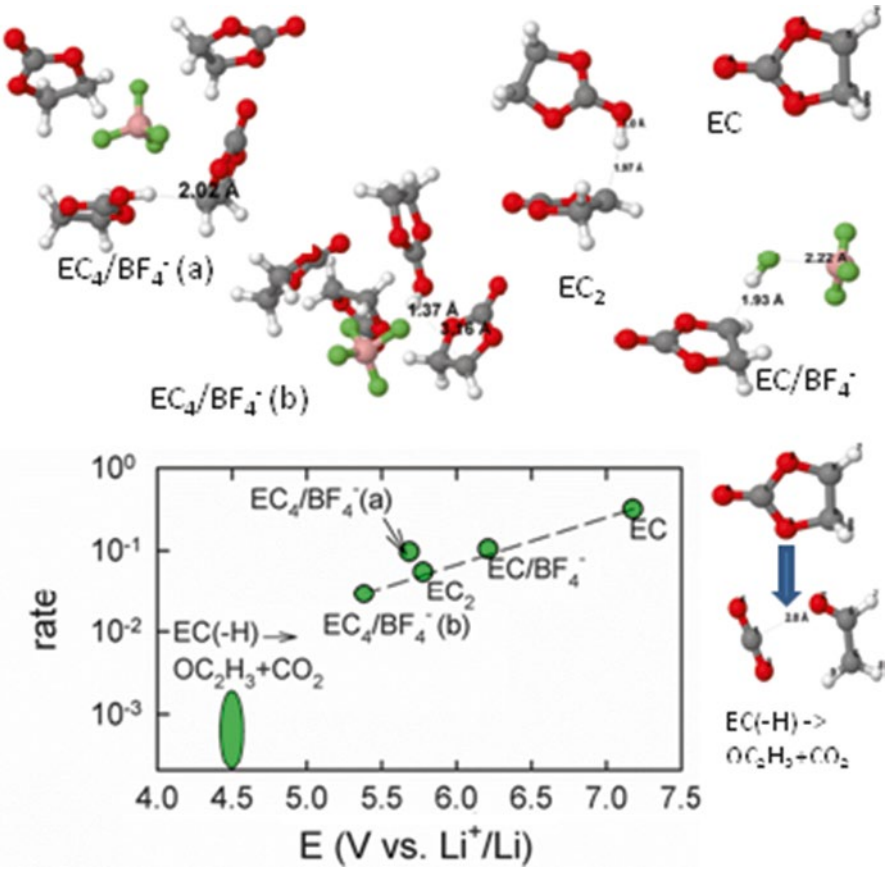

Fig. 8.2 Oxidation potential of model electrolyte clusters vs. the rate estimated from the Marcus electron transfer theory. EC(−H) denotes a neutral EC radical with one proton abstracted from it in the process of the oxidation-induced reaction. Oxidation potentials are from M05-2X/6-31+G** calculations with PCM($\varepsilon=20$) [16]. Rates were calculated in this work

$$\Delta G_a = \frac{\left(\lambda + \Delta G_0\right)^2}{4\lambda}, \tag{8.5}$$

where λ is the reorganization energy, which is set to the vertical oxidation potential (E_v); and ΔG_0 is the potential difference between the reactant and a product. Thus, for oxidation reactions ΔG_0 is set to the adiabatic oxidation potential, $\lambda+\Delta G_0=E_v-E_a$, where E_a is the adiabatic oxidation potential of the complex. Figure 8.2 shows the estimated rates for the oxidation reaction occurring in the model electrolyte complexes. The reorganization energies were calculated in this work using M05-2X/6-31+G(d,p) theory in conjunction with PCM($\varepsilon=20$, acetone). Gaussian g09 software was used. The inverse dependence between the oxidation potential and reaction rate was

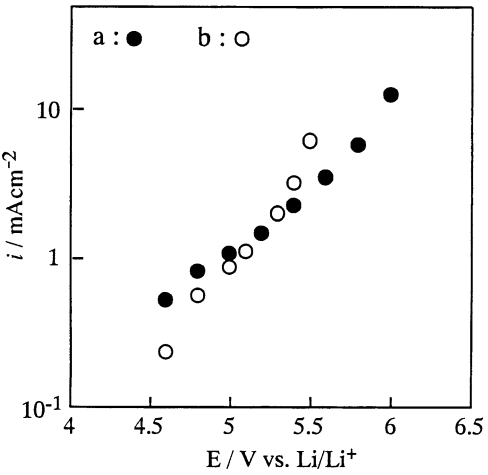

Fig. 8.3 Current (i) applied potential $i \pm E$ relationship of the anodic oxidation of various organic electrolytes. Electrolyte: (a) 1 M $LiPF_6$/(EC:DEC) (1:1); (b) 1 M LiClO4/(EC:DEC) (1:1). Microelectrode: carbon, 10 mm in diameter [41]. "Reprinted with permission from [41] Copyright 2001 Elsevier"

observed. It indicates that the oxidation stability of electrolyte exponentially depends on the time scale of the measurements. A good correlation is observed between the dependence of the oxidation potential on the reaction rate from the DFT calculations shown in Fig. 8.2 and the experimentally measured [41] current (i) − potential (E) dependence for the anodic oxidation of the carbonate-based organic electrolytes on the carbon microelectrode. Higher level G4MP2 calculations in conjunction with SMD solvation model yielded oxidation stability of EC_2/BF_4^- clusters around 5 V, which is slightly below DFT results presented in Fig. 8.2.

In summary, the oxidation stability in common battery electrolytes is represented by a variety of reaction pathways that have reaction rates that differ by more than order of magnitude. Figure 8.2 indicates that the long-term (very low rate) stability of an EC/BF_4-based electrolyte is expected to be around 4.5–5 V. This estimate is obtained for the two-step process involving the oxidation of the EC_4/BF_4^- complex followed by the EC(−H) ring opening, which yields CO_2 and OC_2H_2. Because it is a two-step reaction with an intermediate, the application of Marcus theory is not valid and the rate estimates have large error bars. Note that the common procedure for determining electrolyte oxidation stability by taking a value at a certain current cutoff in LSV measurements yields a value of 6.2 V for a glassy carbon electrode in contact with 0.65 M Et_4NBF_4 electrolyte [42]. This value corresponds to the oxidation of the EC/BF_4^- complex, which has a low barrier for electron transfer reaction. Most of the published QC work has focused on understanding the oxidation stability of isolated solvents, which corresponds to a high-rate oxidation process, while long-term electrolyte stability in batteries and supercapacitors is related to the low-rate processes that occur at significantly lower voltages. Therefore, examination of the distribution of the most probable oxidation reactions and the associated electron transfer rates is needed to construct the current–stability relationship, such as one shown in Figs. 8.2 and 8.3, in order to meaningfully relate the results of the QC calculations to the operation of batteries and supercapacitors.

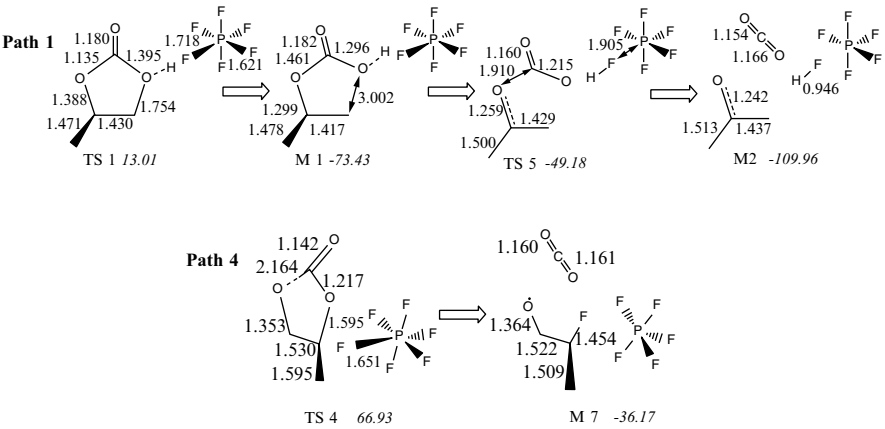

Fig. 8.4 Optimized structure, geometric parameters (in Å), and relative free energy (in kJ/mol) of the oxidation decomposition path of PC-PF_6^- in an implicit solvent. Reprinted with permission from [35] Copyright 2011 American Chemical Society

8.2.3 Oxidation Decomposition Products

While the chapter by Scheers and Johansson focuses on electrolyte redox stability, understanding oxidation decomposition reactions is also very important, as it provides insight into reactions leading to the formation of the passivation layer and gas generation during battery operation. Xing et al. [20, 43] have investigated the decomposition of isolated EC and PC molecules, building on pioneering work by the Phil Ross group [7] published in 2001. A recent DFT study [35] of the PC-PF_6^- and PC-ClO_4^- oxidation-induced decomposition pathways has clearly shown that the presence of anions near PC molecules alters the decomposition kinetics, resulting in the formation of different products. Specifically, the oxidative decomposition of PC-PF_6^- at room temperature favored CO_2 and acetone radical formation, as shown for the low-barrier path 1 in Fig. 8.4. This result is in agreement with experimental evidence [44] at room temperature in which the formation of fluoro-organics was not observed. The reaction shown in path 1 indicates that in the process of PC-PF_6^- oxidative decomposition the PF_6^- anion acts like a catalyst and is not incorporated in the final SEI film. At higher temperatures, however, reaction path 4 with the second lowest barrier is expected to get activated, yielding fluoro-organics consistent with the observations from thermal runaway scenarios [45]. DFT calculations [35] of the initial oxidative decomposition of PC-ClO_4^- yielded the formation of $HClO_4$, CO_2, and acetone radicals, showing that it is the most kinetically favorable with an endothermic $\Delta G = -118$ kJ/mol.

Because of the lower oxidation stability of the EC_2 complex compared to the EC–BF_4^- complex, the oxidation-induced decomposition of EC_2 was investigated [36]. While the lowest barrier and most exothermic path yielded CO_2 and OC_2H_3 radical cations, a higher barrier path led to formation of oligo(ethylene carbonate).

Because of a high barrier for the reaction leading to oligo(ethylene carbonate) formation, this reaction is expected to be sluggish with a low yield. It is consistent with the formation of a thin passivation layer on the cathode surface. Poly(ethylene carbonate) formation on cathode surfaces as a result of the oxidation-induced decomposition of an EC-based electrolyte was also recently suggested from experimental studies [46].

The first ab initio modeling study [47, 48] of the initial stages of the EC decomposition on an $Li_xMn_2O_4(100)$ surface by Kevin Leung revealed important differences between the EC oxidation-induced decomposition mechanism observed in the cluster studies [16, 35–37] and the EC reaction with the low voltage cathode surface. Figure 8.5 shows the essential steps of the EC reaction on a periodic spinel surface under ultrahigh vacuum conditions without dielectric screening. The first step with a barrier ~0.5 eV corresponded to EC–Mn(IV) bond formation (geom. D) followed by the formation of intermediate E, with a broken C_C–O_E bond. No charge transfer occurs at this point. The last step, E to F, led to a very exothermic transfer of two electrons and a proton to the oxide surface. Despite that (100) is not the lowest energy surface of the spinel [49], this DFT study [47, 48] demonstrated a possible mechanism for the oxygen removal from the surface and H-transfer from EC to the cathode surface that is likely related to the surface degradation.

8.3 Molecular Dynamics Simulations of Bulk Electrolytes

8.3.1 Organic Liquid Electrolytes

MD simulations are suitable for simulating bulk electrolytes and electrolyte–electrode interfaces because they access material properties in a nanometer time scale. Ab initio simulations explicitly consider electronic orbitals or electron density and were used to investigate relatively small systems containing tens of molecules for up to 100 ps [50, 51]. Because of the high computational cost associated with solving the electronic problem, most MD simulations of electrolytes use classical force fields where interactions within a molecule and between molecules are presented by simple distance-dependent functions that are often parameterized based on quantum chemistry data obtained for clusters [52] or small model systems [50]. Two types of classical force fields were used in the electrolyte simulations: (1) a polarizable force field, where the presence of ions such as Li^+ polarized the neighboring solvent and anions by inducing atomic dipoles or by shifting charges in response to the electric field, and (2) nonpolarizable force fields, which had fixed charges on molecules to represent the molecular multipoles that did not change over the course of the simulations.

MD simulations were used to study a number of electrolytes of potential interest to lithium battery applications: EC:DMC/$LiPF_6$ [52], EC/LiTFSI [53, 54], DMC/LiTFSI [55], GBL/LiTFSI [55], and acetonitrile doped with $LiPF_6$, $LiClO_4$, $LiBF_4$, LiDFOB, LiTFSI [56–58], oligoethers/Li salts [59–61], acetamide/LiTFSI [62],

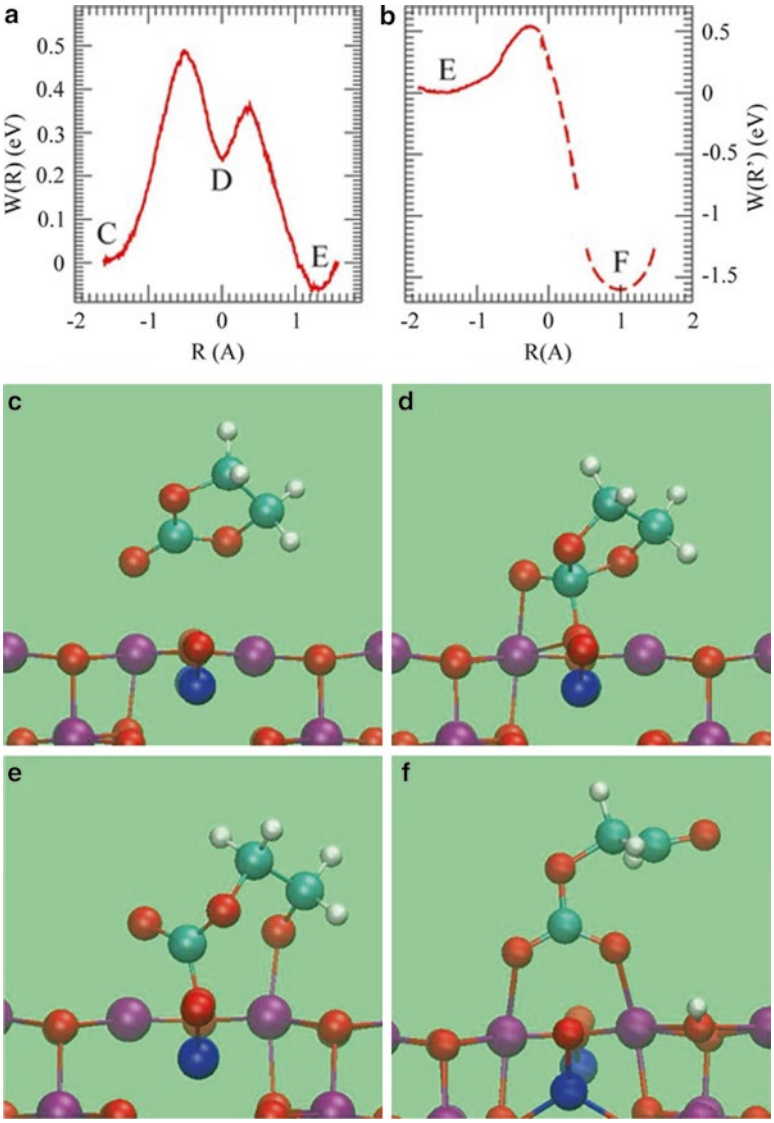

Fig. 8.5 (**a**) Potentials of mean force for two segments of the EC oxidation reaction. (**c**) Intact EC (configuration *C*) on the $Li_{0.6}Mn_2O_4$ (100) surface. (**d**) Intermediate *D*. Note that the EC C_C atom sits atop a surface oxygen ion that is not bonded to a Mn immediately below. (**e**) Intermediate *E*, with a broken C_C–O_E bond. The surface Mn(III) ion coordinated to the OE now becomes a Mn(IV). (**f**) Product *F*; a proton and two electrons are transferred to the surface. Reprinted with permission from [48] Copyright 2013 American Chemical Society

$EC/LiBF_4$ [63], $PC/LiBF_4$ [63, 64], $PC/LiPF_6$ [64], $DMC/LiBF_4$ [63], oligoethers/$LiPF_6$ [65–67], and PC/LiTFSI [54]. Most simulations focused on understanding the lithium cation coordination by solvent molecules and cation–anion aggregation. They provided valuable complementary information to the Raman spectroscopy

and NMR studies of the composition of the lithium solvation shell. While reviewing simulation results, it is important to pay attention to the reported simulation time, because some of the earlier classical MD simulations by Li et al. [68] and Soetens [63] were only 200 and 100 ps long [63, 68], and the ab initio MD simulations of EC/$LiPF_6$ and PC/$LiPF_6$ by Ganesh et al. [51] lasted less than one EC-lithium residence time (~0.5 ns) [52], which is significantly less than the lithium-anion residence time of 2–3 ns for similar electrolytes at 298 K [52]. Recent MD simulations [52, 55–57], however, were performed for tens of nanoseconds to ensure a complete equilibration and extraction of accurate conductivity values. It is recommended that MD simulation trajectories be longer than the cation–anion or lithium-solvent residence time in order to obtain equilibrium between ion aggregates and solvent-separated ion pairs (SSIP) as well as provide a reliable estimate of the composition of the Li^+ cation solvation shell.

Early study of one $LiBF_4$ in PC, EC, and DMC by Soetens [63] provided initial insight into the structure of the lithium solvation shell. Four strongly bound solvent molecules in a tetrahedral arrangement around a lithium cation were reported [63], which is qualitatively consistent with the recent MD studies [52, 53, 55] and ab initio simulations [69]. For example, MD simulations [52, 70] of EC:DMC/$LiPF_6$ and EC:PC/$LiPF_6$ electrolytes predicted that the total number of solvents and anions in the coordination shell was around 4.2–4.4. Analysis of time-of-flight neutron diffraction measurements was carried out for $^6Li/^7Li$ isotopically substituted 10 mol% $LiPF_6$-propylene carbonate-*d*6 (PC-*d*6) solutions, which revealed that the first solvation shell of Li^+ consists on average of 4.5(1) PC molecules with an intermolecular Li + O(PC) distance of 2.04(1) Å [71].

A link between the composition of a Li^+ solvation shell and the activation energy for the Li^+ desolvation and composition of the SEI has been recently examined [72–74]. The prevalence of PC compared to EC in the Li^+ coordination shell was observed in the gas-phase QC studies, using soft ionization technique electrospray ionization (ESI-MS) and MD simulations of EC:PC(1:1)/$LiPF_6$ electrolyte [70]. These data together with the DFT calculations of the first reduction in EC_nPC_m/Li^+ ($n+m=3,4$) clusters indicated a preferential reduction of PC on the graphite anode. Analogous ESI-MS results [74] were obtained in the EC:DMC/$LiPF_6$ mixtures, with a Li^+ preferring EC over DMC in the gas phase in agreement with QC data [52]. In the condensed phase, the oxygen NMR shift for a carbonyl of EC was larger than for DMC, likely related to the stronger interaction between Li^+ and EC compared to DMC [52]. In MD simulations of EC:DMC/$LiPF_6$, a similar probability was found for finding EC and DMC in the Li^+ first coordination shell, indicating a difference between the composition of the Li^+ solvation shell in the gas phase and the condensed phase [52]. Takeuchi et al. [75] and Borodin et al. [52] found that the Li^+ binding pattern to a PF_6^- anion was also found to be different in the gas and condensed phases. The monodentate structure was typically most stable in the condensed phase, whereas the configuration was multidentate in the gas phase. A preference for EC over DMC was observed for the interfacial Li^+ located at the positively or the negatively charged electrodes as is discussed below [76], making a link between the preferential Li^+ solvation by EC vs. DMC and the EC preferential reduction on the graphite anode [74].

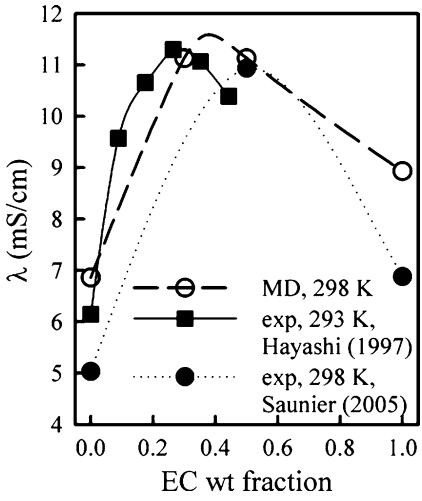

Fig. 8.6 Concentration dependence of ion conductivity from MD simulations [52] and experiments [79, 80]. Reprinted with permission from [52]. Copyright 2009 American Chemical Society

MD simulations with polarizable force fields predicted ion diffusion coefficients [52, 53, 55, 77] typically within 40 % of experiments for DMC/LiTFSI, EC/LiTFSI, PC/LiTFSI, DMC/LiTFSI, EC:DMC/$LiPF_6$, and (EO_n)/LiTFSI, where EO is an ethylene oxide repeat unit, $n = 2,5,12$. MD simulations using polarizable force fields also predicted electrolyte conductivity within 20–40 %. A comparison between MD simulations [52] using a polarizable force field and experiments is shown in Fig. 8.6. MD simulations employing a nonpolarizable force field [54], on the other hand, predicted ion diffusion a factor of 2–4 slower for EC/LiTFSI and PC/LiTFSI and 5–7 times slower for PC/$LiBF_4$ and PC/$LiPF_6$ [64]. Conductivity was predicted a factor of 5 lower for PC/$LiPF_6$ [78] and a factor of 2 lower for PC/LiTFSI [54] and EC/LiTFSI [54] in MD simulations using nonpolarizable force fields. However, when a nonpolarizable force field was parameterized based upon ab initio simulations of a small periodic electrolyte, good agreement with experiments and polarizable simulations for both coordination number and ion transport was obtained [50].

Because MD simulations yield both structural and dynamics properties, it is possible to extract both the fraction of solvent separated ion pairs SSIP (or ions not complexed by counterions) and the iconicity, which characterizes the degree of ion-uncorrelated motion. In [52] the fraction of SSIP, or the degree of solvent dissociation α_s (static), defined as the fraction of Li^+ and PF_6^- with no counterion in their first solvation shell, i.e., $r(\text{Li–P}) > 4.4$ Å for all pairs, is shown in Fig. 8.7. The fraction of free ions increases nearly linearly as the EC fraction increases in the electrolyte, and increasing the temperature slightly decreases the fraction of free ions. Ionicity, or the degree of dynamic correlation (α_d), was extracted from MD simulations using ion self-diffusion coefficients and conductivity (λ), as given by (8.6) and (8.7), in order to compare with α_s (static):

$$\alpha_d = \frac{\lambda}{\lambda^{N-E}}, \tag{8.6}$$

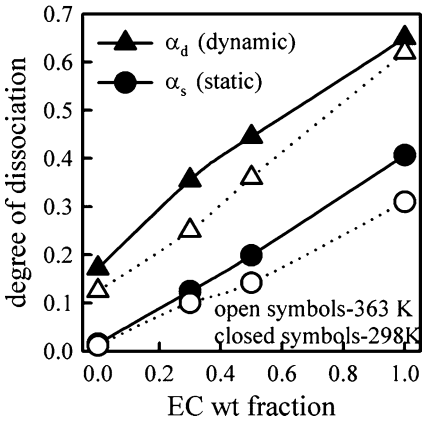

Fig. 8.7 The dynamics (α_d or ionicity) and static (α_s) degree of ion dissociation (fraction of solvent separated ion pairs) for EC:DMC/$LiPF_6$ at 298 K at an ~1-M salt concentration. Reprinted with permission from [52]. Copyright 2009 American Chemical Society

$$\lambda^{N-E} = \frac{e^2}{Vk_BT}\left(n_+D_+ + n_-D_-\right), \tag{8.7}$$

where k_B is the Boltzmann constant, T is temperature, V is the volume of the simulation box, and D_- and D_+ are the self-diffusion coefficients of the anion and cation, respectively. Figure 8.7 indicates that α_d is always higher than the fraction of free ions from the structural analysis (α_s), indicating an important contribution from the charged ion cluster transport to ion conductivity [52]. Joint pulsed gradient spin echo (pgse)-NMR and conductivity analysis of LiTFSI in multiple electrolytes at solvent:Li ratio of 20 at 298 K for PC/LiTFSI and DMC/LiTFSI yielded α_d values of 0.62 and 0.11, respectively, in accord with MD predictions for EC:DMC/$LiPF_6$, shown in Fig. 8.7, and provided a $LiPF_6$ and LiTFSI yield of similar α_d [81]. This indeed seems to be the case as similar α_d were found for LiTFSI and $LiPF_6$ salts in γ-butyrolactone (GBL) electrolyte [82]. Further analysis of the ion diffusion mechanism in EC:DMC/$LiPF_6$ electrolytes [77] indicated an approximately equal contribution from vehicular motion of the Li^+ with the first solvation shell and solvent exchange for Li solvated by EC. In contrast to the lithium motion in carbonates, in oligoethers, Li^+ moves three to four solvent molecules before its solvation shell is renewed, indicating that the motion of the Li^+ together with its solvation shell dominates over the solvent exchange mode of the lithium transport in oligoethers.

8.3.2 Modeling of Ionic Liquid Electrolytes

Binary room-temperature ionic liquid (RTIL)-based electrolytes have attracted significant attention because of their negligible vapor pressure; good thermal and electrochemical stability in the range of 5.3 V [83]; good dissolution properties with many organic and inorganic compounds and lithium salts; and low flammability [84].

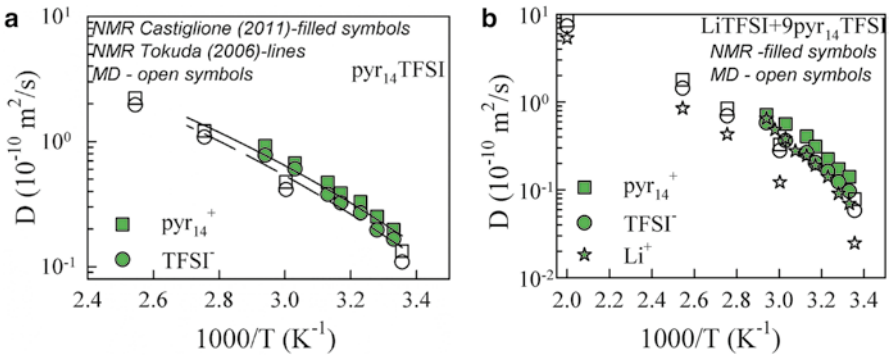

Fig. 8.8 (**a**) Diffusion coefficients of $pyr_{14}TFSI$ from MD simulations [87] and NMR measurements by Castiglione et al. [92] and Tokuda et al. [93]. (**b**) Diffusion coefficients of $LiTFSI + 9pyr_{14}TFSI$ from MD simulations [87] and NMR measurements by Castiglione et al. [92]

A wide variety of possible anions and cations offer a potential to tailor RTIL properties to a particular application. While hundreds of MD simulations of RTILs were reported, only a few MD simulations focused on Li^+ transport in RTIL-based binary electrolytes. Both polarizable [53, 85–88] and nonpolarizable [89, 90] force fields were used in these simulations. MD simulations employing polarizable force fields predicted Li^+ transport in $pyr_{14}TFSI$ doped with LiTFSI below experimental values [86], while MD using nonpolarizable force fields predicted significantly slower ion transport. In particular, MD simulations [90] of bmmimTFSI doped with LiTFSI using a nonpolarizable force field predicted ion transport that was less than an order of magnitude slower than the pfg-NMR data. Figure 8.8 shows the ion self-diffusion coefficients from MD simulations [87] employing an APPLE&P [91] many-body polarizable force field. While the self-diffusion coefficient of $pyr_{14}TFSI$ was found to be in an excellent agreement with the experiments, the Li^+ cation self-diffusion coefficient in the $pyr_{14}TFSI$ doped with LiTFSI was noticeably slower than the experimental data from Castiglione et al. [92], which indicates that further force field refinement is needed. Solano et al. [86] published similar results.

In polarizable simulations of $pyr_{13}TFSI$, $pyr_{14}TFSI$, $pyr_{14}TFSI$, and emimFSI doped with LiTFSI or LiFSI salts [53, 85–88], the Li^+ cation was found to be coordinated, on average, by roughly four oxygen atoms. Both monodentate (one oxygen of TFSI bound to a Li^+) and bidendate (two oxygens of TFSI bound to a Li^+) coordinations were observed with a preference for the monodentate configuration in contrast to the conclusions of infrared and Raman studies of alkyl-substituted imidazolium-TFSI-based IL doped with LiTFSI [94]. Both monodentate and bidentate $Li^+/TFSI^-$ configurations were observed in MD simulations of liquid AN-LiTFSI [56]. The spectroscopic study found that for the LiTFSI mole fractions, $0.08 < x < 0.2$, the $[Li(TFSI)_2]^-$ solvating cage involved bidentate coordinations of Li^+ with two oxygen atoms of one anion in the trans (C_2) conformation and two oxygen atoms of the other anion in the cis (C_1) conformation. While it is possible that the discrepancy is due to deficiencies in the APPLE&P force field, it is also possible that the Raman peak due to the Li^+/

$TFSI^-$ monodentate complex with $TFSI^-$ in the C_2 conformation does not have an appreciable shift in the Raman vs. TFSI not bound to Li^+ and, therefore, this ion pair is not adequately taken into account in the analysis of Raman data, as discussed in Seo et al. [56]. The mechanism of lithium transport in $pyr_{13}TFSI + 0.25LiTFSI$ [53] was found to occur primarily by exchanging $TFSI^-$ anions in the first coordination shell of a Li^+ with a smaller (~30 %) contribution also due to Li^+ cations diffusing together with their first coordination shell. At lower LiTFSI concentrations in 0.9pyr14TFSI + 0.1LiTFSI, Solano et al. [86] concluded that the dominant contribution to the Li^+ transports comes from the exchange of anions.

Solvent-free molten salts were also investigated by MD simulations. They are attractive due to their potential to eliminate ion concentration polarization during battery operation. MD simulations provided insight into the lithium coordination and transport mechanism in a solvent-free molten salt electrolyte comprising $TFSI^-$ tethered to oligoethylene oxide (EO) ($EO_{12}TFSI^-/Li^+$) [59]. The behavior of $EO_{12}TFSI^-/Li^+$ was contrasted with the ion transport and aggregation in a binary solution of EO_{12} doped with LiTFSI salt (EO_{12}/LiTFSI). It was found from the MD simulations and experiments that attaching a $TFSI^-$ anion to the chain end of the oligoether resulted in a reduction of conductivity by one order of magnitude at 423 K and two orders of magnitude at room temperature. In the $EO_{12}TFSI^-/Li^+$ single-ion conducting molten salts only Li^+ exchange solvating groups contributed to ion conduction.

8.3.3 Modeling of SEI Components

The SEI is formed on the battery anode by deposition of electrolyte reduction products; thus, the solubility of these products in electrolytes is important and was studied by Tasaki et al. [95]. They suggested the following order for the SEI-forming salts to be soluble in DMC and EC: lithium dilithium ethylene dicarbonate (Li_2EDC) > lithium methyl carbonate (LiMC, $LiOCO_2CH_3$) > $LiOH > LiOCO_2C_2H_5 > LiOCH_3 > LiF > (LiCO_2)_2 > Li_2CO_3 > Li_2O$. This order agreed with experiments performed in DMC quite well [95].

Ability of SEI model compounds to transport Li^+ determines a battery's interfacial impedance and is critical to enabling high charge–discharge rates especially at low temperature. A number of theoretical studies (DFT models and MD simulations) focused on understanding Li^+ transport in SEI compounds as discussed in [96]. The low barrier of 0.28 eV for the migration barrier of Li^+ diffusion between the planes defined by the Li_2CO_3 units along the open channels [010] was found, while a higher migration barrier of 0.60 eV was found for diffusion across the planes. Chen et al. [97] found that Li^+ diffusion in Li_2CO_3 ranges from 0.23 to 0.49 eV. But, as Shi et al. [96] pointed out, in the interstitial diffusion mechanism a Li^+ must pass through multiple barriers with the highest barrier being 0.54 eV relative to the most stable interstitial structure. Thus, a "knockoff" mechanism for Li^+ diffusion in Li_2CO_3 was proposed by Shi et al. [96], which had a significantly lower overall barrier for Li^+

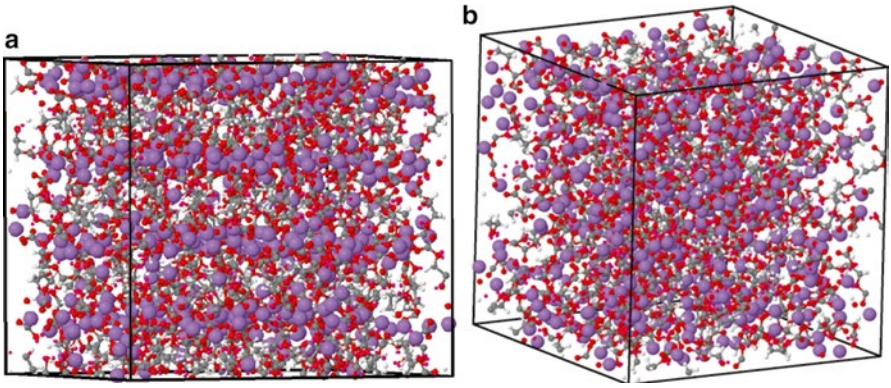

Fig. 8.9 Snapshot from the MD simulations of Li_2EDC of the ordered (**a**) and amorphous (**b**) (molten phase) states at 450 K (Li^+ are highlighted as pink balls)

hopping of 0.31 eV. Because the activation energy for lithium diffusion includes both the formation energy of the Li^+ defect and the activation energy for hopping, the total activation energy for the "knockoff" mechanism was estimated to be around 0.7 V at low voltages, close to lithium metal potential, and it increases as voltage increases according to Shi et al. [96]. Chen et al. [97] also investigated barriers for Li^+ diffusion in the other SEI compounds and found that Li^+ diffusion in Li_2O was 0.152 eV, which is much lower than in LiF (0.729 eV).

MD simulations [59, 98] employing classical polarizable force fields have been used to investigate the structure and transport of two SEI components: dilithium ethylene dicarbonate $(LiCO_3CH_2)_2$, or Li_2EDC, and LiMC, which are often found in outer part of the SEI [99, 100]. While crystals are of room temperature, these compounds might exist in a disordered state in the outer part of the SEI because the high fraction of other components and impurities that might present in the SEI would inhibit the formation of the crystalline ordered phase. MD simulations were performed on the disordered and smectic-like ordered Li_2EDC states, as shown in Fig. 8.9 [98]. MD simulation predictions of the ionic conductivity of Li_2EDC as a function of temperature are shown in Fig. 8.10. Conductivity of the ordered phase was averaged over all three directions. Figure 8.10 indicates that the conductivity of the ordered phase is only slightly higher than the conductivity of the molten state. The experimentally determined conductivity at room temperature is situated slightly below the extrapolated conductivities from MD simulations. Figure 8.10 also shows an activation energy for both the ordered and disordered states around 0.64 eV [98]. This activation energy is similar to the activation energy of 0.7 eV for the inner SEI Li_2CO_3 model compound from the knockoff mechanism [96]. The theoretical predictions for the activation energy for these two SEI compounds are similar to the experimentally measured [101, 102] activation energies for the total interfacial resistance. These results indicate that a 20-kJ/mol activation energy attributed

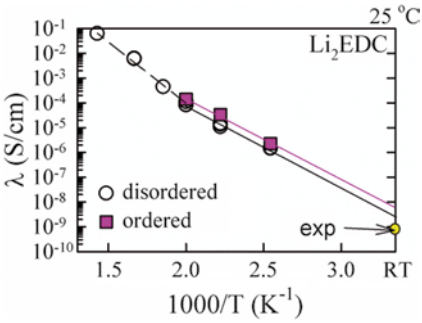

Fig. 8.10 Conductivity form MD simulations using a polarizable APPLE&P force field for melted and ordered Li_2EDC materials. ΔE(ordered) = 64 kJ/mol was obtained by fitting data in the range of 393–500 K from Borodin et al. [98]

during analysis of the impedance data to ion transport in SEI [103] is inconsistent with the activation energy for ion transport in Li_2EDC or Li_2CO_3.

MD simulations also provided details of the Li^+ transport mechanism. At room temperature, the Li^+ transport was suggested to be sub-diffusive on time scales shorter than ~10^{-2} s from analysis of the MD data, which is in a good agreement with the frequency-dependent impedance spectroscopy data, which showed a plateau of resistivity vs. frequency occurring at frequencies lower than 10^2 Hz [98]. Li^+ motion was also significantly more non-Gaussian and heterogeneous in Li_2EDC compared to RTILs, with the motion of the fast-moving Li^+ being spatially correlated, exhibiting chain-like and loop-like hopping by Li^+. The influence of polarization on the Li_2EDC structure and transport was investigated [98]. Turning off polarization resulted in a significant slowing down of ion transport and an increase in the activation energy for ion transport to a much greater extent than was previously observed for RTILs. Finally, initial simulations of Li_2EDC dissolved in EC:DMC(3:7)/$LiPF_6$ reported in [98] indicated a strong aggregation of Li_2EDC that led to the formation of the percolating cluster localized in one part of the simulation cell, which is consistent with a Li_2EDC phase separating from the EC:DMC(3:7)/$LiPF_6$. Interestingly, the Li^+ in the segregated Li_2EDC in EC:DMC(3:7)/$LiPF_6$/Li_2EDC exchanged between anionic EDC^{2-} groups multiple orders of magnitude faster than the Li^+ exchanged anions in the Li_2EDC melt due to a solvent-plasticizing effect in the former. This indicates that trapped solvent could significantly enhance Li^+ transport inside of an SEI.

8.4 MD Simulations of the Electrode–Electrolyte Interfaces

Numerous experimental studies [104–107] indicated that the interfacial impedance could be a limiting factor for charge transport in lithium batteries at low temperature as it exceeds the resistance of the bulk electrolyte. Two major contributions to the interfacial impedance are commonly discussed: (1) the low conductivity and high activation energy of SEI and (2) the resistance associated with the lithium desolvation process as it changes phases from electrolyte to SEI, from SEI to

electrode, or from electrolyte to electrode if the SEI is not formed. The length scale for the desolvation process is on the scale of nanometers and, therefore, could be accessed via molecular simulations. Our preliminary MD simulations of the Li^+ cation desolvation from electrolyte into graphite are presented first, followed by the results for the SEI–electrolyte interface.

The Li^+ desolvation from electrolyte was extensively investigated experimentally for the graphite–electrolyte, $Li_4Ti_5O_{12}$–electrolyte, and ceramic ($Li_{0.35}La_{0.55}TiO_3$ (LLT) and $Li_4Ti_5O_{12}$, or LTO)–electrolyte interfaces [72, 73, 103, 108–113]. Because no SEI is present on the $Li_4Ti_5O_{12}$ anode or ceramic, the desolvation contribution can be straightforwardly extracted from impedance measurements, while on graphite electrodes one has to decouple the desolvation and SEI contributions. Yamada et al. [110] investigated desolvation from EC:DMC/$LiClO_4$ electrolytes into LLT and back and found activation energies 51 and 53 kJ/mol for EC:DMC(1:1) and EC:DMC(1:9) compositions, respectively, which are slightly lower than activation energies in the range of 64–72 kJ/mol found by Xu et al. [73] for EC:DMC = 2.3–11.4 doped with $LiPF_6$. Both groups concluded that activation energy was largely constant in a wide range of EC:DMC concentrations, which raised questions to the simulation community with regard to the underlying physics of the desolvation process.

MD simulations were performed on EC/$LiPF_6$ and EC:DMC(3:7)/$LiPF_6$ 1 M electrolytes using an APPLE&P force field [52, 91] next to the material blocking for the anion and solvent but not blocking to the lithium cation to measure the interfacial resistance and free energy due to lithium desolvation from electrolyte. At the initial stage, graphite was chosen as the electrode material and did not include an SEI or a controlled voltage between the electrodes. The simulation cell is shown in Fig. 8.11. The simulation length ranged from 10 to 15 ns. The free energy profile for the Li^+ desolvation from electrolyte was calculated by integration of the potential of mean force. The free energy $\Delta G(z)$ shows a local minimum of −0.5 kcal/mol at ~5 Å from the graphite, which is indicative of a preferential lithium position in the Helmholtz plane. The free energy sharply increases as the lithium approaches the graphite and is forced to desolvate from the electrolyte at distances closer than 4 Å from graphite. If one assumes that the charge-transfer reaction occurs when a Li^+ is located between outer layer carbon and hydrogen atoms, then a value of $\Delta G(z)$ around 12–19 kcal/mol is obtained, which is consistent with the experimental activation energies of 16.4–17 kcal/mol [73, 103, 109, 111, 113]. MD simulations also predict quite a similar desolvation profile in the immediate vicinity of the graphite surface for EC/$LiPF_6$ and EC:DMC(3:7)/$LiPF_6$, which is consistent with the DMC being desolvated first and EC being desolvated last.

The influence of the applied potential on the electrolyte structural properties was recently examined for EC:DMC/$LiPF_6$ and TMS(sulfolane):DMC/$LiPF_6$ electrolytes near the basal face of graphite electrodes [76, 114]. For the interfacial EC:DMC/$LiPF_6$, electrolyte charging of electrodes resulted in the polar EC replacing the less polar DMC molecule near the electrolyte surfaces, as shown in Fig. 8.12. This effect was observed for both negative and positive electrodes and was experimentally confirmed for the $LiCoO_2$ cathode using the sum frequency generation technique [115]. MD simulations indicated that at negative potentials, the carbonyl

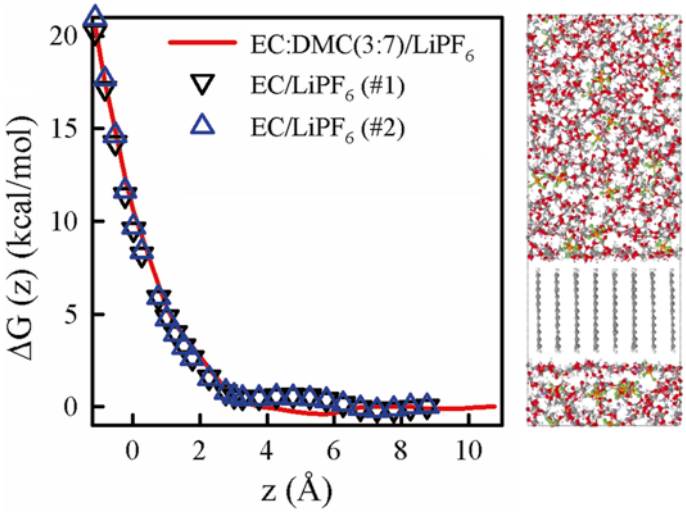

Fig. 8.11 The lithium cation desolvation free energy profile for $EC/LiPF_6$ and $EC:DMC(3:7)/LiPF_6$ 1 M electrolytes next to the graphite at 298 K. $Z=0$ corresponds to position of the hydrogen atoms of the graphite. A snapshot of the simulation box used for calculating the free energy barrier for charge transfer is shown in the *right*

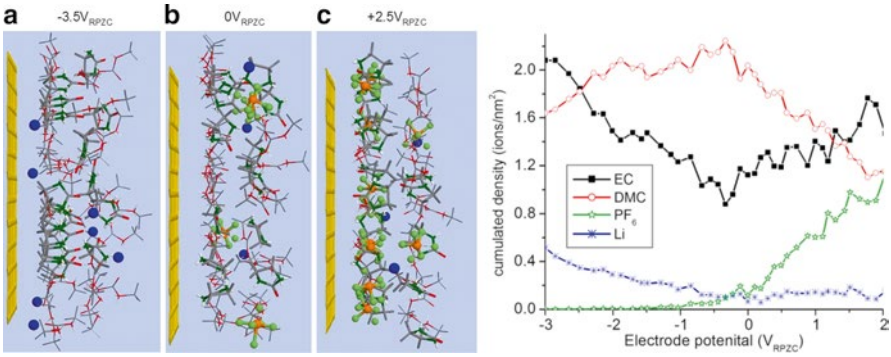

Fig. 8.12 (*left*) Image snapshots showing the electrolyte ordering near interface at a large negative potential (**a**), potential of zero charge (PZC) (**b**), and a large positive electrode potential (**c**); and the cumulated density of electrolyte species in the interfacial layer, i.e., within 6.0 Å from surface, as a function of the electrode potential (shown in the *right*). Reprinted with permission from [76]. Copyright 2012 American Chemical Society

groups from the carbonate molecules are repelled from the surface, while at positive potentials the interfacial layer was enriched with carbonyl groups. The PF_6^- anion rapidly accumulated at the positive electrode with increasing potential; thus, one expects it to be readily available to participate in the oxidation reactions of the solvent–anion complexes discussed above. At the most negative potentials, the Li^+

cation adsorbed at the electrode and was preferentially solvated by EC not DMC. This preference correlates well with the experimental observation [74] of EC reduction dominating the SEI in EC:DMC/$LiPF_6$ mixtures.

In MD simulations [114] of TMS:DMC/$LiPF_6$, a strong enrichment of TMS was found on the negative electrode as the adsorbed Li^+ strongly preferred to be coordinated by TMS vs. DMC, and the relatively polar TMS was able to better respond to the electrostatic potential near a charged surface. In the TMS:DMC/$LiPF_6$ double layer next to the positive electrode, DMC was located approximately 0.8 Å further away from the positive electrode than in EC:DMC/$LiPF_6$, indicating that it might be more difficult to oxidize DMC in TMS-based electrolytes compared to EC-based electrolytes. This finding is consistent with the experimentally reported increased oxidative stability of the sulfone-containing electrolytes [116, 117], of the latter and the good cycling ability of a cell containing a TMS:DMC/$LiPF_6$ electrolyte with a high voltage $LiNi_{0.5}Mn_{1.5}O_4$ spinel positive electrode [118].

The behavior of RTILs at electrified interfaces was extensively studied due to possible applications in double-layer capacitors and has recently been reviewed in a prospective paper [119]. Most studies have focused on understanding differential capacitance behavior as a function of potential or enhancement of the capacitance upon nano-confinement. The composition and ion orientation of RTILs in the innermost layer at the flat surface were found to be strongly dependent on the electrode potential [120]. The ions reoriented as potential were applied. For pyr_{13}TFSI at potentials near the PZC, both the cations and anions adjacent to the surface are oriented primarily perpendicular to the surface; the counterions in first layer orient increasingly parallel to the surface with increasing electrode potential. A camel-shape behavior of differential capacitance was observed with a minimum in DC observed around −1 V relative to the PZC, which corresponded to the point of highest density of perpendicularly aligned TFSI near the electrode. Maxima in the DC observed around +1.5 and −2.5 V_{RPZC} are associated with the onset of "saturation," or crowding, of the interfacial layer [120]. Interestingly, the double-layer structure and capacitance were dependent on the curvature or the atomistic roughness of the surface, especially near the potential of the zero charge. Highly curved surfaces [121, 122] or rough surfaces [123] lead to increased capacitance, as shown in Fig. 8.13. The interfacial packing on the edge surface of graphite shows a dramatically different interfacial structure and charge-storing ability than the atomically flat basal surface.

8.5 Modeling the SEI–Electrolyte Interface

The theoretical studies of the SEI–electrolyte interface are rare [50], while ion transport in electrolytes doped with lithium salts has received significant attention in the form of MD simulations [52, 53, 56, 61, 64, 70, 124–126], ab initio simulations [51, 127], and QC studies [29, 124, 126, 128–134]. The DFT studies of EC-based electrolyte interactions with a graphite anode were recently reviewed by

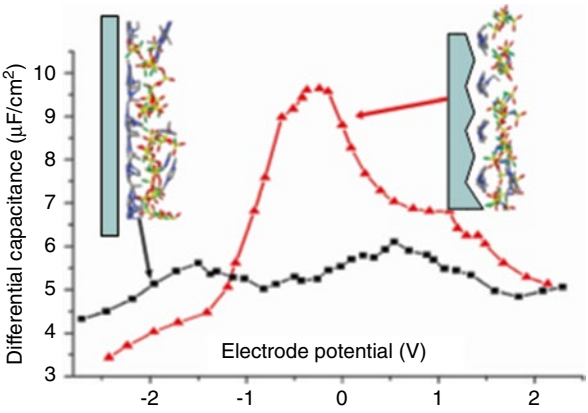

Fig. 8.13 Differential capacitance of 1-ethyl-3-methyl imidazolium (emim) and bisfluorosulfonyl imide (FSI) with a low concentration of LiFSI [123]. Reprinted with permission from [123] Copyright 2011 American Chemical Society

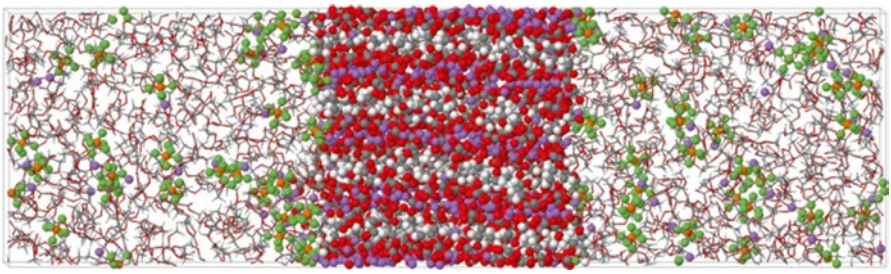

Fig. 8.14 A simulation snapshot showing ordered Li_2EDC in contact with the electrolyte. Solvent molecules are shown as *wireframe*, while Li_2EDC and $LiPF_6$ are highlighted using a *ball* and *stick* model

Leung [48, 135]. Tasaki [95, 136] studied interactions in supercooled Li_2EDC and dilithium 1,2-propylene glycol dicarbonate with graphite at room temperature using MD simulations. Jorn et al. [50] reported on MD simulations of the graphite | Li_2EDC doped and undoped with LiF | EC-$LiPF_6$ electrolyte | SEI | graphite symmetry cell that provided an important initial insight into the SEI–electrolyte interface. Despite long simulation runs (>24 ns) at 453 K, Jorn et al. [50] observed only partial Li^+ desolvation from the electrolyte and adsorption on the SEI surface, raising concerns that the interfacial region might not have been fully equilibrated as Li^+ did not exchange between the SEI and electrolyte. In the preliminary 272-ns simulations of the Li_2EDC | EC:DMC(3:7) $LiPF_6$ (solvent:Li = 10 in electrolyte) interface performed by us at ARL at 393 K, more than 80 Li^+ transfers from electrolyte to SEI and from SEI to electrolyte occurred during the course simulations. A snapshot of the simulated system is shown in Fig. 8.14. The smectic-like ordered Li_2EDC was used in these simulations.

Density profiles have been analyzed from the center of the SEI layer and are shown in Fig. 8.15a. The interface is sharp, with 90 % of the reductions of the

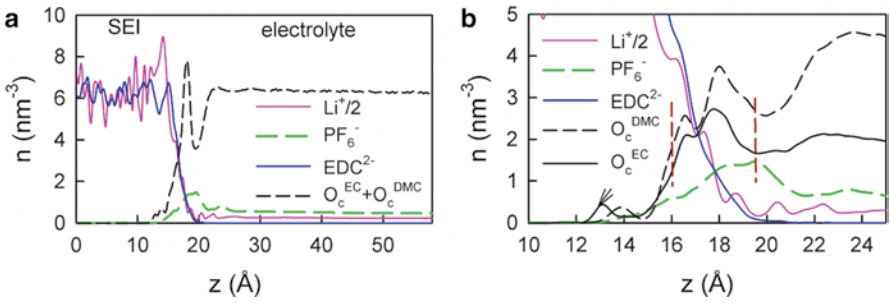

Fig. 8.15 Number density (**a**, **b**) profiles for $Li_2EDC|EC:DMC(3:7)/LiPF_6$ at 393 K over the last 50 ns of MD simulations. The SEI center of mass is located at $z = 0.0$ Å, while the SEI–electrolyte interface is located at ~17 Å

EDC_2^- density profile occurring within 3 Å. The density profile of the solvent carbonyl oxygen shows a well-defined peak at 18 Å and no structuring beyond 22 Å. The position of the peak for the PF_6^- anion density profile at 18 Å roughly coincides with the peak for electrolyte oxygen atoms, as both are due to coordination of the Li^+ cations situated on the Li_2EDC surface. The magnitude of the PF_6^- anion peak is roughly three times the density of PF_6^- in the bulk electrolyte, indicating preferential partitioning of the PF_6^- from the bulk electrolyte to the SEI–electrolyte interface. Jorn et al. [50] also observed high concentration of PF_6^- anions near the SEI surface. As the whole simulated system is charged neutral, the excess of negative charge due to PF_6^- anions around 16–20 Å is compensated by the excess of the Li^+ at 12–15 Å.

In order to obtain further insight into the interfacial structure, the density profiles of carbonyl oxygen atoms of EC and DMC were plotted separately, as shown in Fig. 8.15b. The interfacial region was magnified for clarity in this figure. When the EC and DMC density profiles are traced from the electrolyte toward the SEI, they show that DMC density dips significantly lower at 20 Å compared to the drop in the EC density profile. The first DMC peak is slightly shifted compared to the EC peak. As the solvent further approaches the SEI surface, the DMC profile has a sharper drop compared to the EC density profile. In fact, the EC and DMC density profiles cross at 15 Å. Interestingly, EC penetrates further into the SEI layer than DMC, as indicated by a peak in the EC density profile shown at 13 Å. At this distance, no DMC was observed. We conclude that MD simulations indicate an enrichment of EC compared to DMC near the SEI surface. Moreover, analysis of the composition of the Li^+ cation coordination shell in the interfacial region indicated that upon the initial approach to the SEI from the electrolyte the Li^+ cation initially exchanged DMC for EDC^{2-} oxygen atoms with EC sticking to the Li^+ longer than DMC in the process of desolvating from the electrolyte. Because EC is the last solvent to get exchanged despite the abundance of DMC in bulk electrolyte, one would expect the desolvation free energy to be significantly influenced by this last event of Li-EC desolvation and, thus, largely independent of the EC:DMC composition.

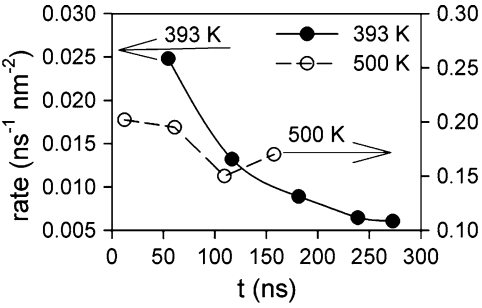

Fig. 8.16 The rate of Li^+ desolvation reaction between EC:DMC/$LiPF_6$ electrolyte and Li_2EDC from MD simulations

The rate of the Li^+ desolvation reaction was estimated from our preliminary simulations. The desolvation event was defined as the change of the Li^+ first coordination shell from being coordinated by solvents or PF_6^- anions to being coordinated by only carbonate groups from EDC_2^- anions. While the rate for the desolvation reaction did not appreciably change over the course of MD simulations at 500 K as shown in Fig. 8.16, at 393 K the rate of desolvation reactions monotonically decreased over the first 200 ns of simulations, thus indicating that long simulation trajectories might be necessary in order to obtain a reliable estimate of it. Using the Li^+ desolvation rates at 393 and 500 K we obtain an estimate for the activation energy for the Li^+ desolvation process of 52 kJ/mol assuming the Arrhenius process. The rate for the desolvation reaction is lower than the rate for the Li^+ conduction in Li_2EDC (64 kJ/mol, see Fig. 8.10) likely due to plasticizing effect of electrolyte on the dynamics of the interfacial SEI layer. The activation energy is, however, similar to the experimentally determined activation energy for the Li^+ desolvation from the EC:DMC-based electrolytes into lithiated spinel titanate ($Li_4Ti_5O_{12}$) of 50–52 kJ/mol but lower than the activation energy for the desolvation into SEI-covered graphite of 60–70 kJ/mol [73, 111].

In summary, it is exciting time for the molecular modeling community as MD simulations have shown promise to quantitatively predict the structure and transport of bulk electrolytes and model SEI components and have been recently expanded to the interfacial properties. DFT methods provide an important insight into the oxidation stability of electrolytes at non-active electrodes and are being extended to active material–electrolyte interfaces. Additional progress in coupling the transport of reactants (redox products) and reaction rates is needed to predict the SEI formation reactions that occur on time scales far longer than current DFT methodologies can handle.

Acknowledgement This work was supported via an Interagency Agreement between the US Department of Energy and the US Army Research Laboratory under DE-IA01-11EE003413 for the Office of Vehicle Technologies Programs including the ARB Program. Discussions with Arthur von Cresce, T. R. Jow, Kang Xu, Kevin Leung, Wesley Henderson, Lidan Xing, Dmitry Bedrov, Samuel Delp, and Brett Lucht are highly appreciated.

References

1. Assowe, O.; Politano, O.; Vignal, V.; Arnoux, P.; Diawara, B.; Verners, O.; van Duin, A. C. T., Reactive Molecular Dynamics of the Initial Oxidation Stages of Ni(111) in Pure Water: Effect of an Applied Electric Field. *J. Phys. Chem. A* **2012,** *116*, 11796-11805.
2. Han, S. S.; van Duin, A. C. T.; Goddard, W. A.; Lee, H. M., Optimization and Application of Lithium Parameters for the Reactive Force Field, ReaxFF. *J. Phys. Chem. A,* **2005,** *109*, 4575-4582.
3. Curtiss, L. A.; Redfern, P. C.; Raghavachari, K., G_n Theory. *Wiley Interdisciplinary Reviews: Comput. Mol. Sci.* **2011,** *1*, 810-825.
4. Trasatti, S., The Absolute Electrode Potential - an Explanatory Note (Recommendations 1986). *Pure Appl Chem* **1986,** *58*, 955-966.
5. Gomer, R.; Tryson, G., An Experimental Determination of Absolute Half-Cell Emf's and Single Ion Free Energies of Solvation. *J. Chem. Phys.* **1977,** *66*, 4413-4424.
6. Isse, A. A.; Gennaro, A., Absolute Potential of the Standard Hydrogen Electrode and the Problem of Interconversion of Potentials in Different Solvents. *J. Phys. Chem. B* **2010,** *114*, 7894-7899.
7. Zhang, X. R.; Pugh, J. K.; Ross, P. N., Computation of Thermodynamic Oxidation Potentials of Organic Solvents Using Density Functional Theory. *J. Electrochem. Soc.* **2001,** *148*, E183-E188.
8. Shao, N.; Sun, X. G.; Dai, S.; Jianel, D. E., Electrochemical Windows of Sulfone-Based Electrolytes for High-Voltage Li-Ion Batteries. *J. Phys. Chem. B* **2011,** *115*, 12120-12125.
9. Dean, J. A., *Lange's Handbook of Chemistry (15th Edition)*. McGraw-Hill: New York, NY, 1999.
10. http://webbook.nist.gov/chemistry/, NIST Webbook.
11. Tissandier, M. D.; Cowen, K. A.; Feng, W. Y.; Gundlach, E.; Cohen, M. H.; Earhart, A. D.; Coe, J. V.; Tuttle, T. R., The Proton's Absolute Aqueous Enthalpy and Gibbs Free Energy of Solvation from Cluster-Ion Solvation Data. *J. Phys. Chem. A* **1998,** *102*, 7787-7794.
12. Westphal, E.; Pliego, J. R., Absolute Solvation Free Energy of Li^+ and Na^+ Ions in Dimethyl Sulfoxide Solution: A Theoretical Ab Initio and Cluster-Continuum Model Study. *J. Chem. Phys.* **2005,** *123(7), 074508*.
13. Eilmes, A.; Kubisiak, P., Relative Complexation Energies for Li^+ Ion in Solution: Molecular Level Solvation Versus Polarizable Continuum Model Study. *J. Phys. Chem. A* **2009,** *114*, 973-979.
14. Bryantsev, V., Calculation of Solvation Free Energies of Li^+ and O_2^- Ions and Neutral Lithium–Oxygen Compounds in Acetonitrile Using Mixed Cluster/Continuum Models. *Theor. Chem. Acc: Theory, Computation, and Modeling (Theoretica Chimica Acta)* **2012,** *131*, 1-11.
15. Marenich, A. V.; Cramer, C. J.; Truhlar, D. G., Universal Solvation Model Based on Solute Electron Density and on a Continuum Model of the Solvent Defined by the Bulk Dielectric Constant and Atomic Surface Tensions. *J. Phys. Chem. B* **2009,** *113*, 6378-6396.
16. Borodin, O.; Behl, W.; Jow, T. R., Oxidative Stability and Initial Decomposition Reactions of Carbonate, Sulfone, and Alkyl Phosphate-Based Electrolytes. *J. Phys. Chem. C* **2013,** *117*, 8661-8682.
17. Ue, M.; Murakami, A.; Nakamura, S., Anodic Stability of Several Anions Examined by Ab Initio Molecular Orbital and Density Functional Theories. *J. Electrochem. Soc.* **2002,** *149*, A1572-A1577.
18. Fu, Y.; Liu, L.; Yu, H. Z.; Wang, Y. M.; Guo, Q. X., Quantum-Chemical Predictions of Absolute Standard Redox Potentials of Diverse Organic Molecules and Free Radicals in Acetonitrile. J. *Am. Chem. Soc.* **2005,** *127*, 7227-7234.
19. Johansson, P., Intrinsic Anion Oxidation Potentials *J. Phys. Chem. A* **2007,** *111*, 1378-1379.
20. Xing, L. D.; Li, W. S.; Wang, C. Y.; Gu, F. L.; Xu, M. Q.; Tan, C. L.; Yi, J., Theoretical Investigations on Oxidative Stability of Solvents and Oxidative Decomposition Mechanism of Ethylene Carbonate for Lithium Ion Battery Use. *J. Phys. Chem. B* **2009,** *113*, 16596-16602.

21. Assary, R. S.; Curtiss, L. A.; Redfern, P. C.; Zhang, Z. C.; Amine, K., Computational Studies of Polysiloxanes: Oxidation Potentials and Decomposition Reactions. *J. Phys. Chem. C* **2011,** *115*, 12216-12223.
22. Ong, S. P.; Ceder, G., Investigation of the Effect of Functional Group Substitutions on the Gas-Phase Electron Affinities and Ionization Energies of Room-Temperature Ionic Liquids Ions Using Density Functional Theory. *Electrochim. Acta* **2010,** *55*, 3804-3811.
23. Shao, N.; Sun, X.-G.; Dai, S.; Jiang, D.-E., Oxidation Potentials of Functionalized Sulfone Solvents for High-Voltage Li-Ion Batteries: A Computational Study. *J. Phys. Chem. B* **2012,** *116*, 3235-3238.
24. Yoshimura, M.; Honda, K.; Kondo, T.; Uchikado, R.; Einaga, Y.; Rao, T. N.; Tryk, D. A.; Fujishima, A., Factors Controlling the Electrochemical Potential Window for Diamond Electrodes in Non-Aqueous Electrolytes. *Diam. Relat. Mater.* **2002,** *11*, 67-74.
25. Wang, R. L.; Moshurchak, L. M.; Lamanna, W. M.; Bulinski, M.; Dahn, J. R., A Combined Computational/Experimental Study on Tert butyl- and Methoxy-Substituted Benzene Derivatives as Redox Shuttles for Lithium-Ion Cells. *J. Electrochem. Soc.* **2008,** *155*, A66-A73.
26. Han, Y. K.; Jung, J.; Yu, S.; Lee, H., Understanding the Characteristics of High-Voltage Additives in Li-Ion Batteries: Solvent Effects. *J. Power Sources* **2009,** *187*, 581-585.
27. Li, T.; Xing, L.; Li, W.; Peng, B.; Xu, M.; Gu, F.; Hu, S., Theoretic Calculation for Understanding the Oxidation Process of 1,4-Dimethoxybenzene-Based Compounds as Redox Shuttles for Overcharge Protection of Lithium Ion Batteries. *J. Phys. Chem. A* **2011,** *115*, 4988-4994.
28. Johansson, P., Intrinsic Anion Oxidation Potentials. *J. Phys. CHem. A* **2006,** *110*, 12077-12080.
29. Johansson, P.; Jacobsson, P., Rational Design of Electrolyte Components by Ab Initio Calculations. *J. Power Sources* **2006,** *153*, 336-344.
30. Armand, M.; Johansson, P., Novel Weakly Coordinating Heterocyclic Anions for Use in Lithium Batteries. *J. Power Sources* **2008,** *178*, 821-825.
31. Scheers, J.; Johansson, P.; Jacobsson, P., Anions for Lithium Battery Electrolytes: A Spectroscopic and Theoretical Study of the $B(CN)_4^-$ Anion of the Ionic Liquid $C_2mim[B(CN)_4]$. *J. Electrochem. Soc.* **2008,** *155*, A628-A634.
32. Ong, S. P.; Andreussi, O.; Wu, Y. B.; Marzari, N.; Ceder, G., Electrochemical Windows of Room-Temperature Ionic Liquids from Molecular Dynamics and Density Functional Theory Calculations. *Chem. Mater.* **2011,** *23*, 2979-2986.
33. Tian, Y.-H.; Goff, G. S.; Runde, W. H.; Batista, E. R., Exploring Electrochemical Windows of Room-Temperature Ionic Liquids: A Computational Study. *J. Phys. Chem. B* **2012,** *116,* 11943–11952.
34. Borodin, O.; Jow, T. R., Quantum Chemistry Studies of the Oxidative Stability of Carbonate, Sulfone and Sulfonate-Based Electrolytes Doped with BF_4^-, PF_6^- Anions. *ECS Transactions* **2011,** *33*, 77-84.
35. Xing, L.; Borodin, O.; Smith, G. D.; Li, W., Density Functional Theory Study of the Role of Anions on the Oxidative Decomposition Reaction of Propylene Carbonate. *J. Phys. Chem. A* **2011,** *115*, 13896-13905.
36. Xing, L.; Borodin, O., Oxidation Induced Decomposition of Ethylene Carbonate from DFT Calculations - Importance of Explicitly Treating Surrounding Solvent. *Phys. Chem. Chem. Phys.* **2012,** *14*, 12838-12843.
37. Borodin, O.; Jow, T. R., Quantum Chemistry Study of the Oxidation-Induced Decomposition of Tetramethylene Sulfone (TMS) Dimer and TMS/BF_4. *ECS Transactions* **2013,** *50*, 391-398.
38. Wang, R. L.; Buhrmester, C.; Dahn, J. R., Calculations of Oxidation Potentials of Redox Shuttle Additives for Li-Ion Cells. *J. Electrochem. Soc.* **2006,** *153*, A445-A449.
39. Kang, S.; Park, M. H.; Lee, H.; Han, Y. K., A Joint Experimental and Theoretical Determination of the Structures of Oxidized and Reduced Molecules. *Electrochem. Commun.* **2012,** *23*, 83-86.

40. Shkrob, I. A.; Zhu, Y.; Marin, T. W.; Abraham, D. P., Reduction of Carbonate Electrolytes and the Formation of Solid-Electrolyte Interface (SEI) in Lithium Ion Batteries. 1. Spectroscopic Observations of Radical Intermediates Generated in One-Electron Reduction of Carbonates. *J. Phys. Chem. C* **2013,** *117*, 19255–19269
41. Egashira, M.; Takahashi, H.; Okada, S.; Yamaki, J., Measurement of the Electrochemical Oxidation of Organic Electrolytes Used in Lithium Batteries by Microelectrode. *J. Power Sources* **2001,** *92*, 267-271.
42. Ue, M.; Takeda, M.; Takehara, M.; Mori, S., Electrochemical Properties of Quaternary Ammonium Salts for Electrochemical Capacitors. *J. Electrochem. Soc.* **1997,** *144*, 2684-2688.
43. Xing, L. D.; Wang, C. Y.; Li, W. S.; Xu, M. Q.; Meng, X. L.; Zhao, S. F., Theoretical Insight into Oxidative Decomposition of Propylene Carbonate in the Lithium Ion Battery. *J. Phys. Chem. B* **2009,** *113*, 5181-5187.
44. Ufheil, J.; Wursig, A.; Schneider, O. D.; Novak, P., Acetone as Oxidative Decomposition Product in Propylene Carbonate Containing Battery Electrolyte. *Electrochem. Commun.* **2005,** *7*, 1380-1384.
45. Hammami, A.; Raymond, N.; Armand, M., Lithium-Ion Batteries: Runaway Risk of Forming Toxic Compounds. *Nature* **2003,** *424*, 635-636.
46. Yang, L.; Ravdel, B.; Lucht, B. L., Electrolyte Reactions with the Surface of High Voltage $Lini_{0.5}mn_{1.5}o_4$ Cathodes for Lithium-Ion Batteries. *Electrochem. Solid State Lett.,* **2010,** *13*, A95-A97.
47. Leung, K., First-Principles Modeling of the Initial Stages of Organic Solvent Decomposition on $Li_xMN_2O_4(100)$ Surfaces. *J. Phys. Chem. C* **2012,** *116*, 9852-9861.
48. Leung, K., Electronic Structure Modeling of Electrochemical Reactions at Electrode/ Electrolyte Interfaces in Lithium Ion Batteries. *J. Phys. Chem. C* **2013,** *117*, 1539-1547.
49. Karim, A.; Fosse, S.; Persson, K. A., Surface Structure and Equilibrium Particle Shape of the $Limn_2o_4$ Spinel from First-Principles Calculations. *Phys. Rev. B* **2013,** *87*, 075322.
50. Jorn, R.; Kumar, R.; Abraham, D. P.; Voth, G. A., Atomistic Modeling of the Electrode–Electrolyte Interface in Li-Ion Energy Storage Systems: Electrolyte Structuring. *J. Phys. Chem. C* **2013,** *117*, 3747-3761.
51. Ganesh, P.; Jiang, D.-e.; Kent, P. R. C., Accurate Static and Dynamic Properties of Liquid Electrolytes for Li-Ion Batteries from Ab Initio Molecular Dynamics. *J. Phys. Chem. B* **2011,** *115*, 3085-3090.
52. Borodin, O.; Smith, G. D., Quantum Chemistry and Molecular Dynamics Simulation Study of Dimethyl Carbonate: Ethylene Carbonate Electrolytes Doped with $LiPF_6$. *J. Phys. Chem. B* **2009,** *113*, 1763-1776.
53. Borodin, O.; Smith, G. D., LiTFSI Structure and Transport in Ethylene Carbonate from Molecular Dynamics Simulations. *J. Phys. Chem. B* **2006,** *110*, 4971-4977.
54. Wu, H.; Wick, C. D., Computational Investigation on the Role of Plasticizers on Ion Conductivity in Poly(Ethylene Oxide) Litfsi Electrolytes. *Macromolecules* **2010,** *43*, 3502-3510.
55. Borodin, O.; Smith, G. D., Development of Many-Body Polarizable Force Fields for Li-Battery Applications: 2. Litfsi-Doped Oligoether, Polyether, and Carbonate-Based Electrolytes. *J. Phys. Chem. B* **2006,** *110*, 6293-6299.
56. Seo, D. M.; Borodin, O.; Han, S.-D.; Boyle, P. D.; Henderson, W. A., Electrolyte Solvation and Ionic Association II. Acetonitrile-Lithium Salt Mixtures: Highly Dissociated Salts. *J. Electrochem. Soc* **2012,** *159*, A1489-A1500.
57. Seo, D. M.; Borodin, O.; Han, S.-D.; Ly, Q.; Boyle, P. D.; Henderson, W. A., Electrolyte Solvation and Ionic Association. I. Acetonitrile-Lithium Salt Mixtures: Intermediate and Highly Associated Salts. *J. Electrochem. Soc* **2012,** *159*, A553-A565.
58. Seo, D. M.; Borodin, O.; Balogh, D.; O'Connell, M.; Ly, Q.; Han, S.-D.; Passerini, S.; Henderson, W. A., Electrolyte Solvation and Ionic Association III. Acetonitrile-Lithium Salt Mixtures–Transport Properties. *J. Electrochem. Soc* **2013,** *160*, A1061-A1070.

59. Borodin, O.; Smith, G. D.; Geiculescu, O.; Creager, S. E.; Hallac, B.; DesMarteau, D., Li^+ Transport in Lithium Sulfonylimide-Oligo(Ethylene Oxide) Ionic Liquids and Oligo(Ethylene Oxide) Doped with Litfsi. *J. Phys. Chem. B* **2006,** *110*, 24266-24274.
60. Siqueira, L. J. A.; Ribeiro, M. C. C., Molecular Dynamics Simulation of the Polymer Electrolyte Poly(Ethylene Oxide)/$Liclo_4$. Ii. Dynamical Properties. *J. Chem. Phys.* **2006,** *125*, 214903-214908.
61. Borodin, O.; Smith, G. D., Molecular Dynamics Simulation Study of Lii-Doped Diglyme and Poly(Ethylene Oxide) Solutions *J. Phys. Chem. B* **2000,** *104*, 8017-8022.
62. Li, S., et al., Molecular Dynamics Simulation of Litfsi-Acetamide Electrolytes: Structural Properties. *J. Phys. Chem. B* **2008,** *112*, 6398-6410.
63. Soetens, J. C.; Millot, C.; Maigret, B., Molecular Dynamics Simulation of $Li^+BF_4^-$ in Ethylene Carbonate, Propylene Carbonate, and Dimethyl Carbonate Solvents. *J. Phys. CHem. A* **1998,** *102*, 1055-1061.
64. Takeuchi, M.; Kameda, Y.; Umebayashi, Y.; Ogawa, S.; Sonoda, T.; Ishiguro, S. I.; Fujita, M.; Sano, M., Ion-Ion Interactions of $LiPF_6$ and $LiBF_4$ in Propylene Carbonate Solutions. J. *Mol. Liq.* **2009,** *148*, 99-108.
65. Brandell, D.; Liivat, A.; Aabloo, A.; Thomas, J. O., Molecular Dynamics Simulation of the Crystalline Short-Chain Polymer System $LiPF_6$ PEO_6 (M-W Similar to 1000). *Journal of Materials Chemistry* **2005,** *15*, 4338-4345.
66. Brandell, D.; Liivat, A.; Kasemagi, H.; Aabloo, A.; Thomas, J. O., Molecular Dynamics Simulation of the Lipf6 Center Dot Peo6 Structure. J. *Mater. Chem.* **2005,** *15*, 1422-1428.
67. Borodin, O.; Smith, G. D.; Jaffe, R. L., Ab Initio Quantum Chemistry and Molecular Dynamics Simulations Studies of $LiPF_6$/Poly(Ethylene Oxide) Interactions J. *Comput Chem.* **2001,** *22*, 641-654.
68. Li, T.; Balbuena, P. B., Theoretical Studies of Lithium Perchlorate in Ethylene Carbonate, Propylene Carbonate, and Their Mixtures. *J. Electrochem. Soc.* **1999,** *146*, 3613-3622.
69. Leung, K.; Budzien, J. L., Ab Initio Molecular Dynamics Simulations of the Initial Stages of Solid-Electrolyte Interphase Formation on Lithium Ion Battery Graphitic Anodes. *Phys. Chem. Chem. Phys.* **2010,** *12*, 6583-6586.
70. von Wald Cresce, A.; Borodin, O.; Xu, K., Correlating Li^+ Solvation Sheath Structure with Interphasial Chemistry on Graphite. *J. Phys. Chem. C* **2012,** *116*, 26111-26117.
71. Kameda, Y.; Umebayashi, Y.; Takeuchi, M.; Wahab, M. A.; Fukuda, S.; Ishiguro, S. I.; Sasaki, M.; Amo, Y.; Usuki, T., Solvation Structure of Li^+ in Concentrated $LiPF_6$-Propylene Carbonate Solutions. *J. Phys. Chem. B* **2007,** *111*, 6104-6109.
72. Xu, K., Electrolytes and Interphasial Chemistry in Li Ion Devices. *Energies* **2010,** *3*, 135-154.
73. Xu, K.; von Cresce, A.; Lee, U., Differentiating Contributions to "Ion Transfer" Barrier from Interphasial Resistance and Li^+ Desolvation at Electrolyte/Graphite Interface. *Langmuir* **2010,** *26*, 11538-11543.
74. von Cresce, A.; Xu, K., Preferential Solvation of Li^+ Directs Formation of Interphase on Graphitic Anode. *Electrochem. and Solid-State Lett.* **2011,** *14*, A154-A156.
75. Takeuchi, M.; Matubayasi, N.; Kameda, Y.; Minofar, B.; Ishiguro, S.; Umebayashi, Y., Free-Energy and Structural Analysis of Ion Solvation and Contact Ion-Pair Formation of Li^+ with BF_4^- and PF_6^- in Water and Carbonate Solvents. *J. Phys. Chem. B* **2012,** *116*, 6476-6487.
76. Vatamanu, J.; Borodin, O.; Smith, G. D., Molecular Dynamics Simulation Studies of the Structure of a Mixed Carbonate/$Lipf_6$ Electrolyte near Graphite Surface as a Function of Electrode Potential. *J. Phys. Chem. C* **2012,** *116*, 1114-1121.
77. Borodin, O.; Smith, G. D., Li^+ Transport Mechanism in Oligo(Ethylene Oxide)S Compared to Carbonates. J. *Solution. Chem.* **2007,** *36*, 803-813.
78. Newman, J.; Thomas, K. E.; Hafezi, H.; Wheeler, D. R., Modeling of Lithium-Ion Batteries. *J. Power Sources* **2003,** *119*, 838-843.
79. Hayashi, K.; Nemoto, Y.; Tobishima, S.; Yamaki, J., Electrolyte for High Voltage Li/$LiMN_{1.9}Co_{0.1}O_4$ Cells. *J. Power Sources,* **1997,** *68*, 316-319.

80. Saunier, J.; Gorecki, W.; Alloin, F.; Sanchez, J. Y., Nmr Study of Cation, Anion, and Solvent Mobilities in Macroporous Poly(Vinylidene Fluoride). *Journal of Physical Chemistry B* **2005,** *109*, 2487-2492.
81. Hayamizu, K.; Aihara, Y.; Arai, S.; Martinez, C. G., Pulse-Gradient Spin-Echo H-1, Li-7, and F-19 Nmr Diffusion and Ionic Conductivity Measurements of 14 Organic Electrolytes Containing $LiN(SO_2CF_3)_2$. *J. Phys. Chem. B* **1999,** *103*, 519-524.
82. Aihara, Y.; Bando, T.; Nakagawa, H.; Yoshida, H.; Hayamizu, K.; Akiba, E.; Price, W. S., Ion Transport Properties of Six Lithium Salts Dissolved in Gamma-Butyrolactone Studied by Self-Diffusion and Ionic Conductivity Measurements. *J. Electrochem. Soc.* **2004,** *151*, A119-A122.
83. Paillard, E.; Zhou, Q.; Henderson, W. A.; Appetecchi, G. B.; Montanino, M.; Passerini, S., Electrochemical and Physicochemical Properties of $PY_{14}FSI$-Based Electrolytes with LiFSI. *J. Electrochem. Soc.* **2009,** *156*, A891-A895.
84. Fox, D. M.; Awad, W. H.; Gilman, J. W.; Maupin, P. H.; De Long, H. C.; Trulove, P. C., Flammability, Thermal Stability, and Phase Change Characteristics of Several Trialkylimidazolium Salts. *Green Chem.* **2003,** *5*, 724-727.
85. Li, Z.; Smith, G. D.; Bedrov, D., Li^+ Solvation and Transport Properties in Ionic Liquid/Lithium Salt Mixtures: A Molecular Dynamics Simulation Study. *J. Phys. Chem. B* **2012,** *116*, 12801-12809.
86. Solano, C. J. F.; Jeremias, S.; Paillard, E.; Beljonne, D.; Lazzaroni, R., A Joint Theoretical/Experimental Study of the Structure, Dynamics, and Li^+ Transport in Bis([Tri]Fluoro[Methane]Sulfonyl)Imide [T]Fsi-Based Ionic Liquids. *J. Chem. Phys.* **2013,** *139*, 034502.
87. Borodin, O.; Vatamanu, J.; Xing, L.; Smith, G.; Bedrov, D., Bulk and Interfacial Properties of Ionic Liquids and Their Mixtures with Lithium Salts. *Meeting Abstracts* **2012,** *MA2012-02*, 3620.
88. Smith, G. D.; Borodin, O.; Russo, S. P.; Rees, R. J.; Hollenkamp, A. F., A Molecular Dynamics Simulation Study of $LiFePO_4$/Electrolyte Interfaces: Structure and Li^+ Transport in Carbonate and Ionic Liquid Electrolytes. *Phys. Chem. Chem. Phys.* **2009,** *11*, 9884-9897.
89. Méndez-Morales, T.; Carrete, J.; Bouzón-Capelo, S.; Pérez-Rodríguez, M.; Cabeza, Ó.; Gallego, L. J.; Varela, L. M., MD Simulations of the Formation of Stable Clusters in Mixtures of Alkaline Salts and Imidazolium-Based Ionic Liquids. *J. Phys. Chem. B* **2013,** *117*, 3207-3220.
90. Monteiro, M. J.; Bazito, F. F. C.; Siqueira, L. J. A.; Ribeiro, M. C. C.; Torresi, R. M., Transport Coefficients, Raman Spectroscopy, and Computer Simulation of Lithium Salt Solutions in an Ionic Liquid. *J. Phys. Chem. B.* **2008,** *112*, 2102-2109.
91. Borodin, O., Polarizable Force Field Development and Molecular Dynamics Simulations of Ionic Liquids. *J. Phys. Chem. B* **2009,** *113*, 11463-11478.
92. Castiglione, F.; Ragg, E.; Mele, A.; Appetecchi, G. B.; Montanino, M.; Passerini, S., Molecular Environment and Enhanced Diffusivity of Li^+ Ions in Lithium-Salt-Doped Ionic Liquid Electrolytes. *J. Phys. Chem. Lett.* **2011,** *2*, 153-157.
93. Tokuda, H.; Ishii, K.; Susan, M. A. B. H.; Tsuzuki, S.; Hayamizu, K.; Watanabe, M., Physicochemical Properties and Structures of Room-Temperature Ionic Liquids. 3. Variation of Cationic Structures *J. Phys. Chem. B* **2006,** *110*, 2833-2839.
94. Lassegues, J. C.; Grondin, J.; Aupetit, C.; Johansson, P., Spectroscopic Identification of the Lithium Ion Transporting Species in Litfsi-Doped Ionic Liquids. *J. Phys. Chem. A* **2009,** *113*, 305-314.
95. Tasaki, K.; Goldberg, A.; Lian, J. J.; Walker, M.; Timmons, A.; Harris, S. J., Solubility of Lithium Salts Formed on the Lithium-Ion Battery Negative Electrode Surface in Organic Solvents. *J. Electrochem. Soc.* **2009,** *156*, A1019-A1027.
96. Shi, S. Q.; Lu, P.; Liu, Z. Y.; Qi, Y.; Hector, L. G.; Li, H.; Harris, S. J., Direct Calculation of Li-Ion Transport in the Solid Electrolyte Interphase. J. *Am. Chem. Soc.* **2012,** *134*, 15476-15487.
97. Chen, Y. C.; Ouyang, C. Y.; Song, L. J.; Sun, Z. L., Electrical and Lithium Ion Dynamics in Three Main Components of Solid Electrolyte Interphase from Density Functional Theory Study. *J. Phys. Chem. C* **2011,** *115*, 7044-7049.

98. Borodin, O.; Zhuang, G. V.; Ross, P. N.; Xu, K., Molecular Dynamics Simulations and Experimental Study of Lithium Ion Transport in Dilithium Ethylene Dicarbonate. *J. Phys. Chem. C* **2013,** *117*, 7433-7444.
99. Xu, K.; Zhuang, G. V.; Allen, J. L.; Lee, U.; Zhang, S. S.; Ross, P. N.; Jow, T. R., Syntheses and Characterization of Lithium Alkyl Mono- and Dicarbonates as Components of Surface Films in Li-Ion Batteries. *J. Phys. Chem. B* **2006,** *110*, 7708-7719.
100. Zhuang, G. V.; Xu, K.; Yang, H.; Jow, T. R.; Ross, P. N., Lithium Ethylene Dicarbonate Identified as the Primary Product of Chemical and Electrochemical Reduction of EC in 1.2 M $LiPF_6$/EC:EMC Electrolyte. *J. Phys. Chem. B* **2005,** *109*, 17567-17573.
101. Jow, T. R.; Allen, J.; Marx, M.; Nechev, K.; Deveney, B.; Rickman, S., (Invited) Electrolytes, Sei and Charge Discharge Kinetics in Li-Ion Batteries. *ECS Transactions* **2010,** *25*, 3-12.
102. Jow, T. R.; Marx, M. B.; Allen, J. L., Distinguishing Li^+ Charge Transfer Kinetics at Nca/Electrolyte and Graphite/Electrolyte Interfaces, and NCA/Electrolyte and Lfp/Electrolyte Interfaces in Li-Ion Cells. *J. Electrochem. Soc.* **2012,** *159*, A604-A612.
103. Xu, K.; Lam, Y. F.; Zhang, S. S.; Jow, T. R.; Curtis, T. B., Solvation Sheath of Li^+ in Nonaqueous Electrolytes and Its Implication of Graphite/Electrolyte Interface Chemistry. *J. Phys. Chem. C* **2007,** *111*, 7411-7421.
104. Zhang, S. S.; Xu, K.; Jow, T. R., Eis Study on the Formation of Solid Electrolyte. *Electrochimica Acta* **2006,** *51*, 1636-1640.
105. Zhang, S. S.; Xu, K.; Jow, T. R., Charge and Discharge Characteristics of a Commercial Licoo2-Based 18650 Li-Ion Battery. *J. Power Sources* **2006,** *160*, 1403-1409.
106. Xu, K., "Charge-Transfer" Process at Graphite/Electrolyte Interface and the Solvation Sheath Structure of Li^+ in Nonaqueous Electrolytes. *J. Electrochem. Soc.* **2007,** *154*, A162-A167.
107. Abraham, D. P.; Heaton, J. R.; Kang, S. H.; Dees, D. W.; Jansen, A. N., Investigating the Low-Temperature Impedance Increase of Lithium-Ion Cells. *J. Electrochem. Soc.* **2008,** *155*, A41-A47.
108. Yamada, I.; Iriyama, Y.; Abe, T.; Ogumi, Z., Lithium-Ion Transfer between Li_xcoo_2 and Polymer Gel Electrolytes. *Sci. Technol. Adv. Mat.* **2006,** *7*, 519-523.
109. Yamada, Y.; Iriyama, Y.; Abe, T.; Ogumi, Z., Kinetics of Lithium Ion Transfer at the Interface between Graphite and Liquid Electrolytes: Effects of Solvent and Surface Film. *Langmuir* **2009,** *25*, 12766-12770.
110. Yamada, Y.; Sagane, F.; Iriyama, Y.; Abe, T.; Ogumi, Z., Kinetics of Lithium-Ion Transfer at the Interface between $Li_{0.35}La_{0.55}TiO_3$ and Binary Electrolytes. *J. Phys. Chem. C* **2009,** *113*, 14528-14532.
111. Ogumi, Z., Interfacial Reactions of Lithium-Ion Batteries. *Electrochemistry* **2010,** *78*, 319-324.
112. Jow, T. R.; Zhang, S. S.; Xu, K.; Allen, J. L., Electrolytes for Low Temperature Operations of Li-Ion Batteries. *ECS Transactions* **2007,** *3*, 51-58
113. Xu, K.; von Cresce, A., Interfacing Electrolytes with Electrodes in Li Ion Batteries. J. *Mater. Chem.* **2011,** *21*, 9849-9864.
114. Xing, L. D.; Vatamanu, J.; Borodin, O.; Smith, G. D.; Bedrov, D., Electrode/Electrolyte Interface in Sulfolane-Based Electrolytes for Li Ion Batteries: A Molecular Dynamics Simulation Study. *J. Phys. Chem. C* **2012,** *116*, 23871-23881.
115. Yu, L.; Liu, H.; Wang, Y.; Kuwata, N.; Osawa, M.; Kawamura, J.; Ye, S., Preferential Adsorption of Solvents on the Cathode Surface of Lithium Ion Batteries. *Angew. Chemie Int. Ed.* **2013,** *125*, 5865–5868.
116. Watanabe, Y.; Kinoshita, S. I.; Wada, S.; Hoshino, K.; Morimoto, H.; Tobishima, S. I., Electrochemical Properties and Lithium Ion Solvation Behavior of Sulfone-Ester Mixed Electrolytes for High-Voltage Rechargeable Lithium Cells. *J. Power Sources* **2008,** *179*, 770-779.
117. Xu, K.; Angell, C. A., Sulfone-Based Electrolytes for Lithium-Ion Batteries. *J. Electrochem. Soc.* **2002,** *149*, A920-A926.
118. Abouimrane, A.; Belharouak, I.; Amine, K., Sulfone-Based Electrolytes for High-Voltage Li-Ion Batteries. *Electrochem. Commun.* **2009,** *11*, 1073-1076.

119. Merlet, C.; Rotenberg, B.; Madden, P. A.; Salanne, M., Computer Simulations of Ionic Liquids at Electrochemical Interfaces. *Phys. Chem. Chem. Phys.* **2013,** *15*, 15781-15792.
120. Vatamanu, J.; Borodin, O.; Smith, G. D., Molecular Insights into the Potential and Temperature Dependences of the Differential Capacitance of a Room-Temperature Ionic Liquid at Graphite Electrodes. J. *Am. Chem. Soc.* **2010,** *132*, 14825-14833.
121. Feng, G.; Jiang, D.-e.; Cummings, P. T., Curvature Effect on the Capacitance of Electric Double Layers at Ionic Liquid/Onion-Like Carbon Interfaces. *J. Chem. Theory and Comput.* **2012,** *8*, 1058-1063.
122. Feng, G.; Li, S.; Atchison, J. S.; Presser, V.; Cummings, P. T., Molecular Insights into Carbon Nanotube Supercapacitors: Capacitance Independent of Voltage and Temperature. *J Phys Chem C* **2013,** 117, 9178–9186.
123. Vatamanu, J.; Cao, L.; Borodin, O.; Bedrov, D.; Smith, G. D., On the Influence of Surface Topography on the Electric Double Layer Structure and Differential Capacitance of Graphite/Ionic Liquid Interfaces. *J. Phys. Chem. Lett.* **2011,** *2*, 2267-2272.
124. Masia, M.; Rey, R., Computational Study of Gamma-Butyrolactone and Li^+/Gamma-Butyrolactone in Gas and Liquid Phases. *J. Phys. Chem. B* **2004,** *108*, 17992-18002.
125. Silva, L. B.; Freitas, L. C. G., Structural and Thermodynamic Properties of Liquid Ethylene Carbonate and Propylene Carbonate by Monte Carlo Simulations. J. *Mol. Struct.-Theochem* **2007,** *806*, 23-34.
126. Wang, Y. X.; Balbuena, P. B., Combined Ab Initio Quantum Mechanics and Classical Molecular Dynamics Studies of Polyphosphazene Polymer Electrolytes: Competitive Solvation of Li^+ and $LiCF_3SO_3$. *J. Phys. Chem. B* **2004,** *108*, 15694-15702.
127. Yu, J.; Balbuena, P. B.; Budzien, J.; Leung, K., Hybrid Dft Functional-Based Static and Molecular Dynamics Studies of Excess Electron in Liquid Ethylene Carbonate. *J. Electrochem. Soc.* **2011,** *158*, A400-A410.
128. Masia, M.; Probst, M.; Rey, R., Ethylene Carbonate-Li^+: A Theoretical Study of Structural and Vibrational Properties in Gas and Liquid Phases. *J. Phys. Chem. B* **2004,** *108*, 2016-2027.
129. Wang, Y. X.; Balbuena, P. B., Theoretical Studies on Cosolvation of Li Ion and Solvent Reductive Decomposition in Binary Mixtures of Aliphatic Carbonates. *Int. J. Quant. Chem.* **2005,** *102*, 724-733.
130. Sutjianto, A.; Curtiss, L. A., Li^+-Diglyme Complexes: Barriers to Lithium Cation Migration. *J. Phys. CHem. A* **1998,** *102*, 968-974.
131. Scheers, J.; Kalita, M.; Johansson, P.; Zukowska, G. Z.; Wieczorek, W.; Jacobsson, P., Anion-Additive Interactions Studied by Ab Initio Calculations and Raman Spectroscopy. *J. Electrochem. Soc.* **2009,** *156*, A305-A308.
132. Jonsson, E.; Armand, M.; Johansson, P., Novel Pseudo-Delocalized Anions for Lithium Battery Electrolytes. *Phys. Chem. Chem. Phys.* **2012,** *14*, 6021-6025.
133. Scheers, J.; Johansson, P., Comment on "Transport and Electrochemical Properties and Spectral Features of Non-Aqueous Electrolytes Containing LiTFSI in Linear Carbonate Solvents" [J. Electrochem. Soc., 158, A74 (2011)]. *J. Electrochem. Soc.* **2012,** *159*, S1-S2.
134. Wang, Y. X.; Balbuena, P. B., Associations of Alkyl Carbonates: Intermolecular C-H Center Dot Center Dot Center Dot O Interactions. *J. Phys. Chem. A* **2001,** *105*, 9972-9982.
135. Leung, K., Two-Electron Reduction of Ethylene Carbonate: A Quantum Chemistry Re-Examination of Mechanisms. *Chem. Phys. Lett.* **2013,** *568–569*, 1-8.
136. Tasaki, K., Solvent Decompositions and Physical Properties of Decomposition Compounds in Li-Ion Battery Electrolytes Studied by DFT Calculations and Molecular Dynamics Simulations. *J. Phys. Chem. B* **2005,** *109*, 2920-2933.

Chapter 9
Prediction of Electrolyte and Additive Electrochemical Stabilities

Johan Scheers and Patrik Johansson

9.1 Introduction

The rapid advent of computational power and re-chargeable lithium batteries was in many ways simultaneous in the early 1990s – but not coupled to each other to a large extent at the time of the breakthroughs. However, as the new computers and computational methods were efficient, these fast became used in the field to model well-known battery materials and phenomena, often with the aim to explain experimental data. Later there were also new battery materials or demands emerging, where computations were foreseen to possibly have a predictive power. As another way of thinking, the models needed to correctly look at complex battery phenomena spurred the development of computational strategies and methods.

One of the more challenging tasks is to model electrolyte electrochemistry properties – directly or indirectly. In the following chapter we outline the aims of using computations to explain and subsequently predict electrolyte and additive electrochemical stabilities. We make a rather thorough history description of the simultaneous methods–materials evolution as we feel that this is largely missing in the current literature and can explain discrepancies noted and also help the interested reader to avoid some pitfalls in the future. From this standpoint we also outline a few of the underlying assumptions generally made. A set of success stories are treated in more detail to exemplify the predictive power and finally we treat the ongoing methods and materials development in terms of new methods and approaches as well as the emergence of predictive modelling of phenomena of, e.g., Li–air battery electrolytes.

J. Scheers (✉) • P. Johansson
Department of Applied Physics, Chalmers University of Technology, Gothenburg, Sweden
e-mail: johan.scheers@chalmers.se

T.R. Jow et al. (eds.), *Electrolytes for Lithium and Lithium-Ion Batteries*,
Modern Aspects of Electrochemistry 58, DOI 10.1007/978-1-4939-0302-3_9,

9.2 Aim and Approaches

9.2.1 The Computational Aim

To be able to understand how computational approaches can and should be used for electrochemical prediction we first of all need to have a correct description of the precise aims. We start from the very basic lithium-ion cell operation that ideally involves two well-defined and reversible reduction and oxidation (*redox*) reactions – one at each electrode/electrolyte interface – coordinated with the outer transport of electrons and internal transport of lithium ions between the positive and negative electrodes. However, in practice many other chemical and physical phenomena take place simultaneously, such as anion diffusion in the electrolyte and additional redox processes at the interfaces due to reduction and/or oxidation of electrolyte components (Fig. 9.1). Control of these additional phenomena is crucial to ensure safe and stable cell operation and to optimize the overall cell performance. In general, computations can thus be used: (1) to predict *wanted* redox reactions, for example the reduction potential (E_{red}) of a film-forming additive intended for a protective solid electrolyte interface (SEI) and (2) to predict *unwanted* redox reactions, for example the oxidation potential (E_{ox}) limit of electrolyte solvents or anions. As outlined above, the additional redox reactions involve components of the electrolyte, which thus is a prime aim of the modelling. The working agenda of different electrolyte materials in the cell –and often the unwanted reactions – are addressed to be able to mitigate the limitations posed in a rational way.

From a practical point of view there are two main approaches to avoid, mitigate, or quench unwanted electrolyte redox reactions: either increasing the electrochemical stability window of the electrolytes or deliberately introducing an additional well-defined redox reaction, i.e., by using additives in what then is coined a *functional* or *role-assigned* electrolyte [1]. Both approaches rely on careful design of the electrolyte from the level of individual species and up, with special attention taken to the specific electrode chemistries.

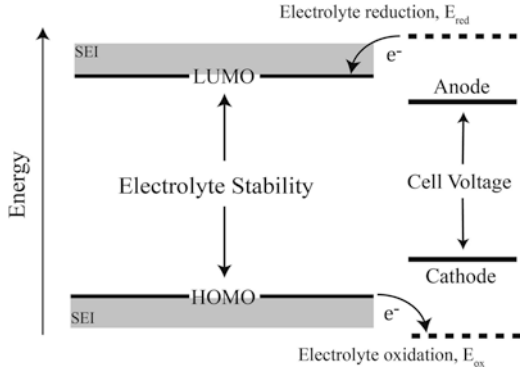

Fig. 9.1 Electrolyte electrochemical stability in relation to electrode potentials

To this end, various computational approaches have proven to be important tools for making a priori predictions of the electrochemical stability of solvents and salts, as well as additives. More precisely the aim of the modelling is to access the electronic energy levels of the molecules/materials, which for many of the methods used are easily accessible, and then directly or indirectly correlate these with the observed experimental data or electrode potentials on an absolute or relative energy scale – to truly test the predictive power of electrochemical stability.

9.2.2 Experimental Data and Verification

In order to be able to assess whether or not and how accurately any computational method and strategy, not only those to be treated here, can be used in a *predictive* manner there is always the need for the "right" experimental data. Also needed is an understanding of the possibilities as well as the problems with the experimental approaches: generality, applicability, and accuracy. This is especially important whenever there is a need to compile experimental data from several literature sources to verify a prediction of a wider selection of modelled compounds or phenomena. After this small section, we hope the main limitations of the experimental data will be obvious and why the use of many different literature sources for corroboration/verification should be avoided – if possible.

Experimental measurements of overall electrolyte electrochemical stability are routinely made by standard electrochemical voltammetry techniques that monitor current flow in response to a controlled potential sweep. One example of such a technique is linear sweep voltammetry (LSV). At a certain potential (voltage) one or several of the electrolyte components are no longer stable towards reduction or oxidation – causing a current to be produced, and the corresponding potential for a certain cut-off current is taken as the electrochemical stability value of the system or one of its components. The procedures used and results obtained from LSV, when applied to non-aqueous liquid electrolytes, have been reviewed by Xu [2]. Xu identified three main strategies to be followed to investigate the redox chemistry of a single electrolyte species: (1) at dilute concentrations (mM) in a supporting medium, used in a cell with inert non-porous electrodes (e.g. Pt or glassy carbon), (2) at concentrations more realistic for practical applications, either in single solvents or as part of more advanced multi-component electrolyte systems, but still in combination with inert electrodes, and (3) using a combination of both a realistic electrolyte in terms of concentrations, solvent mixtures, etc. and a choice of active electrodes commonly used in Li-ion cells.

Electrochemical cells are most frequently set up according to (2) to avoid monitoring currents from competing reactions/phenomena, and thus produce ideal systems solely monitoring the sought intrinsic electrolyte stability. For the direct verification of the most simplistic and yet predictive computations of E_{ox} and E_{red}, these types of experimental setups are easy to interpret, often unambiguous, and thus much preferable.

One should, however, as someone using the computational approach and relying on the experimental data at hand, be very much aware that the choices made above, with the aim to create general and intrinsic data for the redox stability, at the same time excludes many phenomena quite likely to occur in the electrochemical cell that the predictions in reality often are aimed at. One obvious such phenomenon is the role of specific catalytic activities attributable to non-inert porous electrodes – like transition metal oxides used as cathodes in lithium-ion batteries. Another aspect often targeted in (2) and most often in (3) is the synergistic effects among electrolyte components, that do require the use of realistic electrolyte compositions, rather than simplified model electrolytes as in (1), to target the true stability limits [3]. Indeed, it has been pointed out that all possible parameters such as solvent combinations, the presence or not of a salt, salt concentration, the presence of Li^+ or alternative cations – all have an effect on the stability observed – even if, in principle, one and the same main reaction is being monitored [4–7].

As a caveat, the above circumstances have suggested the combination of experimental model systems and computational modelling to be quite inappropriate for determining electrochemical stability limits [4]. While it may be true that in the final stages of electrolyte testing for an intended application the composition and cell environment must mimic the system as closely as possible to obtain accurate electrochemical stability limits, we do still think there is a venue and need for the more simple combined experimental and computational strategy. As this chapter will point out in more detail the predictive computations can in practice, successfully, be used to: (1) assist the analysis of the contributions of individual electrolyte components in detail, (2) establish and also quantify possible synergistic and catalytic effects, and (3) guide electrolyte materials research into exploring new functionalities and areas of application.

Stepping back to the model systems these have specifically been motivated by the added value of avoiding differences imposed by varying experimental setups and operator bias. It is well known that arbitrary choices of LSV cut-off currents and potential sweep-rates [8], in addition to the aforementioned choices of electrodes and electrolyte composition, have an effect on the measured and thus reported stability limits. More subtle differences relate to the use of regular-sized or micro-sized electrodes, potential step or potential sweep measurements, cut-off currents or extrapolation techniques [9]. Indeed, the large number of experimental variables involved makes it difficult to compare experimental data from different sources and to identify the origin of contradicting results. Moreover, these difficulties create a frustrated relationship between predicted and experimental data on electrochemical stability, especially noticeable when trying to create a larger benchmark of the performance of various computational methods to predict electrochemical stabilities. Therefore, whenever possible, electrolyte stability measures should be quoted from the same source.

As we hope is clear, if one remembers the caveat above and understands the limitations, and furthermore care is taken both of the design of the computational approach (strategy, method, and model) and the choice of appropriate experimental data for verification – then prediction of E_{ox} and E_{red} is indeed a useful possibility for rational electrolyte development.

9.2.3 Computational Approaches

Before presenting results there is also a need to introduce the basic construction work behind the most common computational approaches used for predicting electrolyte and additive electrochemical stabilities. We will not cover the applied computational methods per se, since there are many excellent texts on computational chemistry, but outline the basic physical and chemical considerations behind the strategies chosen, methods applied, and models used, for the particular aim of predictions of electrolyte and additive electrochemical stability.

9.2.3.1 Strategies

As much as there are many different aims with using predictive methods – there are many different strategies employed, with strong correlation to the way the scientist(s) in charge endeavour in the project. We simply here outline some of our observations of the field to show the vast variation in strategies.

One strategy is to extensively attack a single, very specific, and hopefully from an experimental point-of-view well understood, reduction, or oxidation reaction with the aim of as accurately as possible obtain a computed numerical value for E_{ox} and/or E_{red}. The most typical example would be EC reduction [10–13]. The aim is not necessarily to obtain a prediction needed for rational development of electrolytes – but perhaps more to confirm and further develop the computational/experimental correlation for certain choices of methods and models or their combinations.

If the method and model combination from studies such as those described above subsequently are applied to a larger variety of reactions – then this strategy has been developed into a predictive one with an orientation towards electrolyte technology field impact rather than an internal scientific. A typical example would be to assess the reduction stability of a variety of electrolyte solvents [14–18].

Yet another strategy is to correlate computational results for a wide variation of reactions in different electrolytes with the corresponding experimental observations, either in absolute or relative values. A typical example would here be the intrinsic stability of various anions in a variety of solvents [8, 19, 20].

Either of the two latter strategies can in addition have the aim of not only addressing the electrochemical stability, but furthermore also outline the reaction mechanism and products obtained once the initial reduction or oxidation has taken place [11, 21].

In more detailed out-sets, the computational setup can either aim at finding the intrinsic stability of a certain species, no influence from the other components of the electrolyte, or it can be directed towards explaining the exact failure for a very special chemistry. This is a strong current strategy development as it also has implications for what battery chemistry or even battery concept the electrolyte components are and should be aiming at.

Moving even further on the predictive track, the real advantage of applying computations is that it is possible to cover many substitutions in a relatively short time

frame – especially compared to synthesizing a wide variety of new compounds. Therefore, one truly and extremely useful predictive strategy is to perform substitutions on a well-known species and predict the corresponding changes in E_{ox} and E_{red} – in absolute or more commonly relative terms [22–27]. In the extreme, and in our opinion best, case, the results of such predictions can and will be used for rational computer-aided design of new electrolyte materials or complete electrolytes – depending on the model employed.

9.2.3.2 Methods

For any method aiming at predicting electrochemical stability there is evidently a need to in some way treat an electronic reference state and also the resulting state, e.g. for oxidation the starting ground state and the resulting radical. This may sound very simple; however, the methods are vast in design.

We will always need to employ methods that can account for the electronic structure of our chosen model in some sense – either (1) totally explicitly by ab initio (Hartree-Fock (HF), Møller-Plesset perturbation theory (MPx), coupled-cluster (CC), etc.) or by density functional theory (DFT) methods with a vast range, and continuously expanding number, of different functionals (B3LYP, M06, etc.), (2) partly explicitly like in semi-empirical (SE) methods (MNDO, AM1, PMx, etc.), or (3) we can even resort to a parameterization such as in classical MD simulations (being a much less prominent method though). All these are of course standard computational methods with generality across any elements and chemistry (for classical MD only if a proper parameter set exists). There is also ab initio MD (AIMD) emerging as a tool in the field.

The algorithms used to handle the electron interactions are complemented by functions to contain the spatial extent of the electron cloud. This is most often made by a *basis set*, which can have different quality, often determined by the number of mathematical functions use to build it – its size.

While it is easy to realize that several electronic states in some way must be treated and that any of the computational chemistry methods above can be used to some extent and with various possibilities – the variety of ways these can be combined and tasks performed within this framework is indeed more troublesome to overview. Nevertheless, in order to be able to follow the development of the topic of this chapter at all, there is a need to describe the main tracks followed traditionally as well as those used only in a few instances so far, but where we see large future possibilities.

The most traditional way to address the stability of any finite molecular model (more on this in Sect. 2.3.3) is to extract and use the molecular orbitals (MOs) resulting from an electronic structure calculation – most often the highest occupied MOs (HOMOs) and the lowest unoccupied MOs (LUMOs) (Fig. 9.1) – and the corresponding eigenvalues. As an example the energy of the HOMO–LUMO gap for a species has often been invoked as a measure of its stability vs. oxidation – quite naturally as it will be a measure of the ease of the transfer of an electron from the

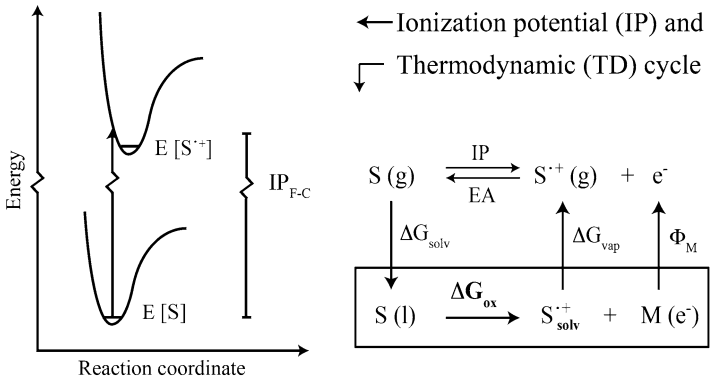

Fig. 9.2 Ionization potential (IP) and thermodynamic (TD) free energy cycle for the oxidation of solvent *S*

ground state to a higher state. The main problem with this approach is, however, the fundamental notion that the LUMO is indeed calculated for the ground state and in addition also some methods, most notably DFT, have vast difficulties to accurately or at least unambiguously calculate the LUMO energies.

A more direct approach is to calculate the electronic energy for both the ground state and the final state. For an oxidation reaction this becomes the same as calculating the ionization potential (IP) and vice versa for a reduction reaction it becomes the electron affinity (EA). This is an important observation as the field of computational chemistry is wide and there are benefits to make from keeping an eye open for the development of assessing these generic properties – even when they are not specifically devoted to electrochemistry.

In practice this type of calculation, rather than just being one single calculation as for extracting the HOMO and LUMO energies, contains several steps – depending on the accuracy level requested. Taking the example of the oxidation modelled by the IP computation; it can simply be obtained by computing the electronic energy of the ground-state followed by calculating the same energy for the radical with the very same model geometry (*vertical transition* – motivated by employing the Franck-Condon (F-C) principle) (Fig. 9.2). This can be refined in several steps; relaxing the excited state to its preferred geometry (releasing the F-C constraints) and subsequently also adding the different vibrational contributions to obtain the enthalpy differences rather than just the electronic.

There are of course more elaborate ways to study the electrochemistry – one way is to have a system in total balance without "removing" electrons out of the system. Creating a thermo-dynamic Born-Haber cycle (TD cycle, Fig. 9.2) for the system of interest is the most common example of such an approach [10, 11, 28, 29]. The main advantage is the reduced need for adjustments for the precise chemistry involved experimentally, as all components treated in the computational model do more or less have exactly the same physical surrounding as in the experiment compared with. Indeed, the TD cycle multi-step method is often quite

predictive – but care needs to be taken when creating the models and choosing the strategy. The TD cycle method is also much more computationally intense than most other methods.

There are also some special cases, e.g., when calculations are directly mixed with experimental data (partly the topic of the next section but appropriate to mention here). One early such study used tabulated free energies of formation to cancel out the metallic work function (Φ_M) by introducing a reference cycle in the TD cycle for Li^+ reduction [28]. In total, this made for a simplification to the conventional TD cycle.

For recent examples of new methods employed, those that propagate in time while including the electronic energies, most notably the implementation of AIMD simulations by Leung et al. [12, 13, 30, 31] to study various properties of EC and its contribution to the SEI, are fascinating. The time-evolution can of course be treated without any electrons, as in classic MD simulations, and still be predictive about the resulting reaction products – while not the direct electrochemistry. An excellent example of the latter is the work by Bedrov et al. [32].

MD simulations, be it classical or AIMD, have an advantage that the other approaches do not: the inclusion of time-evolution and to some extent also kinetics – albeit often trivial. They most often also encompass a matrix, which thus is more than just the molecular model that is the prime aim of the study. This can be thought of as either a part of the method or model construction, but for pedagogic reasons and simplicity we will completely leave the treatment of this to the next section.

9.2.3.3 Models

The methods outlined above do in most cases assume a finite, quite easily defined model system, such as an ion, a molecule or something similar. In the real experimental situation, however, this is of course a large oversimplification. Most computations that we treat in this chapter do, however, heavily rely on treating the phenomena by using only the specie considered as *the* model – often making a molecular entity. In fact, many scientists from a computational background would not even see the problem with this – why we in Fig. 9.3 show an increasing order of model complexity that for real might be needed to properly address the electrochemical stability.

The simplest model, still capable of addressing different electronic states, is an isolated molecular species – be it neutral (as electrolyte solvent or a redox shuttle additive) or charged (like a lithium salt anion or an oxidized redox shuttle). This is by far the most common model employed for any strategy and method combination.

Increasing the complexity a bit – these models are subject to interaction with other components of the electrolyte, which are not electrochemically active by themselves, but perturbs the original model. The most common addition is a lithium ion, which in several cases have shown to alter both the absolute and relative stability of several original models, for solvents (S) like in $[LiS_n]^+$ complexes, where also different solvents can be treated for the same lithium cation to account for different

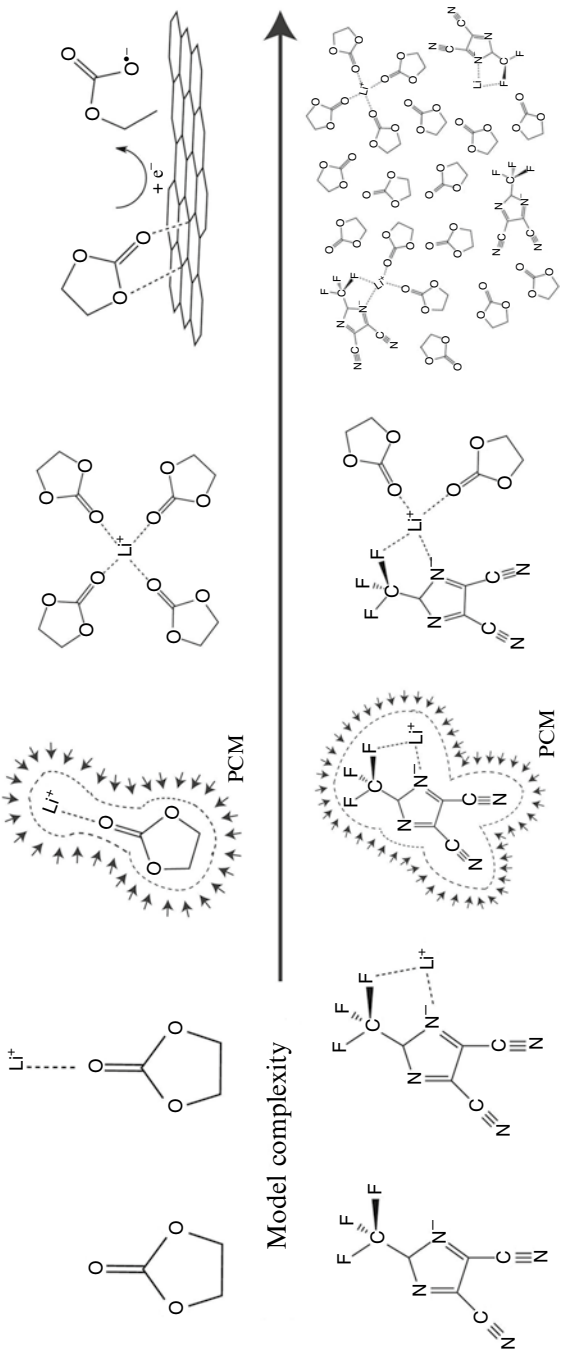

Fig. 9.3 Model systems for the prediction of solvent and salt electrochemical stability

solvent ratios and salt concentrations. Analogous for an electrolyte anion (An) is the use of some kind of Li–An systems. Also a few studies employing An–S models exist as well as Li–An–S models. These systems are all gathered under the framework of "super-molecules." For any attempt to go beyond the redox reaction, to also evaluate the reaction mechanism, super-molecule models are almost compulsory.

All the models above are finite in size and rely on explicit molecular additions subject to the same computational method as the species studied. Another way to take into account and model the "real" surrounding in an electrolyte is to use various continuum methods to implicitly mimic the effect of, e.g., the dielectric constant of the electrolyte. Popular since many years are different variants of the polarizable continuum methods (PCM) applicable to both ab initio and DFT methods and where parameters for a variety of different solvents exist, and with possibilities to tailor for special electrolytes. The use of continuum methods has demonstrated the importance of simulating solvent effects – especially the difference between the gas phase electronic energies and the free energies of solvation (ΔG) via PCM. The use of continuum methods can also be "tweaked" in various ways, e.g., in TD cycles to treat different dielectric constants for different parts of the cycle.

The above models can be combined, in what then is called a "cluster-continuum" approach, sometimes argued to be quite necessary to capture both the specific local and the overall average effects in order to properly and accurately predict EA and therefore E_{red} [11].

While solvent effects are treated by methods like PCM, as an average over the explicit system, these cannot account for local specific phenomena, e.g., a redox reaction at a surface under the influence of solvent interactions. Therefore, larger explicit systems will still be valuable for more elaborate studies, as for electrodes' surface chemistry and physics. Therefore, various types of explicit models, often referred to as clusters – indeed even slabs of graphite in 3D-like constructions to create an anode model – have been used. The size of the explicit models and the methods possible to apply often give rise to practical optimization problems as the models quickly grow in size and complexity and the computational resources are limited. Nevertheless, Leung recently extended his previous AIMD studies of EC reduction [12, 13, 30] to also include oxidation at a $Li_{0.6}Mn_2O_4$ (100) surface [31]. This is, to the best of our knowledge, the first example of introducing an explicit surface together with the very computationally demanding AIMD method for predicting electrolyte solvent oxidation.

9.2.3.4 The Strategy–Method–Model Combination

We hope that despite the enormous diversification in all of the three sub-sections above, altogether resulting in many, many possible combinations – the resulting impression should be positive about the vast promises – rather than confusion. Clearly some selected methods outlined above are today more or less depreciated, while others have just emerged as everyday computational tools for electrochemical stability prediction, both E_{ox} and E_{red}. However, to be able to understand the

implications of older studies (meaning >10 years back) as well as the possibilities available today and in the near future, it is necessary to address all. With a proper base of understanding, we can move on to practical examples including historical reviews, specific case studies, as well as recommendations of best practice.

9.3 Prediction Put in Practice

How do the models, methods, and strategies work in practice? Using the logic of the materials used to build up the electrolyte, which also coincide with their historic advent as targets for the modelling efforts, we start with solvents, continue with lithium salts, and finish of by some examples of additives. By necessity the results reported are a blend of computations following the experiments, thus mainly used to interpret and thus having a secondary role, with more recent works having a predictive role of the computational approach, as a tool for rational design of electrolytes [33]. The latter strategy of computer-aided rational design of materials has become highly appreciated recently c.f. the US materials genome initiative [34].

9.3.1 Solvents

9.3.1.1 Focus and Early Works

When computational studies came into play the lithium batteries had already shifted from metallic lithium to graphite anodes – and the reduction phenomena occurring at these electrodes had fast been recognized as problematic. It is thus natural that the early computational work on predicting solvent electrochemical stability focused on E_{red} and reductive decomposition mechanisms, especially of different cyclic carbonate solvents, EC and PC – as these then, as also today with only a few notable exceptions, were totally dominating. EC in particular has been investigated repeatedly using different approaches, with different co-solvents or additives, and in Li^+ rich or poor environments. The practical and specific goal has been to further the understanding of the electrolyte/graphite anode interface chemistry. The observation that solvent mixtures with EC, but not PC, are effective in forming an SEI on the graphite surface was one of the first problems addressed.

The experimental and theoretical paper on "The behaviour of lithium electrodes in propylene and ethylene carbonate" by Aurbach et al. in 1992 [35] was likely the first to predict electrochemical stabilities of lithium battery materials specifically – using both energy differences and the HOMO–LUMO approach. The energies of EC, PC, and both linear and cyclic radical anions thereof were calculated "free" or coordinated to Li^+ (Fig. 9.4). From the reduction energies the authors suggested EC to be more prone to reduction. However, different interpretations were possible depending on the assumptions made about the reduction products. As visualized in

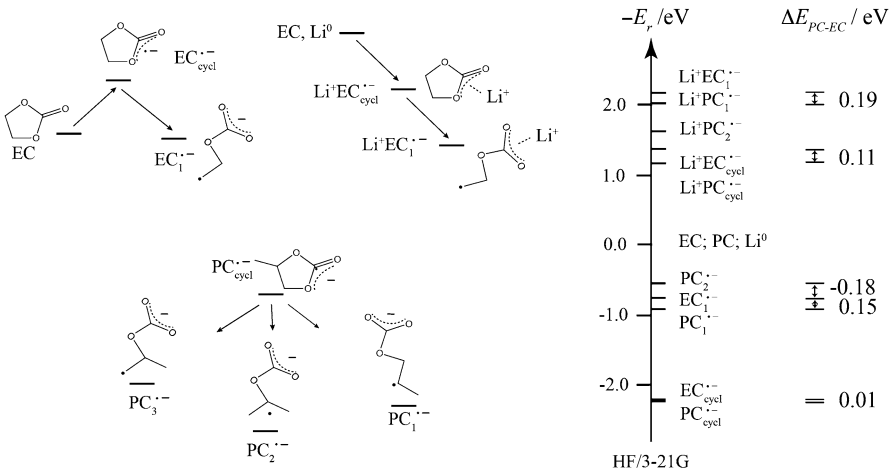

Fig. 9.4 Reduction mechanisms and energies for EC and PC suggested by Aurbach et al. [35]

the bar diagram of Fig. 9.4, only the Li^+-coordinated solvents formed reactions with exothermic energies, where Li^+-coordinated EC vs. PC suggested EC to be more reactive – irrespective of the products being open chain or cyclic. However, for the reduction of the bare solvents EC was predicted to be more, equally, or even less reactive, depending on the final products considered. In addition, the HOMO–LUMO approach predicted a slightly larger energy gap for EC, implying PC to be the more reactive species. With either approach, the energy differences were claimed to be small compared to the experimental reduction potential difference, and hence the authors argued steric effects, rather than electronic, to be decisive origin of the increased stability of PC compared to EC.

With the immense increase in computational power in only a few years, Endo et al. could easily in 1998 extend the scope and thus investigated the initial reduction processes of three different anions and no less than 11 solvents [14]. The driving force for solvent reduction was calculated using enthalpy differences (MNDO). The effects of Li^+ and An coordination were taken into account via modelling of ion–solvent pairs. The preferential reduction of solvent molecules in the coordination shell of Li^+ was highlighted and electron spin resonance measurements presented that suggested electron-transfer equilibria between the reduced species and the remaining solvent molecules of the shell (Fig. 9.5). Comparing the different solvent–Li^+ pairs, the most negative reduction enthalpies (−5 eV) were calculated for the carbonate-based solvents, with an energy span of only 0.2 eV. The reduction enthalpies of carboxyl esters were similar to the carbonates, but separated approximately 0.8 eV from the ethers – the most stable solvents. The pure solvents were only slightly perturbed in the mono-dentate solvent–Li^+ pair configurations and all therefore followed the same trend, albeit with more distinct energy differences for the pairs.

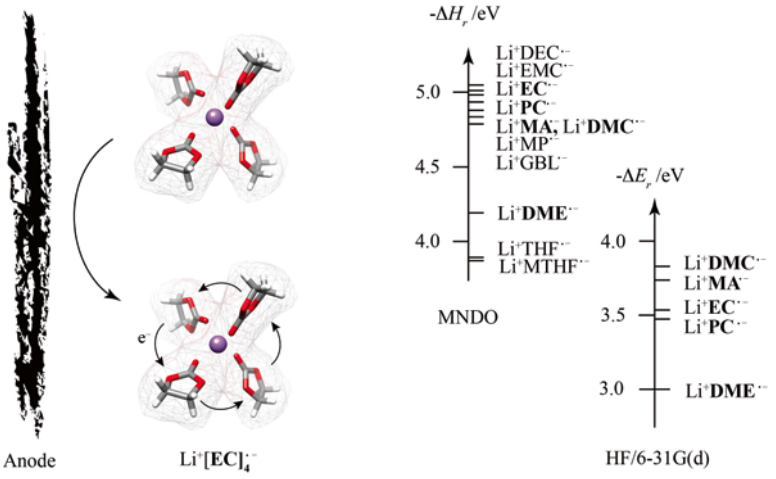

Fig. 9.5 Solvent reduction model proposed by Endo et al. [14, 15] (*left*). Calculated MNDO and HF reduction energies based on solvent–Li^+ pair models (*right*)

In 2000, Endo et al. returned to a subset of solvents (HF) [15]. A notable difference to the earlier work was a more or less reversed E_{red} trend, with the most spectacular result for EC – the least stable previously – now the most stable. Surprisingly, the authors did not address these qualitative differences. With the computational power at hand in 2014, it is easy to check these matters and therefore we here repeated the HF calculations, and obtained a different reduction energy for $[Li(EC)]^+$ (−3.51 eV) compared to the reported, clearly erroneous, value (−2.95 eV). However, as evident from Fig. 9.5, the trends for some of the solvents were still different between the 1998 and 2000 approaches for the solvent–Li^+ pairs. As this was not the case for the solvents, this must originate from the Li^+ interaction description.

The work of Endo et al. in 2000 was made in conjunction with rotating ring disc electrode experiments (for potentials above 3 V). Although no attempt was made to correlate experimental and calculated data for individual species, the authors highlighted the overall agreement with the calculated reduction energies ≤−3 eV. With respect to the E_{red} difference neither the MNDO nor HF ($\Delta E_{PC\text{-}EC}$ = 0.06 eV and 0.04 eV, respectively) approaches offered any significant improvement, but were in good agreement with the 0.11 eV obtained by Aurbach et al. using Li^+-coordinated cyclic reduction products (Fig. 9.4).

As a bit more complex model, Li and Balbuena in 2000 investigated E_{red} of EC and PC (DFT/PCM) [10] by a TD cycle. A potential difference identical to the experimental result referred to Aurbach et al. [35] was obtained. However, the main objective was to investigate an updated two-electron reduction mechanism of EC, following nucleophilic attack from groups at the electrode surface [10]. Here also transition state theory was used to estimate reaction activation barriers, equilibrium constants, and rate constants. The results suggested Li_2CO_3 as the favourable product overall, together with lithium diethylene carbonate at high EC concentrations,

which agreed with contemporary experimental results with Li_2CO_3 and R-CO_2 as main products at low and high EC conc., respectively [36].

With this short exposé into the early works, we have shown the scattering in approaches even initially to cover most of the possible types of strategies, methods, and models. With this in mind, we move on to the modern works with a maintained scatter in approaches, but adding also new dimensions in targets and aims for the predictive calculations – most notable are the work on redox reaction mechanisms and the trend to introduce more complex solvent surroundings.

9.3.1.2 Modern Works on Solvent Reduction

In the years following the early, scattered work on predicting solvent stability, computational studies of both E_{red} and mechanisms intensified. This was a natural response to the challenges of experimental characterization of SEIs and enabled only by the increased availability and applicability of computational methods. In particular Balbuena et al. [11, 37–39] were very active in the field, focusing on the reduction stability of solvents in the first coordination sphere of Li^+. Also Han et al. [40–42] and Tasaki [43–45] made recurring contributions, with Tasaki being the first to introduce an electrolyte/electrode interface. Even today the details of SEI formation and composition are a highly debated subject [46] and have therefore seen application of more advanced and larger system computational studies using AIMD [12, 13, 30] and classic MD [32, 47]. We here focus on the prediction of E_{red} and to some degree also mechanisms, but the detailed mechanisms and suggested SEI products are outside our scope.

Expanding to explicit models, Balbuena et al. used EC and $[Li(EC)_n]^+$ ($n = 1$–4) super-molecules both as pure molecular models and in cluster-continuum models [11]. Two-electron reduction mechanisms of EC with multiple pathways were explored, where detailed energy landscapes supported previous results on the relative stability of cyclic and open-chain products [35] and the stabilizing effect of Li^+-coordination [14, 15]. In addition, the introduction of a continuum demonstrated that the initial reduction step of a single EC molecule can be thermodynamically favourable – in contrast to the EA in gas phase [14]. Furthermore, the possibility of reducing either Li^+ or EC was explored, which identified the reduction of EC as the energetically favoured reaction path. The driving force for one-electron EC reduction was found to decrease with increasing super-molecule size – both the initial EA step with a cyclic reduction product and the overall energy difference forming the reduced open-chain product. The driving force was further decreased in the cluster-continuum model for $[Li(EC)_n]^+$ ($n = 1$–2) [11]. In contrast, only a negligible dependence was observed for the size of the barrier to homolytic EC ring opening.

To test the models against experimentally determined E_{red} for EC, TD cycles were used. The predicted E_{red} varied between −0.95 to +1.05 V vs. Li/Li^+ [11, 37], depending on the model. Underestimated E_{red} – negative or close to zero – were obtained for the smaller $[Li(EC)_n]^+$ ($n = 1$–2) super-molecules, while the cluster-continuum models and the $[Li(EC)_n]^+$ ($n = 4$) super-molecule with E_{red} of 1.05 V and

0.85 V vs. Li^+/Li, respectively, performed better when compared with results obtained with graphite anodes (exp. 0.8–1.0 V [48–50]). However, the EC E_{red} at a gold electrode, 1.36 V vs. Li^+/Li [51] highlights an electrode dependence not accounted for in these calculations. Thus, there is room for selecting suitable experimental references for comparison that comply with calculated results.

Yet more elaborate super-molecular models were studied by Balbuena et al. by introducing a co-solvent to EC in the solvation shell of Li^+, to take into account the presence of additives in real electrolytes. First the effects of VC [37] and later DMC, EMC, or DEC [39], were investigated. A similar approach was taken also for PC with VC as co-solvent [38]. Interestingly, in the super-molecules $Li(EC)_x(VC)_y$ the preferential reduction of EC or VC depended on if the initial cyclic reduction products or the final open-chain products were considered; super-molecules with a cyclic VC anion were found to be the products of lowest energy in the first reduction step, but in the subsequent step the super-molecules with an open-chain EC anion formed the most stable products [37]. These differences, observed for all mixed solvent super-molecules – also for the combination PC and VC [38] – indicate the importance of the choice of reference state for predicting E_{red}. Should the predictions of relative stabilities be based on the initial step only or a multi-step reaction sequence, i.e., in some sense the kinetics or thermodynamics of the reaction process?

For the case of EC and VC, experimental results have demonstrated VC reduction to occur at more positive potentials. Thus, the relative E_{red} predicted from the initial step were in accordance with experimental results. From the overall results the E_{red} trend for cyclic carbonates was $[Li(VC)_x]^+ > [Li(EC)_x]^+ > [Li(PC)_x]^+$. The study on super-molecules containing linear carbonates was limited in scope to $[Li(EC)(S)]^+$, where S = DMC, EMS, DEC, which all showed similar E_{red}. However, a straightforward comparison of the reduction energies of these complexes with the super-molecule data for cyclic carbonates was prevented by the use of different DFT functionals. The authors did make a comparison of the isolated solvents with EC, which predicted the linear carbonates to be more stable both in gas phase and using CPCM [39]. Thus, these results were in contrast with those of Endo et al. (Fig. 9.5) [14, 15].

Finally, in these mixed solvent systems, it was possible to observe the effect of VC on the cyclic and open-chain reduction energies of EC, when VC was only an electrochemically passive co-solvent. However, the results were in conflict depending on the super-molecule size; in $[Li(EC)(VC)]^+$ the formation of both cyclic and open-chain EC was stimulated compared to $[Li(EC)_2]^+$, but in the larger $[Li(EC)_3(VC)]^+$ super-molecule the effect relative to $Li^+(EC)_4$ was negligible. In summary, Balbuena et al. in detail revealed the reduction behaviour of common carbonate solvents as part of the coordination sphere of Li^+, in models more complex than the solvent–Li^+ pairs introduced by Endo et al. [14]. Both groups stressed the importance of Li^+ coordination for predicting solvent reduction.

As a twist to the approach presented above, Han et al. investigated lithium-rich super-molecules $[(Li)_2S]^{2+}$ with S = EC, PC, VC, ES, and GS, assuming a two-step reaction mechanism with the consecutive addition of two lithium ions [40]. Based on open-chain Li^+ coordinated reduction products, the stability trend among the

investigated solvents and additives was ES ~ GS > EC ~ PC > VC for the first reduction step and GS > PC ~ EC ~ VC > ES for the final $[(Li)_2S]^{2+}$ complexes. Although the negligible difference in E_{red} of EC and PC was in accordance with previous results, the increased stability of VC with respect to EC and PC opposed experimental findings.

The same authors also performed an extensive screening of the DFT functional and basis set effect on E_{red} of EC and VC. This time the intermediate cyclic reduction products were included in the mechanism, and based on their energies relative to the solvent ground state, VC was predicted to be more easily reduced irrespective of choice of DFT method [41]. The reference reduction energy difference of EC and VC was 0.17 eV (CCSD(T)/aug-cc-pVQZ). The uniform DFT results were, however, not observed for the subsequent reduction steps. In a later study using CPCM [42] the difference was 0.2 eV, but both results slightly overestimated the experimental 0.06 eV measured by Zhang et al. using a gold electrode [51].

In their work Zhang et al. also predicted E_{red} of several carbonate solvents using TD cycles, but the computational details were sparse, and repeated referencing were instead made to a meeting abstract and a TD cycle similarly used in a second paper for predicting solvent E_{ox} [28]. For the E_{red} calculations, the postulation of several reaction schemes and products was reflected in poor correlation of part of the predicted results with experimental data [51]. For example, a two-electron reduction process with solvent fragmentation into R-CO_2^- and alkyl anions was assumed for both DEC and DMC. One-electron reduction and ring opening with linear products was the base of the calculations for EC and PC, while the ring-structure of VC was kept intact during one-electron reduction, since they found the linear reduced form of VC to be unstable in the absence of Li^+.

The TD cycle method was at the time used by several groups to predict realistic E_{red}. Apart from the solvent reduction and oxidation stabilities predicted by Zhang et al. [28, 51], Balbuena et al. applied it in their first study of the $[Li(EC)_n]^+$ supermolecules [11]. A third relevant contribution came from Vollmer et al. [29], aiming more at assessing the power of the methodology than predicting E_{red} for any specific battery solvent. Therefore, while the solvents investigated were not archetypical Li-ion battery solvents, a selection of 13 solvents and 6 additives was chosen to allow for accurate comparison with experimental E_{red} and EAs.

Vollmer et al. assumed free electrons at rest (with zero energy) and considered the solvent in the liquid phase as a solvated species and investigated a three step TD cycle – where all steps were computationally accessible. The absolute E_{red} obtained was related to the Li^+/Li redox couple by a −1.46 V shift [29]. For the test set the average absolute difference between calculated and experimental E_{red} was 0.26 V. However, three of the modelled solvents (thiourea, hydrazine, and phenylhydrazine) deviated strongly, 2.5–3.3 V. With the two sets of experimental data available, E_{red} and EA, the authors addressed the strength of the individual computational steps and attributed the larger deviations to the involvement of possible side reactions. The real application of the method following this assessment was aimed at three quinone-based additives, VEC, and ES, with direct experimental comparisons resulting in a maximum difference of +0.17 V. For reference, Fu et al. later rigorously

tested the TD cycle to obtain E_{red} for a test set of 270 structurally unrelated organic molecules in acetonitrile [52]. They reported a standard deviation of 0.17 eV between predicted and experimental E_{red}, but also noted nine singular cases where the predictions were off by ±0.5–0.8 eV. These offsets were not as severe as those observed by Vollmer et al., but most of the data of Fu et al. simulated redox processes where the organic molecules were in neutral/cationic form. Thus, the approach may indeed be more suitable for predicting solvent E_{ox}.

In 2004 Vollmer et al. challenged the qualitative result of Balbuena [11] and Endo [15] that Li^+–solvent coordination promotes solvent reduction, using E_{red} of EC, PC, and VEC, and a TD cycle [16]. One-electron reduction potentials were reported for each species with linear or cyclic reaction products, as well as the species' Li^+ coordinated counterparts, and compared with experimental results [51]. The best agreement between calculated and experimental results ($\Delta E \leq 0.3$ V) was obtained with the assumption of non-Li^+ coordinated open chain reaction products. Assuming cyclic reaction products, E_{red} was lower by 1.2–2.4 V. Increased reactivity with Li^+ coordination was demonstrated, as already observed by others, but also a large variation in the magnitude of increase: 0.12–0.77 eV depending on the specific solvent and the solvent anion conformation – cyclic or open chain. Based on a quantitative comparison of predicted and experimental E_{red}, the reduction mechanisms of EC, PC, and VEC were, by taking all information into account, suggested to involve the ring opening of non-Li^+ coordinated solvent molecules.

Non-coordinated solvents were the focus also of Tasaki [17], who stressed the earlier finding of Balbuena et al. [11] that solvent EAs can be exothermic in the absence of Li^+ coordination, when modelled in solution. He also emphasized the possibility of obtaining qualitatively different results in gas-phase with HF or post-HF approaches using cyclopentanone enolate as an example – which has an EA endothermic based on HF, but exothermic and close to the experimental value of −1.6 eV with MP2 and DFT (B3LYP or B3PW91). However, notably all post-HF energies presented by Tasaki were evaluated as single point calculations at the HF/6-31G(d) optimized geometry and were not true minima at the quoted computational level. Also, no exothermic EAs were obtained for any of the battery electrolyte solvents investigated.

Unlike the use of a TD cycle, which implements a reference point to qualitatively assess E_{red}, Tasaki's focus was the relative solvent reduction energies. Based on CPCM, Tasaki listed the ease of one-electron solvent reduction with ring-opening as follows:

$$\mathrm{EC, PC} > \mathrm{VC} > \mathrm{DMC} > \mathrm{EMC, DEC}$$

It was briefly mentioned that the same order of reduction likelihood remained also if one Li^+ was introduced. However, focusing on different possible interpretations, the reduction energy order of VC and DMC was interchanged if considering the cyclic reduction products of EC, PC, and VC. In the gas-phase a difference in the relative stability of the linear carbonates was suggested only with linear products, because of a particularly strong stabilization effect of DMC in a continuum. With

rings intact, the gas-phase approach predicted VC to be the solvent with the lowest barrier to reduction – for us indicating again the caveat of extracting even qualitatively different results when using a single method/model. Including a second-electron reduction step for EC, PC, and VC, using CPCM, VC was found to be substantially more easily reduced, which correlates with the facile SEI forming properties of VC experimentally. While Tasaki for reference included a summary of the results of Balbuena et al. [17], it is interesting that several of the results on the relative reduction stability of EC and VC were in qualitative conflict. Two specific examples are the gas-phase EA, where VC was predicted to be less prone to reduction, and the continuum approach assuming open-chain products, where VC was more prone to reduction. Unlike Tasaki, Balbuena et al. reported energies for structures optimized at the same (high) computational level, and thus the differences can be a result either of the different DFT functionals or Tasaki's approach to use post-HF energies calculated for HF optimized structures – a dimension unaccounted for.

In 2006 surface effects were introduced for the first time when Tasaki et al. simulated solvent reduction at a lithium surface, represented by a 15-atom cluster, a minimum model size to assure adsorbtion and decomposition at the centre of the cluster and to mimicking the body centred cubic structure of metallic lithium [18]. HF intrinsic reaction coordination (IRC) calculations were performed, tracking the reaction enthalpy of the decomposition process from reactant to products via an intermediate transition state. With a selection of common solvents and additives, the cluster and single adsorbent were optimized collectively, simulating reductive decomposition without an explicit transfer of an electron to the adsorbent. All reactions were exothermic, with an endothermic activation step, generating one or two decomposition products – either liberated or adsorbed to the surface. Comparing the activation energies, the relative results were found to be in qualitative agreement with experimental results:

$$\text{VEC}, \text{VVC}, \text{VC} < \text{EC}, \text{ES}, \text{PC} << \text{THF}$$

Smaller activation energies, signalling higher E_{red}, were observed for film-forming additives such as VEC and VC, while larger and comparable activation energies were calculated for EC, PC, and ES. These were in turn much smaller than the activation energy of THF, known to be very stable against reductive decomposition. VEC was unique with two decomposition paths, with the second having an activation energy similar to EC.

With the cluster-adsorbent model, Tasaki et al. added a new dimension to the computations, albeit with important restrictions imposed by unavoidable limitations in computational resources and therefore the authors commented the limited cluster size, the accompanying structural changes of the cluster during reaction, and the low-level method required. Large changes in the cluster structure were in part attributed to a natural flexibility of the metal, while the use of a small basis set without any polarization or diffuse functions, 6-31G, was strengthened by presenting qualitatively similar results for EC, ES, and VC using 6-31+G(d).

Recently, Tasaki et al. investigated the relative reduction stability of EC and PC in graphite, represented by two stacked 72-atom graphene layers [53]. The solvents were part of a solvation shell of Li^+ forming $[Li(EC)_n]^+$ ($n = 1–4$) super-molecules, sandwiched between the graphene layers, and together creating a model of ternary graphite intercalation compounds (GICs); $[Li(EC)_xC_{72}]^+$ and $[Li(PC)_xC_{72}]^+$ ($x = 1–4$). For computational efficiency, the ternary GICs were modelled using non-local DFT with periodic boundary conditions and a numerical basis set. Focusing on the relative exothermic reduction energies obtained for all models, the difference between EC and PC increased with model size from 0.06 to 0.16 eV at $x = 4$, with the more negative E_{red} for the EC-containing GICs. A similar trend was observed for the super-molecules in the absence of the graphene layers, both in gas-phase and with CPCM. At $x = 4$, the predicted gas-phase difference was approximately two times that of the ternary GIC result, while the CPCM result was comparable to the latter.

Other recent contributions including surface effects are the AIMD simulations of Leung et al. [12, 13, 30] – so far focused on details of the reductive decomposition of EC in liquid EC or at graphite, lithium metal, and aluminium oxide surfaces. The simulations have revealed edge effects, identified reaction time-scales, activation free energies, alternative decomposition paths and products. Also, in the supplementary information of [30], based on a snap-shot from a simulation box, the preferential reduction of EC near surfaces have been elegantly demonstrated by calculating the instantaneous energy (via F-C) required to reduce each of the 36 EC molecules positioned between two $LiAlO_2$-coated Li_xC_6 surfaces. However, given the one solvent approach, the prediction of relative solvent E_{red} is still awaiting.

In the absence of surfaces, using both dynamic and static DFT, Leung et al. have also addressed the effects of an explicit EC surrounding on the reduction mechanism. The results suggest that in $EC^-(EC)_n$ complexes an excess electron is localized to one molecule, irrespective of the cluster size. Furthermore, the initial reduction step is less endothermic compared to molecular EC reduction, and the subsequent energy barrier to bond cleavage is smaller, the latter even when compared to the $EC^-[(EC)Li]^+$ dimer [13]. In the dynamic simulations, this was reflected in EC^- bond cleavage occurring within the simulation time-scale only in the absence of Li^+.

Also Bedrov et al. have recently addressed EC with a combination of static and dynamic approaches; high-level DFT with classic MD using a reactive force field [32]. Kim et al., with a similar MD approach, defined an "SEI formation potential" with predicted values of 0.9, 1.1, and 1.0 V vs. Li/Li^+ for DMC, EC, and EC + DMC electrolytes in contact with a lithium metal surface [47].

We believe that we are at the stage where the models used and methods applied to solvent reduction are so elaborate, and the computational resources so vast, that any further development should be directed into converging towards a preferred DFT functional, a preferred cluster size to model a surface, and choosing a cluster-continuum approach for a selected type of super-molecule. Thus with some kind of standardization within the field, chosen based on careful comparisons with

experimental data, and applying this standard should pave the way for more easy interpretation, and this way the predictive power should increase tremendously.

9.3.1.3 Solvent Oxidation Potentials and Mechanisms

While prediction of solvent E_{red} has paved the way for strategies, methods, and models, the focus has gradually shifted towards also treating solvent E_{ox}, and noticeably for more varied solvent chemistries. Also, it is not necessarily so that the same approaches work equally well for predicting E_{ox} as E_{red}. We will here step through the history and current state-of-the-art for prediction of E_{ox} – and do include some recommendations.

To the best of our knowledge the first predictions of E_{ox} for molecular solvents was made by Zhang et al. who applied a SE TD cycle – mixing calculations (DFT/PCM) with experimental data (tabulated free energies of formation) [28]. Doing so, the metallic work function (Φ_M) was effectively cancelled out by introducing a reference cycle for Li^+ reduction, and E_{ox} values of ~5.5 V vs. Li^+/Li were obtained for linear and cyclic carbonates, approximately 1 V more stable than ethers and unsaturated carbonates. Although these results were in line with experimental results gathered from several sources, the authors were forced, by experimental data scarcity, to use the same data for all solvents, leaving only two solvent-dependent energy differences. Therefore, a fully computational TD approach is recommended. In addition, a fixed reference value can replace an explicit second cycle for the Li^+/Li reaction [24, 29].

Similar to the early predictive work of Aurbach et al. on solvent E_{red} [35], the work of Zhang et al. [28] seems to be isolated in time. Although referred to by Han et al., working on predictions for additives for overcharge protection [54], the next dedicated study appeared first with Xing et al. as late as 2009 [21, 55], this time on the detailed oxidation decomposition of PC and EC, respectively. For PC, three main decomposition paths were identified for the initially generated cation radical $PC^{\bullet+}$, with calculated gas phase standard electrode potentials in the interval 4.41–4.51 V vs. Li^+/Li [55]. However, no detailed computational origin of these potentials was given, nor was the energy of PC explicitly stated, as all energies were given relative the energy of $PC^{\bullet+}$. The work on EC also included a number of alternatives or co-solvents, but no E_{ox} relative Li^+/Li was given. However, based on F-C, the HOMO energies, and the adiabatic IP-free energies – the relative oxidation stability was obtained as:

$$EC > PC > DMC > EMC > DEC$$

While the authors concluded this to be consistent with Zhang et al. [28], the predicted order of the latter was in fact different(!): DMC > PC > EC > EMC > DEC. Furthermore, the span of energies by Xing et al., 0.4–0.8 eV, was much larger (0.16 eV in [28]). Moreover, despite EC being predicted to be the solvent most oxidation resistant, Xing et al. argued that a preferential coordination of EC to PF_6^- would facilitate oxidation of EC at the cathode surface. They based this argument

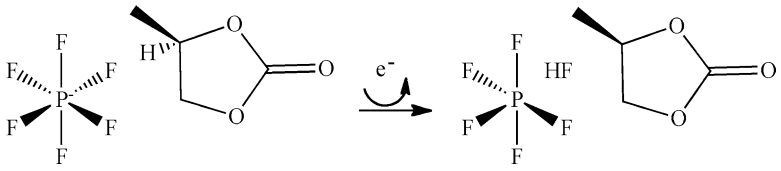

Fig. 9.6 Spontaneous solvent deprotonation and generation of HF when PC is oxidized in the presence of PF_6^-, as predicted by Xing et al. [57]

on differences in calculated solvent:PF_6^- binding energies [21] and experimental indications of EC being the component in EC:DMC and EC:DEC electrolytes more actively oxidized [56].

In a recent paper, the solvent and anion interplay was addressed in more detail by calculating the E_{ox} of PC, PC–PF_6^-, and PC–ClO_4^- via TD cycles [57]. In both gas phase and continua, with high or low dielectric constants, the calculated E_{ox} of PC was lowered in complexes with either PF_6^- or ClO_4^-. The implicitly solvated complexes presented the best fit with experiments [8, 58]. Similar effects were reported also for carbonates, sulfonates, and sulfones in complex with BF_4^- and PF_6^- [59]. The decrease of solvent E_{ox} was for the carbonate solvents attributed to spontaneous solvent deprotonation and formation of HF (Fig. 9.6), while for the sulphur-based solvents, fluorine was instead transferred from anion to solvent. Also demonstrated were general oxidation potential trends when introducing an implicit solvent; for solvent–anion complexes the effect was a potential increase, but the E_{ox} of isolated solvent molecules decreased with increasing continuum dielectric constant. For most species the observed gain or drop in oxidation potential was 1.5–2 eV at $\varepsilon = 20.5$ and varied little with further increase of the dielectric constant [59].

In two papers Shao et al. predicted the E_{ox} of sulfones and functionalized sulfones [60, 61]. Influenced by [28], the solvent E_{ox} was taken as the difference of two free energy cycles – one for solvent oxidation and one for Li^+ reduction – and in part invoking tabulated data as input for the reference cycle [60]. However, new to the approach was the calculation of $\Delta G_{solv}(Li^+)$ at the experimentally determined solvent dielectric constants, which introduced a solvent dependence in the floating, rather than fixed, reference potential. The reference potentials depended on the specific computational approach, but were approximately 2.5–3.0 eV. The reference potential difference between the low ($\varepsilon = 8$) and high ($\varepsilon = 95$) dielectric solvents was 0.5 eV [60]. Thus, both the absolute numbers and the variation with solvent were large compared to the fixed Li^+/Li reference of 1.4–1.5 eV used by other authors [16, 57].

For the five sulfones initially addressed by Shao et al., the HF/PCM approach overestimated and the DFT/PCM approach underestimated the E_{ox}. The MP2/PCM approach gave the best fit with a mean deviation of only 0.29 eV. However, if we now choose to replace the floating reference by a fixed of 1.46 eV, the MP2 approach results in a mean deviation of 1.11 eV, twice of the worst performing DFT approach (Fig. 9.7). Therefore, we stress that the mean deviation of absolute potentials alone is not a measure of the quality of the approach, but the prediction

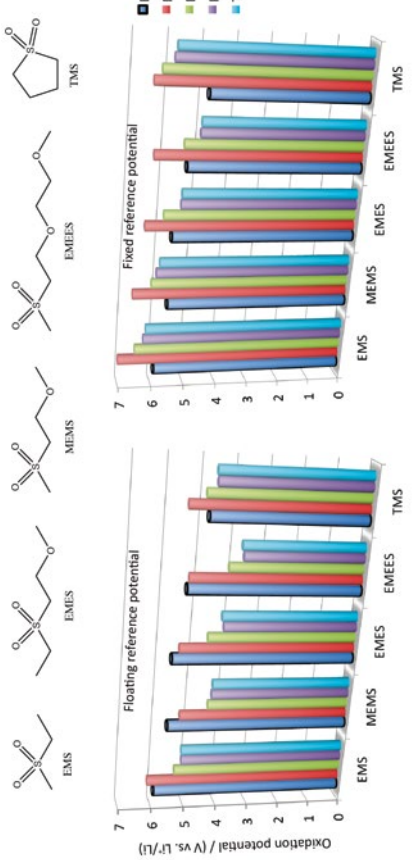

Fig. 9.7 Structures and oxidation potentials for sulfones with the use of floating reference potentials as predicted by Shao et al. [60] (*left*) and with a fixed 1.46 eV reference (*right*)

of relative E_{ox} is more interesting. Making a comparison based on the detailed results provided in the supplementary material of [60], all predict EMS to be the most stable solvent – irrespective of reference. Furthermore, with a floating reference all predict the cyclic sulfolane or TMS to be the second most stable solvent. However, using a fixed reference some approaches predict MEMS to be the second most stable solvent, the reason being the 0.5 eV larger floating reference (resulting from a much lower dielectric constant).

Experimentally the E_{ox} of TMS is inferior to the linear sulfones. We here stress that the use of five experimental potentials from three different sources does add a lot of uncertainty; for example the potential sweep rates differ [62–64]. As demonstrated for PC [8], this can give rise to deviations of the order of 0.5 eV (higher E_{ox} for lower rates). One of the experimental reference studies also clearly shows how the choice of lithium salt does play a role; a 0.4 eV difference is obtained between the 1 M LiTFSI/MEMS (5.6 V vs. Li^+/Li) and the 1 M $LiPF_6$/MEMS electrolytes (5.2 V vs. Li^+/Li) [64], which also for [60] further complicates the comparison of experimental results.

Without any experimental data available for comparison, Shao et al. also proposed and investigated sulfones with different functionalities as solvents [61]. By, e.g., replacing the ether functionality of MEMS with a carbonate, ester, or cyano terminated alkane chain, they in all cases predicted an approximate 0.5 eV increase in E_{ox} (MP2, TD cycle). Other substitutions produced similar effects; a trifluoromethyl group for the terminal methyl group (MEMS or EMES), but if also a fluoro atom was introduced in place of the alkane group directly bonded to the sulphur, this second substitution introduced a further 0.5 eV or 1.0 eV stabilization of the solvents with an ester or cyano functionality, respectively. In addition to the TD cycle, adiabatic gas phase IP computations predicted EMS to be the most stable of the linear solvents and supported the stabilizing effects upon functionalization qualitatively [61].

As an example of studying new solvents by computations, Assary et al. explored the size-dependence of polysiloxane oligoether E_{ox} [26]. No experimental values were provided, but standard organic solvent E_{ox} (B3LYP/CPCM) were computed for reference and compared with the results of Zhang et al. [28]. The Assary et al. values were consequently smaller, but followed the same trend as the results presented by Zhang et al.:

$$\text{EC} \sim \text{PC} > \text{BC} > \text{VEC} \sim \text{GBL} > \text{VC}$$

The values for VEC and γ-butyrolactone (GBL) were new, as were the results for close to 30 mono- and disiloxanes, covering the potential range 3.38–5.14 V vs. Li^+/Li. The most stable solvents being $–NO_2$, –CN, and $–CF_3$ substituted monosiloxanes, all with E_{ox} above 5 V vs. Li^+/Li, but slightly less stable than EC and PC [26].

Very recently, Leung extended his AIMD studies to include solvent oxidation at a $Li_{0.6}Mn_2O_4$ (100) surface [31]. This is, to the best of our knowledge, the first example of introducing an explicit surface for oxidation reactions, with the results suggesting EC to adsorb to the surface and bond breaking to occur before the subsequent exothermic oxidation. In detail, it proceeds with a simultaneous proton

transfer from EC to a surface O atom, followed by reorganization at the surface of the EC fragment – having lost two electrons. Based on the activation energies, a sub-second time scale was suggested for the surface catalyzed EC oxidation. Leung discussed E_{ox} in the introduction of his work, where it was suggested that static DFT approaches overestimate solvent E_{ox} and E_{red}, since the catalytic activity of the electrode surface is not taken into account. However, no alternative E_{ox} was predicted from the AIMD simulations. Instead, for example the activation energy for O–C breakage in ultra-high vacuum versus at the electrode–electrolyte interface was compared, which predicted a lower barrier at the surface. Leung related his results to the work by Xing et al. on solvent decomposition in solvent–anion complexes [57], which also suggested a solvent deprotonation mechanism. Different decomposition products were a natural consequence of having an anion versus an explicit surface accepting the proton, thus showing the importance of a correct model – depending on the sought property.

The approach of Leung above allows for detailed studies of decomposition pathways, but there are also some possible drawbacks with the large freedom in surface design and the choice of reaction pathways: an overwhelming (computational) task. Qualitatively different results may occur on different surface facets and it is in addition also hard to anticipate and account for thin surface coatings, like SEI or SPI, that likely form spontaneously on real electrodes and possibly alter surface properties and decomposition pathways. However, with a continuous increase of computational power and overall development of the methods employed, we foresee that each of these problems will be diminished, and simulations of a much wider number of solvents and scenarios will be possible via this strategy and various models. Thus, this approach will become an increasingly valuable tool to investigate the influence of different surface chemistries on the relative solvent E_{ox} and decomposition pathways – and perhaps be truly predictive, also able to target-specific chemistries and thereby including the "full" battery cell design.

9.3.2 Salts

Prediction of salt electrochemical stability in the context of Li-ion batteries has mainly involved predicting the E_{ox} of novel lithium salt anions, frequently without any focus on the subsequent decomposition reaction products and mechanisms. However, with recent results on oxidation promoted solvent–anion reactions [57] and the rapid development of "solvent-free" ionic liquid (IL) electrolytes, investigations of both anion and cation decomposition products are foreseen by us to become more frequent and important – particularly in connection with the passivation phenomena at the negative electrode. As for solvents, we will here follow the historical development of studies and methods, followed by some more recent works that together with our remarks outline our perspective on the future.

In 1993 Kita et al. presented several predicted anion E_{ox} (MNDO) – upon introducing the new lithium salt LiTFPB [65], a new member of a class of aromatic borate

lithium salts introduced earlier [66]. To investigate the effect of the perfluoroalkyl substitution, the HOMO energies were correlated with available experimental E_{ox} [66]. A linear relationship between calculated and experimental E_{ox} was presented for five anions. TFPB and an analogue with half the number of perfluoromethyl substituents were predicted to be the most stable, offering significantly improved E_{ox} with respect to a non-substituted phenyl borate, $B(C_6H_5)_4^-$, but were not predicted to be as stable as the fluoro substituted $B(C_6F_5)_4^-$. However, neither the predicted oxidation stabilities of TFPB nor $B(C_6F_5)_4^-$ were calculated a priori, but instead extrapolated from calculated results for anions with substituents introduced only in one out of four phenyl ligands. Thus, adding an element of uncertainty to the absolute E_{ox} predicted for these anions. In fact, the oxidation stability of $B(C_6F_5)_4^-$ seems to have been overestimated and that of TFPB underestimated. This is indicated by the very large gap between predicted and measured E_{ox} for $B(C_6F_5)_4^-$ and the approximately 0.7 V difference in experimental oxidation stabilities between a $LiB(C_6F_5)_4$ and a LiTFPB electrolyte, in favour of the latter – with a reservation made for the use of different solvents [65].

MNDO/HOMO energies and experimental E_{ox} for three perfluoroalkylsulfonates, $C_xF_{2x+1}SO_3^-$ with varying perfluoroalkyl chain-lengths, were also presented [65], and accurately predicted the high anionic stabilities observed experimentally for the two larger anions, but the calculated difference of 0.29 V, between the extremes, did not account for the experimental E_{ox} difference of approximately 2 V [65].

The approach was repeated for new salts [67–69]; in 1997 for long-chain sulfonates with updated MNDO to investigate the effects of branching [67], and in 2000 based on HOMO and LUMO energies for imides, imide esters, and a methide anion, using a combination of SE and low-level ab initio approaches [68]. Qualitative trends, but not quantitative results, reproduced experimental E_{ox}, where the methide anion, $(CF_3SO_2)_3C^-$ (TFSM), was found to be the most stable. Moreover, LUMO energies, used to assess relative anion E_{red}, were found to correlate with HOMO levels, such that an anion with lower HOMO value also had a lower LUMO value [68]. In a final paper by these authors, HOMO energies were evaluated for PF_6^- and three perfluoro derivatives, $PF_{6-x}^-(CF_3)_x^-$, using DFT (B3LYP) [69], but a qualitative correspondence between calculated and experimental results was not obvious.

Already in 1995 Benrabah et al. had presented calculated HF/HOMO energies of $CF_3SO_3^-$ (Triflate), $(CF_3SO_2)_2N^-$ (TFSI), and TFSM anions [70]. However, in contrast to the results later reported by Kita et al., they found TFSI to be the most stable and TFSM to be the least stable anion. The important difference was the use of a diffuse function "+" in the basis set or not, often considered to be of importance for accurate modelling of anions [70].

Koch et al. [6] addressed E_{ox} of TFSI, TFSM, PF_6^-, and AsF_6^- with DFT/IP and compared the results with experimental E_{ox} measured for ILs. Both the calculated and experimental results predicted the relative E_{ox}: TFSM>TFSI>AsF_6^->PF_6^-, with a correlation coefficient close to unity. However, the difference between the extremes was only 0.8 eV. Also, they used crystal geometries in place of DFT optimized geometries to calculate the IPs, which must be regarded as highly questionable. Later predictions of E_{ox} have quite unambiguously identified the inorganic fluoro-based anions to be more stable than the organic alternatives – irrespective of approach [8, 20].

This can only agree with the above, if the experimental determination of the stability of the PF_6^-- and AsF_6^--based ILs, which was made at elevated temperatures (80 °C), significantly altered the trend with respect to what is observed with molecular solvents at room temperature [58].

Later, Barthel et al. used MNDO/HOMO to predict the E_{ox} of several new organoborates and found a linear trend vs. the experimental E_{ox} [71]. Fluoro atom substitution decreased the HOMO energies and increased the experimental E_{ox}, however, the methodology somewhat overestimated the E_{ox} differences – as observed for borate anions earlier [65].

Most of the experimental results above were later embraced as references in the seminal computational work by Ue et al. [8], who applied HF/HOMO to more than 20 anions, and DFT/IP to a subset of these. With the experience gained from determining experimental E_{ox} for anions in quaternary ammonium salt electrolytes [58], special emphasis was made to put experimental results from different sources on a similar footing by "correcting" the voltammograms made using different sweep rates. However, lack of control of other experimental parameters was still manifested in large differences of E_{ox} where data sets overlapped, e.g. $CF_3SO_3^-$ (5.1 or 6.0 V vs. Li^+/Li [8]). A single master computational and exp. E_{ox} correlation was not obtainable, but rather for families of chemically similar anions. Qualitatively, the HF/HOMO results reproduced earlier MNDO/HOMO findings, but were not always on par with the DFT/IP results – which were evaluated with optimized excited electronic states and were found to reproduce the experimental E_{ox} trend:

$$AsF_6^- > PF_6^- > BF_4^- > TFSM > TFSI > ClO_4^- > CF_3SO_3^- > B\left(C_2H_5\right)_4^-$$

As already pointed out, these results were quite different to those obtained by Koch et al. with their SE DFT/IP approach [6].

Ue et al. subsequently applied the same approach to study substitution effects in perfluoroborate, $BF_{4-x}(CF_3)_x^-$, and perfluorophosphate, $PF_{6-x}(CF_3)_x^-$, anions [22]. The introduction of a first perfluoro group in either anion family was always predicted to decrease E_{ox} significantly. However, with further substitution and a dominant number of perfluoro groups, an unambiguous picture emerged. The E_{ox} of the borates was regained to a similar value (DFT/IP) or slightly lower value (HF/HOMO) compared to the tetrafluoroborate, but this trend was not obtained for the phosphates. The $P(CF_3)_6^-$ was by both approaches predicted to have a quite substantially inferior E_{ox} to PF_6^-. Moreover, an increase of the perfluoro chain length was predicted to have little effect. Experimental data for $BF_3(C_2F_5)^-$, found this anion to be less resistant to oxidation compared to BF_4^- [22] – in accordance with the predictions. However, $PF_3(C_2F_5)_3^-$ as part of an ionic liquid, has an E_{ox} comparable to PF_6^- [72], which contrasts the predicted trend.

In the spirit of the work by Ue et al., one of us performed further tests and developments of the HOMO and IP (F-C) approaches by implementing new DFT functionals and evaluating the performance of mixed approaches – (HF, MNDO, …)/IP and DFT/HOMO [19, 20]. Also, the effect of introducing a continuum (CPCM) was investigated, and furthermore, E_{ox} were reported with reference to the Li^+/Li redox

couple, following the example of Vollmer et al. [29] and others. The basis of the ab initio HOMO approach, Koopman's theorem, is often stated not to be applicable within the framework of DFT, but DFT Kohn-Sham orbital energies have been demonstrated to correlate very well with both IPs and EAs [73]. For Johansson's test set of 12 anions, representing different functionalities and structures, the DFT/IP approach using the VSXC functional was found to best predict E_{ox}, and thus recommended for future use [20], with no improvement seen for the implicit solvation.

MO energies and different IP approaches has since Ue's and Johansson's work been adopted by several groups for comparison with experimental E_{ox} whenever new Li-salts or ILs have been synthesized [74–77], or to predict the stability of unknown compounds [23, 24, 78, 79].

Recently, a more extensive screening of known and hypothetical anions was made by us, which highlighted the sometimes qualitatively different predictions that can result with the HOMO and IP approaches [27]. The differences were found for cyano- and fluoroborates and phosphates, respectively. The introduction of cyano groups in place of fluoro atoms lead to a big initial drop in oxidation stability according to the HOMO results, while instead the IP results suggested a small improvement. Both methods, however, agreed upon a successive increase of stability with further substitution. It was suggested that the specific DFT treatment of the cyano chemistry was inappropriate, as the discrepancy was not observed in the screening of perfluoro substitution effects by Ue et al. [22] and DFT overestimations of IPs had already been observed for diatomic CN [80].

We conclude this section by reporting on a few approaches to the electrochemical stability of ILs. For these ionic solvents, predictions of the electrochemical stability of both ions are needed to correctly explore the stability limits. Ong et al. focused on a computational efficient screening of foremost IL cations, when they estimated E_{red} and E_{ox} of some 170 cations and 30 anions via DFT/EAs and IPs [25]. Alkylation of proton sites was found to lower cation EAs, thus increase the stability against reduction, with a site-dependence and the strongest effect predicted for the first substitution. In accordance with experimental results, the ammonium, pyrrolidinium, and phosphonium based cations were predicted to be more stable than imidazolium and pyridinium based cations. The introduction of electron-withdrawing cyano, carboxylic acid, perfluoro groups, or fluoro atoms was shown to destabilize the cation, while electron-donating hydroxide, alkyl, or amide groups increased the cation reduction stability. Corresponding substitutions to the $PF_5(CF_3)^-$ anion improved the oxidation stability only when a cyano group replaced a fluoro atom directly bond to the phosphorous centre, probably due to the already very strong electron withdrawing groups present. Also, seemingly unaware of the earlier work by Ue et al. [22], perfluoro groups of different chain-lengths were introduced for PF_6^- and BF_4^-, and here also for TFSI. Improved oxidation stabilities were only predicted for some high molecular weight analogues of BF_4^- [25].

Perhaps most importantly, Ong et al. demonstrated that hundreds of molecules can be screened in a systematic way, with good correspondence also between cation EAs and experimental reduction potentials [25]. In subsequent work they implemented a novel, more expensive, MD-DFT approach to the electrochemical

windows of six possible IL combinations originating from two cations – *N*,*N*-methylpropylpyrrolidinium (C_3mpyr^+) and 1-butyl-3-methylimidazolium (C_4mim^+) – and three anions [81]. Classic MD was performed for unit cells initially containing 128 ion pairs. With 16 ion pairs extracted after equilibration, further time evolution of these structures generated multiple MD-snapshots as input for periodic boundary DFT single point calculations of HOMO and LUMO levels. To compare the results for different ILs, all results were aligned with respect to a common reference – the Hartree potential relative a vacuum slab. In addition to the overall HOMO and LUMO levels calculated, density of states (DOS) revealed the individual cation and anion contributions to the stability limits.

The most striking result of this approach, when compared with regular EA and IP and PCM–HOMO/LUMO calculations, was that the reduction limit sometimes was dictated by the anions and the oxidation limits by the cations. Specific examples include the reduction limit of C_3mpyrTFSI, predicted to be governed by TFSI, in support of electrochemical and spectroscopic findings elsewhere [82], and the lower anodic stability of C_4mim^+ compared to BF_4^- and PF_6^- in the corresponding ILs. Overall, this collective approach to the electrochemical stability of ILs is very appealing and it will be interesting to follow future results. However, it is not clear what possible parasitic effects are introduced when using a liquid structure obtained from MD rather than a structure optimized at the ab initio level used for the HOMO/LUMO calculations. In this respect, the approach suffers a similar drawback as the DFT/IP study by Koch et al. [6], that by using crystal geometries as input, obtained alternative trends for anion oxidation stability with respect to a standard DFT/IP approach [8].

An alternative approach to IL electrochemical windows was put forward by Ballone et al., who implemented a free electron droplet (a 40-electron jellium sphere) as a model electrode in AIMD simulations to investigate the role of the electrode/IL interface on the stability of several ILs [83]. For reference, the predicted stability windows of C_4mimTFSI and C_4mimPF_6 adsorbed on the jellium surface, 3.77 V and 3.48 V, respectively, were in quite good agreement with the corresponding windows, 3.87 V and 3.74 V, reported by Ong et al. using their novel MD-DFT approach [81]. However, as commented and demonstrated by Ong et al. with the use of a different functional, these windows were unduly narrow because of the PBE functional used.

9.3.3 Additives

While the fundamental working scheme of the electrolyte in the electrochemical cell is to support the main reactions, there is for cell optimization a need for certain small amounts of other chemicals to be added to the electrolyte – *additives*. From the battery perspective the exact need is dependent on the cell chemistry and type as well as the intended application. We will here address additive electrochemical stability and how this can be predicted, but we will also select the types of additives treated in order to further exemplify the ways computations can be used – meeting

other demands on the predictions than we so far have seen for solvents or salts. There is also another pronounced difference to the previous sections; many types of additives have as such not been addressed by computational techniques (at least not in the open literature) for at all the same time-period, here rather less than 10 years than the over 20 years mentioned earlier. (We do here consider VC rather as a solvent than an additive). One should remember that this is in the open literature, there was most likely modelling activities at, e.g., Sony earlier, supporting their early work prior to 2000 c.f. Adachi et al. [84]. Anyhow, the need for a description of the time-evolution of computational techniques employed and the diversification in strategies, methods, and models, in the studies reported, is reduced. Therefore, we here rather present a few thorough case studies which we discuss in detail to show on the possibilities today of making predictive calculations useful for further additives development.

9.3.3.1 Active/Passive Role of Electrochemical Stability

Going back to Sect. 2 of this chapter we outlined that we in principle target either *wanted* or *unwanted* redox reactions; this implies even more so to the field of predicting additive electrochemical stabilities via E_{ox} and E_{red}. There are many types of additives used today in practice in lithium ion batteries, making the electrolyte a smart but rather complex cocktail, and where all additives basically are sorted by their target function: chemical stability, flammability, wettability, film formation, thermal stability, overcharge, etc. Any additive that does not have an outspoken electrochemical role in the cell should not impede on the basic wanted redox reaction, i.e., not decrease the electrochemical stability window. This is what we here sort as a *passive* role – the E_{ox} and E_{red} for such additives should simply be outside the ranges set by the solvents and salts. This can of course be predicted much the same way as performed for solvents and salts, with more similarities to the former as most additives are neutral molecules. On the other hand there are additives that certainly should be *active* within the electrochemical ranges set by the cell – typical examples that already have been mentioned are film-forming additives to create the needed SEI (to which of course VC should be counted), but foremost we would here like to focus on *redox shuttle additives*, both for pedagogic reasons, but also because of these compounds immense importance for the battery progress.

9.3.3.2 Redox Shuttle Additives

These compounds are perhaps scientifically the most underrated components of today's battery electrolytes. In order for any battery cells to maintain the best possible safety and life-length, especially when compiled into working batteries and even more so when put into large battery packs, they need to stay within certain cut-off potentials – determined primarily by the intrinsic stability of the electrolyte. As the manufactured cells always are just slightly different, and these differences

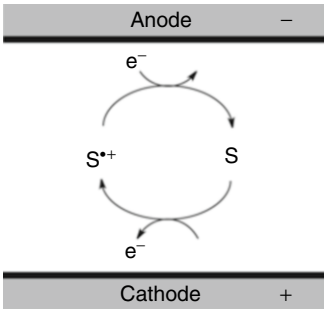

Fig. 9.8 Redox shuttle mechanism

may increase with time, they will also charge and discharge slightly differently, and staying within the desired limits will not be possible without extensive external electronic monitoring – requiring a lot from the battery management system (BMS). This is where parts of this task can be handed over to *redox shuttle additives*, to both simplify the BMS and create electrolytes that become more tolerant to what either would cause overcharge or overdischarge.

Above we in passing noted that some additives "do have other demands on the predictions" – a statement that calls for a bit of explanation. The vast majority of the referenced works so far have been quite satisfied with only qualitative predictions or quantitative ones that either are just relative or, even if absolute, considered OK when they hit approximately the right ball-park. While perhaps the latter is to exaggerate a bit, this is still in stark contrast to the case for redox shuttle additives. In order to ensure cell safety and life-length and at the same instance not decrease the capacity of the cell design, there is an extremely strong emphasis put in the development of these additives to hit exactly the right E_{ox} and E_{red} values – and thus this goes also for the predictive computations employed.

There is also another difference to be noted when comparing to the development of predictions for solvents and salts; while for these electrolyte components the practical materials development quest has most often been to extend the E_{ox} and E_{red} values, the quest for redox shuttles has partly joint in when trying to address high voltage cathode materials, but at the same time the development has also been emphasizing to match "medium" voltage cathode materials like $LiFePO_4$. It should also be noted that the first papers we know of that deals with computational predictions for vast screening of redox shuttle additives, rather than using trial-and-error synthesis, are no older than 2006, see below.

The simple working scheme of any overcharge protection devoted redox shuttle additive is as follows (see Fig. 9.8): the redox shuttle additive, dissolved in the electrolyte, almost always in neutral form (S or S^0), is oxidized to a radical, $S^0 \rightarrow S^{\bullet+} + e^-$, at the desired E_{ox} value, when the charging of the cell is completed and thus matching the positive electrode E_{ox} value. Subsequently the radical by its positive charge migrates through the electrolyte to the negative electrode, where the reaction simply is the reverse, $S^{\bullet+} + e^- \rightarrow S^0$. Hence, the shuttle cycle is completed and can be repeated.

The above may seem very simple as the target basically is a single reaction that involves no other molecules than the main model. However, this is no different to the basic demands on, e.g., the electrolyte anions. Of course, however, there are various designs of molecules that can be employed for constructing redox shuttle additives, some examples where predictive computations have been extensively applied are neutral aromatic molecules like BDB [85], DDB and its derivatives [86–88], anisole and its derivatives [86, 87, 89], while the most notable non-aromatic family of compounds is the TEMPO radical and its derivatives [86, 87, 90]. There are a few studies grasping more than one family of compounds [86, 87, 91], but less frequently this opportunity is taken to monitor the performance of different strategies, methods, or models – but a few notable exceptions will be treated in depth as case studies below. The work by Han et al. is rather unique for its coverage of no less than 108 additives [91], but foremost as the study focuses entirely on high-voltage targets (>4.5 V) – all the above studies, apart from BDB aiming at ca. 4.5 V [85], are directed at $LiFePO_4$ cathodes and thus moderate voltages (ca. 3.5–3.9 V) (Han et al. also already in 2003 covered ten various additives – see [54]).

Case Study: TEMPO and Its Derivatives

We chose this as our first case study due to the many special features of the TEMPO compound(s) and also that the studies made are thorough and exemplifies the level of accuracy that has been reached for predicting the electrochemical stability of additives. There are also a number of delicate computational issues that we do not find described elsewhere for these types of additives. The core TEMPO molecule is a stable radical, with a sterically protected nitroxide. In 2006 only BDB and TEMPO had shown the required stability to act as an overcharge protecting redox shuttle [90].

As examples of the level of accuracy obtainable for TEMPO we basically use two papers from 2006 [86, 90]. As an example of particular methods development, aiming also at other redox shuttle families, the first of these papers also includes the systematic variation of CPCM parameters (B3LYP/6-31G*), something we do not observe in any other papers. Both the solvent radius and the dielectric constant were varied and TEMPO applied as the probe; by varying the radius between 4.0 and 6.0 Å, for a dielectric constant of 60.0, and the dielectric constant between 40.0 and 80.0, for a radius of 5.0 Å, the TEMPO E_{ox} is shown to vary between 3.63 and 3.65 V, and thus being rather insensitive to this variation.

As another feature, the paper in detail discusses the problem of predictive computations to arrive at stable geometries, and instead noting imaginary frequencies. This occurred for no less than 7 out of 17 studied shuttles, whereof one a TEMPO derivative. While the authors did address the issue by increasing the DFT grid quality, we speculate in that the use of another DFT functional, starting geometry or just a larger basis set could prevent this erroneous behaviour, though a freely rotating methyl group often poses a low-lying energy landscape problem. The practical consequence was that the error in energy from having one or more imaginary frequencies denounced the thermal contribution correction sought to better correlate with the experimental data [86].

A third complicating feature found and addressed was that, with the 4-methoxy-TEMPO radical used as the example, some of the shuttles have multiple conformations, e.g., axial or equatorial methoxy group [86]. The solution taken was to predict the E_{ox} value for both conformations and simply report the average, without any Boltzmann distribution based on the small energy difference. The given example of the 4-methoxy-TEMPO radical gave 3.69 and 3.85 V, resulting in an average of 3.77 V (faulty listed as 3.74 in Table 1 [86]). The interesting note to make here is that in solution one conformer may dominate and the difference of 0.16 V is a rather large difference, seen in the light of the E_{ox} values of the other two TEMPO radicals reported: TEMPO 3.64 V and 4-oxo-TEMPO 3.94 V. Thus the maximum substitution effect reported for the TEMPO based shuttles was only twice that of the conformational change.

Of course there can be more chemical substitutions made to the TEMPO basic structure; in [90] an incremental exchange of H to F atoms either on the ring or in the methyl groups were made to move the TEMPO E_{ox} value further away (up) from the $LiFePO_4$ E_{ox} value – deemed valuable for commercialisation. Each such substitution moved the predicted (B3LYP/PCM) E_{ox} value up ca. 0.1 V, which for the practical aim was considered too small an enhancement. This time, this was used as a pre-synthesis screening test, as this exact substitution strategy was not reported with any experimental correlation/verification (while others were).

The main reason for selecting the case of TEMPO and the reference [86] was, however, the excellent RMS and max deviations obtained for the 17 additives test set. By calculating a new measure based on the average orbital energies, corrected to the Li^+/Li redox couple, an "E_{est}" was obtained with a RMS of only 0.05 V and a maximum deviation of 0.15 V for a range which was >1.5 V, which convincingly illustrates just how accurately it is possible to predict the E_{ox} values, when accurate *experimental* data is at hand – as there is nothing especially complicated behind the strategy, method, or model applied.

Case Study: Using a Probe Molecule

When we in Fig. 9.3 in Sect. 2.3.3 outlined the different models that have been used, they all shared the common feature of comprising, either explicitly or implicitly, the components of the electrolyte and sometimes electrodes – and nothing else. This may seem as an obvious choice and perhaps odd to mention, but we will here treat an especially elegant case where another distinct kind of strategy and model was successfully employed [87].

A caveat is that the strategy does not formally treat the electrochemical stability in any redox reaction per se, but rather the overall stability of the oxidized form of the redox shuttle, a property, however, of immense importance for practical application (to be able to fulfil as many cycles as possible in accordance with Fig. 9.8 in Sect. 3.3.2).

The strategy presented in [87] in essence follows this line of thinking: (1) the standard methods that can be accurately used to predict the E_{ox} values (see section "Case study: TEMPO and its derivatives" above) do unfortunately not convey the

additive stability against decomposition within "the reaction cocktail of the Li-ion cell" [87], (2) the calculation of the reaction pathways considering each possible decomposition reaction of each possible additive would effectively prohibit large scale screening of new compounds, (3) the intrinsic reactivity of the additive can instead be estimated by testing with an "atomic reactivity detector" [87].

The physical chemistry idea behind the "atomic reactivity detector" is that a preferred interaction with this probe would naturally reveal an atom in the redox shuttle prone to react. And the strength of the interaction would probe the reactivity of the redox shuttle at large. For the ease of computation the "atomic reactivity detector" would preferably be a rather small molecule and it should interact strongly with the test object. The single strongest criteria, however, is to correlate with the experimental studies of stabilities of a test set.

Having observed that neither the natural choices EC nor Li^+ or PF_6^- worked as probes using the criteria above, the authors next considered to use a species not at all present in *any* electrolyte, but with certain appealing properties. The choice fell on the ethyl radical (ER), $C_2H_5^{\bullet -}$, that via its singly occupied HOMO (i.e., SOMO), localized to the carbon atom of the CH_2 entity, has very strong interactions possible and this for a narrow end of the molecule that can penetrate the additive structure to access all atoms.

While the calculation of the interaction energy with the additives, E_b(ER), is quite straightforward, the experiments correlated against was a long-term experiment for each redox shuttle, to observe the number of 100 % overcharge cycles that could be maintained before the shuttle action ceased [87].

The most amazing feature of this strategy is that when applied to 19 different redox shuttles stemming from, e.g., the DBB, TEMPO, and anisole chemistries, there was a quite binary correlation reported; those that experimentally were stable >100 cycles had $E_b(\mathrm{ER}) \leq 1.73$ eV, while those with a stronger computed interaction (>1.73 eV) all failed before reaching 33 cycles. With this main result the authors dwelled into details of the reactivity, especially how the computed LUMO energies can be used in conjunction with the probe measure, and also how certain chemical substitutions affect both E_{ox} and E_b(ER). Interestingly, there was a rough correlation presented between the two: the higher the E_{ox}, the higher also the E_b(ER), and thus a more unstable shuttle. This we here note as a discouraging result in the perspective of the development of shuttles for high voltage chemistries – but the correlation was not without outliers.

There were also special observations made related to the basic shuttle chemistry; the anisole was suggested to create a more stable species during the oxidation in the experiment and explained its worse correlation, while the radical nature of TEMPO renders this family to perform much worse as the E_b(ER) measure is less suitable. The major criticism that we can put to this case study today is the use of only the B3LYP/6-31G* method, as B3LYP often is regarded by computational chemistry purists as a rather "bad" functional in terms of absolute energies, and furthermore here combined with a rather small basis set. However, as the method is correlated overall vs. adequate experiments, we foresee only minor improvements on average, but perhaps a more modern functional combined with a larger and more flexible basis set would perform much better also for the more problematic cases.

9.3.3.3 Concluding Remarks

The prediction of absolute values is more important for these compounds than elsewhere, partly due to the fact that the experimental data used for the correlation is of higher quality and less ambiguous, and partly due to the work scheme of certain additives. Therefore statistical measures come more into play as well as large screening studies. The rather recent (<10 years) emergence of strategies in the sub-area clearly shows as a less pronounced spread in the methods and models employed. Notably the methods used are not really updated or examined for better alternatives – with a majority or the DFT using the B3LYP functional as its work horse, with Han et al. [91] as an exception using other functionals (BPW91, B3PW91 with CPCM). The strategy employed for assessing the overall stability via a probe molecule for a working redox shuttle in its oxidized state was indeed a successful new way of thinking.

9.4 Summary and Outlook

One of the main goals of the predictive calculations of E_{red} and E_{ox} is to establish trends in solvent, salt, additive, and overall electrolyte electrochemical stability that can be used to guide the selection and combination of electrolyte components. Most conveniently, computational results obtained should – in one way or the other – be converted to a relative potential scale, preferentially vs. Li^+/Li, to ease the comparison of experimental and calculated results. Thus, a grand summary of the work traversed in this chapter would be to present the electrochemical stabilities of the materials covered in this chapter in a master figure relative the Li^+/Li potential. However, because of the many methods and model approaches implemented, and the different procedures used to project the computational results onto an experimental scale, this would be either a hopeless endeavour or end in an overwhelmingly complex figure.

Nevertheless, to still attempt something of the sort, a small sub-space of the results presented in this chapter have been collected in Fig. 9.9, in order to visualize a few of the most important conclusions that can be made. As a suitable sub-space the results of Balbuena et al. on the reduction stability of Li^+-coordinated EC, VC, and PC [11, 37, 38] was chosen, because of the richness of models used and the consistent computation level approach. Balbuena et al. reported their results in both absolute numbers and relative the Li^+/Li potential. In Fig. 9.9 – we have used the relation adopted by these authors, and created and related the absolute and reference frames in a similar fashion as was made in [92].

With Fig. 9.9 as a base we can stress the following: (1) Experimental reference results (potentials and relative trends) from different sources are frequently in contradiction, but map out a potential region where reduction or oxidation occurs, (2) The choice of model, e.g. vacuum, implicitly or explicitly solvated (by 1–4 solvent molecules) species, will show a wide distribution of potential energies, and (3) When settling for a specific model and method combination, e.g. [Li(A)

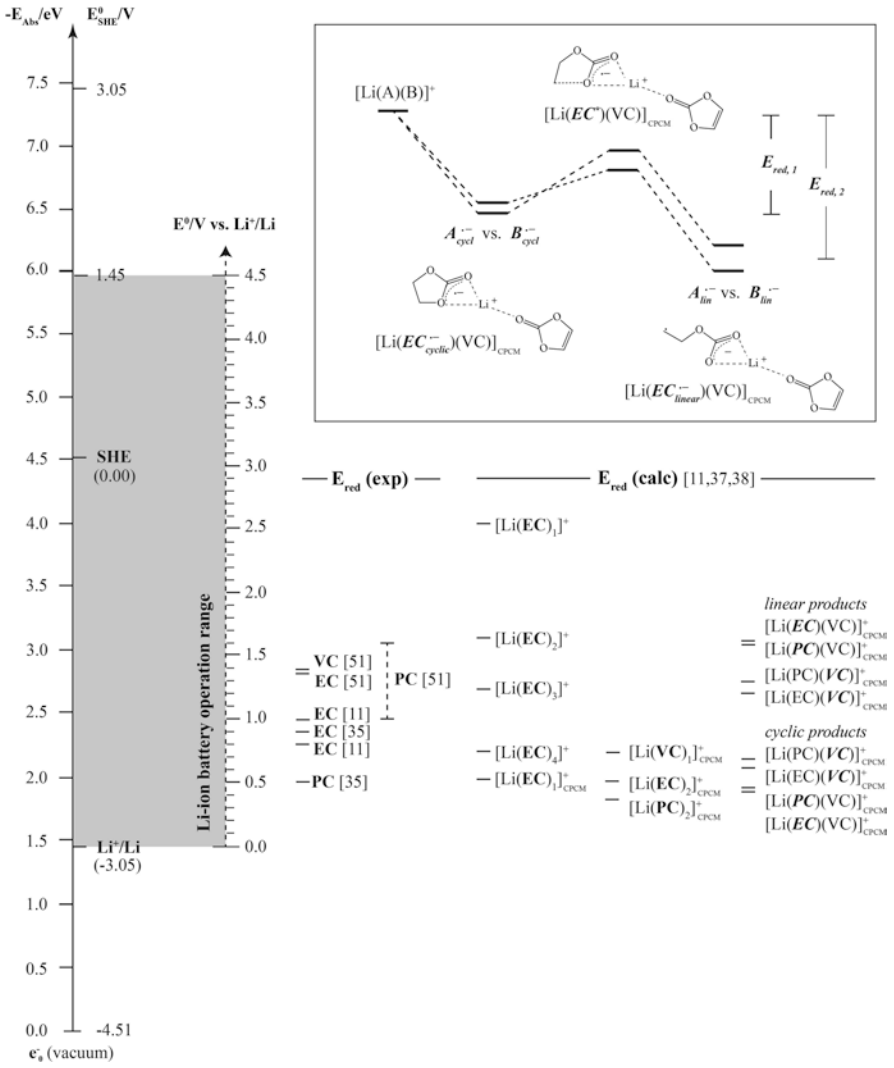

Fig. 9.9 Reduction mechanisms and predicted reduction energies for Li^+-coordinated EC, VC, and PC presented by Balbuena et al. [11, 37, 38], with respect to absolute and relative potential energy scales and experimental reference values reported in [11, 35, 51]

$(B)]^+_{CPCM}$, where A and B are the same or different species, both qualitative and quantitative results for the reduction of A will depend not only if A is partnered with another A or B, but also on the strategy chosen, e.g., how the reduction energy is defined – i.e. the choice of start and end structures, as visualized in Fig. 9.9 by the choice of cyclic or linear reduction products.

Figure 9.9 and all the works behind it illustrates where we are today; the simplest possible forecast of the *future* of predictive computations for electrolyte and additive electrochemical stabilities is that the space and time constraints will be less severe, as it will for any other scientific task mainly relying on hardware and software. The computational power increase, but perhaps even more so the increased availability of the power, open up for many more studies with larger explicit models, preferably using high-level ab initio methods or modern DFT functionals, which then can be treated as cluster-continuum or propagated with time in AIMD. Along these lines we note the extensive work by Borodin et al. on the oxidative stability and decomposition reactions of several classes of electrolytes that appeared just prior to finalizing this text [93].

However, if the synergies among different parts of the electrolyte materials still are poorly understood, as indeed the status in summary in today, and not converge nicely with increased model and method quality, then we will also in the future have large problems in creating reliable predictions of potentials and electrochemical stabilities.

We do also see a possible drawback with the increased ease of applying computations; it might be that some poor studies may result due many more scientists being involved, which either lack battery field knowledge or insight into the strategy–method–model issues. Our modest hope is that the present text may to some extent prevent this from happening.

In some studies we already see examples of what the future will bring; the MD combined with DFT work by Ong in 2011 [81] showed the power of that method to treat electrolytes collectively, which does away with some of the extensive variability seen when treating individual components or smaller clusters (Fig. 9.9). Likewise, the special approach by Ballone in 2012 [83] catched up on the old idea of having a electrode work function ($\Phi_{\text{electrode}}$) in place, but now treated in an elaborate way via performing AIMD on a Jellium model electrode. Also, Leung et al. demonstrated how realistic electrode surfaces, even with specific surface coatings, can be implemented in the AIMD simulations. In addition, Leung recently reviewed the future of this technique for simulating electrochemical reactions at electrode/electrolyte interfaces [94]. It will be very interesting to see how many other groups that during the next few years catch on to these rather different but exciting studies.

Currently, we are in our own group developing a demanding approach (not computationally, but for the wealth of data produced and difficult experimental comparison) to anion electrochemical oxidation stability and mechanism via the reaction products [95]. By using a molecular model and not only calculating the IP, but also deliberately "cutting" apart the resulting anion radical at *all* chemical bonds, we arrive to a large set of possible small fragments of the parent anion that may represent the instantaneous decomposition products. Chemical analysis in situ provides the experimental evaluation of the model.

Not only will the computations change but also the targets and aims. Obviously new solvents, salts, and additives for the lithium ion battery will be targets, but also the next generation batteries, which rely on other chemistries and therefore has other main problems and thus aims with the modelling. One example is the work by

Bryantsev and Faglioni [96] on the auto-oxidation of electrolyte solvents aimed for the construction of Li–air batteries, that via DFT (B3LYP/6-311++G**) and continuum methods attacks the stability of several solvents vs. superoxide, $O_2^{\bullet -}$, using a TD cycle assuming hydrogen abstraction as the solvent decomposition route. One should note that for the Li–air concept the stability vs. $O_2^{\bullet -}$ is indeed the electrolyte stability vs. one of the electrodes, and today the totally dominant problem of Li–air batteries, preventing long-term cycling.

Acknowledgements The writing of this chapter was made possible due to funding to both J.S. and P.J. by several Swedish sources which hereby are gratefully acknowledged: the Swedish Hybrid Vehicle Centre (SHC), Chalmers Area of Advance Transport, the Swedish Energy Agency (STEM), and the Swedish Research Council for Environment, Agricultural Sciences and Spatial Planning (FORMAS). Gothenburg, February 22nd 2014.

References

1. Ue, M. Role-Assigned Electrolytes: Additives, In *Lithium-Ion Batteries*; Yoshio, M.; Brodd, R. J.; Kozawa, A., Eds.; Springer: New York, 2009; 75–115.
2. Xu, K. Nonaqueous liquid electrolytes for lithium-based rechargeable batteries., *Chem. Rev.* **2004**, *104*, 4303–4417.
3. Xu, K.; Ding, S. P.; Jow, T. R. Toward Reliable Values of Electrochemical Stability Limits for Electrolytes, *J. Electrochem. Soc.* **1999**, *146*, 4172–4178.
4. Tarascon, J. M.; Guyomard, D. New electrolyte compositions stable over the 0 to 5 V voltage range and compatible with the $Li_{(1+x)}Mn_20_4$/carbon Li-ion cells, *Solid State Ionics* **1994**, *69*, 293–305.
5. Guyomard, D.; Tarascon, J. M. High voltage stable liquid electrolytes for $Li_{(1+x)}Mn_20_4$/carbon rocking-chair lithium batteries, *J. Power Sources* **1995**, *54*, 92–98.
6. Koch, V. R.; Dominey, L. A.; Nanjundiah, C.; Ondrechen, M. J. The Intrinsic Anodic Stability of Several Anions Comprising Solvent-Free Ionic Liquids, *J. Electrochem. Soc.* **1996**, *143*, 798–803.
7. Egashira, M.; Okada, S.; Yamaki, J. The effect of cation species on the anodic oxidation of organic solvent electrolytes, *Electrochemistry* **2001**, *69*, 455–457.
8. Ue, M.; Murakami, A.; Nakamura, S. Anodic Stability of Several Anions Examined by Ab Initio Molecular Orbital and Density Functional Theories, *J. Electrochem. Soc.* **2002**, *149*, A1572–A1577.
9. Egashira, M.; Takahashi, H.; Okada, S.; Yamaki, J. Measurement of the electrochemical oxidation of organic electrolytes used in lithium batteries by microelectrode, *J. Power Sources* **2001**, *92*, 267–271.
10. Li, T.; Balbuena, P. B. Theoretical studies of the reduction of ethylene carbonate, *Chem. Phys. Lett.* **2000**, *317*, 421–429.
11. Wang, Y.; Nakamura, S.; Ue, M.; Balbuena, P. B., Theoretical studies to understand surface chemistry on carbon anodes for lithium-ion batteries: reduction mechanisms of ethylene carbonate, *J. Am. Chem. Soc.,* **2001**, *123*, 11708–11718.
12. Leung, K.; Budzien, J. L., Ab initio molecular dynamics simulations of the initial stages of solid-electrolyte interphase formation on lithium ion battery graphitic anodes, *Phys. Chem. Chem. Phys.,* **2010**, *12*, 6583–6586.
13. Yu, J.; Balbuena, P. B.; Budzien, J.; Leung, K. Hybrid DFT Functional-Based Static and Molecular Dynamics Studies of Excess Electron in Liquid Ethylene Carbonate, *J. Electrochem. Soc.* **2011**, *158*, A400–A410.

14. Endo, E.; Ata, M.; Tanaka, K.; Sekai, K. Electron Spin Resonance Study of the Electrochemical Reduction of Electrolyte Solutions for Lithium Secondary Batteries, *J. Electrochem. Soc.* **1998**, *145*, 3757–3764.
15. Endo, E.; Tanaka, K.; Sekai, K. Initial Reaction in the Reduction Decomposition of Electrolyte Solutions for Lithium Batteries, *J. Electrochem. Soc.* **2000**, *147*, 4029–4033.
16. Vollmer, J. M.; Curtiss, L. A.; Vissers, D. R.; Amine, K. Reduction Mechanisms of Ethylene, Propylene, and Vinylethylene Carbonates, *J. Electrochem. Soc.* **2004**, *151*, A178–A183.
17. Tasaki, K. Solvent decompositions and physical properties of decomposition compounds in Li-ion battery electrolytes studied by DFT calculations and molecular dynamics simulations., *J. Phys. Chem. B* **2005**, *109*, 2920–2933.
18. Tasaki, K.; Kanda, K.; Kobayashi, T.; Nakamura, S.; Ue, M. Theoretical Studies on the Reductive Decompositions of Solvents and Additives for Lithium-Ion Batteries near Lithium Anodes, *J. Electrochem. Soc.* **2006**, *153*, A2192–A2197.
19. Johansson, P. Intrinsic anion oxidation potentials., *J. Phys. Chem. A* **2006**, *110*, 12077–12080.
20. Johansson, P. Additions and corrections to Intrinsic Anion Oxidation Potentials, *J. Phys. Chem. A* **2007**, *111*, 1378–1379.
21. Xing, L.; Li, W.; Wang, C.; Gu, F.; Xu, M.; Tan, C.; Yi, J. Theoretical investigations on oxidative stability of solvents and oxidative decomposition mechanism of ethylene carbonate for lithium ion battery use., *J. Phys. Chem. B* **2009**, *113*, 16596–16602.
22. Ue, M.; Fujii, T.; Zhou, Z.; Takeda, M.; Kinoshita, S. Electrochemical properties of $Li[C_nF_{(2n+1)}BF3]$ as electrolyte salts for lithium-ion cells, *Solid State Ionics* **2006**, *177*, 323–331.
23. Scheers, J.; Johansson, P.; Jacobsson, P. Anions for lithium battery electrolytes: A spectroscopic and theoretical study of the $B(CN)_4^-$ anion of the ionic liquid $C_{(2mim)}[B(CN)_4]$, *J. Electrochem. Soc.* **2008**, *155*, A628–A634.
24. Scheers, J.; Johansson, P.; Szczeciński, P.; Wieczorek, W.; Armand, M.; Jacobsson, P. Benzimidazole and imidazole lithium salts for battery electrolytes, *J. Power Sources* **2010**, *195*, 6081–6087.
25. Ong, S. P.; Ceder, G. Investigation of the Effect of Functional Group Substitutions on the Gas-Phase Electron Affinities and Ionization Energies of Room-Temperature Ionic Liquids Ions using Density Functional Theory, *Electrochim. Acta* **2010**, *55*, 3804–3811.
26. Assary, R. S.; Curtiss, L. A.; Redfern, P. C.; Zhang, Z.; Amine, K. Computational Studies of Polysiloxanes : Oxidation Potentials and Decomposition Reactions, *J. Phys. Chem.* **2011**, *67*, 12216–12223.
27. Scheers, J.; Jónsson, E.; Johansson, P.; Jacobsson, P. Novel Lithium Imides; Effects of -F, $-CF_3$, and -CN Substituents on Lithium Battery Salt Stability and Dissociation, *Electrochemistry* **2012**, *80*, 18–25.
28. Zhang, X.; Pugh, J. K.; Ross, P. N. Computation of Thermodynamic Oxidation Potentials of Organic Solvents Using Density Functional Theory, *J. Electrochem. Soc.* **2001**, *148*, E183–E188.
29. Vollmer, J. M.; Kandalam, A.; Zapol, P.; Curtiss, L. A.; Chen, C.-H.; Vissers, D. R.; Amine, K., Prediction of reduction potentials with quantum chemical methods, In *Advanced Batteries and Supercapacitors*; Nazri, G.; Koetz, R.; Scrosati, B.; Moro, P. A.; Takeuchi, E. S., Eds.; The Electrochemical Society Proceedings Series, The Electrochemical Society: Pennington, NJ, 2001; pp. 389–394.
30. Leung, K.; Qi, Y.; Zavadil, K. R.; Jung, Y. S.; Dillon, A. C.; Cavanagh, A. S.; Lee, S.-H.; George, S. M., Using atomic layer deposition to hinder solvent decomposition in lithium ion batteries: first-principles modeling and experimental studies, *J. Am. Chem. Soc.,* **2011**, *133*, 14741–14754.
31. Leung, K. First-Principles Modeling of the Initial Stages of Organic Solvent Decomposition on $Li_xMn_2O_4(100)$ Surfaces, *J. Phys. Chem. C* **2012**, *116*, 9852–9861.
32. Bedrov, D.; Smith, G. D.; van Duin, A. C., T. Reactions of Singly-Reduced Ethylene Carbonate in Lithium Battery Electrolytes: A Molecular Dynamics Simulation Study Using the ReaxFF, *J. Phys. Chem. A,* **2012**, *116*, 2978–2985.
33. Johansson, P.; Jacobsson, P. Rational design of electrolyte components by ab initio calculations, *J. Power Sources* **2006**, *153*, 336–344.

34. Patel, P. Materials Genome Initiative and energy, *MRS Bulletin* **2011**, *36*, 964–966.
35. Aurbach, D.; Gofer, Y.; Ben-zion, M.; Aped, P. The behaviour of lithium electrodes in propylene and ethylene carbonate : the major factors that influence Li cycling efficiency, *J. Electroanal. Chem.* **1992**, *339*, 451–471.
36. Aurbach, D.; Levi, M. D.; Levi, E.; Schechter, A. Failure and Stabilization Mechanisms of Graphite Electrodes, *J. Phys. Chem. B* **1997**, *101*, 2195–2206.
37. Wang, Y.; Nakamura, S.; Tasaki, K.; Balbuena, P. B. Theoretical studies to understand surface chemistry on carbon anodes for lithium-ion batteries: how does vinylene carbonate play its role as an electrolyte additive?, *J. Am. Chem. Soc.* **2002**, *124*, 4408–4421.
38. Wang, Y.; Balbuena, P. B. Theoretical Insights into the Reductive Decompositions of Propylene Carbonate and Vinylene Carbonate : Density Functional Theory Studies, *J. Phys. Chem. B* **2002**, *106*, 4486–4495.
39. Wang, Y.; Balbuena, P. B. Theoretical studies on cosolvation of Li ion and solvent reductive decomposition in binary mixtures of aliphatic carbonates, *Int. J. Quant. Chem.* **2005**, *102*, 724–733.
40. Han, Y.; Uck, S.; Ok, J.; Cho, J.; Kim, H. Theoretical studies of the solvent decomposition by lithium atoms in lithium-ion battery electrolyte, *Chem. Phys. Lett.* **2002**, *360*, 359–366.
41. Han, Y.-K.; Lee, S. U. Performance of density functionals for calculation of reductive ring-opening reaction energies of Li^+-EC and Li^+-VC, *Theor. Chem. Acc.* **2004**, *112*, 106–112.
42. Han, Y.; Lee, S. U. Density Functional Studies of Ring-Opening Reactions of Li^+-(ethylene carbonate) and Li^+-(vinylene carbonate), *Bull. Korean Chem. Soc.* **2005**, *26*, 43–46.
43. Tasaki, K. Solvent decompositions and physical properties of decomposition compounds in Li-ion battery electrolytes studied by DFT calculations and molecular dynamics simulations., *J. Phys. Chem. B* **2005**, *109*, 2920–2933.
44. Tasaki, K.; Kanda, K.; Kobayashi, T.; Nakamura, S.; Ue, M. Theoretical Studies on the Reductive Decompositions of Solvents and Additives for Lithium-Ion Batteries near Lithium Anodes, *J. Electrochem. Soc.* **2006**, *153*, A2192–A2197.
45. Tasaki, K.; Goldberg, A.; Winter, M. On the difference in cycling behaviors of lithium-ion battery cell between the ethylene carbonate- and propylene carbonate-based electrolytes, *Electrochim. Acta* **2011**, *56*, 10424–10435.
46. Winter, M. The Solid Electrolyte Interphase – The Most Important and the Least Understood Solid Electrolyte in Rechargeable Li Batteries, *Z. Phys. Chem.* **2009**, *223*, 1395–1406.
47. Kim, S.-P.; Van Duin, A. C. T.; Shenoy, V. B. Effect of electrolytes on the structure and evolution of the solid electrolyte interphase (SEI) in Li-ion batteries: A molecular dynamics study, *J. Power Sources* **2011**, *196*, 8590–8597.
48. Naji, A.; Ghanbaja, J.; Humbert, B.; Willmann, P.; Billaud, D. Electroreduction of graphite in $LiCl0_4$-ethylene carbonate electrolyte . Characterization of the passivating layer by transmission electron microscopy and Fourier-transform infrared spectroscopy, *J. Power Sources* **1996**, *63*, 33–39.
49. Novak, P.; Joho, F.; Imhof, R.; Panitz, J.; Haas, O. In situ investigation of the interaction between graphite and electrolyte solutions, *J. Power Sources* **1999**, *81-82*, 212–216.
50. Yamaguchi, S.; Asahina, H.; Hirasawa, K. A.; Sato, T.; Mori, S. SEI Film Formation On Graphite Anode Surfaces In Lithium Ion Battery, *Molecular Crystals and Liquid Crystals Science and Technology. Section A. Molecular Crystals and Liquid Crystals* **1998**, *322*, 239–244.
51. Zhang, X.; Kostecki, R.; Richardson, T. J.; Pugh, J. K.; Ross, P. N. Electrochemical and Infrared Studies of the Reduction of Organic Carbonates, *J. Electrochem. Soc.* **2001**, *148*, A1341–A1345.
52. Fu, Y.; Liu, L.; Yu, H.-Z.; Wang, Y.-M.; Guo, Q.-X. Quantum-chemical predictions of absolute standard redox potentials of diverse organic molecules and free radicals in acetonitrile., *J. Am. Chem. Soc.* **2005**, *127*, 7227–7234.
53. Tasaki, K.; Goldberg, A.; Winter, M. On the difference in cycling behaviors of lithium-ion battery cell between the ethylene carbonate- and propylene carbonate-based electrolytes, *Electrochim. Acta* **2011**, *56*, 10424–10435.
54. Han, Y.-K.; Jung, J.; Cho, J.-J.; Kim, H.-J. Determination of the oxidation potentials of organic benzene derivatives: theory and experiment, *Chem. Phys. Lett.* **2003**, *368*, 601–608.

55. Xing, L.; Wang, C.; Li, W.; Xu, M.; Meng, X.; Zhao, S. Theoretical insight into oxidative decomposition of propylene carbonate in the lithium ion battery., *J. Phys. Chem. B* **2009**, *113*, 5181–5187.
56. Moshkovich, M.; Cojocaru, M.; Gottlieb, H. .; Aurbach, D. The study of the anodic stability of alkyl carbonate solutions by in situ FTIR spectroscopy, EQCM, NMR and MS, *J. Electroanal. Chem.* **2001**, *497*, 84–96.
57. Xing, L.; Borodin, O.; Smith, G. D.; Li, W., Density functional theory study of the role of anions on the oxidative decomposition reaction of propylene carbonate, *J. Phys. Chem. A,* **2011**, *115*, 13896–13905.
58. Ue, M.; Takeda, M.; Takehara, M.; Mori, S. Electrochemical Properties of Quaternary Ammonium Salts for Electrochemical Capacitors, *J. Electrochem. Soc.* **1997**, *144*, 2684–2688.
59. Borodin, O.; Jow, T. R. Quantum Chemistry Studies of the Oxidative Stability of Carbonate, Sulfone and Sulfonate-Based Electrolytes Doped with BF_4^-, PF_6^- Anions, *ECS Transactions* **2011**, *33*, 77–84.
60. Shao, N.; Sun, X.; Dai, S.; Jiang, D. Electrochemical windows of sulfone-based electrolytes for high-voltage Li-ion batteries., *J. Phys. Chem. B* **2011**, *115*, 12120–12125.
61. Shao, N.; Sun, X.-G.; Dai, S.; Jiang, D.-E. Oxidation potentials of functionalized sulfone solvents for high-voltage li-ion batteries: a computational study., *J. Phys. Chem. B* **2012**, *116*, 3235–3238.
62. Xu, K.; Angell, C. A. High Anodic Stability of a New Electrolyte Solvent : Unsymmetric Noncyclic Aliphatic Sultone, *J. Electrochem. Soc.* **1998**, *145*, L70–L72.
63. Sun, X.-G.; Angell, C. A., New sulfone electrolytes for rechargeable lithium batteries, *Electrochem. Commun.,* **2005**, *7*, 261–266.
64. Sun, X.; Angell, C. A. Doped sulfone electrolytes for high voltage Li-ion cell applications, *Electrochem. Commun.* **2009**, *11*, 1418–1421.
65. Kita, F.; Kawakami, A.; Sonoda, T.; Kobayashi, H. On the new Fluorinated Organic Lithium Salts for Lithium Batteries.pdf, In *Proceedings of New Sealed Rechargeable Batteries and Supercapacitors*; Barnett, B. M.; Dowgiallo, E.; Halpert, G.; Matsuda, Y.; Takehara, Z.-I., Eds.; The Electrochemical Society Proceedings Series, The Electrochemical Society: Pennington, NJ, 1993; 321–332.
66. Horowitz, H. H.; Haberman, J. I.; Klemann, L. P.; Newman, G. H.; Stogryn, E. L.; Whitney, T. A. The anodic oxidation stability of lithium electrolytes, In *Proceedings of the Symposium on Lithium Batteries*; Venkatasetty, H. V., Ed.; The Electrochemical Society Proceedings Series, The Electrochemical Society: Pennington, NJ, 1981; 131–143.
67. Kita, F.; Kawakami, A.; Nie, J.; Sonoda, T.; Kobayashi, H., On the characteristics of electrolytes with new lithium imide salts, *J. Power Sources* **1997**, 68, 307–310.
68. Kita, F.; Sakata, H.; Sinomoto, S.; Kawakami, A.; Kamizori, H.; Sonoda, T.; Nagashima, H.; Nie, J.; Pavlenko, N.V.; Yagupolskii, Y. L. Characteristics of the electrolyte with fluoro organic lithium salts, *J. Power Sources* **2000**, *90*, 27–32.
69. Kita, F.; Sakata, H.; Kawakami, A.; Kamizori, H.; Sonoda, T.; Nagashima, H.; Pavlenko, N.V.; Yagupolskii, Y. L. Electronic structures and electrochemical properties of $LiPF_{(6-n)}(CF_3)_n$, *J. Power Sources* **2001**, *97-98*, 581–583.
70. Benrabah, D.; Arnaud, R.; Sanchez, J.-Y. Comparative ab initio calculations on several salts, *Electrochim. Acta* **1995**, *40*, 2437–2443.
71. Barthel, J.; Buestrich, R.; Carl, E.; Gores, H. J. A New Class of Electrochemically and Thermally Stable Lithium Salts for Lithium Battery Electrolytes, *J. Electrochem. Soc.* **1996**, *143*, 3572–3575.
72. Ignatev, N.; Welzbiermann, U.; Kucheryna, A.; Bissky, G.; Willner, H. New ionic liquids with tris(perfluoroalkyl)trifluorophosphate (FAP) anions, *J. Fluorine Chem.* **2005**, *126*, 1150–1159.
73. Zhan, C.; Nichols, J. A.; Dixon, D. A., Ionization Potential, Electron Affinity, Electronegativity, Hardness, and Electron Excitation Energy: Molecular Properties from Density Functional Theory Orbital Energies, *J. Phys. Chem. A,* **2003**, 107, 4184–4195.
74. Xue, Z.-M.; Chen, C.-H. Density functional theory study on lithium bis[1,2-benzenediolato(2-)-O,O′] borate and its derivatives: electronic structures, energies, and molecular properties, *Electrochim. Acta* **2004**, *49*, 5167–5175.

75. Xue, Z.; Ding, Y.; Chen, C. A DFT study of electronic structures, energies, and molecular properties of lithium bis[croconato]borate and its derivatives, *Electrochim. Acta* **2007**, *53*, 990–997.
76. Xue, Z.-M.; Zhou, W.; Ding, J.; Chen, C.-H. Electronic structures and molecular properties of FLBDOB and its derivatives: A combined experimental and theoretical study, *Electrochim. Acta* **2010**, *55*, 5342–5348.
77. Enomoto, T.; Matsumoto, K.; Hagiwara, R. Properties of fluorosulfate-based ionic liquids and geometries of $(FO_2SOH)OSO_2F^-$ and $(FO_2SOH)_2O_2SOF^-$, *Dalton Trans.* **2011**, *40*, 12491–12499.
78. Armand, M.; Johansson, P. Novel weakly coordinating heterocyclic anions for use in lithium batteries, *J. Power Sources* **2008**, *178*, 821–825.
79. Jónsson, E.; Armand, M.; Johansson, P. Novel pseudo-delocalized anions for lithium battery electrolytes., *Phys. Chem. Chem. Phys.* **2012**, *14*, 6021–6025.
80. Staroverov, V. N.; Scuseria, G. E.; Tao, J.; Perdew, J. P. Comparative assessment of a new nonempirical density functional: Molecules and hydrogen-bonded complexes, *J. Chem. Phys.* **2003**, *119*, 12129–12137.
81. Ong, S. P.; Andreussi, O.; Wu, Y.; Marzari, N.; Ceder, G. Electrochemical Windows of Room-Temperature Ionic Liquids from Molecular Dynamics and Density Functional Theory Calculations, *Chem. Mater.* **2011**, *23*, 2979–2986.
82. Howlett, P. C.; Izgorodina, E. I.; Forsyth, M.; MacFarlane, D. R. Electrochemistry at Negative Potentials in Bis(trifluoromethanesulfonyl)amide Ionic Liquids, *Z. Phys. Chem.* **2006**, *220*, 1483–1498.
83. Ballone, P.; Cortes-Huerto, R. Ab initio simulations of thermal decomposition and of electron transfer reactions in room temperature ionic liquids, *Faraday Discuss.* **2012**, *154*, 373–389.
84. Adachi, M.; Tanaka, K.; Sekai, K. Aromatic Compounds as Redox Shuttle Additives for 4 V Class Secondary Lithium Batteries, *J. Electrochem. Soc.* **1999**, *146*, 1256–1261.
85. Chen, Z.; Wang, Q.; Amine, K. Understanding the Stability of Aromatic Redox Shuttles for Overcharge Protection of Lithium-Ion Cells, *J. Electrochem. Soc.* **2006**, *153*, A2215–A2219.
86. Wang, R. L.; Buhrmester, C.; Dahn, J. R. Calculations of Oxidation Potentials of Redox Shuttle Additives for Li-Ion Cells, *J. Electrochem. Soc.* **2006**, *153*, A445–A449.
87. Wang, R. L.; Dahn, J. R. Computational Estimates of Stability of Redox Shuttle Additives for Li-Ion Cells, *J. Electrochem. Soc.* **2006**, *153*, A1922–A1928.
88. Zhang, Z.; Zhang, L.; Schlueter, J. A.; Redfern, P. C.; Curtiss, L.; Amine, K. Understanding the redox shuttle stability of 3,5-di-tert-butyl-1,2-dimethoxybenzene for overcharge protection of lithium-ion batteries, *J. Power Sources* **2010**, *195*, 4957–4962.
89. Buhrmester, C.; Chen, J.; Moshurchak, L.; Jiang, J.; Wang, R. L.; Dahn, J. R. Studies of Aromatic Redox Shuttle Additives for $LiFePO_4$-Based Li-Ion Cells, *J. Electrochem. Soc.* **2005**, *152*, A2390–A2399.
90. Buhrmester, C.; Moshurchak, L. M.; Wang, R. L.; Dahn, J. R. The Use of 2,2,6,6-Tetramethylpiperinyl-Oxides and Derivatives for Redox Shuttle Additives in Li-Ion Cells, *J. Electrochem. Soc.* **2006**, *153*, A1800–A1804.
91. Han, Y.-K.; Jung, J.; Yu, S.; Lee, H. Understanding the characteristics of high-voltage additives in Li-ion batteries: Solvent effects, *J. Power Sources* **2009**, *187*, 581–585.
92. Trasatti, S. The absolute electrode potential: An explanatory note, *J. Electroanal. Chem.* **1986**, *209*, 417–428.
93. Borodin, O.; Behl, W.; Jow, T. R. Oxidative Stability and Initial Decomposition Reactions of Carbonate, Sulfone, and Alkyl Phosphate-Based Electrolytes, *J. Phys. Chem. C* **2013**, *117*, 8661–8682.
94. Leung, K. Electronic Structure Modeling of Electrochemical Reactions at Electrode/Electrolyte Interfaces in Lithium Ion Batteries, *J. Phys. Chem. C* **2013**, *117*, 1539–1547.
95. Jónsson, E.; Wilken, S.; Kerner, M.; Johansson, P. Manuscript in preparation.
96. Bryantsev, V. S.; Faglioni, F., Predicting autoxidation stability of ether- and amide-based electrolyte solvents for Li-air batteries, *J. Phys. Chem. A,* **2012**, *116*, 7128–7138.

Chapter 10
Aprotic Electrolytes in Li–Air Batteries

Kah Chun Lau, Rajeev S. Assary, and Larry A. Curtiss

Abstract Compared to Li-ion batteries, the Li–air battery is a relatively new concept and much of its problems remain to be solved. One of the key problems is the stability of the electrolytes, which is the subject of this chapter in which we review experimental and computational studies on this subject. The electrolyte stability is of concern during both charge and discharge at both the cathode and anode. In addition to electrochemical reactions, there can also be chemical reactions on the surfaces not directly involving electron transfer. Most experimental and computational studies so far have focused on the stability of solvents during charge and discharge at the cathode. Although there is strong evidence that the carbonates are decomposing at the cathode to form solid products such as Li_2CO_3, it is still not yet completely clear how the reduced O_2 species are directly related to the decomposition mechanism. Recent experimental and computational work has focused on the stability of ether-based electrolytes. Ether-based electrolytes have been found to have increased stability for oxygen reduction products during discharge as most studies do not see evidence for solid decomposition products. However, ethers still have stability issues arising from other decomposition mechanisms such as oxidation during charge and chemical decomposition on the lithium oxide surfaces. In addition, decomposition reactions may occur at the anode, involving an oxygen crossover effect. Meanwhile, independent of whether the solvent decomposition reaction proceeds via O_2^{2-}, LiO_2, or another Li–air reactive species, it is now clear that a solvent that is resistant to attack by reduced O_2 species must be discovered in order to achieve a practical Li–air cell with a long cycle life. Besides the problems of solvent electrochemical stability, the electrochemical selectivity also has to be resolved.

K.C. Lau • R.S. Assary • L.A. Curtiss (✉)
Materials Science Division, Argonne National Laboratory,
Argonne, IL 60439, USA
e-mail: curtiss@anl.gov

T.R. Jow et al. (eds.), *Electrolytes for Lithium and Lithium-Ion Batteries*,
Modern Aspects of Electrochemistry 58, DOI 10.1007/978-1-4939-0302-3_10,

10.1 Introduction

Research and development of the science and technology of advanced, reliable, and clean electrical storage devices is of great importance due to the diminishing fossil fuel supplies and environmental concerns such as pollution from vehicles using conventional fuels. One area of specific interest is the development electrical energy storage systems for electric vehicles. In this case the cost of materials is a major factor in the research and development. In order to make the transition from hybrid electric automobiles to plug-in hybrid electric vehicles, a sustainable electrical energy storage battery technology that enables acceptable driving ranges (300 miles between charges) is critical. This will require much higher specific energy (energy per unit weight) and energy density (energy per unit volume) than can be obtained from the traditional Li-ion batteries. Therefore, there has been an increasing amount of research on energy storage systems that can go beyond the Li-ion battery limits.

One such technology that is of great interest is the Li–air battery, which is based on the Li–O_2 electrochemical couple introduced in 1996 [1]. It has recently been the subject of intense research by many groups [2–7]. However, to go beyond the current Li-ion battery technology to a practical Li–air battery involves many formidable challenges including achieving a fundamental understanding of the unknown Li–O_2 electrochemistry, development of new and improved materials, and mastering the critical aspects of cell design. There are several types of electrolytes being pursued in the Li–air battery development and the choice is intricately related to solving these challenges. Among the types of electrolytes being considered are: (1) aqueous electrolytes, (2) mixed aqueous/aprotic electrolyte, (3) solid electrolytes, and (4) a fully aprotic (nonaqueous) liquid electrolyte.

For Li–air batteries based on aprotic solvent electrolyte, the majority of electrochemical reactions occur either in the organic solution-phase or at its interface with an electrode. Thus, aprotic electrolytes have an advantage over aqueous electrolytes due to their wide electrochemical window. A liquid (molecular or ionic liquid) or solid solvent that can dissolve the solutes (lithium salts, discharge products) can be used. Despite their wide electrochemical windows, one of the key challenges facing the development of a successful Li–air battery is finding an appropriate aprotic electrolyte that is stable during both charge and discharge. In addition, the properties of the electrolyte may play a key role in electrochemical selectivity in the growth of lithium oxides. The electrolyte stability is of concern both during charge and discharge at both the cathode and anode. In addition to electrochemical reactions occurring, there can also be chemical reactions on the surfaces not directly involving electron transfer.

In this chapter we restrict our review to research that has been done on the stability of fully aprotic liquid electrolytes for Li–air batteries. The review includes both experimental and computational aspects of this work, although the emphasis is on theoretical aspects. In the second section we review the basics of Li–air batteries and the electrochemical reactions involved in their operation and how they relate to the electrolyte. In the third section we review electronic structure methods for investigations of electrolytes. In the fourth section we discuss some of the initial Li–air

papers that used conventional Li-ion electrolytes. In the fifth section we discuss new electrolytes being investigated. Conclusions and future work are presented in the final section.

10.2 The Li–O_2 Couple in Aprotic Electrolytes

The design of a typical aprotic Li–air battery is shown in Fig. 10.1. The cell is composed of a metallic Li-anode, an electrolyte consisting of dissolved Li-salt in an aprotic solvent, and a porous O_2-breathing cathode that contains carbon particles

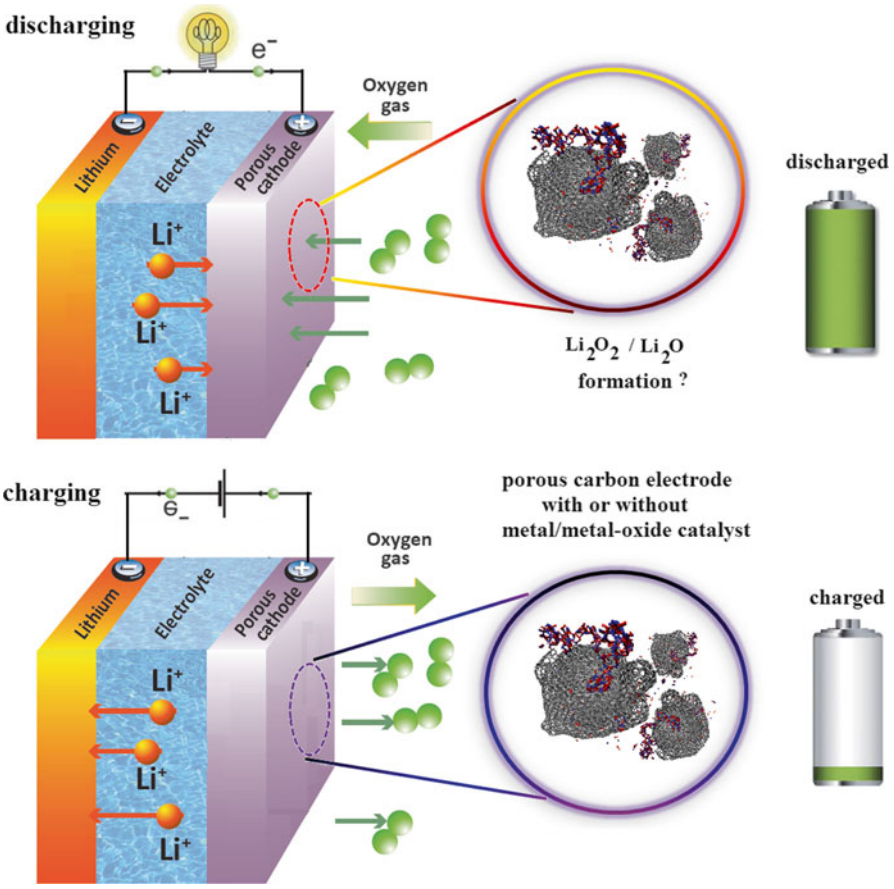

Fig. 10.1 A schematic illustration of a reversible Li–O_2 battery, in which lithium reacts with oxygen to form lithium oxide discharge products on the surface of porous carbon electrode (with or without metal oxide electrocatalysts). Ideally, the reverse charging process is to decompose lithium oxide into Li and O_2 gas

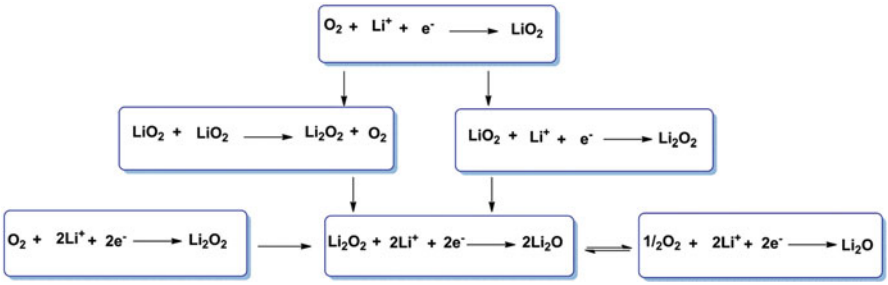

Fig. 10.2 Possible chemical and electrochemical routes for Li–O_2 couples

bound by a binder, and in some cases an added metal catalyst. Assuming that no parasitic side reactions take place, the fundamental chemistry of the battery is a Li–O_2 electrochemical couple. In this case, the potential specific energy that theoretically can be delivered from a Li–air cell is derived from the "active materials" involved in a complete electrochemical cycle (i.e., Li, O_2 in charged state and Li_2O_2, Li_2O in the discharged state), can be much greater than the standard Li-ion battery [3]. One of the major challenges here is achieving the rechargeability, which occurs at three-phase boundary involving the electrode, electrolyte, and O_2 boundary. In this chapter, we focus on aprotic electrolytes and address the critical issues and some of the recent research progress pertaining to this issue in this review article.

For Li–air batteries, an ideal aprotic electrolyte requires low viscosity, a high dielectric constant, high oxygen solubility, low water solubility, and good lithium ion mobility. In addition, the electrolytes should be stable during a wide electrochemical window, low volatility, and chemically inert towards the electrode materials. At present, formulating an optimal electrolyte is requires finding the right blend of both physical and chemical properties between the Li-salt and the solvent. The solvation of the ions of the salt within the dielectric media of an aprotic solvent, involves acid base chemistry [7, 8]. According to the standard acid–base theory, the metal cation (e.g., Li^+) acts as Lewis acid (electron pair acceptors), and the solvent molecules typically act as Lewis bases (electron donors).

For a Li–air electrochemical cell, the presence of the oxygen reduction reaction (ORR) and oxygen evolution reaction (OER) during the discharge–charge cycle makes finding the electrolyte with optimal acid base chemistry even more difficult. This is because multiple different electron-transfer reactions that could occur during the discharge and charging process that could result in several oxidation state of oxygen such as is shown in Fig. 10.2. The theory of Hard and Soft Acids and Bases (HSAB) [9] classified Lewis acids and bases into hard and soft subcategories. Hard acids tend to interact strongly with hard bases, while soft acids interact strongly with soft bases. In addition, hard acids/bases generally have a relatively small ionic radius and are difficult to polarize, while soft acids/bases generally have larger radii and are more easily polarized.

In the Li–air system, the metal (Li^+) ions in the electrolyte appear to act as Lewis acids in the reduction of O_2 to O_2^- (superoxide), which is the initial electron

transfer reaction (Fig. 10.2). Electrochemically, the reduction of oxygen can lead to O_2^- (superoxide), O_2^{2-} (peroxide), and O^{2-} (monoxide/oxide) with three distinct oxidation states. Following this model, O_2^- has a relatively large radius and low charge density that makes it a moderately soft base. Li^+ are hard Lewis acids and have a high affinity for hard Lewis bases such as the O_2^{2-} and O^{2-}. In general, the Pearson model of HSAB theory is consistent with the thermodynamics of the Gibbs formation energy of Li_2O and Li_2O_2. The close proximity of Lewis hard base feature of O_2^{2-} (peroxide) and O^{2-} (monoxide/oxide) ions is analogous to their close vicinity in thermodynamic stability in Gibbs formation energy, i.e., $\Delta G \sim -2.91$ eV/Li (Li_2O) and ~ -2.96 eV/Li (Li_2O_2) [10].

Since superoxide is a moderately soft base the superoxide will either decompose or undergo a fast second reduction to form the hard base, O_2^{2-} peroxide as shown in Fig. 10.2. Relative to a superoxide, peroxide is relatively a stronger Lewis base and tends to be associated with the strong base Li^+. Similarly, the other reduction product of O2, the O^{2-} is a hard base with a strong affinity for Li^+. Consequently based on the HSAB theory, the stable O_2 reduction products in aprotic electrolyte solutions are Li_2O_2 and Li_2O for Li–air system. The resulting products will depend on the interplay between the solvated ionic species and solvent used in the electrolyte, their reactions with the O_2^-, O_2^{2-}, and O^{2-}. Currently little is known about this interplay, and these hypothesized mechanistic routes for the formation of LiO_2/Li_2O_2/Li_2O (Fig. 10.2) remain to be investigated and understood at the molecular level. These types of studies will be required to fully optimize the performance of the electrolytes for Li–air batteries. The remainder of the review focuses electrolyte stability issues, which has been the focus of more studies.

10.3 Overview of Theoretical Methods for Electrolytes

There are a variety of methods for use in modeling of electrolytes in Li–air batteries, which have already been widely used in modeling of electrolytes and related SEI formation in Li-ion batteries [11–18]. The methods that have been used for electrolytes in Li-ion batteries largely have utilized electronic structure or molecular dynamics methods. Since Li–air modeling reported so far has largely been based on electronic structure methods, a brief review of different levels of theory is given in this section.

Density functional theory [19], which has proven to be a quite accurate and robust method for calculating properties of molecules and crystals, is a primary method of choice for the modeling of electrolytes in Li–air batteries. There are now a large number of functionals available for modeling of molecular properties such as structures, energies, and spectroscopic quantities [20]. In general, most functionals perform well for the calculation of structures and spectroscopic quantities. Hybrid density functional methods are a class of approximations to the exchange-correlation functional that include some parameterization based on accurate experimental data, such as the widely used B3LYP method [21]. With an appropriate basis set, methods

such as B3LYP provide the most overall accuracy for energies such as ionization energies, electron affinities, reaction energies, and reaction barriers [22–25]. Accurate ionization energies and electron affinities are needed for the calculation of oxidation and reduction potentials of electrolyte components including the solvent molecules and the salts. The reaction energies and barriers are needed for the investigation of the stability (decomposition) of the electrolyte upon reduction or oxidation and for reactions with surfaces. Since the molecules in the electrolyte are solvated by the solvent molecules and salt molecule it is necessary to take this into account using some type of solvation model. A continuum model such as the SMD or PCM methods [26, 27] is commonly used. Usually solvation is an additive correction to the density functional energy calculated for the gas-phase optimized geometry. This method fails to take into account changes in geometry due to solvation, which may be important in some systems. In addition, in some cases it may be necessary to add a small number of explicit molecules if the continuum solvation model is not adequate. An alternative approach is to use ab initio molecular dynamics (AIMD), a method of performing time-dependent simulations using potentials generated from first-principles [28]. The method is significantly more expensive, but explicitly includes the solvation molecules.

As mentioned above, density functional theory is usually quite accurate. However, occasionally for the calculation of reaction energies and barriers it may have significant errors. Thus, higher level wave function methods may be required. One approach that is very useful when more accurate energies are required is one of the Gaussian-*n* methods. The Gaussian-*n* (G*n*) theories [25, 29, 30] have been developed over the last two decades with the goal of approaching exact molecular energies using a set of calculations based primarily on ab initio molecular orbital theory with different levels of accuracy and basis sets. The approach used in the G*n* theories is referred to as a composite approach wherein a very high level correlation method [e.g., CCSD(T)] based on a moderate sized basis set such as 6-31G(d) is combined with energies from lower level calculations (e.g., MP4, MP2) with larger basis sets. The latest version, G4 theory [29, 30], has an accuracy that approaches 1 kcal/mol. An approximation to G4 theory that bypasses the MP4 calculations called G4MP2 theory [30] can save much computational time, yet gives very accurate energies. Other ab initio approaches for the accurate calculation of thermochemical data that have found use in electrolyte computation include the MP2 and CCSD(T) methods [31] with sufficiently large basis sets.

10.4 Organic Carbonate Solvents: Lessons Learned

In contrast to the Li-ion battery, the practical considerations of aprotic electrolytes used in Li–air battery are not limited to thermal stability, ionic transport, inertness towards electrode materials, and practical electrochemical window, but also include the reversibility issue of the formation of “active materials” that involves the subtle electrochemical reactions between the aprotic electrolytes and the reduced O_2

species with several different oxidation states or Li/O_2 reactive species. Initially, the stability issues of an aprotic electrolyte was not recognized, and carbonate-based organic electrolytes (propylene carbonate (PC), ethylene carbonate (EC), etc.) were widely used in Li–air battery, mostly because the organic solvents are the popular solvents in Li-ion battery application. In addition, the oxygen solubility requirements for Li–air batteries were based on carbonate solvents [32, 33].

One of the first papers to recognize the need for an electrolyte that is stable and inert towards the reduced oxygen species was the work by Mizuno et al. [34] reported at year 2010. Before the study by Mizuno et al. [34], Li_2O_2 was generally be assumed or claimed to be the only discharge product in many publications [32, 35–40]. The lithium–air cell with carbonate-based electrolyte could perform for up to 100 cycles and with capacity retention of over 60 %. However, closer characterization revealed that the prevalent reaction products after discharge and charging process on the cathode are decomposition product of carbonates such as (Li_2CO_3) and lithium alkyl carbonate (R–O–(C–O)–OLi, R = alkyl group), not the desired Li_2O_2 or Li_2O products. The CO_2 gas was generated by the decomposition of these carbonate-based discharge products during charging process, but not O_2 gas [34] Since then, other groups have confirmed by various means that the carbonate-based solvents are not stable under oxygen-rich electrochemical environment [10, 41–44]. Additional evidence comes from Fourier transform infrared (FT-IR) and Raman spectroscopy data, indicating that the primary discharge product in carbonate-based electrolytes is not lithium peroxide, Li_2O_2, but various carbonate species, such as R–O–(C–O)–OLi and Li_2CO_3. In situ differential electrochemical mass spectrometry (DEMS) experiments combined with ^{18}O isotopic labeling [10] reveal that, during charging of the discharged battery, CO_2 is evolved as a predominant oxidation product, most probably from the oxidative decomposition (during charging) of lithium carbonates and alkyl carbonates, and subsequently the decomposition of the solvent during cycling eventually leads to cell failure. Thus, when carbonates are used as solvents side reactions lead to the continuous and irreversible consumption of electrolytes, and therefore the battery is considered to be fundamentally non-rechargeable.

To understand the nature of this reaction mechanism involving attack of oxygen reduction products on the carbonates several studies have been carried out and reported. It was found that PC is susceptible to the attack of superoxide radical (O_2^-) based on Density Functional theory (DFT) study and coupled-cluster calculations by Bryantsev and Blanco as shown in Fig. 10.3 [45]. Subsequent reactions lead to decomposition to form carbonate species as discharge products. Interestingly, similar decomposition pathways for other organic solvents, e.g., ethylene carbonate (EC) and dimethyl carbonates (DMC) are also found [45] with computed activation barriers ~12.4–15.5 kcal/mol. According to Bryantsev et al. [45], the nucleophilic attack by O_2^- at ethereal carbon atoms is a common mechanism of degradation of organic carbonate solvents (Fig. 10.3). However, it is noteworthy to point out that in Li–air batteries, the superoxide (O_2^-) species could also exist as lithium superoxide (LiO_2) [8, 46, 47].

A recent DFT and high-level quantum chemistry calculation by Zhang et al. [44] has been reported that considers four possible intermediates during ORR of O_2,

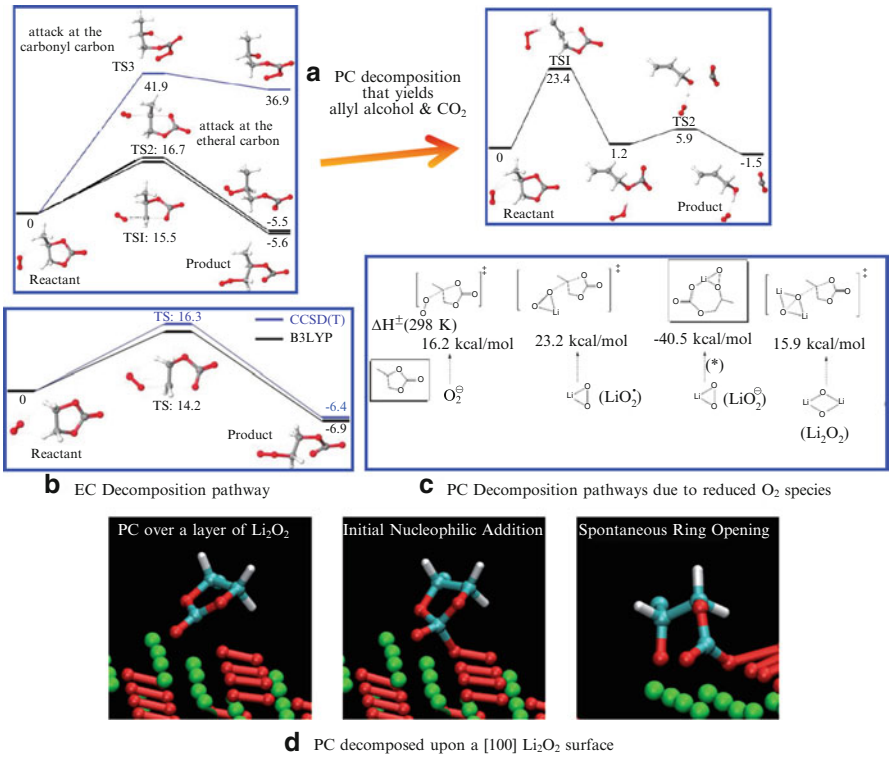

Fig. 10.3 (**a**) Reaction free energy profile for nucleophilic attack of O_2^- at the carbonyl and ethereal carbon atoms of PC and the reaction pathway towards the formation of allyl alcohol (CH_2=$CHCH_2OH$) and CO_2 calculated within the continuum solvent model based on DFT from [45]. (**b**) Reaction energy profile for O_2^- attack on the ethereal carbon atoms of EC based on DFT and CCSD(T)-level of calculations from [49]. (**c**) The DFT results on the barriers for activations of PC decomposition by other possible reduced O_2 species, e.g., LiO_2, LiO_2^-, and Li_2O_2 besides O_2^- from [44]. (**d**) The PC decomposition due to the reactivity of PC with a [100] Li_2O_2 surface through the nucleophilic addition to the carboxylic carbon from [48]. Reproduced with permission from [44, 45, 48, 49]

i.e., O_2^-, O_2^{2-} (Li_2O_2), LiO_2, and LiO_2^-. Consistent with the finding of Bryantsev et al. [45], the first step in the decomposition of PC to Li_2CO_3 or other lithium alkyl carbonates is the "ring-opening" (or C–O bond breaking) for PC reduction mechanism. The energy barriers for this first decomposition step in reactions of PC with Li_2O_2, LiO_2^-, LiO_2, and O_2^- and the transition state structures are shown in Fig. 10.3. In general, the calculated energy barriers for all four species are quite small, ranging from no barrier to 23 kcal/mol, with LiO_2^- being the most reactive. The apparent barrier for the second step in this reaction, i.e., C–O bond breaking is relatively smaller and the reaction is thermodynamically favorable. This suggests that upon "ring-opening" of PC, the reaction is thermodynamically downhill, and therefore, Li_2CO_3 and other products such as formaldehyde and acetaldehyde can be formed,

assuming that a second electron transfer can occur. In addition, the reactions of the electrolyte at lithium oxide/peroxide surfaces could also be responsible for the degradation of the solvent, in addition to the O_2^- that has been postulated by may be present in the electrolyte. Interestingly, such surface reaction has recently been proposed using DFT study [27]. According to Laino et al. [48], it reveals that PC is easily decomposed upon the formation of Li_2O_2 surface (i.e., [100] surface) on the cathode with a "barrier-less" reaction (Fig. 10.3), in contrast to the reaction by a Li_2O_2 molecular unit in PC solution which has barrier as high as ~40 kcal/mol among various reaction paths (e.g., hydrogen abstraction and nucleophilic reactions). For the reactivity of Li-rich, O-rich, and other stoichiometric thermodynamically favorable Li_2O_2 surfaces against PC reactivity, such surfaces reactions remain to be explored in the future.

10.5 Ether-Based Solvents

Much attention is now focused on the search for other solvents that are resistant to the attack by reduced O_2 species and can avoid other decomposition problems. One of the popular alternatives is ether-based solvents (polar aprotic solvent). Ethers are attractive for the Li–air system because they combine the following attributes: stable to oxidation potentials in excess of 4.5 V vs. Li/Li^+, inflammable, high thermal stability, and low cost. The ethers with larger molecular weights, in particular, tetraethylene glycol dimethyl ether (tetraglyme or TEGDME) is stable in contact with Li metal, and are less volatile and polar. Shorter chain ether molecules such as the 1,2-dimethoxyethane (DME) were found to be unreactive towards the ORR intermediate products (i.e., O_2^-) by Aurbach et al. [50] in the electrochemistry study of noble metal electrodes in aprotic organic solvents. Additionally, DME has one of the highest O_2 solubilities reported for Li–air solvents [51] and it is stable at high pH values. These above attributes make DME a potential candidate as a solvent in Li–air batteries and recent reports suggest that they are relatively more stable than organic carbonates in the presence of likely bases such as O^{2-} and O_2^{2-} [52, 53]. However, the question whether the ether-based electrolytes are suitable for Li–air batteries remains to be seen; and the pros and cons of this electrolyte will be discussed in the following sections.

The use of ether-based electrolytes in Li–air battery was first studied by Read and coworkers [32]. According to Read et al. [32], ethers have the high oxygen solubility and high oxygen diffusivity, which are the crucial factors in Li–air cell performance. Following the previous study of Read et al. [12], the effects of ethers as additives and co-solvents in Li–air have been carried out by researchers in PNNL [54]. According to their investigation, the crown ethers (i.e., 12-crown-4, 15-crown-5) have large effects on the discharge performance in nonaqueous Li–air battery, based on their ratio composition in organic carbonate-based solvents [54]. The changes of the cell performance are determined by the combined effects of the variations in the electrolyte's contact angle on carbon electrode, O_2 solubility, electrolyte viscosity,

ionic conductivity, and stability of complexes formed between the crown ether molecules and Li-ions. Despite of these systematic studies [32, 54], the stability of ethers under ORR and OER environment of Li–air cell was not known. To explore this important property, the stability of the ethers in the presence of reduced O_2 species has been the subject of studies in recent years. To probe whether the ether-based electrolytes are stable against the attack of reduced O_2 species (such as superoxide), recently an interesting experiment has been carried out by Black et al. [43]. In their experiment, the metastable superoxide is generated from the reaction of KO_2 with dicyclohexyl-18-crown-6 (crown ether) in solution, which complexes with the K^+. Thus the metastable solvated LiO_2 can be formed in situ through metathesis with a lithium salt (e.g., $LiPF_6$). According to this experiment, no decomposition of TEGDME of by O_2^- radical, generated from a chemical route, was observed. However, the decomposition of poly(vinylidenedifluoride) PVdF (or Kynar Flex) binder through dehydrofluorination was observed along with the formation of H_2O_2. Consistent with other reports [5, 41, 44, 45], Black et al. [43], concluded that the PC is vulnerable to O_2^- attack. Accompanied by the reaction of O_2^- (from KO_2/crown ether) with Li^+ through the evolution of O_2 gas in 1.0 M $LiPF_6$–TEGDME solution, gradual precipitation and crystallization of Li_2O_2 was observed and has been verified using X-ray diffraction (XRD) spectra [43]. The evidence of degradation and decomposition of TEDGME due to O_2^- attack was not found from their NMR analysis [43]. According to Laoire et al. [46], the O_2^- superoxide formed as the first reduction product is complexed by the solvated Li^+, probably becoming a stable species with a finite lifetime in solution.

Several groups have found evidence that the major discharged product when using ether-based solvents in the lithium–air cell is Li_2O_2. Abraham et al. [46] has characterized the discharge products in TEGDME using XRD as shown in Fig. 10.4. Besides using $LiPF_6$ as the Li-salt, $LiCF_3SO_3$–TEGDME electrolyte has recently proven to be a promising electrolyte. Based on a $LiCF_3SO_3$–TEGDME–O_2 cell, a high performance Li–air battery has recently been reported [55]. With a metal or metal oxide catalyst-free electrode, the Li–air cell can operate over many cycles (~30 cycles) under capacity levels as high as 5,000 mAh/g_{carbon} with an average discharge voltage of 2.7 V, which leads to a very high theoretical energy density of 13,500 Wh/kg. Consistent with other TEGDME-based electrolytes, Li_2O_2 has also been confirmed as the major discharge product for the Li–air cell based on $LiCF_3SO_3$–TEGDME electrolyte, characterized using (Fig. 10.4) the ex situ XRD analysis during the discharge and charging cycle of the cell.

Similar to the TEGDME solvent, Li_2O_2 has been found as the major discharge product for a DME-based electrolyte upon Li–O_2 cell discharge [53] by McCloskey et al. In this case, the presence of Li_2O_2 formed during the first discharge on the cathode was both characterized using ex situ XRD and Raman spectroscopy (Fig. 10.4). In conjunction to this observation, a comparison study on Li–O_2 electrochemistry with other carbonate-based electrolytes (i.e., PC, EC, DMC) was also carried out using quantitative DEMS, coupled with isotopic labeling of oxygen gas ($^{18}O_2$). An irreversible decomposition of carbonate-based solvents was observed during cell discharge, while DME appears to be stable during the electrochemical

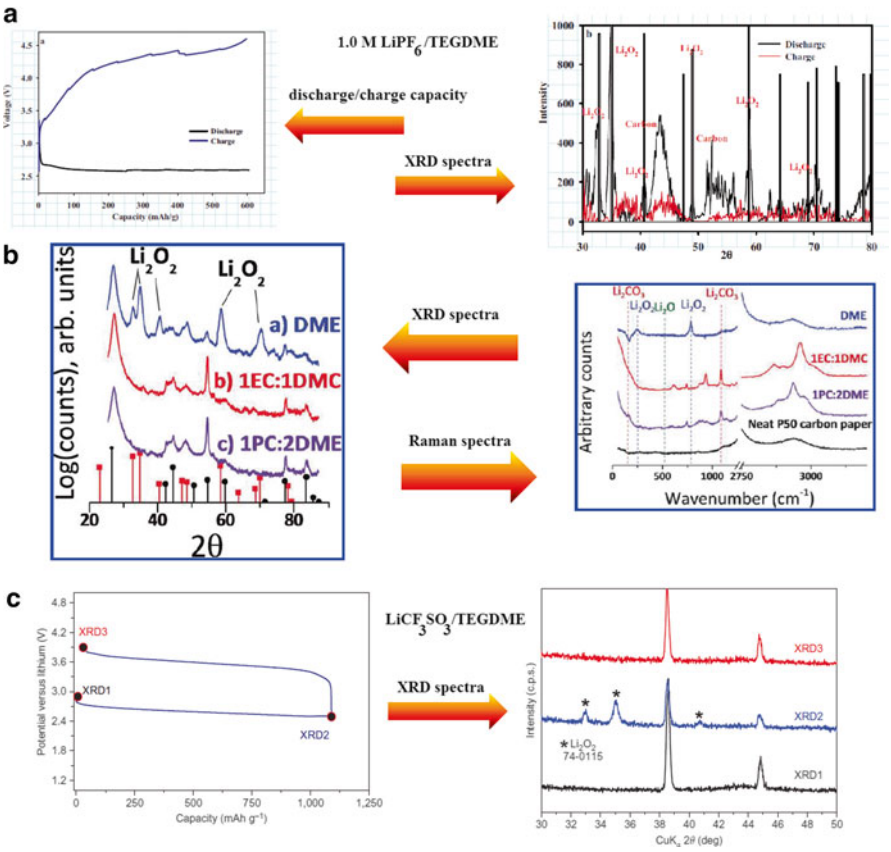

Fig. 10.4 (**a**) Discharge (*black*) and charge (*red*) capacity (in mAh/g) of Li–air cell with carbon electrode cycled at 0.1 mA/cm^2 and its XRD spectra from [46]. (**b**) XRD and Raman spectra of discharged carbon cathodes from cells employing DME, 1EC:1DMC, 1PC:2DME with LiTFSI as salt. (**c**) A sequence of ex situ XRD analysis carried out in its pristine state (XRD1), after complete discharge (XRD2) and after complete recharge (XRD3) of a $LiCF_3SO_3$–TEGDME Li–air cell from [55]. Reproduced with permission [10, 46, 55]

window of ~1.7 V to ~4.6 V vs. Li/Li$^+$. Through the galvanostatic discharge–charge curves and DEMS measurements coupled with the isotopic labeling of oxygen gas, the number of electrons per oxygen consumed during first discharge for DME-based electrolyte was found to be ~2.05 ± 0.05, close to the values expected for the exclusive formation of Li_2O_2 (i.e., a 2e$^-$/O_2 process as defined: $2(Li^+ + e^-) + O_2 \leftrightarrow Li_2O_2$). While for PC and DMC-based electrolytes (i.e., PC–DMC = 1:1), the e$^-$–O_2 ratio is greater than 2 which indicates that parasitic electrochemical or chemical processes consume some of the O_2 during the first discharge of the cell.

Besides TEGDME- and DME-based ethers, a recent study from Zhang and coworkers [44] provided evidence that a oligoether substituted silane, i.e., tri

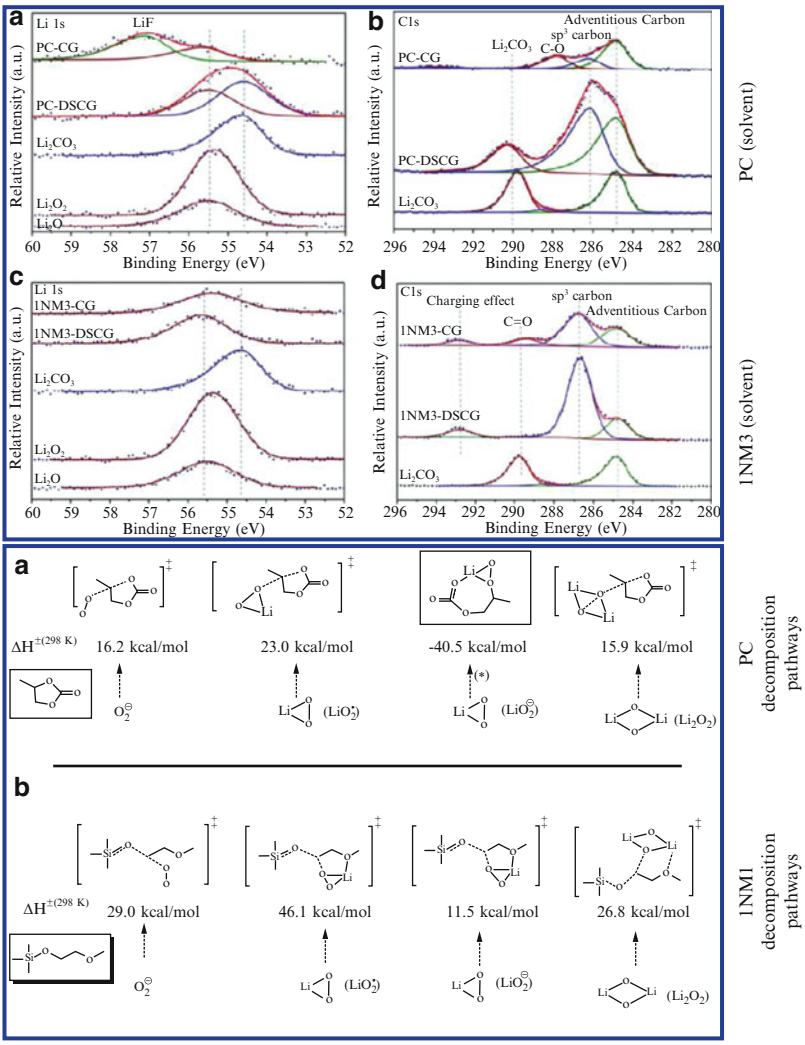

Fig. 10.5 (*Top*) XPS spectra of Li 1s and C 1s core peaks of the cathode carbon electrodes after discharge and charge when using PC or 1NM3 as solvent in the electrolyte. Standard compounds Li_2O_2, Li_2O, and Li_2CO_3 are listed at the bottom of each spectrum for reference from Ref. JPCC2011. (*Bottom*) DFT results on the barriers for activations of PC and 1NM1 decomposition by few possible reduced O_2 species, e.g., O_2^-, LiO_2, LiO_2^-, and Li_2O_2 from [23]. Reproduced with permission [44]

(ethylene glycol)-substituted trimethylsilane (1NM3) (i.e., 1.0 M $LiPF_6$/1NM3 electrolyte with Super P carbon black, electrolytic manganese dioxide as a catalyst and PVDF binder) was stable in the presence of reduced oxygen species. Based on the X-ray photoelectron spectroscopy (XPS) (Fig. 10.5) characterization, the authors found formation of lithium oxides (Li_2O, Li_2O_2) during the first discharge, and no Li_2CO_3.

In contrast, XPS showed that 1.0 M $LiPF_6$/PC in the same cell configuration, decomposed to form Li_2CO_3 during the first discharge cycle. Therefore, the difference in solid discharge products formed in 1NM3 and PC is likely responsible for the large difference in initial charge overpotential observed during the cell cycling. In addition, the higher stability of 1NM3 against the reduced O_2 species compared to PC is supported by their theoretical studies [44, 56].A comparison of reaction barriers for the initial decomposition reaction of 1NM1 (used as a model for 1NM3) and PC by likely oxygen reduced species in solution is shown in Fig. 10.6. The computed energy barriers for the reactions between reduced oxygen species such as O_2^-, LiO_2, LiO_2^-, Li_2O_2 with 1NM3 or PC suggest that ethers are more stable against oxygen reduction products than PC (Fig. 10.5). A similar theoretical finding has also been reported recently for various glyme series of solvents, $CH_3O(CH_2CH_2O)_NCH_3$ ($_N$ = 1–4), where nucleophilic attack of superoxide anion is used as a proxy reaction to assess the stability of solvent [57]. The reversibility and cycling stability of 1NM3-based (or glymes) Li–air cells remains unsatisfactory. This can be attributed to the failure to decompose all of the lithium oxide on charging process since some of the lithium oxide especially the insulating Li_2O layers that might require a higher potential for decomposition. It may also be due to other sources of electrolyte decomposition such as chemical decomposition on cathode surfaces during discharge or by oxidative instability at the cathode surface. In addition, lithium anodes are known for their corrosive properties, and electrolyte decomposition could occur at the anode especially in the presence of O_2 from a crossover effect.

Despite the evidence for the increased stability of ether-based electrolytes that promotes the Li_2O_2 formation compared to carbonate-based electrolytes as discussed above, there is some evidence for degradation of ether-based electrolytes in Li–air cells. Based on a recent theoretical study [58], the decomposition of DME through the chemical reaction with the major discharge product (i.e., Li_2O_2) is possible and this may subsequently influence the cell performance including the crystal growth, nanomorphologies of discharge products and charge overpotential of subsequent cycles. Based on surfaces of Li_2O_2 nanoparticles as reaction sites [47, 58], the DFT studies suggest that the most favorable decomposition of ether solvents occurs on certain sites on the Li_2O_2 surfaces and involves hydrogen abstraction followed by reaction with oxygen, which leads to oxidized species such as aldehydes and carboxylates as well as LiOH. The most favorable site is a Li–O–Li bridging site that may be present as a defect site on a surface of Li_2O_2 discharge product. The decomposition route involving proton abstraction requires a much larger enthalpy of activation. According to McCloskey et al. [10] in a recent study, the irreversible decomposition of ether-based electrolyte (DME) through oxidative decomposition upon cell charging could be problematic. As shown in Fig. 10.6, the evidence of the possible decomposition of DME at high voltage is implied by the gas evolution and electric current vs. cell voltage during the linear oxidative potential scan of a discharged DME-based Li–air cell [10]. Four distinct peaks (at ~3.2, ~3.4, ~3.8, and > ~4.5 V) are observed in this potential scan, with the first three evolving exclusively O_2 and the last coincident to O_2 and CO_2 evolution. The large molar concentration of ^{18}O isotopes present in the CO_2 indicates that $Li_2{}^{18}O_2$ formed during discharge

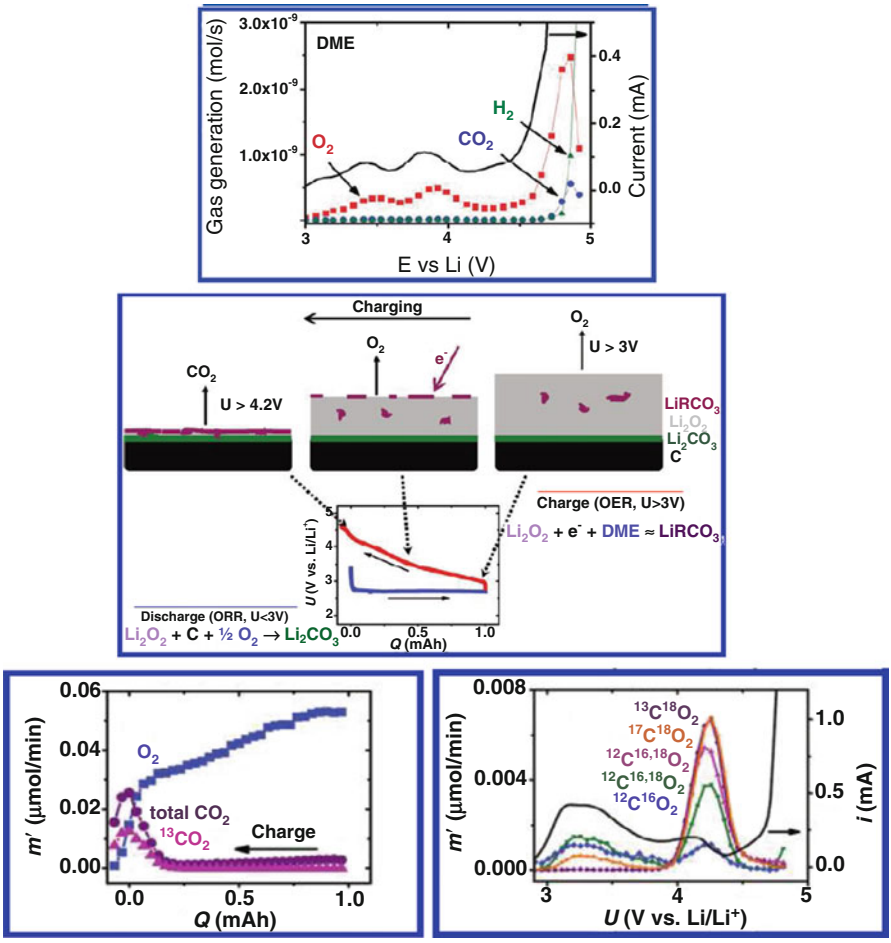

Fig. 10.6 (*Top*) Gas evolution and current vs. cell voltage during a 0.075 mV/s linear oxidative potential scan of a discharged DME-based cell from [10]. (*Center*) A schematic diagram of the stability concern of carbon cathode interface both to Li_2O_2 (during discharge) and to the highly oxidizing electrolyte environment (during charge) as suggested by McCloskey and coworkers [59]. (*Bottom left*) Quantitative evolution rates (m') for O_2, $^{13}CO_2$, and $^{12}CO_2 + {}^{13}CO_2$ during the charging process as measured by quantitative DEMS. (*Bottom right*) m' of various CO_2 isotopes as a function of charging potential U following a 1 mAh discharge at 200 μA of current with 1.2 bar of $^{18}O_2$ and a ^{13}C cathode discussed in [36]. Reproduced with permission [10, 59]

participates in the DME oxidation reaction at high voltages (~4.5–4.6 V). Therefore both DME and other ethers may be unsuitable solvents for secondary Li–air batteries at high voltages.

Besides the possible problem of the high voltage breakdown of DME electrolytes due to the undesirable oxidation process, McCloskey et al have recently noted the presence of solid carbonate deposits (e.g., Li_2CO_3 or $LiRCO_3$ with R = alkyl) during the discharge and CO_2 evolution the during charging as unwanted parasitic

reactions [59]. According to McCloskey et al. [59], Li_2O_2 can react with carbon to form Li_2CO_3 ($\Delta G \sim -534$ to -542 kJ/mol at 300 K). This was shown through isotopic substitutions and the DEMS measurements of galvanostatic discharge–charge experiments using 1.0 M LiTFSI/DME electrolyte with different carbon cathodes (Avcarb P50 C paper, XC72, Super P, Ketjenblack). The results show that some CO_2 is always produced during charging process when the potential is ~4 to 4.5 V referenced to Li/Li^+ [59]. As shown in Fig. 10.6, both $^{13}CO_2$ and $^{12}CO_2$ are evolved in the ~4 to 4.5 V peak, implying that solid carbonate deposits can possibly come both from reaction of Li_2O_2 with the carbon cathode (which is made from ~99 % ^{13}C) and from decomposition of the DME electrolyte. Roughly 50 % of the CO_2 evolved in the high potential peak at the end of charging is $^{13}CO_2$. In addition, some $^{12}CO_2$, and nearly no $^{13}CO_2$, is evolved between 3 and 4 V [59]. Thus, this suggests that CO_2 evolution is due to the electrochemical oxidation of Li_2CO_3 (or possibly $LiRCO_3$) produced on the cathode. On the other hand, the evolution of CO_2 that is composed almost exclusively of $^{12}CO_2$ (Fig. 10.6) might indicate that the electrolyte is decomposed. However according to McCloskey and his coworkers [36], the reaction is more likely to be due to reactions of Li_2O_2 with the electrolytes during charging since there is no measurable electrolyte oxidation between 3 and 4 V under O_2 while in the absence of Li_2O_2. According to McCloskey et al. [59], this reaction is likely to also simultaneously deposit carbonates at Li_2O_2/electrolyte interface until ultimately it can be decomposed into CO_2 when potential reaches ~4 to 4.5 V.

Interestingly, the presence of CO_2 in the cycling process of Li–air cell can have different interpretations. A recent study by Wang et al. [60], found that 1.0 M LiTFSI/DME electrolytes have evidence of unwanted degradation. They carried out characterization by Raman, FTIR, XRD, and XPS measurements. The changes in the fresh and discharged DME electrolytes were also examined by FTIR. All results showed that the mixture of EC and DEC undergo decomposition to form Li_2CO_3 and $CH_3CH_2OCO_2Li$ in the presence of O_2 reduction species such as superoxide ion. Although the DME-based electrolyte seemed to be more stable to O_2 reduction species during first discharge, it also decomposed after a long time exposed due to the formation of ether peroxide. Subsequently, the Li_2O_2 formed at initial discharge becomes Li_2CO_3 by reacting with H_2O and CO_2 due to the degraded ethers [60]. According to Bruce and his coworkers, the mechanism is likely to be due to the electrolyte decomposition [52]. According to their recent study [52] none of the ethers were found to be stable towards reduced O_2 species From the XRD spectra shown in Fig. 10.7, Li_2O_2 was observed as the main products in the first-cycle discharge, but the percentage of Li_2O_2 in total products was found to decrease significantly after cell cycling; and subsequently at the fifth discharge, no Li_2O_2 was observed from the discharge product in 1.0 M $LiPF_6$–TEGDME cell (Fig. 10.7). Here, it is noteworthy to point out that each characterization tool might have limitations, especially the XRD and FTIR. In particular this can be seen from the direct comparison among the XRD and FTIR shown in Fig. 10.7. From XRD, the Li_2O_2 can be interpreted as the only discharge product in the first-discharge cycle, but FTIR show that the Li_2O_2 that forms on the first discharge cycle is accompanied by electrolyte decomposition and yield a mixture of Li_2CO_3, HCO_2Li, CH_3CO_2Li,

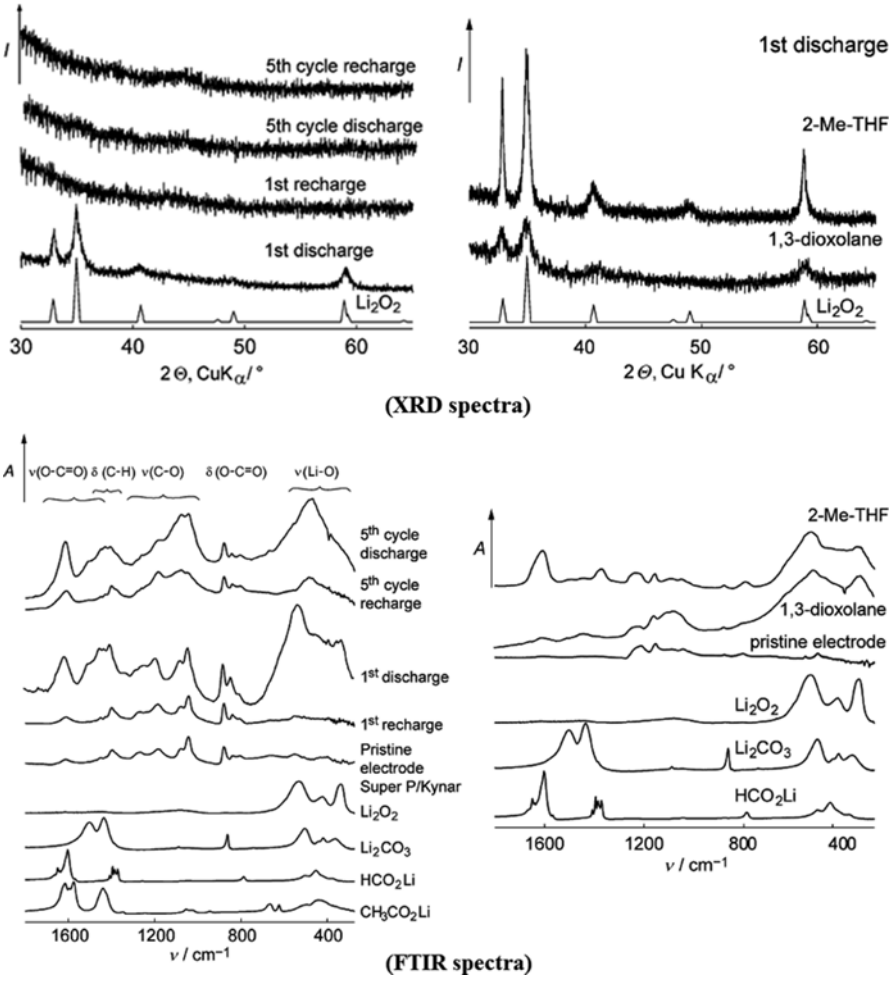

Fig. 10.7 (*Top*) Powder XRD spectra of discharge product of the composite cathode (Super P/Kynar) cycled in 1.0 M LiPF6–TEGDME cell (*left*) and the composite cathode (Super P/PTFE) in either 1.0 M $LiPF_6$–1,3-dioxolane or 2-methyltetrahydrofuran (2-Me-THF) (*right*). (*Bottom*) FTIR spectra of the corresponding composite cathode (Super P/Kynar) cycled in 1.0 M LiPF6/TEGDME cell (*left*), and the composite cathode (Super P/PTFE) in either 1.0 M $LiPF_6$–1,3-dioxolane or 2-methyltetrahydrofuran (2-Me-THF) (*right*). Reproduced with permission [52]

possibly esters, CO_2, etc. (Fig. 10.7). According to Freunberger et al. [52], the cyclic ether (e.g., 1,3-dioxolane and 2-methyltetrahydrofuran (2-Me-THF)) are also not stable as hoped. For 1,3-dioxolane, the decomposition product consists of polyethers/esters, Li_2CO_3, HCO_2Li, and $C_2H_4(OCO_2Li)_2$, whereas for 2-Me-THF the main discharge products are found to be HCO_2Li, CH_3CO_2Li (Fig. 10.7).

To prove the presence of HCO_2Li and CH_3CO_2Li observed in FTIR, the porous cathodes were washed with D_2O and the solution then subjected to ^1H NMR spectroscopy. By inferring HCO_2Li and CH_3CO_2Li to HCO_2D and CH_3CO_2D in the porous cathode, which, on reaction with D_2O, forms the corresponding formic and acetic acids, the discharge cathode in several ether-based electrolytes from their was analyzed. As provided by their NMR analysis, the presence of HCO_2Li and CH_3CO_2Li was identified through NMR. This further suggest that the discharge compounds observed in the FTIR spectrum from the electrode at the end of the first discharge does not consist of Li_2O_2 alone, but other mixture of organic compounds. In addition to the possible decomposition of the ether-based solvents, the undesirable side reactivity of Li_2O_2 with Li-salt in the electrolytes might possibly be a concern. As pointed out by Veith et al. [61] recently, it is very likely that all discharge chemistries of Li–air cells undergo similar decomposition of the salt species in the electrolyte. Based on the TEGDME solvent in various combination with several possible Li-salts (i.e., $LiBF_4$, $LiPF_6$, $LiClO_4$, LiTFSI), it is found that the major discharge product is consists of components of the Li-salt, instead of mainly dominated by Li_2O_2. However, it remains to be investigated systematically, since similar observation has not been yet found in previous works that utilized the similar electrolytes [46, 55]. Thus further systematic investigation on the reactivity and mechanism of Li-salt with the reduced O_2 species will be important for future development of electrolytes in Li–air battery. In addition to oxidative or catalytic decomposition of electrolyte at the cathode, it is also likely that electrolytes undergo reductive decomposition in the presence of molecular oxygen. This reaction would slowly decompose both the electrolyte and the Li-metal anode [62]. Therefore, controlling the reactions of ethers with at the lithium anode through suitable membranes or passivation films will be essential for achieving good performance of Li–O_2 cells based on ether electrolytes. Another area which requires attention is the reactivity of carbon surfaces towards electrolytes and discharge products. Carbon defects in the cathode can decompose electrolytes (ether) through C–O bond cleavage, suggesting significant chemical decomposition of electrolytes occurs during discharge [59]. Therefore controlling electrolyte decomposition reactions at the cathode is essential for a successful design of lithium-air battery in the future.

10.6 Conclusions and Future Outlook

Li–air batteries potentially can offer substantial increase in specific energy relative to today's most advanced Li-ion battery. At present, much remains to be learned about the fundamental chemistry behind Li–air batteries. Among these is the role of the electrolyte in the electrochemical formation and decomposition of lithium oxides. Compared to Li-ion batteries, the Li–air_{air} batteries are a relatively new concept and many problems remain to be solved. One of the key problems is the stability of the electrolytes on which this chapter is focused. The electrolyte stability is an issue

during both charge and discharge at both the cathode and anode. In addition to electrochemical reactions occurring, there can also be chemical reactions on the surfaces not directly involving electron transfer. Most studies so far have focused on the stability of solvents during charge and discharge at the cathode.

Recent experimental and theoretical investigations of decomposition of organic carbonate electrolytes during the operation of Li–air batteries highlight the importance of fundamental understanding. Although there is strong evidence that the carbonates are decomposing at the cathode to form solid products such as Li_2CO_3, It is still not yet completely clear that how the reduced O_2 species are directly related to the decomposition mechanism of the electrolytes. The evidence for whether O_2^-, LiO_2, or Li_2O_2, etc. is the most influential factor in parasitic reactions of carbonate electrolyte degradation is not yet definitive. Recent experimental and theoretical work has focused on the stability of ether-based electrolytes. Ether-based electrolytes have been found to have increased stability for oxygen reduction products during discharge as most studies do not see evidence for solid products on the cathode. However, ethers still have stability issues arising from other decomposition mechanisms such as involving oxidation during charge, chemical decomposition on the lithium oxide surfaces, and electrochemical reactions involving O_2 at the anode. These other mechanisms are currently under study, both by theory and experiment. A number other computational papers on Li–air electrolytes have appeared since writing this paper that have examined other issues involving ether-based electrolytes as well as some screening studies [63–66].

One problem in developing an understanding is that the current ex situ experimental characterization techniques have limitations. As a result, some side-reaction products might not be detectable by using a single technique, but multiple characterization tools are required to get the conclusive results as to the reaction products in Li–air batteries. To understand the fundamental mechanism and the underlying competing reaction pathways of electrolyte degradation, one needs a detailed knowledge of the major reaction mechanisms in the system from a combination of theory and experiment, including the identification of rate determining steps and intermediate reactive species that occur during the ORR and OER processes at the interfaces of the Li–air cell.

Meanwhile, independent of whether the solvent decomposition reaction proceeds via O_2^{2-}, LiO_2, or another Li–air reactive species, it is now clear that a solvent that is resistant to attack by reduced O_2 species must be discovered in order to achieve a practical Li–air cell with a longer cycle life. Besides the problems of solvent electrochemical stability, the electrochemical selectivity and chemical stability has to be resolved. Thus, regardless of whether ether-based electrolytes are completely inert towards the reduced O_2 radical species, the search for more stable electrolyte will remains an active investigation area in Li–air in the near future. Since we wrote.

Acknowledgements This work was supported by the Joint Center for Energy Storage Research funded by the US Department of Energy under Contract DE-AC0206CH11357.

References

1. Abraham, K. M.; Jiang, Z., A Polymer Electrolyte-Based Rechargeable Lithium/Oxygen Battery. *J. Electrochem. Soc.* **1996,** *143*, 1-5.
2. Girishkumar, G.; McCloskey, B.; Luntz, A. C.; Swanson, S.; Wilcke, W., Lithium Air Battery: Promise and Challenges. *J. Phys. Chem. Lett.* **2010,** *1*, 2193-2203.
3. Christensen, J.; Albertus, P.; Sanchez-Carrera, R. S.; Lohmann, T.; Kozinsky, B.; Liedtke, R.; Ahmed, J.; Kojic, A., A Critical Review of Li/Air Batteries. *J. Electrochem. Soc.* **2011,** *159*, R1-R30.
4. Bruce, P. G.; Freunberger, S. A.; Hardwick, L. J.; Tarascon, J.-M., Li-O2 and Li-S Batteries with High Energy Storage. *Nat Mater.* **2011,** *11*, 19-29.
5. Shao, Y.; Park, S.; Xiao, J.; Zhang, J.-G.; Wang, Y.; Liu, J., Electrocatalysts for Nonaqueous Lithium-Air Batteries: Status, Challenges, and Perspective. *ACS Catal.* **2012,** *2*, 844-857.
6. Kraytsberg, A.; Ein-Eli, Y., Review on Li-Air Batteries Opportunities, Limitations and Perspective. *Journal of Power Sources* **2011,** *196*, 886-893.
7. Shao, Y.; Ding, F.; Xiao, J.; Zhang, J.; Xu, W.; Park, S.; Zhang, J.-G.; Wang, Y.; Liu, J., Making Li-Air Batteries Rechargeable: Material Challenges. *Advanced Functional Materials* **2013,** 23, 987-1004.
8. Laoire, C. O.; Mukerjee, S.; Abraham, K. M.; Plichta, E. J.; Hendrickson, M. A., Influence of Nonaqueous Solvents on the Electrochemistry of Oxygen in the Rechargeable Lithium Air Battery. *J. Phys. Chem. C* **2010,** *114*, 9178-9186.
9. Pearson, R. G., Hard and Soft Acids and Bases. *J. Am. Chem. Soc.* **1963,** *85*, 3533-3539.
10. McCloskey, B. D.; Bethune, D. S.; Shelby, R. M.; Girishkumar, G.; Luntz, A. C., Solvents' Critical Role in Nonaqueous Lithium Oxygen Battery Electrochemistry. *J. Phys. Chem. Lett.* **2011,** *2*, 1161-1166.
11. Bedrov, D.; Smith, G. D.; van Duin, A. C. T., Reactions of Singly-Reduced Ethylene Carbonate in Lithium Battery Electrolytes: A Molecular Dynamics Simulation Study Using the Reaxff. *J. Phys. Chem. A* **2012,** *116*, 2978-2985.
12. Johansson, P., Electronic Structure Calculations on Lithium Battery Electrolyte Salts. *Phys. Chem. Chem. Phys.* **2007,** *9*, 1493-1498.
13. Leung, K., First-Principles Modeling of the Initial Stages of Organic Solvent Decomposition on Lixmn2o4(100) Surfaces. *J. Phys. Chem. C* **2012,** *116*, 9852-9861.
14. Marquez, A.; Vargas, A.; Balbuena, P. B., Computational Studies of Lithium Intercalation in Model Graphite in the Presence of Tetrahydrofuran. *J. Electrochem. Soc.* **1998,** *145*, 3328-3334.
15. Vollmer, J. M.; Curtiss, L. A.; Vissers, D. R.; Amine, K., Reduction Mechanisms of Ethylene, Propylene, and Vinylethylene Carbonates: A Quantum Chemical Study. *J. Electrochem. Soc.* **2004,** *151*, A178-A183.
16. Xing, L.; Borodin, O., Oxidation Induced Decomposition of Ethylene Carbonate from Dft Calculations - Importance of Explicitly Treating Surrounding Solvent. *Phys. Chem. Chem. Phys.* **2012,** *14*, 12838-12843.
17. Xing, L.; Borodin, O.; Smith, G. D.; Li, W., Density Functional Theory Study of the Role of Anions on the Oxidative Decomposition Reaction of Propylene Carbonate. *J. Phys. Chem. A* **2011,** *115*, 13896-13905.
18. Zhang, Z.; Zhang, L.; Schlueter, J. A.; Redfern, P. C.; Curtiss, L.; Amine, K., Understanding the Redox Shuttle Stability of 3,5-Di-Tert-Butyl-1,2-Dimethoxybenzene for Overcharge Protection of Lithium-Ion Batteries. *Journal of Power Sources* **2010,** *195*, 4957-4962.
19. Parr, R. G.; Yang, W., *Density Functional Theory of Atoms and Molecules*. Oxford University Press: New York, 1989.
20. Cohen, A. J.; Mori-Sánchez, P.; Yang, W., Challenges for Density Functional Theory. *Chem. Rev.* **2012,** *112*, 289-320.
21. Becke, A. D., A New Mixing of Hartree–Fock and Local Density-Functional Theories. *J. Chem. Phys.* **1993,** *98*, 1372-1377.

22. Curtiss, L. A.; Redfern, P. C.; Raghavachari, K., Assessment of Gaussian-4 Theory for Energy Barriers. *Chem. Phys. Lett.* **2010,** *499*, 168-172.
23. Curtiss, L. A.; Raghavachari, K., Gaussian-3 and Related Methods for Accurate Thermochemistry. *Theor. Chem. Acc.* **2002,** *108*, 61-70.
24. Curtiss, L. A.; Redfern, P. C.; Raghavachari, K., Assessment of Gaussian-3 and Density-Functional Theories on the G3/05 Test Set of Experimental Energies. *J. Chem. Phys.* **2005,** *123*, 124107.
25. Curtiss, L. A.; Redfern, P. C.; Raghavachari, K., Gn Theory. *Wiley Interdisciplinary Reviews: Computational Molecular Science* **2011,** *1*, 810-825.
26. Marenich, A. V.; Cramer, C. J.; Truhlar, D. G., Universal Solvation Model Based on Solute Electron Density and on a Continuum Model of the Solvent Defined by the Bulk Dielectric Constant and Atomic Surface Tensions. *J. Phys. Chem. B* **2009,** *113*, 6378-6396.
27. Miertus, S.; Scrocco, E.; Tomasi, J., Electrostatic Interaction of a Solute with a Continuum. A Direct Utilization of Ab Initio Molecular Potentials for the Prevision of Solvent Effects. *Chem. Phys.* **1981,** *55*, 117-129.
28. Car, R.; Parrinello, M., Unified Approach for Molecular Dynamics and Density-Functional Theory. *Phys. Rev. Lett.* **1985,** *55*, 2471-2474.
29. Curtiss, L. A.; Redfern, P. C.; Raghavachari, K., Gaussian-4 Theory. *J. Chem. Phys.* **2007,** *126*, 084108.
30. Curtiss, L. A.; Redfern, P. C.; Raghavachari, K., Gaussian-4 Theory Using Reduced Order Perturbation Theory. *J. Chem. Phys.* **2007,** *127*, 124105.
31. Shavitt, I.; Bartlett, R., *Many-Body Methods in Chemistry and Physics: Mbpt and Coupled-Cluster Theory*. Cambridge University Press, Cambridge: 2009.
32. Read, J., Ether-Based Electrolytes for the Lithium/Oxygen Organic Electrolyte Battery. *J. Electrochem. Soc.* **2006,** *153*, A96-A100.
33. Kowaluk, I.; Read, J.; Salomon, M., Li-Air Batteries: A Classic Example of Limitations Owing to Solubilities. *Pure Appl. Chem.* **2007,** *79*, 851-860.
34. Mizuno, F.; Nakanishi, S.; Kotani, Y.; Yokoishi, S.; Iba, H., Rechargeable Li-Air Batteries with Carbonate-Based Liquid Electrolytes. *Electrochemistry* **2010,** *78*, 403-405.
35. Ogasawara, T.; Debart, A.; Holzapfel, M.; Novak, P.; Bruce, P. G., Rechargeable Li2O2 Electrode for Lithium Batteries. J. *Am. Chem. Soc.* **2006,** *128*, 1390-1393.
36. Debart, A.; Paterson, A. J.; Bao, J.; Bruce, P. G., Alpha-MnO2 Nanowires: A Catalyst for the O-2 Electrode in Rechargeable Lithium Batteries. *Angew. Chem. Int. Ed.* **2008,** *47*, 4521-4524.
37. Débart, A.; Bao, J.; Armstrong, G.; Bruce, P. G., An O2 Cathode for Rechargeable Lithium Batteries: The Effect of a Catalyst. *Journal of Power Sources* **2007,** *174*, 1177-1182.
38. Thapa, A. K.; Ishihara, T., Mesoporous a-MnO2/Pd catalyst air electrode for rechargeable lithium–air battery. *Journal of Power Sources* **2011,** *196*, 7016-7020.
39. Débart, A.; Paterson, A. J.; Bao, J.; Bruce, P. G., A-MnO2 Nanowires: A Catalyst for the O2 Electrode in Rechargeable Lithium Batteries. *Angew. Chem. Int. Ed.* **2008,** *47*, 4521-4524.
40. Yang, Y.; Sun, Q.; Li, Y.-S.; Li, H.; Fu, Z.-W., Nanostructured Diamond Like Carbon Thin Film Electrodes for Lithium Air Batteries. *J. Electrochem. Soc.* **2011,** *158*, B1211-B1216.
41. Freunberger, S. A.; Chen, Y.; Peng, Z.; Griffin, J. M.; Hardwick, L. J.; Barde, F.; Novak, P.; Bruce, P. G., Reactions in the Rechargeable Lithium-O2 Battery with Alkyl Carbonate Electrolytes. J. *Am. Chem. Soc.* **2011,** *133*, 8040-8047.
42. Xu, W.; Viswanathan, V. V.; Wang, D.; Towne, S. A.; Xiao, J.; Nie, Z.; Hu, D.; Zhang, J.-G., Investigation on the Charging Process of Li2O2-Based Air Electrodes in Li–O2 Batteries with Organic Carbonate Electrolytes. *Journal of Power Sources* **2011,** *196*, 3894-3899.
43. Black, R.; Oh, S. H.; Lee, J.-H.; Yim, T.; Adams, B.; Nazar, L. F., Screening for Superoxide Reactivity in Li-O2 Batteries: Effect on Li2O2/Lioh Crystallization. J. *Am. Chem. Soc.* **2012,** *134*, 2902-2905.
44. Zhang, Z., et al., Increased Stability toward Oxygen Reduction Products for Lithium-Air Batteries with Oligoether-Functionalized Silane Electrolytes. *J. Phys. Chem. C* **2011,** *115*, 25535-25542.

45. Bryantsev, V. S.; Blanco, M., Computational Study of the Mechanisms of Superoxide-Induced Decomposition of Organic Carbonate-Based Electrolytes. *J. Phys. Chem. Lett.* **2011,** *2*, 379-383.
46. Laoire, C. O.; Mukerjee, S.; Plichta, E. J.; Hendrickson, M. A.; Abraham, K. M., Rechargeable Lithium/Tegdme-Lipf[Sub 6]/O[Sub 2] Battery. *J. Electrochem. Soc.* **2011,** *158*, A302-A308.
47. Lau, K. C.; Assary, R. S.; Redfern, P.; Greeley, J.; Curtiss, L. A., Electronic Structure of Lithium Peroxide Clusters and Relevance to Lithium-Air Batteries. *J. Phys. Chem. C* **2012,** *116*, 23890-23896.
48. Laino, T.; Curioni, A., A New Piece in the Puzzle of Lithium/Air Batteries: Computational Study on the Chemical Stability of Propylene Carbonate in the Presence of Lithium Peroxide. *Chem. Eur. J.* **2012,** *18*, 3510-3520.
49. Bryantsev, V. S.; Blanco, M.; Faglioni, F., Stability of Lithium Superoxide LiO2 in the Gas Phase: Computational Study of Dimerization and Disproportionation Reactions. *J. Phys. Chem. A* **2010,** *114*, 8165-8169.
50. Aurbach, D.; Daroux, M.; Faguy, P.; Yeager, E., The Electrochemistry of Noble Metal Electrodes in Aprotic Organic Solvents Containing Lithium Salts. *Journal of Electroanalytical Chemistry and Interfacial Electrochemistry* **1991,** *297*, 225-244.
51. Read, J.; Mutolo, K.; Ervin, M.; Behl, W.; Wolfenstine, J.; Driedger, A.; Foster, D., Oxygen Transport Properties of Organic Electrolytes and Performance of Lithium/Oxygen Battery. *J. Electrochem. Soc.* **2003,** *150*, A1351-A1356.
52. Freunberger, S. A.; Chen, Y.; Drewett, N. E.; Hardwick, L. J.; Bardé, F.; Bruce, P. G., The Lithium–Oxygen Battery with Ether-Based Electrolytes. *Angew. Chem. Int. Ed.* **2011,** *50*, 8609-8613.
53. McCloskey, B. D.; Scheffler, R.; Speidel, A.; Bethune, D. S.; Shelby, R. M.; Luntz, A. C., On the Efficacy of Electrocatalysis in Nonaqueous Li-O2 Batteries. J. *Am. Chem. Soc.* **2011,** *133*, 18038-18041.
54. Xu, W.; Xiao, J.; Wang, D.; Zhang, J.; Zhang, J.-G., Crown Ethers in Nonaqueous Electrolytes for Lithium/Air Batteries. *Electrochemical and Solid-State Letters* **2010,** *13*, A48-A51.
55. Jung, H.-G.; Hassoun, J.; Park, J.-B.; Sun, Y.-K.; Scrosati, B., An Improved High-Performance Lithium-Air Battery. *Nat Chem* **2012,** *4*, 579-585.
56. Assary, R. S.; Curtiss, L. A.; Redfern, P. C.; Zhang, Z.; Amine, K., Computational Studies of Polysiloxanes: Oxidation Potentials and Decomposition Reactions. *J. Phys. Chem. C* **2011,** *115*, 12216-12223.
57. Okamoto, Y.; Kubo, Y., Ab Initio Calculations for Decomposition Mechanism of Ch3o(Ch2ch2o)Nch3 (N = 1-4) by the Attack of $O2^-$ Anion. *J. Phys. Chem. C* **2013,** 117, 15940-15946.
58. Assary, R. S.; Lau, K. C.; Amine, K.; Sun, Y.-K.; Curtiss, L. A., Interactions of Dimethoxy Ethane with Li2O2 Clusters and Likely Decomposition Mechanisms for Li-O2 Batteries. *J. Phys. Chem. C* **2013,** *117*, 8041-8049.
59. McCloskey, B. D.; Speidel, A.; Scheffler, R.; Miller, D. C.; Viswanathan, V.; Hummelshoj, J. S.; Norskov, J. K.; Luntz, A. C., Twin Problems of Interfacial Carbonate Formation in Nonaqueous Li-O2 Batteries. *J. Phys. Chem. Lett.* **2012,** 10.1021/jz300243r, 997-1001.
60. Wang, H.; Xie, K., Investigation of Oxygen Reduction Chemistry in Ether and Carbonate Based Electrolytes for Li-O2 Batteries. *Electrochimica Acta* **2012,** *64*, 29-34.
61. Veith, G. M.; Nanda, J.; Delmau, L. H.; Dudney, N. J., Influence of Lithium Salts on the Discharge Chemistry of Li-Air Cells. *J. Phys. Chem. Lett.* **2012,** *3*, 1242-1247.
62. Assary, R. S.; Lu, J.; Du, P.; Luo, X.; Zhang, X.; Ren, Y.; Curtiss, L. A.; Amine, K., The Effect of Oxygen Crossover on the Anode of a Li–O2 Battery Using an Ether-Based Solvent: Insights from Experimental and Computational Studies. *ChemSusChem* **2013,** *6*, 51-55.
63. Bryantsev, V. S.; Uddin, J.; Giordani, V.; Walker, W.; Addison, D.; Chase, G. V., The Identification of Stable Solvents for Nonaqueous Rechargeable Li-Air Batteries. *J. Electrochem. Soc.* **2013,** *160*, A160-A171.

64. Bryantsev, V. S., Predicting the Stability of Aprotic Solvents in Li-Air Batteries: Pk(a) Calculations of Aliphatic C-H Acids in Dimethyl Sulfoxide. *Chem. Phys. Lett.* **2013,** *558*, 42-47.
65. Bryantsev, V. S.; Faglioni, F., Predicting Autoxidation Stability of Ether- and Amide-Based Electrolyte Solvents for Li-Air Batteries. *J. Phys. Chem. A* **2012,** *116*, 7128-7138.
66. Bryantsev, V. S., Calculation of Solvation Free Energies of Li+ and O-2(-) Ions and Neutral Lithium-Oxygen Compounds in Acetonitrile Using Mixed Cluster/Continuum Models. *Theor. Chem. Acc.* **2012,** *131,* 1250.

Index

T.R. Jow et al. (eds.), *Electrolytes for Lithium and Lithium-Ion Batteries*, Modern Aspects of Electrochemistry 58, DOI 10.1007/978-1-4939-0302-3,